The production and preservation of fish-derived carbonates in shallow sub-tropical marine carbonate provinces

Michael A. Salter

A thesis submitted in partial fulfilment of the requirements
of the Manchester Metropolitan University
for the Degree of
Doctor of Philosophy

School of Science and the Environment
Manchester Metropolitan University
August 2013

ABSTRACT

Recent studies have demonstrated that marine bony fish (teleosts) precipitate inorganic calcium carbonate in their gut as a by-product of osmoregulation, subsequently excreting it into the open water column as loosely aggregated millimetre-scale pellet. These studies have primarily focused on physiological aspects of this process and the fate of resulting carbonates in pelagic settings, which is likely to be dissolution at depth. However, the implications of such carbonate production in shallow tropical and sub-tropical carbonate provinces has also begun to be considered, and it is thought that fish may contribute significant quantities of morphologically distinctive mud-grade high-Mg calcite in certain habitat settings. However, most studies of carbonate mud in modern sub-tropical settings do not report particles that are obviously fish-derived, and questions concerning fish-derived carbonate characteristics and post-excretion stability thus arise.

The present work therefore provides more detailed characterisation of the carbonate products of an expanded range of Caribbean fish species and determines their short-term preservation potential in a sub-tropical carbonate province (the Bahamas). Following collection of carbonates from 22 fish species (all starved), precipitates were characterised using scanning electron microscopy and a suite of complimentary chemical analysis techniques. The form in which these carbonates are likely to be incorporated into surface sediments was investigated by disaggregating pellets and characterising the liberated particles by performing detailed image-based grain size analyses, with additional experiments demonstrating the likely rate and extent of pellet disaggregation by placing them in agitated seawater. Finally, short-term preservation potential was determined in a series of experiments whereby excreted precipitates were exposed to surface seawater and shallow sub-surface porewater conditions for several months.

Results indicate that, at the point of excretion, fish-derived carbonates are morphologically and mineralogically more varied than previously thought, although most morphotypes (*e.g.*, ellipsoids, dumbbells, spheres, rhombohedra) are seemingly unique in shallow sub-tropical marine settings.

High-Mg calcite, typically containing 20–35 mol% $MgCO_3$, is the dominant product of about half the species investigated, but Mg calcite with lower $MgCO_3$ contents (in the range 2–20 mol%) is also common, as is aragonite, which can represent up to 27 wt% of carbonates excreted by some species. In addition, amorphous magnesium carbonate (AMC) and magnesium-rich amorphous calcium carbonate (ACC), both of which are strongly hydrated, represent the dominant precipitation products of some species, with a hydrated crystalline phase (monohydrocalcite) occasionally accompanying the latter. A non-carbonate phase, brucite, is nearly ubiquitous as a volumetrically minor phase. Where analysed, all of these phases are further found to differ from other carbonate sediments in the Bahamas with regard to their stable carbon and oxygen isotope compositions; a consequence of the important role of metabolic HCO_3^- in the precipitation process.

Detailed grain size analyses indicate that most morphotypes are released from pellets upon disaggregation as individual mud-grade particles that retain their distinctive forms. However, extreme agitation can result in polycrystalline forms releasing their fibre-like components; these particles being less distinctive than their parent forms. In contrast, some particles are intergrown and do not disaggregate beyond particle clusters that are up to fine sand sized. Moreover, excreted pellets do not necessarily always disaggregate, with moderate agitation in seawater resulting in a significant proportion of carbonate being retained as intact pellets, albeit smaller (typically fine sand sized) and more well-rounded than initial pellets (typically fine to coarse sand sized). In quiescent settings pellet diminution is less extensive, and it is thus hypothesised that a significant proportion of fish-derived carbonates excreted in the Bahamas is preserved as sand-grade pellets.

Despite the highly distinctive nature of fish-derived carbonates, particles that can be attributed to production by fish nevertheless remain elusive in studies of Bahamian surface sediments. It is thus necessary to invoke post-excretion processes of dissolution and/or recrystallisation to explain the apparent disparity between production rates and occurrence as sedimentary particles. Indeed, it is demonstrated here that AMC, brucite, and large quantities of ACC undergo complete dissolution in seawater within a few days of excretion, with the remaining ACC apparently crystallising to form fine sand-grade (50–200 μm diameter) polycrystalline calcite spheres over similar timescales.

Monohydrocalcite, also undergoes complete dissolution or alteration (to calcite) during 3 month exposures to artificial seawater, and is predicted to alter in a similar manner in natural settings.

Conversely, anhydrous crystalline phases remain largely unchanged after porewater and seawater exposures lasting several months, although two important post-excretion processes are observed. Firstly, high-Mg calcite ellipsoids appear to undergo partial dissolution (with preferential loss of $MgCO_3$) and possible recrystallisation, and, based on these observations, it is predicted that longer exposure times will result in changes being pervasive, possibly obscuring the piscine origin of initial crystals. Secondly, carbonate pellets containing minor amounts of aragonite at the point of excretion appear, in some cases, to stimulate post-excretion growth of abundant aragonite needles that are morphologically similar to aragonite needles that dominate Bahamian carbonate muds. It is further apparent that these processes are inhibited in uncleaned samples, possibly due to surface adsorption of organic compounds, but the evidence after 3 month exposures indicates that inhibiting factors might eventually be overcome.

Based on these results and modelling of carbonate excretion across shallow platform areas of the entire Bahamian archipelago, it is predicted that about 18 % of excreted carbonates will dissolve after excretion, while a further 53 % may alter beyond recognition within a very short period (perhaps on the order of years). Moreover, characterisation of carbonates produced by three species of normally feeding fish indicates they produce only amorphous carbonates, despite producing crystalline phases when starved. This difference, attributed to the inhibition of $CaCO_3$ crystallisation by dietary phosphate, indicates that loss of fish-derived carbonate to dissolution might be considerably higher than 18 % under normal natural circumstances.

The sedimentary significance of fish-derived carbonates thus remains enigmatic, but results presented herein indicate that they follow very different preservation pathways depending on their excreted form, and that they may make previously unrecognised contributions to: i) the carbonate sand fraction (as peloids); and ii) aragonite needle muds (as crystals grown post-excretion).

ACKNOWLEDGEMENTS

During the three years I have spent producing this thesis innumerable people have offered their invaluable support, both scientific and otherwise.

Chiefly among these people, I must first extend a great many thanks to my supervisors, Chris Perry and Rod Wilson, for their continuing support and guidance; a constant source of reassurance. Also to Cathy Delaney, who seamlessly took over as my Director of Studies following the departure of Chris to pastures new, and has been unerring in her support and encouragement.

In addition I am indebted to numerous staff in the laboratories at Manchester Metropolitan University and the University of Exeter for their technical support and advice. In particular, thanks to Vladimir Vishniyakov, Gary Miller, Sue Hutchinson, David McKendry, and Dave Groom in Manchester, and Jon Whittamore and Rob Ellis in Exeter. A special mention must go to Erin Reardon for providing many stimulating discussions and for her unfailing willingness to help with analytical procedures in Exeter when I could not be there myself. Fellow postgraduate students, both in Manchester and in Exeter, are also thanked for their support and useful insights.

Alistair Harborne at the Marine Spatial Ecology Laboratory, University of Queensland, is thanked for his contribution to Chapter 7, in which he combined his fish biomass and habitat data from the Bahamas with data arising from this thesis to provide carbonate production estimates in a range of Bahamian platform settings. I am also grateful to Stephen Crowley (University of Liverpool) and Paul Dennis (University of East Anglia), who kindly performed stable isotope analyses, including calculations necessary to derive the values as reported herein (Chapters 5 and 7).

Finally on the technical side of things, I must thank all of the staff at the Cape Eleuthera Institute, without whom the collection of carbonate samples would have been very much more difficult. Particular thanks go to Annabelle and Edd Brooks, Aaron Shultz, Dave Phillipp, Thiago Soligo, Tyler Sclodnick, Marie Tarnowski, Skylar Miller, Justin Lewis, and Sarah Briggs.

For personal support, my first and foremost thanks go to Fiona, who has always been there for me and was (nearly) always happy to humour me whenever I would get carried away discussing the subtleties of biochemical processes operating in fish. Without you none of this would have been possible. Also to my parents for always encouraging me and instilling in me a determination and a desire for knowledge, without which this thesis would never have been completed. They, and the rest of my family, have provided ever-dependable support and encouragement. Finally to my Grandfather, whose sad passing shortly before submission of this thesis provided the final impetus for me to complete the work as something that I hope he will be proud of. This work is completed in your memory.

CONTENTS

Abstract **i**

Acknowledgements **iv**

List of tables **xi**

List of Figures **xii**

1. Background and rationale for study **1**

1.1 Significance and origins of mud-grade carbonates in modern and ancient shallow sub-tropical marine sedimentary settings 1

1.2 Marine teleosts (bony fishes) as a source of mud-grade carbonates 4

1.3 Stability of carbonates in modern marine environments 10

1.3.1 Carbonate solubility 11

1.3.2 Carbonate stability in surface seawater 18

1.3.3 Porewater chemistry 20

1.3.4 Observed early diagenetic changes in carbonate minerals 24

1.3.5 Considerations on the post-excretion fate of fish-derived carbonates 31

1.4 Aims and objectives 33

1.4.1 Phase 1 33

1.4.2 Phase 2 34

1.5 Study area 35

2. The sedimentary significance of fish-derived carbonates: Characterisation from an expanded range of Caribbean fish species **40**

2.1 Introduction 40

2.2 Materials and methods 42

2.2.1 Sample collection 42

2.2.2 Morphological analyses 44

2.2.3 Mineralogical and chemical analyses 45
2.3 Results 48
2.3.1 Crystal morphology 51
2.3.2 Mineralogy and chemical composition 64
2.4 Discussion 73
2.4.1 Fish-derived carbonates and their classification 73
2.4.2 Crystal growth mechanisms 75
2.4.3 Crystal growth sequences 78
2.4.4 Relevance of fish-derived carbonates in carbonate muds 81
2.4.5 Post-excretion pathways 83
2.5 Conclusions 86
3. Inorganic phases of fish-derived carbonates and the presence of water and organic matter: Infrared analysis and implications for stability in shallow marine settings 88
3.1 Introduction 88
3.2 FTIR analysis of inorganic carbonates 92
3.3 Methodology 97
3.3.1Transmission FTIR 98
3.3.2 Attenuated total reflectance FTIR 99
3.3.3 Post-processing of spectra 100
3.3.4 Scanning electron microscopy 100
3.4 Results 100
3.4.1 Spectra generated by monocrystalline ellipsoids and small dumbbells 104
3.4.2 Spectra generated by spheres, dumbbells, and other morphotypes 108
3.4.3 Spectra generated by precipitates that lack definable form 114
3.4.4 Peak deconvolution: H–O–H bending and the CO_3^{2-} asymmetric stretch 116
3.4.5 Non-carbonate phases 120
3.5 Discussion 122
3.5.1 Previously unrecognised phases and their likely post-excretion fates 122

3.5.2 Implications for the stability of Mg calcite due to low crystallinity 125

3.5.3 Crystalline phases: excreted products or artefacts of sample preparation 126

3.5.4 Water and organic phases 129

3.6 Conclusions 130

4. Pilot study comparing the carbonate precipitation products of starved and fed fish 133

4.1 Introduction 133

4.2 Methodology 135

4.3 Results 136

4.3.1 Ellipsoid producing species 136

4.3.2 Dumbbell and nanosphere producing species 142

4.4 Discussion 145

4.4.1 Mechanisms driving variations in precipitation products 146

4.4.2 Implications for the sedimentary significance of fish-derived carbonates 148

4.5 Conclusions 151

5. Stable isotope composition of fish-derived carbonates: Carbon and oxygen 153

5.1 Introduction 153

5.2 Methodology 157

5.3 Results 161

5.4 Discussion 167

5.4.1 Precipitation processes 167

5.4.2 Relevance to studies of bulk surface sediments in the Bahamas 171

5.5 Conclusions 173

6. Size-fraction analysis of fish-derived carbonates: Implications for their deposition in and around shallow sub-tropical marine carbonate provinces 175

6.1 Introduction 175

6.2 Terminologies 178

6.3 Materials and methods 179

6.3.1 Sample collection 179

6.3.2 Particle size measurements 180
6.3.3 Data plotting 184
6.3.4 Simulation of wave-generated agitation 186
6.3.5 Sedimentary pellet examination 187
6.4 Results 189
6.4.1 Pellet size analysis 189
6.4.2 Disaggregated particles 194
6.4.3 Pellet evolution under agitated conditions 197
6.4.4 Sedimentary pellets 202
6.5 Discussion 204
6.5.1 Transport and deposition in leeward platform settings 204
6.5.2 Transport and deposition in other platform settings 213
6.6 Conclusions 216
7. Short-term preservation pathways of fish-derived carbonates upon exposure to seawater and porewater conditions 219
7.1 Introduction 219
7.2 Methodology 221
7.2.1 Sample collection 221
7.2.2 Seawater and porewater exposure experiments 222
7.2.3 Analytical procedures 234
7.2.4 Estimating the proportions of various precipitation products 241
7.3 Results 243
7.3.1 Sediment, seawater and porewater characterisation 243
7.3.2 Seawater and porewater exposures 249
7.3.3 Stable isotope compositions: Carbon and oxygen 297
7.4 Platform-wide gut carbonate production modelling 300
7.5 Discussion 305
7.5.1 Short-term fate of fish-derived carbonates 305

7.5.2 Implications of manganese precipitation in artificial seawater 313

7.6 Conclusions 317

8. Summary of the present work and recommendations for the future 319

8.1 Introduction 319

8.2 Summary of outcomes of present work 320

8.2.1 Characterisation 320

8.2.2 Short-term post-excretion fate (months) 325

8.2.3 Longer-term preservation potential: A hypothesis 331

8.2.4 Geological implications 334

8.3 Recommendations for future work 340

8.4 Precipitation products: An overview with respect to teleostal phylogenies 346

References 352

Appendices 379

Appendix I – X-ray diffraction data 379

Appendix II – Composition data (energy-dispersive X-ray spectroscopy) 385

Appendix III – Compositional data (liquid ion chromatography) 422

Appendix IV – Representative ATR-FTIR spectra (all species) 428

Appendix V – Full stable isotope (carbon and oxygen) data 433

Appendix VI – Grain sizes (pellets and crystals; full data set) 435

Appendix VII – Pellet size data (before and after pellet agitation) 484

Appendix VIII – Estimated volumetric abundances of different precipitation products 499

Appendix IX – Carbonate production rate data 500

Related publications 504

List of tables

1.1	Summary of the mineralogical, compositional, and morphological characteristics of fish-derived carbonates determined prior to this study.	6
2.1	List of fish species sampled in this study and the key data arising from each.	50
2.2	Relative quantities of aragonite and calcite present in fish-derived carbonates at the point of excretion.	65
3.1	Infrared spectroscopic data reported in literature for calcite, Mg calcite and aragonite.	94
3.2	Infrared spectroscopic data reported in literature for various hydrated Ca- and Mg-bearing carbonate phases (including amorphous calcium carbonate).	95
3.3	Infrared spectroscopic data reported in literature for various anhydrous Ca- and Mg-bearing carbonate and hydroxy phases.	96
3.4	Table summarising the key data output from FTIR analyses with respect to phases present in samples produced by each fish species investigated.	103
4.1	Summary of key compositional data arising from analysis of carbonate samples produced by fed and starved fish.	142
5.1	Average ^{13}C and ^{18}O stable isotope compositions of carbonates produced by different fish species.	162
6.1	Terminology used to refer to various fish-derived carbonate particle types.	179
6.2	Species from which carbonates for grain size analyses were collected, and the estimated abundances of different crystal forms in each.	185
6.3	Size data for pellets at the point of excretion from six different Caribbean fish species.	190
6.4	Key data arising from size analyses of particles released upon pellet disaggregation.	196
7.1	List of species from which carbonates were collected for preservation experiments and a summary of the known excretion products.	222
7.2	Dissolved inorganic carbon system parameters and associated calcite and aragonite saturation states relating to seawater and porewater samples used in this study.	245
7.3	Dissolved ion ratios (for Mg^{2+}, Ca^{2+}, and Mn^{2+}) in freshly prepared artificial seawater, and changes in these ratios following addition of sedimentary mud-grade carbonates and fish-derived carbonates.	248
7.4	Summary of results from particle size analyses for recently excreted ellipsoidal fish-derived carbonates and the same carbonates following exposure to different post-excretion environments.	254

7.5	Ratios of carbonate to phosphate infrared peak intensities generated by high-Mg calcite ellipsoids (produced by schoolmaster snapper) at the point of excretion and after exposure to a range of seawater conditions.	260
7.6	Estimated amount of amorphous carbonates produced by fish as a proportion of total carbonates excreted in a range of platform settings in the Bahamas.	302
7.7	Estimated amount of high-Mg calcite ellipsoids produced by fish as a proportion of total carbonates excreted in a range of platform settings in the Bahamas.	304
8.1	Dominant precipitation products produced by fish belonging to different families and sub-orders within the order Perciformes.	350

List of figures

1.1	Sources and sinks of shallow platform carbonate mud.	3
1.2	Schematic diagram showing carbonate formation in the piscine gut.	5
1.3	Changes in solubility of Mg calcite with increasing magnesium content.	13
1.4	Schematic diagram showing interactions between calcite surface defects and potential dissolution/growth inhibitors.	15
1.5	Plot of ion concentration product against pCO_2, with equilibrium positions for various carbonate minerals shown. Also shown are positions of 'normal' surface seawater and surface seawater overlying the interior of the Great Bahama Bank.	19
1.6	Schematic diagram showing porewater projected porewater saturation states in a variety of sedimentary settings.	21
1.7	Summary of early diagenetic textures in fine-grained carbonates.	27
1.8	Electron microscope images comparing fresh and altered skeletal sedimentary particles to illustrate typical early diagenetic textures in fine-grained carbonates.	29
1.9	Electron microscope images showing a range of synsedimentary recrystallisation textures and associated carbonate cements.	29
1.10	Location map of the study area and the main sedimentary environments of Eleuthera Sound.	36
1.11	Typical subaqueous environments around Cape Eleuthera and Eleuthera Sound	37
1.12	Images of some of the fish species used in this study (pisci-invertivores and macroinvertivores)	38
1.13	Images of some of the fish species used in this study (apex predators, omnivores, herbivores, planktivores, and pisciivores)	39
2.1	Chart showing grain size ranges of main forms of fish-derived carbonate.	49

2.2	Secondary electron (SE) images of various ellipsoidal fish-derived carbonates.	53
2.3	SE images of various dumbbell-shaped fish-derived carbonates.	55
2.4	SE images of various spherical and needle-shaped fish-derived carbonates.	59
2.5	SE images of rhombohedral fish-derived carbonates and precipitates lacking definable form.	61
2.6	SE images of various forms of platy magnesium-rich precipitates excreted along with some fish-derived carbonates.	63
2.7	X-ray diffraction patterns of carbonates produced by bluehead wrasse and checkered puffer.	66
2.8	Backscatter electron images of carbonate pellets containing Mg calcite rhombohedra and magnesium-rich precipitates lacking definable form.	68
2.9	Plot of measured $SrCO_3$ contents against $MgCO_3$ contents for various fish-derived carbonate morphotypes, differentiating between aragonite and Mg calcite particles.	71
2.10	Schematic diagram showing possible morphogenetic sequences in fish-derived carbonates.	79
2.11	Comparison of fish-derived carbonate grain size distribution against those of other known carbonate mud producers and a typical mud fraction of Bahamian surface sediment.	82
2.12	Reported $MgCO_3$ compositional ranges for several known tropical marine carbonate mud producers compared with measured $MgCO_3$ contents of various carbonate crystal forms produced by a range of tropical fish species.	85
3.1	Infrared-active vibration modes of the carbonate ion in carbonate minerals.	93
3.2	ATR-FTIR spectra for some commonly occurring skeletal carbonates in the Bahamas and fish-derived carbonates.	102
3.3	Representative FTIR spectra for ellipsoid- and dumbbell-shaped fish-derived Mg calcite.	105
3.4	Representative FTIR spectra for a range of fish-derived carbonate products that include Mg calcite, aragonite, monohydrocalcite, and amorphous phases	111
3.5	FTIR spectra for assorted fish-derived carbonates in addition to those shown in Figs. 3.3 and 3.4.	112
3.6	Representative FTIR spectra for carbonates produced by bluehead wrasse.	115
3.7	Component peaks of the carbonate ν_3 vibration for various fish-derived carbonates.	117
3.8	FTIR spectra indicating the presence of brucite in some fish-derived carbonates.	121
4.1	Electron microscope images and associated FTIR and energy-dispersive X-ray spectra for carbonates produced by recently fed fish (schoolmaster snapper).	138

4.2 Electron microscope images and associated FTIR and energy-dispersive X-ray spectra for carbonates produced by recently fed fish (black grouper). 139

4.3 Relationship between phosphorus and $MgCO_3$ contents in gut precipitates excreted by recently fed fish (schoolmaster snapper). 141

4.4 Electron microscope images and associated FTIR and energy-dispersive X-ray spectra for carbonates produced by recently fed fish (great barracuda). 144

4.5 Diagram showing proposed cyclical variations in precipitation product characteristics according to time since last feeding event. 148

5.1 $\delta^{13}C$ and $\delta^{18}O$ values for carbonates produced a range of naturally fed fish species. 162

5.2 Comparison of $\delta^{13}C$ and $\delta^{18}O$ values determined for fish-derived carbonates produced by naturally-fed and sardine-fed fish. 165

5.3 Effect of sample preparation on stable isotope ratios in fish-derived carbonates. 166

5.4 Hypothesised pathways of ^{13}C from dietary source to precipitated carbonates. 170

5.5 Comparison of the $\delta^{13}C$ and $\delta^{18}O$ values of fish-derived carbonates with available data for surface sediments and other carbonate sources in the Bahamas. 172

6.1 Screenshots showing pellet size measurement technique using JMicroVision software. 182

6.2 Screenshot showing crystal size measurement technique using JMicroVision software. 183

6.3 Facies map of Eleuthera Sound showing surface sediment sampling locations. 188

6.4 Optical microscope and electron microscope images showing fish-derived carbonates (produced by bluehead wrasse, schoolmaster snapper, and great barracuda) in their excreted forms as: i) intact pellets; ii) crystals within intact pellets; and iii) particles and crystals released following pellet disaggregation. 191

6.5 Optical microscope and electron microscope images showing fish-derived carbonates (produced by bonefish, checkered puffer, and black grouper) in their excreted forms as: i) intact pellets; ii) crystals within intact pellets; and iii) particles and crystals released following pellet disaggregation. 192

6.6 Histograms showing grain size distributions of fish-derived carbonates as intact pellets and as particles released upon pellet disaggregation. 193

6.7 Electron microscope images showing fish-derived carbonates excreted as: a) particles encrusted on ingested skeletal fragments; and b) crystals apparently aggregated about a pre-existing organic structure (*i.e.*, mucus matrix). 194

6.8 Grain size distribution of fish-derived carbonate pellets at the point of excretion and after periods of moderate agitation in artificial seawater. 198

6.9 Optical microscope images of fish-derived carbonate pellets at the point of excretion and after periods of moderate and gentle agitation in artificial seawater. 199

6.10 Electron microscope images showing the component carbonate particles of presumed faecal pellets and pseudopellets in the surface sediment collected from two sites in Eleuthera Sound. 203

6.11 Conceptual model for the transport and depositional fates of fish-derived carbonates in a leeward setting in the Bahamas. 207

6.12 Plot of fish-derived carbonate pellet length against width shown along with the dimensions of sedimentary carbonate pellets and peloids reported in the literature. 210

7.1 Experimental arrangement for natural seawater exposures. 223

7.2 Experimental arrangement for artificial seawater exposures. 227

7.3 Schematic diagram showing design of porewater exposure chambers. 230

7.4 Diagram showing installation of porewater exposure chambers. 233

7.5 Calibration curve for osmolality against salinity to enable accurate determination of salinity of small seawater samples. 237

7.6 Schematic representation of analytical arrangement for determination of TCO_2. 239

7.7 Grain size distribution and X-ray diffraction pattern for surface sediment at the porewater exposure site. 249

7.8 Summary diagram showing main morphological changes observed in fish-derived carbonates during seawater and porewater exposures. 250

7.9 Photographs showing typical fish-derived carbonate pellets at the end of natural seawater exposures and disaggregated pellets resulting from exposure to non-aerated seawater. 252

7.10 Electron microscope images of ellipsoidal fish-derived carbonates (produced by schoolmaster snapper) following exposure to natural seawater and porewater. 256

7.11 Electron microscope images of ellipsoidal fish-derived carbonates (produced by schoolmaster snapper) following exposure to artificial seawater. 257

7.12 ATR-FTIR spectra for ellipsoidal fish-derived carbonates (produced by schoolmaster snapper) following exposure to various seawater and porewater solutions. 259

7.13 Histograms showing distribution of $MgCO_3$ contents in ellipsoidal high-Mg calcite (produced by schoolmaster snapper) after seawater and porewater exposures. 262

7.14 Electron microscope images of carbonates (produced by yellowfin mojarra) following exposure to natural seawater and porewater. 267

7.15 Electron microscope images of needle-like forms grown in porewater exposure chambers in association with cleaned carbonates produced by yellowfin mojarra. 268

7.16 ATR-FTIR spectra for fish-derived carbonates (produced by yellowfin mojarra) following various post-excretion exposures to natural seawater solutions. 270

7.17 Photographs illustrating the rapid dissolution in natural seawater of carbonates produced by bluehead wrasse. 273

7.18 Electron microscope images showing morphologies of fish-derived carbonates (produced by keeltail needlefish) following exposure to natural seawater and porewater. 276

7.19 Electron microscope images showing morphologies of fish-derived carbonates (produced by bluehead wrasse) following brief exposure to natural seawater. 278

7.20 ATR-FTIR spectra for fish-derived carbonates (produced by keeltail needlefish) following various post-excretion exposures to natural seawater solutions. 281

7.21 Electron microscope images showing morphologies of fish-derived carbonates (produced by bonefish) following brief exposure to natural seawater. 285

7.22 Electron microscope images showing morphologies of fish-derived carbonates (produced by bonefish) following exposure to porewater and artificial seawater. 286

7.23 Histograms showing the size range of spheres (produced by bonefish) at the point of excretion and after exposure to natural seawater and porewater. 288

7.24 ATR-FTIR spectra for fish-derived carbonates (produced by bonefish) at the point of excretion. 291

7.25 ATR-FTIR spectra for fish-derived carbonates (produced by bonefish) following exposure to natural seawater, porewater, and artificial seawater. 294

7.26 Comparison of fish-derived carbonate stable isotope (carbon and oxygen) compositions at the point of excretion and after 91 days in porewater conditions 298

7.27 Schematic representation of the main changes observed in fish-derived carbonates during short-term exposure to seawater and porewater, and the factors that might have influenced these changes. 309

7.28 Bahamian porewater chemistry from this study and from other studies, plotted as a function of pH against total alkalinity. 312

8.1 Schematic representation of the precipitation products described in this study. 322

8.2 Diagram summarising the chemical and mechanical processes that influence the short-term post-excretion fate of fish-derived carbonates, and how these processes might influence preservation styles over longer time-scales. 327

8.3 Phylogenetic tree showing marine fish lineages (*i.e.*, including lower classes than teleosts), and known osmoregulatory traits within each. 336

8.4 Summary of the key chemical differences between Cretaceous and modern seawater, and the hypothesised effects of these on carbonate production by fish. 339

8.5 Phylogenetic positions of fish that have been studied with regard to precipitation of gut carbonates, and the relationship of these positions with known precipitation products. 349

Chapter 1: Background and rationale for study

1.1 SIGNIFICANCE AND ORIGINS OF MUD-GRADE CARBONATES IN MODERN AND ANCIENT SHALLOW SUB-TROPICAL MARINE SEDIMENTARY SETTINGS

Carbonate muds form a volumetrically significant component of many modern carbonate sediments and ancient limestones (Matthews, 1966; Purdy and Gischler, 2003; Pomar and Hallock, 2008). Consequently, they are important in controlling the depositional character (grain size, texture etc.) of the sediments that accumulate in these environments, and can have important applications from the perspective of interpreting palaeo-environments (Flügel, 2004). The mineralogical composition of marine carbonate muds, and in particular the presence and abundance of magnesian calcites (Mg calcites), can be an important factor in determining sediment diagenetic pathways. Specifically, Mg calcite mud can influence the preservation of sedimentary textures and fabrics (Husseini and Matthews, 1972), and thus influence porosity and permeability patterns in limestones. Understanding the provenance and genesis of carbonate mud is therefore important, yet in limestones this is often hampered by pervasive recrystallisation (to micrite and microspar) or obliteration of fine-grained carbonate particles that often occurs during syn-depositional and burial diagenesis (Reid *et al*., 1992; Walter *et al*., 1993; Reid and MacIntyre, 1998). Thus carbonate mud sources in modern settings must necessarily be used as analogues for sources in ancient settings.

Carbonate muds in contemporary depositional systems have been attributed to various sources: i) direct physico-chemical precipitation from seawater, which possibly includes aragonite needles and carbonate particles associated with 'whitings' (Shinn *et al*., 1989; Robbins and Blackwelder, 1992); ii) mechanical and/or biological degradation of skeletal grains, such as calcareous green algae, coccolithophores, and foraminifera (Lowenstam and Epstein, 1957; Matthews, 1966; Stockman *et al*., 1967; Stieglitz, 1972; Fütterer, 1974; Debenay *et al*., 1999); and iii) bacteriogenic precipitation,

such as that occurring within intertidal and shallow sub-tidal microbial mats (Greenfield, 1963; Chafetz and Buczynski, 1992). These sources are summarised in Fig. 1.1 along with marine bony fish, which have recently been recognised as a potentially important source of carbonate mud in shallow marine settings (Perry *et al*., 2011; Salter *et al*., 2012; see section 1.2 for details). Despite this reasonably good understanding of mud sources, there is considerable debate as to the relative importance of each to carbonate sediment budgets in modern shallow marine environments (*e.g.*, Broecker and Takahashi, 1966; Neumann and Land, 1975; Shinn *et al*., 1989; Milliman *et al*., 1993; Broecker *et al*., 2000). This problem arises in large part from the difficulties in assigning sedimentary mud-grade carbonates to a distinctive source; this being due both to grain degradation (itself a process invoked in the generation of mud-grade carbonate; Matthews, 1966); and/or the early recrystallisation of fine-grained carbonates (Reid *et al*., 1992; MacIntyre and Reid, 1995; 1998; Reid and MacIntyre, 1998). Furthermore, some mud-grade carbonates, such as the aragonite needle products of whitings and calcareous green algae, can be difficult to distinguish due to morphological and chemical similarities (Boardman and Carney, 1991). Indeed, in recent studies of modern fine-grained carbonate sediments, 20–30 % of the mud fraction (and as much as 60% in some samples) typically remained 'unidentified' (Gischler and Zingeler, 2002; Gischler *et al*., 2013).

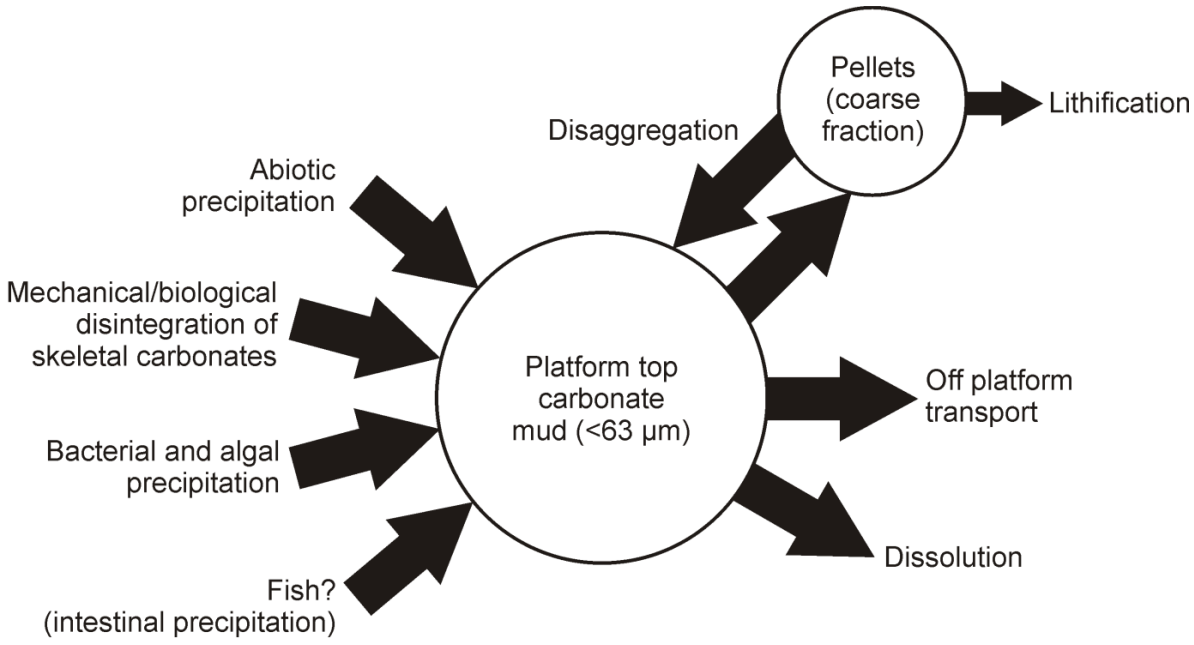

Figure 1.1 *Sources and sinks of shallow platform carbonate mud (modified after Neumann and Land, 1975). Recent studies have shown that marine fish may represent a previously unrecognised source. Relative contributions probably vary according to specific platform settings and are not estimated here.*

One of the classic environments in which work on carbonate mud production has been conducted is the Bahamian platform, where several studies (*e.g.*, Lowenstam and Epstein, 1957; Cloud, 1962) have identified aragonite as the predominant mud fraction mineral. This has led to much work on the production of aragonite mud, and while this remains a topic of debate, its sources are now reasonably well understood (Schlager, 2003). However, many studies also identify high-Mg calcite as an important mineral component of shallow tropical muds, not only in the Bahamas, but also in many other contemporary carbonate settings (*e.g.*, Chave, 1962; Taft and Harbaugh, 1964; Matthews, 1966; Husseini and Matthews, 1972; Gischler, 2011), where it can constitute up to 90% of the mud fraction (Reid *et al*., 1992). Gischler *et al.* (2013) compared mud-grade sediments from several carbonate platforms in the Atlantic, Pacific, and Indian Oceans, and confirmed that compositions are geographically variable, but that in most cases these sediments are biogenic in origin. However, they additionally interpret mud-grade sediments from northern Belize and the Bahamas as being largely inorganically-derived, with abiotic precipitates occurring as high-Mg calcite in the former, and aragonite in the latter. Despite this geographical clustering of carbonate mud types, it is clear that carbonate muds in most shallow tropical and sub-tropical settings should

be considered as a mixture of both biogenically- and inorganically-derived aragonite and high-Mg calcite. Accordingly, multiple origins of carbonate mud should be considered when attempting to reconstruct palaeo-environments, depositional regimes and diagenetic pathways.

1.2 MARINE TELEOSTS (BONY FISHES) AS A SOURCE OF MUD-GRADE CARBONATES

In a recent study, Perry *et al.* (2011) identified marine bony fish (teleosts) as a previously unknown, but prolific, primary source of morphologically distinctive high-Mg calcite mud-grade carbonate (at least at the point of excretion from the fish). Moreover, they emphasised the potential significance of this material in carbonate sedimentary budgets by showing that compositionally and morphologically similar high-Mg calcites occur in the finest fraction of surface sediments from a range of habitats sampled around the island of Eleuthera, the Bahamas.

The genesis of these carbonates, shown schematically in Fig. 1.2, involves primary precipitation within the intestines of bony marine fish (teleosts), and occurs as a by-product of their osmoregulatory requirement to continuously drink seawater in order to remain hydrated (an osmotic gradient exists between teleostal blood and the seawater that surrounds them, meaning they are constantly losing water). Intestinal HCO_3^-, which is metabolically-derived and is secreted at high rates through epithelial cells that line the intestinal lumen, is typically present at concentrations in the range 30 to >100 mM (*i.e.*, much greater than normal seawater, which typically contains approximately 1.5 to 2.0 mM; Morse *et al*., 1985). Within the resulting highly alkaline intestinal fluids (pH 8.3–9.3), high concentrations of imbibed Ca^{2+} and Mg^{2+} react with this HCO_3^- and precipitate out of solution as solid-phase inorganic carbonates (Walsh *et al*., 1991; Wilson and Grosell, 2003; Wilson *et al*., 1996; 2002; 2009; Grosell, 2006; Mekuchi *et al*., 2010). From a physiological point of view, this process is thought to facilitate intestinal water absorption by reducing the osmolality of intestinal fluids, and to limit calcium absorption, which could otherwise cause renal stone formation (Wilson *et al*., 2002; Wilson and Grosell, 2003).

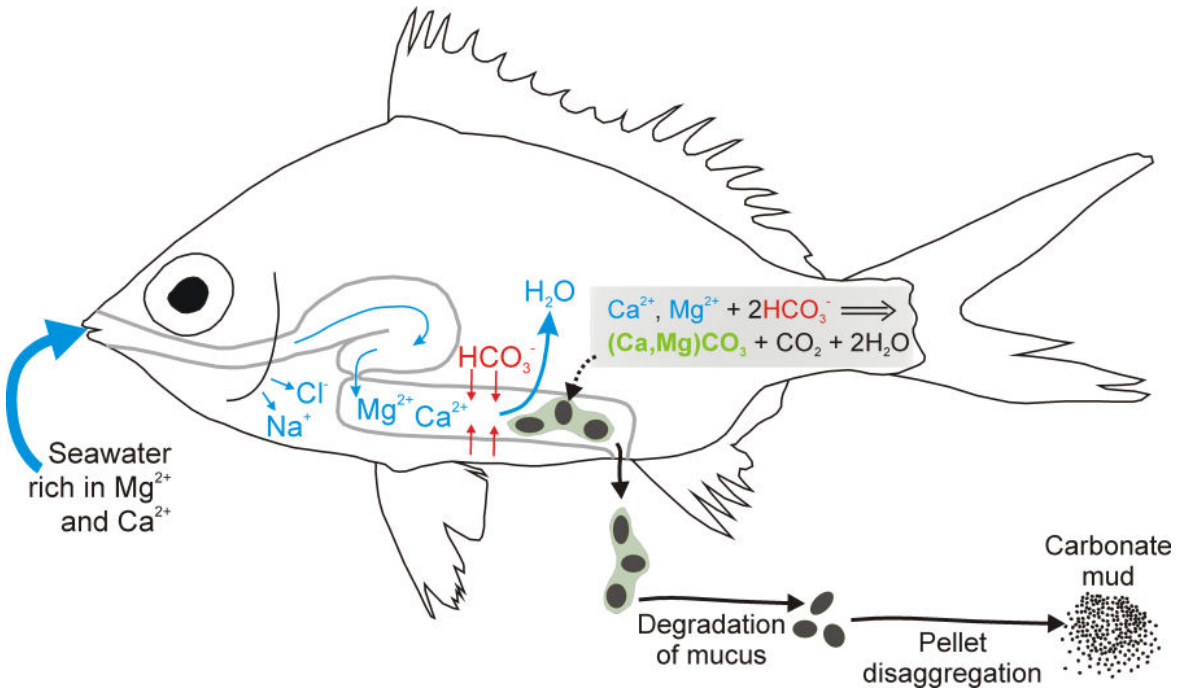

Figure 1.2 *Fish-derived carbonates form as intestinal precipitates resulting from the mixing of Ca^{2+} and Mg^{2+} in imbibed seawater with metabolically-derived HCO_3^- secreted through the intestinal lumen. Carbonates are typically excreted as loosely aggregated pellets of mud-grade high-Mg calcite.*

The resulting carbonate crystals are ultimately excreted as mucus-coated pellets along with faecal matter; the pellets themselves comprising loosely aggregated crystals of mainly high-Mg calcite (Walsh *et al*., 1991; Wilson *et al*., 2009; Perry *et al*., 2011). The nature of these crystals varies among fish species, but they are typically characterised by high magnesium contents (18–39 mol% $MgCO_3$), small particle sizes (<0.5 to >30.0 μm in length), and seemingly unique (in marine settings) morphologies that include ellipsoids, spheres, and dumbbells (Perry *et al*., 2011). Following excretion, mucus coatings rapidly degrade in natural seawater (Wilson *et al*., 2009) and it is thought that pellets ultimately disaggregate and release individual mud-grade particles (Fig. 1.2; Perry *et al*., 2011). Consequently, fish-derived carbonates have the potential to play an important role in the oceanic carbonic acid system where excreted in pelagic settings (Wilson *et al*., 2009), and to accumulate as sedimentary mud-grade particles in shallow settings (Perry *et al*., 2011). However, despite long being known from a physiological perspective (Shehadeh and Gordon, 1969; Humbert *et al*., 1986; 1989; Walsh *et al*., 1991; Wilson *et al*., 1996; 2002; 2009;

Grosell *et al*., 2005), the potential sedimentary significance of these primary precipitates has, until recently (Perry *et al*., 2011), remained completely unrecognised.

In addition to the study by Perry *et al*. (2011), which characterises carbonates produced by eleven fish species common in the Bahamas, other studies describe the nature of carbonates produced by several marine fish species of different geographical origin (Humbert *et al*., 1986; 1989; Walsh *et al*., 1991; Wilson *et al*., 2009; Faggio *et al*., 2011; Mekuchi *et al*., 2010). Most of these are aimed at elucidating the relationship between carbonate precipitation and physiological processes taking place within marine fishes, and while they provide little or no detailed information on crystal size or morphology, they each contribute chemical and mineralogical data (summarised in Table 1.1). Wilson *et al*. (2009), Faggio *et al*. (2011) and Mekuchi *et al*. (2010) examined carbonate precipitates produced by European flounder (*Platichthys flesus*), sea bass (*Dicentrarchus labrax*), and Japanese eel (*Anguilla japonica*), respectively. X-ray diffraction (XRD) analyses identify the major mineral phase produced by all three species as Mg calcite. Wilson *et al*. (2009) also show that Mg calcite contains about 10 mol% $MgCO_3$, while the latter two studies employ other analytical techniques (X-ray fluorescence and energy dispersive X-ray spectroscopy, respectively) to measure $MgCO_3$ contents that fall within the range detailed by Perry *et al*. (2011).

Table 1.1 *Summary of the mineralogical, compositional, and morphological characteristics of fish-derived carbonates determined to-date.*

Study	Number of species (and location)	Mineralogy	$MgCO_3$ content (mol%)	Morphology
Perry *et al*. (2011)	11 (Bahamas)	High-Mg calcite + minor calcite + minor aragonite	18–39	Ellipsoids, spheres, dumbbells
Wilson *et al*. (2009)	1 (UK)	High-Mg calcite	10	Needles
Walsh *et al*. (1991)	1 (Florida)	High-Mg calcite? (initially identified as Mg-kutnahorite)	19	Ellipsoids
Mekuchi *et al*. (2010)	1 (Japan)	High-Mg calcite*	23	Not reported
Humbert *et al*. (1989)	1 (Germany)	Calcite* (+ vaterite; artefact?)	0	Spheres and rhombohedra
Faggio *et al*. (2011)	1 (Italy)	Calcite (High-Mg?)*	~30	Not reported

*X-ray diffraction patterns shown in these studies exhibit reasonably sharp peaks corresponding to calcite and high-Mg calcite, but with the main peak (d_{104}) emanating from a broad hump. This could indicate the presence of a poorly crystalline or amorphous carbonate phase.

Walsh *et al*. (1991) also attempted to characterise the mineralogy of carbonates precipitated within the gut of the gulf toadfish (*Opsanus beta*). In contrast to other studies, they tentatively identify the mineral phase of these carbonates as calcian kutnahorite, $(Ca,Mg,Mn)(CO_3)_2$. However, they also state that there is no detectable manganese in their samples, despite this being the compositional feature used to define kutnahorite; in the absence of manganese the mineral is better described as dolomite, $CaMg(CO_3)_2$ (Frondel and Bauer, 1955). X-ray diffraction peak positions reported by Walsh *et al*. (1991) do not include peaks characteristic of dolomite ordering patterns, and it is thus equally possible to match the reported peaks with the X-ray diffraction pattern for Mg calcite. In this case, $MgCO_3$ content (20 mol%; determined from the d_{104} peak position – see Chapter 2 for details regarding calculation) would fall within the range of values reported by Perry *et al*. (2011). Thus the carbonates precipitated within the guts of at least 15 different fish species, including those from both tropical and temperate regions, are consistently dominated by high-Mg calcites containing 10–39 mol% $MgCO_3$.

Only the results of Humbert *et al*. (1989) differ from these data; XRD patterns for carbonates produced by silver eel (*Anguilla anguilla*) are indicative of pure calcite (*i.e.*, magnesium is absent), whilst electron diffraction patterns reveal the presence of vaterite (although it is stated that the latter could be an artefact of phase transition after exposure to histological fluids during sample preparation). Although this is the only study thus far to identify fish-derived carbonates as pure calcite, Perry *et al*. (2011) clearly demonstrate that mean $MgCO_3$ contents are species-dependent, and that some species produce minor amounts of calcite alongside high-Mg calcite. It is therefore possible that the silver eel possesses unique (among species studied to-date) physiological traits that result in the inhibition of Mg^{2+} uptake in precipitating calcite crystals, and that, on a global scale, marine teleosts therefore represent a primary source of calcite with very wide ranging magnesium contents. In addition to these calcite phases, Perry *et al*. (2011) document the presence of "minor amounts of aragonite" (although the precise amount has not been formally quantified) in precipitates excreted by some species, as well as a commonly occurring, but as yet unidentified, phase that forms networks of plate-like precipitates. Finally, X-ray diffraction patterns presented in

some studies (Humbert *et al*., 1989; Faggio *et al*., 2011; Mekuchi *et al*., 2010) also indicate the presence of poorly crystalline or amorphous carbonate in the products of some fish species, although peaks indicative of this are not generated by all fish-derived carbonates (Wilson *et al*., 2009; Perry *et al*., 2011).

Further to considering excreted carbonate products as potential sedimentary components in shallow sub-tropical marine settings, Perry *et al*. (2011) attempted to quantify the significance of this newly recognised carbonate source by measuring production rates. These data were combined with fish population and habitat survey data to estimate total annual production rate in: a) the Bahamas (6.1 x 10^6 kg over an area of ~112,000 km^2); and b) per habitat within the Bahamas. The resulting production rates were incorporated in a carbonate mud budget for the Bahamas (based on existing information of production rates by known mud sources) to show that, in certain habitats, fish represent a volumetrically significant source of carbonate mud (*e.g.*, approximately 70 % in fringing mangrove settings, and 25 % in hardground settings). It is further pointed out that these estimates of carbonate production by fish are probably conservative. In part, this is because data from patch reefs (where fish biomass is typically high) are excluded from the modelling. Moreover, carbonate production rates per weight of fish are based on production by starved fish held in tanks that are restrictive to movement. Actively feeding and swimming fish are likely to have metabolic rates at least 2.5 times higher than resting fish (Kerr, 1982), and because carbonate production rate is directly related to drinking rate (Wilson *et al*, 2002; Genz *et al*., 2008), which is considered to be a function of metabolic rate (Wilson *et al*., 2009), it is likely that, during normal life conditions, fish will produce carbonates at significantly higher rates than determined by Perry *et al*. (2011).

Despite this work being supported by the finding that numerous high-Mg calcite crystals that closely resemble fish-derived carbonates (both compositionally and morphologically) are present in most surface sedimentary environments in the Bahamas (Perry *et al*., 2011), various general investigations that attempt to assess the relative importance of carbonate mud sources in shallow tropical and sub-tropical carbonate settings (*e.g.*, Gischler, 2011; Gischler *et al*., 2013) have failed

to document the presence of similar crystals (but see Gischler *et al*., 2013; their Figs. 3 F and 4 A – those images respectively show spherical particles and high-Mg calcite 'scalenohedra', both of which closely resemble some fish-derived carbonates documented by Perry *et al*., 2011). In part, this could be due to those studies not specifically targeting fish-derived carbonates, and thus looking in places where they might be less likely to occur. Alternatively, it could be due to the fact that fish-derived carbonates have only recently come to the attention of sedimentologists (Perry *et al*., 2011), and that these general studies have observed such carbonates but not been able to assign them to source. However, the latter is perhaps unlikely given the distinctive appearance of many fish-derived carbonates and their broad morphological similarity to bacterially-derived carbonates (Buczynski and Chafetz, 1991); had such particles been observed as common components of the mud fraction they might have been tentatively assigned to bacterial products rather than written off as 'unidentified grains'.

Nevertheless, the apparent absence or paucity of such crystals is perplexing, and several key questions thus arise regarding the production and post-excretion fate of fish-derived carbonates, these including: 1) Are the morphologies and compositions of carbonate crystal produced by the 11 species documented thus far (Perry *et al*., 2011) representative of gut precipitates produced by other marine fish species in shallow platform settings?; 2) Do excreted pellets disaggregate completely to release mud-grade particles, as suggested by Perry *et al*. (2011), or do they remain fully or partially intact, thus contributing to coarser sediments as well as, or instead of, the mud fraction?; 3) Do crystals remain stable and persist in their excreted form in open marine and porewater environments, or do they dissolve or otherwise alter (*e.g.*, recrystallise) following their transfer from the precipitating environment (the gut) to a considerably different chemical environment (marine seawater and porewater)? In summary, it can be said with certainty that fish produce large volumes of these carbonates, but their fate and depositional potential is far less clear.

1.3 STABILITY OF CARBONATES IN MODERN MARINE ENVIRONMENTS

It is well known that calcium carbonate solubility increases with decreasing temperature and increasing pressure (Garrels and Christ, 1965; Krauskopf and Bird, 1995; Langmuir, 1997), partly due to increases in pCO_2 and H_2CO_3 concentration driven by these factors. Ultimately, deep waters become undersaturated with respect to $CaCO_3$ minerals, and compensation depths, below which dissolution rates exceed rates of mineral supply, have been determined for each of the main carbonate phases. These depths vary spatially and temporally, but in the North Atlantic they are typically positioned at ~2–3 km for aragonite (Berger, 1978) and approximately 5 km for calcite (Tucker and Wright, 1990). High-Mg calcite is typically the most soluble of the carbonate phases that commonly occur in marine settings; solubility increasing with magnesium content (see section 1.3.1). Given the high magnesium content of most fish-derived carbonates, their compensation depths are likely to be shallower than most other commonly occurring marine carbonate minerals (*e.g.*, Wilson *et al*., 2009; Woosley *et al*., 2012) and they are therefore unlikely to persist as abundant sedimentary particles at depth. In contrast, warm shallow waters are typically highly supersaturated with respect to commonly occurring marine $CaCO_3$ polymorphs (Bathurst, 1975). Coupled with the fact that fish-derived carbonate production rates are highest in warm waters (increasing up to 2.33-fold for every 10 °C increase in temperature; Wilson *et al*., 2009), this means the sedimentary significance of fish-derived carbonates is likely to be greatest in shallow tropical and sub-tropical marine settings.

However, as discussed above, carbonates that are obviously fish-derived remain elusive in such settings (Gischler, 2011; Gischler *et al*., 2013), and the stability of excreted forms must therefore be questioned. Indeed, studies of fish-derived carbonates have so far described carbonates collected directly from the intestinal tract (*e.g.*, Humbert *et al*., 1989; Walsh *et al*., 1991; Wilson *et al*., 2009), or within a few hours of excretion (Faggio *et al*., 2011; Mekuchi *et al*., 2010; Perry *et al*., 2011); their longer term post-excretion fates in seawater remaining unknown. Given that precipitation of these carbonates takes place in a chemically distinct environment from the seawater

into which they are excreted, rapid post-excretion alterations would not be surprising. Indeed, Macintyre and Reid (1995; 1998) show that very early recrystallisation (*i.e.*, textural alteration without concomitant change in mineralogy) of both high-Mg calcite and aragonite can occur even when these minerals remain *in situ* at their sites of precipitation as skeletal parts of living organisms (and thus the chemical conditions to which they are exposed have presumably not changed).

One of the major aims of this study is therefore to investigate the short-term preservation potential and style(s) of fish-derived carbonates in surface and sub-surface carbonate sedimentary settings in the shallow sub-tropical environments of the Bahamas. In order to inform this investigation, the following sections provide a brief overview of theoretical considerations with respect to the behaviour of carbonate minerals in seawater and porewater, and of observed early diagenetic changes to various carbonate phases exposed to such settings.

1.3.1 Carbonate solubility

Numerous investigators have attempted to determine solubility products (pK_{sp}) for various common carbonate minerals as a measure of their solubility, and within the last 40 years these have generally been in good agreement, with log K_{sp} values for calcite and aragonite at surface temperature and pressure being about -8.48 and -8.30, respectively (Plummer and Busenberg, 1982; Sass *et al*., 1983; Millero *et al*, 1984). By taking into account variations in temperature, pressure, and salinity, it is possible to use these values to calculate thermodynamic solubility products (K^*_{sp}) for a mineral *X* in solution *Y* (*e.g.*, seawater), and ultimately the saturation state of solution *Y* with respect to mineral *X*. For example, the saturation state of a solution with respect to calcite ($\Omega_{calcite}$) can be written as:

$$\Omega_{calcite} = \frac{{}^{m}Ca^{2+} + {}^{m}CO_3^{2-}}{K^*{}_{calcite}} \qquad \textit{equation } 1.1$$

(after Morse and Mackenzie, 1990), where ${}^{m}Ca^{2+}$ and ${}^{m}CO_3^{2-}$ represent the concentrations of Ca^{2+} and CO_3^{2-} in solution, and resulting values of $\Omega_{calcite}$ indicate supersaturation (> 1), equilibrium (=

1), or undersaturation (< 1). For Mg calcite, $K^*_{calcite}$ is replaced by $K^*_{Mg\text{-}calcite}$ for a given $MgCO_3$ content and $^{m}Mg^{2+}$ is taken into account. In seawater, $[Ca^{2+}]$ and $[Mg^{2+}]$ are usually assumed to be present in fixed ratios (Dittmar, 1884) and are calculated from salinity. The concentration of carbonate, however, is variable, and measurements of various parameters of the carbonic acid system are necessary in order to calculate its value. It is beyond the scope of the present study to reproduce these calculations, which are covered in detail elsewhere (Dickson *et al*., 2007); it is sufficient to say here that carbonate concentration can be calculated when any two dissolved inorganic carbon (DIC) parameters are known, these being: total alkalinity (TA), pH, total CO_2 (TCO_2), partial pressure of CO_2 (pCO_2), and fugacity of CO_2 (fCO_2).

The calculated solubility products for calcite and aragonite indicate that calcite is the most stable $CaCO_3$ phase at surface conditions, with aragonite being the least stable (*i.e.*, metastable). The situation with Mg calcite is more complex because solubility increases with $MgCO_3$ content (Fig. 1.3). However, no simple relationship exists between $MgCO_3$ content and solubility, and the ability to predict Mg calcite solubility is thus hampered. In general, synthetic Mg calcites are the most stable and exhibit a reasonably strong relationship between solubility and $MgCO_3$, such that a solubility minimum occurs at about 2 mol% $MgCO_3$, and steadily increases thereafter causing Mg calcite solubility to exceed that of aragonite at about 19 mol% $MgCO_3$. The 'best fit' for biogenic Mg calcite predicts that solubility will exceed that of aragonite at about 10–15 mol% $MgCO_3$, although the relationship between solubility and $MgCO_3$ content is less tight, suggesting that other factors may influence Mg calcite solubility. Reasons for higher solubility of biogenic Mg calcites are not clear, but could include the presence of excess water, SO_4^{2-}, OH^-, and HCO_3^- (Morse *et al*., 2007). Indeed, the presence of SO_4^{2-} has been shown to strongly influence solubility on its own, and is typically incorporated at higher concentrations in biogenic precipitates than in synthetic precipitates (Busenberg and Plummer, 1985). The influence of SO_4^{2-} and Mg^{2+} that causes higher solubility is not well understood, but both can result in changes in lattice structure (Bischoff *et al*., 1983; Busenberg and Plummer, 1985), thus causing rotation of CO_3^{2-} and, consequently, increased lattice strain and defect density (Bischoff *et al*., 1985), both of which can result directly in

increased solubility (Morse *et al*., 2007). Indirect causes of increased solubility (*i.e.*, factors that promote incorporation of impurities) are varied, but can be inorganically- (*e.g.*, high precipitation rates – Busenberg and Plummer, 1985) or organically-controlled (*e.g.*, biogenically controlled incorporation of magnesium to 'stiffen' skeletal material – Becker *et al*., 2005).

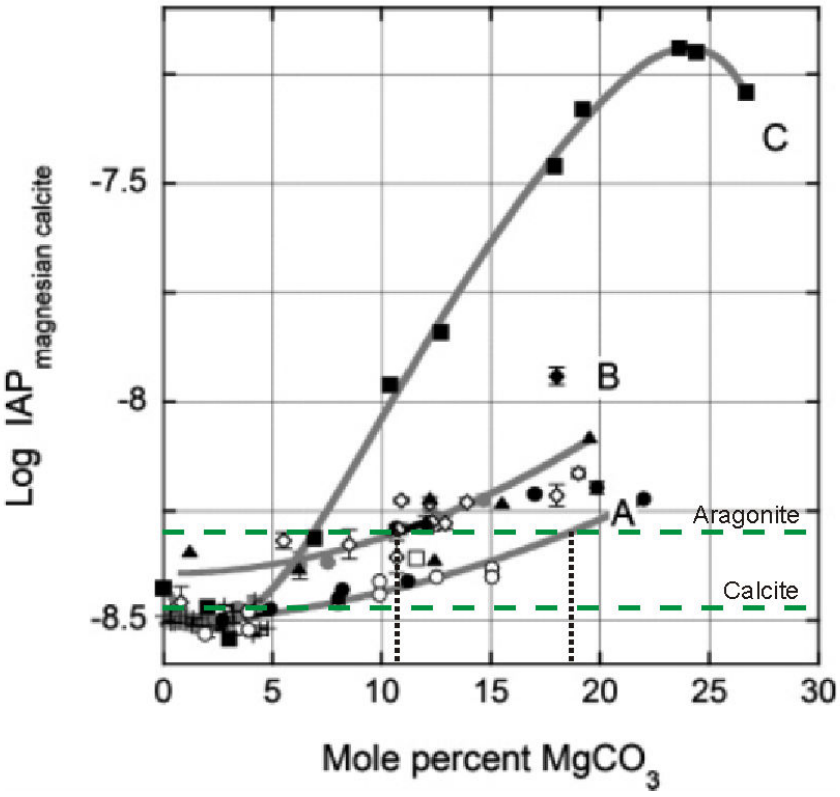

Figure 1.3 *Solubility of Mg calcite based on: A) synthetic Mg calcite (grey circles – Busenberg and Plummer, 1989; open circles – Bischoff et al., 1987; black circles – Mucci and Morse, 1984; and open squares – Lafon, 1990); B) natural Mg calcite (crosses [inorganic] – Busenberg and Plummer, 1989; open diamonds – Busenberg and Plummer, 1989; black triangles – Bischoff et al. 1987; and black diamonds – Walter and Morse, 1984); and C) uncleaned, unannealed natural Mg calcite (black squares – Plummer and Mackenzie, 1974; refit by Thorstenson and Plummer, 1977). Green dashed lines show solubility of calcite and aragonite. Figure reproduced from Morse et al. (2007), with aragonite and calcite data from Sass et al. (1983).*

It should be noted that the above discussion refers to thermodynamic solubility of carbonates; other factors which may result in measurement of apparent solubilities, such as small crystal size, and the presence of reactive organic matter, are overcome by cleaning and annealing samples (Walter and Morse, 1984; Bischoff *et al*., 1987; Busenberg and Plummer, 1989). However, such treatment may result in measured solubility products that are not representative of solubility in nature. Indeed, in their study on the solubility of Mg calcite, Plummer and Mackenzie (1974) left samples untreated

and found substantially higher solubilities than other studies (Fig. 1.3). If lattice strain and defects (which would have been reduced by annealing samples) are responsible for increased solubility, these results are likely reflective of solubility in nature. However, the major controls are not clear, and it is possible that other factors, such as the presence of a few very small (<0.1 μm diameter) crystals, could have caused Plummer and Mackenzie (1974) to grossly over-exaggerate the solubility of Mg calcite (Morse and Mackenzie, 1990).

An additional kinetic problem to understanding carbonate solubility is the presence of reaction inhibitors in a solution. For example, studies of carbonate reactivity in dilute solutions find that trace metals such as manganese and nickel can have a strong inhibiting effect even at micromolar concentrations, thought to be due to selective binding at high-energy surface sites (*e.g.*, kinks and steps; Fig. 1.4) (Sjöberg, 1978; Gutjahr *et al*., 1996; Vinson *et al*., 2007). Trace metals in seawater, however, are considered to be less influential due to increased concentrations of Mg^{2+}, which presents strong competition for site occupancy (Franklin and Morse, 1983). Nevertheless, reaction inhibitors can be present in seawater, with PO_4^{3-} (and HPO_4^{2-}) considered to be the most influential (Morse, 1974), adsorbing at the crystal surface in a similar mechanism to trace metals (Berner and Morse, 1974). However, the influence of phosphate is not uniform among carbonate phases; whereas it is thought to inhibit dissolution of calcite, Morse *et al*. (1979) show that it can increase the rate of aragonite dissolution. In either case the degree of influence may depend on the distance from equilibrium between solution and mineral (Morse and Arvidson, 2002). The fact that Mg calcite lattices can be distorted by the incorporation of Mg^{2+} means it is likely to have more surface defects, and thus more sites for phosphate adsorption. The inhibiting effect of phosphate could therefore be greatest in high-Mg calcite. In surface seawater, phosphate adsorption is unlikely to be an important factor in dissolution kinetics due to very low concentrations (typically < 1 μM; Broecker, 1974), but in porewater, where concentrations can reach 30 μM due to liberation during organic matter decomposition (Gaudette and Lyons, 1980), it may be important in controlling carbonate dissolution rates, and thus diagenesis.

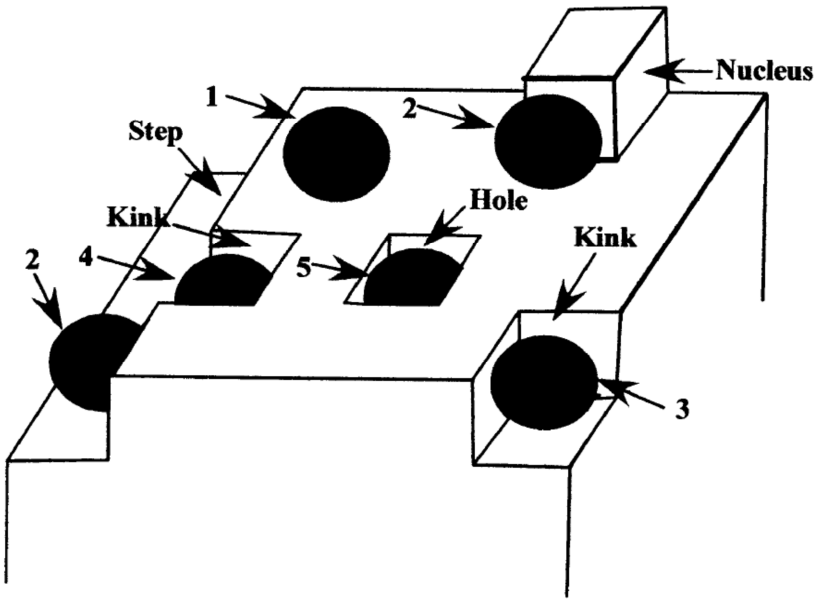

Figure 1.4 *High-energy sites that can occur at the calcium carbonate mineral surface as defects. Solid circles show potential positions for adsorbed ions (e.g., Mg^{2+}, PO_4^{3-}, Mn^{2+}), and numbers represent the likely number of bonds. These high-energy sites can also act as preferential sites for microbial attachment. Diagram reproduced after Morse and Arvidson (2002).*

A final complicating factor is the distribution of incorporated magnesium and the manner in which Mg calcite dissolves as a result. Biogenic calcite can be compositionally heterogeneous, with $MgCO_3$ contents in neighbouring crystal domains differing by as much as 10 mol% (Milliman *et al*., 1971). This may result in a given sample having heterogeneous solubility, and may also mean that solubility products determined for the bulk $MgCO_3$ content are not actually representative of the solubility of Mg calcite of that composition. Furthermore, in order to determine solubility products properly, it is necessary to treat the subject sample as a one-component phase. However, Mg calcite, even where the distribution of magnesium is uniform, is usually thought of as a two-component phase containing $CaCO_3$ and $MgCO_3$, and it has been shown that these dissolve incongruently (Plummer and Mackenzie, 1974). As such, determination of solubility products is hampered by that fact that $MgCO_3$ content may change during experiments, and to overcome this many workers have found it necessary to extrapolate reaction rates from the initial stages of dissolution, which are thought to be congruent (Plummer and Mackenzie, 1974; Bischoff *et al*., 1987). This problem has received much attention in the literature (for an overview, see Morse and Mackenzie, 1990; p.120), but most reported solubility products are calculated by extrapolation on

the assumption that initial dissolution was congruent; few have done this in response to measured congruent and incongruent stages of dissolution.

Given the above considerations, predicting the solubility behaviour of a given Mg calcite phase in seawater is hindered by many factors, these including: i) problems associated with determining solubility products accurately; ii) unknown factors that control excess free energy, such as precipitation kinetics, crystal size, compositional heterogeneity, defect density, and the presence of impurities; iii) unknown influences of reaction inhibitors; and iv) unknown dissolution kinetics (*i.e.*, congruent versus incongruent). Nevertheless, magnesium content does appear to be an important control on solubility, and the high measured $MgCO_3$ contents of many fish-derived carbonates suggests they are likely to be more soluble than most commonly occurring carbonates in marine settings.

Indeed, in a recent attempt to confirm this, Woosley *et al*. (2012) found that micron-scale ellipsoidal Mg calcite (48 mol% $MgCO_3$) produced by Gulf toadfish (*Opsanus beta*) was 1.95 times more soluble than aragonite, with the authors estimating a North Atlantic lysocline depth of approximately 500 m (compared to 2500 m for aragonite). However, although this result seems reasonable given the high magnesium contents, three issues lead to uncertainty in the meaning of this result. Firstly, the $MgCO_3$ content of these carbonates is close to the extreme high limit for fish-derived carbonates identified by Perry *et al*. (2011). Secondly, samples were not annealed prior to experiments, and it is possible that very small crystals influenced measured solubility products. Both of these factors could result in an apparent solubility that is higher than typical for the bulk of fish-derived carbonates. Thirdly, and more importantly, the methodological approach used by Woosley *et al*. (2012) is claimed to be the same as that used by Plummer and Mackenzie (1974), among others. However, the latter used distilled water saturated with CO_2 (0.97 atm) to induce dissolution, whereas the solubility of fish-derived carbonates was determined using seawater at ambient atmospheric conditions (*i.e.*, approximately 0.38×10^{-3} atm). Although Woosley *et al*. (2012) report that their experiments induced dissolution of carbonates, their results show that

solution pH decreased with time. This would suggest that they actually induced precipitation (*i.e.*, CO_3^{2-} and/or HCO_3^- was removed from solution, thus lowering its pH), in which case the apparent solubility product would refer to the precipitated phase(s) (and is possibly influenced by partial dissolution of initial sample material). Because the composition and mineralogy of the precipitated phase is not known, proper interpretation of the measured solubility product is difficult. Further work on the solubility of fish-derived carbonates is thus clearly necessary.

However, even with more well-refined investigations, understanding the solubility of fish-derived carbonates could be further hampered by interactions with organic matter. For instance, the interactions between carbonates and the mucus coatings in which they are excreted (Perry *et al*., 2011) have yet to be investigated, but it is possible that these coatings form a physical barrier that prevents interaction of crystals with seawater following excretion (Morse, 1974). Furthermore, it is known that some microbes preferentially attach to high-energy surface sites of calcite minerals and are capable of inhibiting dissolution, even under conditions of considerable undersaturation (Lüttge and Conrad, 2004). It is possible that such microbes are associated with mucus coatings in which fish-derived carbonates are excreted. Even if these mucus coatings have no bearing on carbonate solubility, another possible influence is internally encased organic matter. Walsh *et al*. (1991) show that organic matter may be present inside some crystals (they propose such organic matter might have acted as a nucleus to carbonate precipitation), while Perry *et al*. (2011) show that some fish-derived carbonates are hollow, possibly due to removal of organic matter that initially filled them. Decomposition of such encased organic matter could result in conditions that promote dissolution from within (see section 1.3.3 for details regarding the geochemistry of organic matter decomposition), in which case the solubility of these phases in seawater may be irrelevant. Organic matter thus represents an additional control on carbonate solubility, with the potential to influence it in either direction, through both physical and chemical interactions.

Finally, given that broad X-ray diffraction patterns generated by some fish-derived carbonates possibly indicate that amorphous calcium carbonate is produced by some fish species (Humbert *et*

al., 1989; Mekuchi *et al*., 2010), it is worth considering its likely stability in open marine conditions. With a measured solubility product (log K_{sp}) of -6.04 to -6.40 at 25 °C (Brečević and Nielsen, 1989; Clarkson *et al*., 1992), amorphous calcium carbonate is considerably more soluble than calcite (log K_{sp} = -8.48) and even the most soluble Mg calcite (K_{sp} = -7.25), and is likely to be unstable in seawater. However, it is known that impurities such as organic matter, PO_4^{3-}, and Mg^{2+} may act to stabilise these phases (Dickens and Brown, 1970; Clarkson *et al*., 1992, Addadi *et al*., 2003). Although the solubility of stabilised amorphous carbonates has not been documented, most workers still consider it to be a highly unstable phase that either dissolves or 'matures' to crystalline forms of $CaCO_3$ upon removal from stable conditions, usually within a matter of minutes to days (Beniash *et al*., 1997; Raz *et al*, 2002; Radha *et al*., 2010). If amorphous carbonates are produced by marine fish, it is thus unlikely they will persist in the marine environment, but whether they crystallise or dissolve is unknown. Furthermore, it is worth mentioning that its presence at the point of excretion means solubility measurements of fish-derived carbonates may be hindered by the presence of mixed phases of different stabilities.

1.3.2 Carbonate stability in surface seawater

Surface seawater in and around the Bahamas is typically characterised by elevated TA values (*i.e.*, greater than ~2400 $\mu M \cdot kg^{-1}$; Lee *et al*., 2006) and, in combination with usually high temperature (24–28 °C) and salinity (36–40 ppt), this means surface seawater in this region is highly supersaturated with respect to calcite and aragonite (ignoring factors such as reaction inhibitors and promoters), with typical values being in the range 6–7 and 4–5, respectively (Morse *et al*., 1985). A plot of ion concentration product (ICP) as a function of pCO_2 is shown in Fig. 1.5 with equilibrium positions for calcite, aragonite, and high-Mg calcite with 15 mol% $MgCO_3$ superimposed. The ICP of modern surface seawater is substantially greater than that for Mg calcite at equilibrium, even when compared with the highest measured solubility for Mg calcite. Surface seawater in the Bahamas is thus likely to be supersaturated with respect to high-Mg calcite with substantially more

than 15 mol% $MgCO_3$, and may therefore be supersaturated with respect to many or all fish-derived carbonates.

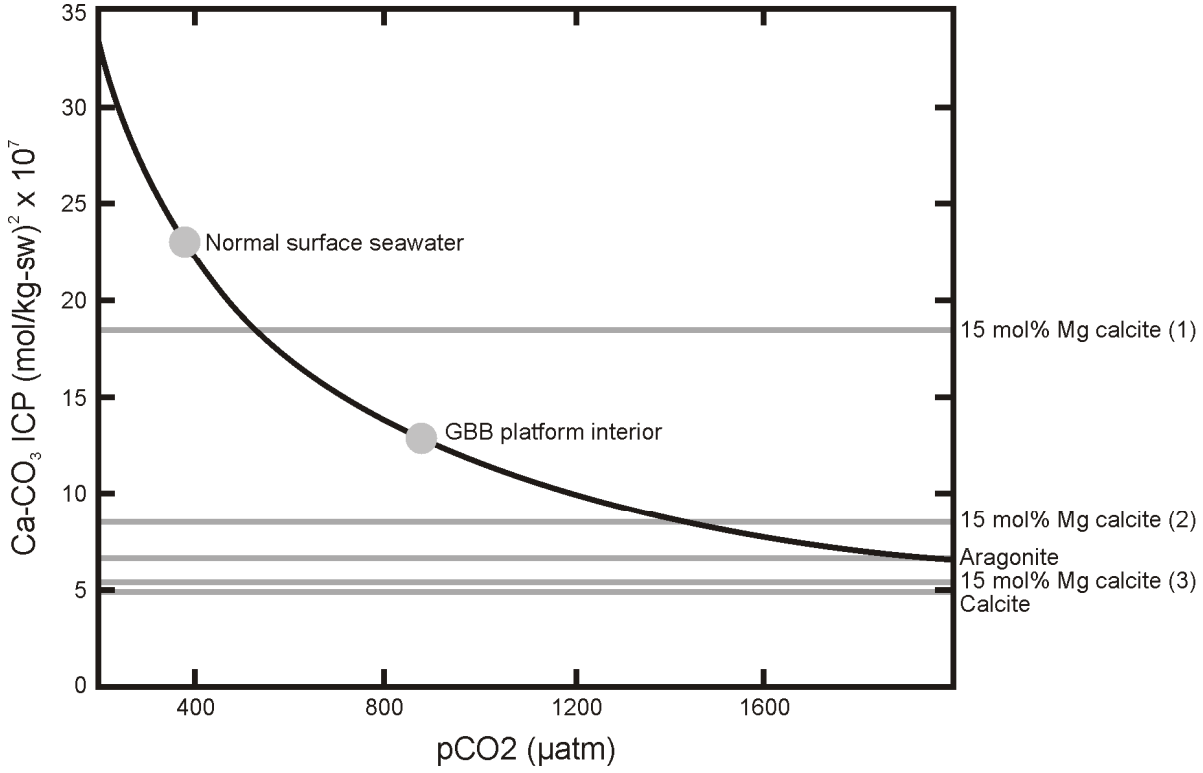

Figure 1.5 *$CaCO_3$ ion concentration product (ICP) against pCO_2 for seawater of salinity 35, temperature 25 °C, and TA 2300 µmol·kg^{-1} (after Morse et al., 2006). Grey lines show equilibrium ICP values for calcite, aragonite, and 15 mol% Mg calcite (1 – highest reported ICP for biogenic Mg calcite, after Plummer and Mackenzie, 1974; 2 – 'best-fit' ICP for biogenic Mg calcite; 3 – synthetic Mg calcite). The pCO_2 value for water overlying the Great Bahama Bank interior is close to that for present-day normal surface seawater, but is shown here at about 880 µatm as equivalent to the difference in alkalinity from normal seawater.*

However, shallow platform settings in the Bahamas can be characterised as having limited terrestrial inputs and restricted seawater circulation, and as a result, seawater overlying platform interiors (*e.g.*, the Great Bahama Bank, or GBB) can have long residence times (Cloud, 1962; Morse *et al.*, 1984). These waters commonly return low values for TA, probably as a consequence of carbonate precipitation and associated depletion of dissolved CO_3^{2-} without replenishment, and for the purposes of calculating ICP values these low TA values are equivalent to waters having elevated pCO_2. This means they are much closer to, or possibly lower than, equilibrium values for 15 mol% Mg calcite (Fig. 1.5), and fish-derived carbonates produced in these settings could potentially be exposed to conditions of undersaturation. It thus appears that, in surface seawater

settings within the Bahamas, preservation potential of fish-derived carbonates may vary spatially according to local flow dynamics.

1.3.3 Porewater chemistry

The processes that influence carbonate stability in shallow sub-surface settings are rather more complex than for surface seawater, and are governed by four fundamental factors: 1) sediment grain size; 2) sediment and interstitial water composition; 3) organic matter content; and 4) bioturbation (Berner, 1966; Morse *et al*. 1985; Walter and Burton, 1990; Walter *et al*., 1993; Burdige and Zimmerman, 2002; processes are summarised in Fig. 1.6). Perhaps the most important of these factors is organic matter content and the manner in which it decomposes. Under aerobic conditions, organic matter degradation will proceed by bacterially mediated oxidation, and can be represented as eq. 1.2:

$$CH_2O + O_2 \rightarrow CO_2 + H_2O \rightarrow H_2CO_3 \qquad \textit{equation } 1.2$$

$$CaCO_3 + H_2CO_3 \rightarrow Ca^{2+} + 2HCO_3^- \qquad \textit{equation } 1.3$$

$$CaCO_3 \rightarrow Ca^{2+} + CO_3^{2-} \qquad \textit{equation } 1.4$$

In a system where fluid flow is restricted (*e.g.*, fine-grained sediment), this reaction can result in porewater undersaturation with respect to carbonate phases, and dissolution either by utilisation of H_2CO_3 (eq. 1.3), or as a direct result of undersaturation (eq. 1.4), both of which can act to increase porewater TA. However, this process can be complicated by the C:N:P ratio of the original organic matter, and eq. 1.2 is perhaps better represented as:

$$\begin{aligned}(CH_2O)_x(NH_3)_y(H_3PO_4)_z + O_2 &\qquad \textit{equation } 1.5\\ &\rightarrow xCO_2 + xH_2O + yNH_3 + zH_3PO_4\\ &\rightarrow xH_2CO_3 + yNH_3 + zH_3PO_4\end{aligned}$$

The ability of this reaction to cause $CaCO_3$ dissolution is moderated by the production of ammonia and phosphate, both of which can act to increase TA, and decomposition of organic matter with high nitrogen and/or phosphorus content is consequently less likely to result in dissolution of $CaCO_3$. These oxidation reactions will proceed in any oxygenated waters, but it is worth

mentioning that in sediments characterised by coarse grain size and high rates of porewater exchange with overlying surface waters, undersaturation is unlikely to be maintained for long enough to cause dissolution.

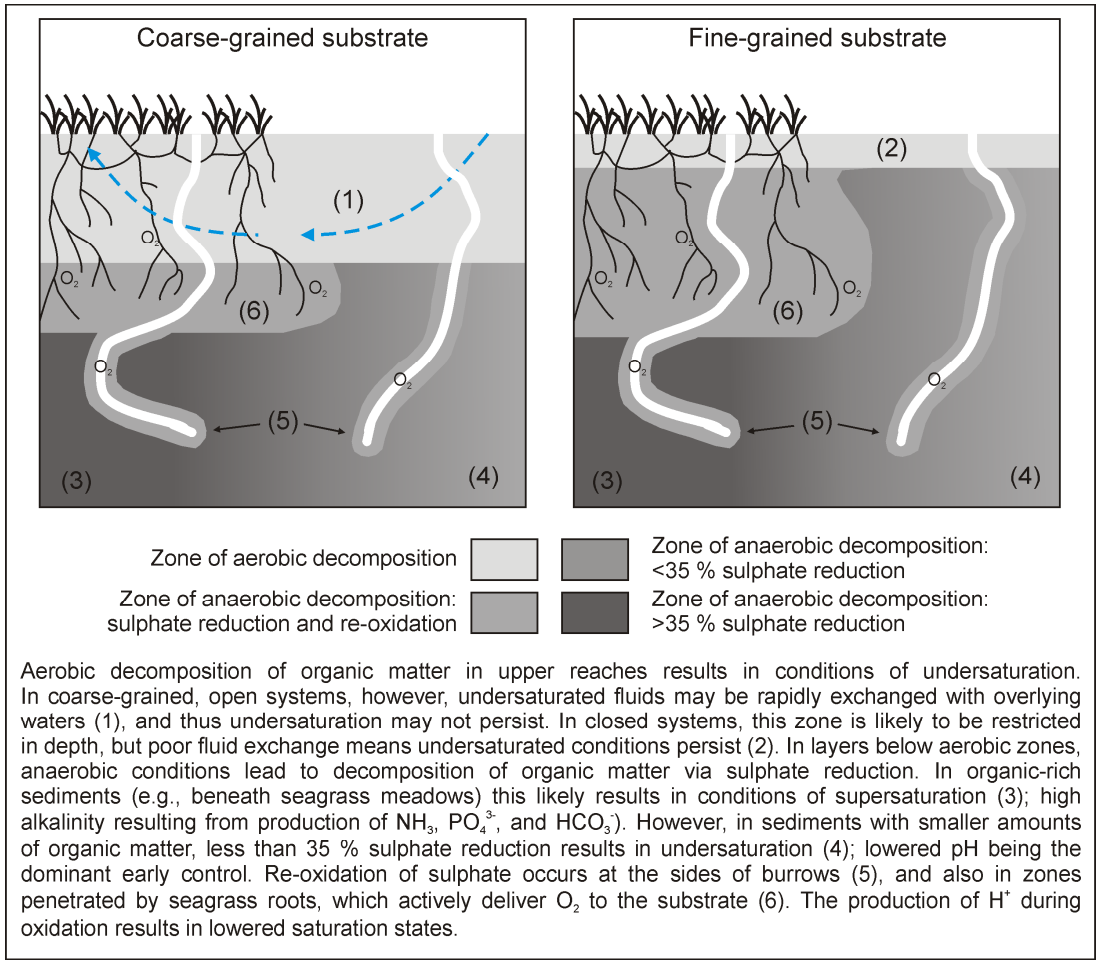

Figure 1.6 *Different sedimentary settings according to grain size (coarse vs. fine) and organic matter content (seagrass bed vs. no seagrass), and a summary of the likely saturation states to be encountered in each. Diagrams show approximately the upper 10–20 cm of surface sediment, but are not meant to be to scale.*

In anoxic sediments, where oxygen is not available as an electron acceptor, organic matter degradation proceeds via reduction of metals, nitrates, or sulphates. In carbonate-rich sediments, the most important of these is sulphate reduction (Morse and Mackenzie, 1990), which, assuming a C:N:P ratio of 106:16:1 for marine plankton (Redfield *et al*., 1963), can be represented as follows:

$$\frac{1}{53}(CH_2O)_{106}(NH_3)_{16}H_3PO_4 + SO_4^{2-} \rightarrow CO_2 + HCO_3^- + HS^- + \frac{16}{53}NH_3 + \frac{1}{53}H_3PO_4 + H_2O$$ *equation* 1.6

In the initial stages of sulphate reduction, pH is lowered to a fixed value of 6.9 as liberated CO_2 titrates CO_3^{2-} (Ben-Yaakov, 1973), thus causing porewater undersaturation with respect to aragonite and high-Mg calcite. However, the production of HCO_3^-, PO_4^{3-}, and NH_3 mean that TA increases as more sulphate is reduced, and at approximately 35 % sulphate reduction porewaters becomes supersaturated again (Morse and Mackenzie, 1990). The stability of carbonate minerals in sub-surface sediments thus depends on the amount of organic matter available to be reduced.

At this stage there exist several potential routes to further porewater chemistry alterations, these depending on sediment character, porewater composition and the rate and intensity of bioturbation. In metal-rich sediments, iron and/or manganese oxide may react with sulphide produced as a result of eq. 1.6, which can be simplified and rewritten as, for example:

$$9CH_2O + 4SO_4^{2-} + 4FeOOH \rightarrow 4FeS_{(s)} + 9HCO_3^- + H^+ + H_2O$$ *equation* 1.7

Precipitation of metal sulphides is accompanied by buffering of pH to higher values and an associated increase in $CaCO_3$ saturation states. However, platform-top carbonate-rich sediments of the Bahamas typically contain low concentrations of iron and manganese (Morse *et al*., 1985), and the fate of sulphides produced in eq. 1.6 must either be to remain in a dissolved state in porewaters, diffusion into overlying seawater, or oxidation by O_2. Whereas the two former possibilities will have little bearing on $CaCO_3$ saturation states, oxidation of reduced sulphur by O_2, which can be delivered to the sediment either via seagrass rhizomes, or via sediment mixing resulting from bioturbation, and is thought to affect 23–94 % of all reduced sulphur in nearshore environments (Ku *et al*., 1999; and references therein), releases hydrogen ions:

$$H_2S + 2O_2 \rightarrow SO_4^{2-} + 2H^+$$ *equation* 1.8

causing the lowering of TA and pH and thus reducing porewater saturation state with respect to $CaCO_3$ (Boudreau, 1991).

The above-described processes provide only a brief insight into what is a complex and much debated topic, but they serve to demonstrate the highly variable nature of shallow sub-surface porewaters. In the Bahamas, platform-top sediments are variable, and include: i) coarse-grained and mobile ooid shoals at platform margins, where limited amounts of organic matter and efficient fluid exchange mean porewaters are probably close to being in equilibrium with overlying surface waters; ii) coarse-grained stable sediments with some mud and varying amounts of organic matter (*i.e.*, some areas are populated by dense seagrass meadows whereas other areas have sparse vegetation cover), where porewater exchange with overlying waters may be less efficient than in (i), and organic matter decomposition will be variously aerobic and anaerobic and will vary in extent according to specific local conditions; and iii) muddy organic-rich sediments of mangrove systems, where sulphate reduction is likely to be an important mode of organic matter decomposition and may result in highly undersaturated conditions where sulphides are re-oxidised (*i.e.*, in the zone of bioturbation).

These relations are confirmed in a study by Morse *et al*. (1985), where porewaters associated with muddy sediments and fine-grained sediments beneath seagrass beds tend to have the lowest saturation states, whereas those associated with ooid shoals and other coarse-grained sediments tend to have higher saturation states. Despite many of these porewaters remaining supersaturated with respect to Mg calcite containing 18 mol% $MgCO_3$, elevated TA values in the absence of significant sulphate reduction indicates that some dissolution has occurred. Moulin *et al*. (1985) have empirically confirmed such dissolution taking place in the uppermost 10 cm of surface sediments in response to experimentally-induced aerobic decomposition of organic matter, also showing that high-Mg calcite is the first responder to thus lowered saturation states.

Clearly, the short-term preservation potential of fish-derived carbonates in the Bahamas is likely to be varied. Perry *et al*. (2011) show that sinks in which these carbonates are likely to have the

greatest impact as contributors to surface sediment (in terms of relative abundance of carbonate mud produced) include fringing mangrove systems and reefal habitats (probably including patch reefs, although this has not been shown). Given that the above-described influences of organic matter degradation on porewater chemistry can be highly influential even within the top few centimetres of sediment (Morse *et al*., 1985), it is likely that fish-derived carbonates produced in these settings will be exposed to a range of different conditions very shortly after excretion, and will thus experience different fates according to depositional setting.

1.3.4 Observed early diagenetic changes in carbonate minerals

The preceding sections describe chemical processes and interactions that present important controls on the stability of carbonate minerals in marine sedimentary settings. However, such considerations only describe whether or not a crystal and the solution that surrounds it are in equilibrium; they do not necessarily predict the fate of a given crystal. For example, while conditions of undersaturation with respect to a certain mineral might be expected to promote dissolution of a mineral, it is well known that diagenetic alterations can occur that move a system towards equilibrium without the need for wholescale dissolution (*e.g.*, Folk, 1965; Bathurst, 1975; Flügel, 2004). Such alterations within the carbonate mineral system involve recrystallisation and neomorphism; terminologies that are widely, but sometimes inconsistently, used in carbonate literature, and can also have different meanings in other geological and metallurgy contexts. Their use herein follows definitions given by Folk (1965), whereby recrystallisation is used to describe textural alterations without concomitant changes in composition or mineralogy (*e.g.*, change from low-Mg calcite micrite to low-Mg calcite microspar; increasing stability by increasing grain size and thus reducing surface free energy), and neomorphism is used to describe solid solution polymorphic changes that may or may not accompany textural changes (*e.g.*, transformations involving low-Mg calcite, high-Mg calcite, and aragonite; increasing stability by alteration to a less soluble phase).

Diagenesis in carbonate systems is conventionally thought of as a series of processes that occur over geological timescales in response to changing pressure, temperature, and solution composition

as sediments are buried or exhumed, or on shorter timescales as sediments are transported to deeper oceanic settings (*e.g.*, Bathurst, 1975; Tucker and Wright, 1990; Flügel, 2004). In shallow marine settings, several authors have described sedimentary textures which they attributed to diagenetic alteration (Illing, 1954; Purdy, 1963), but these micritic textures were later explained as borings that had been infilled by micritic precipitates (Bathurst, 1975), thus removing the need to invoke processes of recrystallisation or neomorphism in these settings, which have since been thought of as sediment sinks where most carbonates represent a stable phase (Berner, 1966; Bathurst, 1975).

However, apparent discrepancies between carbonate production and accumulation rates in modern settings, as well as indications provided by porewater chemistry, have motivated numerous of recent studies focussing on syn- and early post-depositional changes that occur in carbonates in shallow carbonate provinces (Morse *et al*., 1985; Moulin *et al*., 1985; Walter and Burton, 1990; Rude and Aller, 1991; Walter *et al*., 1993; Patterson and Walter, 1994a; MacIntyre and Reid, 1995; 1998; Reid and Macintyre, 1998; Perry, 2000; Hover *et al*., 2001; Sanders, 2003). The findings of these studies indicate that dissolution of carbonates is a dominant syn- and early post-depositional process operating within the upper few decimetres of shallow platform sediments, resulting in the loss of up to 50 % of initially deposited sediment (Walter and Burton, 1990); high-Mg calcite being the first responder. In addition, other workers have begun to identify recrystallisation and neomorphism as a widespread process that operates within similar boundaries (Patterson and Walter, 1994a; Hover *et al*., 2001), and even prior to deposition (*i.e.*, while crystals are still part of the skeletal structure of living organisms – Macintyre and Reid, 1995; 1998). These studies, along with others from freshwater settings (Melim and Spilde, 2011), indicate that diagenetic alteration of reasonably stable carbonate phases (*e.g.*, aragonite and high-Mg calcite with 15 mol% $MgCO_3$) can occur on the order of weeks to months after initial precipitation.

Few of these studies have focussed on Mg calcite containing more than about 15 mol% $MgCO_3$. However, given their typically very high $MgCO_3$ contents, it is likely that fish-derived carbonates have relatively low stability and must therefore have the potential to undergo alteration during very

early stages after excretion. This is perhaps to be expected given their environments of precipitation. Furthermore, amorphous carbonates are known to be highly unstable and usually dissolve or crystallise within hours to days of removal from conditions where they are stable (Beniash *et al*., 1997; Radha *et al*., 2010). Given this potential for rapid alterations to occur in fish-derived carbonates, an overview of the compositional, mineralogical, and textural changes associated with early alterations of fine-grained carbonates is provided here and summarised in Fig. 1.7. However, the number of studies that documents these features in shallow marine settings is limited, so examples from other settings are also included.

Dissolution of fine-grained carbonates usually results in crystals developing rounded terminations, irregular shape, and pitted surfaces. This is shown to occur in aragonite and high-Mg calcite needles in their life positions as components of *Halimeda* and *Archaias* skeletal matter, respectively (Macintyre and Reid, 1995; 1998), and as a syndepositional process in aragonite and high-Mg calcite needles of *Halimeda* and *Peneropolid*, respectively (Hover *et al*., 2001). Given that dissolution of high-Mg calcite can be incongruent (Plummer and Mackenzie, 1974), one might anticipate a reduction in the $MgCO_3$ contents of partially dissolved high-Mg calcite crystals. Patterson and Walter (1994a) report a significant decrease in Mg/Ca ratio (equivalent to a change from 30 to 15 mol% $MgCO_3$) during a 500 day experiment where *Neogoniolithon* red algae were exposed to porewater, which could be a result of incongruent dissolution. However, preferential dissolution of more magnesium-rich Mg calcite (*i.e.*, if initial carbonates were compositionally heterogeneous), or associated brucite, was not ruled out. In addition, such changes are not reported from partially dissolved high-Mg calcite by Hover *et al*. (2001), although the starting $MgCO_3$ content of their initial crystals was lower. The study by Patterson and Walter (1994a) also found that initial high-Mg calcite (with up to 30 mol% $MgCO_3$) typically lost mass at a rate of 1–6 % per year. In contrast, *Halimeda* grains showed no significant change in mass, although mineralogical investigation suggested 5–15 wt% of exposed samples was high-Mg calcite, suggesting that a similar amount of aragonite either dissolved or underwent neomorphism to account for mass balance.

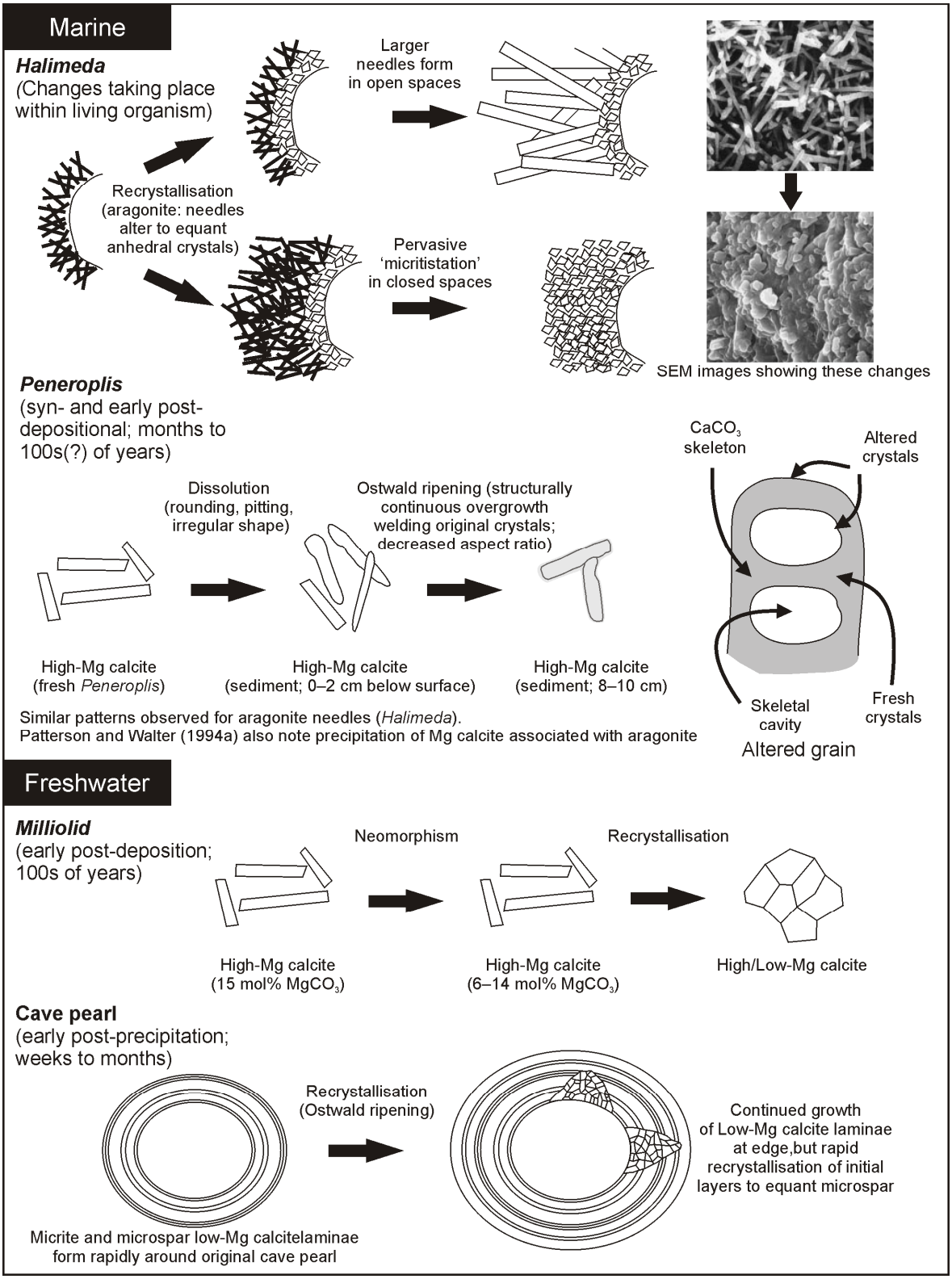

Figure 1.7 *Diagrammatic representation of some early diagenetic textures documented for mud-sized carbonate crystals from shallow subtropical marine settings and freshwater settings (sub-tropical vadose/phreatic and cave pools). See text for detailed descriptions. Data from: Macintyre and Reid, 1995 (living Halimeda); Patterson and Walter, 1994a; Hover et al., 2001 (syndepositional Mg calcite and aragonite needles); Towe and Hemleben, 1976; Budd and Hiatt, 1993 (Milliolid rods/needles); and Melim and Spilde, 2011 (cave pearls).*

Recrystallisation is typically manifest as equant crystals that obliterate original textures. Within the uppermost 10 cm of surface sediments in shallow marine carbonate provinces, grain enlargement can be achieved through recrystallisation by the development of concentric overgrowths associated with initial needles of high-Mg calcite and aragonite (Hover *et al*., 2001). Overgrowths, which are on the order of 10s of nanometres thick, are structurally continuous with original needles and are thought possibly to form via dissolution of original grains at terminations followed by reprecipitation as overgrowths (possibly with slightly lower $MgCO_3$ content), with crystals thus tending towards more equant morphology. This process also acts to 'weld' initial crystals together, thus further increasing grain size and also making original grains less easily discernable (Fig. 1.8). Recrystallisation of high-Mg calcite and aragonite can also occur in living specimens (Macintyre and Reid, 1995; 1998), with euhedral needles or rods (1–3 μm in length) transforming to smaller anhedral equant crystals (0.1–0.5 μm in diameter) and forming a rather cryptocrystalline texture. This second style of recrystallisation is thought to be a result of the breakdown of crystals along sub-micron crystal domain boundaries (Reid and Macintyre, 1998), and proceeds along a migrating front in a manner not dissimilar to fresh water recrystallisation of micrite and microspar laminae to massive microspar that obliterates original structures, and which can occur in a matter of weeks (Melim and Spilde, 2011). Unlike alterations described by Hover *et al*. (2001), where the likely driver is undersaturation in subsurface porewaters, neither of these examples have an obvious cause. It is noted that recrystallisation in *Halimeda* tends to be more extensive in windward settings, and is possibly biogenically controlled as a skeletal strengthening mechanism, although Reid and Macintyre (1998) show that recrystallisation continues in a similar manner post-mortem. The latter study shows that post-mortem recrystallisation is more extensive and involves a second stage whereby initial recrystallisation textures undergo further recrystallisation to coarser-grained (but typically sub-micron) equant crystals (Fig. 1.9). It is worth mentioning, however, that not all post-mortem textures comprise equant grains; skeletal cavities can be infilled with a 'micritic' cement that exhibits more euhedral needle-like morphologies.

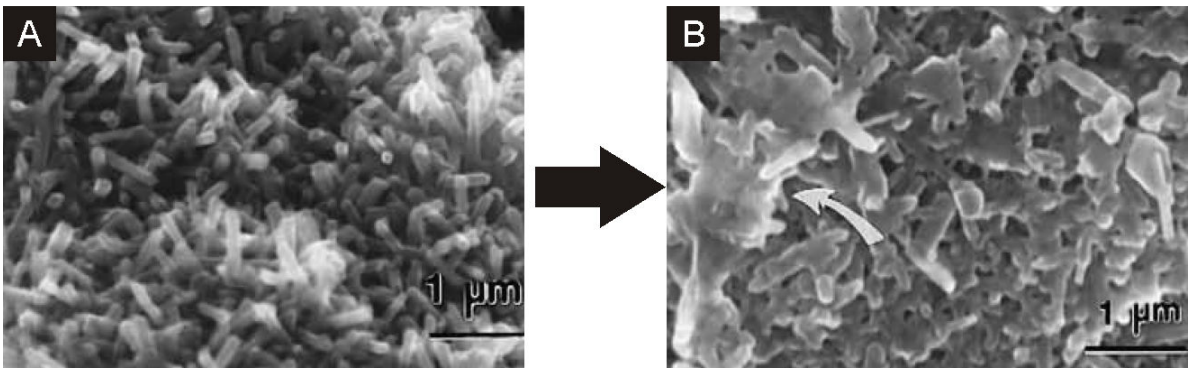

Figure 1.8 *Scanning electron microscope images of fresh (A) and altered (B) Peneropolid foraminifera tests; the latter having been collected from surface sediment in the Bahamas (0–2 cm below the sediment–seawater interface). In fresh tests, needle-like euhedral crystals are easily discernable. In altered tests, recrystallisation has 'welded' crystals together, making them less clearly-defined and, in some cases, forming uniform aggregates (white arrow). Crystals in altered tests also show evidence of dissolution (irregular shape). Reproduced after Hover et al. (2001).*

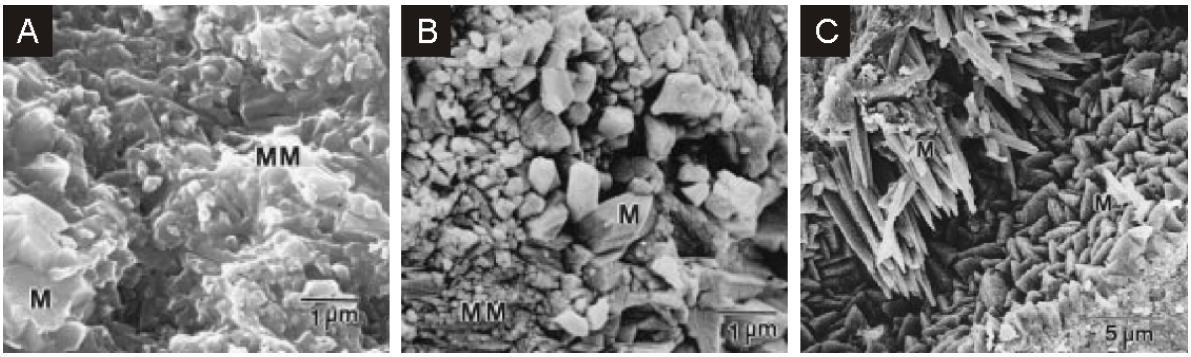

Figure 1.9 *Early recrystallisation textures of common mud-grade crystals in shallow sub-tropical marine settings. A) Halimeda fragment with cryptocrystalline aragonite 'minimicrite' (MM; a recrystallisation product from original needles). B) Post-mortem syndepositional alteration includes continued alteration of needles to 'minimicrite', which in turn recrystallises to coarser-grained micrite (M). C) Skeletal cavity in Halimeda ('minimicrite' sections of skeletal cavity walls at top left and bottom right), infilled by precipitated aragonite (needles; upper left portion) and Mg calcite (dendritic crystals; lower right portion). These are not necessarily recrystallisation structures, but are shown here as an example of the types of crystals that can form in syndepositional settings. Images reproduced after Reid and Macintyre (1998).*

Neomorphism is not evident in the studies of Macintyre and Reid (1995; 1998) and Hover *et al*. (2001), in which recrystallisation of high-Mg calcite does not involve loss of magnesium. However, Reid and Macintyre (1998) find that syndepositional alteration of Mg calcite (*Archaias*) can result in significant amounts (up to 44 %) being replaced by aragonite (and *vice versa* in the case of *Halimeda* aragonite). Patterson and Walter (1994a) observe a similar pattern in the case of aragonite from *Halimeda*, with 5–15 % of the initial mass converting to rhombohedral Mg calcite overgrowths during a 500 day porewater exposure experiment. Preserved aragonite needles show

dissolution features, suggesting that neomorphism may have occurred via a dissolution-reprecipitation process. Initially similar crystals exposed to freshwater diagenetic environments also show evidence for neomorphism, with high-Mg calcite incrementally transforming to low-Mg calcite via intracrystalline alterations (with a change of 0.01–0.1 mol% $MgCO_3$ per alteration event), but without concomitant textural alteration. However, neomorphism is apparently not sufficient to stabilise crystals on its own, as a second stage of alteration involves recrystallisation to equant grains (Towe and Hemleben, 1976; Budd and Hiatt, 1993). These freshwater alterations are apparently much slower than those described above, taking on the order of 100s–1000s of years.

In addition to the more obvious alterations described above, Patterson and Walter (1994a) noted that $\delta^{13}C$ and $\delta^{18}O$ stable isotope values for high-Mg calcite (*Neogoniolthon*) shifted towards equilibrium with porewater after a 500 day exposure experiment, with an estimated 25 wt% of exposed crystals altered per year. No concomitant textural change was reported, but neomorphism may have occurred (*i.e.*, lower $MgCO_3$ contents). It is also possible that intracrystalline equilibration of stable isotopes occurred without any textural or compositional change, thus highlighting the potential value of stable isotopes as tracers of alteration. However, in the case of some carbonates, such as *Halimeda* aragonite, initial stable isotope values are close to equilibrium with porewater, and consequently undergo no discernable change during exposure to porewater.

Finally, it is worth mentioning the distribution of early alteration features, both at the scale of skeletal fragments and at platform scale. Hover *et al*. (2001) find that intra-skeletal sections of altered *Halimeda* and *Peneropolid* fragments maintain textures similar to fresh fragments; only exposed outer sections tending to host altered crystals. This is consistent with the proposal by Reid and Macintyre (1998) that micro-boring activity facilitates more pervasive alteration by creating conduits that bring internal skeletal fragments into contact with porewater. How this might influence fish-derived carbonates is open to question, as the open-ness of intact pellets to fluid flow is unknown. As has been discussed in previous sections, the degree of saturation in different platform settings is likely to be highly variable, and alteration textures may thus vary spatially. One

speculated example, based on the observations of Purdy (1968), is that sediment grains in muddy environments in the Bahamas are less susceptible to the development of cryptocrystalline textures than grains in sandy areas.

In summary, alteration of fine-grained carbonates is temporally and spatially variable, but it has been shown to be a widespread process operating in shallow marine settings, affecting crystals that should theoretically be substantially more stable than many fish-derived carbonates. Alteration typically results in textural changes that include: i) development of irregular morphologies; ii) pitted surfaces; iii) decreasing aspect ratios; iv) development of overgrowths; and v) 'welding' of initial crystals. Dissolution may result in a reduction in grain size, but recrystallisation typically results in increasing grain size. However, this will depend somewhat on the structure of initial crystals; those that comprise multiple sub-domains may actually undergo an apparent reduction in grain size. Other textural changes may involve the development of euhedral overgrowths or cavity-filling cements. The latter two processes may be accompanied by mineralogical or compositional transformations, although these may occur in initial crystals without textural change. Common compositional changes involve reduction in magnesium content of high-Mg calcite, but changes can also be subtle, sometimes only involving stable isotope equilibration.

1.3.5 Considerations on the post-excretion fate of fish-derived carbonates

From the above considerations it is apparent that fish-derived carbonates are a metastable phase in shallow marine settings, and may be one of the first responders to conditions of undersaturation. In the event that they rapidly recrystallise or undergo neomorphism, the present study aims to characterise the textures associated with these changes, thus providing criteria for identifying and assessing the contribution of fish-derived carbonates in older sediments, and potentially in the rock record. In the event that dissolution is the main mechanism by which fish-derived carbonates alter, the present study aims to determine the rate of dissolution and the textures it yields. The study will also aim to constrain the timing of dissolution, which may have implications for the sedimentary significance of these carbonates. For example, if dissolution is rapid and occurs in the open water

column, liberated Ca^{2+}, Mg^{2+}, and CO_3^{2-} will disperse in seawater and have little effect on sedimentary processes, whereas dissolution in the shallow sub-surface will influence porewater chemistry, both by buffering it to higher alkalinity, and by influencing the ratios of dissolved ions in a unique manner (*i.e.*, their very high magnesium contents means dissolution will contribute more Mg^{2+} to porewater than most other carbonates that occur commonly in shallow marine settings). In the latter scenario, fish-derived carbonate could play an important role in controlling diagenetic processes operation in shallow porewaters.

In addition, the influence of mucus coatings in which fish-derived carbonates are excreted will be considered in this study. Numerous studies involving both the *in vitro* precipitation of natural carbonates (*e.g.*, those associated with algal mats; Chafetz and Buczynski, 1992) and synthetic precipitation experiments (*e.g.*, Meldrum and Hyde, 2001; Rivadeneyra *et al*., 2006; González-Muñoz *et al*., 2008) indicate that bacteria and various organic compounds can be of great influence in carbonate precipitation systems. Indeed, Buczynski and Chafetz (1991) describe a suite of bacteriogenic carbonate crystal morphologies and propose that the occurrence of such morphologies in nature may be characteristic of microbially-influenced precipitation. That the crystal morphologies described by Perry *et al*. (2011) closely resemble the morphologies documented in many of these studies suggests that bacteria and/or other organic matter may play an important role in the nucleation and growth of fish-derived carbonates. However, the extent to which such factors continue to influence these crystals after excretion is unknown. Whilst it is possible that the mucus membrane might protect carbonates from rapid alteration and perhaps even stimulate further growth of these crystals – it has been shown that both living and dead bacterial cells can fix calcium and aid its precipitation (Greenfield, 1963) – it is equally plausible that its post-excretion degradation might create a microenvironment that promotes dissolution (*e.g.*, following similar processes to those described in section 1.3.3). Thus it is important to determine not only the nature of fish-derived carbonates after exposure to seawater and shallow porewaters, but also the post-excretion influence of associated organic matter.

1.4 AIMS AND OBJECTIVES

The present project has two major aims: 1) To expand the range of tropical fish species (and functional groups) for which fish-derived carbonates have been characterised, thereby providing an improved understanding of the primary carbonate products available for incorporation within sedimentary systems; and 2) To determine the short-term preservation potential of these various crystalline products in shallow tropical marine settings.

1.4.1 Phase 1

In order to meet the first aim, specific objectives of Phase 1 of this project are to provide: i) a more extensive and expansive description of the morphological, mineralogical and compositional characteristics of the primary precipitation products at the point of excretion from a range of tropical marine bony fish species (Chapters 2–5); and ii) a detailed grain size distribution analysis of carbonate particles falling within the major categories identified in (i) (Chapter 6). These objectives draw on data from an expanded range of fish species (increasing the total number of Bahamian species studied from 11 to 22), and are designed to provide a suite of characteristic (and potentially diagnostic) features of fish-derived carbonate particles. This work could aid interpretations regarding the origin of similar particles present in bulk samples of modern surface sediments, thereby facilitating the appropriate integration of fish-derived carbonates within future carbonate mud budget calculations.

Furthermore, a suite of complementary chemical analyses, including X-ray powder diffraction, Fourier-transform infrared spectroscopy, energy-dispersive X-ray spectroscopy, and mass spectrometry will be utilised to provide further detail on the varied phases present in excreted carbonate and will help to resolve the identification of other, as yet unknown, phases. In addition to providing important information about excreted products, the outcomes of this work could provide a key insight into precipitation processes that operate within the piscine gut, thus potentially aiding future investigations aimed at elucidating the factors that influence species-dependent precipitation

products; itself a potentially important aspect from the perspective of sedimentologists trying to understand the significance of fish-derived carbonates on platform-wide scales.

The results of Phase I will be combined with knowledge of physico-chemical conditions of shallow sub-tropical platform settings in the Bahamas to provide a conceptual model of the post-excretion transport and deposition dynamics of fish-derived carbonates.

1.4.2 Phase 2

The second aim of this project is directed at understanding the post-excretion behaviour of fish-derived carbonates in natural settings via a series of empirical studies (Chapter 7). Specific objectives are to: i) determine the fates of various types of fish-derived carbonate when exposed to open marine conditions during the first few days following excretion; ii) determine the fates of these same carbonates when exposed to seawater for several months; and iii) determine the fates of fish-derived carbonates when exposed to pore fluids in a shallow platform-top burial environment. These objectives are designed to determine the changes that take place in fish-derived carbonates: i) during the period between excretion and incorporation within sediment; and ii) in the early stages of burial within the shallow sediment.

In order to best understand the post-excretion behaviour of the full range of fish-derived carbonates, these experiments will focus on a range of categories of excretion product as described in Phase 1. As such, this second phase of the project investigates the early post-excretion fates of crystals across a wide spectrum of sizes and magnesium contents, and will thus determine whether species-dependent morphological, mineralogical, and compositional variability results in different preservation potentials and pathways. This part of the study also examines the potential control exerted on post-excretion fates by the organic coatings in which carbonates are excreted.

Results obtained in Phase 2 are central to understanding the short-term sedimentary significance of fish-derived carbonates in modern shallow tropical marine settings. Moreover, if fish-derived crystals are preserved in these environments on short time-scales, either as excreted or in altered

forms, this work will provide an essential platform to future work aimed at determining their longer-term (and potentially geological) significance. For example, if rapid and pervasive recrystallisation occurs, Phase 2 of this work will identify the associated changes and provide preliminary criteria for identifying fish-derived carbonates in older sediment samples.

1.5 STUDY AREA AND FISH SPECIES

All of the fish species used in this study were collected from shallow water carbonate platform environments in areas of Eleuthera Sound adjacent to Cape Eleuthera, on the leeward side of Eleuthera Island, the Bahamas (24° 50'N, 76° 20'W; Fig. 1.10 A). The characteristically warm (24–28 °C) and shallow (up to 8 m in depth) waters overlying this area are sheltered from the west by the presence of large ooid shoals (Fig. 1.10 B), but they are nevertheless influenced by strong tidal currents. Consequently they tend to have reasonably short residence times and less highly elevated salinities (typically 36–37 on the practical salinity scale) compared to waters overlying the Great Bahama Bank (west of Andros); an area which is the focus of a large number of sedimentological investigations (*e.g.*, Cloud, 1962; Purdy *et al*., 1963).

Sedimentary environments around Cape Eleuthera are summarised in Figs. 1.10 and 1.11. They are dominated by active and stabilized oolitic sands and skeletal sand veneers, with pelletal sands and pelleted lime muds dominating the more restricted bays and inlets (Dravis, 1979). The loose veneers formed by these sediments are what characterise the substrate of Eleuthera Sound, which is predominantly bare or sparsely vegetated. It does, however, host extensive seagrass meadows and variously concentrated populations of calcareous green algae, as well as numerous and widely distributed small patch reefs, which range in size from a few coral heads to reef clusters typically smaller than 250 m^2 (the paucity of hard substrates means that large and well-developed patch reefs are rare). In addition, an extensive fore reef zone runs along the southern margin of Eleuthera Sound, which is bordered by the deep-water embayment of Exuma Sound (Fig 1.10 A and B), but associated crestal reef zones do not occur in this area; the only shallow reefs being small fringing reef tracts off the western shore of Cape Eleuthera.

These reefs and seagrass meadows, along with several large mangrove-flanked creeks and inlets that feed into Eleuthera Sound, support a large fish population that includes many species that are widespread and common in the Bahamas. For this study, fish with various dietary habits were captured in nearshore areas (mainly creeks and patch reefs) around Cape Eleuthera. These included a total of 24 species belonging to 17 families, all of which are listed in Figs. 1.12 and 1.13.

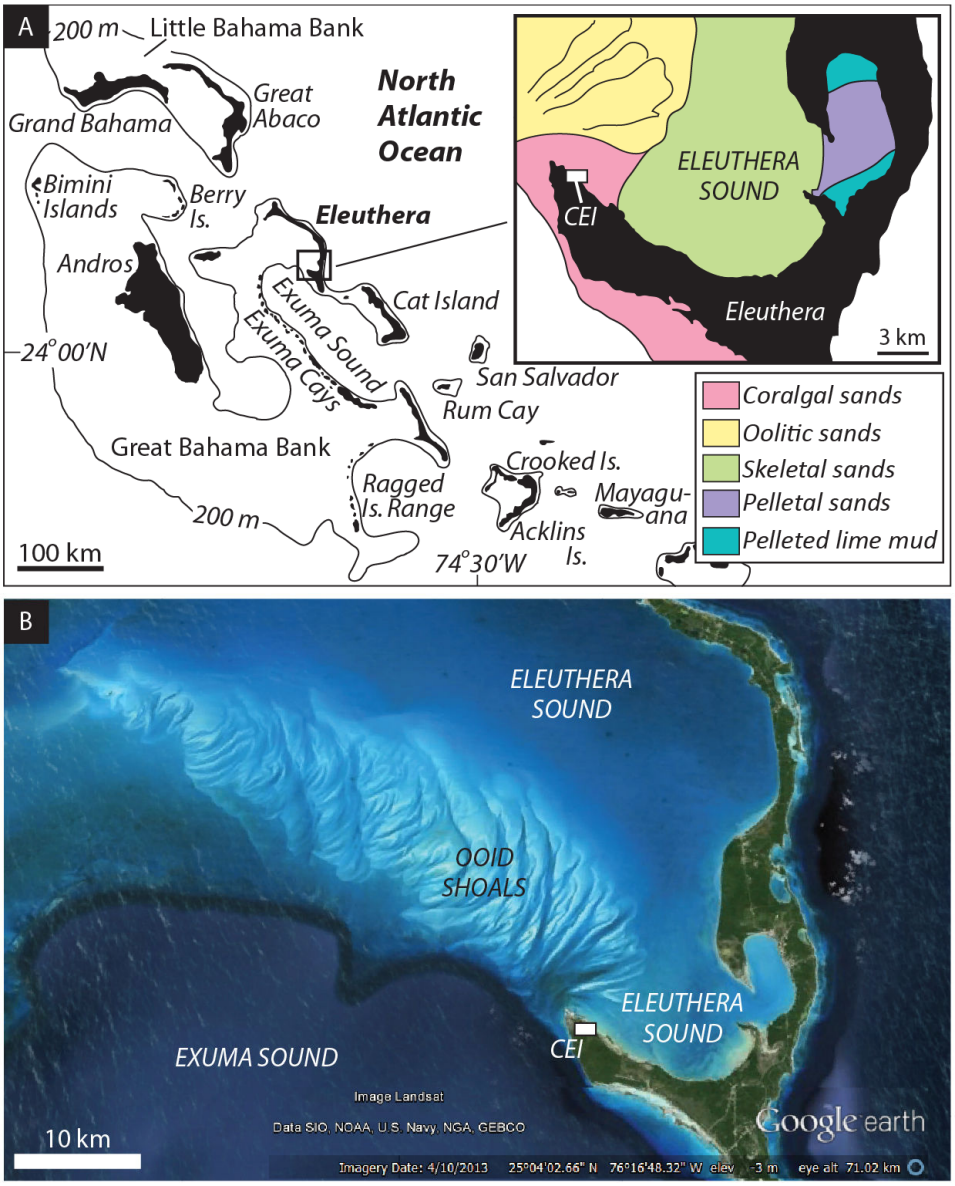

Figure 1.10 *A: Location map showing the study area in the Bahamas and the main sedimentary environments of Eleuthera Sound (inset, modified after Dravis, 1979). The field station on Cape Eleuthera where work was conducted is marked 'CEI' (Cape Eleuthera Institute); B: Satellite image of Eleuthera Bank and Exuma Sound. Note the ooid shoals that extend northwest from Cape Eleuthera, where they flank the southern edge of Eleuthera Bank and provide shelter for areas of Eleuthera Sound to the north and east (modified from Google Earth 7.1.2.2041, 2013).*

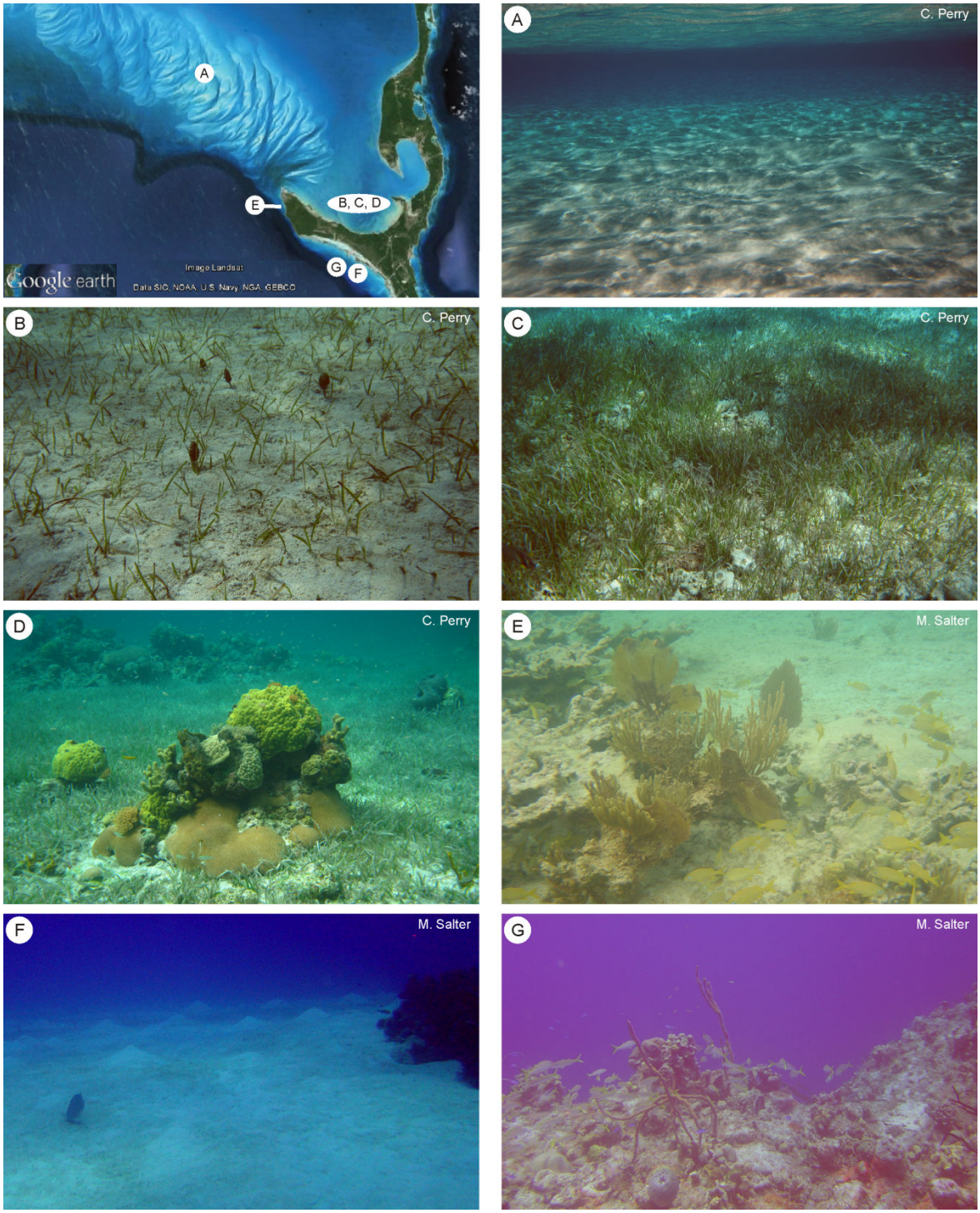

Figure 1.11 *Photographs of typical shallow water environments surrounding Cape Eleuthera. Satellite image (Google Earth 7.1.2.2041, 2013) shows approximate location of each. A) Ooid shoals (0–10 m in depth) – bare sands, typically medium-grained, occurring as 'mega-wave' formations (some are mobile, others are stabilised). B, C, D) Typical inner shelf habitats (0–8 m in depth) – (B) sparse seagrass and calcareous green algae (dark rounded thalli are Rhipocephalus sp.) on loose skeletal sands; (C) dense seagrass colonises and stabilises the substrate in some areas; (D) numerous small patch reefs are distributed widely throughout Eleuthera Sound. E) Fringing reefs (0–3 m in depth) on the western coastline of Cape Eleuthera are, at present, characterised by very low amounts of live coral cover. The platform gradually deepens from the ooid shoals and fringing reefs towards Exuma Sound, with substrates generally similar to those shown in B, C, and D, although extensive fields of bare sand in these regions can be intensely bioturbated (mounds in F). Slopes reach depths of approximately 15–25 m before dropping abruptly to depths >400 m in Exuma Sound. Fore reef zones at this boundary are characterised by low coral cover (G; looking into Exuma Sound).*

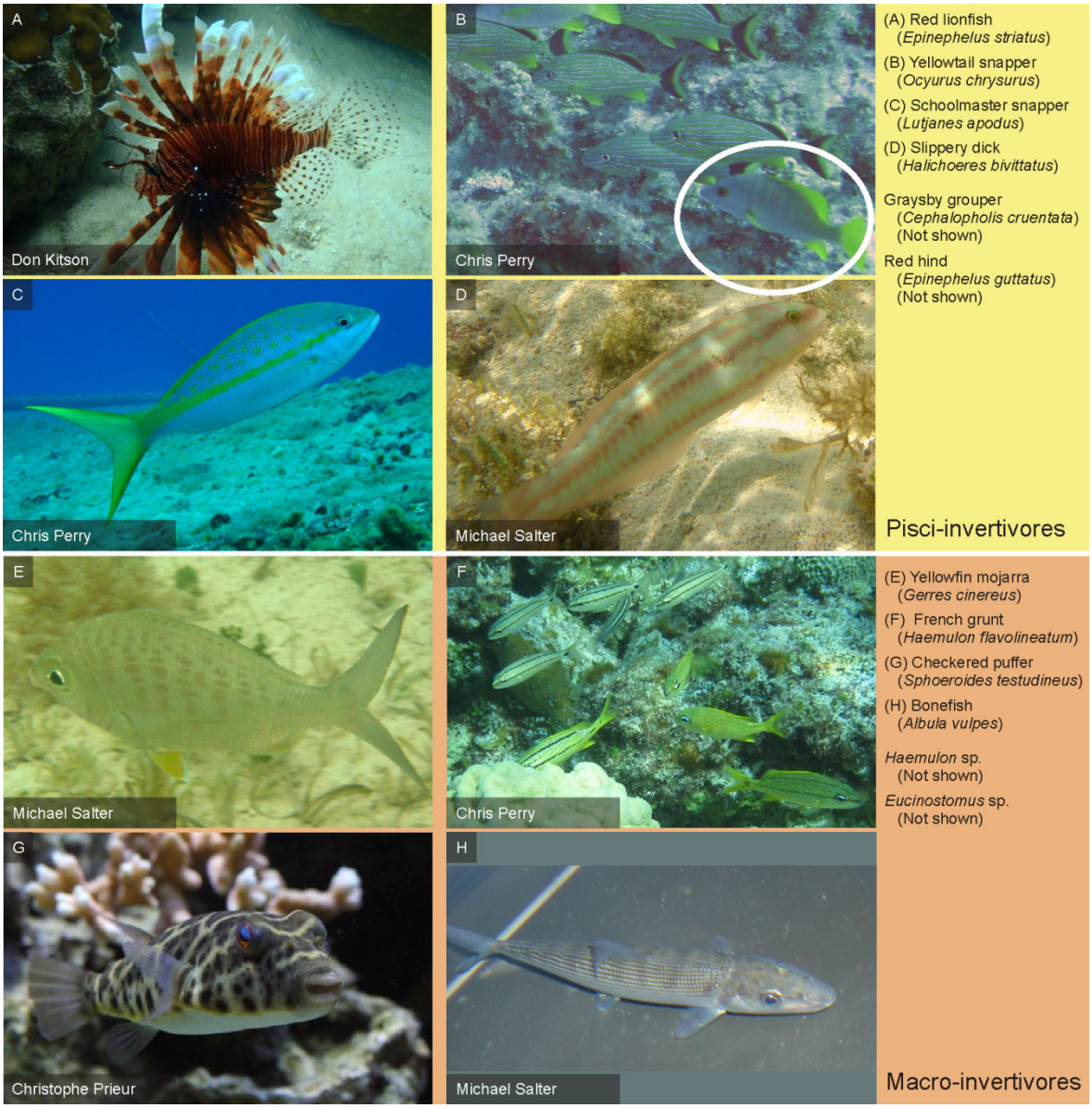

Figure 1.12 *Photographs of a selection of the fish species used in this thesis that belong to the pisci-invertivore and macro-invertivore functional groups. The full range of species used from each group is listed on the right. Note that an unknown species of flounder (not listed here) was also used and probably belongs to one of these two functional groups. The circled fish in image (B) is the species referred to on the right; other fish in this image are Haemulon sp. Note photographer credits; all images were sourced from www.fishbase.org (Froese and Pauly, 2013), with the exception of those taken by Michael Salter and Chris Perry.*

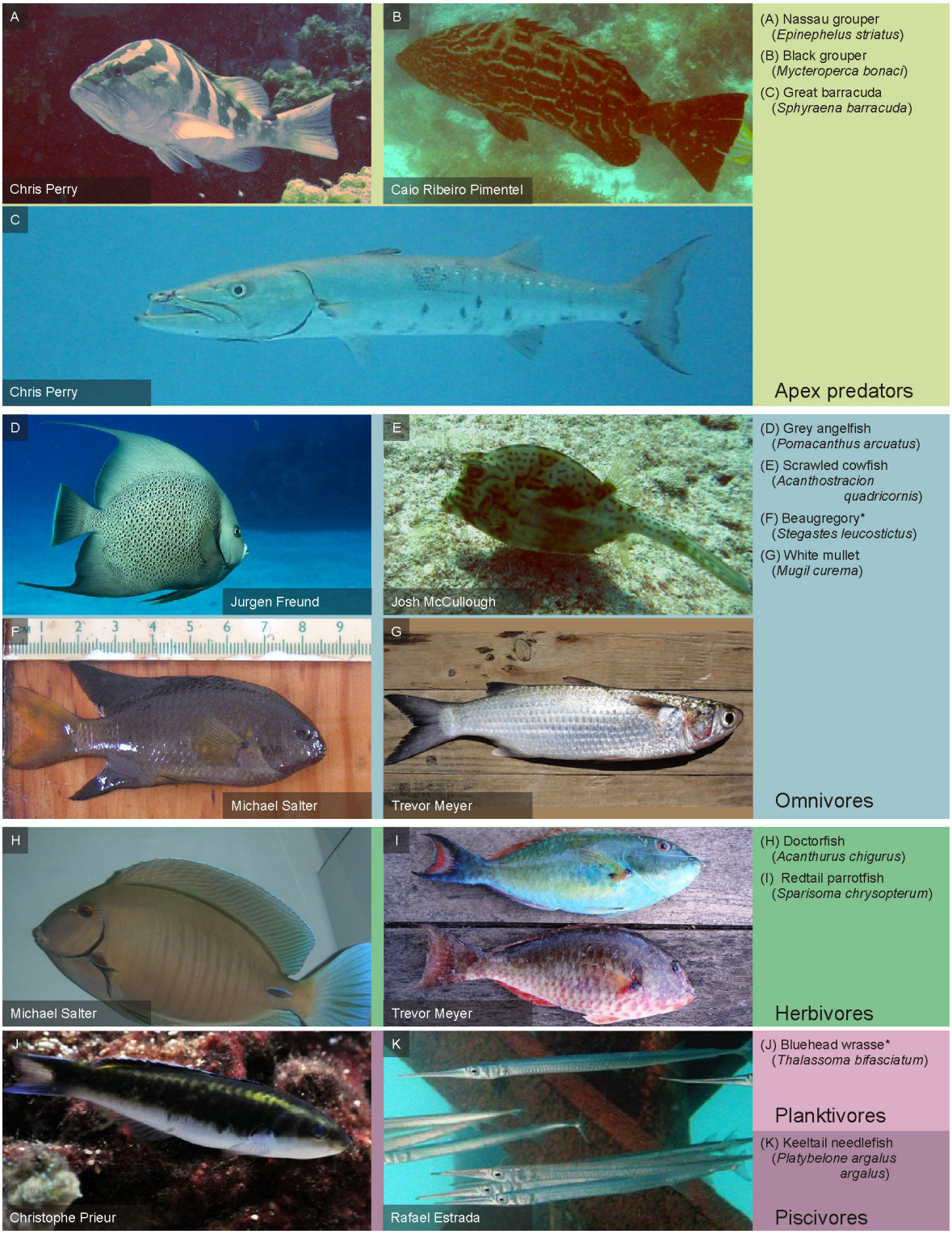

Figure 1.13 *Photographs of a selection of the fish species used in this thesis that belong to the apex predator, omnivore, herbivore, planktivores, and piscivore functional groups. The full range of species used from each group is listed on the right, but note that beaugregory is sometimes considered to be a herbivore, and bluehead wrasse is sometimes considered to be a macro-invertivore. Note photographer credits; all images were sourced from www.fishbase.org (Froese and Pauly, 2013), with the exception of those taken by Michael Salter and Chris Perry.*

Chapter 2: The sedimentary significance of fish-derived carbonates: Characterisation from an expanded range of Caribbean fish species

Parts of this chapter have been published in Sedimentology, v.59, p 2172–2198 (2012); see related publications.

2.1 INTRODUCTION

Previous studies of gut precipitates in marine teleosts have largely focused on their role in osmoregulation (Wilson *et al*., 1996; 2002). Only recently have the implications of these precipitates for ocean chemistry (Wilson *et al*., 2009) and shallow carbonate sediment production (Perry *et al*., 2011) begun to be explored, and only one study has provided detailed descriptions of their morphology, mineralogy, and composition (Perry *et al*., 2011). The latter finds that gut precipitates are typically high-Mg calcite, and that the size and morphology of these crystals is highly variable among 11 common Caribbean fish species, with dominant morphotypes including ellipsoids, dumbbells, and spheres that range from <1 to >30 μm in length, but other crystal forms including non-defined nano-scale products and micron-scale rosette-like clusters. Magnesium contents were shown to be highly variable in these products and typically range from 18 to 39 mol% $MgCO_3$. In addition to Mg calcite, that study also qualified the presence of minor amounts of aragonite (but did not ascribe this phase to a particular crystal morphotype) in the excreted products of some species, and a more recent study (Foran *et al*., 2013) documents the products of another species (gilthead bream, *Sparus aurata*) as magnesium-rich amorphous calcium carbonate (ACC) made up of nano-scale spheres.

Although the study by Perry *et al*. (2011) clearly demonstrated the potential for fish-derived carbonates to be a significant component of sedimentary carbonates in some platform-top settings

of the Bahamas, the variability in excreted products among 12 fish species rather hampers the proper interpretation of these carbonates with respect to their sedimentary significance in shallow platform settings. For example, the solubility of Mg calcite is widely considered to increase with increasing magnesium content (Plummer and Mackenzie, 1974; Walter and Morse, 1984; Bischoff *et al*., 1987), and the solubility of ACC can be up to 120 times greater than that of calcite (Brečević and Nielsen, 1989). The solubility of fish-derived carbonates may therefore actually vary considerably according to producing species, and whereas some products may be quite stable in platform-top sedimentary settings, others may be susceptible to rapid dissolution. Short-term preservation potential of the various excreted products is considered elsewhere (Chapter 7 of this thesis), but before doing so it is necessary that the full range of excreted products is better understood.

The present chapter therefore aims to achieve this by: i) expanding the range of common Caribbean fish species from which excreted carbonates can be characterised (to include species from all of the main functional groups); ii) providing extensive mineralogical, compositional, and morphological descriptions of the products excreted by this expanded range of Caribbean species; and iii) using a range of techniques to confirm the presence of additional precipitate phases, quantify them, and ascribe them to morphotypes. With regard to the final point, aragonite may be particularly problematic if it occurs as a minor component in pellets dominated by Mg calcite. Previous analytical approaches (X-ray diffraction) that qualify its presence require bulk samples, and as such are not capable of relating phases to crystal forms. Conversely, single crystal analytical approaches (scanning electron microscope-based energy-dispersive X-ray spectroscopy) enable determination of composition, but because aragonite and calcite can be compositionally similar, and because no obvious candidate for aragonite based on morphology has yet been described, the source of the aragonite signal in bulk analyses remains elusive. However, the lattice structure of aragonite means it is able to accommodate strontium more readily than calcite (Banner, 1995), and it is possible that strontium content will facilitate identification of the former. The present study therefore includes data on trace elements obtained from individual crystals.

Finally, to enable meaningful modelling of carbonate production by marine fish that includes variable such as crystal morphology, mineralogy, and composition, it is necessary to understand the reasons for variations in excreted products among species. While there are numerous potential drivers for this variability, many of which are beyond the scope of this study, several factors are reported here, such as dietary habits and body mass, in an attempt to begin to explain species-dependent differences in crystal products.

2.2 MATERIALS AND METHODS

2.2.1 Sample collection

Sampling was carried out over two periods at the Cape Eleuthera Research Institute (CEI), Eleuthera, the Bahamas, in November to December 2009 (sea surface temperature of ~25 to 27 °C) and July 2010 (sea surface temperature of ~28 to 30 °C). Seawater salinity during both periods was between 36 and 37 (practical salinity scale). Twenty-three species of fish were captured from a range of shallow (<10 m) nearshore environments (patch reefs and inlets) in Eleuthera Sound using baited traps, seine nets and by hook and line. Immediately after capture fish were transferred to tanks within the aquaculture facility at CEI. Fish were kept individually and in groups (arranged by size where possible), and all were left for two days prior to sampling to allow the excretion of any food material ingested prior to (or during) capture. Oxygen levels in each experiment tank were maintained via quartz sand airstones linked to a central compressed air supply, and a continuous flow of one-pass seawater (pumped from ~70 m offshore at a depth of ~1 to 2 m) ensured that temperature and salinity remained close to ambient within local near-surface waters. Seawater flow was filtered to 5 μm to minimise influx of external material, thus preventing fish from ingesting material during sampling. Tanks were also fitted with false mesh floors to prevent fish re-ingesting excreted carbonate pellets (which typically sink after excretion). One species, yellowfin mojarra, was sampled during both sampling periods and acted as a control by ensuring that any variation in environmental conditions did not result in the production of different crystal forms.

Carbonates are excreted as mucus-coated pellets (see Perry *et al*., 2011) and were collected within 24 hours of excretion with plastic Pasteur pipettes. They were immediately rinsed in distilled water to remove salts before being soaked for 6 hours in 5.25 % sodium hypochlorite (commercial bleach) to remove the organic components of mucus coatings. This treatment has no discernible effect on carbonate mineralogy or grain texture and causes no detectable dissolution (Gaffey and Bronnimann, 1993). However, along with other techniques commonly used to remove organics from carbonates, hypochlorite treatments have been shown to cause minor changes in the trace element chemistry of aragonite (Love and Woronow, 1991), although the effect on calcite and Mg calcite is not known. Bleach was carefully removed with plastic Pasteur pipettes before two additional rapid rinses in distilled water to ensure removal of all dissolved salt and bleach residues. Following the final rinse, precipitates were collected on 47 mm diameter, 0.45 μm pore size cellulose nitrate membranes or 47 mm diameter, 1 μm pore size glass fibre filters. Although pore sizes of these filters exceed the width of many individual crystals (Perry *et al*., 2011), pellets are able to tolerate gentle handling without disaggregating during the cleaning and filtration process, and thus most individual crystals of all sizes were retained. Precipitates were oven-dried on the membranes at 50 °C. Using this methodology precipitates were readily liberated from filters/membranes and prepared either for morphological and/or compositional analysis.

The 24 fish species used for this study were selected to cover a range of key functional fish groups (Table 2.1) that includes apex predators, macroinvertivores, piscivores, pisci-invertivores, omnivores, and herbivores, as described by Randall (1967) and Newman *et al*. (2006). Thus the sample set provides data from a range of common and ecologically important fish that occur within most shallow tropical marine settings. Functional groups not included are microinvertivores (*e.g.*, *Chaetodon* sp.) and planktivores, although several authors (Feddern, 1965; Clifton and Motta, 1998; White and Samhouri, 2011) consider bluehead wrasse to be largely planktivorous. Only two species did not excrete endogenously precipitated carbonates. Of these, it is noted that only a single specimen of doctorfish, *Acanthurus chirurgus*, was collected, and the absence of excreted carbonates does not necessarily apply to the entire species. Indeed, recent work indicates that

sexually mature female fish may produce carbonates at significantly lower rates than males due to the uptake of large amounts of imbibed Ca^{2+} via the gut, driven by elevated oestrogen levels (Al-Jandal *et al*., 2011), and this could explain the apparent absence of any intestinally precipitated carbonates (sexing of fish was not carried out as this is difficult without histological information). The same may also apply to white mullet, *Mugil curema*, which also did not excrete endogenously precipitated carbonates.

2.2.2 Morphological analysis

Crystals were examined for morphological analysis using Scanning Electron Microscopy (SEM) within a Field Emission Gun (FEG) Zeiss Supra 40VP system. Loose pellets were tipped onto either adhesive carbon-coated tabs or a thin coating of silver epoxy resin upon 12 mm aluminium pin stubs (both methods yielding similar SEM image quality). All samples produced good secondary electron (SE) images when examined in high vacuum at a working distance of 5 to 7 mm, accelerating voltage of 2 keV, and aperture width of 30 μm. At least 15 pellets (and in most cases upwards of 40) were examined per species, and for most species these were produced by at least four (and up to 30) individual fish. However, characterisation is based on the products of fewer individuals in the case of seven species (n = 1 for Nassau grouper, scrawled cowfish, red hind, flounder sp., and grunt sp.; n = 2 for redtail parrotfish and grey angelfish).

Cross-sections of some larger particles were examined in polished resin blocks. These were made by placing sample pellets into foil moulds with a 2 ml mixture of 30 % low viscosity resin (TAAB Transmit LM) and 70 % acetone. Acetone acted to lower the resin viscosity, thus ensuring proper impregnation of pellets. Air was removed from pellets by placing the moulds in a vacuum chamber at 94.7 kPa for 1 hour, during which time the acetone evaporated. Following this a further 2 ml of resin was added and moulds were returned to the vacuum chamber for another hour. The resin was cured at 70 °C for 18 hours before sequential polishing down to 5 μm using Buehler P800, P1200, and P4000 silicon carbide abrasive grinding papers. A gold-palladium coating of several nm thickness was applied prior to analysis. Resin-embedding was only successful for samples with the

largest crystals; sub-micron scale crystals, such as small ellipsoids, being easily ripped out of the resin during the polishing process.

2.2.3 Mineralogical and chemical analyses

2.2.3.1 Energy-dispersive X-ray spectroscopy (EDX)

Compositional analyses of individual crystals utilised the SEM-integrated Oxford Instruments ISIS energy-dispersive X-ray spectroscopy (EDX) system, which allows standardless quantification of analytical results using EDAX ZAF quantification software. This system was used in combination with a backscatter electron (BSE) detector at a working distance of 15 mm, accelerating voltage of 15 keV, and aperture width of 120 μm. Images produced using BSE, although lacking the clarity of SE images, were sufficient to identify and select the desired crystal types for analysis. EDX spectroscopy requires flat polished sample surfaces for the most precise quantitative chemical analysis. However, the very-fine-grained nature of fish-derived carbonates makes it difficult to achieve perfectly flat surfaces, even when resin-embedded, and thus the EDX analyses herein should be considered as semi-quantitative. However, average results for samples from individual fish species are generally in close agreement with liquid ion chromatography and X-ray diffraction results, and are thus taken as a good approximation of the accurate $MgCO_3$ mol%. It is also noted that the maximum resolution of EDX analysis in this system is ~1 μm. Given that many of the crystals are <1 μm in length, slight errors could be introduced due to analytical incorporation of other phases surrounding the subject crystal. Thus for the smallest crystals analyses were only conducted if they were surrounded by morphologically similar crystals.

Single crystal compositional analyses were used mainly for determination of Ca:Mg ratios in various crystal forms, and in this manner EDX has an advantage over analytical approaches where the bulk sample is analysed (*e.g.*, liquid ion chromatography, atomic absorption spectroscopy, and inductively-coupled plasma mass spectrometry) of being able to confirm compositional differences among crystal forms in mixed samples. Given this benefit, EDX was also used as a semi-

quantitative approach for determining trace element concentrations in known crystal forms, despite its lower sensitivity compared to other approaches.

2.2.3.2 X-ray diffraction (XRD)

X-ray diffraction (XRD) analysis was conducted on selected samples in order to: i) confirm mineral phases; ii) provide data to support the chemical compositions determined using EDX and liquid ion chromatography; and iii) provide information on the crystallinity of the various precipitates. Samples were selected to cover a range of crystalline products: spheres, dumbbells, and polycrystalline ellipsoids produced by checkered puffer; and rhombohedra and platy and amorphous magnesium carbonates (with <2 mol% $CaCO_3$) produced by bluehead wrasse. Various other crystal types, including monocrystalline ellipsoids, small dumbbells, and polycrystalline spheres (all HMC and VHMC) have been analysed previously (Perry *et al*., 2011) and those data are incorporated here.

X-ray diffraction analyses for this study were carried out using a Philips PW1710 X-ray diffractometer equipped with a Philips PW1729 X-ray generator (Cu*K*α radiation). Sub-samples weighing approximately 100 mg were ground in an agate pestle and mortar and dispersed evenly over a glass plate with an adhesive coating. Samples were scanned with a step width of 0.02° 2θ at 1 second per step, and a silicon standard was used to check the goniometer position. Peak positions were compared with data from the RRUFF database (Downs, 2006) to confirm the crystalline phases present.

In the case of Mg calcite, a systematic relationship exists between $d_{(104)}$ values and the amount of magnesium substituted for calcium in the crystal lattice, and numerous calibration curves have been published (Goldsmith *et al*., 1961; Bischoff *et al*., 1983; Zhang *et al*., 2010; see Appendix I, Table AI 1; Fig AI 1). These curves, based on abiotic synthetic calcites and Mg calcites with up to 50 mol% $MgCO_3$, facilitate the estimation of $MgCO_3$ content in natural calcites, although several caveats apply. Firstly, estimates of $MgCO_3$ content for biogenic Mg calcites may vary by up to ±5 mol% due to: i) line broadening associated with small (<1 μm) crystal size, defect density and

relatively poor crystallinity; ii) compositional heterogeneity; and iii) lattice distortion and disorder resulting from cation substitution (Bischoff *et al*., 1983). Secondly, the influence of incorporated trace elements, such as Sr^{2+}, on calcite unit cell parameters is not well constrained and may introduce further errors. The calibration curve of Goldsmith *et al*. (1961) and Bischoff *et al*. (1983) is based on the assumption of a linear solid-solution series between calcite and magnesite via stoichiometric dolomite. In order to address the problem of lattice disorder, Zhang *et al*. (2010) produced a different curve based on synthetic disordered HMC and disordered dolomite. At $MgCO_3$ contents greater than ~20 mol% the two curves diverge, and at very high $MgCO_3$ contents (>40 mol%) values derived from these curves can differ by more than 10 mol%. As the degree of lattice disorder is not determined for fish-derived carbonates, a range of possible values based on both curves are presented here.

In addition to Mg calcite, previous studies have used XRD to confirm the presence of minor amounts of aragonite in fish-derived carbonates. However, the relative proportions of calcite and aragonite were not quantified. Several attempts have been made at using XRD patterns to estimate the relative proportions of these phases (Lowenstam, 1954; Chave, 1962; Davies and Hooper, 1962; Sepulcre *et al*., 2009). The approach of Davies and Hooper (1962) is claimed to yield results accurate to within 1 % and is consequently one of the most widely used (*e.g.*, Morse *et al*., 1985; Labonne and Hillaire-Marcel, 2000; Jiménez-López *et al*., 2001). Their approach uses the integral of the $d_{(104)}$ calcite diffraction peak as a percentage of the combined total peak integral of calcite $d_{(104)}$, aragonite $d_{(111)}$, and aragonite $d_{(021)}$, plotted against a calibration curve (Appendix I, Fig. AI 2) to determine the weight percent calcite in a sample. This approach is employed here to estimate the weight percent aragonite in fish-derived carbonate samples analysed in this and previous (Perry *et al*., 2011) studies.

2.2.3.3 Liquid ion chromatography

Cation (Ca^{2+} and Mg^{2+}) concentrations were measured by liquid ion chromatography[1] (Dionex ICS-1000, Sunnyvale, CA, USA) using samples of cleaned excreted carbonates suspended in deionised water and dissolved using 0.02 N hydrochloric acid, followed by appropriate dilution. Occasionally, samples contained numerous fragments of calcium phosphate scales and fin rays, and/or marine carbonate particles (excreted during sampling; the gut sometimes having taken longer than anticipated to become completely void of materials ingested prior to capture). The presence of such materials would alter Mg^{2+}/Ca^{2+} ratios measured by liquid ion chromatography and they were therefore removed with forceps prior to analysis.

2.3 RESULTS

Detailed SEM examination of fish-derived carbonates indicates that five predominant crystal morphologies are produced: ellipsoids, dumbbells, spheres, needles, and euhedral rhombohedra. These range in length from <0.1 to >50 μm, depending on morphology, but are predominantly 0.5 to 2 μm in length (Fig. 2.1). Analytical investigations indicate that, in addition to the mainly VHMC (18–39 mol% $MgCO_3$) products detailed by Perry *et al*. (2011), the excretion of predominantly LMC and/or HMC with 4–10 mol% $MgCO_3$ is recorded in seven out of the 22 species that produced carbonates. Of these, three species (all small specimens with a body mass of <13 g) excreted pellets dominated by 'amorphous', or sometimes platy, Mg-rich carbonates (lacking Ca) alongside subsidiary LMC and/or HMC. Below is a detailed description of the morphological and compositional characteristics of the different carbonate crystal products (the key findings are summarised in Table 2.1).

[1] Liquid ion chromatography analyses were performed by Dr. E. Reardon at the University of Exeter.

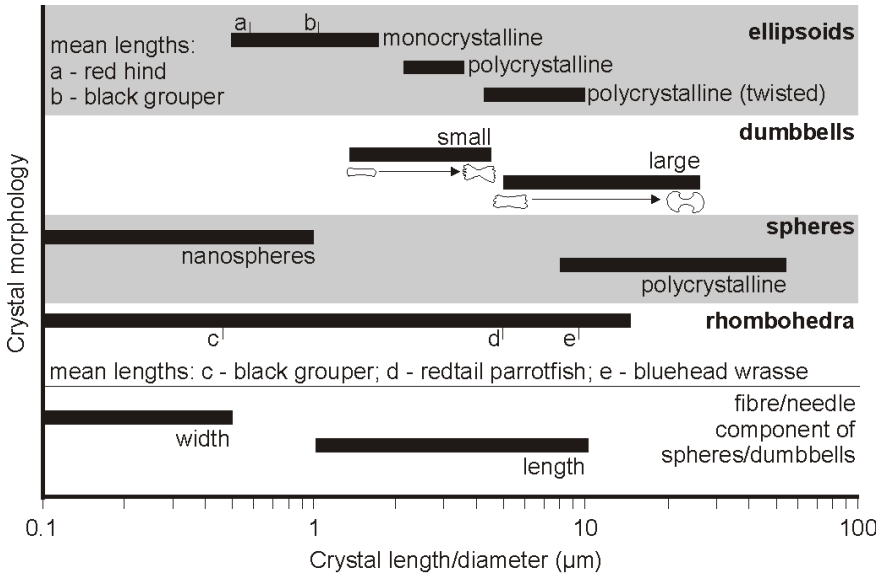

Figure 2.1 *Chart showing the range of grain sizes in which the main fish-derived carbonate crystal morphologies occur.*

Table 2.1 *List of the fish species sampled in this study and the key data arising from each.*

Species	Funct'l Group	Dominant (●) and subsidiary (^) crystal morphologies													$MgCO_3$ content (mol%)				Body mass of fish (g)
		m	e	r	w	d	s	x	l	p	a	b	n	Notes	EDX Dominant	EDX Subsidiary	LC	XRD*	
Lutjanes apodus (schoolmaster snapper)	P-I	●		^							^				22–37	-	20–34	30.4–39.6[a]	4.6–322
Ocyurus chrysurus (yellowtail snapper)	P-I	●												coarse surface	34	-	26–33	26.4–30.1[a]	13–946
Cephalopholis cruentata (graysby grouper)	P-I	●				^									34	-	25–32	30.3–36.0[a]	58–185
Mycteroperca bonaci (black grouper)	AP	●		^	^	^				^	^	^			19–30 (m/r/w)	10–14 (d)	24–35	24.5–43.2	424–1653
Epinephelus striatus (Nassau grouper)	AP	●		^											-	-	-	19.8–31.1	1318
Haemulon flavolineatum (French grunt)	M-I	●				^									20 (e)	6 (d)	22–24	-	11–25
Flounder sp.	?	●													36	-	-	-	81
Epinephelus guttatus (red hind)	P-I	●				^					^	^			39	-	33–35	-	205
Pterois volitans (red lionfish)	P-I	●								^				'mesh' coating	35	-	24–32	-	25–381
Haemulon sp. (grunt sp.)	M-I			●	●										29	-	34	-	101
Sphyraena barracuda (great barracuda)	AP	^			●	^				^	^	^	●		25–35 (n/w)	3 (d/s)	22–33[†]	20.8–26.4	41–11364
Gerres cinereus (yellowfin mojarra)	M-I	●				^	^	^	^						16–23 (m)	3–9 (d/s/x/l)	14–29	18.2[a]	107–202
Platybelone argalus argalus (keeltail needlefish)	P	●		●	●	^	^				^				11–16 (m/r/w)	2–5 (d/s)	16–22[†]	-	10–47
Pomacanthus arcuatus (grey angelfish)	O					●	●							some twisted	2.3 (all)	-	-	-	429–460
Acanthostracion quadricornis (scrawled cowfish)	O					●	●					^			5 (s)	-	-	-	390
Sphoeroides testudineus (checkered puffer)	M-I		●			●	●					^		some twisted	1–3 (all)	9–14 (few d/s)	3–10	6.4 & 17.3[a]	118–207
Sparisoma chrysopterum (redtail parrotfish)	H		●			^	●	●	●			^		some twisted	1.5 (all)	~4 (few s)	-	-	43–49
Thalassoma bifasciatum (bluehead wrasse)	Pk/M-I					●			^	●	●	●			~5 (d/b)	100 (p/a)	57–65[‡]	5.1[a]	1.1–7.7
Halichoeres bivittatus (slippery dick)	P-I					●				●	●	●			~5 (d/b)	100 (p/a)	-	-	1.5–5.9
Stegastes leucostictus (beaugregory)	H/O					●				●	●	●			~4 (d/b)	100 (p/a)	23–68[‡]	-	4.5–12.9
Albula vulpes (bonefish)	M-I					^	●				^	^	●		19–23 (s)	35 (n)	32–35	13.5[a]	759–1506
Eucinostomus sp. (mojarra sp.)	M-I					●	●			^		^			19 (d/s)	-	22	-	11–30

Functional group codes: P-I = piscivore-invertivore; M-I = macroinvertivore; AP = apex predator; P = piscivore; O = omnivore; H = herbivore; Pk = planktivore
Dominant morphology codes: m = monocrystalline ellipsoid; e = polycrystalline ellipsoid; r = rod; w = small dumbbell/wheatsheaf; d = large dumbbell; s = sphere; x = spherulite; l = lath/needle-like; p = platy (commonly forming rosettes or mesh-works); a = amorphous; b = rhombohedron; n = nanosphere.
* XRD range limits represent estimates based on different calibration curves, applicable to all values of $MgCO_3$ >20 mol% (see methodology). Results are based on one analysis for samples from all species except schoolmaster, barracuda, black grouper, and Nassau grouper. Upper and lower limits for these species are based on combined data from two analytical runs.
[a] Minor amounts of aragonite also detected in XRD.
EDX results are shown as mean values; where a range of values is shown this represents the range of mean values from different samples
LC results are shown as the range of values based on analysis of multiple samples. Where only one value is shown, only one sample was analysed
†Upper limit of LC results that represents likely upper limit of $MgCO_3$ mol% in Mg calcite phases. Higher $MgCO_3$ values are likely due to presence of a magnesium carbonate phase.
‡LC values for $MgCO_3$ content based on combined influence of Mg calcite crystals and amorphous Mg carbonates

Category I	Sub-category Ia	Category II	Category III	Category IV

(Categories refer to classification of fish species based on their carbonate products – see discussion)

2.3.1 Crystal morphology

2.3.1.1 Ellipsoids

Ellipsoids are the dominant crystalline product excreted by nine species, constituting >99 % of crystals in samples produced by each. In four additional species, which produce crystals that are more heterogeneous in composition, they represent the dominant crystal form alongside significant quantities of other crystal types, typically dumbbells and/or spheres (described below). In the majority of samples examined ellipsoids take the form of monocrystalline prolate ellipsoids (Fig. 2.2 A). Individual crystals are typically <2 μm in length (the majority across all monocrystalline ellipsoid-producing species are in the range 0.5–1.2 μm) and are morphologically very uniform within most species.

In a few species, specifically yellowfin mojarra and keeltail needlefish, the crystal products are more heterogeneous, with pellets comprising a mixture of not only monocrystalline ellipsoids, but also polycrystalline dumbbells and spheres. Despite this, monocrystalline ellipsoids produced by these two species are morphologically identical to those produced by other ellipsoid-producing species. In most species ellipsoids are well-defined (Fig. 2.2 A). However, in pellets excreted by red hind, and occasionally those excreted by other species, ellipsoids can be rather difficult to discern due to large quantities of surrounding nano-particulate carbonates. Other, more subtle, variations across species relate to the surface texture of crystals. Ellipsoidal crystals precipitated within schoolmaster snapper are consistently very smooth-surfaced (Fig. 2.2 A), while those excreted by yellowtail snapper commonly have numerous surface protrusions that create a coarse surface appearance (Fig. 2.2 B). In addition to individual ellipsoids, most ellipsoid-producing species also excrete occasional crystals that have the appearance of two or more intergrown ellipsoids that share a common centre and have long axes aligned perpendicular to one another (Fig. 2.2 A, inset).

It is notable that carbonate samples produced by keeltail needlefish and black grouper also comprise rods of up to 2 μm in length and dumbbells of up to 2.5 μm in length. Rods are typically

longer than ellipsoids, with straighter sides and blunted or flat terminations. Occasionally rod-like crystals exhibit long edges that are curved, the resultant morphology having the appearance of combined ellipsoids and rods. Other rods appear to have splayed terminations and fall somewhere between rod and small dumbbell morphologies. When viewed together it is tempting to invoke that these various forms are components of a morphogenetic sequence, each representing a different stage in crystal development (see Fig. 2.10).

Morphologically different to the above described monocrystalline ellipsoids are polycrystalline ellipsoids that are the dominant crystal form produced by redtail parrotfish. These comprise blade-like or platy sub-micron crystals that are aggregated to form ellipsoidal particles, occurring as one of two distinct forms: i) prolate ellipsoids, similar in shape to monocrystalline ellipsoids; or ii) elongate 'twisted' ellipsoids, in which crystals are arranged about the long axis in a helical manner (Figs. 2.2 C, D). Both forms are larger than monocrystalline ellipsoids: the former averaging 2.9 μm in length (range 2.2–3.6 μm long); the latter averaging 4.9 μm in length (range 4.0–5.8 μm long). Occasional broken surfaces of 'twisted' ellipsoids reveal a hollow internal structure (Fig. 2.2 D). Similar polycrystalline forms are also produced by checkered puffer (Fig. 2.2 C), although ellipsoids from this species tend to be larger (up to 10 μm in length) with more rounded ends, and individual crystals are aligned parallel to the long axes of particles, in contrast to the oblique alignment in ellipsoids produced by redtail parrotfish. The helical arrangement of crystals about the long axes of particles appears to be a common feature of many particle morphologies produced by these two species, and also by grey angelfish.

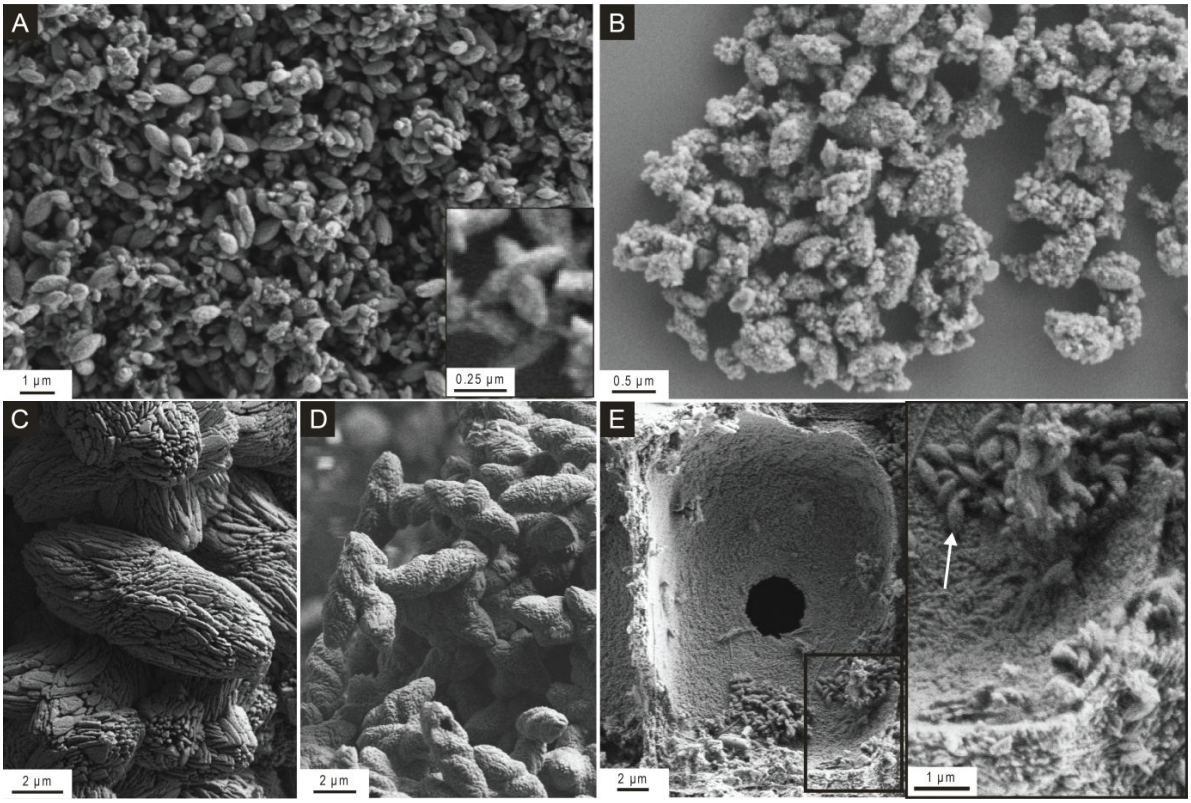

Figure 2.2 *Secondary electron (SE) images of various ellipsoidal crystalline forms produced by: A) schoolmaster snapper; B) yellowtail snapper (after gentle sonication); C) checkered puffer; D) redtail parrotfish; and E) yellowtail snapper. A, B) The majority of ellipsoidal forms examined herein are <2 µm in length and monocrystalline. Many exhibit smooth surfaces (A), but those produced by some species can exhibit rather coarse surfaces (B). C, D) Checkered puffer and redtail parrotfish both produce larger polycrystalline ellipsoids, at least some of which are hollow (D, centre bottom). Individual crystals that make up these ellipsoids are commonly arranged in a helical manner about the long axis. E) Monocrystalline ellipsoids (white arrow) exhibit the same characteristics when precipitated in the presence of ingested carbonate particles, such as Amphiroa shown here. All of these forms typically occur as individual particles, but it is not uncommon for intergrown clusters of two or more ellipsoids to occur (inset, A).*

2.3.1.2 Dumbbells

Dumbbell-shaped particles are present as the dominant crystal form in some species (*e.g.*, great barracuda), and occur as an abundant to rare subsidiary form in samples produced by many other species. The basic dumbbell structure comprises a narrow central core that broadens or splays perpendicular to the long axis, in both directions, resulting in a particle that, in many cases, resembles a double-headed broccoli (Figs. 2.3 A–F). However, the degree of broadening varies greatly, with end members resembling narrow wheatsheafs (Fig. 2.3 B) and broad ‘semi-spheres’ (Fig. 2.3 F). The structure of dumbbells is highly variable, both across and within species, with both monocrystalline and polycrystalline forms occurring.

Dumbbells are typically larger than ellipsoids, ranging from 1.3–25 μm in length, and in any sample comprising assorted crystal forms they are, on average, significantly larger than associated monocrystalline ellipsoids. Based on size relationships and chemical composition, there appear to be two distinct categories of dumbbell: 1) small wheatsheafs and dumbbells with lengths in the range 1.3–4.4 μm (mean lengths are 2.1 and 2.9 μm in precipitates excreted by *Haemulon* sp. and great barracuda, respectively) and typically having high magnesium contents (typically >20 mol% $MgCO_3$; see section 2.3.2); and 2) larger wheatsheafs and dumbbells, which are common subsidiary forms produced by many species, typically occurring with lengths in the range 5–25 μm and magnesium contents in the range 2–14 mol% $MgCO_3$. Perhaps best illustrating this difference in the chemical compositions of these two categories of dumbbell are precipitates excreted by black grouper and keeltail needlefish: both species produce monocrystalline ellipsoids, small dumbbells, and large dumbbells, with the former two morphotypes having consistently higher magnesium contents than the latter.

In samples where larger dumbbells are a common subsidiary form, the dominant form may be ellipsoids (*e.g.*, samples produced by yellowfin mojarra and keeltail needlefish) or spheres (*e.g.*, samples produced by checkered puffer and bonefish). In either case the length of large dumbbells is commonly very variable (*e.g.*, in the range 5.2–18.4 μm in keeltail needlefish and 5.4–19.6 μm in checkered puffer). A general observation suggests that, within the small and large categories, the degree of broadening increases with particle length (Fig. 2.1).

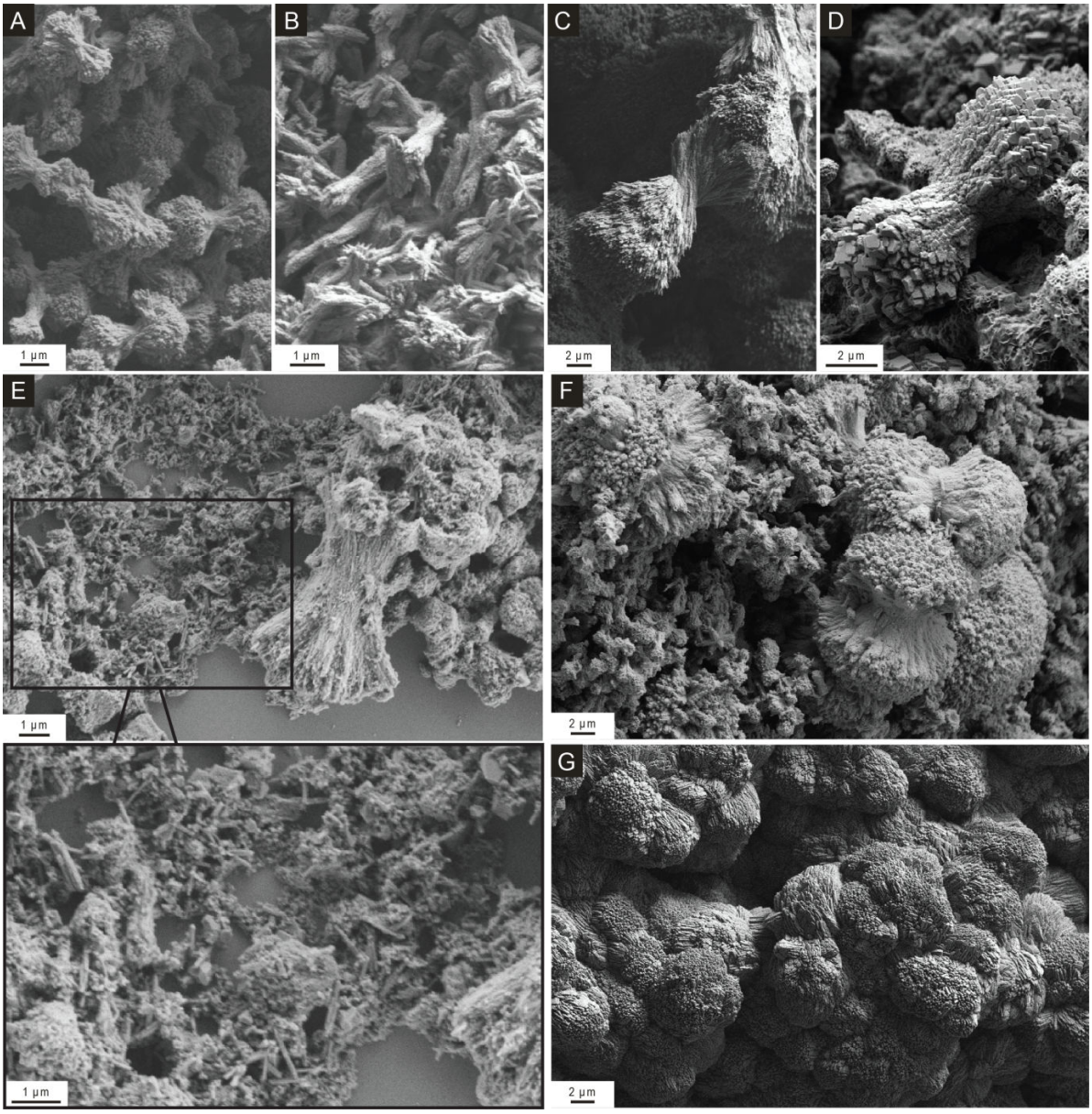

Figure 2.3 *SE images of various dumbbell-shaped precipitates excreted by A) great barracuda; B) grunt sp.; C) grey angelfish; D) mojarra sp.; E) great barracuda (after gentle sonication); F) great barracuda; G) checkered puffer. Some species excrete small (<3 µm) polycrystalline aggregates that can be predominantly dumbbell-shaped (A) or comprise assorted rods, wheatsheafs and dumbbells (B). Larger dumbbells (>4 µm) typically comprise fibres originating from a central point (C, E), but can also comprise numerous sub-micron rhombohedra (D) or micron-scale blade-like crystals (G). Fibrous dumbbells appear to release individual crystals (expanded portion of E) after short periods of gentle sonication. The largest dumbbell-shaped particles can exhibit a high degree of crystal spreading, such that either end assumes a semi-spherical shape (F). Individual crystals of these particles can be significantly broader than the fibres of other dumbbells. Note that the 'semi-spheres' in image F are present alongside much smaller dumbbells of the type shown in image A. In some examples large dumbbells appear to coalesce to form single multi-lobate particles (G).*

The most commonly observed type of dumbbell is polycrystalline, comprising needles or fibres that radiate from a common central point to create a double-headed broccoli-like form. These crystal aggregates form dumbbells across the spectrum from 'wheatsheaf' to 'semi-sphere' and are present

in samples from nearly all species that produce any dumbbell type. In many examples individual crystals are very thin (typically <0.1 μm in width) (Fig. 2.3 C), but occasionally they are broader (up to 0.5 μm in width), especially in the largest dumbbells (Fig. 2.3 F). It is common in the largest dumbbells of this type for the two 'heads' to splay to such a degree that they eventually grow back on themselves, often merging to form a near-complete sphere. A second type of polycrystalline dumbbell is that which comprises an aggregation of sub-micron equant rhombohedra (Fig. 2.3 D). These most commonly occur in samples produced by checkered puffer, *Eucinostomus* sp., bluehead wrasse, slippery dick and beaugregory, but in most samples they are subsidiary to other dumbbell types. Broadening in these particles appears to be controlled by the size of individual rhombohedra, increasing away from the dumbbell core.

As with ellipsoids, some of the large dumbbell-shaped particles produced by redtail parrotfish, checkered puffer, and grey angelfish have a twisted appearance (Fig. 2.3 C), with individual crystals being arranged helically about the long axis. In carbonate particles excreted by redtail parrotfish the polycrystalline aspect commonly involves rather blade-like or platy crystals (as with ellipsoids excreted by this species), whilst dumbbells produced by grey angelfish comprise fibres radiating and twisting from a common centre. Dumbbells excreted by checkered puffer occur in three main forms. Commonly they are twisted, comprising blade-like or platy crystals; the only discernable difference from ellipsoids (*e.g.*, Fig. 2.2 C) being their larger size and dumbbell-shaped outline. In addition, non-twisted forms also occur, typically comprising either fibres or sub-micron rhombohedra (as described above). Dumbbells made up of blade-like crystals do not broaden to the same degree as those consisting of radial fibres, and thus do not form sphere-like morphologies. However, it is not uncommon for these dumbbells to coalesce and form large multi-lobate structures that can constitute entire pellets (Fig. 2.3 G).

2.3.1.3 Spheres

Spherical forms are the dominant crystalline product excreted by several species, including bonefish, checkered puffer, grey angelfish, and scrawled cowfish. They also occur as subsidiary

forms in carbonates produced by several other species, including redtail parrotfish and yellowfin mojarra. Spheres are typically the largest of the particle morphologies, occurring with diameters in the range 8 to >50 μm. In many samples sphere diameter may typically be reasonably uniform within individual pellets but commonly varies from one pellet to the next; mean diameter within individual pellets ranging from ~10 to ~30 μm (Fig. 2.4 A). Occasionally spheres occur as discrete particles (this is mostly restricted to the largest spheres), but most commonly they are intergrown with other spheres (Figs. 2.4 A, B). The nature of these pellets differs somewhat from those comprising ellipsoids; while ellipsoids appear to be held together by the interlocking of individual crystals, spheres appear to have coalesced during growth to form chains of intergrown particles. Consequently, in many cases, spherical forms are not complete spheres, and the degree to which they are 'coalesced' can influence their appearance markedly. At one end of the spectrum a pellet can appear to consist of a large number of spheres that are each in limited contact with one or more neighbouring spheres (Figs. 2.4 A, B). Individual spheres become more difficult to distinguish as the degree of 'coalescence' increases, and, at the opposite end of the spectrum, it is no longer appropriate to describe particles as spheres. Instead pellets have the appearance of a single, multi-lobate particle, similar in manner to coalesced dumbbells (Fig. 2.3 G).

In the majority of examples, sphere (or lobe) surfaces comprise many radially arranged needles or fibres that are typically <0.2 μm in width (Fig. 2.3 B), and they are thus polycrystalline structures. The nature of these fibres is similar to those that make up polycrystalline dumbbells, and, when viewed end-on, a polycrystalline fibrous dumbbell can be difficult to distinguish from a sphere. There are also numerous examples of coalesced 'double-spheres' that closely resemble 'semi-spherical' forms of the dumbbell category, and at least some of these may relate to dumbbells that have grown back over themselves. In support of this, several apparent spheres with missing segments reveal an internal structure that indicates they are composed of several well-developed, intergrown dumbbells (Fig. 2.3 C).

In carbonates produced by checkered puffer and bonefish, the internal structure of spheres indicates, however, that the continued growth of dumbbells is not the only mechanism of sphere formation. Occasional broken surfaces reveal a dense and continuous radial structure of fibres emanating from the central point of some spheres (Figs. 2.4 B, E). In contrast, cross-sections of other, externally identical, spheres reveal an outer layer of radially arranged fibres (each ~1 μm in length) and a hollow, or partially hollow, centre (Figs. 2.4 D, F). Internal structure variations are not particular to species; both bonefish and checkered puffer produce spheres with dense and hollow internal structures. Cross-sections of spheres and pellets produced by checkered puffer, revealed in polished surfaces of resin-embedded pellets, indicate that individual pellets comprise spheres that have either dense internal structures, or hollow centres (Figs. 2.4 E, F). Where spheres are partially hollow, the material that occupies the centre is commonly rather peloidal in character, at least in carbonates produced by bonefish. This can include, or be dominated by, nanospheres that are typically <0.5 μm in diameter (Fig. 2.4 D).

In addition to their presence within hollow spheres, nanospheres represent the dominant morphotype in some pellets. In either situation, their occurrence is limited to two species; bonefish and great barracuda. They range in size from <0.1–1.0 μm diameter (typically being <0.4 μm). As with the relationship between small and large dumbbells, the continued growth of nanospheres to directly form larger spheres appears unlikely given the near-complete absence of spheres in the 1–5 μm diameter range. Thus nanospheres and larger spheres appear to be discrete crystal forms. The microstructure of nanospheres is difficult to ascertain at this scale, but they appear to have smooth surfaces. Occasional broken surfaces reveal hollow interiors. Commonly they appear to ‘coalesce’ in a similar manner to larger spheres, occasionally to such an extent that they amalgamate into a single uniform structure (Fig. 2.4 G).

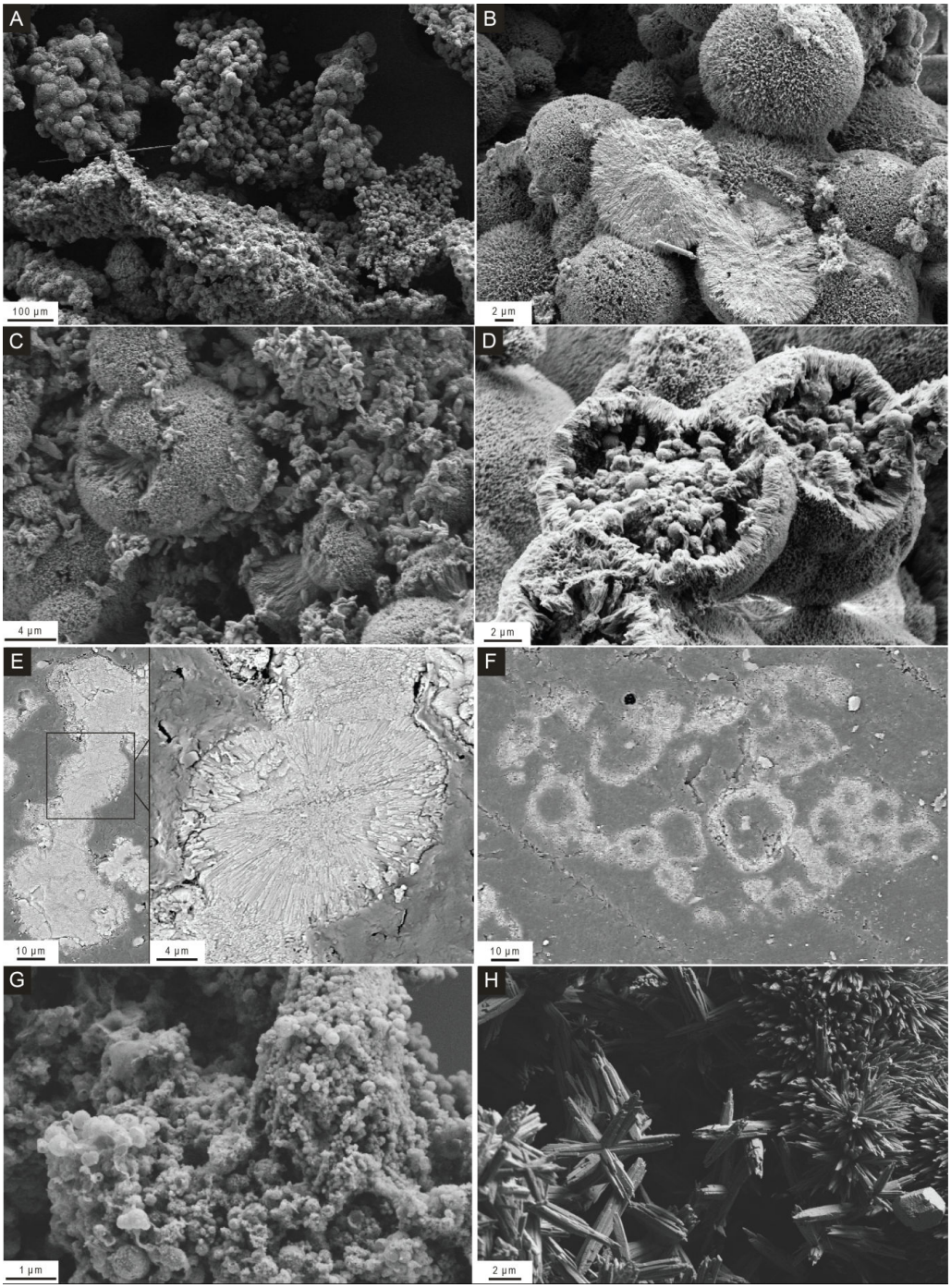

Figure 2.4 *SE images of various forms of spherical precipitates. A) Pellets comprising intergrown spheres (bonefish). Note that sphere diameters are reasonably uniform within pellets, but can vary considerably among pellets. B) Typical outward appearance of spheres (bonefish), with surfaces comprising the terminal points of densely-packed radially-arranged fibrous crystals. In this example fibres radiate from a central point, as evidenced by two spheres in cross-section (centre bottom). C) Partial sphere, left of centre (yellowfin mojarra). Missing segments reveal an internal structure that appears to comprise several intergrown dumbbells. D) Partial sphere revealing an outer layer of radial fibres <1 µm in length, and a hollow centre containing nanospheres (bonefish). E, F) Backscatter electron images of resin-embedded pellets (checkered puffer). E) Solid spheres comprising radial fibres; F) Hollow spheres. Individual pellets dominated by spheres typically comprise only one of these types. G) Nanospheres (bonefish). Occasionally nanospheres appear to coalesce, forming a single structure (top right). H) Spherulitic forms (right) are less densely packed than typical spheres and comprise a radial arrangement of blade-like crystals (redtail parrotfish). Also shown are intersecting/intergrown fibrous needles with multiple blunt terminations (left).*

In addition to the spheroidal forms described above, spherulitic particles are commonly produced by yellowfin mojarra and redtail parrotfish (two species that produce a large variety of crystal forms). In size and radial growth structure these are similar to large spheres. However, individual crystals are less densely-packed and much more blade-like in form, with flat faces and pointed terminations (Fig. 2.4 H). Blades are up to 0.5 μm in width, and complete spherulites are typically in the range 4–10 μm in diameter. Commonly they 'coalesce' to form lobate structures that are similar, but less densely packed, than those formed by typical spheres.

2.3.1.4 Euhedral rhombohedra

Rhombohedral particles of moderate to strong crystal habit (Fig. 2.5) are a common, albeit volumetrically minor, product of many species. These crystals are morphologically varied, often dependent on the species by which they are produced. Redtail parrotfish, for example, produces rhombohedra of very strong crystal habit that are typically up to 5 μm in length (Fig. 2.5 E). Typically they occur as individual crystals distributed randomly through pellets that are dominated by other crystal morphologies. Crystals of similar morphology are also sometimes present in the carbonate products of other species. Scrawled cowfish excrete carbonate precipitates that are dominated by spheres, with rhombohedra identical to those produced by redtail parrotfish commonly occurring in clusters on sphere surfaces. Black grouper also produces similar rhombohedra present alongside the dominant monocrystalline ellipsoids (Fig. 2.5 D). In some pellets excreted by the latter, rhombohedra are randomly distributed among ellipsoids; in others they can occur in localised high concentrations. In either situation crystals are smaller and more prismatic than those produced by redtail parrotfish.

The rhombohedral crystals excreted by bluehead wrasse, slippery dick, and beaugregory differ significantly from those described above. In all three species rhombohedra are subsidiary to a magnesium carbonate phase (see compositional results), but nonetheless they represent a significant proportion of the excreted carbonates. In most pellets the magnesium carbonate forms a 'matrix' in which rhomobohedral crystals are uniformly distributed (Fig. 2.5 A). Most of these

crystals are larger than rhombohedra produced by other species, typically occurring in the range 5–15 μm in length. Whilst they exhibit well-defined crystal faces, these are typically repeated in a series of steps (Figs. 2.5 A–C), with the overall effect of moderate crystal habit tending towards sphere- or dumbbell-like morphologies (*e.g.*, Fig. 2.2 B). In addition to these monocrystalline rhombohedra, these fish species also commonly produce dumbbells that comprise sub-micron rhombohedra (similar to that shown in Fig. 2.3 D).

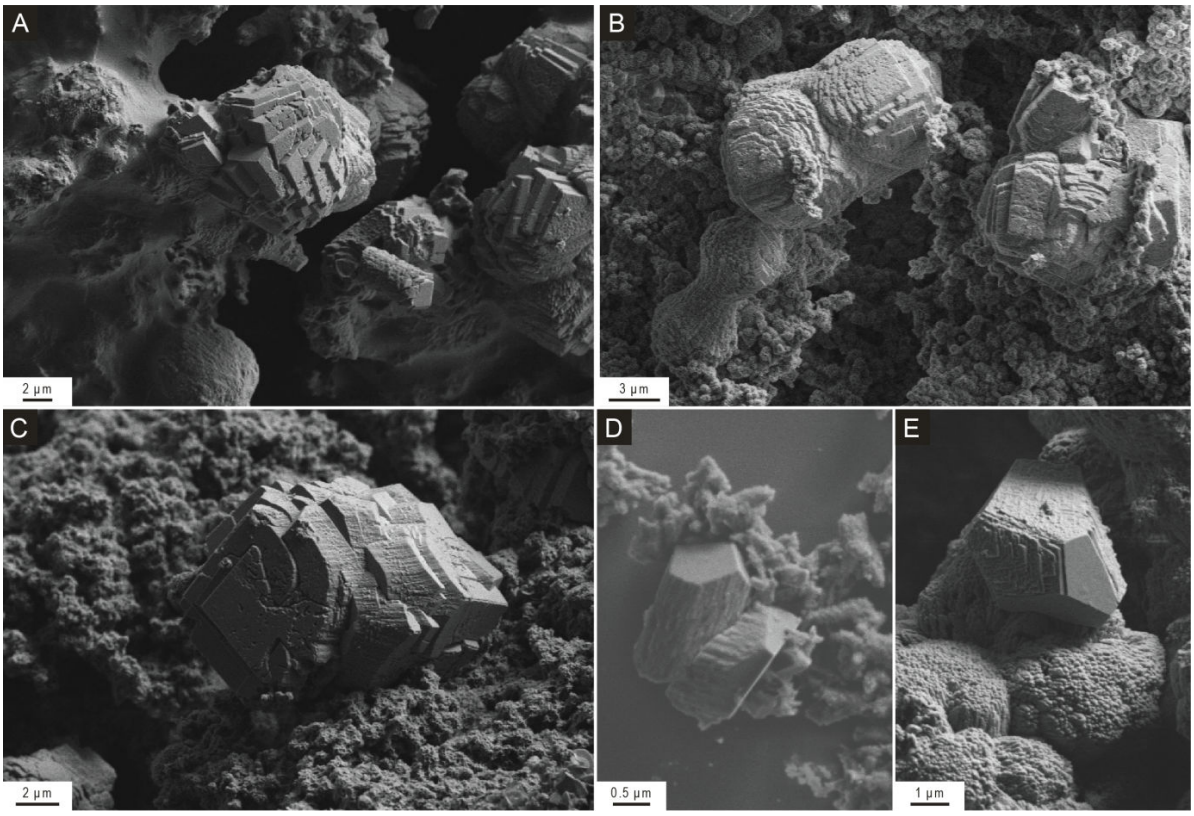

Figure 2.5 *SE images of representative examples of rhombohedral crystals produced by: A, B) slippery dick; C) bluehead wrasse; D) black grouper; and E) redtail parrotfish. In many examples produced by slippery dick, bluehead wrasse, and beaugregory, rhombohedra have step-like structures (A, B, C) and tend towards dumbbell-shaped (B; centre and left) and equant, sub-spherical (B; right) particles. Rhombohedra produced by these three species are typically associated with a magnesium carbonate 'matrix' that can be amorphous in appearance (A; left) and/or consist of nanospheres with a mesh-like structure (B, C; also Fig. 2.6 C). Rhombohedral crystals produced by other species are typically smaller and of different structure, which varies according to species (D, E).*

2.3.1.5 Rods and needles

Rod-shaped crystals are commonly produced by many species. Samples in which monocrystalline ellipsoids are the dominant form often also comprise monocrystalline rods. These are typically

slightly longer than ellipsoids, having an average length of >1 μm. Most examples are straight-sided with flat terminations, or at least are blunt relative to the pointed terminations of ellipsoids. Occasionally terminations also appear frayed, indicating that some rods are partially fibrous. Indeed, such crystals produced by black grouper appear to show a succession of developmental stages, where rods with flat or blunt terminations develop into those with fibrous and frayed tips, which in turn begin to splay to form possible precursors to dumbbell-like forms.

In most other cases where the term 'rod' could be applied as a descriptor on the basis of straight-sided morphology, particles are polycrystalline, being similar in size and texture to polycrystalline dumbbells. They are therefore considered end-members of the range of polycrystalline dumbbells, that is, those which exhibit little or no splay away from the long axis. A rod- or needle-like form of rather different character is occasionally excreted by redtail parrotfish and is also occasionally observed in samples from bluehead wrasse. Needles occur in the range 2–10 μm in length and are straight-sided (Fig. 2.4 H). The long faces differ from those of the rods described above by being of strong crystal habit. Rather frayed terminations are a manifestation of individual needles comprising several blade-like crystals. Needles and their component crystals are similar to the individual crystals that comprise spherulites. Indeed, in pellets excreted by redtail parrotfish needles and spherulites commonly occur in close proximity to one another. In many cases needles are intergrown in a manner reminiscent of spherulites, but are far less densely packed, usually with no more than three intersecting particles.

2.3.1.6 Platy and 'amorphous' material

In addition to the common crystal morphologies described above, all of which are Mg calcite or aragonite (see following section), samples from many species also comprise a magnesium carbonate phase. Typically this is a minor phase, occurring rarely and with rather sporadic distribution. In most cases it occurs as clusters of platy crystals (up to 2 μm in length) that interlock to form rosette-like structures on pellet surfaces (Fig. 2.6 A). However, in samples produced by red lionfish, what is presumably a similar phase is more extensive and forms a pervasive mesh-like

coating that covers nearly all of the dominant Mg calcite ellipsoids (Fig. 2.6 B). In addition, platy crystals can form clusters of discrete 'nano-rosettes' (Fig. 2.6 C).

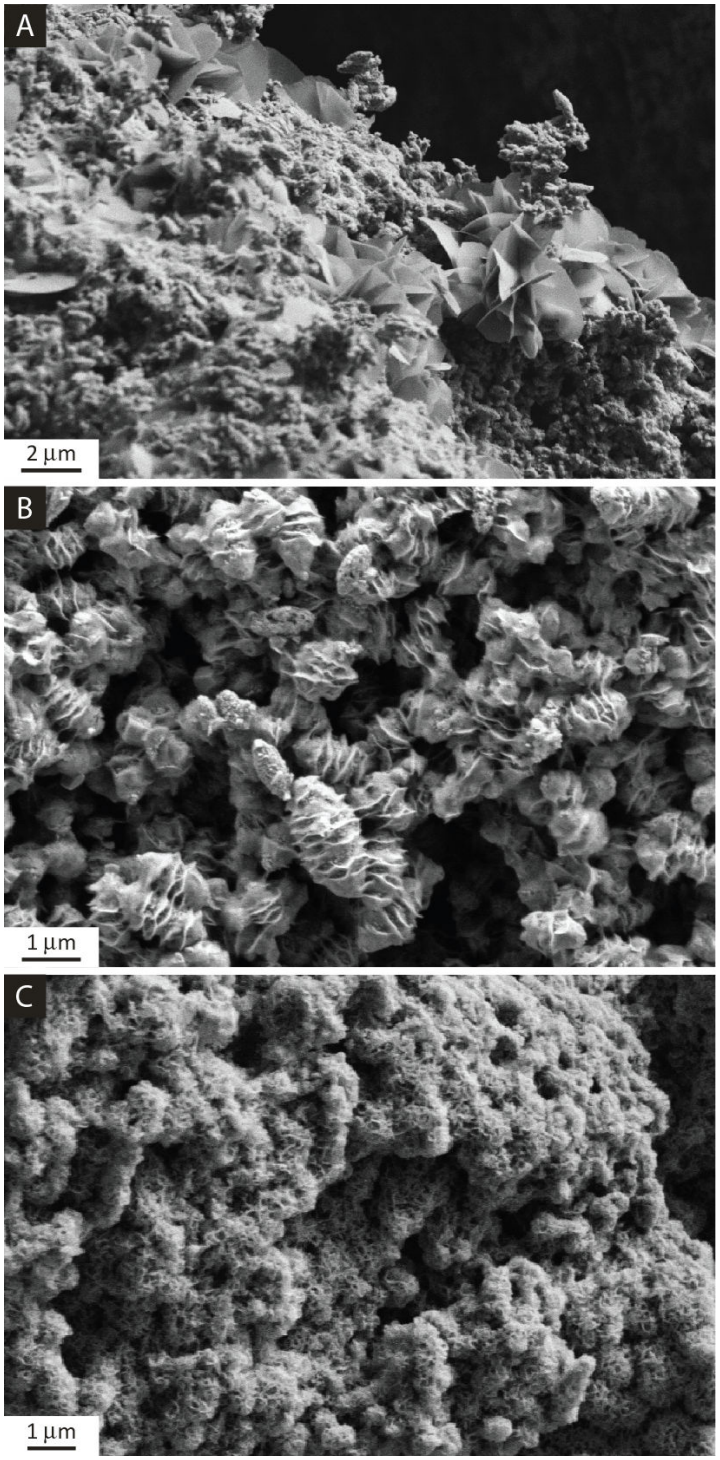

Figure 2.6 *SE images of various forms of platy magnesium carbonate. A) Micron-scale plates occasionally form localised rosette-like structures on pellet surfaces (shown on pellet produced by black grouper). B) Mesh-like coatings covering dominant Mg calcite particles are rare in samples produced by most species, but pervasive in those produced by red lionfish. C) Nanospheres comprising submicron mesh-like structure are common products from some species (shown in pellet produced by beaugregory).*

In samples produced by bluehead wrasse, slippery dick, and beaugregory, magnesium carbonate represents the major phase (Fig. 2.8). In these species it assumes three morphological forms: nanoscale plates that form extensive 'meshworks'; nanospheres or rosettes that comprise nanometer-scale plates (Fig. 2.6 C); and a solid phase that lacks any clearly definable form (Fig. 2.5 A) and commonly exhibits desiccation cracks.

2.3.2 Mineralogy and chemical composition

2.3.2.1 X-ray diffraction (XRD)

X-ray diffraction (XRD) patterns indicate that for carbonates excreted by each of 10 fish species (this study and Perry *et al*., 2011) the dominant mineral phase is Mg calcite. This is based on them having lattice structures in the R-3c space group, with diffraction peaks close to those of pure calcite (Fig. 2.7 and Appendix I, Figs. AI 3–5). The d_{104} diffraction peak is also consistently shifted to values greater than 29.4 °2θ, further indicating Mg calcite as the dominant mineral phase. Estimates of $MgCO_3$ content based on d_{104} values are shown in Table 2.1. Given that the degree of lattice disorder in fish-derived crystals is unknown, values based on the curves for ordered (Goldsmith *et al*., 1961; Bischoff *et al*., 1983) and disordered (Zhang *et al*., 2010) Mg calcites are used here to interpret $MgCO_3$ contents >20 mol%. These indicate that the $MgCO_3$ component of fish-derived Mg calcite varies with fish species and ranges from 5.1 to 43.2 mol%. However, SEM observations indicate that the majority of individual fish-derived crystals are <2 μm in length, while EDX results (see below) indicate there is substantial compositional heterogeneity in carbonates from most species. This may explain the reasonably broad diffraction peaks (Fig. 2.7) typical of fish-derived carbonates, although this could also reflect the fact that these carbonates are of a reasonably low degree of crystallinity. In either case, broad peaks introduce potential errors in estimations of $MgCO_3$ contents (Bischoff *et al*., 1983). Combined with problems of estimating $MgCO_3$ content at >20 mol% and the unknown influence of trace elements, these potential errors mean that crystal chemistry based on diffraction peak positions should be taken as semi-quantitative estimates of $MgCO_3$ content.

The presence of small amounts of aragonite in samples from some species is indicated by small diffraction peaks at 26.3 and 27.3 °2θ (Fig. 2.7; Appendix I, Figs. AI 3–5). Measurements of peak integrals indicate that the aragonite component varies in abundance from 0 to approximately 27 wt.% (Table 2.2), with the smallest quantities occurring in samples dominated by monocrystalline ellipsoids and the largest quantities in samples dominated by dumbbells and spheres. The form of aragonite crystals in these samples is not known, but given this pattern of occurrence it appears likely they are associated with spheres and dumbbells.

Table 2.2 *Relative quantities of aragonite and all forms of calcite in precipitates produced by various fish species. Derived from integrated peak areas of XRD patterns based on the approach of Davies and Hooper (1962).*

Species	Wt.% aragonite	Wt.% calcite + Mg-calcite	Dominant crystal morphology
Schoolmaster snapper	8	92	Monocrystalline ellipsoids
Yellowtail snapper	6	94	Monocrystalline ellipsoids
Graysby grouper	4	96	Monocrystalline ellipsoids
Black grouper	0	100	Monocrystalline ellipsoids
Nassau grouper	0	100	Monocrystalline ellipsoids
Yellowfin mojarra	10	90	Monocrystalline ellipsoids + dumbbells + spheres
Bonefish	20	80	Spheres + nanospheres
Checkered puffer	12	88	Spheres + polycrystalline ellipsoids
Great barracuda	27	73	Small dumbbells + nanospheres + spheres + dumbbells
Bluehead wrasse	7	93	Rhombohedra + 'amorphous' material

Aragonite is the main subsidiary crystalline phase detected, but additional diffraction peaks generated by some samples possibly indicate the presence of small quantities of other phases. In samples produced by bonefish and checkered puffer, small peaks at 20.55 and 41.69 ° 2θ (Fig. 2.7) are in good agreement with peaks generated by monohydrocalcite, although confirmation of this is difficult because other characteristic peaks for this phase overlap with those of calcite and are thus obscured. 'Amorphous' and/or nano-scale platy material that dominates pellets excreted by bluehead wrasse appears to be a form of magnesium carbonate (see EDX results below). However, the positions of X-ray diffraction peaks produced by these samples indicate only the presence of Mg calcite (~5 mol% $MgCO_3$), presumably referring to rhombohedral crystalline material. The absence of peaks indicative of any other phases suggests that the magnesium carbonate component

does not produce a diffraction pattern and is thus a truly amorphous phase. It is also worth pointing out that nanospheres produced by several species (*e.g.*, great barracuda and bonefish) closely resemble the morphology of amorphous calcium carbonate described in various other studies (Brečević and Nielsen, 1989; Foran *et al*., 2013). Because these forms typically occur alongside other morphotypes, the generation of diffraction patterns by these samples does not rule out the possibility that nanospheres are amorphous carbonates.

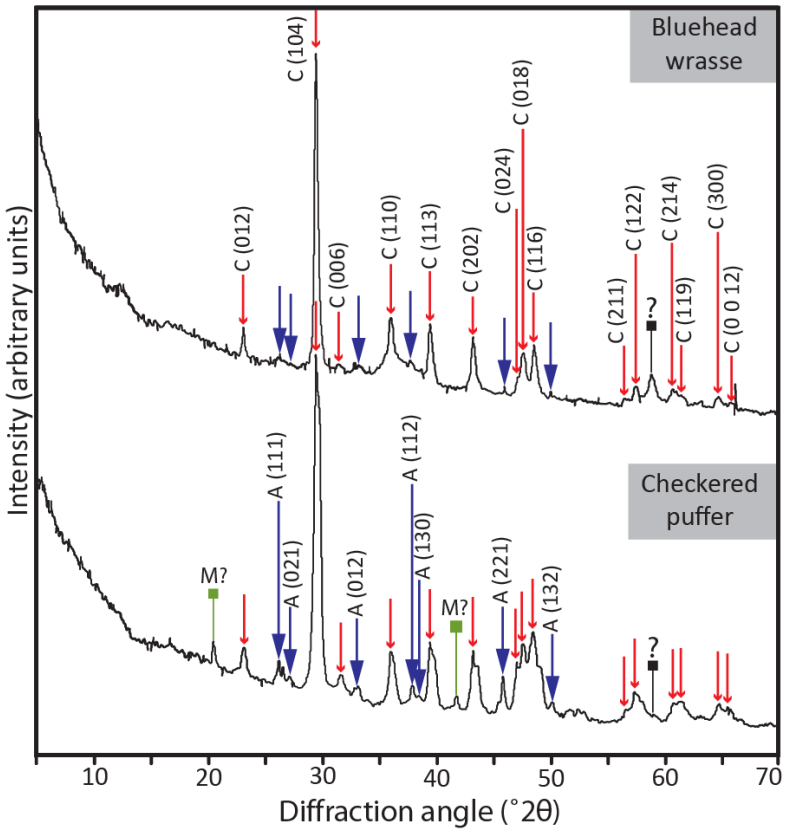

Figure 2.7 *X-ray diffraction patterns of carbonates produced by bluehead wrasse and checkered puffer. Large arrowheads (blue) indicate aragonite (A) peaks; small arrowheads (red) indicate Mg calcite (C) peaks. Note the broad* $d_{(104)}$ *peak for crystals produced by checkered puffer relative to that for crystals produced by bluehead wrasse, probably indicating the presence of crystals with a broad range of* $MgCO_3$ *contents. Small peaks at 20.55 and 41.69 °2θ (generated by the excreted products of checkered puffer; green squares) are in close agreement with peak positions for monohydrocalcite. An additional peak that appears on both spectra at 58 °2θ (black squares) is not assigned.*

2.3.2.2 Energy-dispersive X-ray spectrometry (EDX)

$MgCO_3$ contents based on EDX analyses are generally in close agreement with estimates based on XRD analyses, thus confirming that magnesium detected by EDX is incorporated within the crystal

lattice rather than being adsorbed or occluded at crystal surfaces. This analytical technique allows crystal chemistry to be determined on a crystal-by-crystal basis, thus addressing some of the issues apparent in XRD analysis. Mean values of mol% $MgCO_3$ for carbonate samples excreted by 21 fish species, based on 50+ individual EDX analyses per species, are shown in Table 2.1 (see Appendix II for full data set). Carbonates excreted by 13 out of 21 species have high magnesium contents, falling within the range detailed by Perry *et al*. (2011) of 18–39 mol% $MgCO_3$. However, eight species are found to excrete carbonates with lower $MgCO_3$ contents, seven of which produce carbonates with a markedly different morphology and chemical composition (the carbonate products of keeltail needlefish, which have only slightly lower $MgCO_3$ contents than those previously reported for fish-derived carbonates, are morphologically similar).

Four species (checkered puffer, redtail parrotfish, grey angelfish, and scrawled cowfish) produce carbonates with $MgCO_3$ contents that are consistent with LMC; typical values being in the range 1 to 5 mol%. Each of these species produces a wide range of crystal forms. In any given sample the Mg content may vary by a few mol% from one crystal to the next, but there is no relationship between crystal morphology and $MgCO_3$ content. However, it is noteworthy that some polycrystalline fibrous dumbbells produced by checkered puffer have higher $MgCO_3$ contents (up to 14 mol%), which may explain the presence of a shoulder on the d_{104} XRD peak for samples produced by this species, the position of which corresponds to a $MgCO_3$ content of 17 mol%.

The products of three other species (bluehead wrasse, slippery dick, and beaugregory) differ greatly from those of the majority of species both in texture (see previous section) and in composition. The rhombohedral crystalline forms produced by these species typically have relatively low $MgCO_3$ contents (averaging approximately 5 mol%, but in the range 2–17 mol%) that are consistent with LMC and are in good agreement with XRD data (Fig. 2.7). In contrast, the dominant amorphous or mesh-like ‘matrix’ phase has little or no calcium and appears to be a magnesium carbonate. These results, combined with XRD data, indicate that this is probably an amorphous form of magnesite or, given that EDX analyses are not capable of detecting the presence of hydrogen, any one of

numerous hydrated magnesium carbonate and/or hydroxide phases (*e.g.*, hydromagnesite, dypingite, nesquehonite). This phase is readily apparent in backscatter electron (BSE) images as a much darker phase than the associated Mg calcite crystals (Fig. 2.8). BSE imaging also reveals the limited presence of a similar phase in some samples produced by other species, such as keeltail needlefish, in which Mg calcite monocrystalline ellipsoids represent the dominant phase.

Larger-scale platy and rosette-like phases observed as a subsidiary form in carbonates produced by many species (Fig. 2.6) have a similar Mg-rich composition. The texture and composition of the latter is similar to some forms of nesquehonite ($MgCO_3 \cdot 3H_2O$) (Kloprogge *et al*., 2003) and dypingite ($Mg_5(CO_3)_4(OH)_2 \cdot 5H_2O$) (Power *et al*., 2007). The former occurs naturally as an evaporative mineral (Kloprogge *et al*., 2003), and can form abiotically in highly alkaline environments enriched in magnesium, such as the hydromagnesite playas of the Cariboo Plateau, British Columbia, Canada (Power *et al*., 2007). The occurrence of dypingite is less well-documented but it has been shown to be associated with microbial activity in similar settings (Power *et al*., 2007).

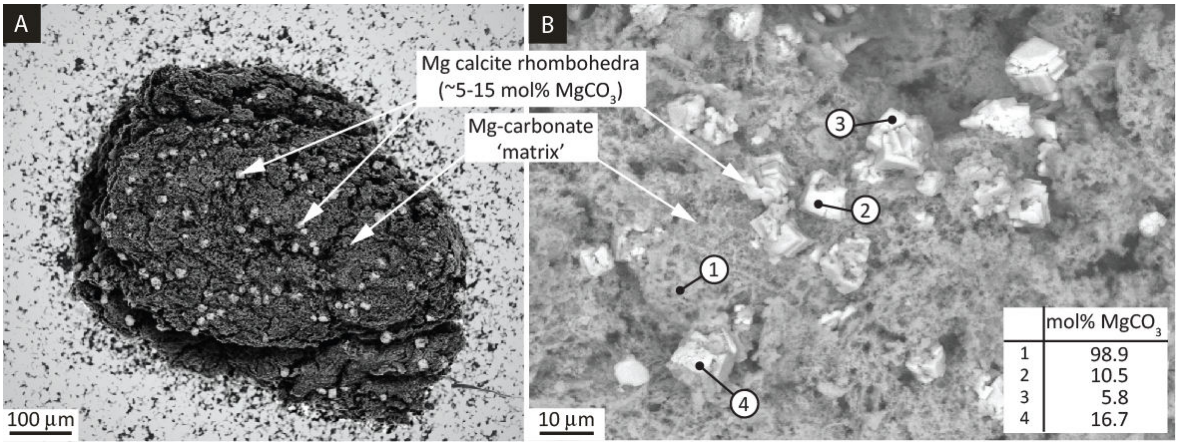

Figure 2.8 *Backscatter electron images of carbonate pellets produced by: A) beaugregory; and B) bluehead wrasse. Pale areas represent Mg calcite crystals; dark areas represent 'amorphous' and platy Mg-carbonates. Mg calcite crystals are typically uniformly distributed throughout the Mg-carbonate 'matrix' (A). Note the corresponding $MgCO_3$ contents, measured by EDX analysis (B).*

The findings of the present study also indicate that $MgCO_3$ content of Mg calcite phases can actually vary more widely within samples from individual species than originally reported (Perry *et*

al., 2011). For example, the carbonate products of yellowfin mojarra are dominated by monocrystalline ellipsoids that have a mean $MgCO_3$ content of 21.1 mol%. Subsidiary products occurring alongside these include larger (~4–20 μm) polycrystalline dumbbells and spheres that have consistently lower $MgCO_3$ contents (mean 5.5 mol%). Similarly, the products of keeltail needlefish are dominated by small (~1–2 μm) ellipsoids, rods and dumbbells with a mean value of 13.2 mol% $MgCO_3$, but also comprise larger (~5–20 μm) dumbbells and spheres with an average of 2.5 mol% $MgCO_3$. Thus for $MgCO_3$ values to be truly representative it is more appropriate to present them as mean values per crystal form for each species (Table 2.1).

In addition to variations according to species and crystal form, $MgCO_3$ content appears, in some samples, also to vary among pellets that share a common dominant morphology and are excreted by the same species. For example, monocrystalline ellipsoids produced by schoolmaster snapper have an overall mean $MgCO_3$ content of 34.2 mol% (n = 62 crystals, 7 pellets), but mean values for individual pellets range from 20.8–43.2 mol%. Samples produced by this species were collected from tanks holding several fish specimens, and it could therefore be the case that the $MgCO_3$ component of crystals varies with individual fish. Indeed, a separate group of schoolmaster snapper (comprising only the smallest individual fish of this species) produced HMC crystals with an overall mean $MgCO_3$ content of only 22.1 mol%. Several species show similar variations, usually to a lesser extent, among pellets, but many species produce pellets in which $MgCO_3$ content is reasonably consistent. For example, mean values range from 17.5–21.5 mol% (n=50 crystals, 5 pellets) in *Eucinostomus* sp.

A crude quantification of trace elements by EDX analysis reveals characteristic trace element signatures in some crystal forms. Strontium, phosphorus, and sulphur are frequently detected in varying concentrations in fish-derived carbonates. These elements may be present due to: i) substitution of cations (Sr^{2+}) or anions (SO_4^{2-}, PO_4^{3-}); ii) adsorption on crystal surfaces; or iii) presence as inclusions of either other mineral phases (*e.g.*, strontianite), fluids, or residual organic matter (Ishikawa and Ichikuni, 1981; Pingitore *et al*., 1992; Mekuchi *et al*., 2010). Despite

theoretical considerations to the contrary, the incorporation of strontium in the calcite crystal lattice as a substituent of Ca^{2+} is a common occurrence (Carpenter and Lohmann, 1992; Pingitore *et al*., 1992); concentration increasing with $MgCO_3$ content in Mg calcite (Mucci and Morse, 1983). It is therefore assumed that Sr^{2+} in fish-derived carbonates is incorporated in the crystal lattice, and it is reported here as mol% $SrCO_3$. The mode of occurrence of phosphorus and sulphur is unknown and they are reported as atomic percentages.

Strontium was measured in various crystal forms produced by numerous species and detected values were found to range from 0.00 to 1.75 mol% $SrCO_3$. When these values are plotted by crystal form against $MgCO_3$ content (Fig. 2.9), two distinct groups are revealed. In one of these, $SrCO_3$ in monocrystalline ellipsoids, small dumbbells, and some larger dumbbells and spheres increases linearly with $MgCO_3$ in a similar manner to that documented for the incorporation of strontium in calcite (Morse and Mackenzie, 1990; Carpenter and Lohmann, 1992), never exceeding 1 mol% and with mean values of approximately 0.3 mol% at 10 mol% $MgCO_3$ and 0.6 mol% at 30 mol% $MgCO_3$. In contrast, the other group, which comprises needle-like forms and some polycrystalline dumbbells and spheres, is characterised by low $MgCO_3$ contents (typically <5 mol%) and variable, but in many cases reasonably high (up to 1.75 mol%) $SrCO_3$ contents. These data lend further support to XRD data that suggest aragonite is present in fish-derived carbonates as needle-like forms and polycrystalline spheres and dumbbells, although the latter two morphotypes can also occur as Mg calcite. In terms of weight percent strontium, typical values for needles and spheres produced by redtail parrotfish are in the range 0.6 to 0.9 wt%, whereas values for monocrystalline ellipsoids produced by black grouper are typically lower than 0.5 wt%. These values are in good agreement with data for marine biogenic aragonite and calcite, respectively (Veizer, 1983).

It is also worth pointing out that, whereas $MgCO_3$ contents of most needle-like forms are lower than 2.5 mol%, $MgCO_3$ content in strontium-rich spheres and dumbbells is commonly between 2 and 5 mol%. These values are high compared to many common marine sedimentary carbonates

(*e.g.*, Speer, 1983), and may reflect: i) preferential surface adsorption of magnesium compared to that in needles; ii) the presence of both aragonite and Mg calcite in these morphotypes; or iii) the partial incorporation of signals generated by adjacent Mg calcite crystals (these morphotypes are commonly associated with Mg calcite ellipsoids, whereas needle-like forms tend not to be).

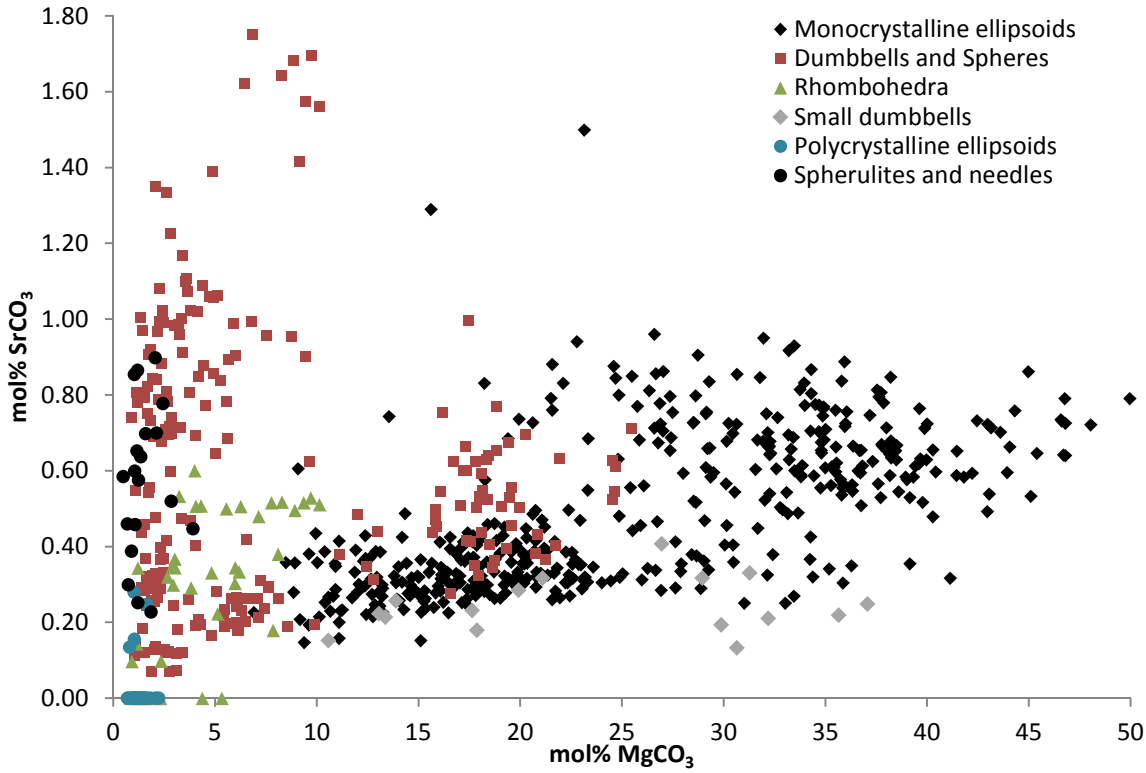

Figure 2.9 *Mol% values for strontium plotted against magnesium for various crystal forms. The linear increase of $SrCO_3$ with $MgCO_3$ in ellipsoids and some spheres and dumbbells is in good agreement with data for Mg calcite from other studies. However, the highest $SrCO_3$ contents correspond with low $MgCO_3$ contents. These data are not typical for Mg calcite but are in good agreement with existing data for aragonite. Thus it appears that needles-like forms, and some polycrystalline dumbbells and spheres, are at least partly aragonitic.*

Phosphorus contents in most crystal forms produced by most fish species are very low, with typical atomic % values in the range 0.08 to 0.19. Expressed as a ratio of phosphorus to cations, or P/(Mg + Ca), this yields typical values in the range 0.003 to 0.008. Two notable exceptions are to be found in the precipitation products of great barracuda and bonefish. In the former, most crystal forms have phosphorus contents similar to those described above, but nanospheres, which dominate some pellets, have consistently elevated concentrations, with an average atomic % of 5.80, and average phosphorus to cation ratio of 0.274. Nanospheres produced by bonefish also have elevated

phosphorus concentrations, albeit to a lesser degree than those produced by great barracuda (average atomic % is 0.30 in one sample and 2.80 in another; corresponding phosphorus to cation ratios being 0.016 and 0.093, respectively). Interestingly, spheres produced by bonefish also appear to have slightly elevated phosphorus concentrations (average atomic % is 0.32, and average phosphorus to cation ratio is 0.013), although it is difficult to rule out the possibility that these results are not due to phosphorus-rich nanospheres inside larger spheres.

It is worth pointing out here that, despite being starved for 48 hours prior to sample collection, the phosphorus-rich nanospheres produced by great barracuda were excreted alongside large amounts of skeletal matter from organisms that were presumably ingested prior to capture. This fact may be of some significance with respect to phosphorus concentrations; such high levels of which were not detected in any other samples produced by this species (see Chapter 4 for further details). In contrast, the elevated phosphorus contents of precipitation products excreted by bonefish were consistent in all samples.

Sulphur is present in very small amounts in most crystal forms produced by most species. Typical values are less than 0.05 atomic %, with mean values for each species never exceeding 0.1 atomic %. Amorphous Mg-carbonates and associated Mg calcite rhombohedra produced by bluehead wrasse and beaugregory consistently contained no detectable sulphur.

2.3.2.3 Liquid ion chromatography

Ion chromatography of dissolved carbonate samples produced by selected species reveals the bulk ionic concentrations of calcium and magnesium. Assuming all calcium and magnesium originates from the initial Mg calcite, these data can provide quantification of the bulk $MgCO_3$ mol% for carbonates derived from each fish species. The results, shown in Table 2.1 (and in full in Appendix III), are generally in close agreement with those derived from EDX (for dominant crystal forms) and XRD. Many species excrete HMC and VHMC (typically in the range 14–35 mol% $MgCO_3$), whilst checkered puffer excretes LMC and HMC (in the range 3–10 mol% $MgCO_3$). Of the samples examined using this technique, only those produced by bluehead wrasse, beaugregory, and

some produced by great barracuda and keeltail needlefish have magnesium contents significantly higher than the $MgCO_3$ contents indicated by EDX and XRD. This is due to the presence of large amounts of amorphous magnesium carbonate in addition to Mg calcite crystals, and these values are therefore not representative of $MgCO_3$ content in Mg calcite crystals.

As with EDX data, ion chromatography indicates that, whilst the $MgCO_3$ contents of carbonates produced by different individuals of the same species are generally comparable, there is clear variation (of up to 12.5 mol%) between individual fish within species. In addition, where analyses of multiple samples produced by a single fish (or group of fish) were carried out, it is apparent that these can exhibit significant differences (of up to 7.8 mol%) in $MgCO_3$ content. In each case there were no measured fluctuations in seawater temperature or salinity during sampling, and all samples were carefully checked to ensure the absence of foreign particles. Thus the possibility arises that there could be some temporal variation in Mg^{2+} incorporation in crystals produced by some fish specimens. It is possible that such temporal and inter-specimen variations explain some of the discrepancies in measured $MgCO_3$ contents using different techniques (*e.g.*, bonefish; Table 2.1). It should be noted, however, that in many cases where multiple samples collected on different days were analysed, temporal variation in $MgCO_3$ content was limited to 0 to 2 mol%.

2.4 DISCUSSION

2.4.1 Fish-derived carbonates and their classification

By combining morphological and compositional (specifically $MgCO_3$ content) data it is possible to categorise fish species based on the carbonates they produce (Table 2.1). Firstly, all monocrystalline ellipsoids are HMC or VHMC with typical $MgCO_3$ contents in the range 20–35 mol%. Small wheatsheafs and dumbbells typically have similar $MgCO_3$ contents. In samples where crystals of these morphologies represent >99 % of the precipitates, subsidiary forms (larger polycrystalline dumbbells and spheres) in the same samples have consistently lower $MgCO_3$ contents, in the range 3–14 mol%. All species producing carbonates of these descriptions fall into Category I (*i.e.*, black grouper, Nassau grouper, schoolmaster snapper, yellowtail snapper, graysby

grouper, red hind, flounder sp., grunt sp., French grunt, great barracuda, red lionfish). Yellowfin mojarra and keeltail needlefish produce a suite of crystals that are morphologically similar to those of Category I and exhibit comparable compositional relationships (high magnesium content in ellipsoids and small dumbbells versus low magnesium content in larger polycrystalline dumbbells and spheres). However, samples are significantly more heterogeneous. Moreover, ellipsoids and small dumbbells produced by these two species have significantly lower $MgCO_3$ contents (22.1 and 13.2 mol%, respectively) than the equivalent products of most Category I species. Thus yellowfin mojarra and keeltail needlefish are assigned to Sub-category Ia.

Category II consists of checkered puffer, grey angelfish, scrawled cowfish, and redtail parrotfish. Each of these species produces a wide range of crystal morphologies, with the notable absence of monocrystalline ellipsoids. Polycrystalline spheres dominate most samples, while other common products include polycrystalline ellipsoids and dumbbells, rhombohedra, spherulites, and needles. Only the products of these species include forms that appear twisted about the long axis. Compositionally the products of these species differ to those of Category I species in their relatively low magnesium contents. Typically this falls in the range 0.8–7 mol%, with variability apparently being random, and not determined by species and/or crystal morphology.

The three species that constitute Category III are bluehead wrasse, slippery dick, and beaugregory. The two features that define this category are the dominant presence of a magnesium carbonate phase, and the Mg calcite phase being dominated by rhombohedral crystals with relatively low magnesium contents (mean values in the range 5–12 mol%). Other crystal morphologies are occasionally present (polycrystalline dumbbells and spheres, and rare needles), but, as with Category II, monocrystalline ellipsoids are absent. Two species that do not fit any of the above categories are bonefish and *Eucinostomus* sp., both of which predominantly produce polycrystalline spheres and large dumbbells with $MgCO_3$ contents of 19–23 mol%; significantly higher than equivalent products excreted by species in any other category. These species are assigned to Category IV.

2.4.2 Crystal growth mechanisms

Given the diverse range of crystal morphologies produced by fish it is clearly of interest to consider the potential controls on crystal growth and form, as this may provide an insight into why certain species produce different crystal forms. Although rarely described from natural settings, various $CaCO_3$ polymorphs, with morphologies similar to those described here, have been identified as common products in carbonate precipitation experiments (Devery and Ehlmann, 1981; Morse *et al*., 1997; Meldrum and Hyde, 2001; Kralj *et al*., 2004; Rivadeneyra *et al*., 2006; Gayathri *et al*., 2007). Nearly all of the fish-derived carbonates identified in this study are Mg calcites and thus it is clear that the precipitating solutions must contain at least some Mg^{2+}. Where inorganic precipitation is concerned, theoretical considerations invoke that the presence of Mg^{2+} in solution should inhibit the growth of calcite, instead favouring the formation of aragonite (Reddy and Wang, 1980; Falini *et al*., 1994). However, Mg calcites with similar morphologies to fish-derived carbonates have been precipitated inorganically; the inhibition of calcite growth being overridden in solutions with very high degrees of supersaturation, and by varying factors such as the concentrations of various impurities (Sr^{2+}, SO_4^{2-} etc.), and the availability of CO_3^{2-} (Sawada *et al*., 1990; Fernández-Díaz *et al*., 1996; Kralj *et al*., 2004). It is worth pointing out that the inorganic chemistry of intestinal fluid in marine bony fish is very different to that of the seawater they ingest. In particular the processing of ingested fluid a) reduces the salinity to about one third of oceanic seawater, b) reduces [Ca^{2+}] from 10 mM in seawater to about 2 to 5 mM due to continual precipitation, c) accumulates [Mg^{2+}] from 52 mM in seawater to over 200 mM in some cases due to absorption of water into the blood without parallel removal of Mg^{2+} ions, and d) creates supersaturated conditions as a result of alkaline pH (8.3–9.2) combined with very high alkalinity (from 30 to over 100 mM) as a result of substantial HCO_3^- secretion (Marshall and Grosell, 2005; Wilson *et al*., 1996; 2002; 2009).

While it is possible that fish-derived carbonates are products of inorganic precipitation in a biologically facilitated environment (*i.e.*, within the fish), it is difficult to envisage precipitation

taking place in the intestine without at least some organic influence. Indeed, the majority of precipitation experiments that result in ellipsoidal, dumbbell-shaped, and spherical carbonate particles (comparable to those identified here) have involved the presence of various organic compounds or microbial strains, which are considered to be important controlling factors (Buczynski and Chafetz, 1991; Meldrum and Hyde, 2001; Rivadeneyra *et al*., 2006; Sánchez-Román *et al*., 2007; González-Muñoz *et al*., 2008). The presence of organic additives in a precipitating solution alongside Mg^{2+} has also been shown to suppress aragonite growth and facilitate precipitation of Mg calcite (Meldrum and Hyde, 2001). Furthermore, Meldrum and Hyde (2001) show that when Mg^{2+} and organic additives are combined in the precipitating solution, Mg calcite crystals can exhibit curved or roughened crystal faces and form polycrystalline aggregates. The resultant particle morphologies can be very similar to those observed herein to be produced by fish and it is thus possible that similar factors are important controls on crystal morphology in both systems. The development of polycrystalline aggregates can be a result of calcite growth inhibition (Prieto *et al*., 1994), perhaps caused by high Mg^{2+} concentrations (Kralj *et al*., 2004), leading to the binding of sub-critical nuclei in order to facilitate continued growth. This process, which results in the growth of multiple aggregated crystals, may be enhanced by the presence of organic compounds, and possibly also by high pH levels (Van der Leeden and Van Rosmalen, 1987), the latter being characteristic of marine teleost intestinal fluids (Wilson *et al*., 1996; 2002).

Carbonates produced in precipitation experiments where calcification is bacterially-mediated (Rivadeneyra *et al*., 2006), as well as those formed in nature in marine algal tidal flats in Baffin Bay, Texas, and in organic-rich inland lakes on San Salvador, the Bahamas (Buczynski and Chafetz, 1991) can bear a striking resemblance to many fish-derived carbonates. It is thus tempting to invoke a major role for intestinal bacteria in the formation of fish-derived carbonates. Indeed, many crystal morphologies described herein (particularly nanospheres, ellipsoids, and twisted) are reminiscent of coccoid, bacillus, and spiriform bacteria, respectively, and it is possible that individual bacteria create microenvironments conducive to carbonate precipitation, within which they eventually became encased; a mechanism initially suggested by Greenfield (1963), and later

by Chafetz and Folk (1984). Such a process would go some way to explaining why some of the fish-derived carbonates appear to be hollow (*e.g.*, Figs. 2.2 D and 2.4 G); encased bacteria having decomposed to leave a void in the crystal.

The large body of literature concerning $CaCO_3$ precipitation experiments considers various organic and inorganic influences on carbonate crystal growth and indicates that any of the above-mentioned factors, in various combinations, can result in mineralogies and crystal morphologies similar to those excreted by fish. A further consideration is that of the partitioning of varying amounts of trace elements (*e.g.*, Mg^{2+}, Sr^{2+}). In solutions where the precipitation of Mg calcite is favoured over aragonite, the amount of Mg^{2+} incorporated in the calcite crystal lattice increases with the Mg^{2+}/Ca^{2+} ratio of the precipitating solution (Mackenzie *et al*., 1983; Meldrum and Hyde, 2001), and is independent of reaction rate (Mucci and Morse, 1983; Mucci *et al*., 1985). The Mg^{2+}/Ca^{2+} ratio in the intestinal fluid of marine fish is much higher than in ambient seawater (*e.g.*, as indicated above, this can be >100 instead of ~5) and this also varies depending on species due to different rates of absorption of water, Ca^{2+}, and Mg^{2+} as well as different rates of secretion of HCO_3^- ions (Marshall and Grosell, 2005). This variability of gut fluid chemistry between species could explain why, for example, Category II crystals typically have much lower $MgCO_3$ contents than Category I crystals. It may also be the case that such factors exert some influence on crystal morphology. Indeed, nearly all monocrystalline ellipsoids are VHMC, suggesting that crystals with this morphology might only form in solutions with high Mg^{2+}/Ca^{2+} ratios. However, the fact that individual carbonate pellets are often compositionally heterogeneous indicates that either: i) Mg calcite crystals of various compositions can precipitate out of a single solution, suggesting that factors other than Mg^{2+}/Ca^{2+} ratio must also influence magnesium uptake; or ii) there exist highly localised variations in precipitating conditions.

Clearly the controls on morphological and compositional development in Mg calcite are complex, and it appears that a crystal with any specified morphology and composition can be derived via several pathways. However, with regard to carbonate precipitation in fish, it is reasonable to

speculate that important drivers in the development of various crystal forms may include: i) the presence of various organic components (mucus, microbial communities, organic compounds associated with digestion); ii) high degrees of supersaturation; iii) precipitating solutions with unique (in nature) ionic concentrations, that are species-dependent; iv) metabolic rates and associated rates of HCO_3^- secretion in the intestine; and v) high pH levels within the intestine. Preliminary observations in the present study indicate that fish body mass and functional group (and diet) may not be significant controls on crystallisation. For example, numerous species sampled in this study produced morphologically and chemically uniform crystals across a large body mass range (*e.g.*, yellowtail snapper: 13.5–946 grams), whilst macroinvertivores are included in all identified categories of crystal form. However, it is not possible to completely rule out body mass as a factor, and it is interesting that all fish specimens that produced Category III precipitates had a body mass of <13 grams (smaller than nearly all specimens of other species). Thus Category III precipitates could be species-controlled, but it may also be possible that they are a product unique to very small fish (*i.e.*, body mass-controlled). Further work to determine the factors influencing crystal growth and form in different fish species is on-going and the nature of these interacting controls will be discussed elsewhere.

2.4.3 Crystal growth sequences

Perry *et al*. (2011) speculated that the range of crystal morphologies observed in their study could belong to a morphogenetic sequence, with a general succession of ellipsoid to splayed ellipsoid to dumbbell to sphere. Further observations in the present study lend support to this, and a modified model of crystal development is proposed that could account for various additional crystal morphologies (Fig. 2.10).

In samples produced by many species the starting point for crystal development appears to be monocrystalline ellipsoids, typically being the smallest crystal form in samples containing multiple morphologies. That many samples are dominated by monocrystalline ellipsoids suggests that continuation of crystal development from this form is suppressed. Indeed, several authors consider

ellipsoidal carbonate forms precipitated experimentally to be the result of growth inhibition by the surface adsorption of organic additives (Rodríguez-Clemente and Gómez-Morales, 1996). High magnesium contents in these crystals are another possible factor inhibiting crystal growth. It is interesting in this respect that yellowfin mojarra and keeltail needlefish, both of which produce ellipsoids with relatively low magnesium contents, produce a much greater variety of crystal forms than other ellipsoid-producing species. It is possible that with lower magnesium contents crystal development is inhibited to a lesser degree, and a wider range of crystal forms is subsequently produced.

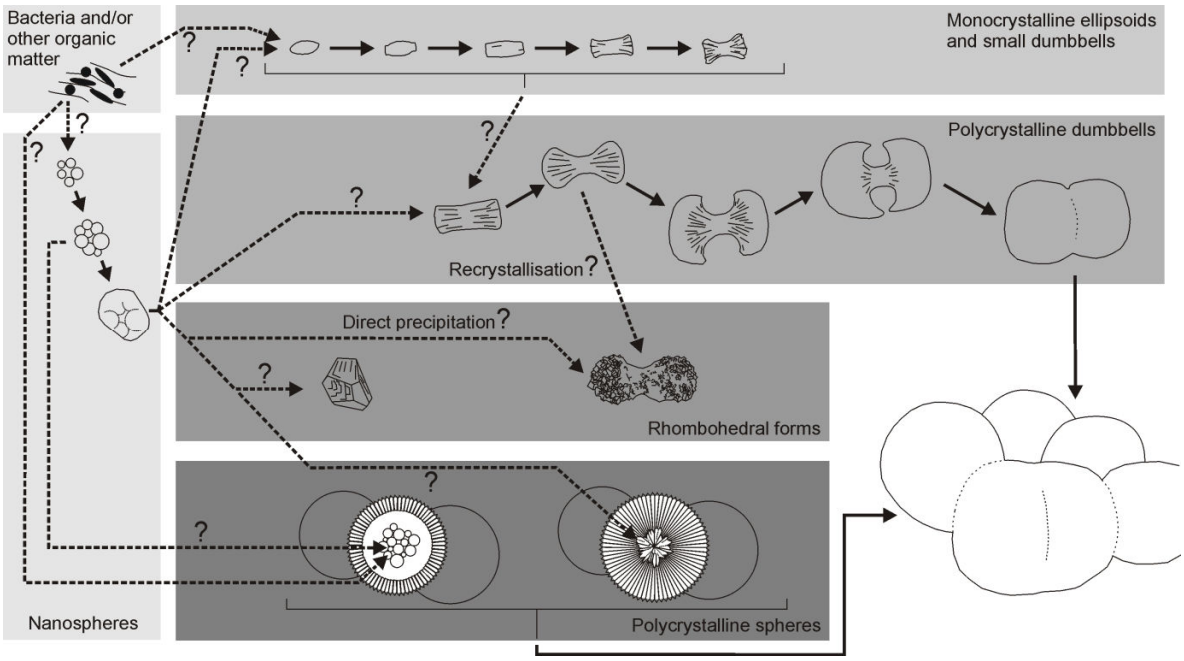

Figure 2.10 *Schematic diagram showing possible morphogenetic sequences in fish-derived carbonates (dashed arrows represent inferred relationships; solid arrows indicate possible relationships as directly evidenced by SEM images).*

Evidence in samples from some species (such as black grouper and keeltail needlefish) indicates that as crystal growth progresses ellipsoids begin to develop straighter edges, with pointed terminations gradually becoming increasingly blunt and eventually beginning to splay, ultimately forming small dumbbells. In this succession of crystal forms the average magnesium content remains unchanged. A similar sequence is observed in larger polycrystalline forms, with dumbbells eventually growing back on themselves to form spherical morphologies. These larger forms typically have significantly lower magnesium contents than ellipsoids in the same samples. There is

little morphological evidence to suggest a link between smaller forms and larger dumbbell forms, but if this is the case presumably it must be accompanied by a change in precipitating conditions and/or crystal growth mechanism that causes decreased uptake of magnesium. Ultimately polycrystalline spheres derived from dumbbells coalesce to form multi-lobate structures that are similar in outward appearance to truly spherical forms (*i.e.*, those produced by bonefish, checkered puffer and scrawled cowfish).

Despite similarities in final appearance, there is no evidence to suggest that polycrystalline spheres belong to the same growth sequence as dumbbells and it is therefore necessary to invoke a separate developmental pathway. Carbonate precipitation taking place within the intestine of the Japanese eel has been shown to involve radially fibrous polycrystalline spheres developed via the aggregation of needles around 'globules' of organic matrix (Humbert *et al*., 1989). Those results also show that spheres eventually begin to coalesce within the organic matrix to form pellets or multi-lobate structures similar to those described here (Fig. 2.4 A). For spheres with partially hollow centres, where fibrous radial growth occurs only at the rim of the sphere (Fig. 2.4 D), it is reasonable to speculate that coalesced nanospheres and/or globules of organic matter (perhaps intestinal mucus, or clumps of bacteria) could have acted as nuclei for needle aggregation.

Rhombohedral forms of calcite are a common result of abiotic precipitation experiments (Devery and Elhmann, 1981; Lopez *et al*., 2009). However, Humbert *et al*. (1989) and Pedley *et al*. (2009) demonstrate that calcite rhombohedra may develop from the coalescence of nanospheres (as discussed previously, a potentially biogenically-mediated morphology). Thus fish-derived rhombohedra could equally be the result of direct precipitation out of the intestinal fluids, or the coalescence of organically-derived carbonates. The process that leads to the formation of dumbbell-shaped aggregations of sub-micron rhombohedra may be similar to that which drives the formation of polycrystalline fibrous dumbbells (*i.e.*, some factor which favours the binding and aggregation of crystallites). However, the possibility also exists that they are the result of very early recrystallisation of polycrystalline fibrous dumbbells. If this is the case then elucidating the timing

of this process is of great importance in order to understand the post-excretion preservation potential, discussed below.

Nanospheres occasionally appear to coalesce to form larger structures (Fig. 2.4 G) and it is reasonable to speculate that they are precursors to some, if not all, crystal growth sequences. Indeed, Pedley *et al*. (2009) invoke a model wherein nanospheres coalesce to form larger crystals with well-defined rhombohedral faces, while Gayathri *et al*. (2007) show that nanosphere-like forms are precursors to monocrystalline ellipsoids. Furthermore, the experimental precipitation work of Gayathri *et al*. (2007) also shows that carbonate crystal morphologies evolve with time through a sequence of ellipsoid to dumbbell to sphere, thus lending further support to the morphogenetic sequences inferred herein.

2.4.4 Relevance of fish-derived carbonates in carbonate muds

The great majority of fish-derived carbonates comprise individual crystals or polycrystalline particles of <4 μm, and typically <2 μm, in length. Polycrystalline spheres and dumbbells are commonly larger, up to 40 μm in diameter, but exposure to brief periods of gentle sonication indicates that these might ultimately break down into their component crystals (<1 μm) in a natural depositional setting. Figure 2.11 shows the grain size distribution of fish-derived carbonates in the context of other major known carbonate mud producers within shallow tropical marine environments, and in the context of a typical carbonate mud fraction from a Bahamian surface sediment sample (Neumann and Land, 1975). The latter shows a rather bimodal grain size distribution, with the majority of material occurring in the 16 to 63 μm and <4 μm fractions.

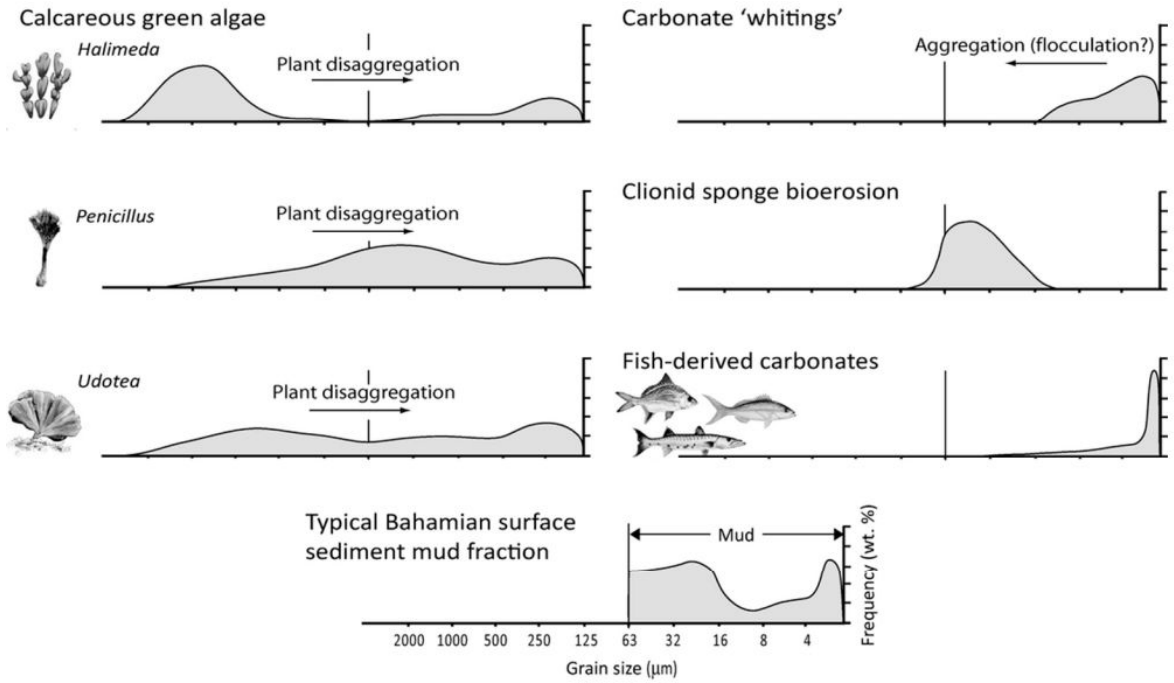

Figure 2.11 *Comparison of fish-derived carbonate grain size distribution against those of other known carbonate mud producers and a typical mud fraction of Bahamian surface sediment. Calcareous green algae and surface sediment data from Neumann and Land (1975); whiting data from Shinn et al. (1989) and Macintyre and Reid (1992); Clionid sponge data from Fütterer (1974).*

Various potential skeletal origins for this very fine carbonate material have been discussed in the literature. For example, the mechanical and biological degradation of larger clasts, such as coral chips resulting from micro-boring by sponges and algae (Fütterer, 1974), and the attrition of skeletal material such as bivalve and gastropod shells (Matthews, 1966), is doubtless responsible for the generation of some material in the <4 µm fraction. In addition, numerous marine organisms that precipitate skeletal carbonates in the form of aggregated anhedral equant nanograins and needles of <10 µm include several species of calcareous green algae (Lowenstam and Epstein, 1957; Loreau, 1982), and the tests of some species of foraminifera (Debenay *et al*., 1999). Upon post-mortem degradation of organic binding material, such organisms can release their individual component crystals to generate significant quantities of carbonate mud grains of <4 µm length (Lowenstam and Epstein, 1957; Stockman *et al*., 1967; Neumann and Land, 1975; Multer, 1988; Debenay *et al*., 1999). Abiotic precipitation of aragonite and Mg calcite needles of <4 µm length in whitings (Shinn *et al*., 1989) also represents a possible source of mud fraction carbonate. The

present study presents clear evidence that an additional and direct pathway for the production of such carbonate is from fish, the vast majority of which is directly precipitated Mg calcite and is <4 μm in size.

Many of the crystal morphologies described herein are not, however, typical of those commonly described in studies of tropical carbonate muds (*e.g.*, Stieglitz, 1972; Gischler and Zingeler, 2002; Gischler *et al*., 2013), although detailed investigations of the morphologies of the very finest size fraction carbonates are not exhaustive. However, Perry *et al*. (2011) document the presence of Mg calcite grains in Bahamian mud samples from a range of depositional settings that are morphologically and compositionally very similar to some of those precipitated within the intestines of marine fish. In light of this, and in the absence of morphologically similar grains originating in other known major mud producers, marine fish are considered a likely contributory source of this material. This is perhaps not unexpected given the high measured production rates (approximately 10–60 g $CaCO_3$ per kg body mass per year, varying according to body mass; Perry *et al*., 2011), coupled with the fact that fish-derived carbonates precipitated and excreted alongside ingested carbonate particles (*i.e.*, as occurs under normal dietary regimes) appear compositionally and morphologically similar to the crystals described herein (*e.g.*, monocrystalline ellipsoids excreted alongside an *Amphiroa* fragment; Fig. 2.2 E). It is therefore likely that marine fish in their natural environments will precipitate and excrete carbonate crystals as described in the present work (but see Chapter 4 for further consideration of carbonates produced during normal feeding).

2.4.5 Post-excretion pathways

A key question arising from the present work relates to the preservation potential of the fish-derived carbonates identified. HMC is typically more soluble in seawater than other $CaCO_3$ polymorphs that commonly occur in marine settings, with numerous studies finding decreasing stability with increasing $MgCO_3$ content (see Chapter 1 for detailed discussion). Mean $MgCO_3$ contents in modern Mg calcite muds are typically in the range 10–13 mol% (*e.g.*, Bosence *et al*., 1985; Reid *et al*., 1992), and it is considered that ~15 mol% represents the upper limit at which Mg

calcite is thermodynamically stable in open shallow marine conditions at ~25 °C (Bertram *et al*., 1991). Indeed, the magnesium contents of many known producers of HMC mud are <15 mol%, with only some species of crustose coralline algae consistently producing Mg calcite with >15 mol% $MgCO_3$ (Fig. 2.12; Chave, 1954).

Fish-derived carbonates documented in the present study clearly exhibit a wide range of $MgCO_3$ contents, with some being very high (*e.g.*, >25 mol%) at the point of excretion (Table 2.1; Fig. 2.12). It is thus reasonable to suppose that a proportion of this material may be relatively unstable in seawater, and therefore subject to processes of recrystallisation and/or dissolution. However, factors that influence Mg calcite solubility are numerous and complex, and solubility where $MgCO_3$ content exceeds ~25 mol% remains poorly constrained (Morse *et al*., 2007); solubility predictions based on $MgCO_3$ content alone are thus not necessarily straightforward. Moreover, the finding here that Mg calcite produced by fish can have substantially lower $MgCO_3$ contents than previously documented (Perry *et al*., 2011; Fig. 2.12), as well as the fact that aragonite can represent a significant proportion of some fish-derived carbonates, suggests that these precipitates are actually likely to occur over a wide range of stabilities, and that different crystal forms may consequently undergo very different post-excretion preservation pathways.

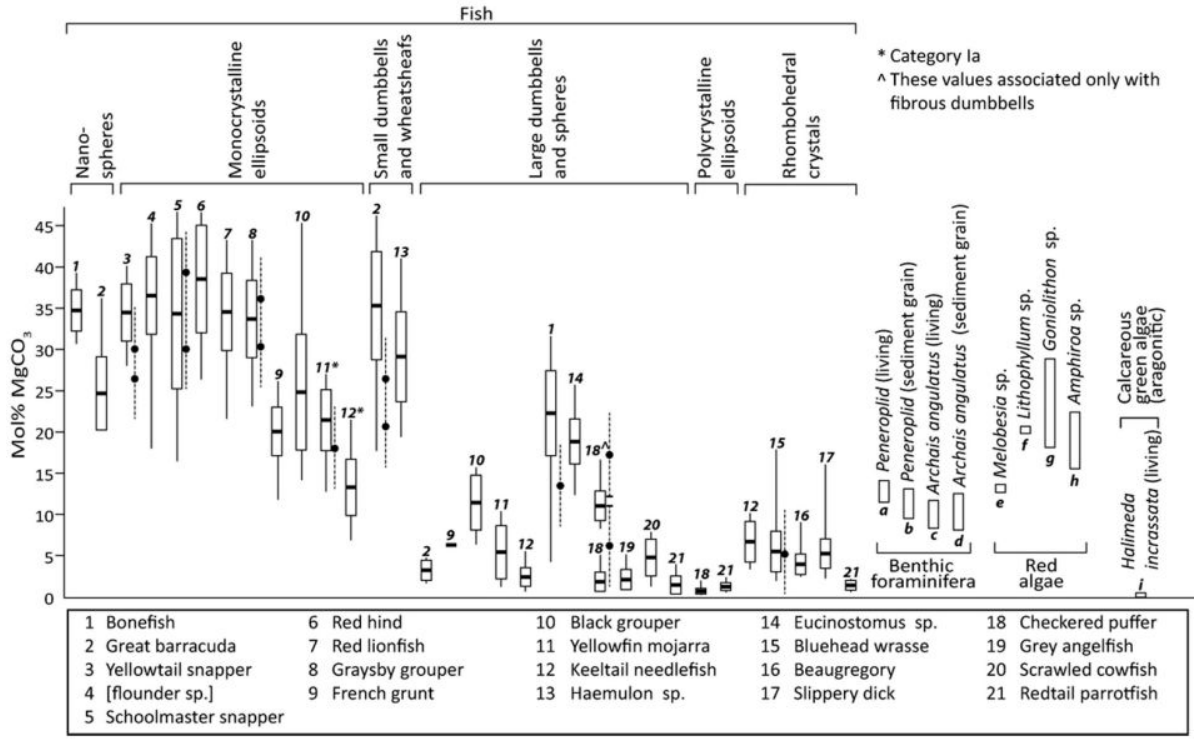

Figure 2.12 *Reported $MgCO_3$ compositional ranges for several known tropical marine carbonate mud producers compared with measured $MgCO_3$ contents of various carbonate crystal forms produced by a range of tropical fish species (this study). Fish data are based on EDX analyses and show mean $MgCO_3$ content per crystal form ± 1 standard deviation (white boxes), and the full range of measured values (solid lines). Where measured, data based on XRD analyses are shown (solid circles; dashed lines represent error of ± 5 mol%) adjacent to EDX data for the dominant crystal form produced by the species. Data on $MgCO_3$ content ranges of other carbonate mud producers based on: a, b – Hover et al. (2001); c – Macintyre and Reid (1998); d – Reid and Macintyre (1998); e – Smith (1972); f – Chave (1954); g – Chave (1954); Walter and Morse (1984); h – Chave (1954); Schmalz (1967); i – Hover et al. (2001).*

Assuming conventional understanding of carbonate stabilities in seawater applies to fish-derived carbonates (Chapter 1), crystals containing <15 mol% $MgCO_3$ (*i.e.*, most large polycrystalline dumbbells and spheres, rhombohedral forms, and polycrystalline ellipsoids) should be reasonably stable in shallow sub-tropical seawater, as should aragonite needles and dumbbells. In contrast, crystals with >15 mol% $MgCO_3$ (*i.e.*, most nanospheres, monocrystalline ellipsoids and small dumbbells) should have greater dissolution potential, as should amorphous carbonate phases (*i.e.*, phases lacking definable form, and possibly nanospheres). However, it is worth drawing attention to the fact that crystal morphologies and compositions described in this study are representative only of fish-derived carbonates collected and processed within 24 hours of excretion. The sustained presence of the mucus envelope and associated microbes may continue to influence crystal development and/or recrystallisation for some time after excretion, and the final form in which

fish-derived carbonates are fully exposed to seawater and/or surface sediment porewater may be different to that described here. Further work is clearly necessary to properly understand the solubility behaviour of fish-derived carbonates and the post-excretion influence of associated organic matter; these themes are considered further in Chapter 7.

2.5 CONCLUSIONS

Marine bony fish are a prolific source of marine carbonate and the results of the present study indicate that marine fish could make important sedimentary contributions to shallow marine carbonate muds. At the point of excretion, these carbonates exhibit a diverse array of crystal morphologies and are typically <4 μm in length. The dominant mineralogy in most fish carbonate samples analysed is high-Mg calcite, but low-Mg calcite and magnesium carbonates (*i.e.*, phases containing <2 mol% $CaCO_3$) represent previously unrecognised major products in samples excreted by some species; the latter probably occurring as an amorphous phase. In addition, aragonite commonly represents a minor phase, but can constitute up to 27 wt% of excreted carbonates in some samples, where it takes the form of euhedral needles as well as polycrystalline spheres and dumbbells. X-ray diffraction evidence also suggests that minor amounts of monohydrocalcite may be present in some samples, while morphological evidence suggests that nanospheres present in the excreted products of some species could be amorphous calcium carbonate.

Many of the crystals described herein are morphologically unique among known producers of marine carbonate mud, and more so for the very high magnesium contents (up to 40 mol%) of some crystal forms. In addition to previously described morphologies, euhedral needles and rhombohedra are common. However, their small size and commonly very high magnesium content raises important questions about the stability of fish-derived carbonates in seawater, such as whether or not they dissolve or recrystallise, and when such processes might take place. It is reasonable to hypothesis that these aspects could have important implications with respect to the contribution these crystals actually make to carbonate depositional regimes. However, the finding

that low-Mg calcite (containing as little as ~0.5 mol% $MgCO_3$) can be a dominant phase suggests fish-derived carbonates probably occur over a wide range of stabilities and may follow different preservation pathways.

Based on the different crystalline products identified, different fish species can be classified as producing different categories of carbonate crystals; each category presumably an expression of different precipitating conditions within the intestine. An improved understanding of the controls on precipitation products will therefore be important in order to elucidate the reasons for different fish species producing different crystal types, thus allowing improved modelling of carbonate production across fish populations, and ultimately an improved understanding of the significance of potentially differential preservation processes. From the present study it is apparent that body mass, functional group (and thus diet), and possibly gut morphology are not important factors controlling precipitation type. It is more likely that the variation of precipitating conditions within species can be attributed to one or more of the following: i) different rates of cation sequestration; ii) different organic controls on precipitation (gut microbial populations, composition of the mucus membrane etc.); iii) different metabolic rates; or iv) different degrees of supersaturation. Three major areas of future research are identified: 1) the need to understand the wider geographical significance and diversity of fish carbonate production both in other tropical, but also sub-tropical to temperate regions; 2) the need to more fully understand the intra-species controls on the form and diversity of crystal products; and 3) the need to investigate preservation potential of fish-derived carbonates with respect to the variety of crystal morphologies and the chemical compositions.

Chapter 3: Inorganic phases of fish-derived carbonates and the presence of water and organic matter: Infrared analysis and implications for stability in shallow marine settings

3.1 INTRODUCTION

Primary precipitation of carbonates in the intestines of marine teleosts has been the focus of numerous recent studies investigating physiological adaptations in fish (Wilson *et al*., 2002; Grosell *et al*., 2005) and the potential post-excretion significance of these precipitates as a source of sedimentary carbonates in shallow tropical marine carbonate provinces (see Perry *et al*., 2011; and Salter *et al*., 2012 – based on data in Chapter 2). The latter studies document various forms of intestinally precipitated carbonate produced by a range of Caribbean fish species and demonstrate that, in certain platform settings in the Bahamas, they are produced in volumetrically significant quantities with respect to other known sources of carbonate. Mostly these carbonates occur as high-Mg calcite with smaller quantities of low-Mg calcite and aragonite. In addition, some fish species have been shown to excrete amorphous carbonates, and most precipitates also comprise small quantities of an unknown platy magnesium-rich phase similar to some hydrated magnesium carbonates, such as nesquehonite, and magnesium hydroxy carbonates, such as dypingite (Salter *et al*., 2012; Foran *et al*., 2013).

The presence of amorphous phases in fish-derived carbonates is interesting and potentially provides an insight into precipitation processes operating within the piscine gut, as well as having implications for the post-excretion fate of these carbonates (see Chapter 1), yet their properties and the full extent of their occurrence are poorly understood. In Chapter 2 it was shown that magnesium-rich amorphous carbonates (typically containing more than 95 mol% $MgCO_3$) lacking any definable form are produced as a dominant phase by several species. In addition, several other

species were found to produce abundant carbonate nanospheres. Crystalline carbonates have apparently not previously been documented exhibiting such morphotypes, yet amorphous carbonates are frequently found to occur in these forms (Aizenberg *et al*., 1996; Tlili *et al*., 2001; Ajikumar *et al*., 2005; Foran *et al*., 2013). Indeed, a recent study (Foran *et al*., 2013) showed that one fish species (Gilthead bream, *Sparus aurata*) from the Gulf of Eilat, Israel, produced predominantly amorphous carbonate nanospheres when starved. This raises the possibility that fish-derived nanospheres described in Chapter 2 are actually amorphous carbonates, and that amorphous phases represent a more common excretion product than previously thought, although this remains to be confirmed.

If amorphous carbonates do represent an abundant phase in these precipitates, their high solubilities (Brečević and Nielsen, 1989) will likely have direct implications for their stability and preservation in open marine settings. Addadi *et al*. (2003) discuss the fact that amorphous carbonates can occur in two states – stable or transient – the former, which tends to be hydrated, either remaining as an amorphous phase or dissolving; the latter, which tends to contain little or no water, rapidly crystallising to more stable anhydrous phases. However, the hydration state and post-excretion fate (preservation, crystallisation, or dissolution) of fish-derived amorphous carbonates remains unknown. In addition to having implications for the sedimentary fate of fish derived carbonates, the highly unstable nature of many amorphous carbonates (Loste *et al*., 2003; Cheng *et al*., 2007) may have implications for previous characterisations of fish-derived carbonates. Previous studies (Perry *et al*., 2011; Salter *et al*., 2012) have described fish-derived crystalline phases that have been prepared by soaking excreted pellets in sodium hypochlorite for 6 hours (see Chapter 2). Whilst this approach is found to have little or no effect on crystalline carbonate phases (Gaffey and Bronnimann, 1993), its effect on amorphous carbonates is not well known. However, the possibility exists that such approaches might induce crystallisation of initially amorphous phases, and it is thus necessary to verify that previously documented mineralogies were not artefacts of sample preparation.

Assuming the various carbonate phases described by Salter *et al*. (2012) are representative of fish-derived carbonates produced in nature, the numerous phases and forms they comprise likely means their post-excretion stability is highly variable (see Chapter 2). However, in most cases the high magnesium contents and small size of these crystals probably means they have high solubilities compared with most other carbonate forms common in shallow marine settings (*e.g.*, Land, 1967; Plummer and Mackenzie, 1974; Bischoff *et al*., 1987; Morse and Mackenzie, 1990), and this supposition is apparently confirmed in solubility studies of similar fish-derived carbonates (Woosley *et al*., 2012), albeit from a single fish species and with very high magnesium contents (see Chapter 1 for further discussion relating to this work). X-ray diffraction patterns generated by fish-derived carbonates have previously been shown to be characterised by broad peaks (Humbert *et al*., 1989; Mekuchi *et al*., 2010; Perry *et al*., 2011; Salter *et al*., 2012) which may be indicative of other factors that influence solubility, such as poor degree of crystallinity or abundant lattice defects (Bischoff *et al*., 1983). In addition, most biogenic Mg-calcites probably contain some H_2O and OH^- and it is likely that this further influences solubility (Mackenzie *et al*., 1983; Bischoff *et al*., 1987; Morse and Mackenzie, 1990). However, none of the above properties have yet been confirmed for fish-derived carbonates.

In addition to properties that are inherent to the precipitates themselves, the presence of organic matter and/or liquid water associated with these crystals could further influence the solubility of fish-derived carbonates following excretion. The mucus coating in which pellets are excreted has been observed to persist only for a few days before it breaks down and dissipates in seawater (see Chapter 7), and appears to have little influence on the solubility of carbonates (Woosley *et al*., 2012). However, many fish-derived carbonate crystals have been described as having hollow interiors (Walsh *et al*., 1991; Salter *et al*., 2012). Walsh *et al*. (1991) tentatively identify mucosal organic matter within these hollow crystals, whereas Salter *et al*. (2012) note the similarity in morphology between fish-derived crystals and the products of microbial precipitation (Buczynski and Chafetz, 1991), and suggest the possibility that the bacterial cells that induce precipitation are ultimately entombed within crystals. In either case, incidental trapping of liquid water within

hollow crystals must also be a possibility. Any of these scenarios are likely to influence crystal stability. For example, trapped organic material would not be readily dispersed like external mucus coatings, and instead it is possible that its decomposition within crystals could result in lowered calcite saturation states that promote dissolution from within, as has been similarly suggested for carbonates associated with travertines (Chafetz and Folk, 1984).

Many of the properties discussed above are difficult to detect or confirm with analytical approaches utilised in Chapter 2. However, one potentially useful approach lies in the use of Fourier transform infrared (FTIR) spectroscopy, which generates spectra based on the wavelengths at which subject molecules vibrate. As such, this approach is useful for characterising numerous organic and inorganic phases, and can be applied to both liquid and solid samples. The spectral patterns for numerous carbonate phases are generally well known, as is also the case for water and organic matter. This technique facilitates rapid characterisation and requires small sample sizes, and is therefore particularly useful in the analysis of fish-derived carbonates.

The present chapter builds on previous work to further characterise fish-derived carbonates using FTIR spectroscopy. In particular, this study has two major aims:

1. To further characterise fish-derived carbonates at the point of excretion with respect to their mineralogy and crystal properties. Specifically, this will include:
    i. Confirmation of phases present in samples produced by a wider range of Caribbean fish species than previously reported from X-ray diffraction studies;
    ii. Identification of unknown phases, such as the platy magnesium-rich phase present in many samples and any previously undetected phases; and
    iii. Characterisation of crystals with regard to their degree of crystallinity and the presence of water.
2. To investigate the possibility that large amounts of organic matter and/or liquid water are trapped inside hollow crystals.

The data arising from this study will inform considerations regarding precipitation processes operating within the piscine gut and the preservation potential of excreted phases in shallow sub-tropical marine settings.

3.2 FTIR ANALYSIS OF INORGANIC CARBONATES

FTIR spectroscopy operates on the principle that molecules absorb energy at different wavelengths according to their bond arrangement and the manner in which they vibrate. A set of vibrations for a given molecule will thus absorb energy at different wavelengths that can yield characteristic spectral patterns for different materials. In brief, these wavelengths can be determined for an unknown sample by firing a broadband infrared beam through the subject and measuring the infrared wavelengths received at a detector beyond the sample as a percentage of that initially emitted. Where no infrared-active material obstructs the path of the beam, a plot of absorbance against wavelength (conventionally converted to wavenumbers) will produce a horizontal line at zero absorbance. However, where the beam interacts with a material that is infrared-active, molecules in that material will absorb infrared energy at specific wavelengths that cause them to vibrate in a variety of stretching and bending modes. As such, a spectral pattern generated by a given sample will show absorbance peaks centred over certain wavenumbers according to the molecules it contains and the arrangement of their bonds. The reader is referred to Farmer (1974) for more complete details and theory regarding the principles of FTIR spectroscopy.

Inorganic carbonates are reasonably well characterised by FTIR spectroscopy in the mid-infrared region (~4000–400 cm^{-1}). The main vibration modes of the carbonate ion are symmetric and asymmetric stretching (ν_1 and ν_3, respectively) and out–of–plane and in–plane bending (ν_2 and ν_4, respectively), as shown schematically in Fig. 3.1. Each of these vibrational modes absorbs energy at specific wavelengths according to carbonate phase, which thus generate unique spectral patterns and facilitate easy identification of carbonate phases present in an unknown sample. The same principles apply to other molecules and it is therefore possible to use FTIR spectroscopy to determine the presence of, for example, water and organic matter.

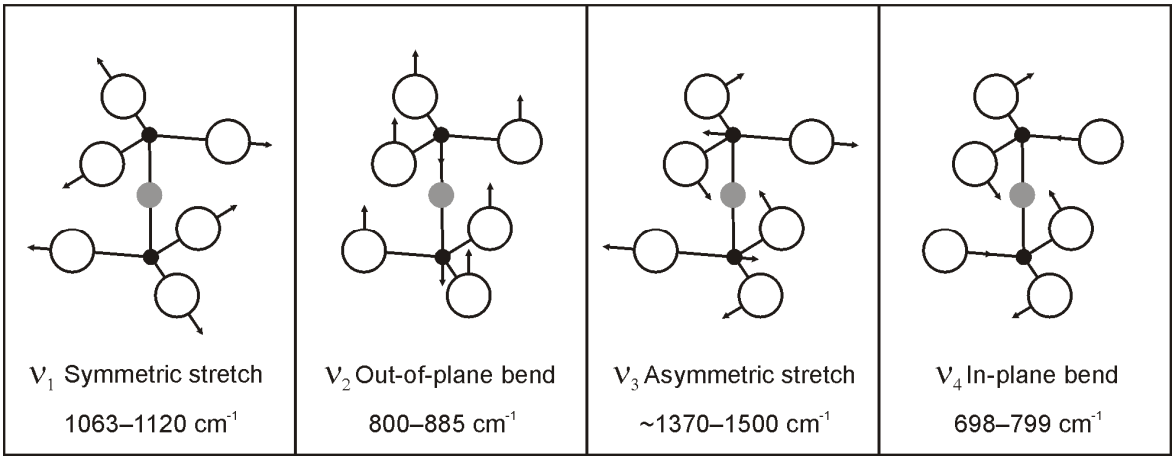

Figure 3.1 *Infrared-active internal vibration modes of the CO_3^{2-} ion in calcium and magnesium carbonates. Wavenumber ranges for all carbonate phases are shown for each mode. CO_3^{2-} ions are represented by open circles (oxygen) arranged about a black circle (carbon); grey circles represent cations. Modified after White (1974).*

The FTIR spectra for anhydrous carbonate phases that are common in shallow marine settings, such as calcite, aragonite, and Mg calcite, are reasonably well documented and are widely included in spectral databases. Hydrous phases, however, are less well known. Given the possible occurrence of hydrated phases and other phases that are not well know in fish-derived carbonates, a spectral database of various relevant phases is compiled here based on available information in the literature (Tables 3.1–3.3).

Table 3.1 *Infrared spectroscopic data reported in literature for calcite, Mg-calcite, and aragonite (see Table 3.3 footnote for details regarding methods, symbols, and references).*

Phase	Method	CO_3^{2-} vibrational modes						Other vibrations	Ref.
		ν_1 (cm^{-1})	ν_2 (cm^{-1})	ν_3 (cm^{-1})	ν_4 (cm^{-1})	$\nu_1 + \nu_3$ (cm^{-1})	$\nu_1 + \nu_4$ (cm^{-1})	Lattice modes	
Calcite, $CaCO_3$	ATR		871	NR	711				1
	ATR		868	1395	712				2
	ATR		872	1374	711	2511?	1795		18
	ATR		871	1392	711		1795		19
	KBr		877	1420	713			227, 311, 354	3
	KBr		877	NR	713				4
	KBr		876	NR	713				5
	KBr		870	1420	710				10
	KBr		870	1430	715				11
	KBr		874	1430	710				12
	KBr		876	1435	712	2545	1812		13
	KBr	1087?	881	1432	712				14
	KBr		877	1425	713				15
	KBr		877	1419	713				17
synthetic (syn)	KBr	1084	849[§], 876	1426	712	2513	1798		21
natural (nat)	KBr	1083	849[§], 876	1429	712	2513	1796		21
2 mol% $MgCO_3$ (syn)	KBr	1084	849[§], 876	1435	713	2516	1798		21
2 mol% $MgCO_3$ (nat)	KBr		849[§], 876	1431	713	2516	1797		21
6 mol% $MgCO_3$ (syn)	KBr	1086	849[§], 874	1429	714.5	2519	1799		21
5 mol% $MgCO_3$ (nat)	KBr	1086	849[§], 877	1435	713.3	2517	1798		21
11 mol% $MgCO_3$ (syn)	KBr	1086	849[§], 875	1449	715.3	2525	1802		21
16 mol% $MgCO_3$ (nat)	KBr	1088	851[§], 877	1429	719.5	2525	1802		21
23 mol% $MgCO_3$ (syn)	KBr	1084	876	1437	721.4	2529	1800		21
43 mol% $MgCO_3$ (nat)	KBr	1092	854[§], 883	1451	731	2538	1815		21
Aragonite, $CaCO_3$	ATR	1084	856	1413	703, 714		1792		2
	KBr	1083	854	1440, 1488	700, 713			315, 273, 237, 220	3
	KBr	1083	859	NR	701, 713				4
	KBr	1080	855	1475	700, 715				11
	KBr	1080	855	1470	696, 710				12
	KBr	1085	875	1470	699, 712				13
	KBr	1087	866	1430, 1550	703, 715				14
	KBr	1085	858	1471	699, 713				15
	KBr	1083	857	1489, 1511	700, 713				17

Table 3.2 *Reported infrared wavenumbers for hydrous Ca- and Mg-bearing carbonate (and related) phases (see Table 3.3 footnote for details regarding methods, symbols, and references).*

Phase	Meth.	CO_3^{2-} vibrational modes					Other vibrations				Ref.
		ν_1 (cm^{-1})	ν_2 (cm^{-1})	ν_3 (cm^{-1})	ν_4 (cm^{-1})	$\nu_1 + \nu_4$ (cm^{-1})	HOH bend	OH^- stretch‡‡	OH^- stretch††	Lattice modes	
ACC, $(Ca,Mg)CO_3 \cdot H_2O$	ATR	~1080	~865b	NR	711_{bh}	NR	~1645	~3400			1
*1:1 Mg:Ca solution	ATR	1072	863	1396, ~1470			1645	~3300			2
*2:1 Mg:Ca solution	ATR	1073	856	1385, ~1450			1642	~3300			2
*4:1 Mg:Ca solution	ATR	1074	861	1382, ~1450			1645	~3300			2
*10:1 Mg:Ca solution	ATR	1073	858	1375, ~1450			1645	~3300			2
	KBr	1067	864b	1425, 1490	725_{bh}	1793	1640	3230, 3375			3
	KBr	NR	876	NR	713_{bh}			~3500			5
	KBr	1075	860	1405, 1480	705, 735_{bh}		1645				10
	KBr	NR**	866	1406, 1474			1655	NR			22
	KBr	NR**	866	1420, 1474			1653	NR			23
	KBr	NR**	873	1425, 1470			1635	~3430			23
Ikaite, $CaCO_3 \cdot 6H_2O$	NaCl†	1085	876	1411, 1425	720, 743		1644	3216, 3404, 3468		800?	6
Monohydrocalcite	NaCl†	1063	872	1401, 1492	698, 762			3236, 3327, 3400			6
$CaCO_3 \cdot H_2O$	NR	1068	873	1408, 1487	700, 727, 766		1700	3235			24
Nesquehonite	NaCl†	1099	854	1427, 1467, 1518	719			3350, 3460, 3508			6
$MgCO_3 \cdot 3H_2O$	KBr	1097	~855	1415, 1470, 1518	~710		1640	~3400	3568		7
$Mg(OH)(HCO_3) \cdot 2H_2O$‡	ATR	1098	855	1419, 1439, 1462	710		1636, 1683	3012–3483*	3560, 3605		8
Dypingite	ATR	1071	852, 882	1380–1508*	755, 799			~3400	3647, 3686	948, 1008	9
$Mg_5(CO_3)_4(OH)_2 \cdot 5H_2O$	ATR	1078	NR	1312–1585*	NR			~3400	3649, 3682	947, 1012	9
Artinite	ATR	1076	844	1376–1535*	NR			~3400	3649, 3685	947, 1017	9
$Mg_2CO_3 \cdot (OH)_2 \cdot 3H_2O$	ATR	1083	NR	1325–1439*	722, 762			~3400	3651, 3685	952, 995	9
Hydromagnesite	NR	1119	800, 854, 885	1424, 1482	601		1644	3448	3648		16
$Mg_5(CO_3)_4 \cdot (OH)_2 \cdot 4H_2O$	KBr	1110, 1120	~800, ~860, ~900	1420, 1475, 1515	~600		~1650	~3100, 3463, 3525	3658		7
Brucite	KBr								3700–3704		25
$Mg(OH)_2$	NR								3698	440, 565, 627	26
	KBr								3698	445, 571, 645	27

Table 3.3 *Reported infrared wavenumbers for selected additional anhydrous Ca- and Mg-bearing carbonate phases (see footnote for details regarding methods, symbols, and references).*

Phase	Method	CO_3^{2-} vibrational modes						Other vibrations	Ref.
		ν_1 (cm^{-1})	ν_2 (cm^{-1})	ν_3 (cm^{-1})	ν_4 (cm^{-1})	$\nu_1 + \nu_3$ (cm^{-1})	$\nu_1 + \nu_4$ (cm^{-1})	Lattice modes	
Vaterite, $CaCO_3$	ATR	1085	868	NR	747				2
	KBr	1089	873, 877	1418, 1487	738, 746			383, 332, 282, 250, 232	3
	KBr	1085	870	1420, 1490	750				11
	KBr	1090	878	1450	741				14
	KBr	1089	877	1450	744				17
Dolomite, $CaMg(CO_3)_2$	KBr		881	1439	729				15
	KBr		881	1450	730	2530	1818		13
	KBr		881	1437	728	2524	1823		20
synthetic	KBr	1100	853[§], 883	1445	729	2529	1818		21
natural	KBr	1101	853[§], 882	1443	728	2526	1821		21
Huntite, $Mg_3Ca(CO_3)_4$	KBr	1112	870, 893	1445, 1511	743				15
	KBr	1113	869, 891	1452, 1467, 1512, 1530	743	2544, 2583	1828		21
Magnesite, $MgCO_3$	KBr		887	1450	748		1818		13
synthetic	KBr	1108	855[§], 886	1448	748	2537	1831		21
natural	KBr	1113	855[§], 885	1456	748	2535	1827		21

Cell values Empty cell = peak not present; NR = value/peak not reported. **Method** KBr = Transmission FTIR, sampled mounted in KBr disc; ATR = Attenuated internal reflectance FTIR; NaCl[†] = Transmission FTIR, samples mounted in NaCl windows and analysed at -80 °C. **OH^- stretch** [††]OH^- strongly bonded in hydroxy mineral phases, generally very sharp peaks; [‡‡]OH^- associated with water in various states, generally broad peaks. **Additional notes** *numerous peaks within this range; [‡]a different formula is proposed for nesquehonite based this on IR spectrum. The authors observe additional peaks (not shown in the table) at 934 cm^{-1}, which they assign to the MgOH deformation mode, and in the region 624–680 cm^{-1}, 836 cm^{-1}, 1027 and 1052 cm^{-1}, and 1511, 1528, and 1584 cm^{-1}, these being attributed to ν_4, ν_2, ν_3, and ν_1 vibrational modes of HCO_3^-, respectively; **If present, this peak is obscured by a relatively intense phosphate peak; [§]Small satellite peak assigned to vibration of $^{13}CO_3^{2-}$; $_{bh}$ = peak present as an indistinct broad hump.

References 1 – Gong *et al*., 2012; 2 – Loste *et al*., 2003; 3 – Andersen and Brečević, 1991; 4 – Compere and Bates, 1973; 5 – Politi *et al*., 2004; 6 – Coleyshaw *et al*., 2003; 7 – White, 1971; 8 – Frost and Palmer, 2011; 9 – Frost *et al*., 2008; 10 – Dupuis *et al*., 1984; 11 – Sato and Matsuda, 1969; 12 – Nakamoto *et al*., 1957; 13 – Huang and Kerr, 1960; 14 – Weir and Lippincott, 1961; 15 – Adler and Kerr, 1963; 16 – Janet *et al*., 2007; 17 – Sterzel, 1969; 18 – Bullen *et al*., 2008; 19 – Boels *et al*., 2010; 20 – Ramasamy *et al*., 2009; 21 – Böttcher *et al*., 1997; 22 – Raz *et al*., 2002; 23 – Aizenberg *et al*., 1996; 24 – Neumann and Epple, 2007; 25 – Ahlrichs, 1968; 26 – Frost and Kloprogge, 1999; 27 – Schroeder, 2002.

3.3 METHODOLOGY

Infrared spectra were obtained for fish-derived carbonates by both transmission and attenuated total reflectance (ATR) FTIR. The former is routinely employed in the analysis of carbonates (and other materials), and involves mounting carbonates in a KBr pellet through which an infrared beam is transmitted. However, this approach can be problematic, especially with regard to the aims of the present study. Specifically, KBr is strongly hygroscopic and it can be difficult to prevent adsorption of atmospheric moisture during preparation of the KBr pellet. Atmospheric moisture absorbs infrared energy at broadly similar wavelengths to those of water adsorbed in carbonates, and contamination in this manner will thus generate absorbance peaks in the resulting spectra that interfere with some of the areas of interest in this study. Furthermore, to obtain the best results in transmission FTIR it is necessary to grind sample materials until individual particles are <2 μm in length. However, excessive grinding can result in changes in mineralogy or degree of crystallinity in some carbonates (Lane, 1999; Chu *et al*., 2008; Ramasamy *et al*., 2009; Regev *et al*., 2010); an effect that may be particularly prominent in fish-derived carbonates given their possible low stability, and may consequently result in the generation of misleading spectra.

ATR-FTIR adopts a similar approach to that used in transmission FTIR, but rather than the infrared beam interacting with a sample as it is passed through a KBr pellet, the beam is instead reflected internally in an optically dense crystal of high refractive index. Infrared energy is absorbed by sample material that is placed in contact with the surface of this crystal. This approach means that neither sample grinding, nor mounting (in KBr), is necessary, and the problems associated with transmission FTIR are consequently avoided. However, the spectra generated using this approach can result in absorbance peaks being centred over slightly lower wavenumbers than those derived from transmission FTIR (Loste *et al*., 2003). Because ATR-FTIR is a relatively new analytical approach, spectral patterns for most carbonate phases tend to be poorly characterised compared with equivalent data derived from transmission FTIR (*e.g.*, Table 1.1). Another spectral difference between the two approaches is peak intensity, which tends to be higher at lower wavenumbers in

comparison to equivalent peaks in transmission IR spectra. Peak intensity ratios have been used as a proxy for degree of crystallinity in carbonate minerals (Politi *et al*., 2004), but in most cases those studies have used transmission IR data.

Given the above information, both transmission and ATR FTIR approaches are employed in the present study: transmission FTIR is used to determine the carbonate phase(s) present in samples and their degree of crystallinity, based on comparisons with existing spectral data; ATR-FTIR is used to confirm the presence of water. All carbonate samples were collected and processed using the approach described in Chapter 2.

3.3.1 Transmission FTIR

Carbonate samples were prepared by gently grinding approximately 0.3 mg in an agate mortar with approximately 40 mg of spectrophotometric-grade KBr. The resulting homogeneous mixture was held in a manual hydraulic press under a load of 2 tonnes for approximately one minute, thus inducing recrystallisation of the KBr to form a semi-transparent disc of 7 mm diameter, in which the ground carbonates were evenly dispersed. Infrared absorption spectra were obtained over the mid-infrared region (500–4000 cm^{-1}) using a Nicolet FTIR spectrometer at the University of Southampton. Analyses were performed at a resolution of 4 cm^{-1} and final spectra obtained by the co-addition of 32 scans.

The spectrometer background was calibrated against ambient atmospheric conditions at the beginning of each analytical session and following every three analyses thereafter. To check for other potential sources of contamination, spectra were obtained both for blank KBr discs and for KBr discs containing a dispersion of geological calcite at the beginning and end of each analytical session. Low intensity hydration peaks were sometimes present in these spectra, presumably due to water adsorbed to KBr during sample preparation. Hydration peaks in some fish-derived carbonate samples were typically of greater intensity than these and were presumably due to the presence of hydrous phases. However, proper interpretation of these peaks was complicated by the potential for absorbed moisture in the KBr.

3.3.2 Attenuated total reflectance FTIR

Spectra generated using ATR-FTIR were collecting using a Nicolet 380 FT-IR spectrometer coupled with a Thermo Scientific SMART iTR ATR sampler equipped with a diamond reflecting cell. Samples were analysed by placing two or three carbonate pellets directly onto the ATR crystal, where they were gently crushed and held securely in place by an in-built clamp. Because observations made using SEM reveal that the components of fish-derived carbonates produced by some species can vary among pellets, three sub-samples were analysed for each species to ensure spectra were representative of bulk samples. Analyses were performed at a resolution of 2 cm^{-1} and final spectra were obtained by the co-addition of 32 repeated scans.

Although spectra generated using this approach differed slightly from those obtained using transmission FTIR, in most cases the distribution of absorbance peaks was generally similar and suggests that grinding associated with sample preparation for transmission FTIR had little effect on the nature of samples. To verify this, several samples were gently ground in an agate mortar for 20 seconds (*i.e.*, the same amount of grinding used in the preparation of KBr pellets). ATR-FTIR spectra obtained for these ground samples were identical to those obtained for samples that underwent no grinding, thus confirming that CO_3^{2-} vibrational modes determined using transmission FTIR are representative of fish-derived carbonates in their excreted forms (and not of altered forms that might have resulted from grinding).

Spectra were also collected for several carbonate samples of other biogenic origin to provide comparison with fish-derived carbonates. These included skeletal carbonates of *Porites* coral, gastropod (both aragonite), and foraminifera tests (high-Mg calcite). Samples were prepared in a similar manner to fish-derived carbonates. Following collection from surface sediments of Eleuthera Sound, the Bahamas, samples were repeatedly rinsed in distilled water and organic matter was removed by soaking in a 5.25 % solution of sodium hypochlorite for six hours. Following more rinses in distilled water, samples were dried in a low temperature oven at 50 °C. They were then prepared for analysis by gentle grinding in an agate mortar.

3.3.3 Post-processing of spectra

All spectra were further processed after collection using the spectrometer software (OMNIC Version 7.2). This included baseline correction, peak intensity measurement, and peak deconvolution to determine positions of overlapping peaks. Peak deconvolution followed the approach of Frost *et al*. (2008). A Gaussian-Lorentzian peak fitting function was used to resolve the positions of the minimum number of peaks necessary to generate a spectral pattern similar to that of the originally obtained spectrum. Peak deconvolution was performed on two or more spectra for samples generated by each fish-species to ensure derived component peaks were reproducible.

3.3.4 Scanning Electron Microscopy

High magnification electron microscope images were collected from sub-samples of each sample analysed using FTIR spectroscopy. Sample preparation and instrumental arrangement were as described in Chapter 2 (section 2.2.2).

3.4 RESULTS

Carbonate pellets produced by 16 fish species have been characterised using a combination of transmission FTIR and ATR-FTIR. Carbonate vibrational modes are generally in good agreement with similar carbonate phases of other biogenic origins (Fig. 3.2), and for most species it is possible to assign these to calcite or Mg calcite. In addition, it is evident that some fish species produce small amounts of aragonite, and the results are thus in good agreement with X-ray diffraction data of previous studies (Humbert *et al*., 1989; Mekuchi *et al*., 2010; Perry *et al*., 2011; Salter *et al*., 2012). Other phases identified from FTIR spectra include amorphous calcium and magnesium carbonates (referred to hereafter as ACC and AMC, respectively) present in samples produced by at least 6 fish species and, identified here for the first time, monohydrocalcite, $CaCO_3 \cdot H_2O$, and brucite, $Mg(OH)_2$.

Further to confirming the inorganic solid phases present, FTIR data also indicate the presence of water and organic matter in samples produced by all species, these typically producing more

intense signals compared with other biogenic carbonates (Fig. 3.2). Because excreted carbonates often contain mixed phases, it is not always possible to assign water to a particular phase. However, the most intense signals are typically produced where amorphous phases are present, thus confirming they are hydrated. Spectra for some samples (especially those produced by bonefish) also indicate the presence of phosphate, which is presumably the source of phosphorus reported in Chapter 2. Finally, although clearly defined peaks corresponding with the CO_3^{2-} ν_4 vibration are generated by most samples, thus confirming the presence of crystalline phases, these peaks are typically very weak. The ratio of peak intensity between the ν_2 and ν_4 absorption bands ranges from about 6.8 to 15.3 for samples containing only calcite or Mg-calcite. By comparison, Politi *et al*. (2004) and Chu *et al*. (2008) find this ratio to be 3.0 for well-crystallised calcite, and higher for carbonates of lower crystallinity. It thus appears that fish-derived carbonates are very poorly crystalline, although for some samples these spectral patterns may also be due to the combined presence of crystalline and amorphous phases, as has been similarly shown by Politi *et al*. (2004).

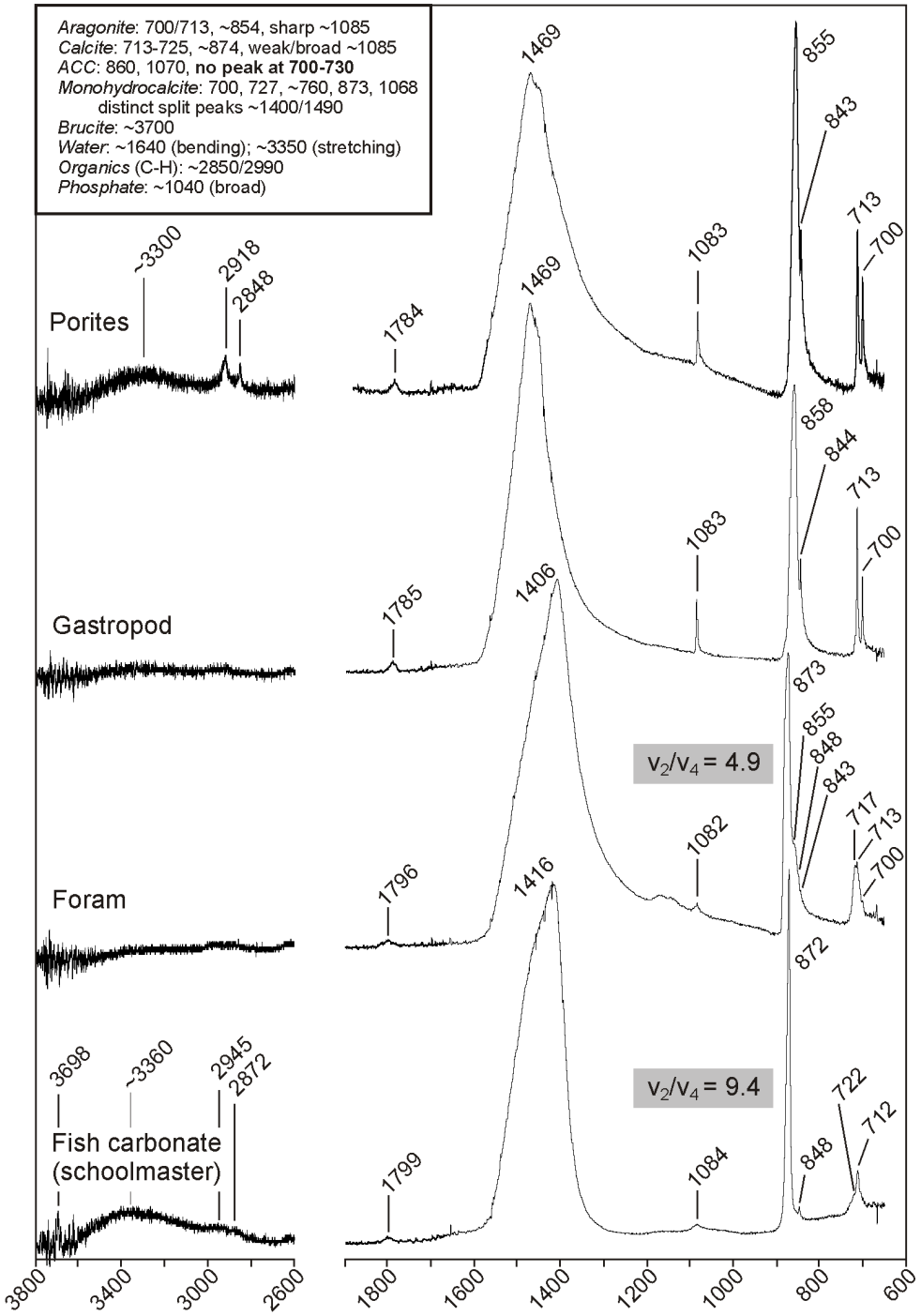

Figure 3.2 *ATR-FTIR spectra for some common marine sedimentary carbonates and a fish-derived carbonate sample produced by schoolmaster snapper. Spectra between 3800 and 2600 cm^{-1} are 4x vertically exaggerated relative to those at lower wavenumbers. Spectra for Porites and gastropod carbonate are in good agreement with existing spectral data for aragonite (Table 3.1). The spectrum for the foram test is indicative of a calcite structure, with overlapping peaks at 713 and 717 cm^{-1} indicating the presence of pure calcite and Mg calcite, respectively. In addition, very weak peaks at 855 and 700 cm^{-1} indicate the presence of aragonite as a minor phase. The spectrum for fish-derived carbonate is similar to that for the foram test, indicating that calcite and Mg calcite are dominant phases. Note that fish-derived carbonate spectra typically generate a stronger water stretching band (centred over ~3360 cm^{-1}) than other common marine carbonates. A similar, but weaker, peak generated by Porites aragonite is probably due to water associated with residual organic matter, the presence of which is indicated by sharp peaks at 2918 and 2848 cm^{-1}. Also note the difference in v_2/v_4 peak intensity ratio between fish-derived and foram-derived calcite; the higher value for fish-derived calcite indicating a lower degree of crystallinity. Inset at top left are the key peak positions that identify the various phases relevant here.*

The various phases identified in this study are summarised for samples produced by each fish species in Table 3.4. Representative spectra are shown in Figs. 3.3 to 3.6 (see also Appendix IV). Based on these data, fish are grouped into three categories: 1) those that produce calcite or Mg-calcite with a limited amount of water; 2) those that produce calcite and amorphous phases with abundant water; and 3) those that produce predominantly amorphous phases with abundant water and minor amounts of calcite. Results for each of these categories are described in more detail below.

Table 3.4 *Phases identified in carbonate samples produced by 16 different species of fish, and the main solid forms with which they are associated. Particle morphologies based on data of Salter et al. (2012).*

Fish species	Dominant particle morphologies	Calcite*	Aragonite	Monohydro-calcite	ACC–AMC†	Brucite	Water	Organic matter	Phosphate‡
Schoolmaster snapper	ME	••				◊	•	•	
Yellowtail snapper	ME	••				◊	•	•	o?
French grunt	ME	••				•	•	•	
Black grouper	ME + Ro	••				o	•	•	o
Graysby grouper	ME	••				◊	•	•	
Nassau grouper	ME	••				•	•	o	
Red hind	ME	••	•			•	•	•	
Lionfish	ME	••				•	•	o	
Great barracuda	Dmb (sml) + NSph	••	o?		o?	◊	•	•	o
Yellowfin mojarra	ME + Dmb + Sph	••	o			•	•	o	
Keeltail needlefish	ME+ Dmb+ Sph+ Amo+ Pl	••	o		•	••	••	o	
Redtail parrotfish	Sph+ PE+ Nee+ Amo+ Rho	•	•	•	•	•	••	•	•
Checkered puffer	Sph + PE + Rho + Amo	oo	o?	oo	o	o	••	o	
Bonefish	Sph + NSph + Amo	oo		o	oo	o	••	o	oo
Bluehead wrasse	Amo + Rho + Sph + Pl	•			••	•	••	•	•
Slippery dick	Amo + Rho + Sph + Pl	•			••	•	••	•	•

Morphology codes: ME = monocrystalline ellipsoid; PE = polycrystalline ellipsoid; Ro = Rod; Dmb = Dumbbell [(sml) = small]; Sph = sphere; NSph = nanosphere; Nee = needle; Rho = rhombohedron; Amo = amorphous solids; Pl = platy crystals, often interlocking to form rosettes.

Key to symbols: •• = common in all samples; • = minor presence in all samples; oo = common in some samples; o = minor presence in some samples; ◊ = not detected in samples produced by this species using FTIR, but platy crystals that are presumably of this phase observed in SEM images; *calcite represents all calcite and Mg calcite; †indicates the presence of any amorphous carbonate in a solid–solution series between amorphous $CaCO_3$ and amorphous $MgCO_3$; ‡Form of phosphate unknown, but may be amorphous, either as a discrete phase or co-precipitated with ACC, PO_4^{3-} substituting for CO_3^{2-}. Shading denotes category (palest = 1; darkest = 3 – see text for explanation of categories).

3.4.1 Spectra generated by monocrystalline ellipsoids and small dumbbells (Category 1)

3.4.1.1 Carbonate phases

Carbonates that comprise monocrystalline ellipsoids generate transmission FTIR spectra with CO_3^{2-} vibrational modes indicative of Mg calcite (Fig. 3.3; Table 3.1). Sharp peaks at 874–875 cm^{-1} are assigned to the CO_3^{2-} ν_2 vibration in calcite, with subsidiary peaks at ~850 cm^{-1} probably due to ν_2 vibrations associated with $^{13}CO_3^{2-}$ (Golyshev *et al*., 1981; Böttcher *et al*., 1997). Carbonate ν_1 vibrational modes are infrared-inactive in calcite (Adler and Kerr, 1963) and they are not usually observed in FTIR spectra (Table 3.1). However, the selection rules that dictate such inactivity breaks down when calcite becomes structurally disordered due to the presence of magnesium (White, 1974), and weak bands at 1084–1087 cm^{-1} are thus attributed to the presence of Mg calcite. Peaks centred over ~1450 $cm^{-1}$are assigned to the CO_3^{2-} ν_3 vibration mode. The maximum intensity of these peaks is centred over wavenumbers in the approximate range 1450–1479 cm^{-1}, which are rather high for calcite (Table 3.1). However, interpretation of this peak is complicated by its asymmetry, which suggests it is a composite of several component peaks. Peak deconvolution is used to further explore this peak in section 3.4.4, where it is shown that at least one component peak is in good agreement with available data for Mg calcite.

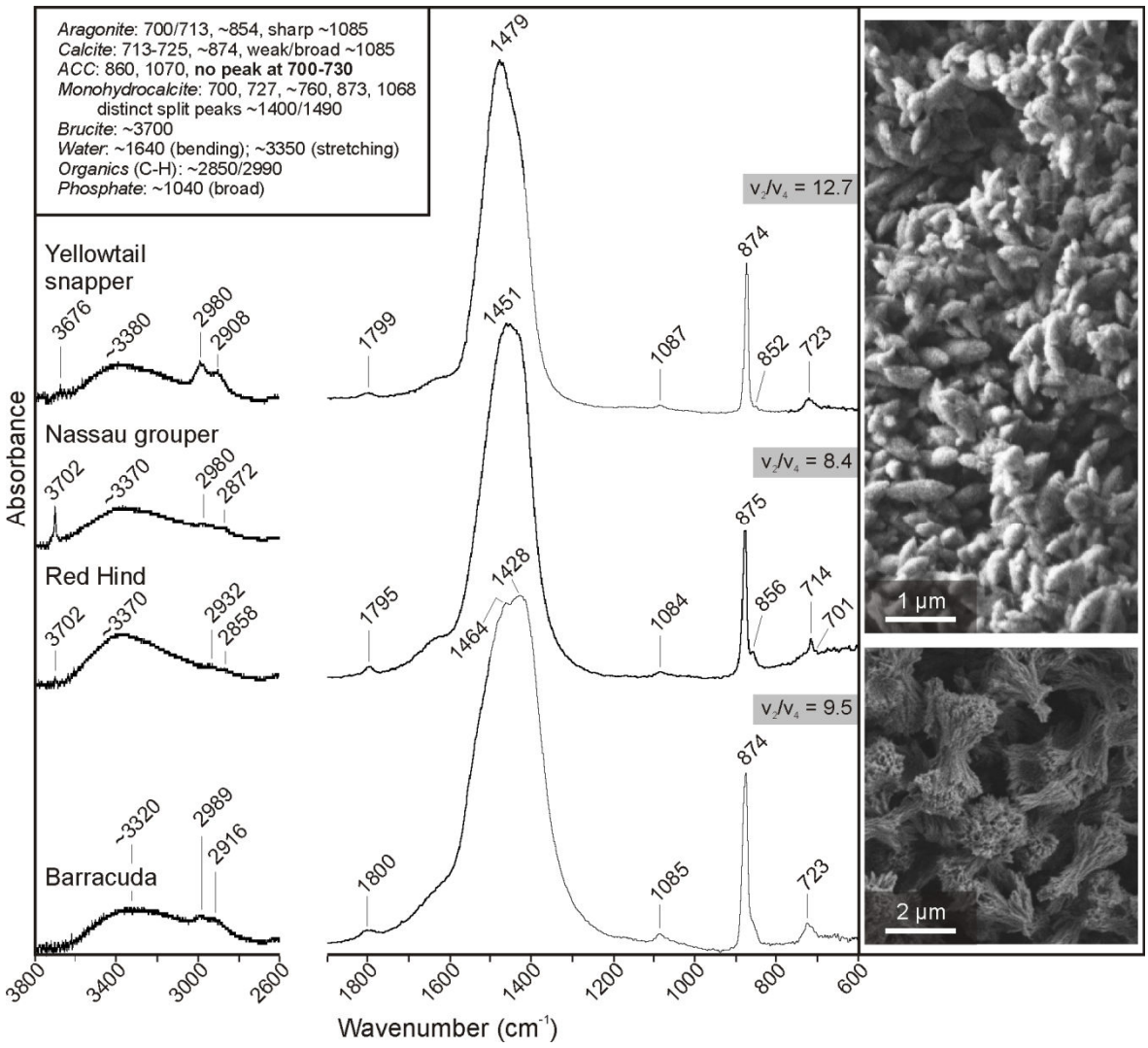

Figure 3.3 *Representative FTIR spectra for fish-derived carbonates that have ellipsoidal (top three spectra) and small dumbbell (bottom spectrum) morphologies (as shown in SEM images, right). Spectra between 3800 and 2600 cm^{-1} are derived from ATR-FTIR, these being 4x vertically exaggerated relative to spectra between 1900 and 600 cm^{-1}, which are derived from transmission FTIR. See text for peak assignments. Ratios of the intensity of ν_2/ν_4 are shown in grey boxes and indicate poor crystallinity of these calcites. The sharp peak generated by some samples at 3701–3703 cm^{-1} is assigned to the OH stretching mode of brucite (Fig. 3.8). Inset at top left are the key peak positions that identify the various phases relevant here.*

Peaks in the range 714–727 cm^{-1} are due to CO_3^{2-} ν_4 vibrational modes, and their presence confirms that all samples contain a crystalline phase. However, they are typically very weak in comparison to equivalent peaks generated by marine carbonates of different origin (*e.g.*, Fig. 3.2; foram test), and the ratio of maximum intensity between ν_4 and ν_2 peaks is consequently much higher for fish-derived calcite than for well crystallised biogenic calcite (Politi *et al*., 2004). Two possibilities may explain these low ν_4 intensities and consequently high ν_2/ν_4 ratios: 1) extremely poor crystallinity of fish-derived Mg calcite; and/or 2) the combined presence of an amorphous phase with calcite. A

similar scenario to the latter has been demonstrated in sea urchin spines, which generate low intensity ν_4 peaks (Politi *et al*., 2004). The CO_3^{2-} ν_2 peak at 874 cm^{-1} is typically sharp and intense in spectra generated by these carbonates (Fig. 3.3), thus appearing to rule out the presence of ACC (which should generate a broader, less intense peak centred over lower wavenumbers). However, this broader peak is not always apparent when crystalline phases are also present (*e.g.*, Politi *et al*., 2004), and the presence of an unexplained component of the CO_3^{2-} ν_3 peak centred over ~1450 cm^{-1} (see section 3.4.4 below) might be explained by the presence of ACC. It is worth noting, however, that morphological forms typical of ACC, such as nanospherical clusters and material lacking any definable form, are extremely rare in these samples, and poorly crystalline Mg calcite therefore probably best explains the observed spectral patterns.

Another feature of peaks assigned to the ν_4 vibration in fish-derived carbonates is the reasonably wide range of wavenumbers they are centred over (714–727 cm^{-1}). Böttcher *et al*. (1997) identify a relationship between ν_4 peak position and magnesium content in Mg-calcite, whereby:

$$\nu_4\ (\mathrm{cm}^{-1}) = 39.4X_{Mg} + 712.2 \qquad \textit{equation } 3.1$$

Accordingly, ν_4 peaks at 723–727 cm^{-1} (as found for samples produced by schoolmaster snapper, yellowtail snapper, lionfish, graysby grouper, and great barracuda) correspond to magnesium contents of approximately 27–38 mol% $MgCO_3$, and are in good agreement with previously determined values (Perry *et al*., 2011; Salter *et al*., 2012 – see Chapter 2). In contrast, some samples produced by black grouper, red hind, Nassau grouper, and French grunt generate ν_4 peaks centred over 714 cm^{-1}, corresponding to magnesium contents of approximately 5 mol% $MgCO_3$. While it is possible that variations in CO_3^{2-} ν_4 peak position reflect variable magnesium contents in these samples, such low values have not previously been obtained for these morphotypes using other approaches (Salter *et al*., 2012). This apparent disparity is puzzling, but it is worth pointing out that equation 3.1 was derived using synthetic and geological samples of Mg calcite; biogenic samples, and perhaps poorly crystalline fish-derived carbonates in particular, may not adhere strictly to the rules that dictate this relationship. In view of this uncertainty, data arising in the

present study are unreliable as a proxy for magnesium content, and calcite and Mg calcite phases are referred to only as Mg calcite (Mg calcite is preferred over calcite due to the presence of at least some magnesium in most calcite crystals analysed in Chapter 2, as well as the ubiquitous presence of a peak assigned to a CO_3^{2-} ν_1 vibration, which is forbidden in pure calcite).

Apart from poorly crystalline Mg calcite (and possible ACC), spectra generated by some samples also indicate the presence of minor amounts of aragonite. For example, the spectrum for carbonates produced by red hind (Fig. 3.3) has very low intensity peaks at 856 cm^{-1} and 701 cm^{-1}, corresponding with ν_2 and ν_4 vibrational modes for aragonite, respectively. In the spectrum for great barracuda carbonates, a shoulder at ~859 cm^{-1} may be due to minor aragonite but, in absence of a peak close to 700 cm^{-1}, it is difficult to rule out the possibility that this peak is due to ACC. Note that carbonate samples produced by great barracuda and analysed in this study comprised only small dumbbells. Samples comprising nanospheres (see Chapter 2) were not analysed here, but are confirmed as being amorphous carbonates in Chapter 4.

3.4.1.2 Water and organic phases

Several peaks in these spectra indicate the presence of other phases in addition to inorganic carbonates. Small peaks between 2850 and 3000 cm^{-1} are due to symmetric and asymmetric stretching of C–H in various organic molecules (Derrick *et al*., 1999). Their occurrence is common, but they are typically of very low intensity and in many cases are completely absent (*e.g.*, yellowtail snapper vs. red hind; Fig. 3.3). The fact they are generally more intense than equivalent peaks generated by other carbonates (Fig. 3.2) suggests that organic matter is more abundant in cleaned fish-derived carbonates, despite being prepared in the same manner. This could mean it is more tightly bound to the latter, possibly as a consequence of being trapped inside hollow crystals or adsorbed to crystal surfaces. However, if this is the case, the apparent absence of organic phases in some samples is perplexing. It is worth pointing out that the ages of the 'other carbonates' (foram test, gastropod, and *Porites* coral) used in this study are unknown, but they are presumably substantially greater than for the newly precipitated fish-derived carbonates, and their associated

organic matter would probably have degraded long before samples were retrieved. Consequently, there would have been a significantly larger amount of organic material to remove from fish-derived carbonates during cleaning, and thus greater potential for the retention of residual organics. Given the absence of organic matter in some fish-derived carbonate samples, the latter is the most satisfactory explanation.

Unlike organic phases, water is present in all samples, as evidenced by weak OH^- stretching bands centred over ~3300–3400 cm^{-1}. The presence of water in samples where organic content is not discernible indicates that it is associated with the carbonates themselves rather than organic matter. However, the low intensity of water bending and stretching peaks means it is difficult to ascertain whether it is in a liquid form (*i.e.*, fluid inclusions), or is somehow bound to a carbonate phase (*e.g.*, adsorbed on the surface of Mg calcite, or forming a hydrous component of minor ACC).

3.4.2 Spectra generated by spheres, dumbbells, and other morphotypes (Category 2)

3.4.2.1 Carbonate phases

FTIR spectra reveal that carbonates falling within Category 2 comprise multiple crystalline phases that include calcite (Fig. 3.4; all species), plus aragonite (Fig.3.4; redtail parrotfish) and monohydrocalcite (Fig. 3.4; bonefish, checkered puffer, and redtail parrotfish); only the products of keeltail needlefish appearing to comprise a single crystalline phase (compare spectra in Fig. 3.4 with data in Tables 3.1–3.3). The presence of monohydrocalcite is confirmed by peaks centred over ~770 and 1068 cm^{-1}, thus verifying the tentative XRD-based identification of monohydrocalcite as a minor phase in carbonates produced by checkered puffer (Chapter 2). Indeed, some samples produced by checkered puffer appear to comprise only monohydrocalcite, with SEM images indicating this phase is morphologically similar to calcite produced by this species (Fig. 3.5). However, where multiple phases are present (*i.e.*, most samples), other peaks associated with this phase overlap with calcite (ν_2) and aragonite (ν_4) peaks, and thus hamper interpretations regarding the presence of these phases. Peak intensities in most cases (as well as XRD data; Chapter 2)

confirm the presence of calcite, but in some cases (*e.g.*, bonefish and checkered puffer; Fig. 3.4) the unknown source of a peak at ~700 cm^{-1} (aragonite or monohydrocalcite) precludes the possibility of confirming whether a shoulder at ~857 cm^{-1} is due to aragonite or an amorphous phase. The presence of aragonite in these samples is not unexpected (it is confirmed in XRD patterns – Perry *et al*., 2011; and Chapter 2), but it is not always possible to confirm this using FTIR data. As with ellipsoids and small dumbbells, ν_2/ν_4 peak intensity ratios are typically high, but the presence of multiple phases (including amorphous carbonates; see below) precludes meaningful interpretation of these values.

A characteristic feature of all of these spectra is the presence of broad peaks of high intensity (relative to that for monocrystalline ellipsoids and small dumbbells) over the water stretching and bending regions (Fig. 3.4) at approximately 3300–3400 cm^{-1} and 1640 cm^{-1}, respectively. Interpretation of these peaks is hindered by the presence of multiple phases, and several possibilities can be considered. One possibility is that water is associated with monohydrocalcite, which is hydrous by definition. However, this phase typically generates a differently shaped water stretching peak, and a water bending peak centred over 1701 cm^{-1} (see Fig. 3.5). Furthermore, the peaks that identify the presence of monohydrocalcite (at approximately 700, 770, and 1068 cm^{-1}) are generally weak, indicating it is usually a minor phase which should therefore generate less intense water stretching peaks. Moreover, similarly shaped water stretching and bending peaks are generated regardless of whether monohydrocalcite is present or absent. Another possibility is that other crystalline phases (calcite and aragonite) are strongly hydrated, although hydration to this extent would be highly unusual. The presence of liquid water as fluid inclusions can also be ruled out by careful assessment of the water bending peak positions using peak deconvolution (Figs. 3.5–3.7), which indicates that these peaks are typically centred over 1640–1655 cm^{-1}. These data suggest that the O–H bond strength is greater in these samples than in liquid water, which typically generates water bending peaks over wavenumbers lower than 1635 cm^{-1} (Grdadolnik, 2002).

A final possibility is that water bending and stretching bands are generated by hydrated amorphous carbonates. As has already been mentioned, CO_3^{2-} bands generated by such phases can be obscured when samples also contain crystalline phases with overlapping peaks (*e.g.*, calcite; Politi *et al*., 2004). However, close examination of the carbonate ν_2 and ν_4 bands indicates they are weaker and broader in these samples than is typical of fish-derived Mg calcite described in section 3.4.1 (*e.g.*, checkered puffer; Fig. 3.4), whilst the positions of water bending peaks are in good agreement with existing data for amorphous carbonates (Table 3.2). Furthermore, analysis of multiple samples produced by bonefish indicates that crystalline phases are nearly absent from some; spectra instead confirming the presence of amorphous carbonate, as indicated by the absence of a carbonate ν_4 peak, the shifting of ν_1 and ν_2 peaks to lower wavenumbers, and component peaks of the ν_3 band (centred over 1391 and 1455 cm^{-1}; derived from peak deconvolution) that are in good agreement with available data for ACC (Table 3.2; Fig. 3.5). In these samples, water stretching and bending modes must be associated with the amorphous solid (as mentioned above, peak positions suggest O–H bonds are too strong to be generated by liquid water), which must therefore be hydrated. Given the similar shape and intensity of water bending and stretching modes common to precipitates containing some crystalline phases, it appears likely that a hydrated amorphous phase is also present in these samples; its carbonate vibrations being obscured by crystalline carbonate vibrations.

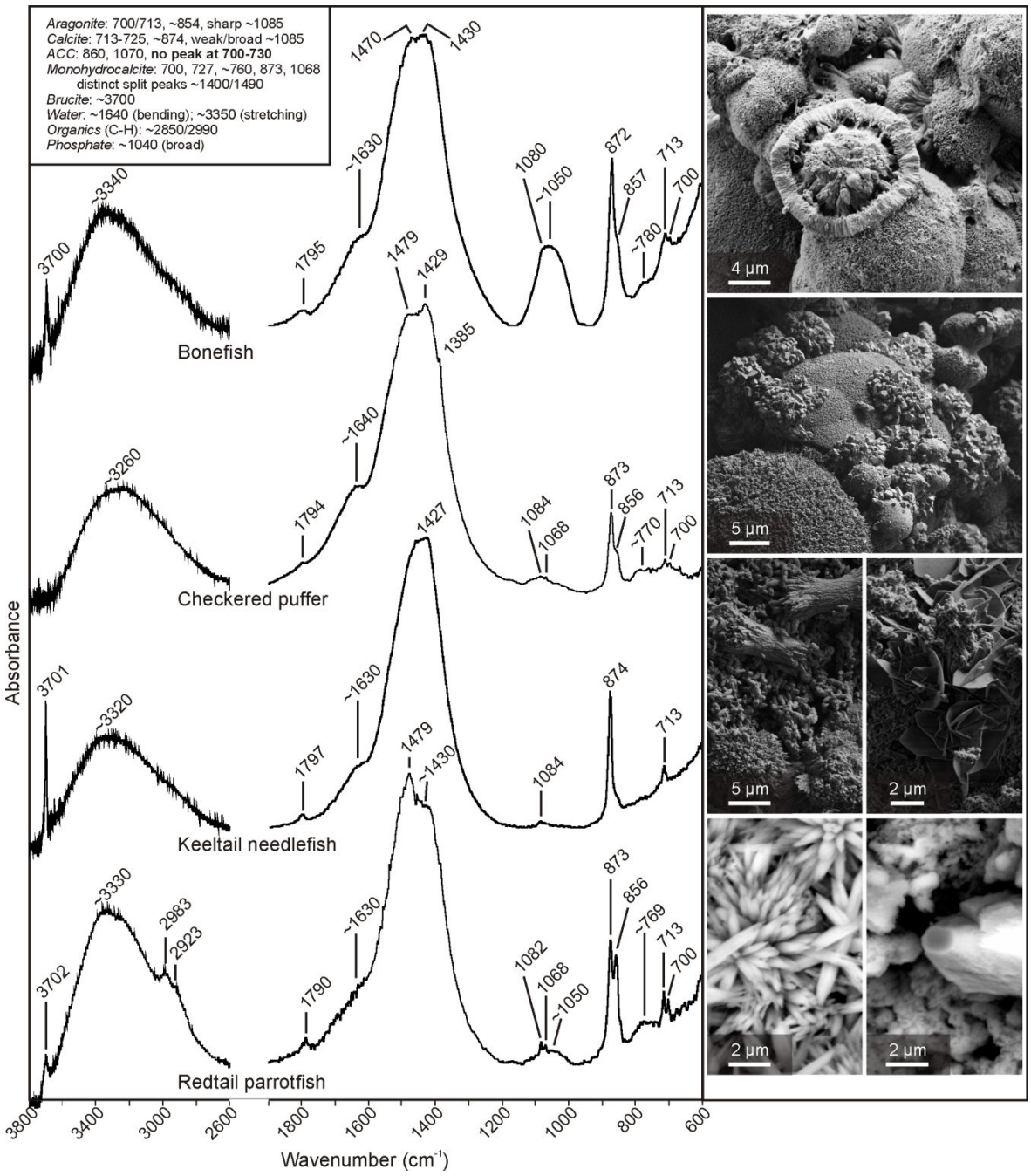

Figure 3.4 *Transmission (low wave numbers) and ATR (high wavenumbers) FTIR spectra and SEM images of fish-derived carbonates produced by four different fish species. SEM images to right of each spectrum show representative crystal forms. Many pellets also contain nanospheres and/or a phase that lacks definable form (e.g., see Fig. 3.5). Spectra demonstrate the presence of calcite in all cases along with aragonite (redtail parrotfish) and monohydrocalcite (bonefish, checkered puffer, and redtail parrotfish). Intense hydration peaks (at ~3300 and ~1630 cm^{-1}) indicate the presence of a hydrous phase in all samples, partly due to monohydrocalcite, but probably also due to hydrous amorphous carbonates (see Fig. 3.5). Peaks at 3702 cm^{-1} are due to brucite (see Fig. 3.8), while those at ~1050 cm^{-1} are due to phosphate, and those at 1385 cm^{-1} are due to nitrate contamination of KBr pellets. See text for further details. Inset at top left are the key peak positions that identify the various phases relevant here.*

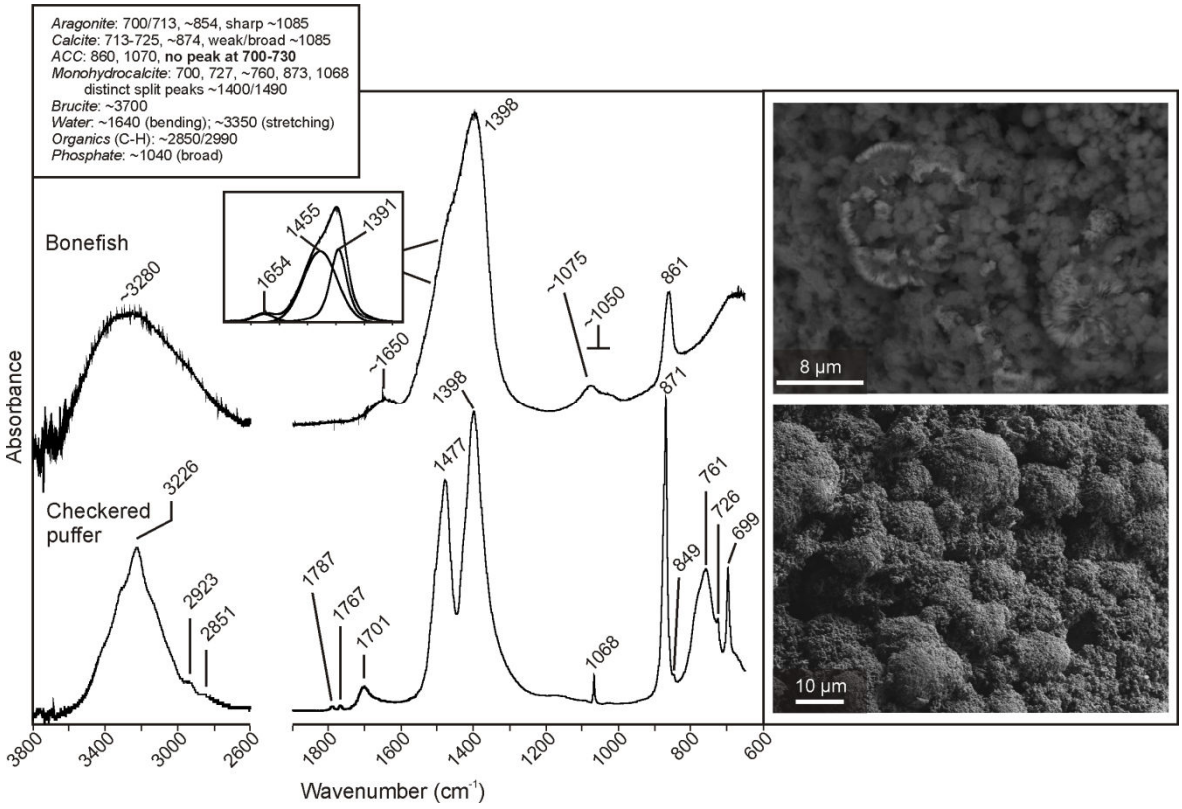

Figure 3.5 *Variations of ATR-FTIR spectra for carbonates produced by bonefish and checkered puffer (compare with Fig. 3.4). SEM images on the right show corresponding crystal morphologies (top image is backscatter electron; bottom is secondary electron). These spectra indicate that carbonates produced by bonefish can be dominated by amorphous carbonates at the point of excretion (note the lack of v_4 peak), which are presumably represented by the more magnesium-rich (i.e., darker in BSE image) nanospheres. Inset spectrum shows results of peak deconvolution for the main CO_3^{2-} v_3 peak – component peaks are in good agreement with available data for ACC (Table 3.2). Precipitates produced by checkered puffer can be dominated by monohydrocalcite. Note the distinctive shape of water stretching peak at ~3200 cm^{-1} compared to that generated by amorphous bonefish carbonates. Monohydrocalcite appears to comprise spherical and lobate forms similar to those also documented for calcite produced by this species. Inset at top left are the key peak positions that identify the various phases relevant here.*

Infrared data, however, reveal little about the compositional and morphological properties of these hydrated amorphous carbonates. Salter *et al.* (2012) showed that amorphous carbonates produced by bluehead wrasse typically contain more than 95 mol% $MgCO_3$, and as such they are amorphous magnesium carbonates (or AMC). In contrast, Foran *et al*. (2013) showed that a different fish species produced magnesium-rich ACC. AMC has not previously been characterised using FTIR spectroscopy, but Loste *et al*. (2003) find little change in spectral patterns of ACC containing varying amounts of $MgCO_3$. It is thus possible that spectral patterns of ACC and AMC will be similar, and it is necessary to utilise visual observations and compositional data to reveal more details regarding these amorphous phases.

The amorphous phase produced by checkered puffer was not readily apparent using SEM; it is possible that it was not present in the pellets that were examined, or that it was present but hidden from view inside hollow crystals (as shown to be produced by this species in Chapter 2). However, examination of carbonates produced by keeltail needlefish and redtail parrotfish reveals that some pellets comprise, and can even be dominated by, a phase that lacks any definable form, being similar in appearance to AMC produced by bluehead wrasse (see Fig. 2.5 A). This phase presumably represents the amorphous carbonate detected using FTIR, and compositional analyses show that it is magnesium-rich (typically containing > 70 mol% $MgCO_3$; *i.e.*, lower than in AMC from bluehead wrasse). It is thus best referred to as Ca-rich AMC. In contrast, precipitates produced by bonefish do not contain a morphologically similar phase, but instead contain abundant nanospheres (see Fig. 2.4 G) that are morphologically similar to some previously documented ACC (Aizenberg *et al*., 1996; Tlili *et al*., 2001; Ajikumar *et al*., 2005; Foran *et al*., 2013). Backscatter electron images reveal that nanospheres contain a greater abundance of lighter elements than associated crystalline phases (*i.e.*, they appear darker; Fig. 3.5), and compositional analyses confirm that this is due to higher magnesium concentrations, typically 30–40 (but up to 57) mol% $MgCO_3$. Their size and morphology suggests that nanospheres probably represent the amorphous phase produced by bonefish, and their composition indicates they are Mg-rich ACC. It is interesting to note that spheres present alongside nanospheres are commonly only partially formed, usually isolated from other spheres, and are surrounded internally and externally by nanospheres (Fig. 3.5), thus giving the appearance of spheres crystallising from amorphous nanospheres.

3.4.2.2 Phosphates

In addition to carbonate vibrations, several samples generate a broad peak (of varying intensity) centred over ~1050 cm^{-1} (Fig. 3.4; bonefish, checkered puffer, and redtail parrotfish), in some cases accompanied by a peak centred over ~550 cm^{-1}. Vibrations at these wavelengths are attributed to phosphate, and the particularly intense peaks associated with bonefish precipitates are in good agreement with previous compositional analyses that indicate relatively high phosphorus concentrations in these samples (Chapter 2). Phase determination of this phosphate is hampered by

the loss of signal quality at wavenumbers lower than about 500 cm^{-1}, but peaks lack the well-defined sharp maxima that are typical of well-crystallised apatite-type phases, and their broad character is more typical of amorphous calcium phosphate (Skrtic *et al*., 2003; Combes and Rey, 2010). Where phosphate is associated with amorphous carbonates (*e.g.*, Fig. 3.5), it is presumably present either as discrete amorphous calcium phosphate (ACP), or as a single amorphous phase in which it is co-precipitated with carbonate. It is possible that amorphous phases represent the only phosphate 'sink' in these samples, although it is worth noting that samples containing only crystalline phases can also generate high intensity phosphate peaks of similar shape to those shown here (*e.g.*, Chapter 7), suggesting that it may be retained in those samples either as a discrete ACP phase, or as ions adsorbed on crystal surfaces.

3.4.2.3 Organic phases

As with ellipsoidal Mg calcite, some samples comprising spheres, dumbbells, and ACC/AMC generate weak vibrations at about 2930 and 2850 cm^{-1}, indicating the presence of a minor organic component. However, many samples do not generate these peaks (Figs. 3.4 and 3.5), indicating that the presence and abundance of organic matter varies among samples. It is thus difficult to explain the presence of organic matter as a result of it being trapped within precipitates or adsorbed at their surfaces (samples would probably generate more consistent peaks if this was the case). Instead it is likely that organic phases detected here are due to remnants of mucosal coatings retained in pellets following sample preparation.

3.4.3 Spectra generated by precipitates that lack definable form (Category 3)

Carbonates excreted by bluehead wrasse, slippery dick, and beaugregory were shown in Chapter 2 to be dominated by AMC along with a relatively minor quantity of rhombohedral, dumbbell-shaped, and spherical low-Mg calcite. FTIR analyses of samples produced by the first two of the species (beaugregory samples were not analysed), confirm the amorphous nature of these carbonates, and also reveal that they are strongly hydrated (Fig. 3.6). Samples that generate weak bands at ~711 cm^{-1} probably contain a minor amount of calcite, as further evidenced by the

emergence of a weak band at ~872 cm^{-1} (Fig. 3.6; top spectrum), while other samples can generate more well-defined calcite peaks, indicating a greater abundance of this phase in some cases (Fig. 3.6; bottom spectrum). Note that the main component peaks of the ν_3 carbonate vibration are centred over 1460 and 1415 cm^{-1} (Fig. 3.6; inset), although the higher wavenumber peak position is variable – it can be centred of wavenumbers as high as 1512 cm^{-1} (Fig. 3.7). Unlike equivalent peaks generated by ACC from bonefish, these component peaks differ considerably from data available for ACC (Table 3.2), possibly due to the substantially higher magnesium contents.

As with Category 2, Category 3 carbonates produced by bluehead wrasse and slippery dick can generate broad peaks assigned to phosphate (these are typically weak), and peaks associated with organic compounds that are of varying, but always low, intensity (Fig. 3.6).

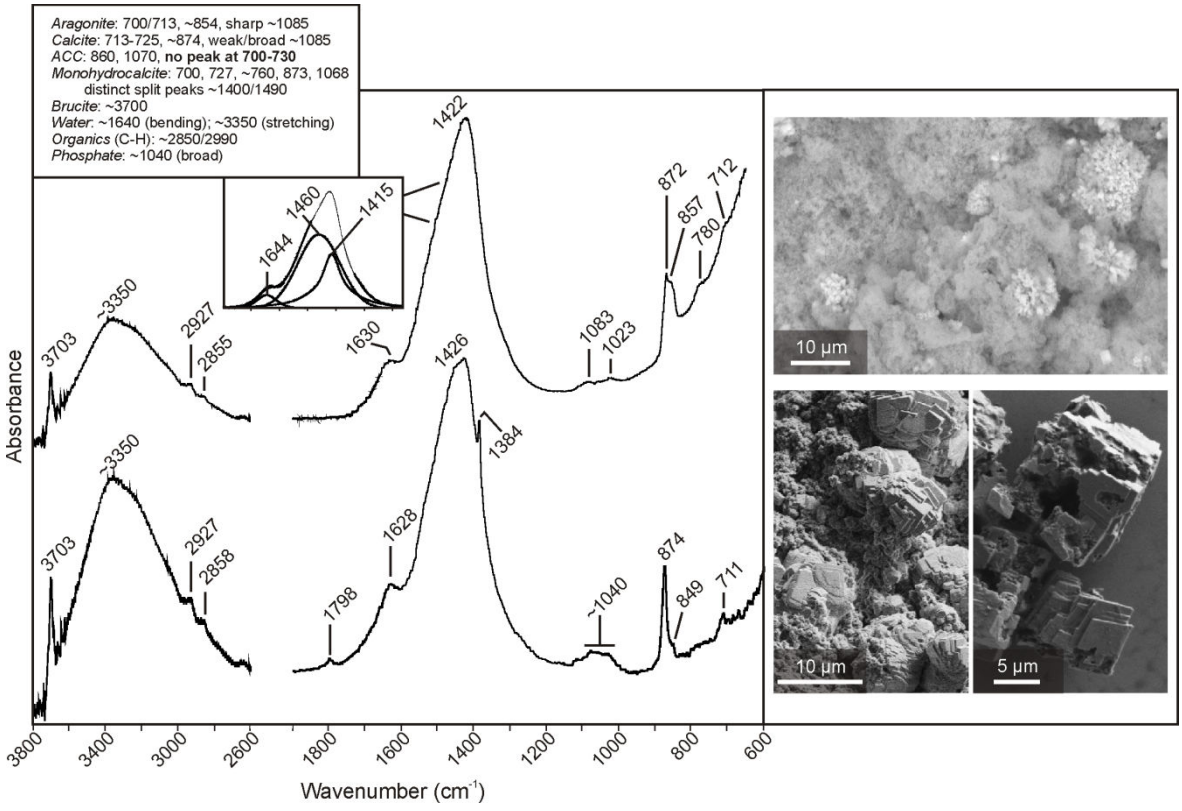

Figure 3.6 *ATR-FTIR and transmission FTIR (lower wavenumbers of bottom spectrum) spectra for carbonates produced by bluehead wrasse (those produced by slippery dick generate similar spectra). SEM images to right show corresponding crystal morphologies; both samples being dominated by Mg-rich precipitates lacking definable form (darker phase in BSE image; top), but the bottom sample containing a greater abundance of rhombohedral crystals. The top spectrum indicates the sample is dominated by amorphous carbonate (note ν_4 limited to weak hump, and relatively broad ν_2 shifted to 857 cm^{-1}), whereas the bottom spectrum indicates a greater abundance of crystalline precipitates. Note also the presence of brucite (peaks at 3703 cm^{-1}), phosphate (broad peaks at ~1040 cm^{-1}, and nitrate contamination of the KBr pellet (peaks at 1384 cm^{-1}). Inset at top left are the key peak positions that identify the various phases relevant here.*

3.4.4 Peak deconvolution: H–O–H bending and the CO_3^{2-} ν_3 asymmetric stretch

Several spectra show a weak shoulder on the carbonate ν_3 peak centred over approximately 1640 cm^{-1}. This peak is assigned to water bending mode, and its position can be used as an indicator of bond strength, and thus the state in which water occurs. However, because it appears as a shoulder rather than a discrete peak it is necessary to resolve individual peaks that make up the carbonate ν_3 peak and the H–O–H bending peak using peak deconvolution software. This is done using ATR-FTIR spectra to ensure the water vibrations are representative of water associated only with fish-derived carbonates and not background contamination. Because the carbonate phases identified in the above sections are reasonably well-characterised using ATR-FTIR (Tables 3.1–3.3), it is also useful to compare the resulting component carbonate ν_3 peak positions with documented values. Results of these analyses are shown in Fig. 3.7.

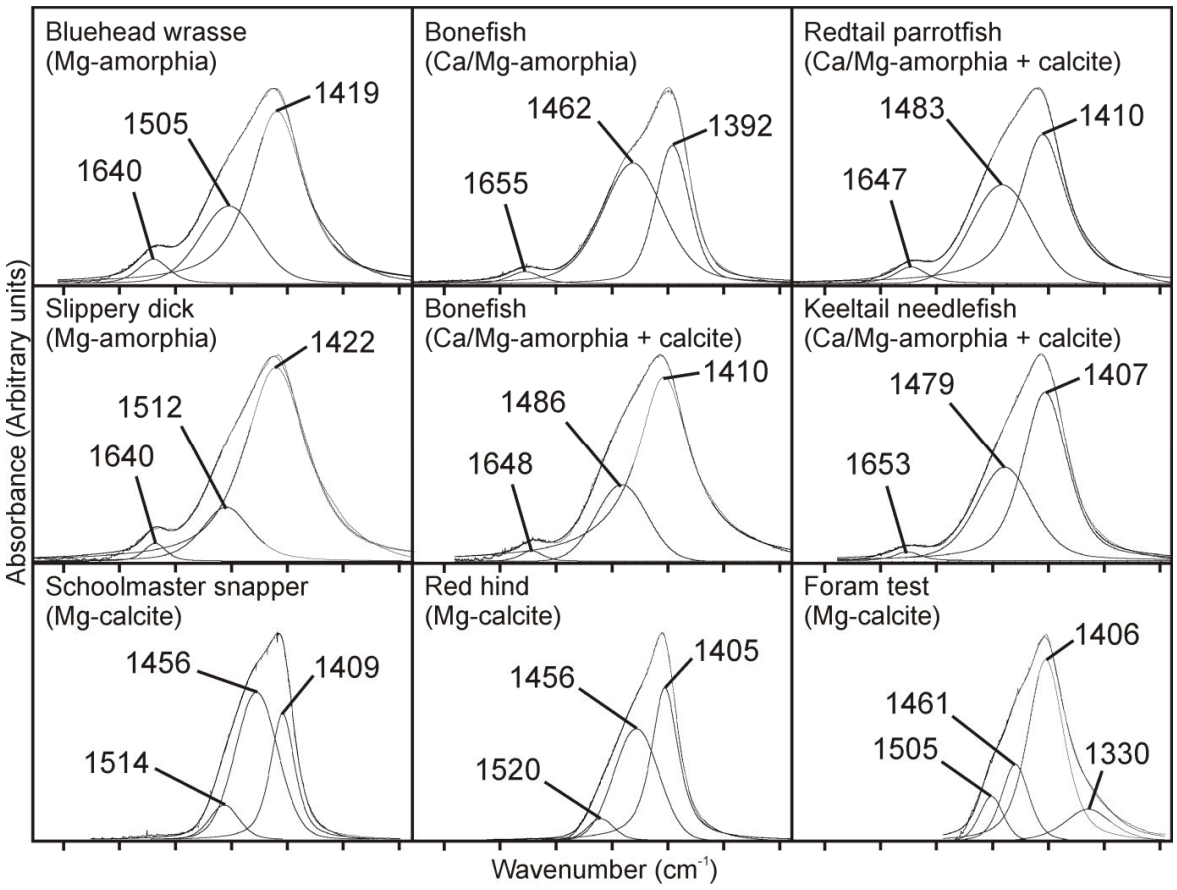

Figure 3.7 *Component peaks of carbonate ν_3 asymmetric stretching modes (1390–1500 cm^{-1}), water bending modes (1640–1655 cm^{-1}), and presumed combination modes (bottom three spectra only; 1330 and 1505–1520 cm^{-1}) derived from peak deconvolution based on ATR-FTIR spectra. Top six boxes show peaks corresponding to amorphous carbonates or mixed amorphous carbonates and calcite. Water bending peaks centred over wavenumbers greater than 1640 cm^{-1} indicate that water is more strongly bonded than is typical in liquid states and must occur primarily as a solid phase associated with amorphous carbonates. The arrangement of component ν_3 peaks for these spectra is complicated by the presence of multiple phases and is discussed in the main text. Fish-derived carbonates dominated by a single phase (Mg calcite; bottom row) generate ν_3 peaks that can exhibit variations in overall shape but typically comprise three component peaks consistently centred over similar wavenumbers. These component peaks are in good agreement with biogenic Mg calcite of other origin (e.g., foram test; bottom right). Overall peak shape is determined by variations in relative intensities of component peaks centred over ~1455 and ~1405 cm^{-1}, such variation being tentatively attributed to differences in degree of crystallinity.*

3.4.4.1 Amorphous carbonate ν_3 modes

For magnesium-rich ACC produced by bonefish, component carbonate ν_3 peaks are in good agreement with published data for ACC and Mg-rich ACC (Fig. 3.7; Table 3.2). Corresponding peak positions for AMC produced by slippery dick and bluehead wrasse, however, are shifted to higher wavenumbers than previously documented for ACC; a disparity that is probably due to high magnesium concentrations (typically > 95 mol% $MgCO_3$) in AMC. Böttcher *et al*. (1997) document increasing wavenumbers for the ν_3 peak with increasing magnesium content in

crystalline phases, and it is possible that amorphous phases follow a similar trend, although Loste *et al*. (2003) observe the opposite in their study of Mg-rich ACC. However, in the latter study, maximum magnesium content was 47 mol%, and the resulting CO_3^{2-} response to infrared may have been different to that in AMC. Peaks assigned to the carbonate ν_3 mode for samples containing crystalline and amorphous phases (*e.g.*, those produced by keeltail needlefish and redtail parrotfish) are centred over approximately 1410 and 1480 cm^{-1}, and are thus approximately intermediate between AMC and Mg-rich ACC. This is in good agreement with the idea that ν_3 peaks shift to higher wavenumbers with increasing magnesium content (see compositional data in section 3.4.2.1), but this is suggested with the caveat that the presence of crystalline carbonates (*i.e.*, with overlapping ν_3 peaks) may hamper interpretation of these data.

3.4.4.2 Calcite ν_3 modes

The ν_3 peak generated by ellipsoidal Mg calcites occurs in two asymmetric forms; one that is reasonably broad with a rounded peak, and one that is more angular with a relatively sharp peak. The latter peak type is similar in shape to the ν_3 peak generated by foram-derived Mg calcite, with the exception that the slope towards lower wavenumbers is steeper for fish-derived Mg calcite. Peak deconvolution indicates that for all of these fish-derived Mg calcites ν_3 peaks are a composite of three component peaks positioned at approximately 1405, 1455, and 1515 cm^{-1} (Fig. 3.7). Component peaks resolved for foram-derived Mg calcite are in good agreement (1406, 1461, and 1505 cm^{-1}), with the exception of an additional peak centred over 1330 cm^{-1}. In both cases, ν_3 maximum intensity is centred over higher wavenumbers than has been documented for calcite using ATR-FTIR (Table 3.1), but assuming the findings of Böttcher *et al*. (1997) apply to ATR-FTIR as well as transmission FTIR, this anomaly can be explained by high magnesium contents in these samples.

The difference between rounded and sharper ν_3 peaks for fish-derived Mg-calcite is caused by variations in the relative intensities of component peaks (Fig. 3.7; schoolmaster snapper vs. red hind). For example, the strongest component in rounded ν_3 peaks is the peak centred over

1455 cm^{-1}, whereas the strongest component in sharper ν_3 peaks is centred over 1405 cm^{-1}. The peaks close to 1405 cm^{-1} are most consistent with previously published values for the ν_3 mode of calcite, and are assigned to Mg calcite. The peaks at approximately 1515 cm^{-1} are generally of low intensity and may be due to combination of lattice and internal modes. For example, a possible combination might be:

$$(2 \times 215\ cm^{-1}) + (1085\ cm^{-1})$$

where 1085 cm^{-1} corresponds to the position of ν_1, and 215 cm^{-1} is an estimated position of the lattice translation mode – Gillet *et al*. (1996) demonstrate that the infrared-active lattice translation mode for calcite is centred over approximately 227 cm^{-1} when measured with transmission FTIR, so for ATR-FTIR, which typically yields lowers wavenumbers, value of 215 cm^{-1} is within reason. Peaks centred over approximately 1455 cm^{-1} are more difficult to assign, but it is possible that they are related to the degree of crystallinity. For example, foram-derived Mg calcite is well crystallised compared to fish-derived Mg calcite (as indicated by intensity ratios of ν_2/ν_4; Fig 3.2), and it generates the weakest peak centred over 1455 cm^{-1} (Fig. 3.7). Within fish-derived carbonates, Mg calcite produced by schoolmaster snapper appears to have a lower degree of crystallinity than that produced by red hind (Figs. 3.2 and 3.3), and it accordingly generates the strongest peak centred over 1455 cm^{-1}. It is worth mentioning, however, that Luzinova *et al*. (2011) use ATR-FTIR spectroscopy to identify a similar triplet of component ν_3 peaks generated by coccolithophore-derived calcite and authigenic deep water Mg calcite. Although those authors do not assign peaks to specific vibrational modes, they do note differences in the relative intensities of component peaks accompanied by differences in magnesium content and ^{13}C concentrations. Degree of crystallinity is therefore not the only possible explanation for observed variations in ν_3 component peak intensities, and further work is necessary to clarify these relationships.

3.4.4.3 Water bending modes

The water bending vibration generated by the above described samples is typically centred over 1640 cm^{-1} in AMC (Fig. 3.7; bluehead wrasse and slippery dick), and 1647–1655 cm^{-1} in samples

comprising Mg-rich ACC and/or Ca-rich AMC (Fig. 3.7; bonefish, redtail parrotfish, and keeltail needlefish). In all cases the positions of these peaks are centred over wavenumbers greater than those associated with liquid water (*i.e.*, 1625–1636 cm^{-1}), indicating that water does not predominantly occur as fluid inclusions. The higher wavenumbers associated with calcium-containing amorphous phases possibly indicates water is most strongly bonded in these phases. The water bending shoulder on the carbonate ν_3 peak generated by samples comprising monocrystalline ellipsoids or small dumbbells is very weak and cannot be resolved with precision.

3.4.5 Non-carbonate phases

Finally, many spectra generated by fish-derived carbonates exhibit a sharp peak of varying intensity at wavenumbers ranging from 3700 to 3703 cm^{-1}. This peak is generated by samples produced by most species, but is not present in all samples analysed for each species. However, it is particularly prominent in samples produced by keeltail needlefish and also in some samples produced by bluehead wrasse and slippery dick. This pattern of occurrence is not dissimilar to that of a platy Mg-rich phase observed in SEM images (Fig. 3.4; and Chapter 2); the identity of which has remained elusive thus far.

Assuming the sharp peak at ~3700 cm^{-1} does relate to this platy phase, previous suggestions as to its identity (dypingite and nesquehonite; see Chapter 2) can be ruled out based on OH^- stretching vibrations of those phases being centred over lower wavenumbers (Table 3.2). Other magnesium carbonates, such as hydromagnesite and artinite, can be similarly eliminated. The only documented Mg-rich phase that generates a sharp OH^- stretching band at ~3700 cm^{-1} is brucite, $Mg(OH)_2$ (Ahlrichs, 1968; Frost and Kloprogge, 1999; Schroeder, 2002), which can exhibit platy rosette-like morphologies similar to those described here (Nothdurft *et al*., 2005; their Fig. 2 B). Additional bands generated by this phase are described elsewhere as a broad peak over the OH^- stretching region of water (~3300 cm^{-1}) and very weak MgO translational modes at 627, 565, and 440 cm^{-1} (Frost and Kloprogge, 1999). The former is present in all spectra for fish-derived carbonates, and may include some contribution from brucite (although it is noted that the intensity of these peaks

does not vary with the intensity of peaks at ~3700 cm^{-1}, indicating that most water is probably associated with carbonate phases). With regard to translational modes, most samples that generate a sharp band at ~3700 cm^{-1} also generate a broad hump at ~565 cm^{-1}, whereas this region is typically flat in samples that do not generate a peak at ~3700 cm^{-1} (Fig. 3.8). This is in good agreement with previously obtained spectra for brucite. The band at 627 cm^{-1} is not observed here, but it can apparently be very weak (Frost and Kloprogge, 1999) and may not always be evident, whereas the band at 440 cm^{-1} may be obscured in this study due to spectra being rather noisy at wavenumbers lower than about 500 cm^{-1}. It is thus with some confidence that the platy magnesium-rich phase present in varying, but usually minor, quantities in fish-derived carbonates is identified as brucite.

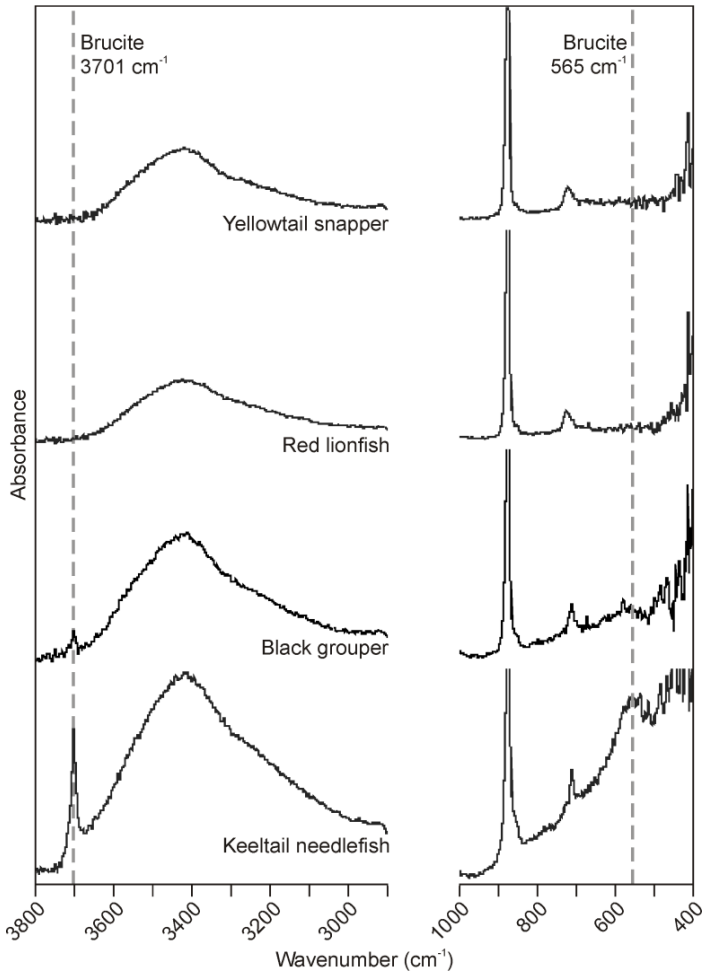

Figure 3.8 *Transmission FTIR spectra confirming the presence of brucite, $Mg(OH)_2$, in some fish-derived carbonates. The sharp peak at 3701 cm^{-1} for precipitates produced by keeltail needlefish, and a similar but less intense peak for precipitates produced by black grouper, is assigned to the OH^- stretching mode of brucite. Both of these samples also generate a broad peak centred over ~565 cm^{-1}, which is assigned to an MgO translation mode. In some samples neither peak is observed (e.g., those produced by red lionfish and yellowtail snapper, shown here), suggesting brucite is not a ubiquitous phase.*

3.5 DISCUSSION

The results of infrared spectroscopy support findings of previous studies (Perry *et al*., 2011; Salter *et al*., 2012) by showing that fish-derived carbonates in their excreted form mostly comprise crystals that have a calcite structure, with some samples also containing small quantities of aragonite. Data also confirm the presence of hydrated amorphous phases, not only as AMC in samples produced by species such as bluehead wrasse (Salter *et al*., 2012 – see Chapter 2), but also as Mg-rich ACC in samples produced by species such as bonefish; the latter probably taking the form of nanospheres described by Salter *et al*. (2012). Minor quantities of monohydrocalcite and brucite are also identified for the first time; the former seemingly restricted to samples that also comprise amorphous phases, whereas the latter sporadically accompanies any carbonate phase. In addition, the identification of monocrystalline ellipsoids and small dumbbells as Mg calcite is verified, but they are shown either to be crystallised to a very low degree, or to be accompanied by a discrete amorphous phase that remains elusive in SEM images. Water is also associated with ellipsoids and small dumbbells, but the vibrations it generates are weak and its mode of occurrence is therefore not clear. These findings and their implications are further discussed below.

3.5.1 Previously unrecognised phases and their likely post-excretion fates

3.5.1.1 Amorphous carbonates

The presence of hydrated amorphous carbonates is shown here to be more extensive than previously thought, occurring as a significant component in the excreted products of at least 6 out of 16 species. In addition, at least one other species investigated in this volume produces AMC (beaugregory; see Chapter 2), and at least three others can produce Mg-rich ACC in certain situations (see Chapter 4), and it is thus known that a proportion (in some cases nearly all) of the carbonates produced by at least 10 out of 21 Caribbean fish species can be amorphous. As discussed in Chapter 1, such phases are usually considered to be highly unstable, and their prolonged existence following excretion is unlikely. Whether they dissolve or crystallise to more stable forms is considered further in Chapter 7. However, if their fate is dissolution, a major

implication of the findings of the present study could be that fish-derived carbonates undergo a substantial and potentially rapid reduction in volume prior to, or during, incorporation within surface sediments.

3.5.1.2 Monohydrocalcite

Monohydrocalcite is rarely reported as a sedimentary mineral, and is usually restricted to minor components in lacustrine (Krumbein, 1975; Taylor, 1975) and polar marine (Dahl and Buchardt, 2006) settings. Its growth can be encouraged in solutions containing high concentrations of inhibitors to the formation of calcite and aragonite (*e.g.*, Mg^{2+} or PO_4^{3-}; Kitano *et al*., 1979), and its formation in the piscine gut, which typically has high Mg^{2+}/Ca^{2+} ratios compared to seawater (*e.g.*, ~40–100 in the piscine gut compared with ~5 in seawater; Wilson *et al*., 2002) is therefore readily explained. Whether it forms as a result of direct precipitation or alteration of initial amorphous phases is less clear, but its presence only in samples produced by species that also produce amorphous phases suggests the latter could be true. Indeed, Rodriguez-Blanco *et al*. (2012) show that monohydrocalcite can form from Mg-rich ACC precursors.

With regard to its preservation potential as a sedimentary component, monohydrocalcite is considered to be metastable with respect to anhydrous carbonate phases in surface marine conditions, having a solubility product (log K_{sp}) of -7.60 (Hull and Turnball, 1973). It is thus considerably more soluble than Mg calcite, but probably stable enough to preclude rapid dissolution (see Chapter 1). However, the high solubility of monohydrocalcite means it readily dehydrates and alters to more stable anhydrous phases in aqueous environments (Taylor, 1975), with resultant phases controlled by solution composition (Yagi and Fukushi, 2011). Specifically, monohydrocalcite is found to transform to aragonite in PO_4^{3-}-free solutions where Mg^{2+} is present (the latter inhibits calcite formation), but to calcite when low concentrations (*e.g.*, 10 μM) of PO_4^{3-} are present (PO_4^{3-} inhibiting aragonite formation and over-riding the inhibitory effect Mg^{2+} has on calcite formation). It is noted here that, in some cases, phosphate is present at elevated concentrations in fish-derived samples containing monohydrocalcite. Although the source of this

phosphate is not known (but see preliminary considerations in Chapter 4), its presence in association with monohydrocalcite is perhaps not surprising; it is known that phosphate will readily adsorb to the surface of monohydrocalcite. It is this process that inhibits its transformation to aragonite (Yagi and Fukushi, 2011), and in the event that surface seawater concentrations of PO_4^{3-} (typically < 0.5 μM) are too low to inhibit transformation of monohydrocalcite to aragonite, it may therefore be the case that inhibition will be controlled by the composition of excreted forms. Because Mg^{2+} and PO_4^{3-} inhibit the formation of calcite and aragonite, their presence will likely retard transformation rates, but monohydrocalcite is nevertheless predicted to alter to anhydrous phases eventually (Rodriguez-Blanco *et al.*, 2012). It is thus likely that fish-derived PO_4^{3-}-rich monohydrocalcite will eventually alter to calcite (or Mg calcite if the original phase contains $MgCO_3$; this has yet to be determined) in sub-tropical platform-top sedimentary environments, whereas PO_4^{3-}-free monohydrocalcite may transform to aragonite. Such potential post-excretion transformation may mean that resulting calcite and/or aragonite are in equilibrium with seawater, and will thus represent reasonably stable phases.

3.5.1.3 Brucite

Brucite is most common in nature as an alteration product of periclase (MgO) in metamorphic rocks, where it usually occurs in association with other Mg-rich minerals such as hydromagnesite, dolomite, serpentinite (Frost and Kloprogge, 1999). However, it also occurs as a rare phase in marine settings, where it has been observed in deep-sea hydrothermal vent structures (Kelley *et al*., 2001) and in shallow settings in association with skeletal carbonates of living specimens of some corals (Nothdurft *et al*., 2005) and red alga (Schmalz, 1965). Because surface seawater is undersaturated with respect to brucite (Morse and Mackenzie, 1990), it is necessary to invoke unique chemical environments to explain its presence in the latter two examples, where it has been attributed to microbially-induced microenvironments characterised by high pH, low pCO_2, and high Mg^{2+}/Ca^{2+} ratios (Nothdurft *et al*., 2005). The formation of brucite in association with piscine gut carbonates is thus readily explained given the elevated pH levels (up to 9.2) and high concentrations of Mg^{2+} (up to 200 mM) reported for precipitating fluids (Wilson *et al*., 2002).

Despite these occurrences of brucite, it is an exceedingly rare mineral phase in marine sediments and is also absent from submerged Holocene corals that are equivalent to living specimens containing brucite (Nothdurft *et al*., 2005). This suggests that brucite is not typically preserved for long durations when exposed to open marine conditions, and it is likely to be removed from excreted fish-derived carbonates via dissolution. However, because it typically occurs as a minor subsidiary phase (see Chapter 2), its loss will not greatly reduce the volume of excreted precipitates entering surface sedimentary environments.

3.5.2 Implications for the stability of Mg calcite due to low crystallinity

As with the phases discussed in section 3.5.1, the post excretion fate of fish-derived Mg calcite is investigated using empirical data in Chapter 7. However, it is worth briefly mentioning here the potential implications of poor crystallinity with respect to the stability of this phase. It is useful first to consider the meaning of the term "crystallinity". Bassinot *et al*. (2004) define crystallinity as a measure of how perfect a crystal lattice is, with well crystallised calcite comprising a single-domain, 'lattice-perfect' crystal, and poorly crystallised calcite comprising numerous 'crystallite' sub-domains, each having a perfect lattice structure that is slightly misaligned with respect to its neighbour.

The above definition means that two particles of similar size but crystallised to different degrees will have different effective crystal sizes (*i.e.*, the individual sub-domains of a poorly crystallised particle being smaller than the single domain of a well crystallised particle). Where poor crystallinity results in crystallite size being less than 1 μm, broad diffraction peaks are generated in X-ray diffraction patterns (*e.g.*, Chapter 2). Several studies have employed the full width at half maximum intensity (FWHM) of the d_{104} calcite peak in X-ray diffractograms as a proxy for degree of crystallinity (Bonneau *et al*., 1980; Gehlen *et al*., 2005), where it has been shown that fresh foram tests can have poor crystallinity, but progressively more dissolved tests have increased crystallinities (*i.e.*, diffraction peaks become narrower). These data have been interpreted as an indication that the most poorly crystalline domains are the first to dissolve, which is not surprising

given that the associated small crystallites will have higher surface energies than well crystallised domains, and will therefore be less stable. Confirmation in the present study that many fish-derived carbonates are poorly crystallised thus indicates that they are likely to be less stable than if they were well crystallised.

3.5.3 Crystalline phases: excreted products or artefacts of preparation?

As discussed in Chapter 1, amorphous carbonates are usually considered to be highly unstable and will rapidly dissolve or crystallise to more stable phases upon removal from, and even within, their environment of formation (Addadi *et al*., 2003; Foran *et al*., 2013). Because several fish species are now known to excrete abundant amorphous carbonates (as demonstrated in the present study and in the recent work of Foran *et al*.; 2013), and because such phases have the potential to rapidly crystallise, it was necessary to test whether crystalline phases documented in earlier work (Perry *et al*., 2011; Salter *et al*., 2012) are naturally occurring products of fish, or whether they are artefacts of sample preparation, wherein prolonging soaking in sodium hypochlorite could have induced crystallisation of initially amorphous phases.

Results of the present study, in which sample preparation involved a 6 hour soaking stage in sodium hypochlorite (as described in Chapter 2), specifically show that some samples primarily comprise crystalline phases, whereas others are dominated by amorphous phases, and numerous samples comprise a mixture of both. In the first instance this would appear to indicate that crystalline phases are not artefacts of sample preparation; if they are, questions arise as to why amorphous phases were selectively crystallised in some samples and not others.

However, it is perhaps possible to explain this by considering the compositions of 'preserved' amorphous phases. Magnesium has been invoked as a potential stabilising agent in ACC (Addadi *et al*., 2003; Loste *et al*., 2003), and its presence in all amorphous phases documented herein may have inhibited their crystallisation. That said, the typically very high magnesium contents of monocrystalline ellipsoids (Chapter 2) suggests any potential amorphous precursor would also have had a high magnesium content (*e.g.*, Long *et al*., 2011). Amorphous carbonates produced by

bonefish (which typically contain 30–50 mol% $MgCO_3$) are therefore unlikely to be preferentially preserved over, for example, amorphous carbonates that might have been produced by schoolmaster snapper due to the inhibitory effect of magnesium alone. However, AMC (*e.g.*, produced by bluehead wrasse) typically contains more than 95 mol% $MgCO_3$. The stability of this phase is not clear (its existence has rarely been documented), but its composition precludes extensive crystallisation as $CaCO_3$. Instead it is possible that these phases might crystallise as $MgCO_3$ phases, but these rarely form at Earth surface conditions, in part due to the high energy of hydration of magnesium (Morse and Mackenzie, 1990). It is thus possible that AMC was preferentially preserved during sample preparation due to its Mg-rich composition inhibiting crystallisation.

The potential selective preservation of ACC produced by bonefish requires further explanation. This phase differs from most other excreted carbonates because it is consistently associated phosphate. The only other fish-derived precipitation products consistently found to contain elevated phosphate concentrations are nanospheres produced by great barracuda and black grouper, which are also ACC (see Chapters 2 and 4). Phosphate is thought to act as a stabilising agent when present in amorphous carbonates (Raz *et al*., 2002; Foran *et al*., 2013), and it is thus difficult to rule out the possibility that ACC produced by these species was preferentially preserved during sample preparation because of its presence. However, pellets produced by bonefish can be variable with respect to their component particles; some being dominated by ACC, some by crystalline spheres, and others by an admixture of the two. If crystallisation was induced during sample preparation, it is difficult to explain why it proceeded to completion in some pellets, but hardly at all in others. Instead it is possible that crystallisation (possibly from an initially amorphous phase) took place in the piscine gut or in the short period between excretion and sample collection; its extent perhaps varying according to the amount of time spent in each environment.

In summary, the present study clearly demonstrates that amorphous carbonates can be preserved when prepared using the approach employed in previous studies (Perry *et al*., 2011; Salter *et al*.,

2012), but also that this preservation might be facilitated only because of specific factors inhibiting crystallisation (in addition to the above-mentioned factors, this might include the fact they are hydrous; Addadi *et al*., 2003). The question that remains is whether other carbonates might have been excreted as amorphous phases with no stabilising agents and/or as anhydrous ACC, and whether such phases might have crystallised to, for example, monocrystalline ellipsoids during sample preparation. To test this rigorously would require analysis of samples immediately after excretion and with minimal cleaning (*e.g.*, the approach adopted by Foran *et al*., 2013), but analytical apparatus necessary to facilitate this was unfortunately not available in the field study area. Clearly such work must be carried out in the future to fully understand the form of carbonates excreted by marine fish.

Available data from other studies (Chapter 7 of this thesis), however, do provide strong evidence that the crystal forms described by Salter *et al*. (2012) are representative of forms that are ultimately incorporated within marine sediments. Specifically, carbonates produced by several fish species were collected following excretion and held in seawater and pore water environments without exposure to non-natural conditions for three months. Following these exposures, samples were cleaned and dried using the approach described in Chapter 2, and subsequent analyses revealed, in brief, that crystalline phases were morphologically and compositionally almost identical to those described at the point of excretion (Salter *et al*., 2012), whereas all 'known' amorphous phases (*i.e.*, those discussed in the above paragraphs) were rapidly lost to dissolution. The wholescale dissolution of 'known' amorphous carbonates suggests that any potential 'unknown' amorphous phases might also have dissolved rather than crystallised. Nevertheless, if such phases did crystallise (*e.g.*, to form monocrystalline ellipsoids), the process almost certainly would have taken place in seawater or pore water; prolonged preservation of ACC in seawater is unprecedented, and as such it is highly unlikely that any potential crystallisation of ACC was induced during sample preparation three months after precipitates were initially excreted. To summarise the interpretation of observations made in Chapter 7, it appears that crystalline forms described by Salter *et al*. (2012) were either 'as excreted', or were the result of rapid crystallisation

of excreted ACC up on exposure to seawater; in either case it is unlikely that soaking in sodium hypochlorite resulted in alteration of excreted forms.

3.5.4 Water and organic phases

Data presented herein indicate that both water and organic phases are common components of excreted and cleaned fish-derived carbonates. The organic component typically generates weak C–H stretching bands over wavenumbers between about 2850 and 3000 cm^{-1}. However, there is no obvious relationship between the presence of these phases and crystal morphology and/or producing species, and in many cases organic matter appears to be absent. This sporadic pattern of occurrence is not suggestive of abundant organic matter being trapped within hollow crystals (*e.g.*, as suggested by Walsh *et al.*, 1991). Instead, it may indicate the presence of residual organic matter left after cleaning, which might rule out ideas regarding organic matter degradation taking place inside crystals and promoting dissolution from within (as discussed in Chapter 1).

The presence of water is revealed in all samples by the generation of O–H bending and stretching peaks; its consistent presence where organics are absent precluding the possibility that it is primarily associated with organic matter. Where amorphous carbonates and monohydrocalcite are present, O–H vibrations tend to be strong, indicating that these are hydrous phases. The precise position of water bending bands can be used to interpret the state of water in these precipitates. For example, ATR-FTIR spectroscopy typically generates bending bands centred over 1595 cm^{-1} for water in vapour form, shifting to higher values of 1625–1636 cm^{-1} for water in liquid form, owing to stronger bonding associated with this phase (Grdadolnik, 2002; Frost and Palmer, 2011). Water bound within a crystal lattice is typically more strongly bonded than water in liquid form and consequently generates bands usually centred over even higher wavenumbers. The precise wavenumber can fall anywhere within a large range and will depend on the mode of water incorporation and the size and charge of cations in the crystal lattice (Falk, 1984). Strong bonding of water in the crystal lattice is well illustrated in the spectrum relating to monohydrocalcite produced by checkered puffer, which generates a water bending peak centred over 1701 cm^{-1}. The

water bending band for carbonates containing an amorphous phase is typically between 1640 and 1655 cm^{-1}, indicating stronger bonding than in liquid water and being in good agreement with existing data for similar phases (Table 3.2).

Water associated with 'anhydrous' crystalline phases is more difficult to interpret, either because water vibrations are obscured due to the presence of hydrous phases (*e.g.*, Fig. 3.4), or because water vibrations are too weak to properly resolve peak positions (*e.g.*, Fig. 3.3). Nevertheless, it is possible to say that monocrystalline ellipsoids are associated with water in some state that generates stronger peaks than the water associated with several other biogenic carbonates (Fig. 3.2), thus indicating water is present in greater abundance in fish-derived carbonates. Several possibilities exist as to the state in which water occurs in these crystals, some also proposed by Gaffey (1995) for echinoid Mg calcite, these including: i) strongly bonded in discrete hydrated carbonate phases, which are either not detectable using XRD (*e.g.*, ACC), or occur with crystallites that are too small or in abundances that are too low to be detected using XRD (*e.g.*, hydromagnesite); ii) a limited number of water molecules between crystallites, their restricted motion in such a position meaning their bonds vibrate at wavelengths closer to adsorbed rather than liquid water; iii) adsorbed on crystal surfaces; or iv) as fluid inclusions, either within hollow crystals, or within crystal lattice defects. The presence of water associated with these Mg calcite crystals is perhaps not surprising given their typically high magnesium contents. Lippmann (1960) proposed that Mg calcite might contain water owing to the difficulty with which Mg^{2+} dehydrates prior to incorporation within the crystal lattice; a theory supported by finding that biogenic Mg calcites exhibit an apparent positive correlation between water and magnesium contents (Mackenzie *et al*., 1983). Morse and Mackenzie (1990) suggest that such incorporation of water may partly explain the high solubility of Mg calcite, although this assertion has yet to be tested.

3.6 CONCLUSIONS

Data derived from FTIR spectroscopy confirms earlier findings (Chapter 2) that fish-derived carbonates are dominated by Mg calcite and minor aragonite; the former having poor crystallinity

and being hydrated to greater degree than other common sedimentary carbonates (at least in the case of monocrystalline ellipsoids). Organic matter trapped within these crystals, however, does not appear to occur in abundance, if at all. Carbonates produced by at least two fish species (bluehead wrasse and slippery dick) are further confirmed to be dominated by hydrated amorphous magnesium carbonates (AMC). In addition, new data indicate that Mg-rich hydrated amorphous calcium carbonate (ACC) nanospheres represent an abundant phase in the excreted products of some species (*e.g.*, bonefish), and that at least 6 fish species (out of 16 investigated) produce substantial quantities of ACC and/or AMC. Phosphorus detected in some samples examined in earlier studies (Chapter 2) is found to occur as phosphate, which is probably present as an amorphous phase co-precipitated with ACC, and/or as ions adsorbed to crystal surfaces. Finally, monohydrocalcite and brucite represent previously unrecognised phases in fish-derived carbonates; the former found to be produced by some species in association with ACC and calcite spheres, the latter sporadically occurring as aggregated rosettes of platy crystals.

These findings add relevance to questions regarding the post-excretion preservation of fish-derived carbonates (see Chapters 1 and 2), with possible implications as follows:

1. Amorphous phases will be highly unstable in seawater and will likely dissolve or mature to crystalline phases such as calcite (possibly involving monohydrocalcite as an intermediate phase);
2. Monohydrocalcite is metastable with respect to anhydrous phases in seawater and will likely dehydrate to form calcite or aragonite;
3. Seawater is undersaturated with respect to brucite, which will probably dissolve following excretion;
4. Poor crystallinity of Mg calcite is associated with high surface free energy, and thus probably increased solubility with respect to well crystallised Mg calcite. The presence of water may similarly increase solubility;
5. Phosphates may act to stabilise phases in which they are present.

These speculative suggestions are based on theoretical considerations and existing data from unrelated studies involving these phases. If correct, their consequences for fish-derived carbonates as sedimentary particles will be of varying significance. For example, wholescale dissolution of amorphous carbonates could substantially lower the volume of excreted precipitates that are incorporated within the surface sediment, whereas dissolution of brucite, which occurs as a volumetrically minor phase, will have little impact on total excreted volumes. In addition, if monohydrocalcite undergoes post-excretion alteration to calcite, the fact that this will take place in seawater (or porewater) should mean newly formed calcite is close to being in equilibrium with surrounding fluids, and may therefore represent a stable product. These proposed implications, which are yet to be tested empirically, will be investigated further in Chapter 7.

Chapter 4: Pilot study comparing the carbonate precipitation products of starved and fed fish

4.1 INTRODUCTION

Chapters 2 and 3 of this thesis provide a detailed assessment of the morphology, mineralogy, and chemical composition of fish-derived carbonates as they are excreted under experimental conditions; information which is used to consider the potential sedimentary significance and fate of fish-derived carbonates in shallow tropical marine settings. While it has been shown that the characteristics of these precipitates do not appear to be influenced by the presence of ingested skeletal carbonates in the intestine (Fig. 2.2 E), it is important to point out that all gut carbonates characterised to-date, whether or not associated with ingested skeletal fragments, were excreted at least 48 hours after the fish that produced them had last eaten. Moreover, no obvious organic faecal matter has been observed or reported to have been excreted concomitantly with carbonates that have been characterised up to now, suggesting that processes associated with active digestion (*e.g.*, enzyme production, nutrient absorption, and organic waste production; Bone and Moore, 2008) were not fully operational during their precipitation. However, such processes must occur during and after feeding events in nature, and a question that is fundamental to the themes of this thesis thus arises: to what extent do processes associated with feeding and digestion influence the mineralogical, morphological, and compositional properties of fish-derived carbonates?

It is known that gut precipitation occurs regardless of whether or not a fish has been feeding (Wilson *et al*., 1996), but no attention has been given to whether or not precipitation processes vary according to feeding state. However, the act of feeding must have the potential to induce considerable changes in the chemistry of precipitating fluids, at least temporarily, and such changes must presumably influence $CaCO_3$ precipitation processes. As an example, the phosphate intake of

marine bony fish is considered here. Phosphate is an important nutrient in the diet of many fish, and piscivorous fish will additionally ingest inorganic phosphate in the form of skeletal matter of their prey (bones and scales). Since phosphate is known to be highly influential with regard to $CaCO_3$ precipitation kinetics (Morse, 1974), generally being found to have an inhibitory effect on crystal growth (Morse *et al*., 2007; and references therein), its presence in the gut after feeding events could inhibit the growth of crystals in forms that have been described elsewhere (Perry *et al*., 2011; Salter *et al*., 2012 – see Chapter 2), perhaps resulting in the production of different carbonate morphotypes and/or phases. Indeed, it is interesting to note that precipitated phosphate can occur in association with amorphous calcium carbonate (ACC) nanospheres produced by bonefish and great barracuda (see Chapters 2 and 3), indicating that phosphate must have been present in the guts of these fish during precipitation of this phase, where it may have inhibited the development of low-phosphate Mg calcite crystals that are otherwise produced by these species (presumably when gut phosphate levels are low).

Phosphate is used as an example here because it is known to have a significant effect on $CaCO_3$ precipitation kinetics even when present at very low concentrations (*e.g.*, <10 μM in seawater; Walter and Burton, 1986). However, various other differences in gut precipitating fluids between fed and starved fish may be equally influential, such as the presence of other nutrients, or the manipulation of pH levels (and thus saturation states) to enhance the efficiency of certain digestive enzymes (Bone and Moore, 2008).

Given this potential for highly significant chemical changes to take place in gut fluids during and after feeding, there is a clear need to describe the properties of the resulting carbonates in order to properly understand their significance and fate in natural environments. Although the experiments described in this thesis do not set out to investigate this issue in detail, gut carbonates isolated from faecal matter excreted by several fish species immediately after their capture are presumed to be representative of carbonates produced under conditions of normal feeding, thus facilitating an initial assessment of the effects of feeding and starvation on precipitation processes.

4.2 METHODS

Carbonate samples were collected from several fish species to investigate potential differences between carbonates produced under normal dietary conditions and carbonates produced during periods of starvation. Fish were caught in nearshore settings around Cape Eleuthera, Eleuthera Island, the Bahamas, in December 2011 using methods outlined in Chapter 2, and for the study presented in this chapter they included groups of schoolmaster snapper (n = 3) and great barracuda (n = 5), along with two individual black groupers held separately. Following capture, fish were immediately transferred to controlled aquaria facilities and carbonates excreted within the first few hours were collected along with other excreted material (*i.e.,* faecal matter). These precipitates are presumed to be representative of those produced under normal natural conditions, and are described hereafter as having being produced by fed fish. Although it is not known when any of these fish had last eaten prior to their capture, the fact that carbonates were excreted alongside faecal suggests that they precipitated while digestive processes were active. Moreover, all fish used in this study were captured using bait (locally caught baitfish), which presumably triggered further digestive processes after being eaten. Because these samples were collected opportunistically (rather than being part of a rigorous experiment), it was only possible to collect one from each individual (group of) fish.

Following the collection of these initial samples, fish were starved for at least two days prior to further sample collection, thus allowing all previously ingested material to be voided from the gut. This approach is identical to that employed throughout the rest of this thesis and in other studies (Perry *et al*., 2011), and precipitates were therefore expected to be similar to those previously described for the species involved (Chapter 2). Following collection, all samples were prepared for analysis following the protocol described in Chapter 2 (section 2.2.1).

Subsequent analyses were designed to compare carbonates produced by fed and starved fish with regard to morphological, mineralogical, and compositional characteristics. Scanning electron microscopy (SEM) was employed to facilitate morphological characterisation, and compositional

analyses were carried out with SEM-integrated energy-dispersive X-ray spectroscopy (EDX). Attenuated total reflectance Fourier transform infrared spectroscopy (ATR-FTIR) was used to support compositional analyses and determine mineralogy. Methods associated with these techniques are identical to those described in Chapters 2 and 3.

4.3 RESULTS

4.3.1 Ellipsoid-producing species

Carbonates produced by starved schoolmaster snapper and both individual black groupers were dominated by monocrystalline ellipsoids and subsidiary rod-shaped crystals, both forms typically being approximately 1 μm or less in length (Figs. 4.1 A and 4.2 A). Additional scarce components of pellets produced by both black groupers were micron-scale rhombohedra. Morphologically, these crystals were identical to those described from these species in Chapter 2. ATR-FTIR analyses of all samples produced by starved fish yield similar results to those obtained in Chapter 3, with poorly crystalline, largely anhydrous Mg calcite being the only phase detected (Figs. 4.1 D and 4.2 D). Compositional analyses reveal that $MgCO_3$ contents are also similar to previously obtained results for these species, with values ranging from 18.9–29.9 mol% for schoolmaster snapper, and 15.2–28.7 mol% for black grouper. Trace amounts of strontium, phosphorus, sodium, and chlorine are also typical.

Carbonates produced by both species immediately after capture were typically excreted as pellets of similar size and shape to those produced by starved fish, some of these comprising ingested particles (*e.g.*, coccoliths, diatoms, and sponge spicules were commonly observed). Alongside pellets, faecal matter excreted by these species included skeletal fragments, such as fish bones (black grouper) and Mg calcite algal fragments (schoolmaster snapper); these being as large as, or in some cases larger than, precipitated carbonate pellets. It is common for these to be partially coated by fish-derived carbonates (Fig. 4.1 B and 4.2 B), which could have either precipitated on skeletal surfaces, or accumulated there as they passed through the gut. Similar situations are also described in Chapters 2 and 6 of this thesis.

Precipitates excreted by fed schoolmaster snapper were morphologically almost identical to those produced by starved fish (*i.e.*, dominated by micron-scale ellipsoids) in all pellets examined. However, a notable difference was the presence of rare micron-scale spheres among ellipsoids in most pellets and skeletal-fragment-encrusting patches (Fig. 4.1 C) – such morphotypes are never observed in samples produced by starved fish. ATR-FTIR analyses of these samples (Fig. 4.1 D) indicate that they are predominantly Mg calcite similar to those produced by starved fish, but the presence of a weak band at ~1650 cm^{-1} indicates that water is more abundant in these samples. In addition, a broad band of moderate intensity centred over ~1040 cm^{-1} indicates the presence of phosphate. These patterns are similar to those generated by amorphous carbonates produced by bonefish (Chapters 3 and 7), and perhaps indicate that the micron-scale spheres observed here (which are morphologically similar to the amorphous phase produced by bonefish) are also amorphous. The fact that these samples represent the only documented production of amorphous spheres by this species, as well as the only occurrence of elevated phosphate, indicates the latter may have inhibited crystallisation.

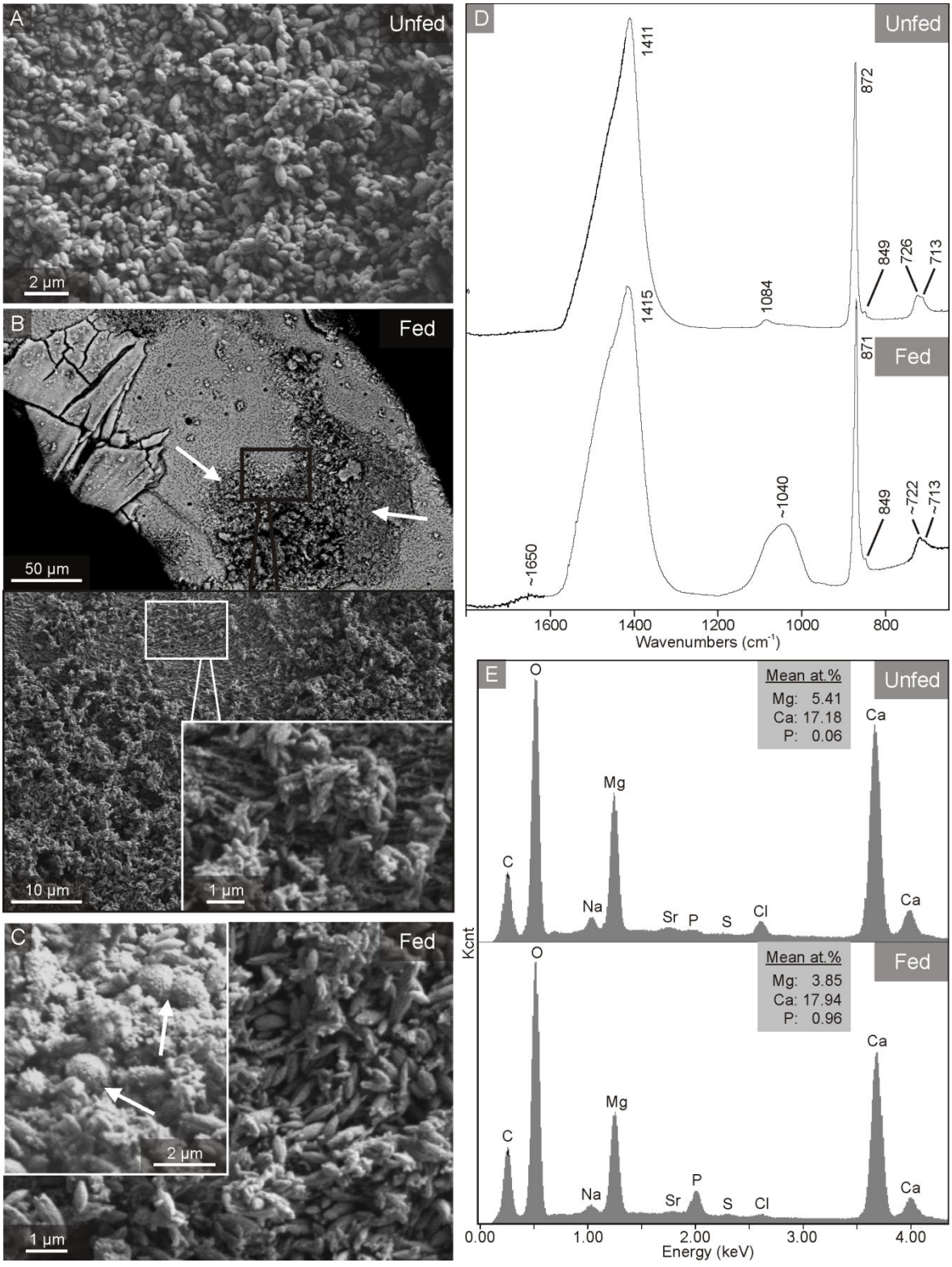

Figure 4.1 *SEM images (A–C), ATR-FTIR spectra (D), and EDX spectra (E) for carbonates produced by starved and fed schoolmaster snapper. Micron-scale ellipsoids are the dominant product of starved fish (A), and similar crystals are produced by fed fish, albeit occasionally occurring as particles encrusted on ingested skeletal fragments (B) alongside more typical pellets (C). Nano- to micron-scale spheres also occur as scarce products of fed fish (C; inset). FTIR spectra (D) indicate that both starved and fed fish produce poorly crystalline calcite, although precipitates produced by the latter additionally contain phosphate (broad peak at ~1040 cm^{-1}) and water (shoulder at ~1650 cm^{-1}). EDX spectra (E) confirm the elevated phosphorus content in the products of fed fish, which contain, on average, 0.96 atomic % P.*

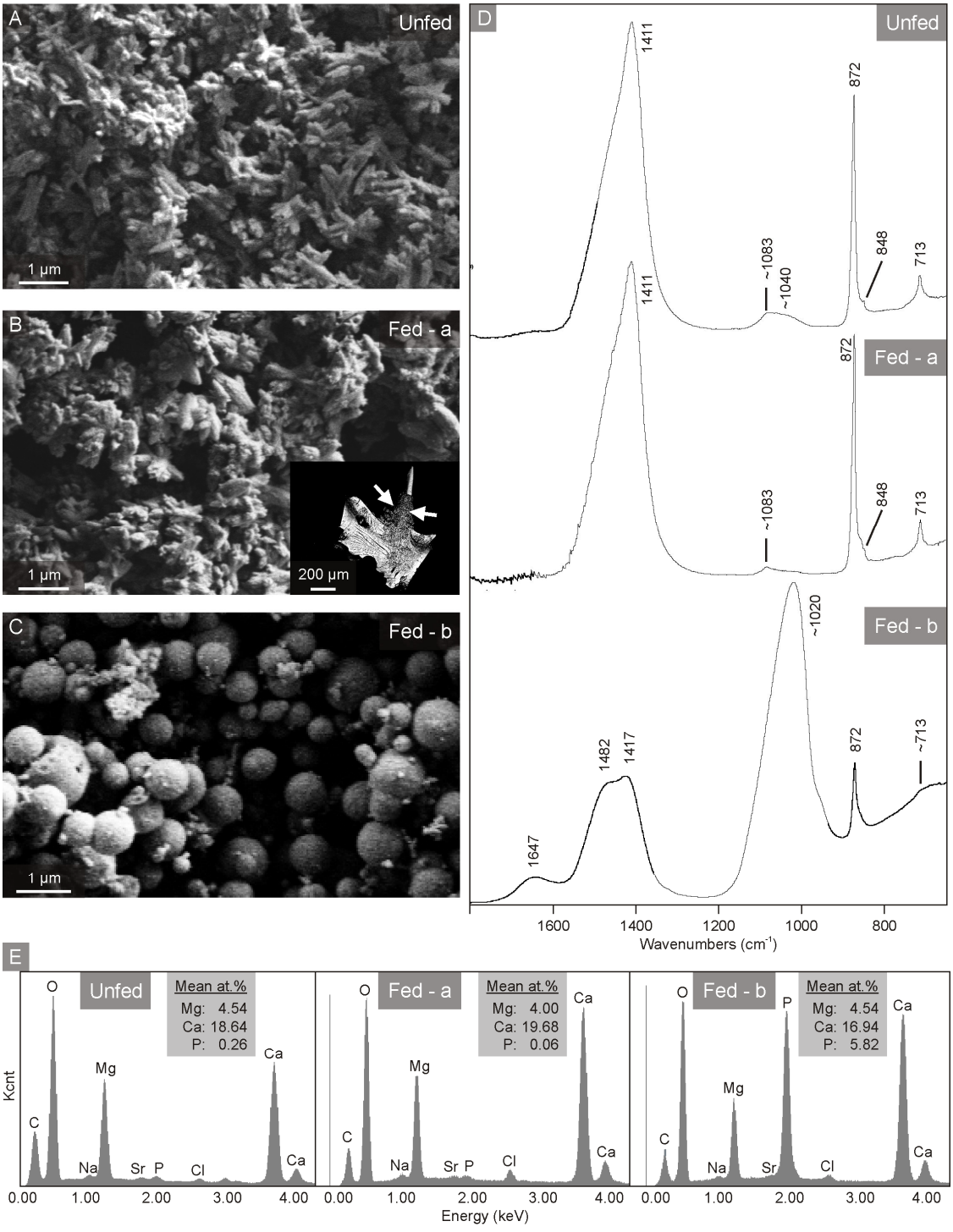

Figure 4.2 *SEM images (A–C), ATR-FTIR spectra (D), and EDX spectra (E) for carbonates produced by black grouper (one starved individual; two separate fed individuals – a and b). Starved fish consistently produced micron-scale ellipsoid- and rod-shaped crystals (A), which FTIR spectra (D; top) indicate to be poorly crystalline calcite with minor phosphate (broad hump at ~1040 cm^{-1}). Precipitation products of one fed individual (a) were morphologically (B) and mineralogically (D) identical to these, except that they were occasionally encrusted on ingested skeletal fragments (B; inset), and typically generated weaker phosphate vibrations (D; middle). However, precipitation products of a second fed individual (b) were dominated by nano- to micron-scale spheres (C) which generated FTIR spectra consistent with the presence of a hydrated amorphous carbonate (note lack of well-defined v_4 peak and presence of a distinct water bending peak at ~1647 cm^{-1}) in association with major phosphate (broad and intense peak at ~1020 cm^{-1}). EDX spectra confirm this pattern of phosphate occurrence, with precipitates of fed individual-b containing, on average, 5.82 atomic % P.*

Compositional analyses (Fig. 4.1 E; Table 4.1) support this finding, indicating that phosphorus is present at elevated levels in all carbonates produced by fed schoolmaster snapper (relative to carbonates produced by starved fish). For example, the mean ratio between phosphorus and total major cations (Mg + Ca) for carbonates produced by starved fish is 0.002 (maximum 0.003), whereas the mean value for carbonates produced by fish under normal dietary conditions is an order of magnitude higher (0.044; minimum 0.009). No compositional differences are apparent between micron-scale spheres and ellipsoids.

Further analysis of compositional data for samples produced by fed and starved schoolmaster snapper reveal differences not only in phosphorus contents, but also in $MgCO_3$ contents. Significant variation of $MgCO_3$ content among precipitates produced by fed fish (one-way ANOVA; df = 12, F = 6.3, p <0.001), is revealed in Tukey post hoc tests to be a result of compositional differences between gut carbonates encrusted on skeletal fragments (mean 15.9 mol% $MgCO_3$) and gut carbonates excreted as pellets free of skeletal fragments (mean 19.4 mol% $MgCO_3$). In contrast, samples from starved fish, which contain few or no skeletal components, have higher $MgCO_3$ contents (mean 23.9 mol%) which do not vary significantly among pellets (one-way ANOVA; df = 7, F = 2.1, p >0.100). Analysis of variance among these three groups (starved fish: pellets; fed fish: pellets; and fed fish: associated with skeletal grains) indicates that all differ significantly from each other (one-way ANOVA; df = 2, F = 29.5, p <0.001).

With regard to phosphorus to cation ratios in samples produced by fed schoolmaster snapper, values are typically quite uniform within pellets but vary significantly among them (one-way ANOVA; df = 12, F = 51.6, p <0.001); the highest values (up to 0.124) occurring in crystals encrusted on skeletal fragments. Separate analyses of skeletal fragments (*i.e.*, in areas where gut precipitates are absent) indicate that they contain only trace amounts of phosphorus (P:Ca+Mg ratios are typically <0.04; *i.e.*, less than a third of the values measured for encrusting gut precipitates), suggesting that elevated values are a real property of gut precipitates on skeletal surfaces, and not due to contamination of the signal by underlying skeletal fragments.

If, as they appear to be, elevated concentrations of phosphorus are generated during normal dietary functioning of fish, a correlation that exists between phosphorus and $MgCO_3$ contents (Fig. 4.3) would appear to suggest the latter is also influenced by normal dietary functioning, either directly, or as a result of the elevated phosphorus concentrations. The variability in compositional data within samples produced by the group of fed fish may also be a result of the feeding effect: analysed pellets could have been produced by different individual fish that experienced different intervals between feeding and excreting those pellets. Alternatively, pellets could have been produced by the same individual fish; those with lower phosphorus to cation ratios probably being precipitated as effects of feeding were beginning to wane. Indeed, the latter possibility is supported by the fact that the highest phosphate and lowest $MgCO_3$ contents tend to occur in carbonates encrusted on skeletal fragments, which suggests that these precipitates might have formed at a time when active digestion was taking place, and thus when the effects of feeding were probably greatest.

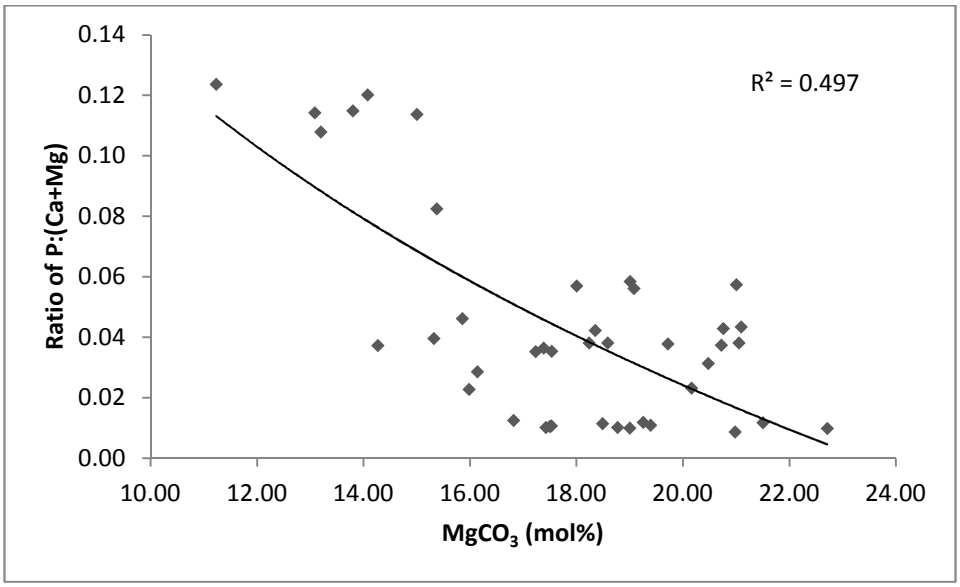

Figure 4.3 *Relationship between phosphorus (phosphate) and $MgCO_3$ contents in gut precipitates excreted by fed schoolmaster snapper.*

Carbonates produced by individual fed black grouper differed substantially from each other. Samples produced by one individual were indistinguishable from those it produced when starved, comprising poorly crystalline high-Mg calcite ellipsoids and rods with very low phosphate contents

(Figs. 4.2 B, D, and E; Table 4.1). In contrast, samples produced by a second individual differed considerably from those it produced when starved, being dominated by nano- to micron-scale spheres (Fig. 4.2 C), which ATR-FTIR analyses reveal to be hydrated amorphous carbonate (*i.e.*, the ν_4 band at ~713 cm^{-1} is limited to a barely discernible hump, and weak band at ~1647 cm^{-1} indicates the presence of water) with very high phosphate content (Fig. 4.2 D). Compositional analyses of the latter confirm that phosphorus content is consistently very high, with the ratio of P:(Mg+Ca) ranging from 0.235 to 0.316 (compared with values in the range 0.005–0.010 for starved fish; Table 4.1). Unlike samples produced by schoolmaster snapper, these high phosphorus concentrations were not accompanied by significantly lower $MgCO_3$ contents.

Table 4.1 *Summary of $MgCO_3$ contents and phosphorus to cation ratios recorded in gut precipitates produced by fed and starved fish.*

Species	Sample	Inter-quartile range of $MgCO_3$ (mol%)	P/(Mg + Ca) (ratio of atomic %)
Schoolmaster snapper	3 or more days after capture	22.3–27.6	0.002–0.004
Schoolmaster snapper	Immediately after capture	18.4–20.9	0.009–0.058
Black grouper[1]	3 or more days after capture	16.1–22.1	0.007–0.024
Black grouper[1]	Immediately after capture	15.0–20.9	0.003–0.007
Black grouper [2]	3 or more days after capture	22.4–25.3	0.005–0.010
Black grouper[2]	Immediately after capture	17.5–24.6	0.235–0.316
Great barracuda (d)	3 or more days after capture	19.5–23.0	0.004–0.009
Great barracuda (n)	Immediately after capture	18.1–22.4	0.217–0.324
Great barracuda (a)	3 or more days after capture	64.5–81.2	0.004–0.007
Great barracuda (a)	Immediately after capture	65.1–85.8	0.058–0.133

[1,2]Data for black grouper reported from samples produced by two individual fish (denoted by '1' and '2'). Data for great barracuda reported for small dumbbells (d), nanospheres (n), and amorphous magnesium carbonate (a).

4.3.2 Dumbbell and nanosphere producing species

Gut precipitates were also collected from a small group (n = 5) of great barracuda. Previous studies of carbonates produced by this species (see Chapter 2) indicated that small dumbbells are typically the dominant precipitation product of starved fish, with large dumbbells and spheres, nanospheres, monocrystalline ellipsoids, and rhombohedra occurring as subsidiary phases along with varying quantities of carbonate that lack definable form. It is worth mentioning that, where present, previously documented nanospheres tended to be rich in phosphate (see Chapter 2), and were thus

similar in both morphology and composition to precipitates produced by fed black grouper (see above). Furthermore, it was noted that those samples were excreted along with abundant skeletal matter (despite fish being starved for 48 hours beforehand) and may therefore have been representative of carbonates produced by fish under conditions of feeding.

Visual examination of carbonates produced by starved fish in this study reveals that they comprise small dumbbells (2–5 μm in length) in a magnesium-rich 'matrix' that lacks any clearly definable form (Fig. 4.4 A); the dumbbells being similar to those previously described for this species. Samples produced within hours of fish being captured, however, are markedly different; nanospheres being the dominant particle type in most pellets, although some pellets are dominated by a magnesium-rich phase along with abundant nanospheres (Fig. 4.4 B–C). These nanospheres are morphologically identical to those documented for this species in Chapter 2, and also to those documented for black grouper (above).

Representative ATR-FTIR spectra for these samples are shown in Fig. 4.4 D. The spectrum for samples from starved fish exhibits a series of peaks that suggest that presence of calcite (including a low intensity, but well-defined peak at 713 cm^{-1}). In addition, a water bending vibration at approximately 1644 cm^{-1}, broadening at the base of the carbonate ν_2 peak, and the upward inflection of the baseline over lower wavenumbers are all typical features generated by the presence of a hydrated amorphous phase. The calcite vibrations are presumably generated by small dumbbells, whilst the amorphous carbonate vibrations are likely generated by magnesium-rich 'matrix' phase. Spectra generated by samples from fed fish differ markedly in two ways. Firstly, the presence of a substantial amount of phosphate is indicated by an intense broad peak centred over approximately 1040 cm^{-1}; such a peak being barely discernable in samples from starved fish. Secondly, the absence of a peak at 713 cm^{-1} (*i.e.*, carbonate ν_4), combined with the broadening of the ν_2 peak and its shift to slightly lower wavenumbers, indicates that the only carbonate phases present in these samples are amorphous.

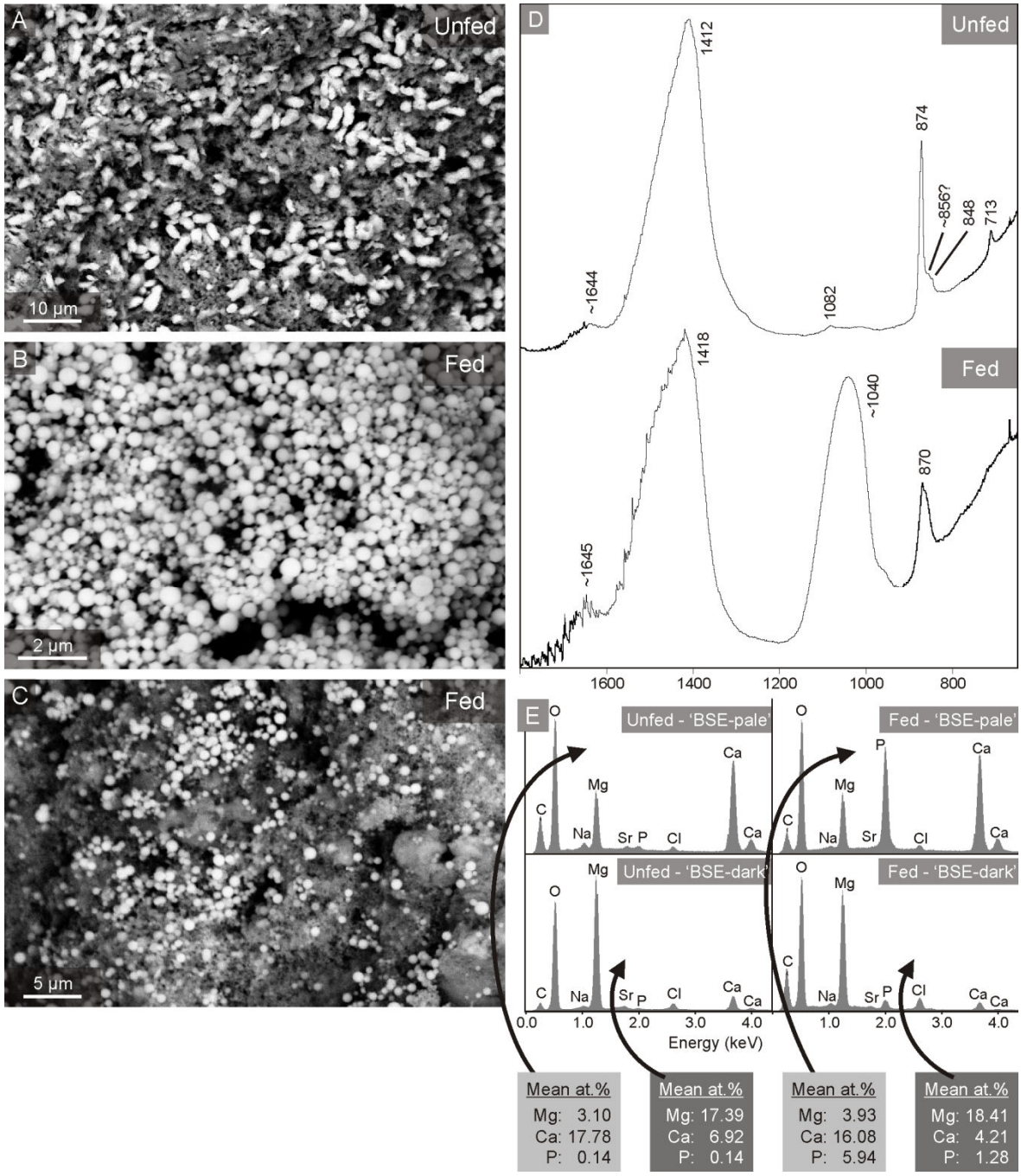

Figure 4.4 *BSE images (A–C), ATR-FTIR spectra (D), and EDX spectra (E) of carbonates produced by fed and unfed great barracuda. Image A shows carbonates excreted by starved fish. Typical pellets in this sample comprise dumbbell-shaped crystals that are 2–5 µm in length (pale areas) in an Mg-rich 'matrix' (dark areas). FTIR spectra (D; top) indicate the presence of hydrated amorphous carbonates (note the water bending peak at 1644 cm^{-1} and the broadening at the base of the carbonate v_2 peak at 874 cm^{-1}) along with calcite (note the presence of a weak but sharp v_4 peak at 713 cm^{-1}); the former presumably relating to the Mg-rich 'matrix' phase and the latter to the dumbbell-shaped phase. Images B and C show nanoscale spheres and an Mg-rich 'matrix' phase produced by fed fish. The former is the dominant morphotype in these samples, and FTIR spectra (D; bottom) indicate they are a hydrated amorphous carbonate (note the absence of a v_4 peak, the broadened v_2 peak at 870 cm^{-1}, and the water bending peak at ~1645 cm^{-1}) associated with a large phosphate component (intense peak at ~1040 cm^{-1}). EDX spectra confirm that neither phase produced by starved fish contains more than trace amounts of phosphorus, whereas nanospheres produced by fed fish contain, on average, 5.94 atomic % (or about 6–7 wt.%). The associated magnesium-rich phase occasionally produced by fed fish also contains phosphorus, but concentrations are elevated to a lesser degree (average 1.28 atomic %).*

The observation that phosphates are elevated in samples collected from fish shortly after their capture is also confirmed in EDX spectra (Fig. 4.4 E; summarised in Table 4.1). These data indicate that small dumbbells produced by starved fish are compositionally similar to high-Mg calcite (mean 21.2 mol% $MgCO_3$), whereas the associated magnesium-rich 'matrix' typically contains in excess of 65 mol% $MgCO_3$ (it is probably best defined as a Ca-rich amorphous magnesium carbonate). Phosphorus in both phases occurs at very low concentrations, with the ratio of phosphorus to major cations never exceeding 0.009 (mean 0.006). Magnesium contents of nanospheres and the 'matrix' phase excreted by fed fish are generally similar to those of small dumbbells and the 'matrix' phase (respectively) excreted by starved fish, with nanospheres containing, on average, 19.7 mol% $MgCO_3$ and the 'matrix' phase typically containing in excess of 65 mol% $MgCO_3$. In contrast, phosphorus contents are considerably higher, with mean values for the ratio of phosphorus to major cations of 0.297 (nanospheres) and 0.092 ('matrix').

4.4 DISCUSSION

Data arising in this study show that two samples produced by fed fish (black grouper and great barracuda) comprised phosphate-rich amorphous calcium carbonate (ACC) nanospheres; these being completely different to the high-Mg calcite precipitation products of: i) the same fish when starved; and ii) any other starved fish of the same species (Perry *et al*., 2011; Salter *et al*., 2012). A third sample (produced by schoolmaster snapper) contained a small quantity of similar phosphate-rich nanospheres (these never being observed in samples from starved fish) alongside the high-Mg calcite ellipsoids typically associated with starved fish of this species, while a fourth sample (produced by different black grouper to that mentioned above) contained crystals identical to those produced by starved fish of this species. Based on these data, it is apparent that the effects of feeding on gut carbonate precipitation processes can be considerable, but they are also highly variable.

4.4.1 Mechanisms driving variations in precipitation products

Prior to this pilot study, phosphate (or phosphorus) has typically been documented as a minor component of carbonates produced by most fish species when starved (see Chapters 2 and 3). Only carbonates produced by bonefish were found to consistently contain higher than trace amounts, although some samples produced by several other species (*e.g.*, checkered puffer, redtail parrotfish, bluehead wrasse, and slippery dick) were also found to contain low (but higher-than-trace) concentrations. The only recorded occurrence of high phosphate concentrations similar to those measured in the present study was in association with amorphous carbonate nano-scale spheres excreted by great barracuda alongside abundant digested skeletal matter. That result, together with the observation in the present study that two out of four sample sets produced by fed fish comprised amorphous carbonate nano-scale spheres with high phosphate concentrations (*i.e.*, markedly different to the phosphate-free high-Mg calcite ellipsoids and dumbbells consistently produced by these species when starved), provides a clear indication that the properties of gut precipitates can be strongly influenced by normal feeding. It is therefore apparent that precipitates produced under normal natural circumstances may differ significantly from those described in Chapter 2, at least when they are produced shortly after feeding.

These observations appear to confirm the hypothesis put forward in section 4.1 wherein: a) dietary phosphate enters the piscine gut; and b) once there, it can strongly influence carbonate precipitation kinetics. In the examples documented in this chapter, elevated intestinal phosphate has seemingly inhibited the precipitation of anhydrous crystalline phases and instead resulted in precipitation of amorphous calcium carbonate (ACC) and amorphous calcium phosphate (ACP); a result that is not surprising given that phosphate is known to inhibit precipitation of both aragonite and calcite (Walter and Burton, 1986; Burton and Walter, 1990; Dove and Hochella, 1993).

However, a key finding of this study is that two sample sets (out of four that were examined) comprised high-Mg calcite crystals that were indistinguishable from those produced when the fish had been starved in captivity for several days. The excretion of these precipitation products

immediately after fish were captured (in one case from black grouper; a species of which a separate individual produced phosphate-rich amorphous precipitates) indicates that the effects of dietary phosphate are variable under normal natural circumstances. Preliminary results from investigations of several temperate fish species indicate a similarly variable influence, with no obvious differences in the products of fed and starved fish in at least a few cases (E.E. Reardon, *Pers. Comm.*).

This variability can perhaps be explained by the timing of precipitation with respect to feeding sessions. Mather *et al*. (1995) find that excretion rates of phosphate waste by the freshwater gizzard shad (*Dorosoma cepedianum*) are highest immediately after feeding, suggesting that dietary phosphate is processed quite rapidly. If the same is true of all teleosts, this rapid phosphate processing might mean that precipitates that form shortly after feeding (when intestinal phosphate levels are highest) may be the most strongly influenced (*e.g.*, precipitates produced by great barracuda and black grouper B in this study), whereas precipitates produced just prior to a feeding event (when intestinal phosphate is presumably at its lowest level) may be less strongly influenced and thus are produced as under conditions of starvation (*e.g.*, as produced by black grouper A in this study). An intermediate stage may be represented by gradually diminishing intestinal phosphate levels (and a consequent reduction in the influence of phosphate on precipitation processes) following the post-feeding phosphate peak, which may result in a mixture of crystalline and amorphous precipitates with moderate phosphate concentrations (*e.g.*, as produced by schoolmaster snapper in this study). This hypothesised cyclic variation in precipitation products that operates in tandem with feeding sessions is shown schematically in Fig. 4.5.

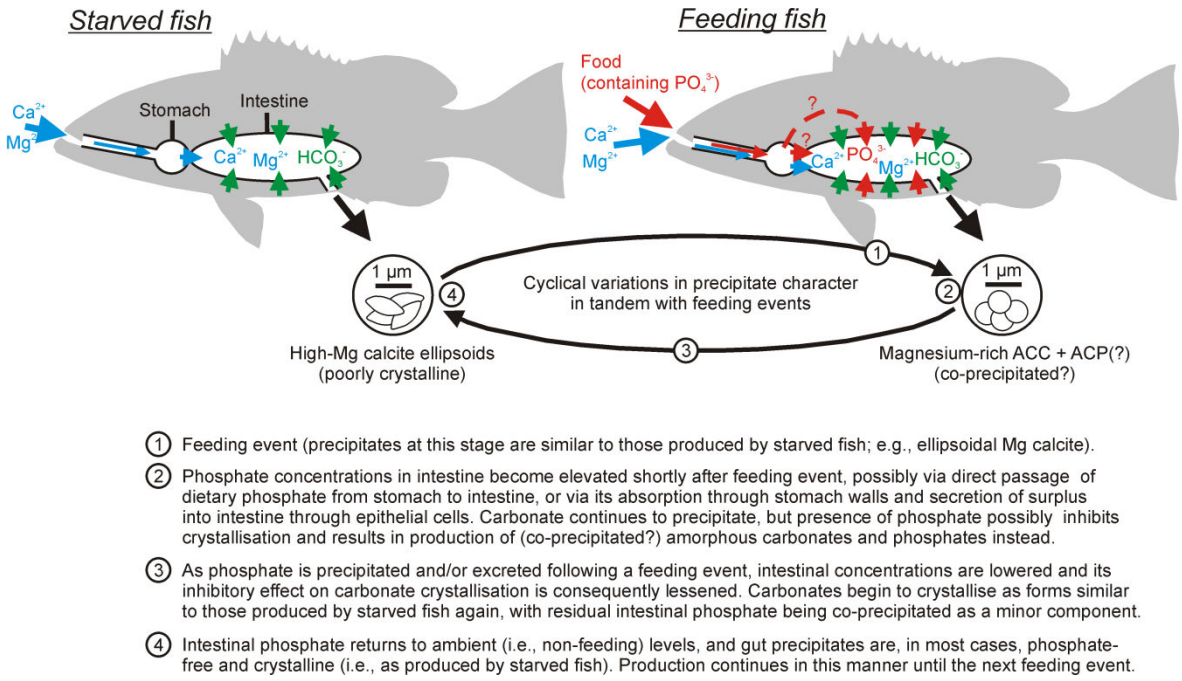

Figure 4.5 *Schematic diagram showing potential dietary control on the nature of intestinal carbonate precipitates.*

However, applying a cyclical variation in precipitation products across whole fish populations is hampered by numerous complicating factors such as feeding rhythms and dietary habits. For example, a fish that meets its dietary requirements by undertaking short and infrequent feeding sessions (*e.g.*, apex predators such as black grouper and great barracuda) may produce cyclically variable precipitation products as speculated above, whereas a fish with an equivalent dietary intake spread over longer (or continuous) feeding sessions (*e.g.*, herbivorous fish; not tested here) may never attain intestinal phosphate levels as high as the short-lived peaks that occur in apex predators; perhaps having moderately elevated levels over much longer periods instead. Although the effects of such variations in dietary habits on gut precipitation products remain to be determined, the potential for a diet-specific influence clearly exists.

4.4.2 Implications for the sedimentary significance of fish-derived carbonates

The production of mainly amorphous nano-scale spheres, apparently as a direct consequence of feeding, may have significant implications for the current understanding of fish-derived carbonate products and their sedimentary significance. Not only does it mean that the crystalline precipitation products described in Chapters 2 and 3 (*e.g.*, ellipsoids and dumbbells) may represent a smaller

proportion of total excreted carbonates than previously thought; it may also have implications for the preservation potential of fish-derived carbonates. For example, in Chapter 7 it is shown that fish-derived amorphous carbonate nanospheres dissolve very rapidly (hours to days) in seawater, while similarly low stability of a comparable fish-derived phase is reported by Foran *et al.* (2013), and also more widely for ACC from other sources (Brečević and Nielsen, 1989; Clarkson *et al*., 1992). In the first instance, it would thus appear that phosphate-rich amorphous phases produced as a consequence of feeding will dissolve and be of little sedimentary significance following excretion.

It is worth pointing out, however, that none of the above-mentioned investigations on preservation potential used amorphous phases with high phosphate contents as their subjects, and the fate of these products therefore remains to be determined. It is speculated here that they might actually persist in open marine conditions for longer than other amorphous phases described in Chapters 2 and 3. In part this speculation depends upon whether phosphate occurs as a discrete ACP phase alongside ACC, or is co-precipitated along with carbonate to form an ACC–ACP solid solution. Given the reasonably consistent compositional data within samples, along with the fact that BSE images show spheres with a uniform pale shade, the latter would seem more likely (discrete ACC and ACP phases would presumably be displayed as contrasting darker and paler shades, respectively, in BSE images due to their different molecular weights). The co-precipitation of phosphate with ACC is widely held to stabilise the latter (Taylor *et al*., 1993; Sawada, 1997; Raz *et al*., 2002; Bentov *et al*., 2010), to the extent that it is used as a stabilising agent for ACC reference materials (Foran *et al*., 2013; their Fig. 3). In the FTIR spectrum for phosphate-stabilised reference ACC shown by Foran *et al*. (2013), the phosphate peak is of moderate intensity. The considerably higher intensity of some of the phosphate peaks shown here could mean these fish-derived carbonates are well stabilised, and it is for this reason that it is suggested they could persist for longer in seawater than other fish-derived ACC.

Despite these considerations, it should be noted that similar ACC precipitates with moderate phosphate concentrations rapidly dissolved when exposed to seawater (see Chapter 7), and a similar fate should not be precluded for these phosphate-rich amorphous phases. Nevertheless, if the above speculation is correct, and these ACC–ACP precipitates do persist after excretion, an additional consideration should be that of crystallisation to more stable forms. As has been stated above, high phosphate concentration may inhibit and/or preclude the crystallisation of carbonate phases, but its presence here raises another possibility not previously considered for fish-derived gut precipitates: that phosphate phases, such as hydroxyapatite, may crystallise instead. It is widely held that the formation of crystalline phosphate phases is inhibited in seawater by the presence of magnesium (Salimi *et al*., 1985; Kibalcyzc *et al*., 1990; Van Capellen and Berner, 1991; Gunnar *et al*., 2004), and it has been demonstrated that ACP exposed to seawater for eight months does not crystallise, whereas it rapidly crystallises to apatite in Mg-free solutions (Martens and Harriss, 1970). However, other studies indicate that crystallisation of ACP can take place in seawater, albeit over longer timescales than investigated elsewhere; crystallisation to apatite taking on the order of 10 years (Gulbrandsen *et al*., 1984).

In the absence of previous studies regarding the preservation potential of co-precipitated ACC–ACP, predicting its fate after production and excretion by fish can only be highly speculative. The above considerations suggest that the presence of phosphate in ACC, whilst inhibiting crystallisation of carbonates, may act to stabilise it as an amorphous phase. If the stabilising influence of phosphate is strong enough that these precipitates can persist in seawater for several years, the possibility also exists that the phosphate component might eventually crystallise. However, it has been shown elsewhere (see Chapter 7) that the stabilising effect of moderate concentrations of phosphate is not sufficient to prevent dissolution of fish-derived ACC in seawater, so rapid dissolution of this phase is also a possibility. Further work is clearly necessary to properly elucidate the effects of feeding on precipitation products in all fish species, and the implications this has for gut carbonate preservation potential in shallow sub-tropical marine settings.

4.5 CONCLUSIONS

This pilot study demonstrates that the mineralogical and morphological properties of piscine gut carbonates can vary according to the feeding state of the fish that produced them; high-Mg calcite ellipsoids and dumbbells produced by starved fish used in this study being replaced with amorphous calcium carbonate (ACC) nanospheres (probably co-precipitated with amorphous calcium phosphate, or ACP) shortly after a feeding event. The major mechanisms thought to be responsible for these changes are as follows:

- Dietary phosphate enters the intestine during and shortly after a feeding event;
- Its presence in the intestine inhibits development of crystalline carbonate phases, and precipitation instead proceeds via the formation of amorphous phases;
- The waning of gut phosphate levels some time after a feeding event means that carbonate crystallisation is no longer inhibited, and various forms of Mg calcite begin to develop.

For the species used in this study, the latter point would appear to occur reasonably soon after a feeding event; two out of the four samples excreted by presumed fed fish being identical or very similar to those produced by starved fish of the same species. These observations are used to form a testable hypothesis wherein fish that undertake infrequent and brief feeding events (*e.g.*, apex predators such as black grouper) may have highly fluctuating gut phosphate levels that result in production of phosphate-rich ACC shortly after a feeding event (when gut phosphate levels are high), and phosphate-poor crystalline phases some time after a feeding event (when gut phosphate levels have waned). However, it is conceivable that fish that feed continuously or over long periods (*e.g.*, herbivores) may have more stable gut phosphate levels, which could mean the effects of feeding on carbonate production are diet-specific.

Amorphous carbonate phases produced as a result of feeding are thought likely to be highly unstable in open marine settings (although this remains to be tested), and the findings of this study therefore represent a potentially important advance in the understanding of fish-derived carbonates

and their relevance in sedimentary systems. Several questions arise that should be the focus of future studies:

- How long after a feeding event do elevated gut phosphate levels persist, and how long does it take for precipitation products to revert to those of starved fish?
- To what extent is the influence of feeding on gut carbonate precipitation determined by the feeding habits of any given fish (*i.e.*, herbivores vs. piscivores)? For example, are the guts of certain 'continuous-feeder' species ever a phosphate-free environment in which the precipitation products of a starved fish might be produced?
- What is the preservation potential of co-precipitated ACC and ACP in shallow sub-tropical marine settings, and how does this vary with magnesium and phosphate content?

Finally, it is re-iterated that carbonates produced within a few hours of fish being captured can be very similar to those produced by starved fish, suggesting that, at least for some species, the characteristics of gut precipitates produced in natural settings may vary temporally; some being as described in earlier studies (Perry *et al*., 2011; Salter *et al*., 2012), and others being more phosphate-rich and amorphous.

Chapter 5: Stable isotope composition of fish-derived carbonates: Carbon and oxygen

5.1 INTRODUCTION

As outlined in Chapter 2, carbonates produced in the intestines of 22 Caribbean fish species and excreted in shallow sub-tropical marine provinces, where they are a potentially significant source of sedimentary mud-grade carbonate (Perry *et al*., 2011; Salter *et al*., 2012), exhibit a remarkable range of distinctive crystal forms and commonly have very high magnesium contents (up to about 45 mol% in high-Mg calcite). Consequently they are seemingly unique as potential components of shallow sub-tropical carbonate surface sediments and should be easily recognisable, at least at the point of excretion, in bulk sediment samples from those areas. However, while Perry *et al*. (2011) find numerous particles that resemble fish-derived carbonates in surface sediments collected from Eleuthera Sound (the Bahamas), similar particles are typically not reported from surface sediments of the Bahamas or other contemporary settings (Matthews, 1966; Stieglitz, 1972; Gischler and Zingeler, 2002; Gischler *et al.*, 2013). As discussed in the first chapter of this thesis, one possible explanation for this apparent disparity in carbonate inputs to platform-top sediments and the observed components of those sediments is that the former undergo rapid alteration after they are produced and therefore either not present or are not recognisable in bulk surface sediment samples.

A further means of characterisation that may aid detection of fish-derived carbonate particles in bulk sediment samples is that of stable carbon (^{13}C) and oxygen (^{18}O) isotope compositions. Stable isotope analysis is widely utilised to characterise sedimentary carbonates and provide insights to the precipitation processes that led to their formation (*e.g.*, Hu and Burdige, 2007; Gischler *et al*., 2009; Swart *et al*., 2009). Of particular relevance here is that stable isotope compositions of bulk surface sediment samples have been compared with those of carbonates associated with *Halimeda*

algae, and those associated with 'whitings' in order to aid assessments regarding which of these potential carbonate mud sources is of greatest sedimentary significance in the Bahamas, with results indicating that bulk sediments, characterised by $\delta^{18}O$ values of about 0.0 to 0.4 ‰ and $\delta^{13}C$ values in the range 2.0 to 6.0 ‰, are isotopically closer to the latter (Shinn *et al.*, 1989; Swart *et al*., 2009). If fish-derived carbonates have stable carbon and oxygen isotope compositions that are distinct from those of other sedimentary carbonates produced in shallow waters of the Bahamas, it is possible they will impart a strong isotopic signature on bulk surface sediments in areas where they are produced in abundance. For example, Perry *et al*. (2011) estimate that 70 % of the carbonate mud produced in fringing mangroves could be fish-derived, and, if these carbonates are not preferentially exported or dissolved in these settings, and assuming no rapid alteration and concomitant shift of stable isotope composition takes place (see Chapter 7), the surface sediment mud fraction in these areas should be dominated by a fish-derived carbonate stable isotope signature.

One of the outcomes of previous investigations on carbonate production in fish was the finding that precipitation is promoted by highly alkaline gut fluids (pH 8.5–9.3) which result from elevated HCO_3^- concentrations that are up to 50-fold greater than ambient sea water (Wilson *et al*., 1996; 2002; Taylor and Grosell, 2006). Intestinal concentrations of Mg^{2+} and SO_4^{2-} are two to four times greater than seawater values; their concentrations increasing due to water absorption across the intestinal epithelium without concomitant absorption of these ions (Taylor and Grosell, 2006). Assuming intestinal HCO_3^- from imbibed seawater undergoes similar concentration increases (it cannot undergo greater concentration increases unless an unknown and significant removal of Mg^{2+} and SO_4^{2-} occurs elsewhere), this is not nearly sufficient to explain the highly elevated intestinal HCO_3^- concentrations that have been reported, and it is thus necessary to invoke an additional source. By way of confirming this, active secretion of HCO_3^- into the intestine has been observed following its production via hydration of endogenous (metabolically-derived) CO_2 (Wilson *et al*., 1996; Grosell *et al*., 2001; 2005).

This process means that the HCO_3^- that drives precipitation of calcium carbonate within the piscine gut is influenced to some degree by dietary carbon intake, and as such it should have a stable isotope ratio ($^{13}C/^{12}C$) that is distinct from that of ambient seawater dissolved inorganic carbon (DIC). For example, $\delta^{13}C$ values in surface seawater DIC vary geographically, but are typically in the range -3.0 to 2.4 ‰ in surface waters of the Bahamas (Patterson and Walter, 1994b; Swart *et al*., 2009). In contrast, $\delta^{13}C$ values for CO_2 in muscle tissues of fish are typically ~1 ‰ enriched relative to their diets (Fry *et al*., 1982), meaning the muscle tissues of herbivorous fishes in the Florida reef tract typically have $\delta^{13}C$ values of about -15 ‰ (Lamb *et al* 2012). Normal fractionation of carbon between stored CO_2 (carbohydrate) and HCO_3^- secreted into the intestine should then result in $\delta^{13}C$ values for intestinal carbon of about -14 ‰ (McConnaughey *et al*., 1997), although other factors, such as enzymatic processes, may influence this (Gillikin *et al*., 2006; and references therein). Assuming seawater DIC contributes only a small portion of intestinal carbon that ultimately precipitates as inorganic carbonate (as indicated by highly elevated intestinal HCO_3^- concentrations), this large predicted difference between the isotopic compositions of seawater DIC and intestinal HCO_3^- suggests carbonates precipitated from the latter will be substantially depleted in ^{13}C compared to carbonates precipitated in equilibrium with seawater.

Furthermore, because most marine organisms that produce $CaCO_3$ skeletons typically incorporate <10 % respired carbon into precipitating fluids, the remainder having an external origin (*i.e.*, seawater), the resulting $\delta^{13}C$ values of skeletal carbonates are typically <2 ‰ lower than if carbonates were precipitated in equilibrium with seawater (McConnaughey *et al*., 1997; Lorrain *et al*., 2004). Conversely, existing compositional data for piscine intestinal fluids (Wilson *et al*., 1996; 2002; Grosell *et al*., 2005; Taylor and Grosell, 2006) suggest that, if imbibed seawater HCO_3^- undergoes similar concentration as Mg^{2+} and SO_4^{2-}, up to about 80–90 % of the HCO_3^- that precipitates as $CaCO_3$ must be of metabolic origin. If other factors with the potential to further influence the isotopic composition of these fluids (*e.g.*, gut microbial activity) are not important, it can thus be expected that $\delta^{13}C$ values of fish-derived carbonates will be considerably lower than values reported from most marine carbonates, regardless of whether they are of abiotic or biogenic

origin. In support of this contention, fish otoliths, although precipitated under different conditions to those that lead to gut precipitate formation, are one of the few sources of marine carbonate known to incorporate similarly large amounts of metabolic CO_2 (McConnaughey *et al*., 1997), and they are characterised as having $\delta^{13}C$ in the range -8.03 to 0.50 ‰; these values departing from calculated seawater equilibrium values by 3.0 to 10.0 ‰ (Kalish, 1991; Gao *et al*., 2012).

A complicating factor with regard to using stable isotope data as a guide to identifying the presence of fish-derived carbonates in surface sediments is that of the potential for them to undergo rapid alteration after excretion. These issues are considered in Chapter 1 and further explored in Chapter 7, but the key point here is that such alteration (*e.g.*, recrystallisation) might be accompanied by shift in stable carbon and oxygen isotope composition towards seawater or porewater equilibrium values, as has been shown to occur in high-Mg calcite exposed to shallow sub-surface porewater for 500 days (Patterson and Walter, 1994a). The potential must exist for fish-derived carbonates to undergo similar changes in natural settings (especially given questions raised about its stability in Chapters 1–3), and stable carbon and oxygen isotope composition may therefore not be an ideal indicator of their presence in bulk sediment samples. This being the case, the present work provides a baseline dataset for the stable isotope composition of these carbonates at the point of excretion, which may be of use in tracking potential post-excretion alterations.

Given these considerations, this chapter aims to determine the stable carbon and oxygen isotope values of gut carbonates produced by a range of fish species, with specific objectives being to:

i) Characterise them with respect to other marine carbonates, thus potentially aiding identification of fish-derived carbonates in sediment samples;
ii) Provide baseline data for future investigations (*e.g.*, Chapter 7) on the preservation pathways of fish-derived carbonates; and
iii) Confirm the metabolic origin of intestinal HCO_3^-.

The work presented here does not, however, attempt to use these data to fully resolve issues of precipitation processes; there being too many unknown or complicating factors, such as: i) the types of precipitation-inducing gut microbes and the direction of their influence on carbon isotope fractionation; ii) the rate of crystal growth, which is known to cause departures from normal fractionation when high (Turner, 1982); and iii) the presence in many gut carbonate samples of multiple carbonate phases (see Chapter 3) that may precipitate with different fractionation factors (*e.g.*, Tarutani *et al*., 1969). Instead it serves as a pilot study for potential future work in this field, which may help to elucidate reasons for the variation in crystal form and composition with species.

Finally, while the results of Chapter 3 appear to indicate that carbonate preparation protocols (described in Chapter 2) have little or no influence on their properties, it has been shown that rinsing fine-grained carbonates in distilled water and allowing them to dry at room temperature can result in alteration of their stable carbon and oxygen isotope compositions (by up to 0.25 and 1.20 ‰, respectively) due to recrystallisation induced by this process (Barrera and Savin, 1987). Although this problem should be avoided by using the protocol outlined in Chapter 2 (because all cleaning and rinsing solutions are largely removed via vacuum filtration before drying), the effect of sample preparation protocols described in Chapter 2 is tested by determining stable isotope compositions for carbonates that have been subject to varying numbers of rinsing and drying cycles.

5.2 METHODOLOGY

Carbon dioxide was prepared for mass spectrometric measurement of carbon ($^{13}C/^{12}C$) and oxygen ($^{18}O/^{16}O$) isotope ratios in fish-derived carbonates by reacting samples with phosphoric acid (specific gravity of 1.91 to 1.92) under vacuum at 25^{o}C for approximately 16hr following a procedure similar to the 'sealed vessel' method described by McCrea (1950) and Swart *et al*. (1991). The CO_2 released by the reaction was recovered using standard cryogenic methods, and mass ratios (*m*/*z* 45/45 and *m*/*z* 46/44) were measured relative to a comparison (reference) CO_2 by dual-inlet, stable isotope ratio mass spectrometry using a VG SIRA10 mass spectrometer. Resultant

delta 45 and *delta* 46 values were corrected for ^{17}O effects following the procedures of Craig (1957) and calibrated to the VPDB (Vienna Pee Dee belemnite) international reference scale (see below) *via* concurrent measurement of calibrated calcite laboratory quality control materials prepared under identical conditions to the unknowns. Oxygen isotope data were subsequently adjusted for the temperature-dependent isotopic fractionation associated with the carbonate-phosphoric acid reaction using a fractionation factor (α) of 1.01025.

The isotopic compositions of unknown samples are reported as differences in the amount ratios of carbon and oxygen isotopes with respect to the same ratios defined for VPDB by reference to NBS 19 (Coplen, 1996). Resultant isotope data are expressed as $\delta^{13}C$ and $\delta^{18}O$ values on the VPDB scale, *e.g.*:

$$\delta_{c}(^{18}O) = \frac{n_{c}\left(^{18}O\right)/n_{c}\left(^{16}O\right) - n_{VPDB}\left(^{18}O\right)/n_{VPDB}\left(^{16}O\right)}{n_{VPDB}\left(^{18}O\right)/n_{VPDB}\left(^{16}O\right)}$$

where: $n_{c}(^{18}O)$ and $n_{c}(^{16}O)$ are, respectively, the amounts of ^{18}O and ^{16}O in calcite in units of moles, and similarly for those values defined for VPDB. Analytical precision for both isotope ratios is estimated to be better than $\pm 0.1\ ^{o}/_{oo}$ (1σ) based on replicate analysis of laboratory quality controls materials[1].

It is worth noting that some samples emitted a pink gas of unknown composition when reacted with phosphoric acid. Evolution of an unknown pink gaseous phase has also been observed following similar treatment of unrelated geological carbonate samples, and the resulting isotope data have been found to deviate from those of samples not generating a pink gas (S.F. Crowley, *Pers. Comm.*). Although the source of pink gas is unknown, it is thought possibly to be derived from sample contamination by organic matter. Indeed, Fourier transform infrared spectra (see Chapter 3) indicate the presence of minor amounts of organic matter associated with some fish-derived

[1] Dr. Stephen Crowley (University of Liverpool, School of Environmental Sciences) and Mr Paul Dennis (University of East Anglia, School of Environmental Sciences) performed all stable isotope analyses and subsequent calculations to derive reported $\delta^{13}C$ and $\delta^{18}O$ values.

carbonates. Fish-derived carbonates emitting a pink gas were therefore not analysed, and data for carbonates produced by Nassau grouper, bluehead wrasse, and keeltail needlefish are consequently omitted. Interestingly, carbonates from the latter two species were the only ones prepared for analysis that are known to contain AMC (see Chapters 2, 3, and 7), although whether or not this phase is related to the emission of pink gas is not known.

Samples used for the analyses described above were collected and processed using the same protocol as described in Chapter 2 (*i.e.*, rinsed with distilled water, soaked in a 5.25 % solution of sodium hypochlorite, rinsed again with distilled water, and transferred to a membrane via vacuum filtration before being dried in a low temperature oven at 50 °C). Complete removal of organic matter is necessary in the preparation of samples for stable isotope analysis as it likely has isotopic signatures that are distinct from associated inorganic carbonates and its presence can thus strongly skew data output. Potential changes in initial stable isotope compositions due to cleaning protocols are therefore unavoidable, and stable isotope data from any naturally occurring carbonates should always be interpreted with this caveat in mind.

Although it is not possible to determine potential changes in stable isotope ratios resulting from initial sample cleaning (*i.e.*, it is not possible to measure the stable isotope composition of inorganic carbonates without first cleaning the sample), the effects of subsequent repeated cleaning and drying cycles (up to 6) are tested here. Carbonate pellets produced by a single fish (schoolmaster snapper) were divided into four sub-sample sets (n = 3), and each was exposed to a different number of preparation cycles (*i.e.*, as described in the above paragraph) between one (*i.e.*, the way in which all other samples in this study were prepared) and six.

Apart from schoolmaster snapper, other species for which carbonates were analysed (after normal preparation in all cases) were black grouper, Graysby grouper, great barracuda, bonefish, yellowfin mojarra, and yellowtail snapper. Dietary preferences differ among these species (Randall, 1967), with the first three feeding almost exclusively on fishes, and the latter three (along with schoolmaster snapper) feeding on a mixture of crustaceans and fishes (but tending to favour

crustaceans). It has been shown that, although values are species-specific, crustaceans typically have similar or only slightly lower (by about 1 to 2 ‰ on average) $\delta^{13}C$ values in their soft parts compared with fishes inhabiting the same waters (Kieckbusch *et al*., 2004; Yeager and Layman, 2011). Consequently, it is predicted that $\delta^{13}C$ values of intestinal HCO_3^- (and thus gut carbonates) will be broadly similar among these species, thus making it difficult to confirm a metabolic source of HCO_3^-. Moreover, any observed differences will be difficult to confidently attribute to dietary factors due to the potential influence on carbon fractionation of other unknown factors that might be species-specific (*e.g.*, different gut microbial populations, or different metabolic rates).

In order to confirm the metabolic origin of HCO_3^-, carbonate samples from one fish species (schoolmaster snapper) were collected after: i) a two day starvation period following capture from the wild (*i.e.*, natural diet); and ii) a two day starvation period after being fed on a diet that was isotopically distinct from their natural diet. For the latter, fish were held in aquaria conditions (one-pass natural seawater at similar temperature and salinity conditions to those of ambient local surface seawater) and fed a diet consisting only of sardines (*Sardinella aurita*; Cap'n Salty, Raffield Fisheries Inc., Port St. Joe, FL; sourced in the Gulf of Mexico) for at least two weeks. Although the stable isotope ratio of organic carbon was not measured in either diet, existing data indicate that the natural diet of schoolmaster snapper (mainly fishes and crustaceans) in the Bahamas is probably depleted in ^{13}C by about -15 to -14 ‰ relative to VPDB (Kieckbusch *et al*., 2004; Lamb *et al*., 2012), whereas zooplankton (the main dietary component of *Sardinella aurita*) in the Gulf of Mexico (where sardines were sourced) is depleted by about -21.9 to -20.5 ‰ relative to VPDB (Thayer *et al*., 1983). Bode *et al*. (2004) find that carbon isotope fractionation in sardines results in a 2 ‰ enrichment in ^{13}C over their dietary intake (*i.e.*, close to the pattern observed in other fish species by Fry *et al*., 1982), and $\delta^{13}C$ values of organic carbon in this experimental diet should therefore have been about -20 to -18 ‰ (*i.e.*, depleted by about 3 to 6 ‰ compared to the natural diet of schoolmaster snapper).

Due to the way in which fish were obtained, it was also necessary to feed some bonefish on a diet of sardines for two weeks prior to sample collection, and carbonates available for stable isotope analysis from this species were mostly from these fish. However, one additional sample from a recently caught, naturally fed bonefish was analysed for comparison. In addition to the fish species listed above, one sample produced by checkered puffer was also analysed. As with some bonefish, it was necessary to feed this fish a diet of sardines prior to sample collection, and the measured stable isotope composition therefore reflects this.

5.3 RESULTS

Carbon and oxygen stable isotope compositions were determined for fish-derived carbonates produced by eight fish species, the results of which are summarised in Table 5.1 and shown in full in Figs. 5.1–5.2 and in Appendix V. In general, carbonates produced by fish that have had only natural diets typically yield $\delta^{18}O$ values in the range -0.5 to 2.0 ‰$_{VPDB}$, and $\delta^{13}C$ values in the range -3.0 to 2.5 ‰$_{VPDB}$, and as such they are isotopically distinct from most other common marine carbonates (Swart *et al.*, 2009). Ignoring species as a factor, it appears that $\delta^{18}O$ values are the most tightly constrained (full range covers 2.41 ‰), whereas $\delta^{13}C$ values are highly variable (full range covers 5.90 ‰). However, by taking species into account it is evident that the opposite is true; all species for which multiple samples were analysed (Table 5.1) producing carbonates that return $\delta^{18}O$ values over ranges covering about 1.5 ‰, whereas $\delta^{13}C$ values occur within reasonably narrow ranges of 0.4 to 0.8 ‰ for all species except great barracuda (range = 2.07 ‰).

Table 5.1 *Key data arising from stable isotope analyses of carbonate samples produced by naturally fed and sardine-fed fish.*

Species	Natural diet			Sardine diet			Δ_{Diet} ‰
	n	$\delta^{13}C$ ‰ (VPDB) (±SE)	$\delta^{18}O$ ‰ (VPDB) (±SE)	n	$\delta^{13}C$ ‰ (VPDB) (±SE)	$\delta^{18}O$ ‰ (VPDB) (±SE)	
Schoolmaster snapper	8*	-1.27 (±0.09)	1.47 (±0.21)	3	-5.75 (±0.49)	0.70 (±0.46)	4.48
Bonefish	1	2.55	1.65	4	-1.84 (±0.41)	0.30 (±0.67)	4.39
Black grouper	3	-0.11 (±0.12)	0.57 (±0.37)	-	-	-	-
Yellowfin mojarra	3	-0.91 (±0.19)	0.59 (±0.47)	-	-	-	-
Yellowtail snapper	1	-1.92	0.65	-	-	-	-
Graysby grouper	1	-0.33	1.23	-	-	-	-
Great barracuda	3	-2.00 (±0.68)	0.66 (±0.49)	-	-	-	-
Checkered puffer	-	-	-	1	-5.71	1.17	-

* Due to an apparent negative correlation between $\delta^{13}C$ and number of cleaning cycles (see Fig. 5.3), $\delta^{13}C$ values from samples rinsed and dried more than twice are discarded here. However, $\delta^{18}O$ values show no variation with number of cleaning cycles, and values from all 14 samples are therefore included here.

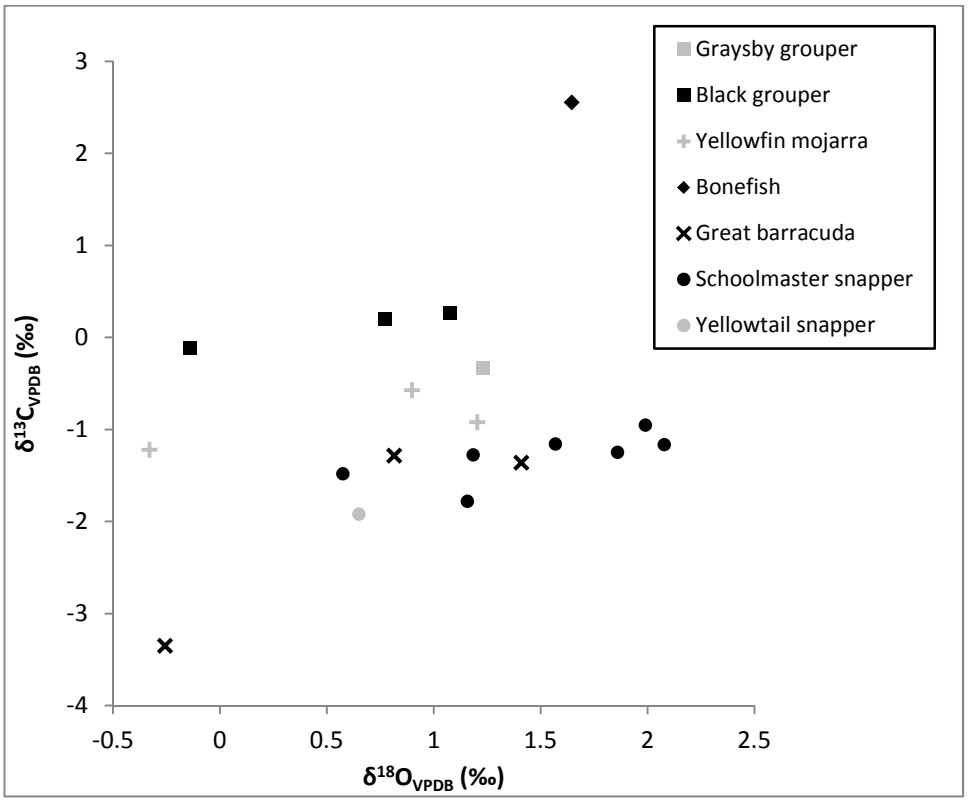

Figure 5.1 *Stable carbon and oxygen isotope compositions of carbonate precipitates excreted by 7 Bahamian fish species. Fish that produced these carbonates were wild-caught a few days prior to sample collection and were not fed between capture and carbonate excretion.*

The large overall range of $\delta^{13}C$ values in combination with the relatively narrow ranges for each species indicates that carbonate $\delta^{13}C$ values vary according to species. Indeed, based on this admittedly small (because of small sample sizes and omission of numerous samples due to contamination; see section 5.2) dataset, it is possible to say that $\delta^{13}C$ values for carbonates from naturally fed fish differ significantly among at least some families. For example, by pooling the results from carbonates produced by all grouper (n = 4) and all snapper (n = 9) species, it can be demonstrated that those produced by the former are significantly enriched in ^{13}C (by about 1 ‰) compared to those produced by the latter (Mann-Whitney U test; p = 0.004). Ambient environmental conditions were similar for all fish at the time of sample collection, suggesting there was some other control on this variation. One possibility is that bulk mineralogies and/or magnesium contents (which have different bicarbonate⁻solid phase ^{13}C fractionation factors; Rubinson and Clayton, 1969; Jimenez-Lopez *et al*., 2006) varied between these families, but morphological and compositional analyses show that their carbonates are characterised in all cases by ellipsoidal Mg calcite with ~30 mol% $MgCO_3$ (see Chapter 2). This result is therefore indicative of some species-specific biological control on $\delta^{13}C$ values, which, in this case, can be readily be explained by dietary differences; the data of Kieckbusch *et al*. (2004) indicating that organic carbon in the diet of groupers (piscivores) is likely to be enriched in ^{13}C by about 1 ‰ relative to the diet of the snappers (pisci-invertivores).

The role of dietary carbon in gut carbonate precipitation is further confirmed by data arising from carbonates produced by sardine-fed fish. Such carbonates produced by schoolmaster snapper yield $\delta^{18}O$ values within a similar range to that of carbonates produced by naturally fed fish, but $\delta^{13}C$ values are strongly depleted (Fig. 5.2); the difference between averages being 4.48 ‰ (Table 5.1). Statistical analysis of the two samples sets (from sardine-fed and naturally fed fish) indicates that this difference is significant (Mann-Whitney U test; p = 0.012), thus supporting previous observations of a metabolic origin for a least some intestinal HCO_3^- in fish (although it is conceivable that the change in diet here induced a change in gut microbial activity which might have influenced ^{13}C distribution). The single data point from carbonates produced by sardine-fed

checkered puffer is within the range of those produced by sardine-fed schoolmaster snapper, and, if the sardine diet causes a similar depletion of ^{13}C in this species, it is predicted that carbonates produced by checkered puffer with a natural diet will have a stable isotope composition within the range of most other fish-derived carbonates documented here.

Carbonates produced by sardine-fed bonefish, however, show no $\delta^{13}C$ depletion compared with values from carbonates produced by other species that were naturally fed, with values in the range -2.81 to -0.91 $‰_{VPDB}$ (Fig. 5.2). This enrichment compared to carbonates produced by sardine-fed schoolmaster snapper is easily explained when the single data point for carbonates from naturally fed a bonefish is taken into consideration; this result being enriched in ^{13}C compared to carbonates produced by naturally fed schoolmaster snapper, therefore suggesting that all carbonates produced by bonefish are enriched in ^{13}C relative to those of other species. In fact, the difference between average values for carbonates from sardine-fed and naturally fed bonefish of 4.39 ‰ (Table 5.1) is remarkably close to the equivalent difference between samples produced by schoolmaster snapper. Assuming the single data point from naturally fed fish to be representative, and that the natural diets of schoolmaster snapper and bonefish are isotopically similar (which would appear likely given the similar depletion in ^{13}C of carbonates caused by the sardine diet), this result indicates that there are likely to be species-specific controls on the distribution of ^{13}C other than just dietary.

It is worth pointing out here that no morphological or compositional (with respect to $MgCO_3$) differences were noted between samples produced by sardine-fed and naturally fed fish, indicating that partitioning of different amounts of ^{13}C has no direct effect on the overall characteristics of precipitation products. However, it is interesting to note that, whereas carbonates produced by most species investigated here are morphologically, mineralogically, and isotopically similar, those produced by bonefish differ from the rest in all of these aspects. This is discussed further below.

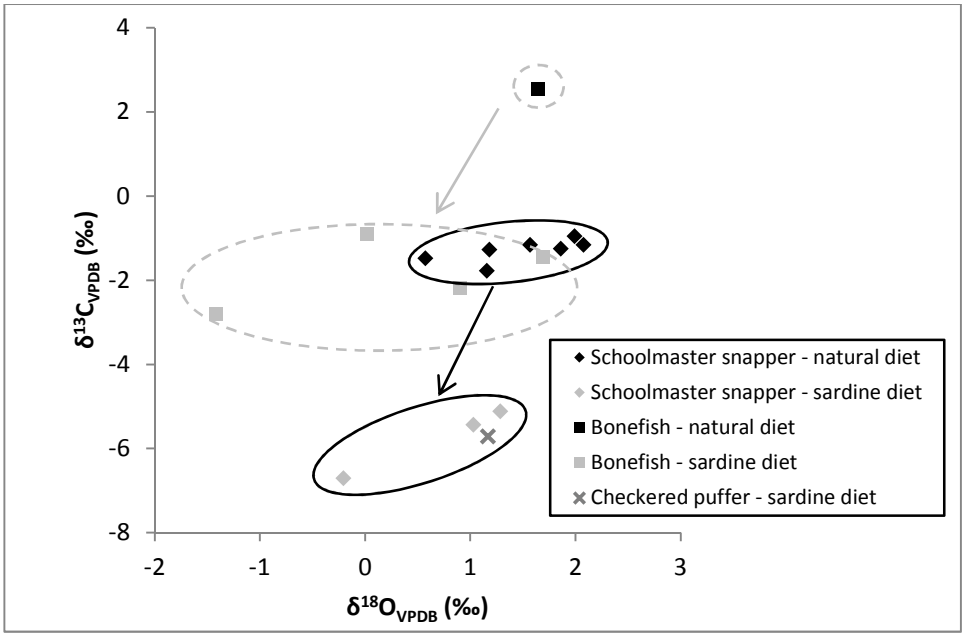

Figure 5.2 *Comparison of stable oxygen and carbon isotope data from carbonates produced by naturally fed fish (black markers) and sardine-fed fish (grey markers).*

An important caveat to mention with regard to the data described above is that of the effects of sample preparation, as alluded to in Table 5.1. Mass spectrometry of carbon and oxygen evolved from high-Mg calcite ellipsoids prepared with varying numbers of repeat cleaning and drying cycles (Fig. 5.3) indicates that the sample preparation protocol described in Chapter 2 causes no significant change in $\delta^{18}O$ values (Kruskal-Wallis one-way ANOVA: df = 3; H = 2.49; p = 0.478), but does cause a significant depletion in $\delta^{13}C$ of ~0.13 ‰ per cycle (Kruskal-Wallis one-way ANOVA: df = 3; H = 9.48; p = 0.024). This finding suggests that the $\delta^{13}C$ values reported above could be ~0.13 ‰ lower than actual values at the point of excretion, at least for samples dominated by Mg calcite with similarly high $MgCO_3$ contents (which is the case for all samples except those produced by bonefish and checkered puffer; see Chapter 2). However, this is difficult to confirm owing to the problems associated with analysing samples without prior removal of organics.

This change in $\delta^{13}C$ is surprisingly large given that most of any dissolved ions should have been removed via vacuum filtration prior to each drying cycles, and therefore should not have reprecipitated to cause alterations in the stable isotope composition of sample material. Progressive removal of organic matter is also an unlikely cause of these changes because it is usually

significantly more depleted in ^{13}C than inorganic carbonates and its removal would therefore have caused $\delta^{13}C$ values to change in the opposite direction. A possibility that cannot be ruled out is that changes are due to incongruent dissolution during each cleaning cycle of a carbonate phase that is enriched in ^{13}C relative to the bulk sample. Partitioning of carbon isotopes has been shown to vary with magnesium content in calcite, with $\delta^{13}C$ values increasing by about 0.024 ‰ per mol% $MgCO_3$ (Jimenez-Lopez *et al*., 2006). However, assuming the data of Jimenez-Lopez *et al*. (2006) are applicable to all calcites, for incongruent dissolution of $MgCO_3$ from high-Mg calcite to result in a 0.13 ‰ depletion in $\delta^{13}C$ per cycle would require significant depletion in $MgCO_3$ content (by about 5 mol% on average), yet this is not observed. Another possible explanation is preferential dissolution of a discrete phase such as amorphous calcium carbonate (ACC). Stable isotope partitioning into ACC has received little or no attention in the literature but it could differ to that in calcite. The presence of such a phase has not been confirmed in samples produced by this species (schoolmaster snapper), but equally it has not been completely ruled out (see Chapter 3).

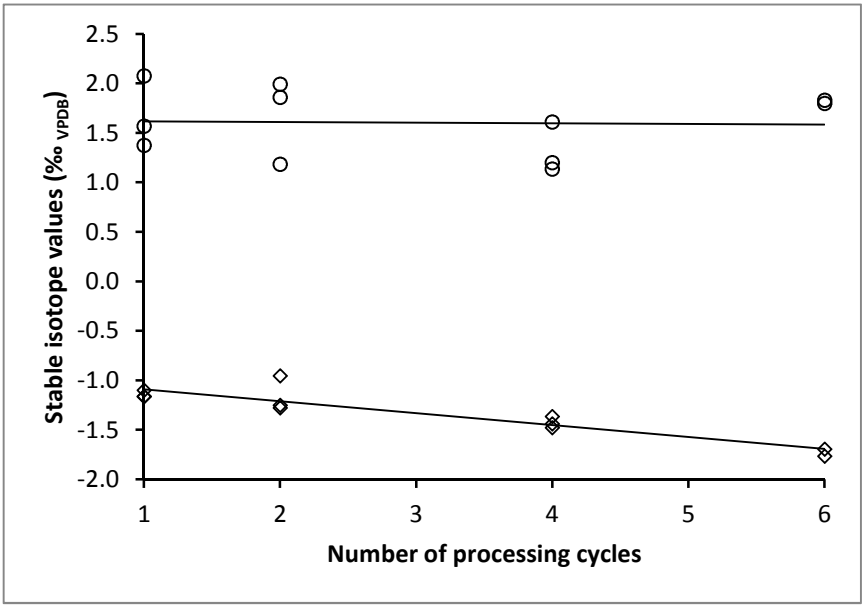

Figure 5.3 *Relationship between isotopic composition and the number of cleaning and drying cycles applied to carbonate samples. Open circles show $\delta^{18}O$ values; open diamonds show $\delta^{13}C$ values. $\delta^{18}O$ appear to remain stable regardless of the number of processing cycles. However, $\delta^{13}C$ appears to become depleted at a rate of ~0.13 ‰ per processing cycle (linear $R^2 = 0.869$).*

5.4 DISCUSSION

5.4.1 Precipitation processes

Data arising in this study indicate that carbonates produced in the gut of starved (but previously consuming a natural diet) fish are isotopically varied among species, but are typically distinct from other sedimentary carbonates, having slightly more positive $\delta^{18}O$ values (typically in the range 0 to 2 $‰_{VPDB}$), and slightly more negative $\delta^{13}C$ values (typically in the range -2 to 0 $‰_{VPDB}$). Interpreting values for $\delta^{18}O$ is hampered by the fact that: a) samples commonly contain crystals with a broad range of $MgCO_3$ contents (Perry *et al*., 2011; Salter *et al*., 2012), and it is known that calcite is about 0.06 ‰ heavier for each mol% $MgCO_3$ it contains (Tarutani *et al*., 1969); b) samples contain variable amounts of brucite (see Chapter 3), the presence of which may influence bulk sample values; and c) several samples (especially those produced by checkered puffer, bonefish , and great barracuda) contain hydrated phases, and the effect of oxygen isotopes associated with water is not known. These factors, along with the fact that some samples probably contain mixed carbonate phases (*e.g.*, samples produced by great barracuda and yellowfin mojarra can contain significant quantities of aragonite; see Chapter 2), may explain the reasonably broad range of measured $\delta^{18}O$ values for carbonates from each species. Nevertheless, average values for per species are in the range 0.7 to 1.4 ‰ (Table 5.1), which are slightly higher than the average of about 0.1–0.4 ‰ for bulk surface sediments from the Great Bahama Bank (GBB), but within the range of extreme reported values (Shinn *et al*., 1989; Swart *et al*., 2009). Shinn *et al*. (1989) and Swart *et al*. (2009) use their data to suggest that most of the surface sediment must be of abiotic origin because biogenic carbonates produced in the same waters typically have significantly more negative values of $\delta^{18}O$, with even high-Mg calcite (which should be enriched in ^{18}O relative to aragonite precipitated from the same solution) having values of about -6 ‰ (Patterson and Walter, 1994a). The data presented here clearly contradict this model of ^{18}O depletion in biogenic carbonates, and it thus appears that HCO_3^- (of combined ambient seawater and metabolic origins) in the piscine gut is somehow enriched in ^{18}O relative to the pooled HCO_3^- that leads to the

formation of other biogenic carbonates. Temperature variations, which are known to be a control on ^{18}O fractionation in $CaCO_3$ (Grossman and Ku, 1986), are probably not an important control here as most marine teleosts are poikilothermous (Morrow and Mauro, 1950).

Values of $\delta^{13}C$ are perhaps easier to interpret. Carbonate precipitates excreted by most species typically yield values in the range -2 to 0 $‰_{VPDB}$, which is substantially lower than average values for bulk surface sediments from the GBB of about 3 to 5 $‰_{VPDB}$. This result is in good agreement with the hypothesis presented in section 5.1, and suggests that a large proportion of the HCO_3^- in intestinal precipitating fluids has a metabolic origin; an assertion that is further supported by the fact that fish fed a ^{13}C-depleted diet for two weeks produced carbonates that are significantly depleted in ^{13}C.

However, if dietary $\delta^{13}C$ values are the sole reason for among-species variation in measured $\delta^{13}C$ values of carbonate precipitates, it is difficult to explain why carbonates produced by great barracuda (a piscivore) tend to yield lower $\delta^{13}C$ values than those produced by grouper species (also piscivores). By the same token, it is difficult to explain differences between carbonates produced by bonefish and schoolmaster snapper. Interestingly, carbonates produced by bonefish, and probably by great barracuda as well, commonly contain ACC (Chapters 2 and 3), whereas this is not an abundant phase in carbonates produced by other species analysed here. The possibility thus arises that the carbonates of these species deviate isotopically from those of other species with similar diets because of different bicarbonate–ACC and bicarbonate–calcite ^{13}C fractionation factors. However, this appears unlikely to be the cause of deviation for both species since the deviations are in different directions (*i.e.*, carbonates produced by great barracuda are more negative than those produced by groupers, whereas carbonates produced by bonefish are more positive than those produced by snappers). Nevertheless, if fractionation factors do differ between these phases, and if the bulk isotopic composition of carbonates produced by one of these species is thus influenced, this may also explain differences in crystalline phases. For example, in Chapter 7 it is shown that the removal of ACC from bonefish carbonates (leaving only well-crystallised calcite)

does not result in a shift in stable isotope composition. It is therefore apparent that ACC either: i) involves similar fractionation factors to calcite; or ii) crystallises as calcite and imparts stable isotope ratio different to that which might be expected if calcite precipitated in equilibrium with precipitating fluids (as has similarly been suggested for dolomite altered from calcite; Degens and Epstein, 1964). Regardless of the potential effect of bicarbonate–ACC fractionation factor, the fact that it is difficult to explain isotopic deviations of both bonefish and great barracuda by this possibility suggests that either: i) the carbon isotope compositions of dietary items are more varied among species than is assumed (*e.g.*, fish species favoured by great barracuda could be isotopically lighter than those favoured by black grouper); or ii) there are other species-specific factors that influence the distribution of ^{13}C in intestinal precipitating fluids, as postulated in section 5.1.

Calcite is usually considered to be enriched in ^{13}C by about 1 ‰ over bicarbonate in the solution it precipitates from (Rubinson and Clayton, 1969). Assuming fish-derived carbonates adhere to this relationship, and by taking into account a 0.024 ‰ enrichment factor for each mol% $MgCO_3$ in calcite (Jimenez-Lopez *et al*., 2006), the $\delta^{13}C$ value for intestinal HCO_3^- for most species investigated here would appear to be in the range -4 to -2 ‰. These values are highly enriched compared to values hypothesised in section 5.1 (approximately -14 ‰). Following the same approach as in that section, the 'best-case' scenario for a Bahamian fish would be to assume a $\delta^{13}C$ value of about -10 ‰ for its muscle tissue (as shown to be the case for some species by Kieckbusch *et al*., 2004), in which case intestinal HCO_3^- could be expected to have a value of -9 ‰, and the resulting high-Mg calcite would have a value of about -7 ‰. The discrepancy of about 5 ‰ between this value and measured values suggests either that: i) fractionation factors between dietary carbon and carbohydrate, carbohydrate and intestinal HCO_3^-, and intestinal HCO_3^- and precipitated calcite differ from those used in the above estimates; ii) enzymatic and/or microbial processes further influence the carbon isotopic signature of intestinal HCO_3^-; iii) carbonate initially precipitates as an isotopically distinct unstable phase that transforms to calcite and imparts an isotopic signature that appears to be in disequilibrium with precipitating fluids; or iv) more seawater DIC is involved in carbonate precipitation than hypothesised in section 5.1. These

scenarios are shown schematically in Fig 5.4. With regard to the latter, assuming an average $\delta^{13}C$ value for seawater DIC of about 1 ‰ (Swart *et al*., 2009), and taking the 'best-case' scenario described above where metabolic HCO_3^- has a $\delta^{13}C$ value of about -9 ‰, the bulk $\delta^{13}C$ value for HCO_3^- 'pooled' from a 50:50 mixture of seawater DIC and metabolic HCO_3^- would be about -4 ‰, and the resulting calcite precipitates would be expected to have a $\delta^{13}C$ value of about -2 ‰. This is much closer to measured values reported herein, but it is difficult to conceive a 50:50 mixture of seawater DIC and metabolic HCO_3^- given the reported degrees in elevation of intestinal HCO_3^- concentration relative to seawater (Wilson *et al*., 1996).

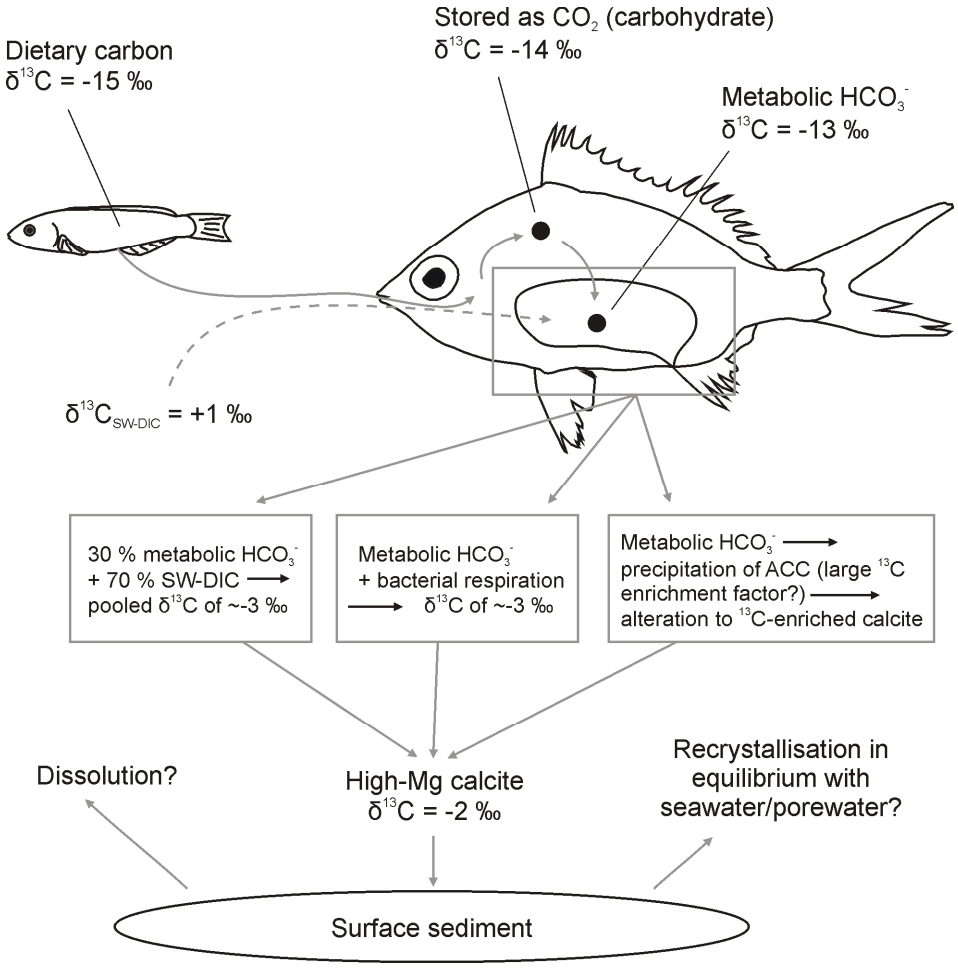

Figure 5.4 *Schematic diagram showing hypothesised pathways of ^{13}C between dietary carbon and excreted gut carbonates. A disparity in metabolic HCO_3^- $\delta^{13}C$ values and those of excreted carbonates that cannot be explained by bicarbonate–calcite fractionation factors alone requires additional factors to be invoked (grey boxes). The absence of isotopically similar carbonates in surface sediments (according to existing literature; e.g., Swart et al., 2009) suggests that fish-derived carbonates are either not a significant component of carbonate production in the Bahamas, or dissolve rapidly after excretion. Other studies (Patterson and Walter, 1994a) indicate another possibility is recrystallisation in equilibrium with surrounding fluid.*

5.4.2 Relevance to studies of bulk surface sediment in the Bahamas

Regardless of the mechanisms that control these stable isotope compositions, the results clearly indicate that carbonates produced by at least 6 naturally fed Bahamian fish are: i) depleted in ^{13}C relative to bulk surface sediments and abiotic carbonates; and ii) enriched in ^{18}O relative to biogenic carbonates with similar $\delta^{13}C$ values (Fig. 5.5). If it is assumed that most other piscivores and invertivores in the Bahamas produce isotopically similar carbonates, and that herbivores and planktivores produce carbonates that are slightly more depleted with respect to ^{13}C (because their diets are more depleted; Lamb *et al*., 2012), then it is reasonable to assume that fish-derived carbonates, where present, should cause deviations in bulk surface sediment isotopic compositions away from values for carbonates precipitated in equilibrium with seawater. Furthermore, given that Perry *et al*. (2011) show there are likely to be large variations in the relative contributions of fish-derived carbonates to carbonate production budgets according to habitat, the degree of this deviation should vary by habitat.

Although the extensive dataset of Swart *et al*. (2009) indicates that surface sediment carbon and oxygen isotope compositions are uniform across the GBB and do not vary by facies, which would appear to indicate that fish-derived carbonates are perhaps not as significant in shallow sub-tropical carbonate sediments as initially suggested, or that production rate is not as varied by habitat (Perry *et al*., 2011), two further possible scenarios may explain this disparity. Firstly, Swart *et al*. (2009), while characterising the facies from which analysed sediment samples were collected, do not discriminate between habitat settings, and it is possible that many of their samples were collected from bare sands or seagrass meadows that characterise a large portion of the GBB (and 95 % of the areal extent of the Bahamian platform; Perry *et al*., 2011). These habitats are thought to represent areas in which fish-derived carbonates represent <1 % of the total mass of carbonate mud production (Perry *et al*., 2011), and should therefore have negligible influence on $\delta^{13}C$ and $\delta^{18}O$ values of bulk sediment. Comparison of results of stable isotope analyses from specific habitats would clearly be more appropriate in this respect and should be a subject of future studies.

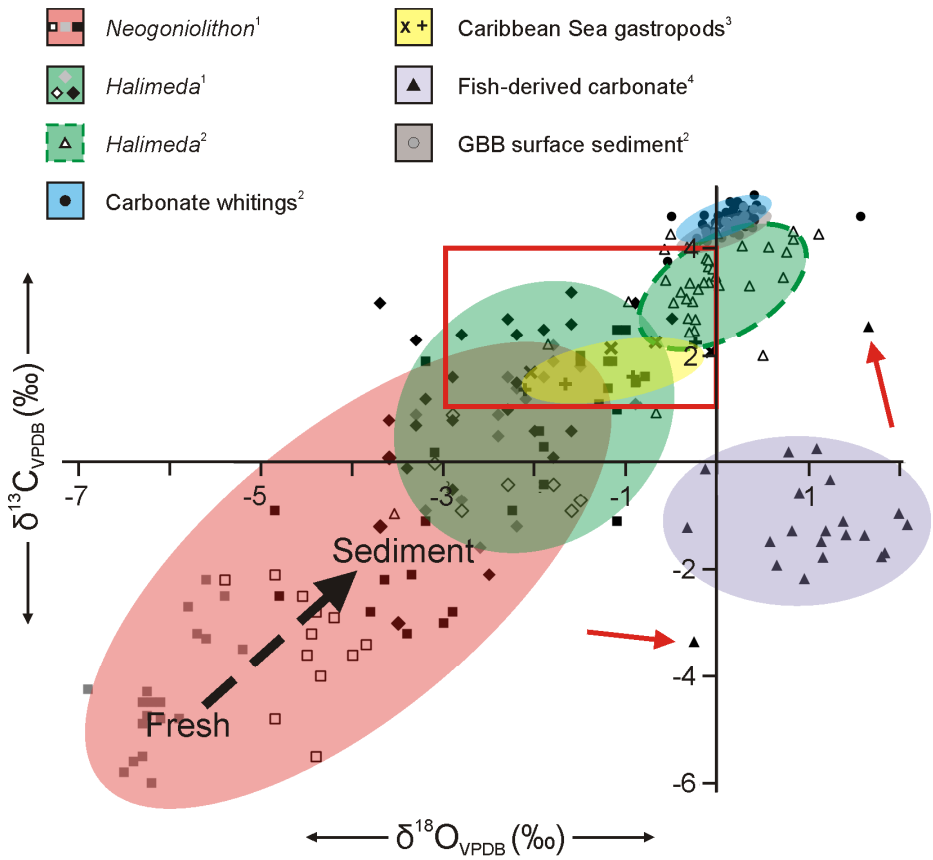

1 - Patterson and Walter, 1994a (grey markers = freshly precipitated; white markers = 500 days in porewater; black markers = fragments from surface sediment)
2 - Shinn *et al*., 1989 (nb. results for surface sediment are similar to Swart *et al.*, 2009)
3 - Lecuyer *et al*., 2012 (**+** = calcite; **x** = aragonite)
4 - This study

Figure 5.5 *Existing data on stable carbon and oxygen isotope compositions for: i) bulk surface sediments in the Bahamas; and ii) various common sources of sedimentary carbonate in shallow platform settings of the same region. These data are plotted alongside all data for carbonates produced by naturally fed fish in the Bahamas (note red arrows pointing to extreme data points). Red rectangle highlights the estimated stable isotope compositions of Mg calcite and aragonite in equilibrium with shallow Bahamian porewaters (after Walter et al., 1993), which most sedimentary (i.e., not freshly precipitated) carbonates are close to.*

Secondly, and perhaps more significantly, studies of high-Mg calcite from *Neogoniolithon* red algae indicate that these carbonates are precipitated under a strong biological influence and are well outside the limits of isotopic equilibrium with surrounding seawater (Patterson and Walter, 1994a). However, it is also shown that they rapidly recrystallise and, in doing so, move towards isotopic equilibrium with the solutions to which they are exposed. This isotopic shift is significant within only 500 days of exposure, and largely complete in *Neogoniolithon*-derived carbonate preserved in surface and shallow sub-surface sediments. If it is assumed that all red alga produce high-Mg calcite similarly depleted in ^{13}C, the carbonate production budget of Perry *et al*. (2011) suggests

that, ignoring recrystallisation, carbonate muds in some habitat settings (*e.g.*, seagrass meadows) should be dominated by an isotope signature depleted in ^{13}C. The fact this is not observed (Shinn *et al*., 1989; Swart *et al*., 2009) suggests most of this high-Mg calcite either dissolves (Moulin *et al*., 1985; Walter *et al*., 1993), or recrystallises as described above (Patterson and Walter, 1994a). It is worth noting that the possibility of biogenic carbonates recrystallising in isotopic equilibrium with seawater or porewater is seemingly not considered by Shinn *et al*. (1989) and Swart *et al*. (2009) when using their data to conclude that platform-top sediments in the Bahamas are largely of abiotic origin. Given that fish-derived carbonates are dominated by high-Mg calcite, and are therefore probably of similar or lower stability than *Neogoniolithon*-derived high-Mg calcite (see Chapters 1–3), it is likely that, if preserved, they will similarly recrystallise and may lose their distinctive isotopic signature in the process.

5.5 CONCLUSIONS

1. At the point of excretion, fish-derived carbonates are depleted in ^{13}C compared to most surface sediments from shallow platform settings in the Bahamas, and enriched in ^{18}O compared to biogenic carbonates from the same area, with values typically in the range -2.0 to 0.0 $‰_{VPDB}$ and 0.0 to 2.0 $‰_{VPDB}$, respectively.
2. Existing data from bulk surface sediment samples from the Bahamas show no evidence for the presence of isotopically distinct fish-derived carbonates. Habitats in which fish-derived carbonate production is thought to be significant may have been overlooked, but other possibilities include removal of the distinctive isotope signatures via: i) preferential dissolution of fish-derived carbonates over other carbonate sources; and ii) recrystallisation in equilibrium with local seawater or porewater DIC.
3. Depletion of ^{13}C is expected due to a metabolic origin of intestinal HCO_3^-, which is confirmed in a sample set collected from diet-controlled fish. However, depletion occurs to a lesser degree than expected based on knowledge of carbon fractionation factors, and one or more of the following additional factors are invoked to explain

measured $\delta^{13}C$ values: i) significant contribution from imbibed seawater DIC; ii) alteration of intestinal HCO_3^- by gut microbial and/or enzymatic activity; and iii) initial precipitation as an unstable phase that has a high ^{13}C enrichment factor, followed by transformation of to calcite while maintaining original stable isotope ratios.

4. The latter point may explain the ^{13}C enrichment observed in carbonates produced by bonefish (which can be dominated by ACC) compared to those produced by other species, although species-specific factors (*e.g.*, unique gut microbial populations) cannot be ruled out.

5. Sample preparation causes no change in $\delta^{18}O$ values. However, at least in high-Mg calcite ellipsoids it appears to cause depletion in $\delta^{13}C$ values of ~0.13 ‰ per processing cycle, possibly due to preferential dissolution of an unknown ^{13}C-enriched phase. The effects of sample preparation on stable isotope compositions thus appear to be small when only one cycle is performed, although further testing is required on a wider range of precipitation products.

6. Further work on gut fluids and processes is necessary to facilitate better understanding of stable isotope pathways prior to and during precipitation, while other studies should aim to elucidate the post-excretion behaviour of fish-derived carbonates with respect to their stable isotope compositions (see Chapter 7 for a pilot study). A larger number of samples and species should also be investigated to better constrain the limits of stable isotope compositions in these carbonates.

Chapter 6: Size fraction analysis of fish-derived carbonates: implications for their deposition in and around shallow sub-tropical marine carbonate provinces

Parts of this chapter have been submitted for publication in the journal, Geology. Revisions based on the comments of four independent reviewers are incorporated here.

6.1 INTRODUCTION

Chapters 2 and 3 of this thesis (see also Perry *et al*., 2011; and Salter *et al*, 2012) have provided detailed descriptions of the various Mg calcite crystal forms precipitated within the intestines of 22 species of marine teleost in the Bahamas. These crystals are typically found to be loosely aggregated mud-grade (<63 μm) components of larger (approximately 1–2 mm diameter) excreted carbonate pellets which, as shown in Chapter 2, readily disaggregate to release these component particles. The sedimentary significance of fish-derived carbonates has thus been considered to-date only with respect to carbonate mud.

Crystal measurements, although not exhaustive, indicate that these mud-grade crystals span more than two orders of magnitude in size, ranging from <0.5 μm diameter (nanospheres) to ~50 μm diameter (spheres) (Salter *et al*., 2012). Assuming normal laws of particle settling apply, this size difference must mean there is potential for differential transport and deposition of fish-derived carbonates according to morphotype. For example, if two spherical particles of equal density are suspended in the same medium, Stokes' Law of particle settling velocity (eq. 6.1; Batchelor, 1967) predicts that particles differing in size by two orders of magnitude will have settling velocities that differ by four orders of magnitude.

Stokes' Law: $$v_s = \frac{2}{9}\frac{\rho_p - \rho_f}{\mu} g R^2$$ *equation* 6.1

where v_s is particle settling velocity ($m \cdot s^{-1}$), ρ_p is the particle density ($kg \cdot m^3$), ρ_f is the fluid density ($kg \cdot m^3$), μ is the dynamic viscosity of the fluid ($kg \cdot m^{-1} \cdot s^{-1}$), g is acceleration due to gravity ($m \cdot s^{-2}$), and R is the particle radius (m). Assuming a particle density of 2710 $kg \cdot m^3$, a fluid density of 1024 $kg \cdot m^3$ (*i.e.*, the densities of calcite and tropical surface seawater, respectively) and seawater dynamic viscosity of 0.9 x 10^{-3} $kg \cdot m^{-1} \cdot s^{-1}$ (approximate value for Bahamian surface seawater; Sharqawy *et al*. 2010), Stokes' Law predicts that a nanosphere of diameter 0.5 μm will settle at velocity 2.56 x 10^{-7} $m \cdot s^{-1}$, and a sphere of diameter 50 μm will settle at velocity 2.56 x 10^{-3} $m \cdot s^{-1}$. To put this in the context of a typical Bahamian platform setting, assuming particles are initially suspended in a quiescent setting one metre above a substrate, this means that a sphere will take approximately 6.5 minutes to settle out from suspension, whereas a nanosphere will take approximately 45 days. While these calculations should not be taken as actual values for the settling velocities of fish-derived carbonates (as shown in Chapter 2, some crystals have hollow interiors, most are not spherical, and densities will vary according to $MgCO_3$ content), they clearly demonstrate the potential for differential transport and deposition of fish-derived carbonates according to morphotype.

In addition to variations in crystal size, further consideration should also be given to the degree and rate of natural pellet disaggregation as a factor controlling the transport and depositional fates of fish-derived carbonates. Salter *et al*. (2012) describe disaggregation as occurring readily during brief sonication of wet pellets, and at pin prick for dry pellets. In natural settings pellet breakdown will presumably proceed as a result of physical disturbances such as agitation and attrition (due to tidal currents and wave action) and/or bioturbation (*e.g.*, reworking of sediment or the mastication and ingestion of pellets by other marine organisms), but the influence of these processes will vary according to platform setting and may not necessarily act to fully disaggregate pellets.

It is useful here to refer to similar particle types that are common constituents of Bahamian platform sediments. On the Great Bahama Bank (GBB), surficial sediments occupying large areas

of the inner platform are assigned to the pellet mud facies (Newell *et al*., 1959; Purdy, 1963), wherein a substantial fraction of sediment comprises carbonate pellets made up of aggregated mud-grade particles. Various types of pellet are recognised but, owing to morphological and compositional similarities and the subsequent difficulties in making confident genetic interpretations, they are usually referred to under the blanket term of peloids (Table 6.1; McKee and Gutschick, 1969; Bathurst, 1975; Flügel, 2004). Among numerous postulated peloid origins summarised by Flügel (2004) are: i) faecal pellets comprising mud-grade particles, formed by the ingestion, aggregation, and excretion of carbonate particles by a range of organisms, particularly sediment-grazers such as polychaete worms, crustaceans, and gastropods (Illing, 1954; Kornicker and Purdy, 1957); ii) aggregated 'pseudopellets', formed by hydraulically controlled aggregation of mud-grade particles on the sediment surface (Fahraeus *et al*., 1974); iii) *in situ* biochemical precipitation of carbonates (Chafetz, 1986); and iv) alteration of original carbonate particles, either rounded (such as ooids; Flügel, 2004), or non-rounded (such as bivalves; Samankassou *et al*., 2005). The latter two grain types are commonly cryptocrystalline, characterised by a pervasive micritic texture that lacks any internal fabric, but in the geological record the original characteristics of any peloid type can be obscured by pervasive alteration (Flügel, 2004). On modern platform interiors of the Bahamas, the pellet-mud facies comprises, on average, 57% sand-grade material, of which faecal pellets and mud-aggregate 'pseudopellets' make up 38%, compared with only 2% cryptocrystalline grains (Purdy, 1963).

Importantly, Illing (1954) notes that faecal pellets from modern platform settings can vary in their cohesive strength, ranging from those that disaggregate readily at pin prick (and in this way are not dissimilar to fish-derived carbonates), to those that are considerably more resistant to breakage. This variation in strength is attributed to varying degrees of induration within these faecal pellets, and Illing (1954) thus demonstrates that pellets with initial characteristics similar to those of fish-derived carbonate pellets (at the point of excretion), held together only by insubstantial cement, organic matter, or the interlocking of constituent particles, do not only maintain their original form in some Bahamian platform settings, but can also become well-cemented and thereby maintain that

form for long periods. It is thus reasonable to suppose that some fish-derived carbonate pellets might behave in a similar manner, and the assertion that fish-derived carbonates are a source of mud-grade carbonates should perhaps be modified to reflect this.

Given these potential controls on transport and deposition of fish-derived carbonates, the aims of this chapter are two-fold: 1) to provide a detailed assessment of grain size variation of the main crystal forms described by Salter *et al*. (2012); and 2) to determine the grain size variations of pellets produced by these species in their excreted form, and to assess the degree and extent of pellet disaggregation by agitation. In view of pellets having possible sedimentary significance, their morphologies are better characterised to aid identification in carbonate sediment samples, and their variation in size with fish species is also considered. Pellet size is a major control on the hydrodynamic properties of such grains, and variation in size with producing organism may mean that pellets produced by different fish will be differentially distributed in platform settings. In addition, modern peloids from the surface sediments of Eleuthera Sound, the Bahamas, are examined for evidence of the occurrence of fish-derived carbonates in sediments other than carbonate muds. These data form the basis of discussion regarding the transport and depositional fates of fish-derived carbonate pellets and their constituent particles in and around Bahamian platform settings. In addition, some of the potential geochemical fates of these carbonates as a result of deposition in different settings are considered.

6.2 TERMINOLOGIES

Numerous terminologies are used in this study to refer to the various excretion and break down products of fish-derived carbonates, some of which have the potential to overlap with terms in common usage for sedimentary carbonates of broader genetic origin. Table 6.1 therefore provides definitions for the terms used in this study and related terms where appropriate.

Table 6.1 *Definition of terms used to refer to various particle types in this study*

Term	Definition
Mucus-bound pellet	Fish-derived carbonate pellets in their excreted form, typically occurring as several individual pellets bound in an organic mucus coating.
Pellet/soft pellet	Following rapid dissipation of the mucus coating, pellets are released as individual particles. Generally referred to as pellets, at this stage they are unlithified, and thus when used in the context of sedimentary particles are described as 'soft pellets' to clearly differentiate from hardened/cemented forms.
Hardened pellet	Where pellets are exposed to solutions that are highly supersaturated with respect to common marine carbonate minerals (*i.e.*, surface seawater in the Bahamas), a hypothesis presented here suggests that 'soft pellets' become cemented and rapidly indurate, thus forming 'hardened pellets'.
Peloid	A non-genetic term used to refer to any sedimentary carbonate pellet for which origin is unknown (after McKee and Gutschick, 1969). Peloids can be unlithified or lithified, referred to as soft and hard peloids, respectively, and are commonly cryptocrystalline (*i.e.*, component crystals are not easily definable; may be micritic).
Faecal pellet	Used here (and more widely) to refer specifically to carbonate pellets formed by the ingestion, aggregation, and excretion of carbonate particles by any of a number of sediment-grazing marine organisms.
Pseudopellet	Defines aggregates of mud-grade particles formed by hydraulic forces (after Fahraeus *et al*., 1974), and possibly flocculation.
Crystal/ morphotype	Individual components of pellets, often released as individual particles on pellet disaggregation.
Particle cluster	Where two or more crystals are intergrown and will not readily break down further to individual crystals, pellet disaggregation results in the release of particle clusters.

6.3 MATERIALS AND METHODS

6.3.1 Sample collection

Carbonate pellets were collected from fish using the same experimental procedure and during the same field sessions as described in Chapter 2. For the purposes of this study, six fish species were targeted such that the main crystal forms were represented in their combined carbonate products. These species and the crystal forms they produce are summarised in Table 6.2. Sub-samples of carbonates produced by all species were held for several days in seawater to ascertain their immediate post-excretion fate (*i.e.*, sinking or floating) and the longevity of mucus envelopes in which pellets are excreted.

6.3.2 Particle size measurements

Various approaches commonly used for sediment grain size analyses include sieving, laser diffraction, Coulter counter and sediment suspension. However, none of these approaches are suitable for the grain size analysis of fish-derived carbonates, at least for the purposes of this study. In the case of pellets, this is because sieve analysis would likely cause pellet fragmentation as a result of attrition of these friable particles, while Coulter counter and laser diffraction approaches rely on subject particles being suspended with a dispersing agent (*e.g.*, sodium hexametaphosphate), which would result in pellet disaggregation, thus obliterating the subject particles. In the case of individual crystals, grain size is typically too small to be assessed in detail by commonly available sieve apertures, and sieve aperture intervals are too large to provide grain size distributions at appropriate resolution. Coulter counter and laser diffraction methods would be more appropriate for the subject grain sizes, but neither approach is capable of discriminating between crystal morphotypes. Furthermore, the use of phosphate-based dispersants has been shown to cause significant surface damage (etching) to some carbonates (Kontrovitz *et al*., 1991), and while this effect has not been observed or quantified with respect to fish-derived carbonates, the possibility exists that such processes could occur during sample preparation, therefore having a direct effect on the resulting data set. For these reasons it was necessary to perform manual particle size measurements using an image-based approach.

A minimum of 300 pellets per species were analysed by collecting digital images with a digital camera (Nikon DS-5M, Nikon Corporation, Tokyo, Japan) coupled to an optical microscope (Nikon SMZ800, Nikon Corporation, Tokyo, Japan). Individual crystals were prepared for Scanning Electron Microscope (SEM)-based image collection by gently sonicating single pellets in 1.0 ml of deionised water for 10 seconds. The resulting crystal–water mixtures were homogenised by shaking, and 30 µl aliquots were dispersed on silicon plates (0.5 cm^2 approximate surface area) pre-mounted on 12 mm aluminium pin stubs. Water was removed by evaporation in a low temperature oven at 35 °C. Using this technique, particles that remain on the silicon plate are

typically well-dispersed, although smaller crystals tend to form clusters (presumably due to electrostatic charges and/or the inability of smaller particles to penetrate the surface tension of shrinking water droplets). However, in most cases it is easy to differentiate particles that failed to disaggregate (which would be subject to measurement as single particles) from those that disaggregated and formed clusters during sample preparation; the latter occurring as single-layer sheets of crystals as opposed to peloidal aggregates that failed to disaggregate. Electron microscope operating conditions were as described in Chapter 2 (section 2.2).

In all cases (*i.e.*, pellet and crystal measurements), samples were obtained from at least three individual fish, and in the case of crystal measurements at least 5 pellets per individual fish were disaggregated. For samples produced by groups of fish held together in a single tank it was assumed that carbonate production rate was uniform for all individual fish and that 15 pellets were representative of carbonates produced by several individuals. For each disaggregated pellet, images were collected at 10 intervals along a straight line connecting two edges of the area where crystals were deposited, allowing at least 450 crystal measurements to be made per species. Initial observations indicated that crystal size distribution was approximately uniform within each morphotype across this area and that crystals had not been sorted by size during preparation. Analysis of variance tests performed on measurement data confirmed that there were no significant within-morphotype size differences between image locations on each stub.

All particle measurements were carried out in the image-processing software package JMicroVision (v1.2.7; Roduit, 2008). This software can be manually calibrated to accurately set the scale of images being analysed by assigning dimensions to individual pixels based on a known dimension within the image. For pellet measurements it was then possible to measure various parameters of individual pellets using the object extraction tool built into the software, which enables automatic detection of pellet and non-pellet areas of images based on user-defined thresholds in the red, green, and blue colour channels (Fig. 6.1). The software then generates size data for each pellet identified. This method was compared with manually-derived data sets using

the same software (*i.e.*, using a line tool to draw and measure a- and b-axes of pellets in a one-dimensional measurement function) for two images and the results were accurate in all cases except where two or more pellets were touching; in these cases the software identified multiple pellets as individual pellets. Pellet measurements were thus generated automatically using the object extraction tool, but the resulting data set for each image was reviewed and data from touching pellets was removed and replaced by data derived manually using 1D and 2D measurement functions.

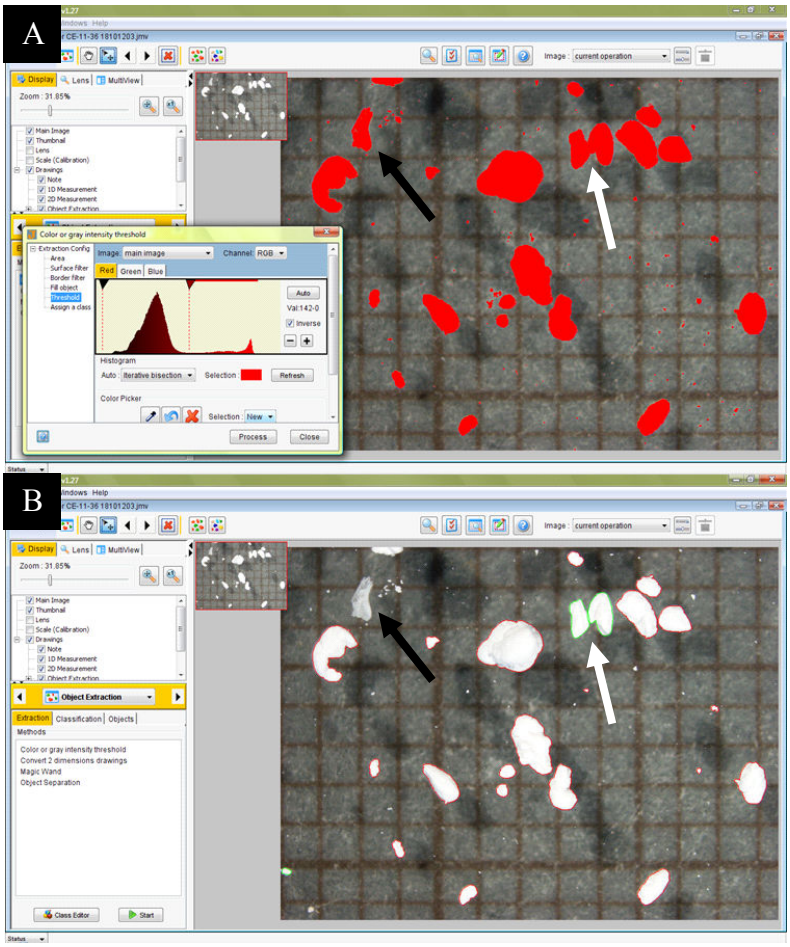

Figure 6.1 *Screenshots from the JMicroVision software (v1.2.7; Roduit, 2008) showing the object extraction method approach for obtaining pellet size data. A) Pellets identified after appropriate setting of colour intensity thresholds (bottom left) are highlighted red. B) Pellets extracted by software are shown with red outlines. Note the fish scale fragment (black arrow) and two touching pellets (white arrow), both of which were initially identified as pellets in (A). These data are removed and, where necessary, replaced by manually derived data (e.g., green outlines to touching pellets).*

For individual crystals, two factors hindered use of the object extraction tool for automated particle measurement: 1) in many cases, particularly where the smallest particles were involved, grains

were touching and could not be identified as individual particles by the software; and 2) greyscale SEM images often lacked sufficient contrast for object extraction to be effective. Disaggregated particles were therefore measured manually using the 1D measurement function built into the software (Fig. 6.2).

In all cases, only morphotypes with clearly definable forms were subject to measurement. Amorphous Mg-carbonate phases were omitted from these analyses because their lack of definable form presented difficulties in measuring individual particles. Furthermore, such phases are rarely (if ever) reported in marine sedimentary environments, possibly because they are reportedly up to 30 times more soluble than aragonite (Brečević and Nielsen, 1989). Indeed, in short-term preservation experiments pellets produced by bluehead wrasse underwent a dramatic reduction in volume after only a few days in seawater as a result of AMC dissolution (see Chapter 7). AMC in its excreted form is therefore probably of little relevance as a sedimentary particle type, and its inclusion in the present study would be superfluous. Similar might be said of ACC nanospheres, which are also likely to be unstable in seawater (*e.g.*, see Chapter 1), but they are included here because of uncertainties regarding their post-excretion fate (especially in light of highly elevated phosphate concentrations in some cases; see Chapter 4).

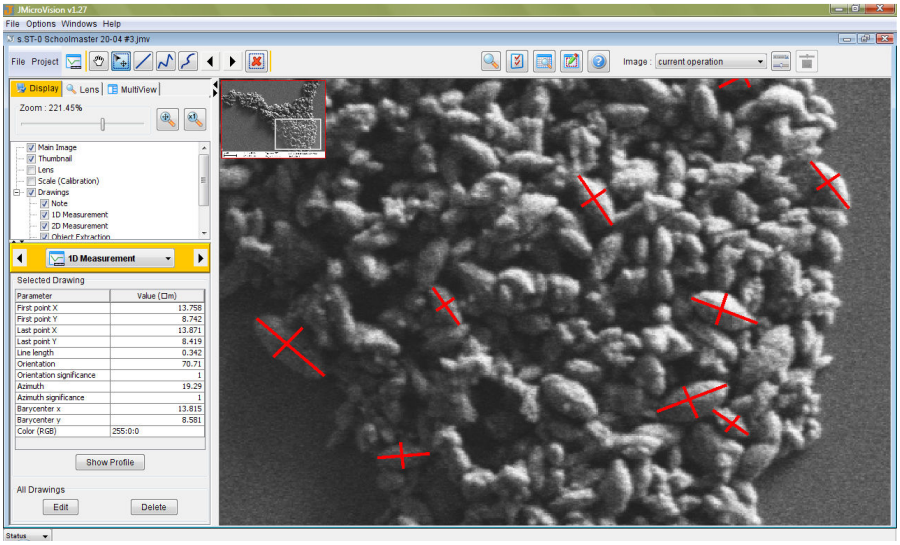

Figure 6.2 *Screenshot from JMicroVision software (v1.2.7; Roduit, 2008), showing 1D measurements of particles released during pellet disaggregation. Both a- and b-axes are measured.*

6.3.3 Data Plotting

The data generated using these approaches are presented as histograms, with grain length bins assigned according to the Udden-Wentworth quarter phi scale and plotted against abundance as a percentage of the number of particles. The Udden-Wentworth scale is particularly useful as it not only includes the silt–clay (4 μm) and sand–silt (63 μm) grade boundaries, but also facilitates plotting of all particles, from sand-grade pellets to clay-grade nanospheres, at appropriate resolutions on the same histogram. All particles released during pellet disaggregation are plotted as relative abundances to show the estimated relative number of particles released from a pellet produced by a given species following its disaggregation. However, because the number of pellets disaggregated for this study was limited, and because dominant crystal form produced by any given species can vary from pellet to pellet, the number of particles measured for each morphotype is not necessarily an accurate reflection of their overall relative abundance. Thus the overall relative number of crystals per morphotype was estimated based on SEM observations of 50 or more pellets per species (Table 6.2). Using this data, the relative abundances of measured particles were corrected such that histograms show actual grain size distributions for each morphotype, plotted relative to each other based on estimated numeric abundances. Three exceptions to this are for some morphotypes produced by bonefish. The data in Table 6.2 indicate that the number of spheres and sphere clusters produced by this species are negligible in comparison to the number of nanosphere clusters. However, this is a result of a large difference in particle size; on a volumetric basis the former are by far the more significant, and their size distributions should therefore be clearly displayed. To improve clarity, they are therefore positively exaggerated. Similarly, the number of individual nanospheres (which are not released in large numbers but are plotted here because they might ultimately be released in large numbers in nature) is negatively exaggerated. In all cases the number of pellets is plotted independently of particles.

Table 6.2 *Fish species used in this study and the crystal forms they produce (after Salter et al., 2012). Numerical data represent estimated percentage of crystals (by number) for each species following pellet disaggregation.*

Species	Body mass of fish (g)	Monocrystalline ellipsoids	Rods	Small dumbbells	Nanospheres	Nanosphere clusters	Spheres	Sphere clusters	Rhombohedra	Polycrystalline ellipsoids	Needles/fibres	Dumbbells	Unclassified particles
Schoolmaster snapper *Lutjanes apodus*	4.6–322	96	4	-	-	-	-	-	*	-	-	-	-
Black grouper *Mycteroperca bonaci*	424–1653	70	25	2	-	-	-	-	3	-	-	*	-
Bonefish *Albula vulpes*	759–1506	-	-	-	**	98 (84)‡	<0.1 (4)‡	<0.2 (8)‡	*	-	2	*	-
Great barracuda *Sphyraena barracuda*	41–11364	7	-	50	35	5†	*	*	*	-	3	*	-
Checkered puffer *Sphoeroides testudineus*	118–207	-	-	-	-	-	5	50	30	10	-	*	5
Bluehead wrasse *Thalasomma bifasciatum*	1.1–7.7	-	-	*	-	-	11	12§	75	-	*	2	-

*Morphotypes present in samples produced by species in question, but in volumetrically and numerically minor amounts. Size data are therefore not included in the results.
†Nanosphere 'clusters' produced by great barracuda typically take the form of nanosphere 'doublets' (*i.e.*, two intergrown nanospheres); clusters of more than two are extremely scarce. In this manner they differ from nanospheres produced by bonefish, which typically disaggregate as clusters comprising numerous nanospheres.
‡The number of spheres and sphere clusters produced by bonefish is negligible compared with the number of nanosphere clusters released after disaggregation. However, their much larger size means the former are by far the most volumetrically significant, and thus relative abundances are adjusted to make their size distributions clearly visible in the histogram (Fig. 6.6).
**Individual nanospheres produced by bonefish are rarely observed after disaggregation; instead they are released as clusters. Their size range is included in the histogram because in nature these clusters might progressively disaggregate to eventually release numerous individual nanospheres. However, the proportion eventually released is unknown. The histogram peak height for this morphotype is therefore arbitrary and does not describe its abundance relative to other morphotypes.
§Particle clusters released after disaggregation of pellets produced by bluehead wrasse typically comprise spheres, but may also include or be dominated by rhombohedral forms.

6.3.4 Simulation of wave-generated agitation

The degree of pellet diminution by wave-generated agitation was assessed by measuring the grain size distributions of carbonate pellets at the beginning and end of a wave-simulation experiment. More than 500 pellets produced by black grouper were measured using the image analysis technique described in section 6.3.2). These pellets were then weighed before being placed in a wave-simulation vessel with artificial seawater for a total of four weeks. Pellets that remained intact were measured after one week, and again after four weeks, to assess diminution caused by agitation during the experiment. A separate sub-sample from the same bulk sample was examined in SEM to confirm that pellets comprised similar crystals to those previously documented for this species (*i.e.*, monocrystalline ellipsoids).

A simple wave simulation vessel was constructed by placing a sterile rectangular plastic box (15 cm long by 10 cm wide) containing 300 ml of artificial seawater (Tropic Marin) on a plate rotating at 22 rpm. A wave was thus generated and travelled longitudinally within the box, causing pellets to roll parallel to this direction at a rate of 22 cycles (*i.e.*, back and forth) per minute. Experimental conditions caused greater pellet movement (both in distance and speed) than that observed for sand-grade particles in most platform settings of Eleuthera Sound under ambient conditions, and best approximated conditions associated with ooid shoals to the north of CEI (Fig. 6.3), and with storm conditions in most shallow platform settings. Whereas experimental conditions caused most pellets to roll along the base of the vessel, the smallest pellets moved by saltation, while liberated crystals were easily suspended, remaining so until re-aggregation allowed them to settle out.

An important aspect of this experiment was to ensure that the solution used for wave simulation did not differ substantially from natural seawater. A solution with an aragonite saturation state lower than that of Bahamian surface seawater might promote higher-than-natural rates of dissolution of carbonates within pellets, possibly accelerating pellet disaggregation. Likewise, an aragonite saturation state that is too high might cause pellet induration to proceed at higher rates than in nature, potentially inhibiting pellet diminution. It was therefore necessary to maintain an

appropriate chemical environment by carefully controlling the temperature, salinity, and pH of the artificial seawater at values close to those of ambient Bahamian surface seawater, these being 26 °C, 37 ppt, and 8.20 (NBS scale), respectively (see Chapter 7 for details regarding these values and the method of seawater preparation). Following the preparation of seawater, pellets were added to the solution and allowed to soak for at least 30 minutes prior to agitation (dry pellets are brittle and may disaggregate in a different manner to wet pellets). The experimental vessel was fitted with an air-tight lid to prevent evaporation of seawater and thus maintain stable salinity, and the entire experimental assemblage was held in an incubator to maintain a stable temperature of 26 °C.

At the one- and four-week pellet measurement intervals, the experimental vessel was removed from the rotating plate and intact pellets were corralled into a small area of the vessel. Pellet images were collected through an optical microscope (as described in section 6.3.1) without removing pellets from the seawater solution, thus preventing pellet breakage or deformation during handling. At the end of the experiment, intact pellets were collected using a pipette, rinsed briefly in deionised water, and soaked in a 5.25 % solution of sodium hypochlorite. Following a second rinse in deionised water they were transferred to a membrane of known dry weight via vacuum filtration. The seawater and liberated carbonate fines that remained in the experimental vessel were centrifuged before the removal of seawater with a pipette. The remaining fines were processed in the same way as intact pellets, but were centrifuged between each stage to ensure no carbonate material was lost. All retained carbonates were then dried on their membranes in a low temperature oven (40 °C) before their weights were recorded.

6.3.5 Sedimentary pellet examination

Surface sediment samples were collected from two shallow water sites in Eleuthera Sound, the Bahamas by scooping the upper two centimetres of the sediment column into a plastic screw top container whilst snorkelling. The sites were located in a muddy embayment (Rock Sound) dominated by pelletal sands and lime muds (site 1), and close to a patch reef within Eleuthera Sound (site 2), where surface sediment is predominantly skeletal sands but also includes carbonate

muds and peloids (Fig. 6.3). These sites were specifically targeted because of their potential to contain fish-derived carbonates. Rock Sound is a low energy sink for mud, probably including that produced in the wider area of Eleuthera Sound, and may therefore contain fish-derived carbonate crystals. Indeed, Perry *et al*. (2011) identified many crystals that are morphologically and compositionally similar to fish-derived carbonates in their investigation of mud-grade sediments in this area. The patch reef is also a reasonably low energy site and holds a large fish biomass. Consequently, many of the carbonate pellets they produce may remain in this vicinity, especially if they do not disaggregate immediately.

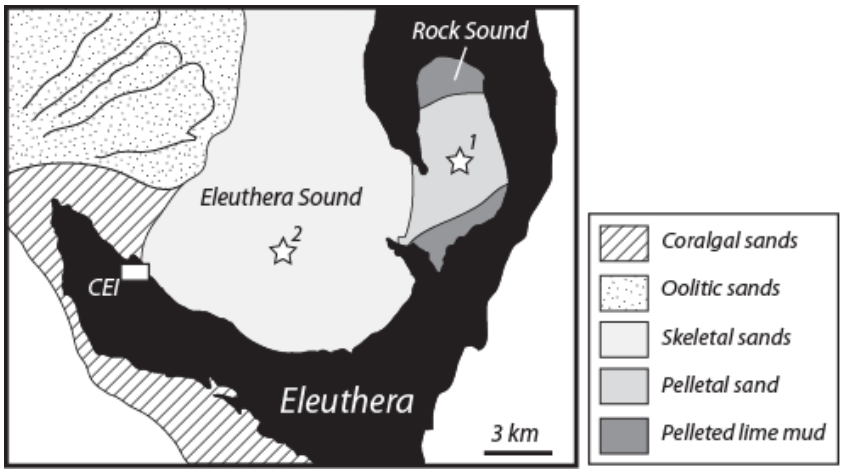

Figure 6.3 *Map of the southern part of Eluethera Island, showing locations of Eleuthera Sound and Rock Sound. Sediment sampling sites are marked by stars; site 1 is the muddy embayment of Rock Sound and site 2 marks the location of a patch reef near which surface sediment was sampled (sediment facies after Dravis, 1979).*

Sediment samples were cleaned and dried using the same approaches described for fish-derived carbonates (see Chapter 2). Particles were then examined under an optical microscope and approximately 30 peloids of varying size (approximately 0.1–0.7 mm in length) from each site were isolated for detailed examination using SEM. Peloids were mounted on 12 mm aluminium pin stubs with adhesive carbon tabs. Morphological and compositional investigations were then carried out using SEM and EDX under the same operating conditions as described in Chapter 2.

6.4 RESULTS

6.4.1 Pellet size analysis

Data show that carbonate pellets from the six fish species examined have broadly sub-spherical to ellipsoidal morphologies (Figs. 6.4; 6.5), but can also be quite irregular in form. At their most extreme, these irregular morphologies include sinuous pellets comprising strands of crystals that appear to have aggregated or grown about existing mucosal structures (Fig. 6.8), although the scarcity and fragility of these pellets suggests they might not remain intact in natural settings. Pellet size ranges from medium silt grade to very fine granules, and varies with species (Table 6.3; Figs. 6.4; 6.5). Commonly, grain size ranges from predominantly very fine to fine sand-grade (*e.g.*, in checkered puffer pellets, 80% of the total number measured 60–230 μm in width) to predominantly fine to coarse sand-grade (*e.g.*, in black grouper pellets, 80% of the total number measured 160–1010 μm in width). Within each species, pellet length is positively skewed (*i.e.*, tails are longer over larger grain sizes) and closely approximated by log-normal distribution, although subsidiary peaks at smaller grain sizes obscure this pattern. These subsidiary peaks (*e.g.*, see black grouper; Fig. 6.6) are due to pellet breakage during sample preparation. Pellets also vary in shape according to species (Table 6.3), with those produced by black grouper tending to be the least elongate (median length/width ratio 1.36) and those produced by great barracuda tending to be most elongate (median length/width ratio 1.50). The full data set for particle and pellet measurements is presented in Appendix VI.

Table 6.3 *Size data for carbonate pellets produced by six Caribbean marine fish species (median values in bold-type).*

		Length data					Width data			L/W ratios		
Fish species	n	Min. (µm)	Max. (µm)	D_{10} (µm)	Median (µm)	D_{90} (µm)	D_{10} (µm)	Median (µm)	D_{90} (µm)	D_{10}	Median	D_{90}
Grouper	331	90	2600	230	**870**	1320	160	**640**	1010	1.13 – **1.36** – 1.78		
Snapper	1189	80	2780	110	**260**	1090	80	**180**	720	1.11 – **1.39** – 1.86		
Barracuda	501	50	1740	150	**380**	740	110	**240**	460	1.17 – **1.50** – 2.09		
Wrasse	300	70	1990	150	**520**	940	110	**360**	620	1.13 – **1.40** – 2.06		
Bonefish	977	70	3630	180	**570**	1490	120	**390**	950	1.14 – **1.44** – 1.96		
Puffer	592	30	1040	90	**180**	320	60	**120**	230	1.11 – **1.40** – 1.84		

There is no evidence to suggest that pellet size varies with fish body mass, either across or within species, although there can be marked variations in pellets produced by different individual fish of the same species. For example, the body mass of bluehead wrasse and bonefish used here differs by more than two orders of magnitude (Table 6.2), but both species produce pellets over a similar size range (Table 6.3; Fig. 6.6). In contrast, the pellets produced by checkered puffer (intermediate in size between bluehead wrasse and bonefish; Table 6.3) are significantly smaller (unequal variance t-test, $p < 0.001$), with a median length of 180 µm. However, these data should be viewed with some caution: whereas pellets produced by both small and large specimens of schoolmaster snapper tend to have similar size ranges (both having median length 230 µm), suggesting little size variation within species, a separate sample set produced by several fish of mixed body mass yielded much larger pellets (median length 650 µm). The shoulder at the coarse end of the histogram for pellets produced by this species is a result of this (Fig. 6.6). It therefore appears that, at least for some species, pellet size varies between individual fish. However, in other species pellet size may be more uniform. For example, the median lengths of pellets produced by five individual black groupers varied only slightly (730–930 µm).

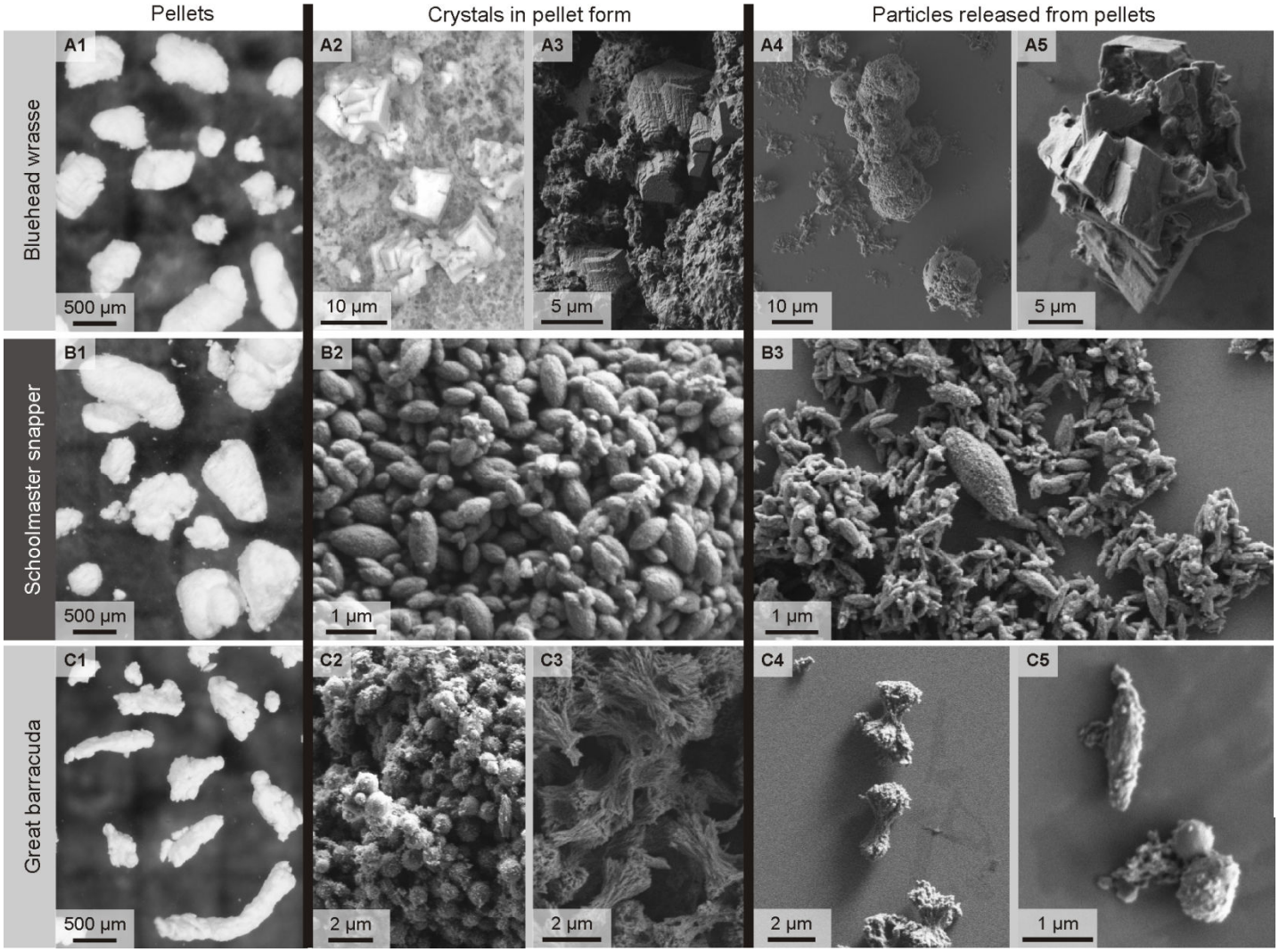

Figure 6.4 *Fish-derived carbonates in their various physical forms. Left column: optical microscope images showing typical pellets produced by three of the species used in this study. Central and right columns are SEM images. Central column shows main crystal forms produced by each species prior to pellet disaggregation: (A2 and A3) Mg calcite rhombohedra (A2) and spheres (A3) in a magnesium carbonate 'matrix' (backscatter electron images: pale areas are Mg calcite; dark areas are the magnesium carbonate 'matrix'); (B2) Monocrystalline ellipsoids; (C2) Nanospheres; (C3) Small dumbbells. Right column shows main crystal forms released following pellet disaggregation. In most cases particles are morphologically similar before and after disaggregation. Many morphotypes are released as individual particles (e.g., rhombohedra [A5], ellipsoids [B3], and dumbbells [C4]), but some are intergrown and can be released as particle clusters (e.g., sphere clusters [A4] and nanosphere 'doublets' [C5]).*

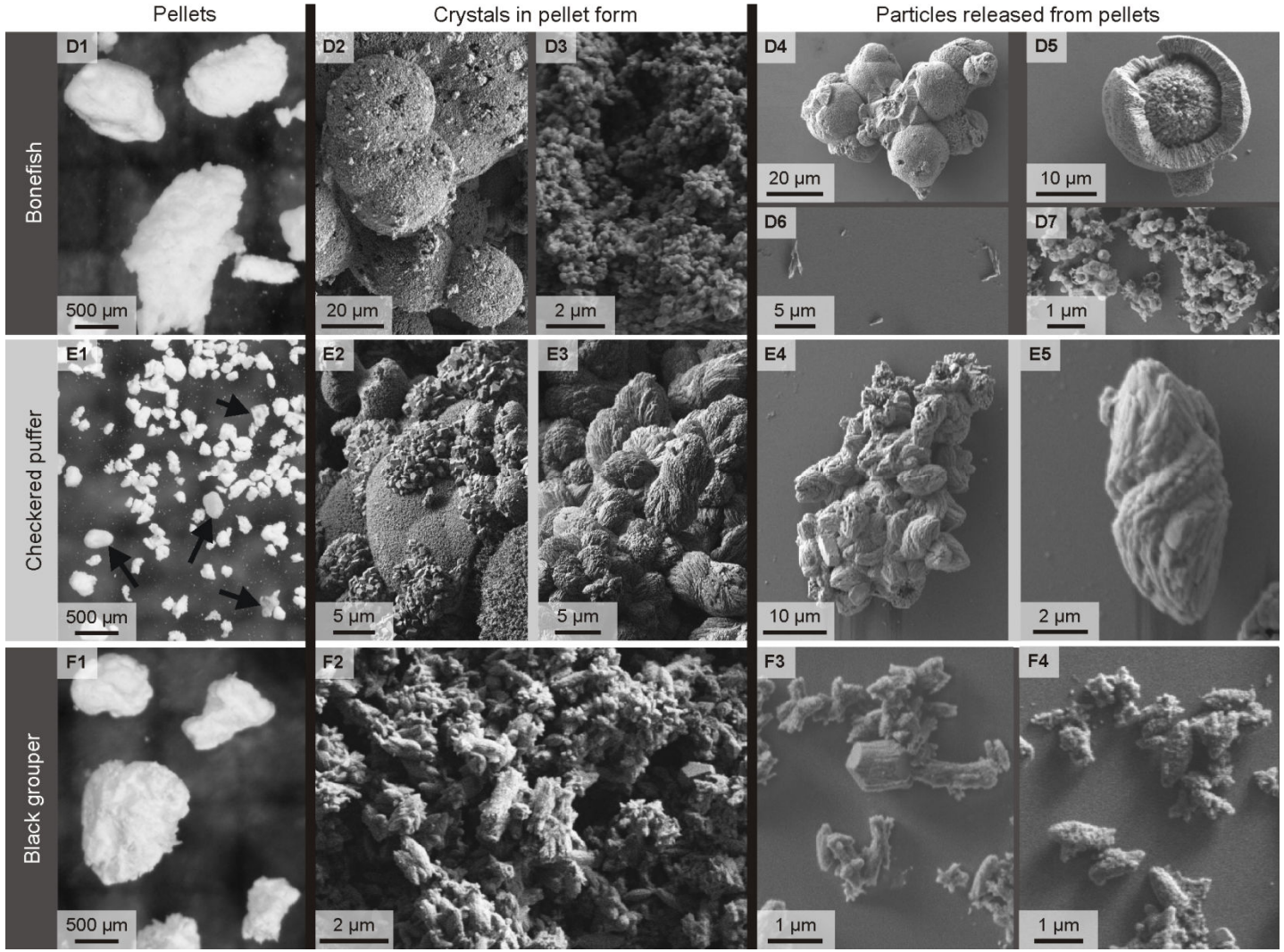

Figure 6.5 *Fish-derived carbonates in their various forms. Layout as Fig. 6.4. Black arrows (E1) point to ingested carbonate particles excreted alongside fish-derived carbonates produced by checkered puffer. Main crystal forms prior to pellet disaggregation: (D2) Spheres (particles shown are intergrown); (D3) Nanospheres; (E2) Intergrown spheres with rhombohedra on sphere surfaces; (E3) Polycrystalline ellipsoids (those shown are tending towards dumbbell-shaped); (F2) Ellipsoids and rods, and a single rhombohedral crystal (right). Following disaggregation, most morphotypes are released as individual particles: (D5) spheres; (E5) polycrystalline ellipsoids; (F3, F4) ellipsoids, rods, and rhombohedra. However, intergrown particles are commonly released as particle clusters: (D4) spheres; (D7) nanospheres; (E7) polycrystalline ellipsoids. Note that some polycrystalline morphotypes can appear fractured following disaggregation (e.g., [D5]) and may have released their component crystals as individual particles (D6).*

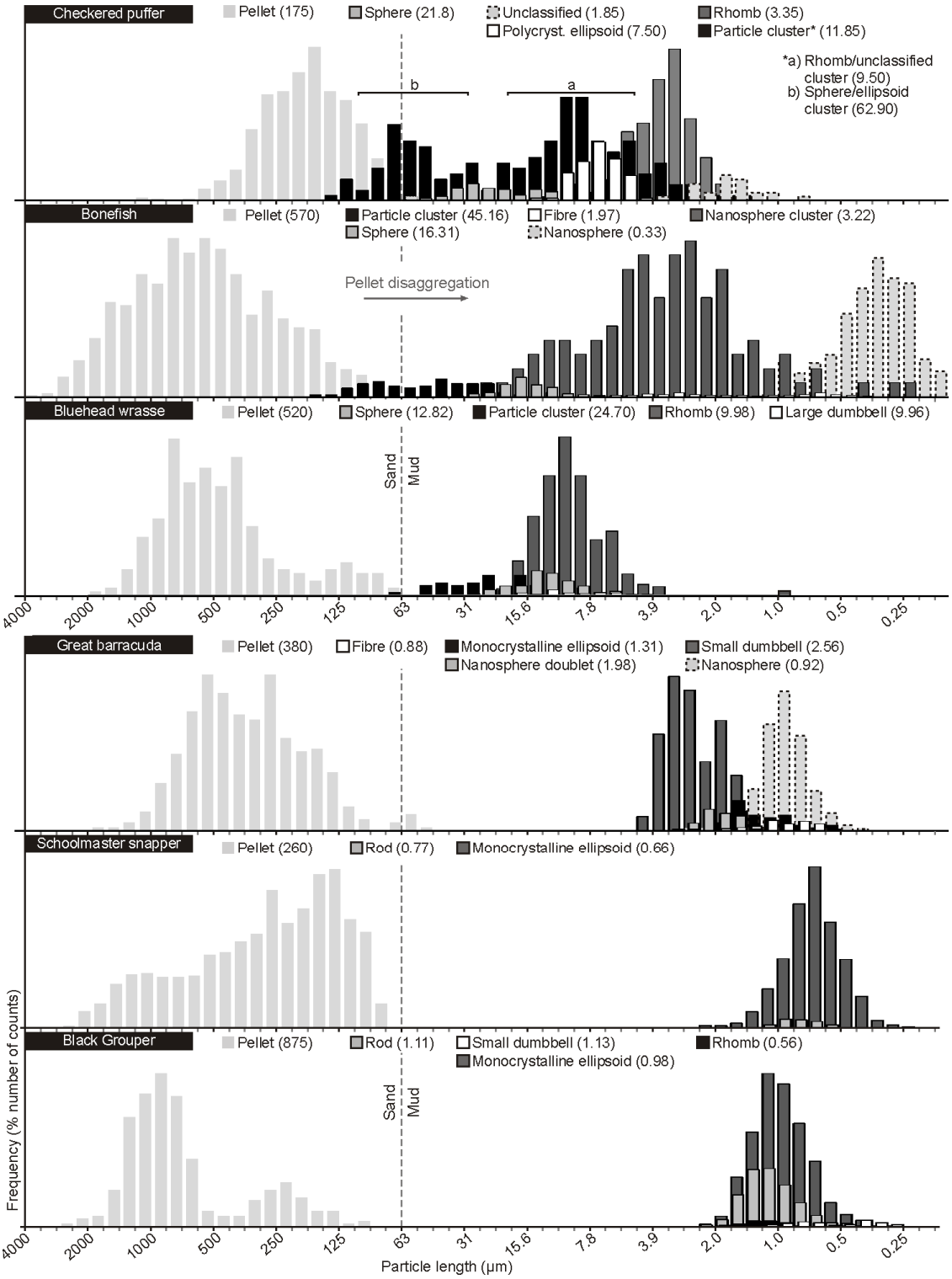

Figure 6.6 *Histograms showing grain size distributions for carbonate pellets and the particles they release on disaggregation. Histogram area for each particle type represents relative abundance by number of particles, with the exception of nanospheres, spheres, and sphere clusters produced by bonefish, which have been adjusted to improve clarity (see methods section for further detail). Pellet histogram area is independent of other particle types and is set arbitrarily. Median length (in µm) for each particle type is shown in parentheses next to the legend on each plot. Note the presence of secondary peaks for pellets produced by some species, which are largely a result of pellet breakage during sample preparation. In addition, particle clusters produced by checkered puffer show two distinct peaks: a) rhombohedra/unclassified grain clusters; and b) sphere/ellipsoid clusters.*

It is worth mentioning that in a limited sample set collected from fed fish, carbonate pellets are similar to those described here with the exception that they commonly contain small amounts of ingested particles (*e.g.*, foraminifera tests and diatom frustules) alongside precipitated carbonates. In a few cases fish-derived carbonates form clusters of crystals aggregated on the surfaces of ingested particles (Figs. 2.2 and 6.7). However, these are always excreted alongside abundant pellets, which appear to form regardless of feeding activity and the presence of dietary material within the gut.

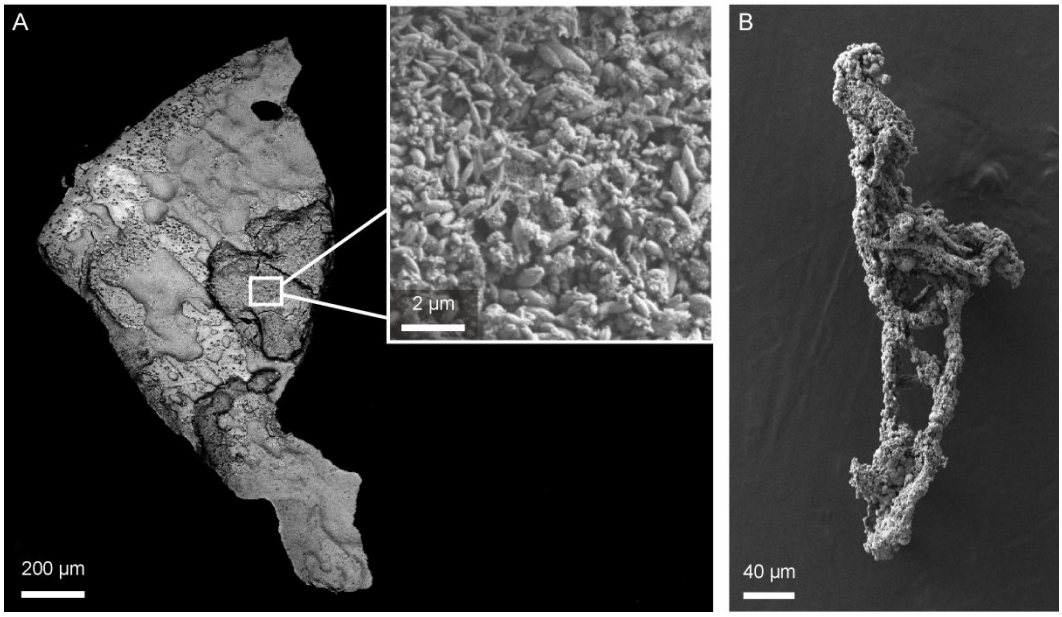

Figure 6.7 *Photomicrographs of fish-derived carbonates excreted in forms that differ from the typical sub-spherical and ovoid pellets.* ***A)*** *Backscatter electron (BSE) image of a high-Mg calcite skeletal fragment ingested by a schoolmaster snapper and excreted shortly after capture of the fish. Note the darker area on the right-hand edge, and another below this leading to the left-hand edge, corresponding to fish-derived carbonates, which appear darker than the ingested fragment in BSE due to their higher magnesium content. Inset shows a higher magnification secondary electron image confirming that these particles are monocrystalline ellipsoids (as previously documented for this species). Fish-derived carbonates produced under normal dietary conditions can sometimes be excreted in this form, but pellets are typical.* ***B)*** *Secondary electron image of a sinuous pellet comprising a network of aggregated crystals that appear to have formed about an organic structure (i.e., mucus coating).*

6.4.2 Disaggregated particles

Upon disaggregation, pellets produced by the six fish species release a diverse range of crystal morphotypes (Figs. 6.4 and 6.5) and generate different size spectrums of crystals (Fig. 6.6). Pellets comprising monocrystalline ellipsoids, rods, small dumbbells, and rhombohedra typically released all crystals as individual mud-grade particles (Figs. 6.4 A5, B3, C4). Nanospheres produced by

great barracuda were also released in this manner, and occasionally as nanosphere doublets (*i.e.*, two intergrown nanospheres). Conversely, spheres, polycrystalline ellipsoids, and some rhombohedral forms can also be intergrown and were released either as individual morphotypes (Figs. 6.5 D5, E5) or as larger (up to fine sand-grade) particle clusters (Figs. 6.4 A4; Figs. 6.5 D4, E4). Nanospheres produced by bonefish are similarly released as intergrown particle clusters, but these are typically smaller (mud-grade). It is worth mentioning that individual nanospheres produced by bonefish were rarely observed. However, their size data are presented here for three reasons: i) it is possible that prolonged disaggregation might ultimately release nanospheres as individual particles; ii) SEM examination of some pellets produced by this species reveals discrete nanospheres in a magnesium-carbonate 'matrix' which would presumably be released on pellet disaggregation; and iii) in some cases it was difficult to determine whether nanosphere clusters comprised truly intergrown crystals, or had formed as a result of the aggregation of individual nanospheres during sample preparation.

Data arising from the size fraction analysis of the products of pellet disaggregation are summarised in Table 6.4 and shown as histograms in Fig. 6.6. All particles released as individual crystals are mud-sized (<63 μm), and similar morphotypes produced by multiple species typically occur within similar size ranges; only rhombohedral forms varied markedly in size among species. Clay-grade particles (<4 μm in width) include monocrystalline ellipsoids, rods, and nanospheres (all typically <1.5 μm in length), small dumbbells produced by great barracuda (median length 2.6 μm), and most polycrystalline ellipsoids (median length 7.5 μm, but typically <4.0 μm in width). The length and character of rhombohedral forms varies with species, but those produced by checkered puffer and black grouper are mostly clay-grade. Other clay-grade particles include fibre-like crystals (Fig. 6.5 D6) and 'unclassified grains' that could not be assigned to previously designated categories; these particles commonly lack a distinctive form, but sometimes exhibit a plate- or blade-like appearance. Fibres and 'unclassified grains' were not observed prior to pellet disaggregation, but their morphologies and the morphotypes with which they are associated suggest that they may be original component parts of polycrystalline morphotypes such as spheres, dumbbells, and

polycrystalline ellipsoids. Most other individual morphotypes are silt-sized (4 to 63 μm), and include rhombohedra with median length 10.0 μm (produced by bluehead wrasse), and individual spheres with median diameters in the range 12.8 to 21.8 μm (produced by several species).

Table 6.4 *Key numerical data arising from the size fraction analysis of all particle types released on pellet disaggregation.*

Fish species	Particle type	n	Min. (μm)	Max. (μm)	D_{10} (μm)	Median (μm)	D_{90} (μm)	D_{90}-D_{10} (μm)
Black grouper	M/cryst. ellipsoid	1562	0.29	2.22	0.64	0.98	1.39	0.75
	Rod	888	0.26	2.10	0.75	1.11	1.50	0.75
	Rhombohedron	32	0.27	1.70	0.34	0.56	1.10	0.76
	Small dumbbell	29	0.44	1.70	0.92	1.13	1.49	0.57
Schoolmaster snapper	M/cryst. ellipsoid	1097	0.24	2.20	0.46	0.66	0.99	0.53
	Rod	32	0.55	1.13	0.61	0.77	0.97	0.36
Great barracuda	Small dumbbell	240	0.94	4.43	1.64	2.56	3.44	1.80
	M/cryst. ellipsoid	37	0.51	1.89	0.73	1.31	1.67	0.95
	Nanosphere	270	0.39	2.38	0.67	0.92	1.25	0.58
	N/sphere doublet	47	1.12	2.95	1.47	1.98	2.42	0.95
	Needle/Fibre	44	0.55	2.91	0.68	0.88	1.46	0.78
Bluehead wrasse	Particle cluster	44	8.28	73.0	14.83	24.70	44.67	29.84
	Rhombohedron	319	0.85	21.09	6.05	9.98	14.28	8.23
	Large dumbbell	24	4.40	18.12	5.75	9.96	15.46	9.71
	Sphere	78	6.33	28.45	8.83	12.82	19.22	10.39
Bonefish	Sphere cluster	64	11.66	177	23.35	45.16	102.3	78.95
	N/sphere cluster	108	0.20	24.00	1.18	3.22	11.07	9.89
	Sphere	313	4.53	45.33	10.18	16.31	23.04	12.86
	Nanosphere	451	0.10	1.17	0.22	0.33	0.63	0.41
	Needle/Fibre	119	0.24	8.75	0.54	1.97	4.73	4.19
Checkered puffer	Particle cluster	188	1.40	150	4.47	11.85	71.0	66.53
	*Sphere/ellipsoid**	*45*	*6.90*	*150*	*18.84*	*62.9*	*90.4*	*71.56*
	*Rhomb/unclass.**	*143*	*1.40*	*114.6*	*3.80*	*9.50*	*42.14*	*38.34*
	Sphere	88	7.30	53.90	9.90	21.80	35.69	25.79
	P/cryst. ellipsoid	73	3.30	14.80	5.20	7.50	10.16	4.96
	Rhombohedron	142	1.70	12.90	2.40	3.35	5.20	2.80
	Unclassified grain	24	0.80	59.50	1.16	1.85	2.60	1.44

*Data for particle clusters produced by checkered puffer are divided into those comprising spheres and/or polycrystalline ellipsoids, and those comprising rhombohedra and/or unclassified particles

Particle clusters were classified as such if they contain two or more intergrown crystals. Many comprise intergrown spheres, and as a consequence they are typically large relative to individual morphotypes. For example, the length ranges of many particle clusters produced by checkered puffer and bonefish traverse the silt–sand boundary (63 μm), with the largest clusters being up to fine sand-grade. Some sphere clusters tended to be smaller (*e.g.*, from bluehead wrasse), probably as a result of growth in relative isolation from other spheres. That is, calcite crystals produced by

this species are typically distributed sparsely in a magnesium carbonate 'matrix' (Fig. 6.4 A2), and may have had limited opportunity to form clusters.

6.4.3 Pellet evolution under agitated conditions

Immediately following excretion, mucus-coated pellets produced by all fish species rapidly settled out of the seawater column; none floated. In quiescent conditions with no agitation, mucus envelopes typically disaggregated within a few days (up to 10 days) and released individual pellets with no visible traces of organic material remaining.

Approximately 500 cleaned carbonate pellets, produced by black grouper and predominantly comprising clay-grade monocrystalline ellipsoids, rods, and some rhombohedra, were measured before and after wave agitation experiments (Fig. 6.8; full data set in Appendix VII). Control pellets had a median length of 0.73 mm (80 per cent of the total number in the range 0.11–1.13 mm) and a median width of 0.54 mm (80 per cent in the range 0.07–0.78 mm). However, it is worth noting that this distribution is bimodal in character: a dominant peak occurs over the larger grain lengths (median 0.85 mm) and is a reflection of true pellet size at the point of excretion; a subsidiary peak over smaller grain lengths (median 0.13 mm) is probably a result of pellet breakage during sample preparation. In either case, initial pellet size is close to that described above (4.4.1) for this species.

After one week under conditions of moderate agitation, pellets approached a unimodal size distribution and were substantially greater in number (from 507 to 968) and reduced in size (median length 0.19 mm, 80 per cent in the range 0.10–0.57 mm; median width 0.11 mm, 80 per cent in the range 0.07–0.36 mm). Continued agitation under similar conditions resulted in still further pellet diminution, and after four weeks median pellet length was 0.14 mm (80 per cent in the range 0.08–0.31 mm) and median pellet width was 0.09 mm (80 per cent in the range 0.05–0.20 mm). Pellet size was thus reduced from predominantly coarse, medium, and fine grade sand to fine and very fine sand and coarse silt during four weeks of moderate agitation.

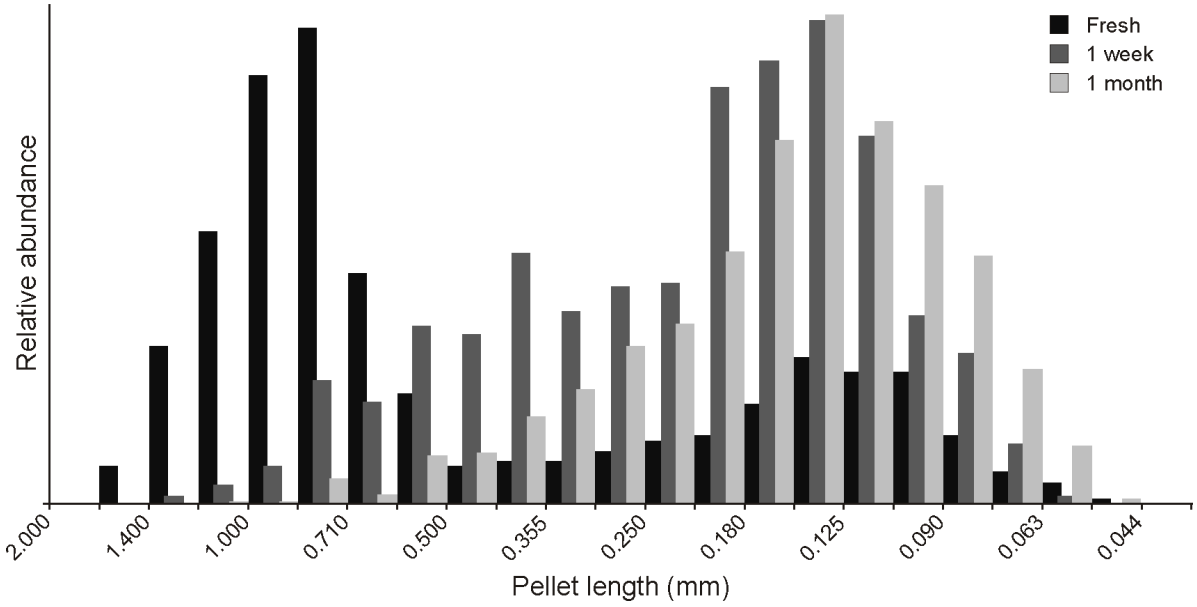

Figure 6.8 *Grain length distributions of fish-derived carbonate pellets (produced by black grouper) at various stages after excretion: i) controls (immediately after excretion; black bars); ii) after one week in moderately agitated conditions (dark grey bars); and iii) after four weeks in moderately agitated conditions (pale grey bars). Note the bimodal distribution of control pellets – the peak at smaller pellet lengths is a result of some pellet breakage during sample preparation and storage. Populations rapidly become unimodal as pellet size diminishes and median length of excreted pellets reduces from 0.85 mm to 0.14 mm. Histograms show relative abundance (number of counts) within each population. Relative histogram areas among populations have been adjusted to improve clarity.*

Concomitant with pellet diminution was a change in pellet morphology. Control pellets were predominantly sub-spherical and ellipsoidal, typically being sub-rounded to sub-angular (Fig. 6.9). Irregularly-shaped pellets were also common. By the end of one week of agitation the latter were rare, but sub-spherical and ellipsoidal pellets remained dominant. Visual observations indicate an increase in degree of rounding: most pellets were rounded to well-rounded after agitation, with sub-angular pellets being rare. In addition, aspect ratio measurements (length/width) indicate a tendency towards pellet elongation during agitation; the median value increasing from 1.36 for control pellets to 1.53 after one week, and 1.55 after four weeks. These data suggest that pellet morphology underwent rapid changes (rounding and elongation) during the first week of agitation but was more stable after this.

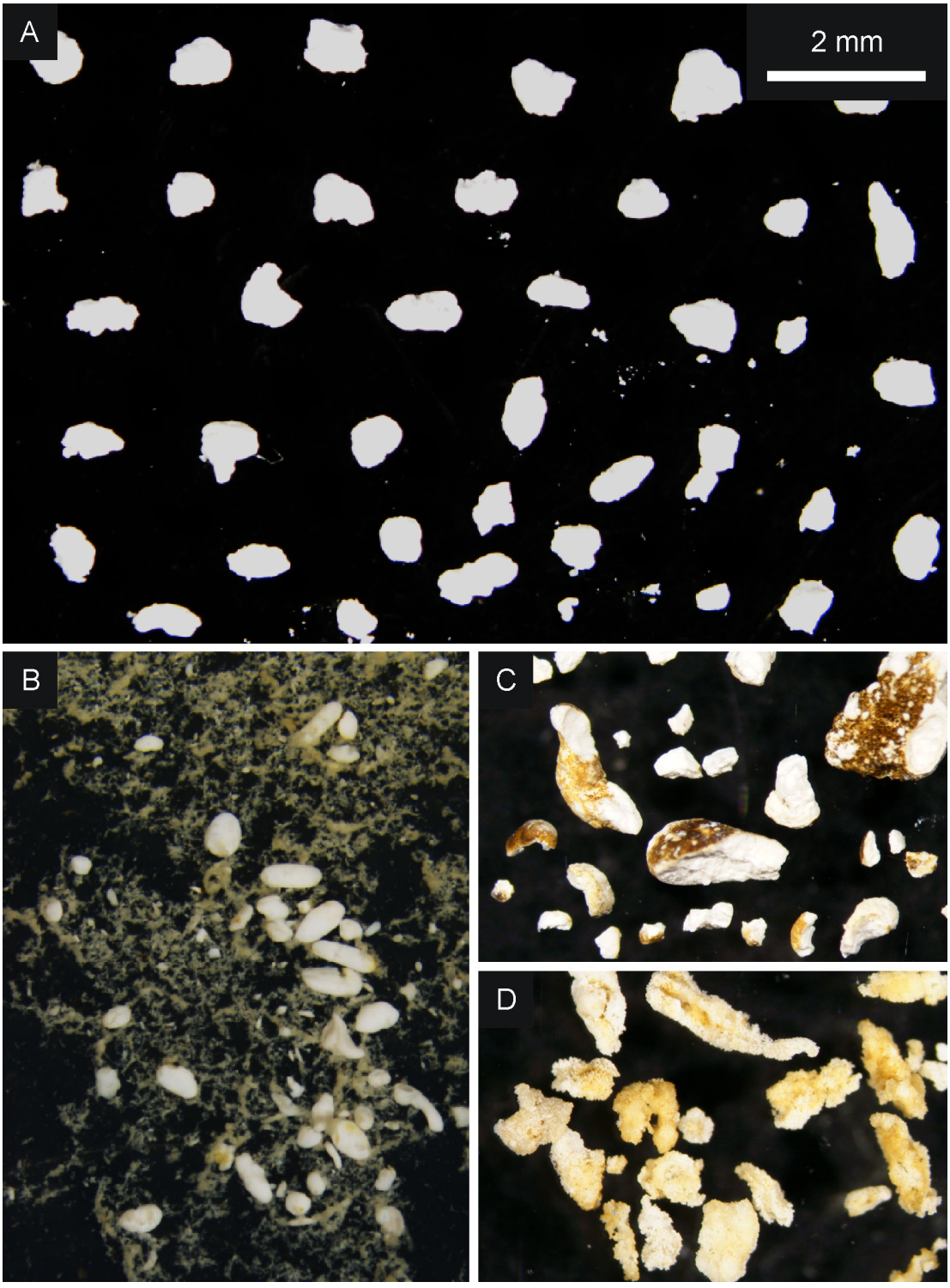

Figure 6.9 *Photomicrographs of fish-derived carbonate pellets at various stages after excretion (scale same in all images): A) Cleaned pellets at the point of excretion, produced by black grouper; B) Pellets from the same sample set shown in (A) after 4 weeks of moderate agitation in artificial seawater. Note the generally smaller size and more rounded nature of the pellets. Also note the 'substrate' of carbonate fines (off-white) formed by re-aggregation of individual crystals liberated from pellets; C) Pellets produced by schoolmaster snapper, after seven months of gentle agitation in artificial seawater. Note the larger size of pellets compared to those in (B), and the more irregularly-shaped, less well-rounded morphologies; D) As (C), but pellets produced by bonefish. The orange-brown colour of pellets (C, D) is a result of superficial manganese precipitation from artificial seawater. These precipitates are not pervasive and have no bearing on pellet robustness.*

Crude visual assessment of the total volume of intact pellets at both measurement intervals indicated it to be substantially lower than that of the initial sample, suggesting that some fraction of carbonates had been released as individual crystals during agitation. Indeed, after 24 hours of agitation, water in the vessel containing fish-derived carbonates was clouded, presumably because of the presence of carbonate fines in suspension. In contrast, water in control vessels (one containing only artificial seawater; the other containing artificial seawater and carbonate sands from the Bahamas) retained a high clarity throughout the experimental period. After one week, the seawater had regained its initial clarity and a 'substrate' of off-white material, rather nebulous in form, had accumulated at the base of the vessel (Fig. 6.9 B). Despite having the appearance of organic material, it was not affected when exposed to a 5.25 (w/v) % solution of sodium hypochlorite. However, it reacted vigorously with, and completely dissolved in, a 3.5 (w/v) % solution of hydrochloric acid, thus indicating that it comprised $CaCO_3$ with little or no organic material. Microscopic examination suggests it comprised loosely aggregated carbonate fines. It is likely that this 'substrate' formed as a result of re-aggregation and consequent settling of the initially suspended individual crystals.

The weight of the carbonate pellet sample prior to agitation was 24.5 mg pellets. After four weeks of agitation, fines and re-aggregated fines made up 16.0 mg and intact pellets made up 8.3 mg, indicating that approximately 66 % of the initial pellet sample had been released as individual crystals under conditions of moderate agitation. In addition, the combined weight of retained carbonates (24.3 mg) indicates that only 0.2 mg (0.8 %) of the original sample was lost during the experiment, suggesting that the extent carbonate dissolution was minor, if it occurred at all. Indeed, the loss of this small amount of material might as easily be explained by the loss of the smallest individual crystals through the membrane during filtration. Solution pH at the end of the experiment (8.11) was close to the starting pH (8.15) and remained stable for 24 hours afterwards with air bubbling through it, indicating that pCO_2 was the same at the beginning and end of the experiment. The dissolved inorganic carbon (DIC) system was thus unchanged from the starting conditions of the experiment, further indicating that precipitation and/or dissolution reaction were

minimal. The small pH decrease possibly suggests net precipitation of carbonate, but another control on this could be the precipitation of manganese from artificial seawater (see Chapter 7 for discussion).

Finally, it is worth pointing out that pellets produced by two different fish species, held for seven months in similar, but very gently agitated, artificial seawater conditions (in experiments designed to investigate the preservation potential of fish-derived carbonates; see Chapter 7), remained largely intact as sub-spherical, ellipsoidal, and irregularly-shaped pellets that were mainly sub-rounded (*i.e.*, similar to the form in which they were excreted; Figs. 6.9 C, D). Although grain size analyses were not performed for these pellets, it is readily apparent that larger pellets (*e.g.*, up to 2 mm in length) are considerably more numerous than they are after four weeks of moderate agitation. For one of the samples, in which pellets comprise spheres (produced by bonefish), this preservation of pellet shape and size is perhaps explained by findings of particle disaggregation experiments (described above). Namely, spheres are commonly intergrown and may disaggregate less readily than the interlocking ellipsoids of pellets produced by black grouper. However, the other sample from this 'gentle agitation experiment' comprised pellets made up of ellipsoids (produced by schoolmaster snapper), and is similar to the carbonate products excreted by black grouper. The retention of pellet shape and size must therefore, and not unexpectedly, be related to the physical conditions to which pellets are exposed. Furthermore, carbonates produced by schoolmaster snapper and retained at the end of seven month 'gentle agitation experiments' had undergone a mass reduction of <4 %, and comprised only a very small fraction (<5 wt%) of fines. It is thus evident that fish-derived carbonates can persist as pellets for periods of at least seven months in physical conditions (*i.e.*, not including reworking due to the activity of marine organisms) similar to those of quiescent open marine platform settings without undergoing considerable changes to their size or morphology, and without substantial loss of mass as fines. In contrast, they can lose approximately two thirds of their mass as liberated fines within one month under conditions of moderate agitation, rapidly diminishing in size and developing less irregular, more elongate, and more rounded morphologies as they do so.

6.4.4 Sedimentary pellets

Examination of approximately 60 friable peloids from two shallow sites in Eleuthera Sound revealed that most are probably faecal pellets and/or pseudopellets, comprising aggregated mud-grade particles from a range of sources. Cryptocrystalline peloids were rare but some hard peloids were identified, usually as components of 'grapestone' grains (*i.e.*, several peloids cemented together).

Pellets from the muddy embayment of Rock Sound are dominated by aragonite needles of strong crystal habit, ranging from approximately 2–6 μm in length (Figs. 6.10 A, B) and having either blunt or pointed (but not rounded) terminations. These are similar to the aragonite needles usually considered to be the main component of carbonate muds in the Bahamas (Lowenstam and Epstein, 1957; Shinn *et al*., 1989) and are probably derived from inorganic precipitation events (*e.g.*, 'whitings') or calcareous green algae (*e.g.*, *Halimeda incrassata*). However, it is worth noting that they are also morphologically indistinguishable from aragonite needles described in Chapter 2 (Fig. 2.4 H). Other particle types from this area are very rare, but include low-Mg calcite rhombohedra (Fig. 6.10 A), which are also similar to some fish-derived carbonates.

Pellets from the surface sediments close to a patch reef are more varied in composition (Fig. 6.10 C, D). Common components include aragonite needles similar to those found in Rock Sound and skeletal carbonate fragments (*e.g.*, foraminiferal tests, *Amphiroa* fragments, and coccoliths), along with scarce tunicate and sponge spicules and diatom frustules. No particles were observed that could confidently be assigned as fish-derived carbonate. However, small clusters of nanospheres (Ca-carbonate containing approximately 20 mol% $MgCO_3$) closely resembling those produced by some fish species were present in some pellets (Fig. 6.10 C). In addition, approximately 35% of the pellet volume comprised high-Mg calcite (containing 13–17 mol% $MgCO_3$) lacking definable form (Fig. 6.10 C, D). Although it is not possible to assign this material to source, it is worth noting that its overall appearance is not dissimilar to carbonates produced by some fish species (Fig. 6.10 E), and its magnesium content is also within the range determined for some fish-derived carbonates.

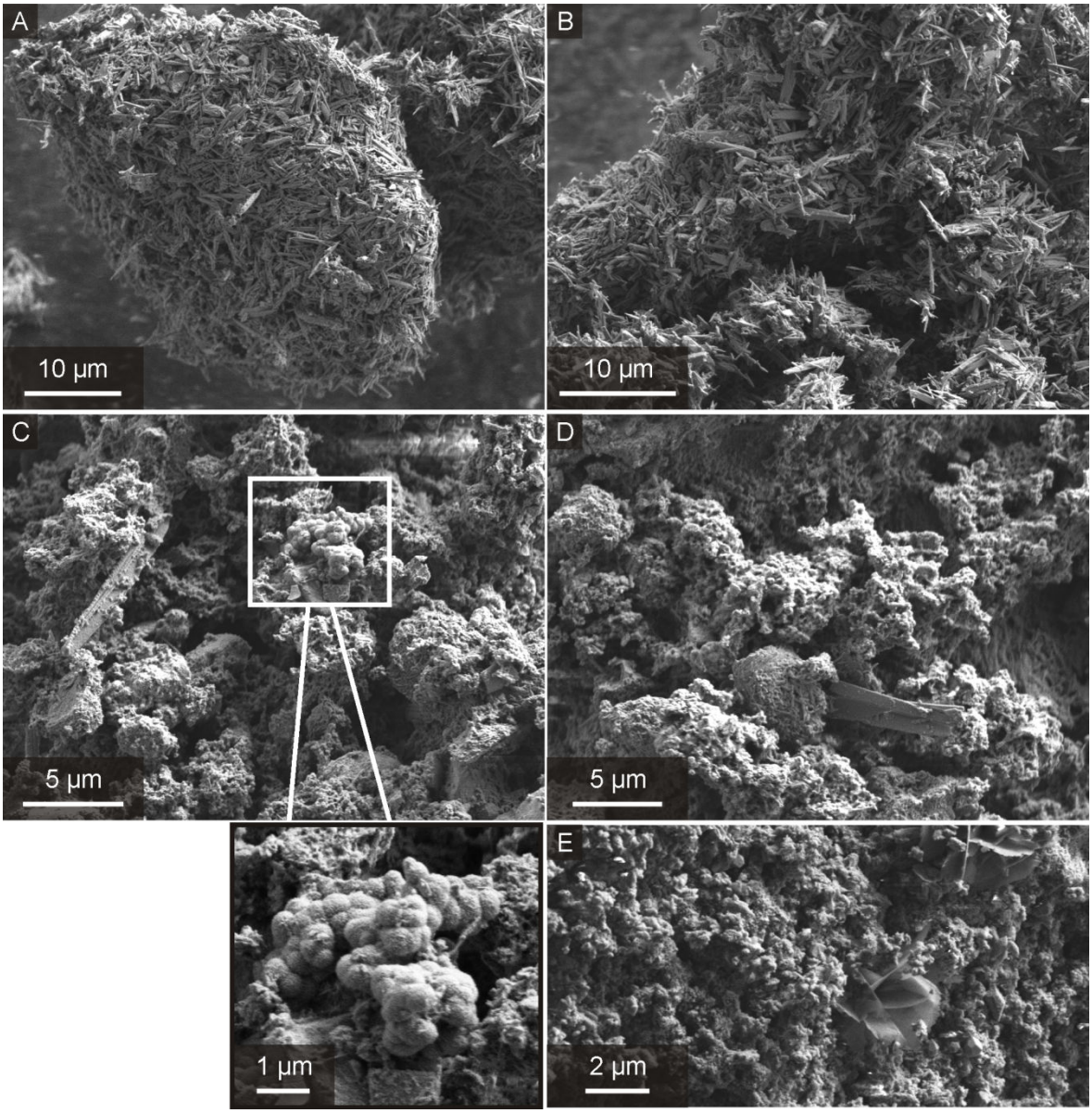

Figure 6.10 *SEM images of faecal pellets and pseudopellets from the surface sediments of two sites in Eleuthera Sound, the Bahamas (A–D) and fish-derived carbonates (E) for comparison. A & B show pellets from the surface sediment of a muddy embayment (Rock Sound), which are dominated by aragonite needles but also include very rare low-Mg calcite rhombohedra (top-centre; A). C & D show pellets from the surface sediment near a patch reef, which are compositionally more varied. C (and inset) shows a cluster of high-Mg calcite nanospheres (scarce) similar to some fish-derived carbonates (see Fig. 6.5 D3 for comparison). D shows a more commonly observed component of these pellets which comprises poorly-defined rounded and stubby high-Mg calcite crystals. These are not dissimilar to the components of some fish-derived carbonate pellets, such as those produced by red hind (E).*

6.5 DISCUSSION

6.5.1 Transport and deposition in leeward platform settings

6.5.1.1 Platform-top processes

Fish-derived carbonates, in their various aggregated and disaggregated states after excretion, have a size range spanning four orders of magnitude (0.1 to >1000 μm in length), while particles released from disaggregated pellets span more than three orders of magnitude (0.1 to 177 μm in length), with particle size closely related to morphotype. This large variation in grain size clearly has implications for the transport potential and depositional fate of these carbonates, and thus for sedimentary facies development, as considered here. Observations made during sample collection indicate that, following excretion, mucus-bound fish-derived carbonate pellets will rapidly sink and settle on the local substrate (as long as they are not ingested by fish or other organisms). The mucus coating typically disaggregates within a few days in seawater and at this point most pellets are loosely bound aggregates of mud-grade carbonates; effectively unlithified faecal pellets (*sensu* Illing, 1954) and referred to hereafter as soft pellets. Agitation experiments conducted herein indicate that pellets will remain in this state until physical disturbances (*e.g.*, wave action or bioturbation) facilitate their break up, at which point pellet diminution and/or the release of component particles will occur, the extent depending on degree of disturbance. As a result, on quiescent 'Bahamas-type' muddy platforms (Purdy, 1963) such as the Great Bahama Bank (GBB), fish-derived carbonates may contribute soft pellets, mud-grade crystals, and mud- to sand-sized particle clusters to Holocene accumulations of shallow platform sediments; grain types which are the main components of carbonate facies that characterise surface sediments of the interiors of leeward Bahamian platforms such as the GBB (Newell *et al*., 1959; Purdy, 1963; Reijmer *et al*., 2009).

Following their release from pellets and any re-suspension, most mud-grade carbonates (<63 μm) will likely settle in quiescent conditions on shallow platform interiors, perhaps aided in some areas by the baffling provided by seagrasses (Scoffin, 1970). For the most part, these particles are

predicted to retain their characteristic morphologies after the break up of pellets, although the present study indicates that particularly vigorous disturbance (*e.g.*, as a result of agitation in a high energy setting or mastication) may facilitate the disaggregation of polycrystalline precipitates to release their less distinctive component fibre- and blade-like crystals (depending on initial morphotype). The small size of many of these crystals means they may remain in suspension for prolonged periods, with many likely to undergo platform-wide dispersal before settling in the most quiescent areas (which, in the case of the GBB, is a large portion of the inner part of the platform leeward of Andros Island). However, the coarsest particles (*e.g.*, spheres) may settle out closer to sites of excretion along with particle clusters and soft pellets. Areas that support high fish population densities, particularly those in low-energy settings (*e.g.*, patch reefs), may accordingly accumulate the largest volumes of coarser-grained fish-derived carbonates.

The reasoning that fish-derived carbonates will contribute soft pellets, particle clusters, and individual mud-grade crystals should be valid for all sheltered platform settings where marine teleosts are abundant. However, facies patterns on the interiors of several sheltered leeward platforms, such as Berry Islands and Crooked-Acklins Platform, contradict this argument; soft pellets and mud are scarce and instead these platforms are grain-dominated, their surface sediments comprising large volumes of hardened peloids (Rankey and Reeder, 2010). Rankey and Reeder (2010) note that the interiors of these grain-dominated platforms are influenced by frequent tidal flushing, in marked contrast to platform interiors dominated by mud and pellet mud facies, which are characterised by overlying waters of long residence time (Morse *et al*., 1984). To explain the differences in surface sediment components between these settings, Rankey and Reeder (2010) proposed that mud produced on tidally flushed platforms is suspended and transported off-bank by wave action and tidal currents. In addition, they speculate that soft peloids are subject to early cementation and hardening due to the highly supersaturated and agitated overlying waters delivered by tidal flushing. Such conditions are not encountered on the interiors of muddy platforms (Morse *et al*., 1984), where hardened peloids are scarce and tend to occur only in agitated and highly supersaturated waters near the platform margins (Purdy, 1963; Neumann and Land, 1975).

It is thus proposed here that the transport and depositional fates of fish-derived carbonates produced in leeward settings vary according to specific platform conditions. End-member platform types are: 1) muddy platforms, characterised by quiescent conditions and poor circulation of overlying waters, where fish-derived carbonates are preserved on the platform top as soft pellets, mud- and sand-grade particle clusters, and mud-grade crystals; and 2) grain-dominated platforms, characterised by overlying waters frequently refreshed by tidal flushing, where fish-derived carbonates are either exported off-platform as liberated fines, or preserved on the platform top as pellets that are rapidly indurated to become hardened peloids (Fig. 6.11).

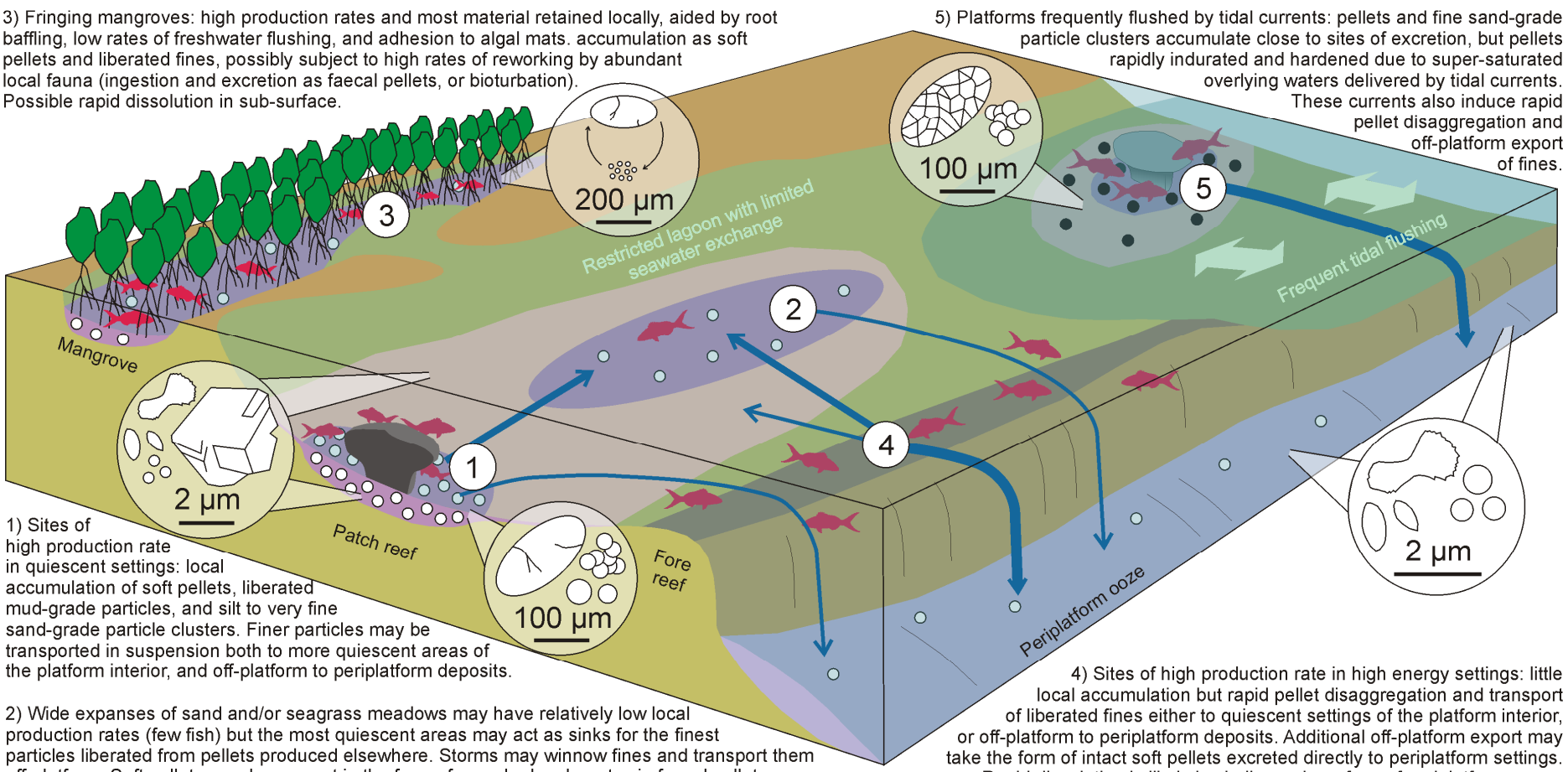

Figure 6.11 *Conceptual model for the transport and depositional fates of fish-derived carbonates in a range of typical leeward platform settings in the Bahamas.*

6.5.1.2 Pellet disaggregation and resultant morphologies

The hypothesis outlined above proposes for the first time that fish-derived carbonates not only contribute to the mud fraction of carbonate sediments in the Bahamas, but also to the sand fraction as pellets and peloids. The data presented herein indicate that pellets comprising clay-grade ellipsoids rapidly diminish in size in moderate to high energy settings, losing approximately two thirds of their mass as liberated fines and becoming substantially more rounded within four weeks. In contrast, pellets left in quiescent conditions for several months remain largely intact and lose <5 % of their original mass as liberated fines. It is thus apparent that fish-derived carbonates excreted in quiescent platform interior settings, such as patch reefs, fringing mangroves, and seagrass meadows, are more likely to be preserved as intact soft pellets. In contrast, a larger proportion of pellets excreted in higher energy settings, such as fore reefs and other highly agitated areas, are likely to be released as individual crystals and particle clusters, with pellets that remain intact likely to be smaller and more well-rounded than at the point of excretion. Of course, this assertion considers only the effects of pellet reworking by purely physical processes and does not account for biophysical processes such as bioturbation and forage-feeding, which, in settings of all energy regimes, are likely to accelerate pellet diminution and/or rework fish-derived carbonates as faecal pellets. Nevertheless, peloids of similar characteristics to these are common in Bahamian surface sediments (Illing, 1954), and the potential thus exists for fish-derived pellets to be similarly preserved in surface sediments.

In the present work, no pellets were found in Bahamian sediments that were unambiguously fish-derived, although the observation that particles broadly similar to some fish-derived carbonates abound in presumed faecal pellets is intriguing, and potentially supports the idea of some fish-derived carbonates being reworked as faecal pellets. If such particles are fish-derived, the fact they are not identical to those described in Chapter 2 is not surprising; these pellets being of presumed faecal origin means their component particles have probably been exposed to mildly acidic conditions (*i.e.*, in the stomachs of organisms that produced them), and as such these particles may have undergone partial dissolution. Of further interest regarding the potential for fish-derived

carbonates to be incorporated in sedimentary peloids is the fact that particles liberated from excreted pellets during agitation experiments appeared to re-aggregate, presumably via flocculation. Although these experiments were carried out under restricted conditions in which the chances of flocculation must have been higher than in open conditions, the observation that liberated particles have the potential to re-aggregate in seawater could mean similarly liberated particles in natural settings will interact with carbonate muds of other origins (*e.g.*, calcareous green algae, skeletal fragments, and whitings; see Chapter 1) and, via a mechanism similar to that described by Fahraeus *et al*. (1974), may form peloids of varied composition. It is thus possible that fish-derived carbonates are incorporated within surface sediments as components of pellets or peloids that form via various mechanisms. However, the limited scope of sedimentary peloid examination in the present study means these hypotheses are not confirmed, and more exhaustive studies of Recent peloids from a range of settings are necessary.

The present study does, however, inform on criteria that might aid identification of fish-derived carbonate pellets in various settings. At the microscopic scale, 'fresh' fish-derived carbonate pellets should be readily apparent based on their component crystal morphologies, many of which are unique among known carbonate sources in shallow sub-tropical marine settings (Salter *et al*., 2012). At larger scales, only spheres larger than about 30 μm in diameter can usually be discerned; pellets containing these morphotypes can be quite distinctive, but others are more difficult to identify. The size of fish-derived carbonate pellets at the point of excretion is generally close to that of faecal pellets in the surface sediments of the GBB interior (Fig. 6.12). Data arising in this study indicate that these pellets do not necessarily undergo substantial diminution in quiescent settings, and it can thus be expected that intact fish-derived pellets will be broadly similar in size to faecal pellets present in these settings. In higher energy settings, fish-derived pellets are probably substantially smaller due to attrition, but they are within the size range of hardened peloids documented in the sediments of tidally flushed platforms (Rankey and Reeder, 2010; Fig. 6.12). Rankey and Reeder (2010) do not speculate on the genesis of peloids at their study sites prior to hardening, but their size, being similar to fish-derived pellets that have undergone diminution, is

consistent with a hypothesis that fish-derived pellets in these higher energy settings may be preserved as hardened peloids.

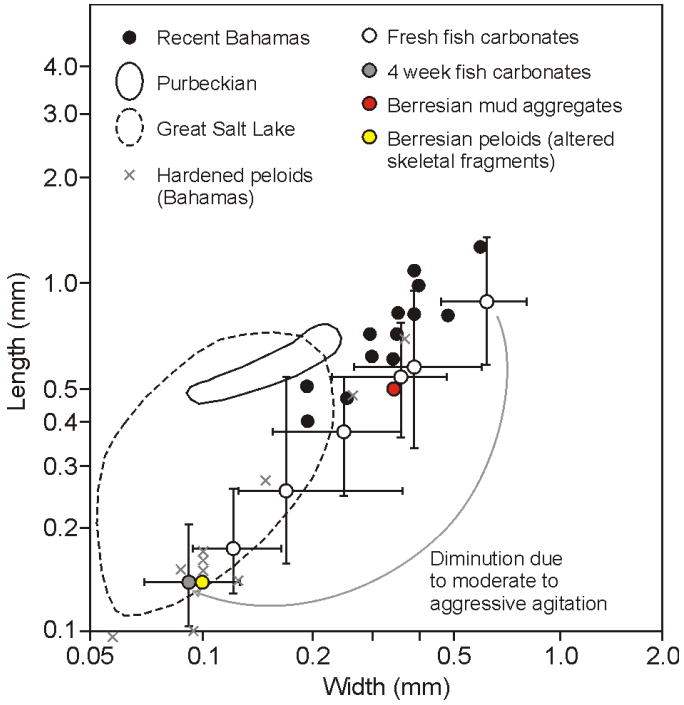

Figure 6.12 *Dimensions of pellets and peloids (modified after Bathurst, 1975). Fish carbonate data from this study (median dimensions shown, with bars showing inter-quartile ranges); Recent Bahamas pellets (considered to be faecal pellets) after Illing (1954) and Cloud (1962); Great Salt Lake pellets (faecal, from brine shrimp) after Eardley (1938); Purbeckian pellets (presumed faecal origin) after P.R. Brown (1961; in Bathurst, 1975); Berresian pellets/peloids after Samankassou et al., (2005); Hardened peloids after Rankey and Reeder (2010).*

Morphologically, pellets and peloids from the surface sediments of the Bahamas are generally spherical or ellipsoidal (Illing, 1954; Rankey and Reeder, 2010); distinctive grains being restricted to elongate tapered faecal pellets produced by the ecologically restricted gastropod, *Batillaria minima* (Kornicker and Purdy, 1957). Fish-derived pellets typically fit into the former category, being spherical to ellipsoidal and lacking distinctive surface or internal structures. The irregular, sub-rounded to sub-angular outlines of recently excreted pellets are not dissimilar to some of the friable aggregates documented by Illing (1954), and the well-rounded, regular outlines of agitated pellets are similar to many other composite grains documented by Illing (1954). The most distinctive fish-derived pellet morphologies are those in which precipitation appears to have proceeded on or around mucosal material within the gut (Fig. 6.7 B). However, such pellets are only rarely observed and are unlikely to be common or well-preserved in sedimentary settings.

Given these similarities in pellet size and shape between fish-derived carbonate pellets and those commonly occurring in shallow platform settings, unambiguous evidence for sedimentary pellets of teleostal origin is likely to lie only in micro-scale features (component crystal forms) and chemical properties (mineralogy and magnesium content). In the geological record, even these lines of evidence are likely to be obscured because, as with carbonate fines, pervasive micritisation can obliterate original features of faecal pellets (Bathurst, 1975), and presumably affects fish-derived pellets in a similar manner. Indeed, the results of Chapter 7 indicate that such processes could, in some cases, begin to occur as early as a few months after excretion.

6.5.1.3 Off-platform export: depositional fate and possible geochemical implications

In addition to proposing a previously unrecognised source of sand-grade pellet and peloid grain types in the Bahamas, the hypothesis regarding the transport and deposition of fish-derived carbonates in leeward platform settings invokes off-platform export of a proportion of the mud-grade particles liberated during disaggregation of initial pellets. Export of muds is expected to occur regardless of platform type, whether controlled by frequent tidal flushing of grain-dominated platforms (Rankey and Reeder, 2010), or storm-driven flushing of muddy platforms (Neumann and Land, 1975; Pilskaln *et al*., 1989). In the Bahamas, large volumes of carbonate mud are exported from the platform tops and deposited on their leeward flanks as periplatform carbonate ooze (Droxler *et al*., 1983; Wilber *et al*., 1990). Up to 70 % of the particles in these periplatform deposits can be clay-grade (Wilber *et al*., 1990) and, based on the data arising from this study, it follows that the export of fish-derived carbonates to these areas is likely to be dominated by liberated clay-grade particles such as monocrystalline ellipsoids, nanospheres, and small dumbbells. Given questions regarding the stability of fish-derived carbonates (Salter *et al*., 2012), and speculation regarding their dissolution in the upper one kilometre of pelagic zones (Wilson *et al*., 2009), their fate following off-platform export merits further consideration.

The preferential export of the finest fraction of fish-derived carbonates might result in them being partially sorted by composition. That is, fish-derived Mg calcite crystals <4 μm in length tend to

contain >20 mol% $MgCO_3$, whereas those >4 μm in length typically contain <15 mol% $MgCO_3$ (Salter *et al*., 2012). This compositional relationship with grain size is likely to be of little relevance on grain-dominated platforms, where the majority of mud-grade particles released on pellet disaggregation are likely flushed off-platform. Conversely, in areas where the finest particles are preferentially exported off-platform, such as mud-rich platforms like the GBB, the delivery of fish-derived carbonate to periplatform sediments is likely to be dominated by particles containing >20 mol% $MgCO_3$. Thus, it is potentially the least stable forms of fish-derived carbonate (*i.e.*, the smallest particles with the highest magnesium contents; see Salter *et al*., 2012, for further discussion) that contribute to periplatform deposits flanking Bahamian platforms, and this may have implications for their capacity to accumulate in such settings.

Empirical evidence indicates that most crystalline forms of fish-derived carbonate are stable in surface waters and in shallow platform-top porewater environments, at least in the short-term (see Chapter 7), but evidence for their stability, and consequent capacity to accumulate, at greater depths is limited. However, solubility measurements of ellipsoidal high-Mg calcite (<1 μm in length and containing approximately 48 mol% $MgCO_3$) produced by a sub-tropical toadfish (*Opsanus beta*) indicate a solubility about twice that of aragonite, which would equate to a lysocline in the North Atlantic at approximately 550 metres depth (Woosley *et al*., 2012). The magnesium content of these toadfish carbonates and, by extension, their solubility (Morse and Mackenzie, 1990; and references therein) is high compared to many Bahamian fish-derived carbonates (Salter *et al*., 2012). In addition, the aragonite lysocline around the Bahamas is depressed by approximately 1500 metres relative to that in the North Atlantic (Droxler *et al*., 1988), and the position of the lysocline for Bahamian fish-derived carbonates containing, for example, 25 mol% $MgCO_3$ is thus likely to be markedly deeper than 550 metres. Periplatform deposits on the leeward slopes of the GBB commonly begin at depths of 140–180 m (Wilber *et al*., 1990). Consequently, the upper slope areas of these periplatform deposits are at substantially shallower depths than the probable lysocline depth for most Bahamian fish-derived carbonate forms, which should therefore accumulate as a stable phase at the surface of such deposits.

Accumulation of fish-derived carbonates in periplatform deposits may have important implications for early diagenetic processes operating within these sediments. Analyses of bulk sediment samples from leeward periplatform deposits indicate that, as with many platform-top settings, they are dominated by aragonite, which can account for up to 96 wt% of sediment in the upper sections (Wilber *et al*., 1990). Pore fluids become undersaturated with respect to aragonite and high-Mg calcite within the upper 10 metres of these deposits, resulting in dissolution of metastable phases and precipitation of low-Mg calcite and dolomite cements (Malone *et al*., 2001). Fish-derived carbonates will likely follow similar fates of dissolution in these shallow burial conditions, where they may represent an important source of magnesium and consequently exert some control on the development of diagenetic cements.

6.5.2 Transport and deposition in other platform settings

6.5.2.1 Mangrove systems

Fringing mangrove systems have been identified as particularly important sites of fish-derived carbonate production because of high fish biomass (Perry *et al*., 2011) and, because they can be partially isolated from the wider platform setting, it is prudent to consider them discretely with respect to the fates of fish-derived carbonates. Mangroves and tidal creeks in the Bahamas can be sedimentologically varied, with surface sediments variously dominated by carbonate muds, peloids, and skeletal sands according to specific local conditions (Newell *et al*., 1959; Mitchell, 1987; Reijmer, 2009). Peloids in these settings are reportedly micritic in texture and are considered to be altered faecal pellets (Mitchell, 1987), although information regarding this is not exhaustive. Indeed, the production of faecal pellets in mangrove systems is to be expected given the numerous sediment-grazing organisms (*e.g.*, fishes, crustaceans, and gastropods) that commonly inhabit them. The presence of peloids and muds in these systems suggests that similar grain types produced by fish are likely to be retained in mangroves, where *Rhizophora* roots can act as highly efficient baffles to sediment transport (Scoffin, 1970; Fukuwara *et al*., 1997), and sediment trapping and stabilisation by microbial mats may further aid retention (Curran and Williams, 1997; Perry and

Taylor, 2007). In Bahamian mangrove systems, limited fresh water flushing may further augment sediment retention in the upper reaches of mangroves (Wolanski *et al*., 1992).

Following local deposition of excreted carbonates, pellet disaggregation is likely to proceed via numerous mechanisms, these including: i) attrition induced by diurnal tidal currents; ii) mastication by marine organisms; or iii) disturbances caused by bioturbation. Sediment-grazing organisms such as fiddler crabs (*Uca* sp.) are often abundant in mangrove systems and may cause significant disturbance to surface sediments. For example, *Uca vocans* has been shown to produce faecal pellets with an average weight of 37 mg at a rate of 8.6 min^{-1}, indicating that a typical mangrove population can forage 43 % of the uppermost millimetre of surface sediments in a single low tide feeding session (Dye and Lasiak, 1986). Such mechanisms will accelerate pellet disaggregation but will also aid the local retention of liberated fines via ingestion and re-excretion as faecal pellets, albeit more heterogeneous in composition than fish-derived pellets because they will likely have been pressed into new pellets alongside other ingested carbonate particles. In addition, bioturbation by infaunal organisms may promote rapid incorporation of a proportion of fish-derived carbonate below the sediment–water interface, possibly resulting in simultaneous disaggregation of pellets.

Although known patterns of sediment transport and deposition within mangrove systems indicate that fish-derived carbonates should be retained locally, evidence from mangroves on the western edge of Andros Island, the Bahamas, contradicts this theory. Specifically, Newell *et al*. (1959) find that the average age of carbonate fines within the uppermost 7 cm of mangrove sediment differs little from that of carbonate fines 69–76 cm below the sediment–water interface (2330 ±100 and 2660 ±100 years, respectively), and is substantially greater than that of carbonate fines on the surface of the wider platform interior (typically a few hundred years).They interpret these data as an indication that carbonate fines in Androsian mangroves are the result of sediment reworking, and that no newly precipitated carbonate sediment is being added at the surface. This is perplexing given that these mangroves hold large fish populations (*e.g.*, Layman and Silliman, 2002) which should provide a continuous supply of newly precipitated carbonates, and suggests that either: i)

fish-derived carbonates are not retained in these systems; ii) production rates are low relative to the supply of reworked older sediment; or iii) fish-derived carbonates are lost to rapid dissolution in these settings.

Net export is difficult to reconcile given that mud-grade sediments dominate the mangrove substrate and suggest good sediment retention, and one of the latter two possibilities must be more likely. Overlying waters in mangrove systems do not differ greatly in their carbonate chemistry from surface waters across the wider platform area (Newell *et al*., 1959; Morse *et al*., 1985) and should not promote rapid dissolution. However, the input and subsequent decomposition of large quantities of organic matter to mangrove substrates causes pH values and aragonite saturation states to decrease rapidly beneath the sediment–water interface (Llalier-Vergès, 1998; Alongi, 2000; Berkeley *et al*., 2007), with, for example, values of 7.30 (NBS) and 1.3, respectively, reported in the upper 3 cm of sediment in the Bahamas (Morse *et al*., 1985). Such conditions have been shown to promote dissolution of macrofossils in Australian mangrove systems (Perry *et al*., 2008) and can presumably also facilitate the dissolution of fish-derived carbonates, which could explain their apparent scarcity in Androsian mangroves. In fact, given their small size and high magnesium contents, it is possible that fish-derived carbonates represent one of the least stable phases in these settings, and are consequently one of the first to dissolve. In this manner they may have an important role in buffering pore fluids and consequently aiding preservation of more stable forms (Plaziat, 1995). Of course, this is highly speculative and further investigations are necessary to elucidate the fates and interactions of fish-derived carbonates in mangroves.

6.5.2.2 Windward settings

Although of limited areal extent in comparison to leeward platform settings, it is also worth giving some thought to the fate of fish-derived carbonates produced in windward settings. These areas of highly agitated waters promote rapid coral growth and the development of extensive reefs (Kornicker, 1963) which can support abundant fishes (*e.g.*, Peckol *et al*., 2003). However, the sediments present in shallow settings are dominated by sand-grade skeletal grains (coralgal facies);

non-skeletal grains and mud-grade carbonates are rare (Ginsburg *et al*., 1958; Purdy, 1963; Reijmer *et al*., 2009). Whilst these settings can hold large fish populations which presumably produce large amounts of fish-derived carbonate, the results of this study indicate that the agitated conditions that facilitate this will also promote rapid pellet diminution. Subsequent deposition of the resulting mud- and fine sand-grade particles is probably hampered in shallow settings by these high energy conditions, and most fish-derived carbonates are likely transported away from production sites, either to more sheltered leeward settings, or to adjacent platform slopes. Periplatform sediment aprons are well-documented on wind- and wave-ward platform slopes in the Bahamas (Mullins, 1983; Mullins *et al*., 1984; Ginsburg *et al*., 1991; Rankey and Doolittle, 2012), and although these can differ in character from equivalent deposits in leeward settings, they have been shown to contain similarly platform-derived fine-grained aragonite and high-Mg calcite (Heath and Mullins, 1984). Windward periplatform deposits are thus likely to be an important sink for fish-derived carbonates produced in shallow windward settings, potentially with similar diagenetic implications as speculated for leeward slope deposits.

6.6. CONCLUSIONS

Detailed measurement of individual fish-derived carbonate particles confirms that the various morphotypes described in Chapter 2 are highly varied in size at the point of excretion, ranging from clay-grade (<4 μm) particles (nanospheres, monocrystalline ellipsoids, and some rhombohedral crystals) to coarse silt-grade (31–63 μm) particles (some polycrystalline spheres), with numerous other morphotypes occurring as intermediate fine–medium silt-grade particles (rhombohedra, dumbbells, and most polycrystalline spheres). Importantly, disaggregation experiments show that, other than individual morphotypes, particles may, in some cases, be released from pellets upon their disaggregation as either: i) clusters of intergrown particles (usually comprising spheres, polycrystalline ellipsoids, or rhombohedra) that do not readily disaggregate further and that typically occur as coarse silt- to very fine sand-sized particles (*i.e.*, 31–125 μm); or ii) component crystals of initially polycrystalline forms (*e.g.*, needles or fibres from polycrystalline spheres, or

blade-like crystals from polycrystalline ellipsoids), these typically being clay-grade. These latter findings indicate that, upon pellet disaggregation, fish-derived carbonates might contribute to surface sediments over a much wider grain size interval than previously thought; not only occurring as distinctive mud-grade particles described in previous studies, but also as distinctive sand-grade particle clusters, as well as less distinctive mud-grade particles that may be difficult to recognise as being fish-derived when observed in bulk sediment samples.

Based on these grain size measurements, it is proposed that many fish-derived carbonates will be deposited in platform-top settings, but also that tidal or storm-driven currents may flush many of these particles off-platform, perhaps favouring those that are clay-grade. This being the case, it is possible that fish-derived carbonates might become partly sorted on a geochemical basis, with larger, lower-Mg particles tending to be retained on-platform, and smaller, higher-Mg particles tending to be exported off-platform, perhaps being deposited along with other platform-top mud-grade carbonates as periplatform carbonate ooze. Given that such deposits around the Bahamas can be dominated by aragonite, input of high-Mg calcite fish-derived carbonates might have important early diagenetic implications, potentially influencing the phase and texture of diagenetic cements.

Of further significance are the findings of investigations concerning pellets in their excreted forms. While cohesion in pellets at the point of excretion is typically weak, suggesting that many will readily disaggregate after excretion and degradation of mucus coatings, experiments involving physical agitation of cleaned pellets show that they do not necessarily disaggregate in all situations. For example, pellets remained largely intact after seven months of very weak agitation (losing <5 % of their initial mass to liberated fines), suggesting that, where produced in quiescent platform settings, there is a good chance they will be preserved close to their excreted form. Moreover, approximately one third of the mass of carbonates retrieved after one month in moderately agitated seawater conditions were intact pellets, albeit much smaller and more well-rounded than those at the point of excretion, suggesting that some fish-derived carbonates may be retained in pellet form even in agitated platform conditions (*e.g.*, fore reefs). Although it is likely that pellets produced in

nature will additionally be subject to reworking by biophysical processes (*e.g.*, mastication, ingestion, and bioturbation), these results clearly indicate some fish-derived carbonates have the potential to be preserved, at least over short timescales, in platform-top surface sediments, either as very fine to very coarse sand-grade particles in quiescent settings where reworking is limited, or as coarse silt- to fine sand-grade particles in agitated settings. Moreover, short-term retention of intact pellet forms may facilitate their induration in certain physico-chemical settings, thus potentially favouring their preservation as peloids in the geological record, although differentiating such particles from peloids of other origins may be difficult.

Chapter 7: Short-term preservation pathways of fish-derived carbonates upon exposure to seawater and porewater conditions

7.1 INTRODUCTION

In chapters 2 and 3, detailed descriptions of the carbonates produced in the guts of a variety of fish species demonstrated that individual Mg calcite crystals can vary significantly in morphology, size (0.1 to >50 μm in length), and magnesium content (0 to 45 mol% $MgCO_3$); this variability occurring both across species and, in many cases, within species. Because of these sometimes high magnesium contents and small grain sizes, questions evidently arise about the preservation potential of these carbonates in marine settings, and whether fish-derived carbonates of different morphological and chemical characteristics might follow different preservation pathways (Salter *et al*., 2012).

The importance and relevance of such questions become clear when considered alongside the documented preservation pathways of other shallow platform carbonates in sub-tropical regions. For example, Perry *et al*. (2011) compiled available data on carbonate mud production in shallow settings of the Bahamas to construct a carbonate mud budget that incorporates all known major sources (their Table S4), thus facilitating estimation of the relative contribution made by each and, consequently, the relative proportions of aragonite, calcite and Mg calcite that might be incorporated within the surface sediment. Their budget suggests that approximately 85 % of carbonate mud produced in these settings is calcite and, predominantly, high-Mg calcite; a result that is in stark contrast to surficial carbonate mud compositions determined in various studies for the Great Bahama Bank (GBB), which typically indicate that more than 70–80 % (Husseini and Matthews, 1972; Milliman, 1974; Shinn *et al*., 1989), and up to 95 % (Cloud, 1962), of the mud-

fraction is aragonite (typically exhibiting needle-like morphology). Although substantial errors are introduced to these budgets due to uncertainties in factors such as the rate and significance of abiotic precipitation (*e.g.*, Morse *et al*., 2003), this disparity in estimated production and observed mud composition requires further explanation. One possibility is that, because it is a metastable phase (Morse and Mackenzie, 1990; and references therein), a large amount of high-Mg calcite produced in these settings may dissolve at a reasonably early stage after they are produced, thus leaving aragonite as the dominant phase in muddy surface sediments. Indeed, Walter *et al*. (1993) demonstrate that more than 50 % of carbonates produced in shallow settings in the Bahamas either dissolve or recrystallise in the upper 10s of cm in shallow marine waters, and the fact that high-Mg calcite with more than about 10–15 mol% $MgCO_3$ is the most soluble of commonly occurring marine carbonates (Walter and Morse, 1984; Bischoff *et al*., 1987) means this will probably be the first phase to respond to conditions of undersaturation, as demonstrated by Moulin *et al*. (1985).

Given the very high magnesium contents of many fish-derived Mg calcite crystals (Perry *et al*., 2011; Salter *et al*., 2012 – see Chapter 2), such large-scale alteration of sedimentary carbonates presumably means that many of these carbonates may undergo similar post-excretion transformations; their poor crystallinity and relatively high water contents (Chapter 3) possibly further increasing their susceptibility. Two important questions thus arise: 1) Does fish-derived Mg calcite undergo alteration after it is excreted in shallow sub-tropical marine settings, and if so at what rate do these alterations proceed?; and 2) In the event that alterations are represented by recrystallisation, what are the alteration textures that characterise preserved fish-derived Mg calcite? It is the aim of this chapter to start to address these questions by exposing fish-derived carbonates to a variety of conditions likely to be encountered during the short-term period (days to months) following excretion, and assessing the resulting textural and chemical changes.

In addition, the potential for post-excretion alteration of several other fish-derived precipitation products identified in Chapter 3 (amorphous carbonates, monohydrocalcite, and brucite) must be even greater than for Mg calcite; these phases being considered to be highly unstable in shallow

sub-tropical surface seawater (see Chapters 1–3). The short-term post-excretion fate of these phases is also investigated here. Moreover, because of the likelihood that at least some of these phases will rapidly dissolve in seawater (see discussion in Chapter 1), thus potentially reducing the amount of excreted carbonate that is of sedimentary significance, the relative abundances of different precipitation products are estimated here and applied to platform-wide fish populations in order to assess the total volume of fish-derived carbonate that is likely to be preserved during the initial stages following excretion.

7.2 METHODOLOGY

7.2.1 Sample collection

The short-term preservation fate of fish-derived carbonates was investigated in experiments designed to simulate three types of post-excretion exposure: 1) up to 12 days in surface seawater; 2) up to 7 months in surface seawater; and 3) up to 3 months in shallow platform-top porewater. Porewater exposure experiments were further divided into those in which organic coatings were left to degrade naturally during exposure and those in which they were removed prior to exposure, thus facilitating the study of interactions between organic and inorganic components of excreted matter.

Carbonate samples for all experiments were collected from a range of common Caribbean fish species selected to ensure most carbonate forms described in previous studies were represented (Table 7.1.; based on the findings of Chapters 2 and 3). Sampling took place at the Cape Eleuthera Institute (CEI), Eleuthera Island, the Bahamas, in May and December 2011, and was conducted according to the methodology described in Chapter 2. Mean surface seawater (and aquaria) temperature (SST) was 26 °C in May 2011 and 22 °C in December 2011, and salinity during both periods varied between 36 and 38 (practical salinity scale). Following sample collection, carbonates were transferred to experimental chambers in their excreted forms (*i.e.*, with mucus coatings intact) unless otherwise stated.

Table 7.1 *Fish species from which carbonates were collected for preservation experiments. Crystal morphologies, mineralogies, and magnesium contents as determined in Chapters 2 and 3.*

Species*	Dominant crystal morphologies and mineralogies	Approximate $MgCO_3$ content (mol %)
Schoolmaster snapper	Ellipsoids (Mg calcite)	22–37
Yellowfin mojarra	Ellipsoids (Mg calcite)	16–23
	Dumbbells + spherulites (Mg calcite + aragonite?)	3–9
Bonefish	Spheres (Mg calcite + monohydrocalcite?)	19–23
	Nanospheres (ACC)	35
Keeltail needlefish	Mg-rich amorphous phase (AMC)	>95
	Rosettes and plates (Brucite)	N/A
	Ellipsoids + rods + small dumbbells (Mg calcite)	11–16
	Dumbbells +spheres (Mg calcite + aragonite?)	2–5
Bluehead wrasse	Mg-rich amorphous phase (AMC?)	>95
	Rhombohedra + dumbbells + spheres (Mg calcite)	<10

*Note – samples were also collected from other species (*e.g.*, Nassau grouper and black grouper) and exposed to seawater and porewater conditions. The results of those experiments are not reported in detail here, but were generally similar to those documented for carbonates produced by schoolmaster snapper.

7.2.2. Seawater and porewater exposure experiments

7.2.2.1 Natural seawater

Surface seawater was collected via a seawater intake that supplies the aquaria at CEI. Seawater was drawn from approximately 70 m offshore, where water depth ranges from 1–2 m, and was transported to the aquaria via a pump and a series of filters (down to 1 μm). Following filtration, a continuous one-pass flow of seawater was directed to a clean, lidded tank from which water for exposure experiments was collected. Prior to use in preservation experiments, seawater was passed through a Nuclepore™ track-etched polycarbonate membrane (47 mm diameter, 1 μm pore size) to ensure the removal of most particulate and biological matter.

Preservation experiments were carried out in 385 mL narrow-necked, sterilised, glass bottles which were thoroughly cleaned prior to use (*i.e.*, sonicated, soaked in a 5.25 % solution of sodium hypochlorite for 24 hours, rinsed with distilled water, and flushed with filtered seawater). During experiments, bottles were filled with 350 mL of filtered seawater which was aerated via a mains-connected air pump and lengths of polyethylene tubing (0.58 mm internal diameter) which supplied air to the base of experimental vessels (Fig. 7.1). This air supply also served to gently agitate

sample material (as would happen in nature due to wave action, tidal currents, and disturbance by marine fauna). Mucus-coated carbonates (wet mass typically in the approximate range 0.2–2.0 g) were collected from fish within 18 hours of excretion and placed directly into experimental vessels, which were covered to prevent ingress of foreign particles (*i.e.*, dust).

Figure 7.1 *Experimental vessels for short-duration (up to 12 days) exposures of fish-derived carbonates to natural surface seawater. Glass bottles are aerated via a mains-connected air pump. Air flow is divided prior to entering bottles and is supplied from the splitter via polyethylene tubing (0.58 mm internal diameter).*

The presence of mucus coatings in experimental vessels means constant aeration of seawater was crucial in these experiments. In natural settings, organic matter should undergo aerobic decomposition in surface seawater via the following reaction:

$$CH_2O + O_2 \rightarrow CO_2 + H_2O \qquad \textit{equation } 7.1$$

Because mucus coatings in open marine conditions are in contact with an effectively infinite volume of water, the above reaction has little effect on bulk seawater chemistry and calcite and aragonite saturation states remain unchanged. However, within non-aerated experimental vessels, equation 7.1 would lead to the rapid accumulation of dissolved CO_2 and consequent lowering of pH and $CaCO_3$ saturation states, potentially resulting in dissolution of inorganic carbonates that would

otherwise not occur in nature. To illustrate the effects of non-aeration, one experimental vessel was left without an air supply following the addition of mucus coated fish-derived carbonates (produced by Nassau grouper). Within a few days, all components of the original sample (which contained numerous mm-scale pellets) had broken down to very fine particles, yet in a parallel experiment in which seawater was aerated (and thus atmospheric CO_2 levels maintained), pellets remained intact during this period.

Another issue with these closed system experiments arises in changes that may occur in the dissolved inorganic carbon (DIC) system as a result of carbonate dissolution and/or precipitation. For example, calcite precipitation in seawater usually proceeds by the following reaction:

$$Ca^{2+} + CO_3^{2-} \rightarrow CaCO_3 \qquad \textit{equation } 7.2$$

Following this removal of CO_3 from solution, DIC species (CO_2, H_2CO_3, HCO_3^-, and CO_3^{2-}) are redistributed via:

$$HCO_3^- \rightarrow CO_3^{2-} + H^+ \qquad \textit{equation } 7.3$$

and

$$HCO_3^- + H^+ \rightarrow CO_2 + H_2O \qquad \textit{equation } 7.4$$

Within experimental vessels, excess CO_2 produced during such reactions would be removed via aeration, but the net effect would be a decrease in seawater pH, total alkalinity, and calcium and aragonite saturation states due to lowered CO_3^{2-} and HCO_3^- concentrations. In the case of carbonate dissolution, the reverse would be true. Consequently, it was necessary to manage seawater chemistry in experimental vessels by removing half of it with a siphon every 48 hours and replacing this with 'fresh' filtered seawater.

An associated problem with this procedure is that typically small (<2 μm) fish-derived carbonate crystals, once liberated from pellets, are likely to be held in suspension due to seawater agitation caused by aeration. In order to minimise loss of liberated fines, air supplies were removed prior to water exchange, thus allowing fine particles to settle out from suspension. However, because aeration was required to prevent organically-derived CO_2 build-up, it was necessary to strike a

balance between material loss and CO_2 accumulation. It was found that removal of air supplies from seawater containing fish-derived carbonates for up to 10 hours resulted in little or no change in solution pH (8.21 ±0.01; NBS), suggesting little accumulation of dissolved CO_2 during this time. Furthermore, while some aerated and agitated samples were slightly cloudy, presumably due to suspended fines, seawater samples were completely clear after 10 hours without agitation, suggesting most fine-grained carbonates had settled out from suspension.

Using the methodology described above, carbonate samples were collected from each fish species and held in different experimental vessels for periods of 2, 4, 8, and 12 days. Each of these sub-samples was the product of 18 hours worth of carbonate production by fish (with a total of five sub-samples per species over a five day period). To ensure the initial characteristics of excreted products did not change during this period, control samples were collected and immediately cleaned and dried at two hour intervals during the intervening six hour periods between collections of samples for seawater exposure. Air supplies were removed from experimental vessels for the final 10 hours of each exposure prior to removal of seawater with a siphon. The remaining solid particles (predominantly carbonate pellets) were soaked in a 5.25 % solution of sodium hypochlorite, which was removed with a siphon after a further 10 hours prior to cleaned carbonates being rinsed with distilled water. Finally, distilled water was removed immediately by vacuum filtration; solid particles being retained on a cellulose nitrate membrane (0.47 mm diameter, 0.45 μm pore size).

7.2.2.2 Artificial seawater

In order to investigate the preservation potential of fish-derived carbonates in surface seawater over longer periods, carbonates excreted by two species that produce different crystal forms (very high-Mg calcite ellipsoids produced by schoolmaster snapper, and high-Mg calcite and monohydrocalcite polycrystalline spheres and ACC nanospheres produced by bonefish) were cleaned and held in artificial seawater for periods of 3 and 7 months. The pre-cleaning of carbonates and the use of artificial seawater was necessitated by the need to conduct these

experiments under controlled conditions in the UK without being able to: a) transport uncleaned carbonates from the Bahamas in aerated and temperature-controlled seawater; and b) transport a sufficient volume of surface seawater from the Bahamas while ensuring its DIC chemistry remained unchanged. While removal of mucus coatings potentially influences post-excretion processes that affect carbonate precipitates (see section 7.3), the advantage of doing this is that it allows the initial weight of inorganic carbonate to be determined and compared with final weights, thus facilitating quantification of the amount of excreted carbonate lost to dissolution or the amount of carbonate precipitated in association with fish-derived carbonates.

Artificial seawater was prepared in a 1 L glass beaker using deionised water and commercial seawater salts (Tropic Marin) to salinity 36 (pss), and brought to 26 °C (mean SST in the Bahamas) in a constant temperature water bath. Following equilibration to atmospheric conditions via a mains-connected air pump and a ceramic air stone, solution pH was typically 8.43 (NBS). Assuming pCO_2 values of about 395 µatm (*i.e.*, the approximate concentration in ambient atmospheric conditions), this pH value indicates total alkalinity and total CO_2 values are considerably higher in this solution than in natural seawater (*e.g.*, total alkalinity of approximately 4700 µmol·kg^{-1} versus approximately 2400 µmol·kg^{-1}, respectively), and consequently higher calcite and aragonite saturation states (as calculated using CO2SYS software – see below). These higher-than-nature values are due to elevated CO_3^{2-} and HCO_3^- concentrations, which were manipulated by the addition of 2.2 mL of a 1.0 M solution of HCl to induce the following reactions:

$$H^+ + HCO_3^- \rightarrow H_2CO_3 \rightarrow H_2O + CO_2 \qquad \textit{equation } 7.5$$

and

$$H^+ + CO_3^{2-} \rightarrow HCO_3^- \qquad \textit{equation } 7.6$$

By thus lowering the concentrations of HCO_3^- and CO_3^{2-}, and by degassing excess CO_2 via aeration, pH values were reduced to 8.20 (NBS) and calculated total alkalinity values and $CaCO_3$ saturation states were altered to within the range of natural seawater values.

Figure 7.2 *Experimental arrangement for artificial seawater exposures. Cleaned carbonate samples were held in beakers with 500 mL of aerated artificial seawater held at a constant temperature of 26 °C in a water bath.*

Following proper preparation of artificial seawater, the stock solution was passed through a Nuclepore™ track-etched membrane (1 µm pore size) before being divided among glass beakers (500 mL per beaker), each aerated via a ceramic air stone (Fig. 7.2). Fish-derived carbonate samples were then added to four beakers (two replicate beakers for samples produced by schoolmaster snapper and a further two replicates for samples produced by bonefish), which were then sealed with parafilm to prevent ingress of dust. In addition, an identical beaker was prepared as a blank seawater experiment to check there were no ambient changes in the DIC system. Solution pH was closely monitored during the first week of exposure, and thereafter at weekly intervals, to ensure the presence of carbonates did not induce changes to the DIC system beyond reasonable limits for natural surface seawater from the Bahamas.

Conditions of freshly prepared artificial seawater were maintained by removing half the solution from each experimental beaker on a weekly basis and replacing it with freshly prepared artificial

seawater, in a manner similar to that described for refreshment of natural seawater (see previous section). Additional seawater preparations were identical to the first except at times when salinity in experimental beakers, increased due to evaporation, approached 37 (PSS), at which point new batches were prepared to an appropriate salinity slightly lower than 36 (PSS). Throughout the experiment salinity was maintained between 36 and 37 (PSS) and pH was maintained between 8.19 and 8.25 (NBS).

After 3 months approximately half of the remaining carbonates, most of which were intact pellets, were removed using a plastic Pasteur pipette and prepared for further analysis following the cleaning protocol described in Chapter 2. The remaining carbonates were left for a further four months before being retrieved and prepared for analysis.

Aside from ensuring the DIC system was close to that of natural surface seawater, it was also necessary to ensure that dissolved ion ratios of artificial seawater solutions were close to those of natural seawater. The relative concentrations of dissolved ions in surface seawater are considered to be globally uniform (*i.e.*, Marcet's Principle), and the CO2SYS program for calculating parameters related to the DIC system (see details below) makes calculations based on the assumption that dissolved ion ratios are the same as widely held for surface seawater. For artificial seawater used in this study, concentrations of a range of major and minor ions (Na^+, Cl^-, Mg^{2+}, Ca^{2+}, K^+, PO_4^{3-}, and SO_4^{2-}) were compared to those of natural surface seawater (Reference seawater, Batch 114, A.G. Dickson, Scripps institute of Oceanography, California, USA) using liquid ion chromatography (see below for methodology) and found to be within 4 %. However, it is worth mentioning that further analyses by inductively-coupled plasma optical emission spectrometry (ICP-OES; see analytical details below) found manganese to be present at concentrations of about 0.01 mM (corrected to salinity 35; PSS). This concentration, although very low, is three orders of magnitude higher than expected seawater values (typically <0.00001 mM; Turekian, 1968). Several studies describe the potential for similarly low, but elevated, concentrations of manganese to interact

strongly with calcite (*e.g.*, Vinson *et al*., 2007); the potential implications of this are discussed further in section 7.5.

7.2.2.3 Porewater exposures

Carbonate samples for porewater preservation experiments were collected from the same range of species as used for natural surface seawater exposure experiments. Following collection at the point of excretion, carbonates were held in natural seawater for 12 days, as described in section 7.3.2.1. In this way samples were exposed only to the chemical conditions they would encounter in nature. Moreover, following excretion in natural systems, it would be unusual for these carbonates to enter a porewater environment immediately, and this holding period thus mimics the period between carbonate excretion and incorporation within the substrate.

After being held in natural seawater, samples produced by each species were divided into three sub-samples: 1) a control sample to facilitate characterisation of crystals prior to porewater exposure; 2) a sample left untreated prior to porewater exposure (two replicates); and 3) a sample that was soaked in a 5.25 % solution of sodium hypochlorite for six hours (to remove organic residues) and rinsed with distilled water prior to porewater exposure (two replicates). The latter sub-set of samples was prepared to allow determination of the post-excretion influence of mucus coatings, if any, during exposures lasting several months. Finally, control samples were collected from each species within two hours of excretion at the beginning and end of the sampling period.

Several factors hamper the burial of fish-derived carbonates in a sediment substrate for later recovery, these including: 1) the very small grain size of most crystal forms; and 2) the typically small (<2 g) sample size. To overcome these problems, samples were buried in small plastic containers with porous walls (Fig. 7.3). Burial chambers consisted of two parts: an open-topped inner chamber (7 mL plastic vial), the sides of which were perforated with more than 40 holes of 0.3 mm diameter covering three quarters of its height (approximately 1 cm at the base was left intact); and a sealed outer chamber (30 mL plastic vial with screw-cap closure), the sides of which were perforated with more than 200 holes of 0.5 mm diameter. The latter was positioned upside-

down during experiments; inner chambers, which were kept upright, being adhered to the insides of their lids using a waterproof marine resin (Marine Weld, JB Weld Co., Sulphur Springs, Texas, USA). Employment of this experimental arrangement facilitated the free exchange of external and internal fluids, as demonstrated in tests using artificial seawater and a dye: experimental chambers containing clear seawater were immersed in a beakers containing dyed seawater and reached equilibrium with the latter within 24 hours. However, the reasonably large diameter of holes in the walls of outer chambers (0.5 mm) means that sedimentary particles with shortest diameters less than 0.5 mm could potentially enter chambers. To prevent mixing of external surface sediments with fish-derived carbonates, the double chamber design meant that incoming external sediments would fall between the inner and outer chambers, while sample material remained uncontaminated within inner chambers (Fig. 7.3). The success of this arrangement was readily discernable upon sample retrieval, with the spaces between inner and outer chambers containing external sediments (up to about 5 mm deep at the base of outer chambers) and inner chambers containing only fish-derived carbonates. Later examination using scanning electron microscopy revealed that only a very limited number of external sediments (*e.g.*, foraminifera tests) reached the inner chambers.

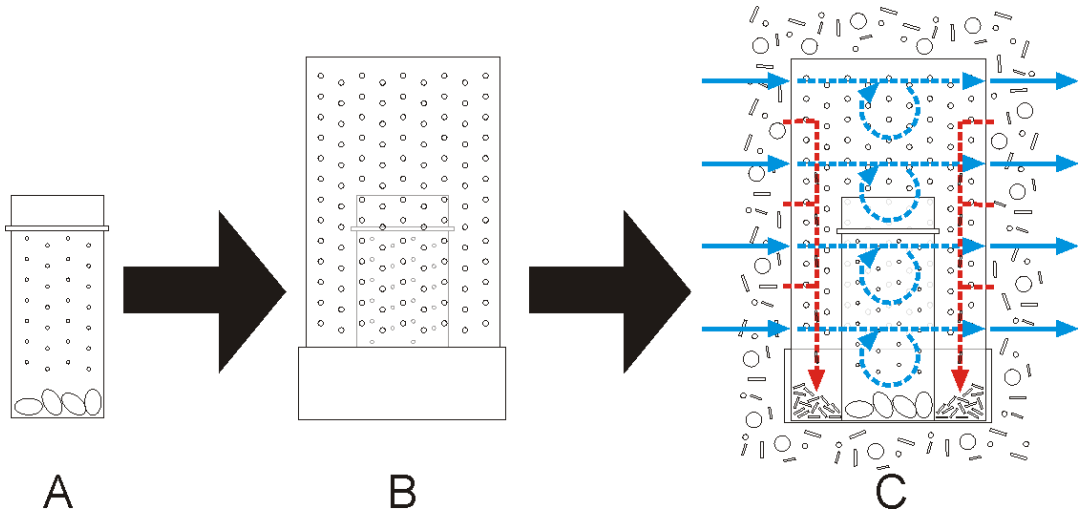

Figure 7.3 *Arrangement of containers in which fish-derived carbonates were buried within a carbonate sedimentary substrate and exposed to shallow porewaters. A) Inner plastic container in which sample material is held. Walls perforated with 0.3 mm diameter holes; B) Outer plastic container, inverted; inner container is adhered to the internal surface of its screw-fitting cap. Walls perforated with 0.5 mm diameter holes. C) Schematic cross-section of containers and sample material when buried in a sediment substrate. Holes in the walls of both containers allow the exchange of internal and external waters (blue arrows), while the inner pot prevents external sedimentary particles from mixing with sample material; the former accumulating in the bottom of the outer container (red arrows).*

Although the waterproof marine resin securing inner chambers to outer chambers contains 5–10 % iron and 10–30 % 'limestone' (JB Weld Co., 2012), both of which have the potential to influence the chemistry of seawater, preliminary tests found it to be chemically inert in seawater. Fully cured resin blocks (with volumes of approximately 0.5 cm^3) were immersed in 30 mL of artificial seawater in a clean glass beaker made airtight with parafilm. Three replicate samples were held for two weeks at 26 °C, along with three beakers containing blank artificial seawater. All seawater was from the same stock solution, prepared as described in section 7.2.2.2, with the exception of lower starting pH (8.05; NBS) and TCO_2 (1424 $\mu mol \cdot kg^{-1}$). Although the DIC system of this artificial seawater differs from that anticipated for porewater (*e.g.*, Bahamian porewaters commonly have elevated TCO_2 values compared to overlying seawater due to elevated pCO_2 values; Morse *et al.*, 1985), the resulting aragonite saturation state (1.92) is within the expected range. At the end of the experiment, no changes were observed in solution pH, salinity, or TCO_2 in any beaker, and resin blocks had the same mass as at the beginning of the experiment.

Using the experimental arrangement described above, carbonate samples were buried in a carbonate substrate in Eleuthera Sound, where they were exposed to porewater conditions for 79 days between December 2011 and March 2012. A burial site was selected to meet four criteria: 1) it was close to an area with a large fish population (and was therefore an area where fish-derived carbonates are likely to be produced in large quantities); 2) it was a reasonably sheltered location, thus increasing the likelihood that samples would remain buried within the substrate (*i.e.*, substrate was stable), and also making it a likely location for naturally produced fish-derived carbonates to accumulate and become incorporated within the sediment (thus being exposed to similar conditions as experimental samples); 3) it was a habitat that is common and widespread in the Bahamas; and 4) it comprised a veneer of loose sediment of sufficient depth to: i) bury sample containers to a depth of approximately 10–15 cm below the sediment–water interface; and ii) securely anchor stakes to which sample containers would be attached.

To meet these criteria, a site was selected adjacent to a patch reef located at 24° 50' 2.35 N, 76° 14' 34.29 W. The sediment–water interface at this site was approximately 3 m below sea level, and the veneer of loose sediment was approximately 30 cm thick (overlying a hard surface, likely either a hardground or limestone bedrock). Loose sediment comprised predominantly fine sand-grade skeletal carbonates; a typical surface sediment composition at many sites within Eleuthera Sound. Within close proximity of this location the substrate supported a sparse seagrass (*Thalassia testudinum*) population, indicating a reasonably stable sediment veneer (*i.e.*, stable enough for seagrass to become established). However, the precise locations where samples were buried typically contained little or no seagrass cover (*i.e.*, at the surface) or rhizomes (*i.e.*, in the sub-surface).

Carbonate samples were transported to the burial location in surface seawater within their sealed experimental chambers. Chambers were installed in burial positions attached to stakes (0.5 inch diameter PVC pipes; two chambers per stake) of 1 m length, which were hammered into the substrate until securely anchored about 2 m apart from each other. Once stakes were anchored, surface sediment was removed from around their bases to form 'bowls' approximately 15 cm deep. Experimental chambers were positioned in these 'bowls' and attached to stakes using cable ties. Finally, the 'bowls' were refilled with sediment such that containers were buried to depths of approximately 10–15 cm below the sediment–water interface (Fig. 7.4). Because it was predominantly sand-grade, the disturbed sediment surrounding experimental chambers was assumed to be permeable and influenced by advective fluid transport, thus allowing interstitial fluids to rapidly re-equilibrate with local porewaters.

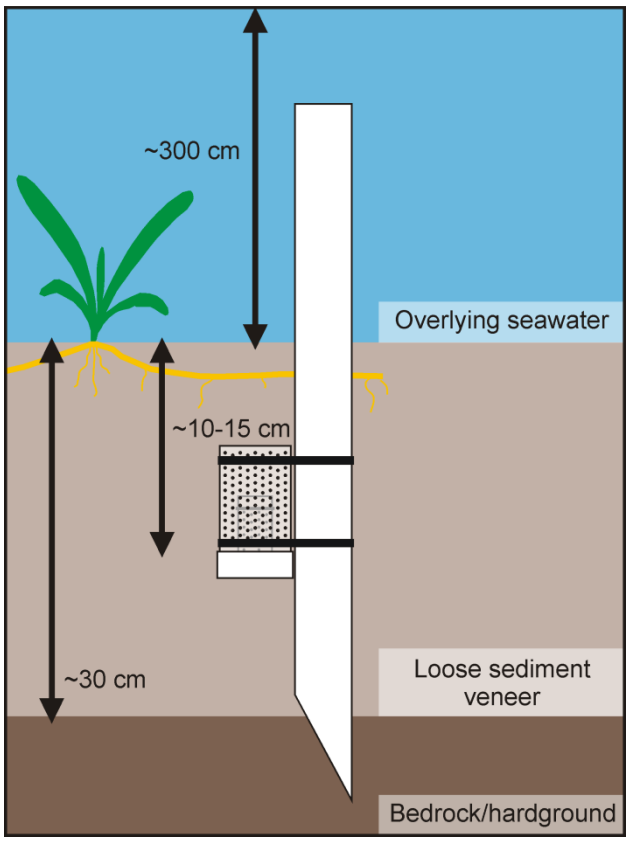

Figure 7.4 *Diagrammatic representation of experimental chambers installed for exposure of fish-derived carbonates to porewaters in a shallow platform top setting in the Bahamas. The burial location was characterised by a very sparse cover of seagrass (Thalassia testudinum), and rhizomes were typically very sparsely distributed in the immediate vicinity of experiment chambers.*

Following 79 days of porewater exposure, experimental chambers were relocated and retrieved in a manner such that carbonate samples and the porewater they were exposed to could be retained for later analysis. This was done by carefully pulling stakes out of the sediment veneer and taking them, one at a time, to the surface (keeping experimental chambers the right way up to ensure sample materials remained within the inner container). Tests conducted prior to experiments indicated that the rate of internal and external fluid exchange associated with experimental chambers, whilst efficient (*i.e.*, complete equilibration within 24 hours, as described above), was slow enough that, in the few seconds between removing samples from the substrate to bringing them above the seawater surface, the amount of overlying seawater mixing with porewaters inside the containers would have been negligible. Above the seawater surface, porewater inside the experimental chambers was unable to overcome surface tension and leak through holes in the outer containers until their lids were loosened. Excess surface seawater was wiped from the outside of

containers before doing this and, once lids were loosened, porewater inside experiment chambers was allowed to flow slowly into 10 mL glass vials, which were filled to the point that little or no headspace remained before being closed immediately with rubber-sealed screw-cap lids. Within a few hours of collection, porewaters were poisoned by addition of 50 µL of a saturated solution of $HgCl_2$ (to prevent biological activity from altering the distribution of carbon), before being stored at 4 °C until further analyses were performed. This methodology follows that described by Dickson *et al*. (2007), with the exception that those authors recommend the volume of $HgCl_2$ should be 0.05–0.02 % of the total sample volume; here 0.5 % of the total volume was added, which acted only to increase the poisoning effect – comparison of analytical results obtained from samples poisoned with 0.02 % and 0.5 % of the sample volume shows that this has no effect on DIC system parameters.

Following the collection of porewater, outer chambers were completely removed and inner chambers, which still held pore fluids and carbonate samples, were closed with screw-fitting caps. Within a few hours the remaining water was removed with a pipette and carbonates were cleaned and dried following the protocol described in Chapter 2.

In addition to porewater and exposed fish-derived carbonates, surface sediment from the burial location was also collected for later characterisation. Sediment was cleaned and dried using the same approach as employed for fish-derived carbonates. Numerous surface seawater samples were also collected from close to the burial site and from elsewhere in Eleuthera Sound. These were poisoned and stored in the manner described above for porewater.

7.2.3 Analytical procedures

7.2.3.1 Carbonate sample analysis

Fish-derived carbonate samples from all seawater exposure experiments were analysed using approaches as described in Chapters 2–5. Specifically, this included morphological and textural characterisation based on SEM imaging, compositional analyses using SEM-based EDX,

mineralogical analyses using ATR-FTIR, and determination of stable oxygen and carbon isotope ratios using mass spectrometry. Crystals were measured using JMicrovision (v1.2.7; Roduit, 2008). In addition, surface sediments from the site of porewater exposure were characterised with the aid of optical light microscopy, wet sieving, and XRD (to determine the ratio of aragonite to calcite, and to estimate the average $MgCO_3$ content of Mg calcite).

7.2.3.2 Porewater and seawater analyses

Seawater and porewater samples from all exposure experiments were analysed in order to: i) determine various parameters with respect to the DIC system; ii) confirm dissolved ion ratios were the same in all samples; and iii) determine salinity. Salinity, temperature, and pressure data can be used in conjunction with any two DIC parameters out of pH, total alkalinity (TA), total CO_2 (TCO_2), partial pressure of CO_2 (pCO_2), and CO_2 fugacity (fCO_2) to calculate all other DIC parameters along with carbonate and bicarbonate concentrations and calcite and aragonite saturation states (Ω_{Ca} and Ω_{Ar}, respectively). These calculations were performed in the CO2SYS program (Pierrot *et al*., 2006), using carbonic acid dissociation constants (K1 and K2) of Mehrbach *et al*. (1973) refit by Dickson and Millero (1987), KSO_4 (the dissociation constant for the reaction: $HSO_4^- = H^+ + SO_4^{2-}$) of Dickson (1990), and pH measured on the NBS (National Bureau of Standards) scale. Analytical procedures used to obtain the necessary input values are described below. CO2SYS allows users to enter temperature and pressure values for conditions under which analyses were performed and conditions at sample origin, and subsequent calculations yield DIC parameters for input (laboratory) and output (*in situ*) conditions. All values reported herein are for output conditions.

The CO2SYS program assumes that the concentrations of dissolved ions are proportional to salinity. These values can be particularly important for calculating calcite and aragonite saturation states, where, for example:

$$\Omega_{calcite} = \frac{{}^{m}Ca^{2+} \cdot {}^{m}CO_3^{2-}}{K^{*}{}_{calcite}} \qquad \textit{equation } 7.7$$

where $\Omega_{calcite}$ is the saturation state of calcite, ${}^{m}Ca^{2+}$ and ${}^{m}CO_3^{2-}$ are the concentrations of calcium and carbonate, respectively, and $K^{*}{}_{calcite}$ is the solubility product for calcite. The carbonate concentration for use in this equation is derived from calculations made in CO2SYS, but calcium concentration is assumed to be proportional to salinity. Whilst dissolved ion concentrations are typically constant in surface seawaters (*e.g.*, the Marcet Principle), they can differ in deeper waters (*e.g.*, calcium concentrations can increase due to $CaCO_3$ dissolution; Millero, 1996) and in waters overlying carbonate banks or interstitial to carbonate sediments (Thorstenson and Mackenzie, 1974; Rosenthal, 1979; Morse *et al*., 1985; Walter and Burton, 1990), thus potentially contravening the assumptions made in CO2SYS. Another potential issue with the use of CO2SYS is that some workers consider interpretations of alkalinity to be complicated for anoxic interstitial waters due to sulphate reduction (*e.g.*, Berner *et al*., 1970). However, Morse *et al*. (1985) find that, at least for pore fluids in which less than 10 % of sulphate is reduced, this does not need to be accounted for in calculations involving carbonate and total alkalinity.

In order to show that the use of CO2SYS for calculations relating to the carbonic acid system was valid, the concentrations of various dissolved cations and anions in all seawater, porewater and artificial seawater used in the present study were determined with respect to a reference standard seawater (Batch 114, A.G. Dickson, Scripps Institute of Oceanography, California, USA). The methodology and results of these analyses are described in section 7.2.3.2.4.

7.2.3.2.1 Pressure, temperature, and salinity measurements

In all experiments, water that carbonates were exposed to was at depths no greater than 3.5 m, and pressure for all calculations was set at 0 decibar accordingly (*in situ* pressure of porewater at 3 m below sea level would have been 3 decibar, but such values have no appreciable effect on DIC system output parameters and are therefore nominally reported as 0 decibar). Temperature was measured either with a mercury thermometer or an electronic thermostat, both achieving similar

results. Salinity was determined using either a conductivity meter (YSI model 85, Yellow Springs, Ohio, USA), a refracting salinometer, or by using osmolality as a proxy; the latter determined using an osmometer (Vapro 5520, Wescor Inc., Logan, Utah, USA) calibrated with Wescor Opti-mole sodium chloride osmolality standards (1000 mmol·kg^{-1}; seawater osmolality is typically between 1000 and 1150 mmol·kg^{-1}, depending on salinity). Data obtained using a conductivity meter was measured on the practical salinity scale (PSS) and was accurate to within 0.1 units. Salinity values that were obtained thus were used to calibrate the latter two approaches (Fig. 7.5).

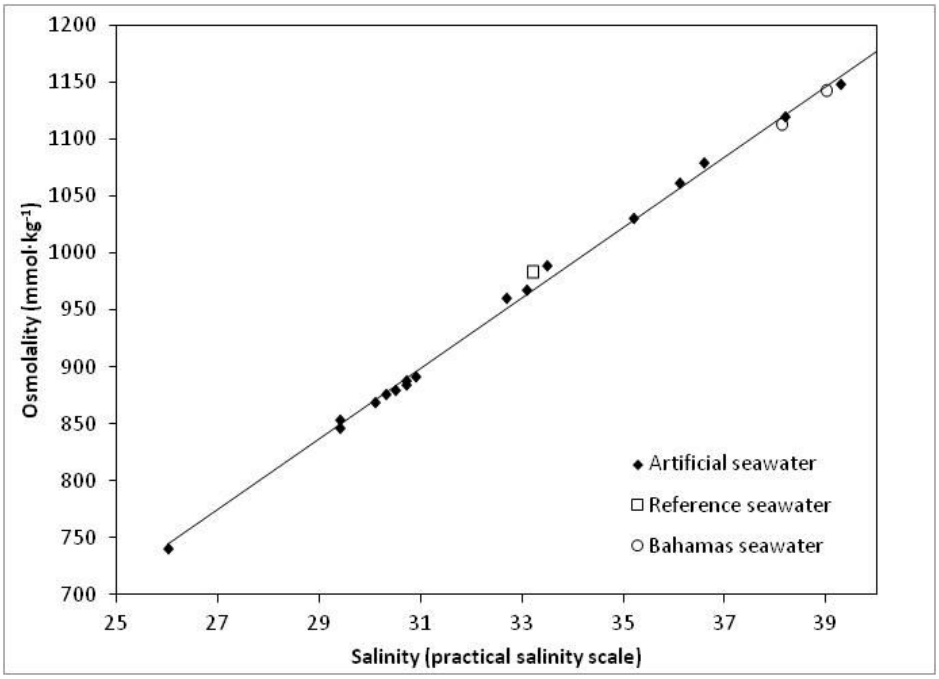

Figure 7.5 *Calibration curve for osmolality against salinity based on measurements made from artificial seawater (R^2 >0.99). Salinity measurements are based on conductivity meter readings, accurate to within 0.1 salinity units. Replicate osmolality readings were accurate to within 6 mmol·kg^{-1}. Data obtained at the same temperature from other seawater samples (Bahamas surface seawater and reference seawater material – Batch 114, A. G. Dickson, Scripps Institute of Oceanography, California, USA) are also plotted and show that the calibration curve is accurate to within 0.5 salinity units for natural seawater solutions.*

7.2.3.2.2 Solution pH measurements

In order to characterise the seawater and porewater with respect to DIC parameters, values were determined for solution pH (NBS) and TCO_2. It is well known that accurate measurement seawater pH is hampered by the contrast in salinity between subject solutions and widely available calibration standards recommended by the National Institute of Standards and Technology, or

NIST (formerly the NBS), and various alternative approaches have been developed to overcome this liquid junction potential problem (*e.g.*, Dickson, 1993; Riebesell *et al*., 2010; Easley and Byrne, 2012). However, it is possible to obtain stable seawater pH values using NBS-calibrated pH electrodes, and the CO2SYS program (Pierrot *et al*., 2006) has the capability to correct for values reported on this scale. In the present study, pH values were determined using combination pH electrodes (either Radiometer pHC 2401, Radiometer Analytical, Villeurbanne, France, or Hanna HI 1230B, Hanna Instruments, Woonsocket, Rhode Island, USA; both returning similar results) in conjunction with handheld pH meters (either Hanna model HI 8314 or HI 9024, Hanna Instruments, Woonsocket, Rhode Island, USA). Electrodes were calibrated against pH 7.00 and pH 10.00 NIST standards. Data obtained in this manner were precise to within 0.005 pH units.

7.2.3.2.3 Total CO_2 measurements

Total CO_2 (TCO_2) in seawater and porewater was measured by acidifying 1 mL samples with a 5 % solution of phosphoric acid. Acidification results in all dissolved carbon species (CO_2, H_2CO_3, HCO_3^-, and CO_3^{2-}) being evolved as gaseous CO_2, which is transported with a CO_2-free carrier gas (nitrogen) to a CO_2 analyser (Qubit S154, Qubit Systems Inc., Kingston, Ontario, Canada) via a $Mg(ClO_4)_2$ filter to remove moisture. This apparatus is shown schematically in Fig. 7.6. The resulting data plot of CO_2 concentration (ppm) x gas flow rate (mL·min) as a function of time (s) yields a peak for each sample analysed, the integral of which can theoretically be used to calculate the total amount of CO_2 evolved per mL of seawater, and thus TCO_2. However, to ensure inter-laboratory standardisation of results, peaks integrals are treated as arbitrary values and are converted to TCO_2 values by calibration against peak integrals derived from a reference standard seawater of known TCO_2. (Batch 114, A.G. Dickson, Scripps Institute of Oceanography, California, USA).

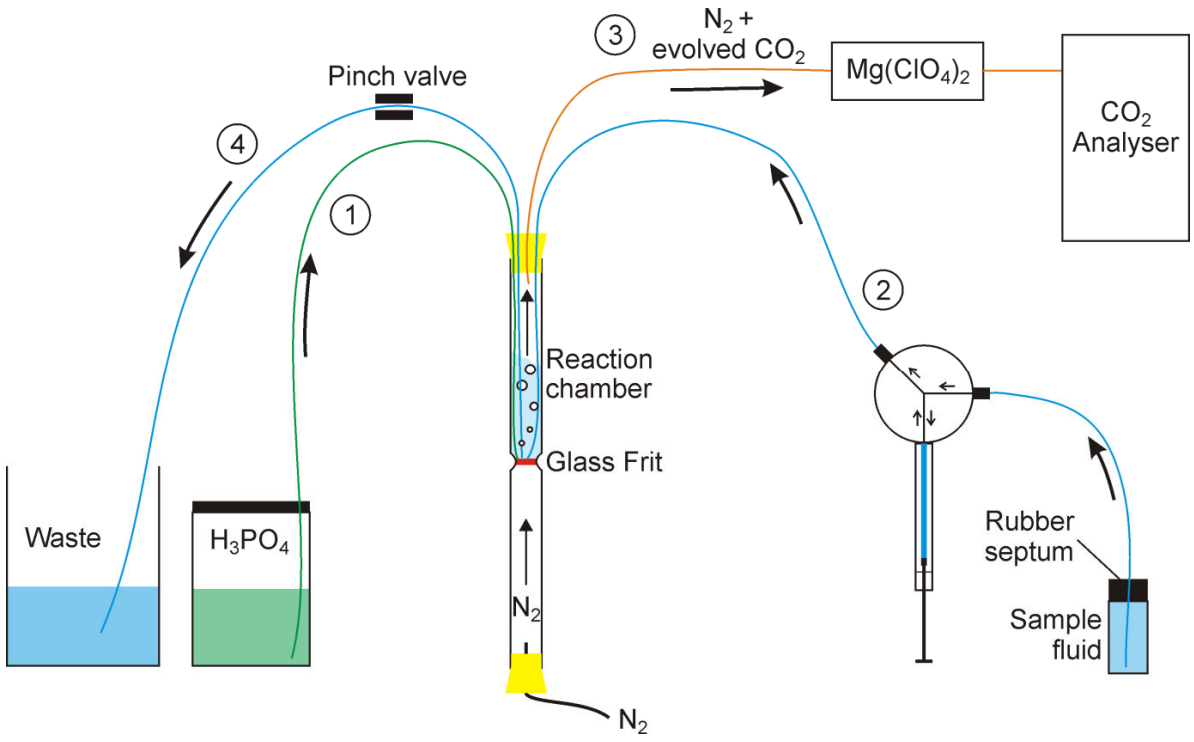

Figure 7.6 *Schematic diagram showing the apparatus used to determine seawater and porewater TCO_2. 1) Phosphoric acid is delivered to a reaction chamber, where its loss through a porous glass frit is prevented by pressure exerted from below by the flow of nitrogen. 2) Sample fluid (1 mL) is accurately delivered to the reaction chamber, where all CO_2 species it contains are converted to gaseous CO_2 following reaction with phosphoric acid. 3) Evolved CO_2 is transported via nitrogen carrier gas for measurement in CO_2 analyser (other lines along which CO_2 could potentially escape the reaction chamber are closed with a pinch valve). Moisture is removed by a magnesium perchlorate filter. 4) Waste fluids are removed from the reaction chamber prior to analysis of the next sample.*

Prepared seawater and porewater samples (*i.e.*, poisoned and stored in refrigeration in glass vials with no head space) were brought to room temperature prior to analysis. Because samples were stored in vials with no head space, and because vials were closed with a rubber septum, they had no opportunity to equilibrate with ambient atmospheric conditions before or during analysis (samples were drawn from vials via an automated syringe that pierced the rubber septum), and the distribution of carbon species should therefore have remained as they were *in situ*. All analyses were performed within two months of sample collection, and analysis of each sample was repeated five times. Values for TCO_2 are reported as the mean of replicate analyses ± one standard deviation, which is typically less than 5 $\mu mol \cdot kg^{-1}$. In combination with the error associated with pH measurements, this yields typical errors in calculated DIC-related parameters of <10 $mmol \cdot kg^{-1}$ (TA), <5 µatm (pCO_2), and <0.08 (Ω_{Ca}).

7.2.3.2.4 Concentrations of major dissolved ions

The concentrations of major ions dissolved in seawater – Na^+, Cl^-, Mg^{2+}, Ca^{2+}, K^+, and SO_4^{2-}; these constituting approximately 99.8 % of the total dissolved ions in normal seawater – were determined for all samples by liquid ion chromatography (Dionex, Sunnyvale, California, USA). Samples were diluted 400-fold with ultrapure water and stored below freezing in 15 mL plastic centrifuge tubes until analyses were performed[1]. Analyses of surface seawater, porewater, and artificial seawater were performed along with reference seawater standards (Batch 114, A. G. Dickson, Scripps Institute of Oceanography, California, USA) and blank ultrapure water stored in the same manner as seawater samples. Ultrapure water contained no appreciable amounts of any ions. Results for all seawater solutions were corrected to salinity 35 (PSS) and were typically in good agreement (± 3 %). This included porewater sulphate values almost identical to those for overlying seawater, indicating that only a limited amount (if any) of sulphate reduction had occurred in sub-surface fluids to which carbonates were exposed. The use of CO2SYS to calculate DIC-related parameters was thus validated.

Further compositional analyses were performed using inductively coupled plasma optical emission spectrometry (ICP-OES; iCAP 6300, Thermo-Fischer Scientific, Maine, USA) in order to check the concentrations of trace elements present in artificial seawater samples. The analytical apparatus was calibrated against a multi-element standard prior to sample analyses, and checked after every five samples thereafter. Artificial seawater, prepared as described in section 7.2.2.2, was diluted 10-fold with deionised water and analysed along with a blank deionised water aliquot. Deionised water returned negligible values for all elements analysed. Sub-array plots generated using this approach were manually checked to ensure that signals produced by different elements did not overlap. Resulting values were generally close to those expected for seawater, except in the case of manganese, which was consistently present at concentrations that were three orders of magnitude higher than expected. Additional samples that had held fish-derived carbonates for periods of one

[1] All liquid ion chromatography analyses were performed by Dr. Erin Reardon at the University of Exeter.

week or more yielded values that were an order of magnitude lower than initial concentrations due to manganese precipitation associated with carbonates (see section 7.3).

7.2.4 Estimating the proportions of various precipitation products

Because of the likelihood that different excretion products will have different preservation potentials (*e.g.*, amorphous versus crystalline carbonate phases), an additional aspect of this work involves estimation of the relative abundances of different precipitation products excreted across shallow platform settings in the Bahamas. Applying the findings of exposure experiments to the resulting precipitation product abundance data facilitates assessments regarding the proportion of excreted carbonates that undergo different preservation pathways to be made.

In order to achieve this, the relative abundance (by volume) of different precipitation products was estimated based on visual observations of numerous pellets produced by the full range of species documented in Chapter 2. These data were obtained during observations contributing to the findings of Chapter 2, and are presented in Appendix VIII. Note that some species found to produce amorphous carbonates in Chapter 3, specifically checkered puffer and redtail parrotfish, are listed as producing no amorphous carbonates because none/very little was observed during visual examination of pellets. Spectral data indicating the presence of amorphous carbonates in the products of these species were obtained after abundance estimates were made, and moreover, an approach has not, as yet, been developed for using these spectral patterns as proxies for estimating relative abundances of component carbonate phases. Likewise, the findings of the present study indicate that amorphous phases might be more abundant in the products of keeltail needlefish and bonefish than previously thought. Furthermore, an unquantified amount of amorphous carbonate produced by the latter species probably crystallises to calcite in seawater (see section 7.3). Because of these uncertainties, the abundance estimates provided here are rather crude and should be refined in similar future studies.

Because the relative abundances of different precipitation products varies markedly among species, it is inappropriate to take an average from the data in Appendix VIII and apply it across all species

that inhabit shallow platform areas in the Bahamas. Instead it was necessary to make assumptions about which species would excrete which precipitation products based on the existing data (Chapter 2). This was done by assuming that precipitation products are similar within families (see section 8.4 for justification), such that they could be predicted for any species not yet investigated, as long as it belonged to a family in which other species have been investigated (*i.e.*, in Chapter 2). For families in which no species have been investigated, however, there exists no basis for making predictions about precipitation products, and it was necessary to use the average abundances in products of investigated families for these fish.

In order to apply abundance data appropriately, it was also necessary to have knowledge of fish community structure across the Bahamas. This information was obtained from fish census data from a range of shallow platform habitats in the Bahamas[2], which included counts of pelagic, reef-bound, and cryptic fish species. Carbonate excretion rates (see below) were applied to these data to facilitate calculation of the total amount of gut carbonate excreted in each habitat, and precipitation product abundance estimates (Appendix VIII) were incorporated to estimate the contribution of each to total carbonate production within these habitats[3]. By taking into account the areal extents of each habitat (Perry *et al*., 2011), it was then possible to estimate the total amount of each precipitation product excreted over the entire Bahamian platform, and thus to assess the implications of the different preservation pathways of each.

Overall carbonate excretion rates were determined by combining previously measured production rates (Perry *et al*., 2011) with new production rate data arising herein. Specifically, new data were collected for 10 fish species (resulting in total combined data from 18 species) using the approach described in Perry *et al*. (2011), whereby excreted carbonate samples were collected over a known period of time (usually 24 or 48 hours) from a fish (or group of fish) of known body mass. Following preparation (*i.e.*, cleaning and drying), the total amount of carbonate produced was

[2] Surveys were conducted by Dr. Alistair Harborne (University of Queensland) at numerous sites in shallow waters surrounding eight islands of the Bahamas. All fish species were recorded along with the estimated size and body mass of all individuals encountered.
[3] Dr. Alistair Harborne utilised the production rates determined herein to perform all calculations regarding carbonate output within each habitat surveyed.

determined either by weighing samples (precise to ± 0.01 mg), or by titrating them. For the latter, samples were placed in 20 mL of deionised water, gently sonicated to encourage disaggregation, and titrated to below pH 4.0 (measured using a Radiometer PHC 2401 pH electrode in conjunction with a Hanna HI 8314 pH meter) by addition of a 0.02 M HCl solution (delivered using 2 mL micrometer syringes, precise to ± 0.001 mL; Gilmont Instruments, Barrington, USA). Following this, the solution was immediately titrated back to the initial pH by addition of a 0.02 M NaOH solution. Throughout the titrations, CO_2-free air was bubbled through the solution to remove excess CO_2 evolved during acidification, and to ensure stable pH measurement during the second titration. The difference between the number of moles of HCl and NaOH added to the solution is equal to the number of bicarbonate equivalents in the original solid sample; this value being used to calculate the molar amount of $CaCO_3$ or $MgCO_3$ in each sample, assuming that each mole of $(Ca,Mg)CO_3$ yields two bicarbonate equivalents when it dissolves. These values were then converted to mass; molecular weights being determined by measuring the amount of Mg^{2+} and Ca^{2+} in the titrated solution using liquid ion chromatography (see section 7.2.3.2.4), and assuming each Mg^{2+} ion corresponds with one mole of $MgCO_3$, and each Ca^{2+} ion with one mole of $CaCO_3$. This method was found to yield similar results to direct weighing of samples, but was preferred in some cases because pellets occasionally contained ingested apatite-type skeletal fragments (*e.g.*, scales and fin rays) which do not dissolve during titration and therefore do not contribute to weight approximations using this approach. Sample weights thus determined, production rates were calculated for each fish by taking into account fish body mass and time taken to produce each sample. These data and the resulting production rate curve are shown in Appendix IX.

7.3 RESULTS

7.3.1 Sediment, seawater and porewater characterisation

7.3.1.1 Natural and artificial seawater chemistry

Measurement of various parameters of the solutions that fish-derived carbonates were exposed to during preservation experiments reveals that the DIC system of surface seawater can undergo small

temporal variations, and that pore fluids at the site of sample burial differ considerably from overlying seawater; the former typically being supersaturated to a lesser degree than the latter. The DIC system of artificial seawater was close to that in Bahamian surface seawater throughout. The results of these analyses are summarised in Table 7.2.

Surface seawater collected from Eleuthera Sound typically has total CO_2 values in the range 2080–2140 $\mu mol \cdot kg^{-1}$). Combined with high pH values (typically 8.24–8.25; NBS), these data indicate high total alkalinity values (approximately 2400–2500 $\mu mol \cdot kg^{-1}$) and high calcite and aragonite saturation states (typically close to 6 and 4, respectively). Calculated pCO_2 values (approximately 345–355 μatm) are close to being in equilibrium with ambient atmospheric levels. In contrast, pore fluids collected from experimental chambers after 79 days of burial exposure typically have higher total CO_2 values (in the range 2150–2350 $\mu mol \cdot kg^{-1}$) and lower pH values (in the range 7.89–8.08; NBS). These data indicate similar total alkalinity values to overlying seawater, but substantially higher pCO_2 values (typically in the range 600–850 μatm), and consequently lower calcite and aragonite saturation states (in the ranges 3–4 and 2–3, respectively). Furthermore, there is considerable variability in the DIC system parameters among pore fluid samples. Assuming these fluids were representative of pore fluids in the surrounding sediments, this suggests there were highly localised variations in pore fluid characteristics at the experiment location. However, this is somewhat difficult to confirm given that fish-derived carbonate samples in each chamber differed in their nature, with different responses to porewater exposure potentially resulting in a unique influence on pore fluid characteristics in each chamber. Nevertheless, it is clear that all samples were exposed to conditions of lower saturation with respect to aragonite than they would have been exposed to in overlying seawater.

Table 7.2 *Seawater and porewater DIC parameters calculated using CO2SYS software.*

	Measurement parameters				Calculated *in situ* parameters					
Sample	Temp (°C)	Salinity (pss)	pH (NBS)	TCO_2 ($\mu mol \cdot kg^{-1}$)	Temp (°C)	pH (NBS)	Total alkalinity ($\mu mol \cdot kg^{-1}$)	pCO_2 (µatm)	$\Omega_{Calcite}$	$\Omega_{Aragonite}$
Surface seawater	22	36.7	8.26	2090.3	24	8.235	2443.4	355.8	5.95	3.92
Surface seawater	22	36.9	8.26	2105.6	24	8.235	2462.4	357.8	6.04	3.96
Surface seawater	22	36.8	8.27	2080.5	24	8.245	2440.7	344.9	6.05	3.99
Surface seawater	22	36.8	8.27	2074.4	24	8.245	2434.2	343.8	6.04	3.98
Surface seawater*	19	38.8	8.30	2137.8	24	8.236	2518.5	357.0	6.27	4.14
Porewater	19	39.1	8.03	2193.9	24	7.97	2406.6	715.6	3.69	2.43
Porewater	19	39.1	8.14	2145.2	24	8.08	2417.9	534.6	4.55	3.00
Porewater	19	39.2	7.98	2154.5	24	7.92	2340.5	791.8	3.26	2.15
Porewater	19	38.7	8.06	2302.7	24	8.00	2536.3	700.2	4.10	2.71
Porewater	19	38.8	8.03	2188.5	24	7.97	2399.2	714.9	3.67	2.42
Porewater	19	38.9	7.99	2348.5	24	7.93	2548.2	844.4	3.62	2.32
Porewater	19	38.9	8.07	2192.4	24	8.01	2425.8	649.6	4.00	2.64
Porewater	19	39.4	7.95	2166.5	24	7.89	2339.4	854.7	3.08	2.03
Porewater	19	38.7	8.12	2210.7	24	8.06	2473.4	580.2	4.48	2.95
Artificial seawater^	19	36.0	8.29	2083.2	26	8.20	2422.2	395.1	5.80	3.84
Artificial seawater^	19	36.0	8.30	2094.4	26	8.21	2411.8	387.3	5.95	3.94
Artificial seawater^	19	36.0	8.29	2087.9	26	8.20	2427.4	396.0	5.81	3.85
Artificial seawater†	19	36.8	8.29	2093.3	26	8.20	2441.3	394.4	5.89	3.91
Artificial seawater†	19	37.0	8.29	2088.3	26	8.20	2437.7	392.8	5.90	3.91
Artificial seawater‡	19	36.8	8.31	2156.4	26	8.22	2576.5	386.2	6.32	4.19
Artificial seawater‡	19	36.8	8.32	2243.2	26	8.23	2631.4	391.7	6.71	4.44

*Surface seawater collected from Eleuthera Sound in March 2012 (all others were collected in January 2013).
^Freshly prepared artificial seawater.
†Artificial seawater after one week in experimental vessels with gut precipitates from schoolmaster snapper.
‡Artificial seawater after one week in experimental vessels with gut precipitates from bonefish.

Analysis of artificial seawater shows that most DIC system parameters were in close agreement with natural surface seawater from Eleuthera Sound during exposure experiments. However, it is worth pointing out that seawater pH, total alkalinity, and total CO_2 increased when gut precipitates produced by bonefish were present; the greatest increases occurring in the replicate containing the largest initial amount of gut precipitate. These data, in combination with infrared analyses and morphological observations (see below), strongly suggest that precipitates produced by bonefish underwent a substantial amount of dissolution during exposure to artificial seawater. Consequently, calcite and aragonite saturation states in these experimental chambers increased to values higher than those of freshly prepared seawater, although experiments were managed to ensure these never

exceeded those that can be found in natural surface seawater in the Bahamas (Morse *et al*., 1985). Conversely, the DIC system in experimental chambers containing precipitates produced by schoolmaster snapper remained stable throughout.

It is worth pointing out here that parts of the outer surfaces of some pellets produced by both schoolmaster snapper and bonefish (and also black grouper; see Chapter 6) rapidly (*i.e.*, within one day) took on an orange-brown hue when placed in artificial seawater (see Figs. 6.9 C & D). In contrast, pellets exposed to natural waters remained white in all cases. Compositional analyses of orange-coloured surfaces revealed the presence of a small amount of manganese (values typically in the range 1.0–2.5 at.%); this being the only chemical difference between these surfaces and control pellets. No additional vibrational bands were generated by these pellets in infrared spectra, suggesting that manganese, the presence of which was restricted to patchy surface coatings, was either: i) not precipitated as a manganese-rich carbonate phase such as kutnahorite, $CaMn(CO_3)_2$; or ii) not precipitated in amounts sufficient to generate vibrations strong enough to be discernable in FTIR spectra. The form of manganese in these samples is thus not known, but possibilities to be considered include: i) surface adsorption on existing gut precipitates; ii) direct precipitation as an undetected manganese-rich phase; and iii) dissolution of gut carbonates and subsequent reprecipitation as a manganese-rich phase.

In order to confirm the source of manganese and whether or not its precipitation significantly influenced the carbonate system parameters of artificial seawater, an experiment was conducted wherein a stock solution of artificial seawater was prepared and divided into four subsets, these including: 1) three replicate aliquots diluted with deionised water for immediate elemental analysis; 2) a 300 mL sample containing 30 mg of fish-derived carbonates; 3) a 300 mL sample containing 30 mg of mud-grade sedimentary carbonate from the Bahamas; and 4) a 300 mL blank sample. The latter three sub-samples were held in sealed glass beakers at 26 °C for one week before replicate aliquots were: i) diluted for elemental analysis; and ii) prepared for measurement of DIC system parameters. The results are presented in Table 7.3.

Elemental data (ICP-OES) show that the ratios of calcium and magnesium to manganese become significantly higher in artificial seawater following addition of fish-derived carbonates (high-Mg calcite monocrystalline ellipsoids), but remain stable in blank seawater and in seawater containing sedimentary carbonate mud. One explanation for this is that the calcium and magnesium concentrations of seawater increased relative to manganese concentrations due to dissolution of fish-derived carbonate. However, in order to achieve the measured ratio changes would require the loss of about 30 wt.% of the initial carbonate to dissolution, yet sample weights remained unchanged at the end of one week. Furthermore, such extensive dissolution should also result in changes in DIC system parameters, yet such changes are not observed. Changes in ion ratios must therefore be due to decreased manganese concentrations in solution as a result of its precipitation; this being favoured in the presence of fish-derived carbonate. This assertion is supported by absolute values for manganese concentration, which are typically 0.010 mM in freshly prepared seawater and seawater containing sedimentary carbonates, and 0.009 mM in seawater containing fish-derived carbonates (all values are corrected to seawater salinity 35 on the practical salinity scale).

Artificial seawater is thus confirmed as the source of manganese precipitated in association with fish-derived carbonates, which probably occurs due to highly elevated manganese concentrations compared to natural surface seawater; expected values at 35 ppt are 0.07×10^{-4} mM (Turekian, 1968) instead of the 0.01 mM measured here. Manganese precipitation is further shown to have no obvious effect on bulk solution DIC system parameters (Table 7.3) that might influence solid–solution interactions (although a small pH decrease is tentatively attributed to manganese precipitation in a separate study; see section 6.4.3). However, the possibility remains that manganese incorporated in solid carbonate phases may influence their stability. Nevertheless, the surfaces of many pellets exposed to artificial seawater remain white and contain no detectable manganese (as shown by EDX analyses). The solubility of crystals in these surfaces is therefore less likely to be influenced by the presence of precipitated or adsorbed manganese, and crystal

morphologies and compositions for carbonates exposed to artificial seawater are therefore reported only from these surfaces in the sections that follow.

Table 7.3 *Ratios of selected dissolved ions concentrations (based on mM values) and DIC system parameters for blank artificial seawater (Tropic Marin) and additional solutions from the same stock following different treatments (see footnotes).*

	Dissolved ion ratios**			DIC system parameters				
Sample	$[Mg^{2+}]/[Ca^{2+}]$ ±1 S.D.	$[Mg^{2+}]/[Mn^{2+}]$ ±1 S.D.	$[Ca^{2+}]/[Mn^{2+}]$ ±1 S.D.	Salinity (pss)	pH (NBS)	TCO_2 (µmol·kg)	Ω_{Ca}	Ω_{Ar}
Expected SW*	5.18	7.29×10^6	1.41×10^6					
Fresh blank	4.69 ±0.05	5.60×10^3 $\pm 0.08 \times 10^3$	1.19×10^3 $\pm 0.02 \times 10^3$	36	8.20	2095.6	5.83	3.86
1 week blank^	4.68 ±0.06	5.56×10^3 $\pm 0.14 \times 10^3$	1.19×10^3 $\pm 0.01 \times 10^3$	36.2	8.20	2087.1	5.82	3.86
1 week w/sed†	4.65 ±0.02	5.49×10^3 $\pm 0.09 \times 10^3$	1.18×10^3 $\pm 0.02 \times 10^3$	36.2	8.19	2063.4	5.64	3.73
1 week w/fish‡	4.58 ±0.04	6.47×10^3 $\pm 0.12 \times 10^3$	1.41×10^3 $\pm 0.02 \times 10^3$	36.2	8.20	2090.1	5.83	3.86

*Expected seawater ion ratios based on data from Turekian (1968).
**Ratios are reported instead of absolute values to normalise data by removing differences caused by variations in salinity.
^Artificial seawater held blank for one week after preparation in a sealed glass beaker. Other treatments were similar but with the addition of 30 mg of mud-grade sedimentary carbonate (†) and 30 mg of gut carbonates produced by black grouper (‡).

7.3.1.2 Sediment composition

The grain size distribution of surface sediment from the porewater exposure location, shown graphically in Fig 7.7, describes a muddy sand which comprises 14.2 wt.% mud-grade carbonate (mostly coarse silt) and more than 60 wt.% fine and very fine sand. The sediment predominantly comprises skeletal carbonates, with the main components in all size fractions being the tests of foraminifera, bivalves, and gastropods, all of which are intact or in a good state of preservation (*e.g.*, bivalves are typically disarticulated but not fragmented). Other particles include occasional coral fragments and ellipsoidal peloids, some of which are dark grey in colour. X-ray diffraction patterns (Fig. 7.7) indicate that surface sediment at this location typically comprises 54–57 wt.% aragonite and 43–46 wt.% calcite, with little variability among size fractions. These values are interesting given those reported by other workers for the Bahamas (*e.g.*, typically >70 wt%

aragonite; Husseini and Matthews, 1972; Shinn *et al*., 1989), but may be explained by the predominance of foram tests in these sediments. The calcite component is predominantly high-Mg calcite containing approximately 19 mol% $MgCO_3$.

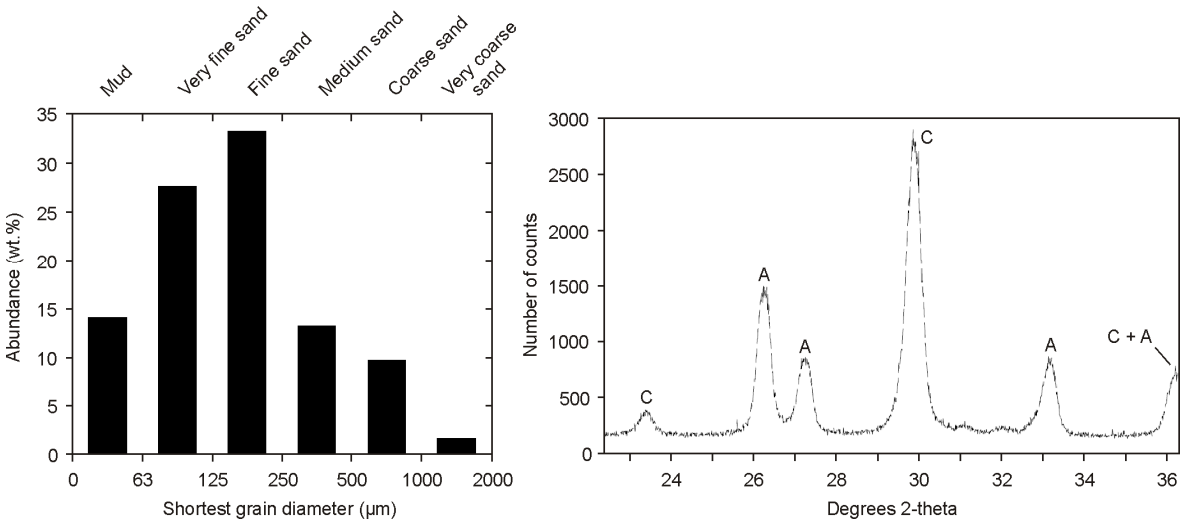

Figure 7.7 *Grain size distribution of sediment from the porewater exposure location (left) and X-ray diffraction pattern of the same sediment (right) showing aragonite (A) and calcite (C). The position of main (d_{104}) calcite peak at 29.98 ° 2θ indicates it is predominantly high-Mg calcite containing 19 mol% $MgCO_3$.*

7.3.2 Seawater and porewater exposures

Morphologies, mineralogies, and compositions of gut precipitates before and after seawater exposures are described in detail in the sections that follow. The wide range of precipitate forms responded very differently to exposure, with all hydroxides (*i.e.*, brucite) and amorphous carbonates rapidly dissolving (or in some cases probably crystallising) within a few days to weeks of excretion, Mg calcite forms remaining largely unchanged, and aragonite needles appearing to develop in some samples. The results are summarised in Fig. 7.8.

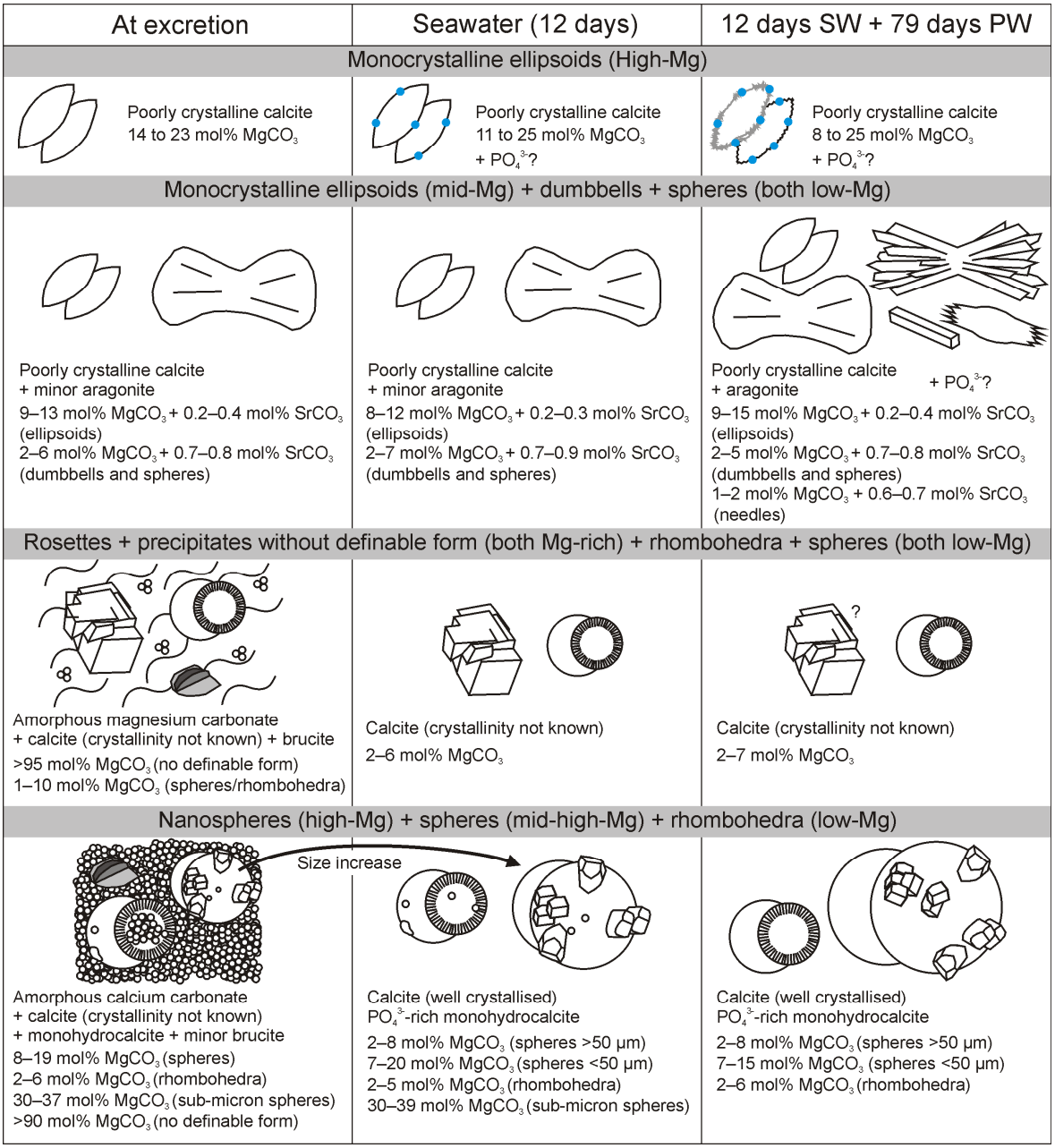

Figure 7.8 *Preservation styles of the main forms of gut precipitate known from Caribbean marine fish species. Solid circles associated with monocrystalline ellipsoids indicate phosphate, the concentration of which possibly increases with exposure time (see main text). Major changes are the apparent development of aragonite needles in samples with numerous spheres and dumbbells, the loss (dissolution) of amorphous magnesium carbonate, the loss (dissolution and possibly some crystallisation) of amorphous calcium carbonate, the loss (dissolution?) of brucite, and the lowering of $MgCO_3$ content in some monocrystalline ellipsoids and concomitant loss of clear particle definition. Note also the increase in size of some spheres produced by bonefish following porewater exposures.*

7.3.2.1 Mucus disaggregation following excretion

Mucus coatings in which carbonate pellets were excreted typically disaggregated rapidly when held in natural surface seawater, such that within 10–15 days it was usually no longer possible to detect

the presence of any organic matter with the naked eye. Following degradation of organic matter, gentle shaking of experimental vessels in some cases resulted in the suspension of numerous fine particles; the water column remaining cloudy for up to an hour before particles settled out of suspension. Where tested, this particle suspension continued to occur after organic matter had been removed with sodium hypochlorite, suggesting that these fine particles were liberated crystals rather than disaggregated organic particles. It is not known whether these crystals were originally held as discrete particles in the organic coating and were released on its disaggregation, or whether they were released following partial pellet disaggregation. However, in most cases the greatest volume of inorganic carbonate remained in the form of intact pellets following disaggregation of organics.

Only in a small number of experimental vessels did carbonate pellets undergo a substantial reduction in size during 12 day exposures to seawater. Some of these were a result of initially amorphous phases (*e.g.*, in pellets produced by bluehead wrasse) undergoing rapid dissolution (see section 7.3.4), whereas others were probably a result of failures in aeration. For example, carbonates produced by Nassau grouper remained as intact pellets with a limited amount of liberated fines in five experimental vessels, but in an additional experimental vessel initial pellets underwent extensive disaggregation within a few days (Fig. 7.9). This difference was noted despite similar physical and initial chemical conditions in each vessel, with the exception that the air supply was removed from the latter prior to pellet disaggregation. This probably resulted in a build up of dissolved CO_2 as organic matter decomposition proceeded, thus lowering the seawater calcite saturation state, presumably to a point where cohesion within pellets was lost due to partial dissolution. Accordingly, all experimental vessels in which air supplies failed for more than a few hours were discounted from further analysis.

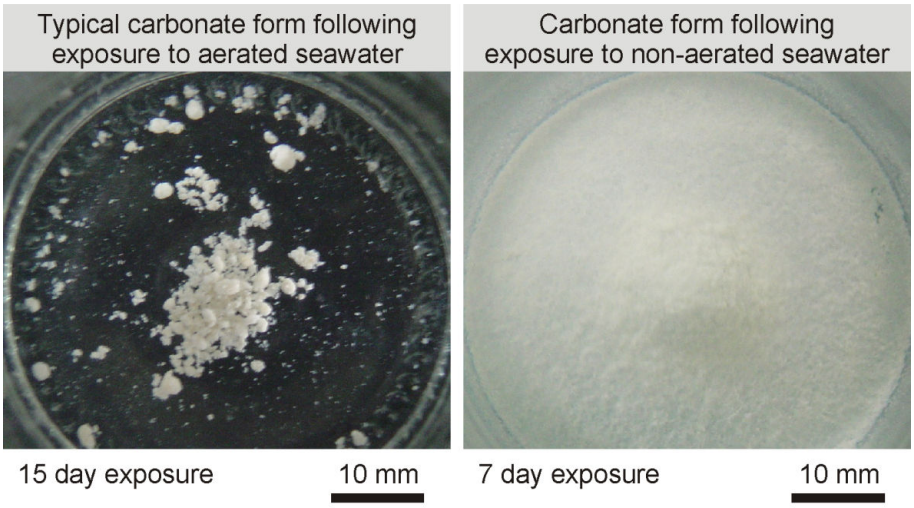

Figure 7.9 *Carbonates produced by Nassau grouper, photographed during seawater exposures in experimental vessels. In most cases, carbonates produced by this (and other) species remain as intact pellets following exposure to gently agitated seawater (left image). However, pellets rapidly disaggregated in some vessels where the air supply was removed (right image), presumably as a consequence of partial dissolution resulting from a lowering of calcite saturation state in response to organic matter decomposition.*

7.3.2.2 High-Mg calcite ellipsoids (produced by schoolmaster snapper[4])

7.3.2.2.1 Morphologies

Control samples (*i.e.*, those cleaned and dried immediately after excretion) produced by schoolmaster snapper are dominated by micron-scale monocrystalline ellipsoids (Fig. 7.10 A). Only in a few pellets are other crystal morphologies present; two pellets (out of more than 50 examined) being dominated by crystals that are more rod-like, with higher aspect ratio and straighter long edges (Fig. 7.10 B, inset), and a few pellets comprising micron-scale rhombohedra as a rare subsidiary form alongside ellipsoids. No other crystal morphologies were observed. Most randomly selected pellet surfaces exhibit clearly defined ellipsoids as shown in Fig. 7.10 A; only in rare cases are ellipsoids less clearly defined due to individual particles having coarser surface features and possibly also due to a greater abundance of nano-scale particles partially obscuring larger ellipsoids (Fig 7.10 B). Crystals left in natural seawater for up to 12 days after excretion

[4] Note that samples produced by black grouper and Nassau grouper are not documented in detail here. These carbonates were similar to those produced by schoolmaster snapper at the point of excretion, and post-excretion changes were generally similar to those reported here.

(mucus envelopes intact) show no morphological differences to those at the point of excretion (Figs. 7.10 C–D).

Following the transfer of these samples to shallow porewater burial sites, and their subsequent retrieval after a further 79 days (total exposure time of 91 days), SEM observations reveal that micron-scale ellipsoids remain the dominant crystal form and are generally preserved as excreted. However, these ellipsoids are commonly not as well defined as those in control samples, with ellipsoids in most randomly selected pellet surfaces having coarse surface features (similar to those shown in Fig. 7.10 B) and/or being obscured by abundant nano-scale particles (Fig. 7.10 E); the latter producing the effect of some ellipsoids being 'welded' together. Interestingly, these textures are not dissimilar to recrystallisation textures observed in Mg calcite needles (Hover *et al*., 2001; see Fig. 1.8 B). However, some sample surfaces, and nearly all internal surfaces of pellets broken after porewater exposure, also show clearly defined ellipsoids with smooth surfaces (Fig. 7.10 F), suggesting that processes resulting in the loss of clear ellipsoid definition were restricted to pellet surfaces. Again, this is consistent with previous observations of alteration in skeletal grains (Hover *et al.*, 2001; see Fig. 1.7). No morphological differences were observed between samples that were cleaned prior to porewater exposure and those that were not, and grain size measurements from all exposures show that no significant changes in ellipsoid length or aspect ratio occurred following excretion (Table 7.4).

Table 7.4 *Mean values for length and aspect ratio of ellipsoidal crystals (produced by two fish species) after various exposures and key output from statistical analyses (one-way ANOVA) comparing these values among exposures. A significant result is returned when p < 0.05.*

Species	Exposure	Mean length (μm)	1 S.D. range (μm)†	Significance	Mean aspect ratio	1 S.D. range†	Significance
Schoolmaster snapper	Control	0.66	0.54–0.81	df = 3	2.46	2.26–2.66	df = 3
	12 day SW	0.69	0.55–0.85	WS* =	2.40	2.19–2.64	F = 1.032
	3 month PW	0.67	0.55–0.81	3.455	2.45	2.27–2.64	p = 0.379
	7 month art. SW	0.68	0.52–0.89	p = 0.754	2.41	2.19–2.65	
Yellowfin mojarra	Control	1.64	1.21–2.23	df = 2	2.33	2.15–2.53	df = 2
	12 day SW	1.69	1.27–2.24	F = 1.098	2.37	2.20–2.56	F = 2.056
	3 month PW	1.55	1.10–2.19	p = 0.335	2.39	2.20–2.60	p = 0.131

*WS refers to the Welch statistic. In this example the results of a Welch test were used as a robust test of equality means instead of one-way ANOVA results because the Levene test for homogeneity of variance returned a p value of <0.05.
†The full range of one standard deviation is asymmetrical about the mean because data were non-normal. All descriptive statistics were generated following Log(10) transformations of data.

The observed changes in ellipsoid textures during porewater exposures are likely to be a result of partial dissolution or recrystallisation. In order to support this contention, dissolution textures that develop in these crystals were determined by briefly exposing them to a weak solution of HCl. Acid exposure was achieved by transferring several pellets to a beaker containing a 5 mL HCl solution (0.01 M) for two seconds before diluting with 100 mL of deionised water and immediately removing all fluid via vacuum filtration; carbonate particles being retained on a cellulose nitrate membrane (0.2 μm pore size). Electron microscope images of these 'etched' carbonates, which partially disaggregated during acid exposure, show two main particle types: i) clearly defined ellipsoids with smooth surfaces that tend to make up larger aggregates (Fig. 7.10 G); and ii) poorly defined ellipsoids with coarse surface texture that tend to make up dispersed particles (Fig. 7.10 H). Presumably, dissolution occurred to greatest extent at the exposed surfaces of pellets; particles being released from these areas as dissolution proceeded. Consequently one would expect dispersed surface particles to be those that show the most extensive dissolution features, whereas intact pellets would be expected to retain particles less affected by dissolution. Indeed, the clearly defined particles typical of control samples appear to make up intact pellet fragments, and it is thus likely that the poor definition and coarse surface texture of dispersed ellipsoids are dissolution

features. The textural similarity between these 'etched' ellipsoids and ellipsoids in the surfaces of pellets exposed to porewater is suggestive of partial dissolution having occurred in the latter.

In addition to ellipsoids, samples exposed to porewater also comprise rare fibrous dumbbells up to 5 μm in length. Although similar particle types have been described as rare subsidiary forms present at the point of excretion alongside dominant ellipsoids produced by several other species (Salter *et al*., 2012), dumbbells have not previously been reported from such samples produced by schoolmaster snapper. Thus while it is possible that these particles were formed as initial intestinal precipitates, their appearance only in porewater-exposed samples may indicate that they developed at some post-excretion stage.

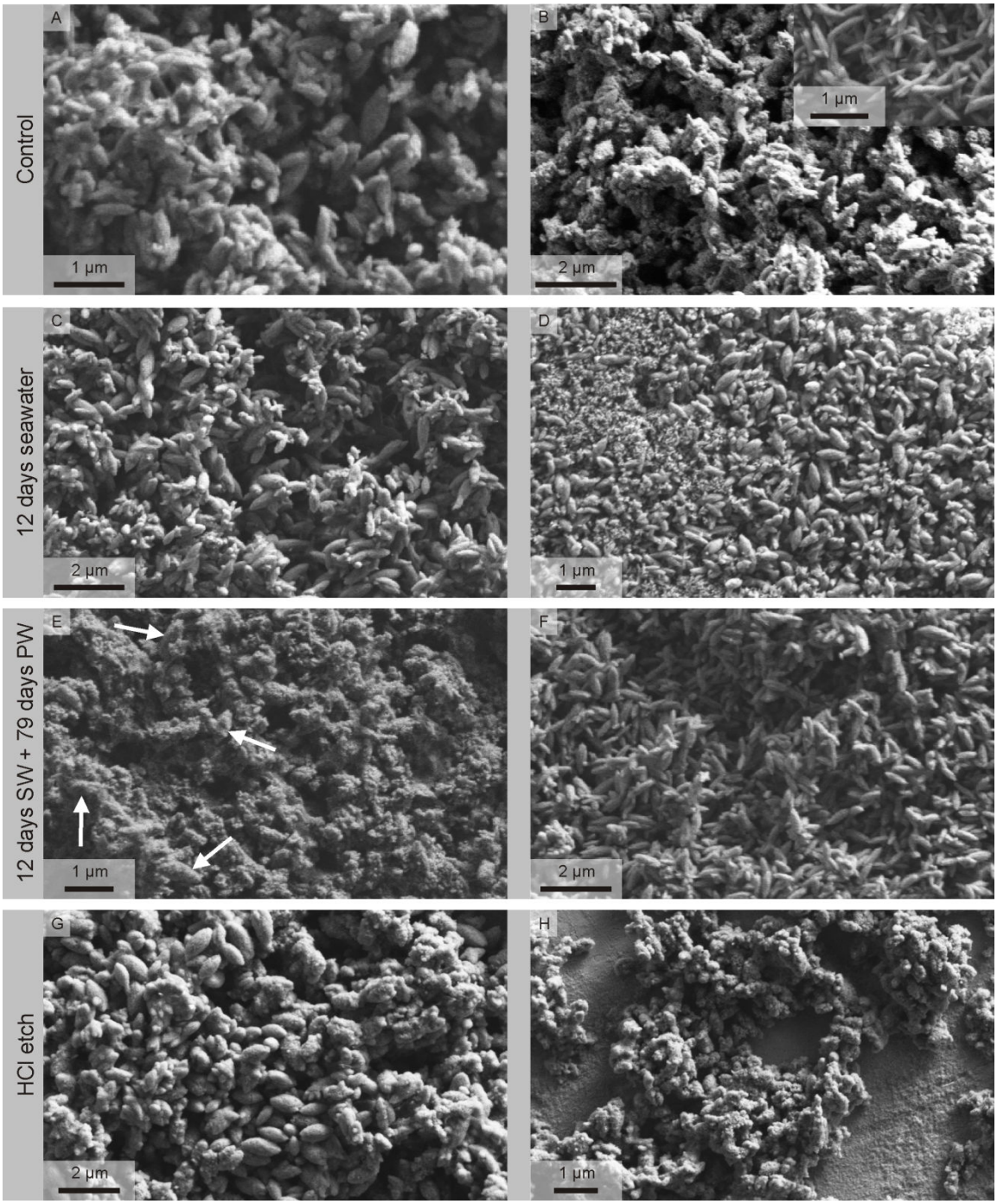

Figure 7.10 *SEM images of carbonate precipitates produced by schoolmaster snapper after different post-excretion exposures: (A–B) Monocrystalline ellipsoids at the point of excretion. Most randomly selected pellet surfaces comprise clearly defined ellipsoids with smooth surfaces (A); other textures are rare, but include poorly defined ellipsoids with coarser surface features (B), and rod-like crystals with relatively high aspect ratios (B, inset); (C–D) Monocrystalline ellipsoids left in seawater for up to 12 days. Crystals are typically identical in morphology to those in (A–B); (E–F) Monocrystalline ellipsoids buried in shallow porewater for 79 days following 12 days in seawater. Pellet surfaces commonly comprise poorly defined ellipsoids (white arrows) that typically have coarse surface features and can be obscured by nano-scale particles (E), although ellipsoids similar to those in control samples are also not unusual (F); (G–H) Control pellets exposed to a weak HCl solution. Intact pellet surfaces typically comprise clearly defined ellipsoids (G); dispersed ellipsoids (presumably liberated from pellet surfaces during dissolution) tend to be less well-defined with coarse surface textures (H).*

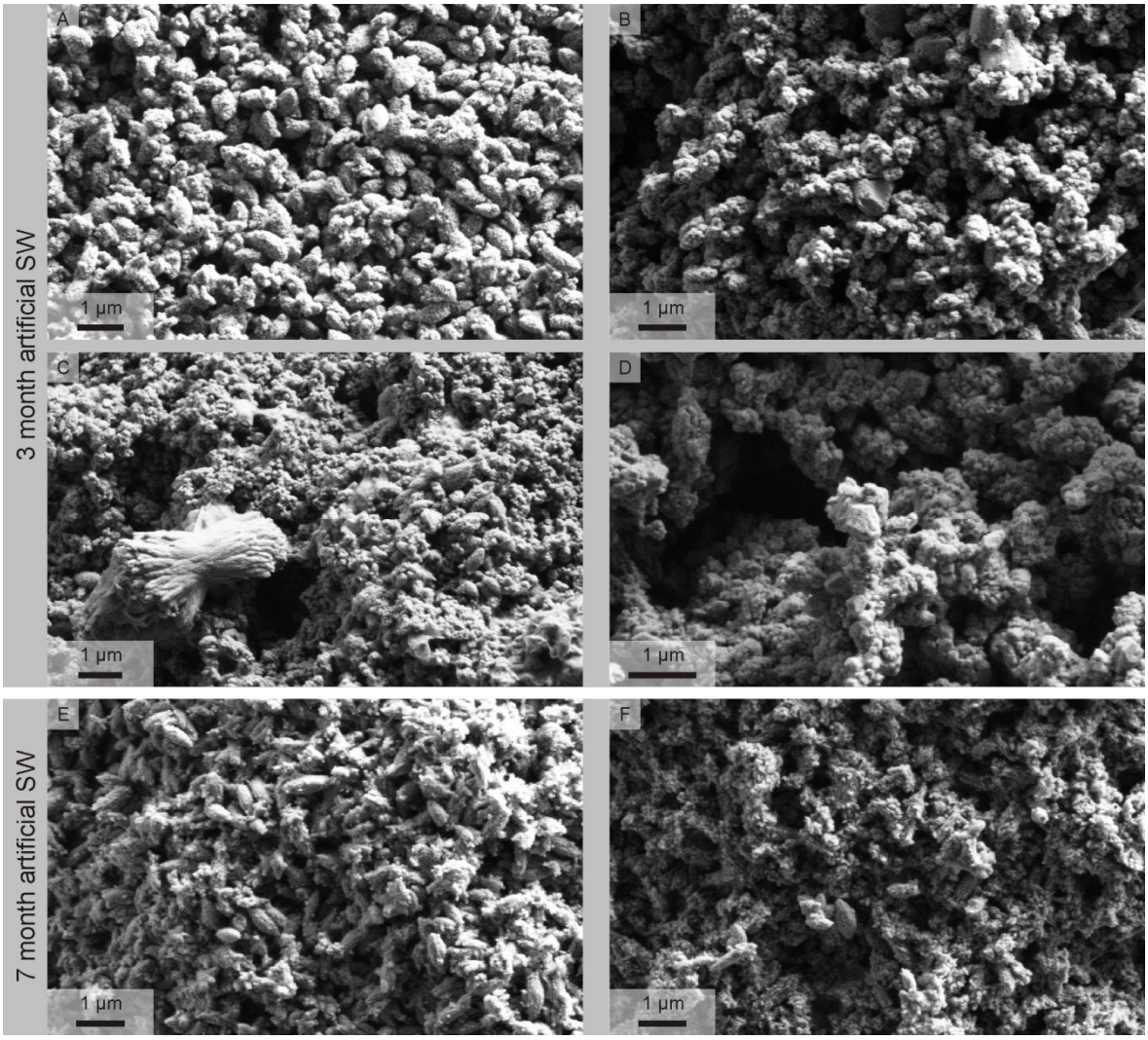

Figure 7.11 *SEM images of carbonate precipitates produced by schoolmaster snapper, cleaned, and left in artificial seawater for 3months (A–D) and 7 months (E–F). Both exposures yield crystals that are morphologically similar: areas of well-defined ellipsoids with smooth surfaces are common, especially on internal pellet surfaces that were exposed after seawater treatments (A & E), but areas of poorly defined ellipsoids with coarse surface texture and associated abundant nano-scale particles dominate in outer pellet surfaces (B–C & F). In addition, small dumbbells (not observed in control samples) are present in some pellets (C), albeit in very small number, and some pellets comprise areas where ellipsoids are apparently absent; precipitates instead comprising rhombohedral crystals (D, centre, centre-top, and bottom right) among a nebulous arrangement of nano-scale particles (D).*

Samples left in artificial seawater show generally similar textures to those exposed to porewater (Fig. 7.11), with smooth-surfaced, well-defined ellipsoids being common after both three month and seven month exposures, but poorly defined ellipsoids with coarse surface texture and associated nano-scale particles being the dominant crystal forms in pellet surfaces. Small dumbbells and rhombohedra are scarce subsidiary particle types in most pellets (Fig. 7.10 C–D), yet they are either rare (rhombohedra) or apparently absent (dumbbells) from control samples.

7.3.2.2.2 Infrared analyses

Infrared analyses of these samples indicate that few, if any, mineralogical changes occurred during various natural and artificial seawater exposures. Spectral patterns generated by carbonates at the point of excretion are similar to those shown in Chapter 3, comprising peaks assigned to poorly crystalline Mg calcite (Fig. 7.12). Spectra for samples exposed to seawater (natural and artificial) and porewater exhibit peaks that are almost identical in shape, position, and intensity (including component ν_3 peaks) to those generated by control samples (Fig. 7.12), indicating that little or no change in bulk mineralogy or crystallinity took place during any exposure. Among-sample variations in infrared data for carbonate vibrations are noted only in ν_4 bands, which typically comprise component peaks at 713 and 724 cm^{-1}, but these differences (which are not well understood, but may be related to variations in magnesium content – see Chapter 3) are not consistent in replicate samples from each exposure and are therefore not considered a result of changes induced by various exposures. Indeed, similar variations are commonly found within control samples.

Broad, low intensity peaks in the water stretching region also show little or no variation in shape or intensity among exposures. However, a sharp peak at 3698 cm^{-1}, assigned to O–H stretch in brucite ($Mg[OH]_2$; see Chapter 3), was present in three out of five replicate control samples (Fig. 7.12), but was absent from all spectra generated by replicate exposed samples, thus indicating that brucite may have dissolved rapidly up on exposure to seawater. Indeed, platy crystals that characterise brucite were not observed during SEM examinations of these samples, although they were also not observed in control samples (suggesting that brucite was never common).

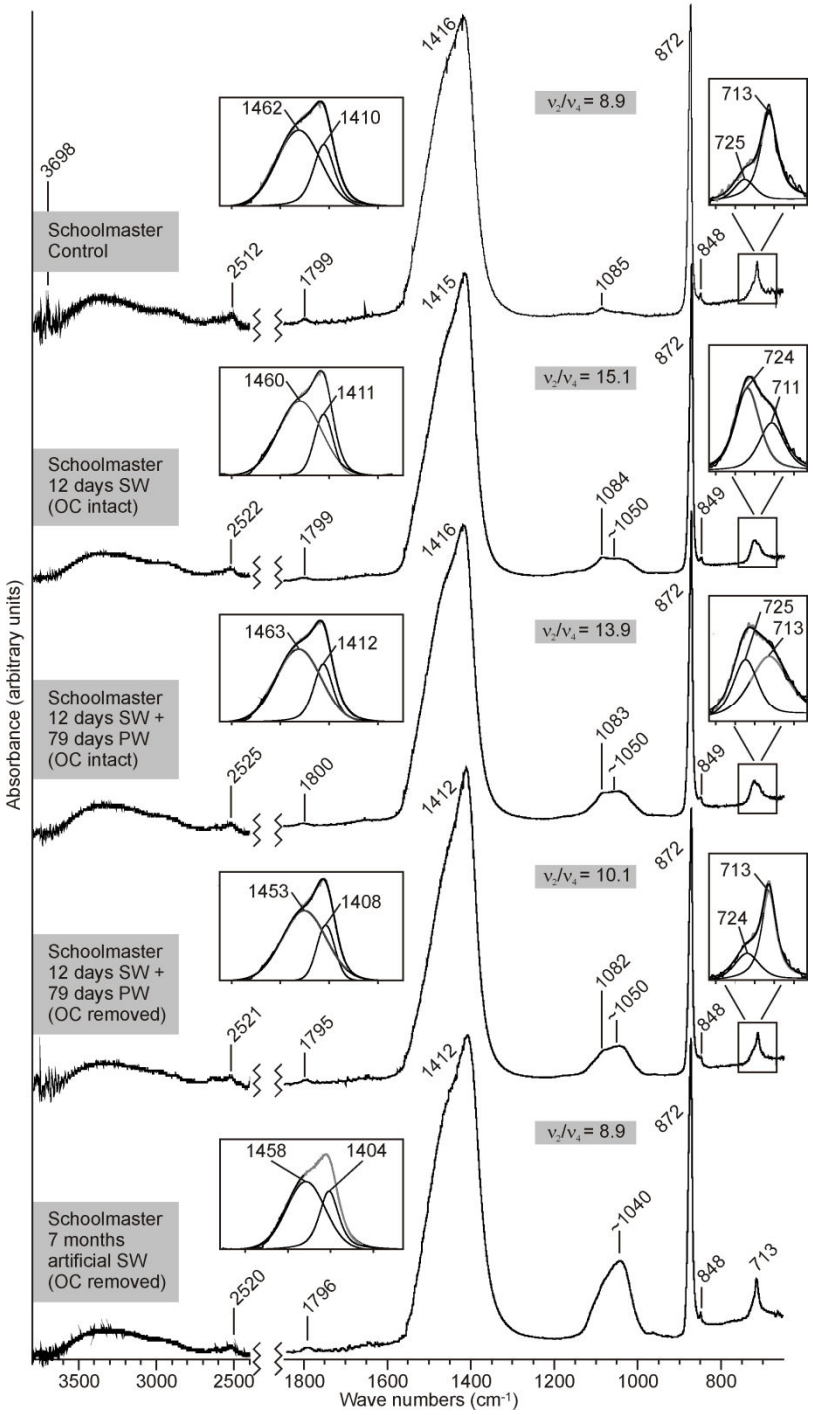

Figure 7.12 *ATR-FTIR spectra for carbonate samples produced by schoolmaster snapper. Samples were exposed to a range of natural and artificial seawater (SW) and natural porewater (PW) solutions for varying durations, with organic coatings (OC) variously intact or removed (as noted, left). Spectra are normalised to the CO_3^{2-} ν_3 band at ~1410 cm^{-1}, with those at higher wave numbers (2400–3800 cm^{-1}) 4x vertically exaggerated. Carbonate vibrations at 1082, 872, ~1410 (including component peaks; left insets), 713, and 725 cm^{-1} show little variation between treatments, indicating no bulk mineralogical changes have taken place. Differences in ν_4 peak shape (713–724 cm^{-1}) are a function of inter-pellet variability rather than being a result of exposure, and probably explain varying ν_2/ν_4 ratios (rather than this being due to variations in crystallinity). Water stretching vibrations at ~3350 cm^{-1} show little variation, but a sharp peak at 3698 cm^{-1} (brucite) is only present in control samples; its disappearance after exposure suggesting rapid dissolution of this phase. Broad peaks at ~1050 cm^{-1} are assigned to phosphate stretching. Increasing intensities of these peaks with exposure time seemingly indicates a relative increase in phosphate content during the course of all experiments.*

Apart from the apparent loss of brucite, the only notable difference in spectra generated by these samples is the appearance of a broad peak centred over approximately 1050 cm^{-1} following various exposures. This peak is assigned to the P–O stretch of phosphate, and increases in intensity with increasing exposure time (quantified in Table 7.5), being absent or weak in control samples, but being of moderate intensity in samples exposed for several months.

Table 7.5 *Ratios of carbonate to phosphate infrared peak intensity (generated by samples from schoolmaster snapper) according to various seawater and porewater exposure times.*

Exposure	CO_3^{2-}/PO_4^{3-} intensity ratio $\left(\frac{CO_3^{2-}\ asymmetric\ stretch}{PO_4^{3-}\ stretch}\right)$
Control (for artificial SW)	33.0
Artificial SW (3 months)	8.3
Artificial SW (7 months)	4.1
Control (for natural SW)	>100
SW (12 days)	21.7
PW (91 days; OC intact)	10.6
PW (91 days; OC removed))	11.3

This finding appears to indicate that phosphate was incorporated within carbonates during exposure. However, it is known that fish-derived carbonates can sometimes be excreted with elevated phosphate concentrations, probably in response to feeding (see pilot study in Chapter 4). In the case of natural seawater exposures, carbonates used for control samples were collected on two separate days at the beginning and end of the sample collection period, whereas samples used for various seawater exposures were accumulated over several days in between these times. Some sample material used for exposures was thus not retained for control purposes and, although unlikely, it is difficult to rule out the possibility that some of these products may have contained elevated phosphate at the point of excretion without similar phosphate elevation in control samples. For example, this could have occurred if one (or several) individual fish producing phosphate-rich carbonates did not contribute to either control sample.

However, the fact that artificial seawater exposures yield similar increases in phosphate content with increasing exposure time (Table 7.5) suggests that this pattern may not be an artefact of sampling. For these exposures, two control samples (both generating similar spectra with very low

intensity phosphate peaks) were pooled and transferred to artificial seawater; no additional material was used. Following three month exposures, replicate samples generated a phosphate peak nearly four times the intensity of control phosphate peaks (relative to the carbonate ν_3 peak), and after seven months replicates generated a peak approximately nine times the intensity of controls. This suggests that the relative amount of phosphate increased in these samples during the experiment.

7.3.2.2.3 Compositional analyses

Compositional analyses utilising EDX were performed on multiple crystals in each of at least five pellets for each exposure. The results show that average magnesium content per control pellet ranges from 18.1 to 20.6 mol% $MgCO_3$, with extreme values of 14.4 and 23.4 mol%. Pellet averages are broadly similar to these in seawater and porewater treatments where samples were not cleaned prior to exposure, with values in the range 16.3 to 20.5 mol% $MgCO_3$ (12 days seawater) and 16.7 to 22.3 (12 days seawater plus 79 days porewater). Overall results are displayed as histograms in Fig. 7.13. It is worth noting that the extreme lowest measured $MgCO_3$ contents in both uncleaned porewater exposure replicates (11.1 and 12.6 mol% $MgCO_3$) are lower than in control samples and 12 day seawater exposures (14.4 and 13.5 mol% $MgCO_3$), but analysis of variance suggests there is no significant difference between any of these treatments (one-way ANOVA; df = 2, F = 2.360, p = 0.099), thus indicating that there was no pervasive lowering of $MgCO_3$ content during exposures. Nevertheless, the possibility must exist that extreme low values in porewater-exposed samples are a result of localised lowering of $MgCO_3$ content.

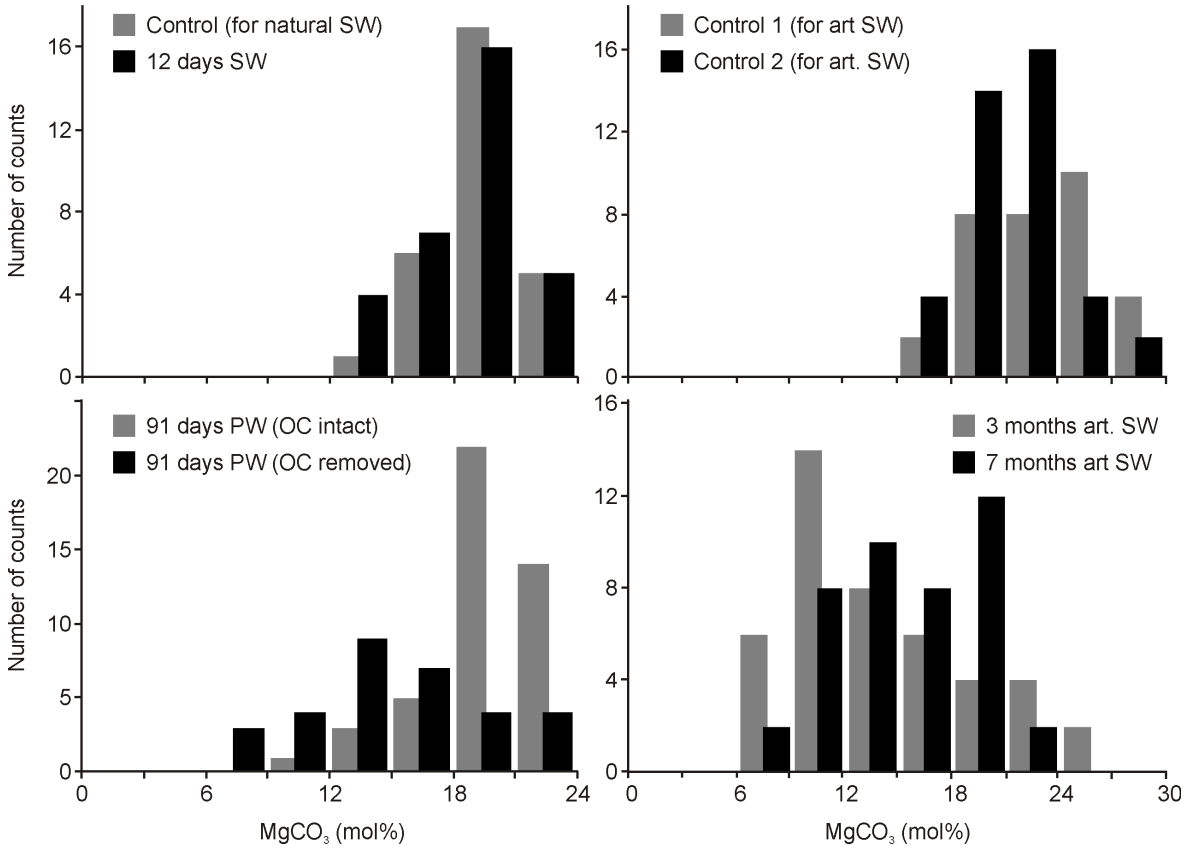

Figure 7.13 *Histograms showing distribution of $MgCO_3$ contents in ellipsoidal Mg calcite (produced by schoolmaster snapper) after various natural seawater (SW) and porewater (PW) exposures (left), and artificial SW exposures (right). Note the increased proportion of lower values for carbonates exposed to porewater with organic content (OC) removed. A similar, but more pronounced shift is observed in samples exposed to artificial seawater (also with OC removed).*

Indeed, compositional data obtained from pellets that were exposed to porewater after organic coatings had been removed lend support to this idea. Average $MgCO_3$ contents per pellet in both replicate samples range from 13.5 to 19.5 mol%, with an extreme low value of 8.0 mol% (five analyses returned values in the range 8.0 to 11.0 mol%). However, not all crystals had lower values, with the maximum value of 22.4 being within the range of maximum values returned from other samples. The resulting distribution of $MgCO_3$ contents is quite different from those of other exposures (Fig. 7.13), and one-way analysis of variance that includes these data indicate they are significantly lower (Welch one-way ANOVA; df = 3, Welch statistic = 11.395, $p < 0.001$), with Tamhane post-hoc tests indicating that cleaned porewater-exposed samples have significantly lower $MgCO_3$ contents than all other treatments. This result is interesting as it indicates not only that magnesium contents in some initially high-Mg calcites appear to be reduced to lower values

within a short period of exposure to porewater conditions, but also that the effect is significantly more pronounced when organic coatings are removed, suggesting that the retention of organic coatings may inhibit the processes that result in loss of magnesium.

Compositional analyses of samples exposed to artificial seawater further support the finding that magnesium contents of high-Mg calcite ellipsoids may decrease rapidly following excretion. Control sample averages of 24.2 and 22.0 mol% $MgCO_3$ (with a minimum value obtained of 17.3 mol%) are considerably higher than those of the same sample material exposed to artificial seawater for three months (11.1 mol%) and 7 months (12.2 mol%), with minima from both exposures of <6 mol% $MgCO_3$ (Fig. 7.13). Analysis of variance confirms that samples exposed to artificial seawater both have significantly lower $MgCO_3$ contents than control samples (Welch one-way ANOVA; df = 3, Welch statistic = 107.320, $p < 0.001$), with Tamhane post-hoc testing revealing no significant difference among the two control samples or among the two seawater exposed samples. However, because these samples were cleaned prior to exposure, it remains a possibility that such decreases would not occur, or would be retarded, in nature.

Regarding phosphorus, compositional analyses reveal that ellipsoids at the point of excretion have an average P/(Ca + Mg) atomic ratio of 0.004 (with maximum values not exceeding 0.006; *i.e.*, similar to results obtained in Chapter 2 for most fish-derived carbonates), whereas in ellipsoids exposed to seawater for 12 days, the average value for this parameter is 0.018 (with a maximum value of 0.040). Likewise, porewater-exposed samples yield average P/(Ca + Mg) ratios of between 0.017 and 0.027, with maximum values up to 0.080 and minima not lower than 0.008. This pattern of phosphorus contents suggests phosphate increases might have occurred in nearly all analysed crystals following seawater and porewater exposures, thus supporting the findings of FTIR analyses (see above).

7.3.2.2.4 Other observations

Neither of the replicates exposed to seawater for 7 months showed any change in mass during this time, suggesting that if any dissolution took place, it was either limited to a very small fraction of the total initial sample, or it was accompanied by reprecipitation. Furthermore, the preserved total mass indicates that relative phosphate abundance cannot have increased due to preferential dissolution of carbonate and preservation of phosphate (*i.e.*, in order to generate apparent phosphate increases in this manner would require a large proportion of $CaCO_3$ to preferentially dissolve). Increased phosphate concentrations, if not present in precipitates at the beginning of experiments, must therefore be due to precipitation (possibly via surface adsorption) of dissolved phosphate present in seawater solutions. The limited amount and rate of dissolution is further supported by artificial seawater pH measurements, which remained stable (8.20 ± 0.02) throughout the experiment.

7.3.2.3 High- and low-Mg calcite ellipsoids, dumbbells, and spheres (produced by yellowfin mojarra)

7.3.2.3.1 Morphologies

Carbonates collected at the point of excretion (control samples) from yellowfin mojarra are similar to those described for this species in earlier studies (Perry *et al*., 2011; Salter *et al*., 2012), being characterised by pellets that comprise micron-scale monocrystalline ellipsoids and larger (up to 20 μm in length) fibrous dumbbells and spheres (Figs. 7.14 A–B). Monocrystalline ellipsoids are commonly up to 3 μm in length, with smaller (~1 μm) crystals being dimensionally and texturally similar to those produced by schoolmaster snapper, but larger crystals tending to have straighter edges and more rounded terminations. Variation among pellets is evident only in differences in relative proportions of ellipsoids and dumbbells; some pellets being dominated by the former, some by the latter. The only other morphotypes observed are spherulitic structures (approximately 5–10 μm in diameter) that comprise radially arranged needle-like crystals, but these are very rare.

Samples left in mucus envelopes and exposed to surface seawater for up to 12 days comprise crystals that are morphologically identical to control samples (Figs. 7.14 C–D). Material from the same sample sets exposed to shallow porewater for a further 79 days retain morphologically similar crystals (Fig. 7.14 E), but additionally contain a greater abundance of needle-like forms (occurring both as spherulites and as individual needles; Fig. 7.14 F), although these remain rare. Ellipsoids in samples from all exposures have similar lengths and aspect ratios (Table 7.4).

The most obvious change in crystal morphologies is apparent in both replicate samples that were cleaned prior to 79 day shallow porewater exposures. Approximately 30 % of the pellets in these samples comprise crystals similar to those observed in control samples (Fig. 7.14 G). In contrast, the remaining 70 % of pellets typically comprise ellipsoids and dumbbells along with abundant needle-like forms; these commonly being 4–10 μm in length and <1 μm in width, having straight edges and variously blunt, pointed, or frayed terminations, and exhibiting short cross-sections that are close to square-shaped (Fig. 7.14 H). Morphological variants of needles include spherulites, dumbbells, individual needles, and ellipsoid-shaped crystals, some of which are shown in Fig. 7.15.

The morphological similarity between many of these needles and those observed as a dominant component of carbonate muds from some settings in Eleuthera Sound (*e.g.*, Fig. 6.11 B) raises the question as to whether the needles observed in association with yellowfin mojarra precipitates might be a result of sample contamination by mud-grade sediment surrounding the burial chambers. However, this possibility is easily eliminated by several observations: 1) it seems unlikely that contamination by surrounding sedimentary needles should occur in both cleaned samples produced by yellowfin mojarra, yet not in any other samples produced by this or other species; 2) although individual needles closely resemble those that occur in surface sediments, the ellipsoid- and dumbbell-shaped aggregates they can form (Figs 7.15 A–D) have not been observed in surface sediments and instead seem to be uniquely associated with fish-derived carbonates; and 3) perhaps mostly importantly, many of the needle-like forms in these samples have grown on or around crystals that are almost certainly fish-derived (*e.g.*, monocrystalline ellipsoids; Fig. 7.15 C),

thus indicating that they have formed in association with these carbonates rather than representing an added contaminant.

This being the case, it is worth emphasising that needles are much more abundant in samples that were cleaned prior to porewater exposure than they are in samples that were not cleaned. This would appear to indicate that organic coatings, where left intact, may have a significant inhibitory effect on the post-excretion development of aragonite needles, despite its rapid degradation such that it can no longer be seen with the naked eye within a few days of excretion.

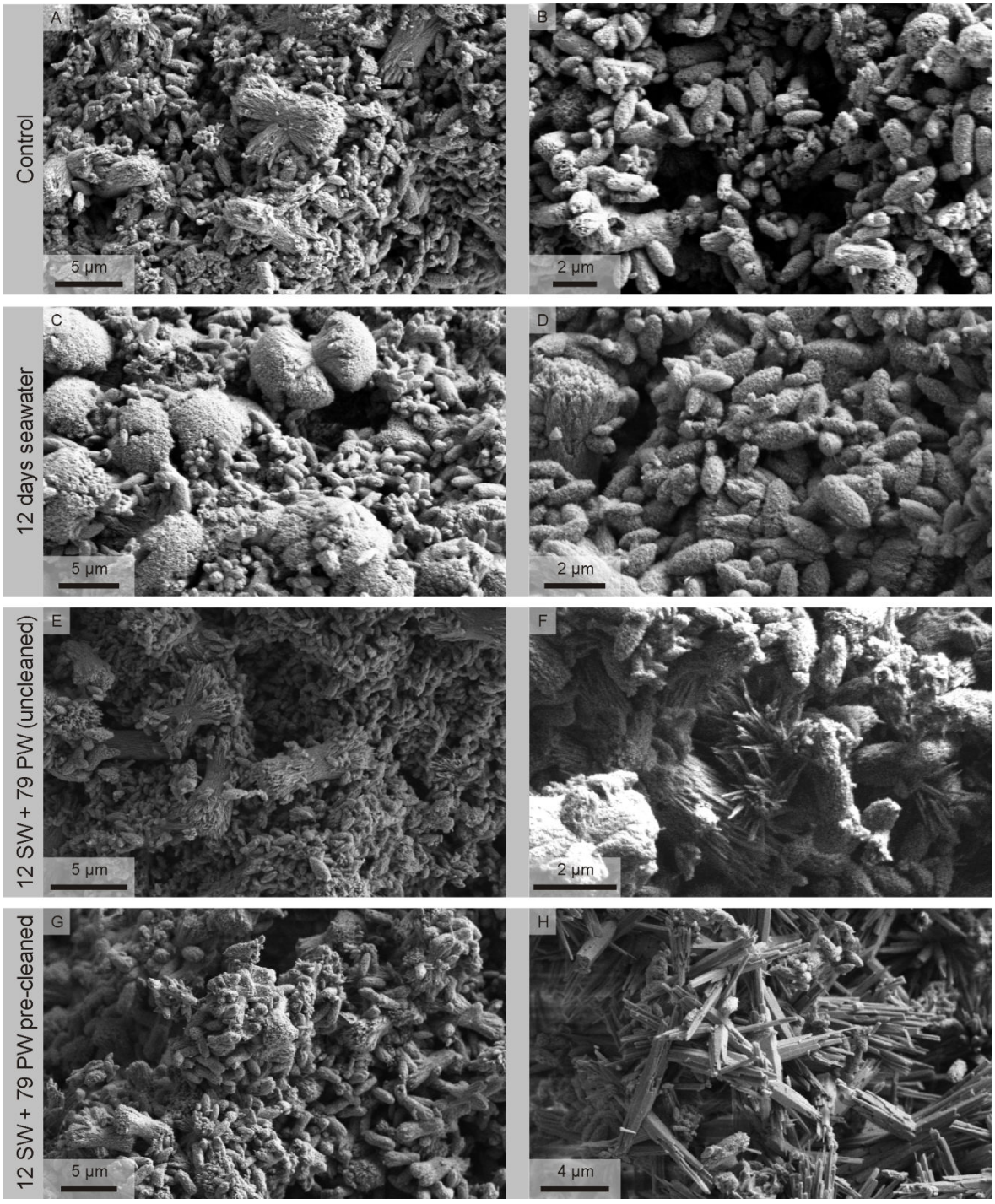

Figure 7.14 *SEM images of control sample carbonates and seawater- and porewater-exposed carbonates produced by yellowfin mojarra. Precipitation products in control samples typically comprise micron-scale ellipsoids and larger polycrystalline dumbbells (A), with larger ellipsoids (up to 3 µm in length) also being common; these tending to have more rounded terminations (B). These precipitation products remain unchanged after 12 days in seawater (C & D) and after 79 days in porewater (E & F), but note that needle-like morphologies are more abundant after porewater exposure (F). Crystals in uncleaned porewater-exposed samples (E & F) are generally similar to those in pre-cleaned samples (G & H), but note the considerably greater abundance of needle-like forms in the latter (H).*

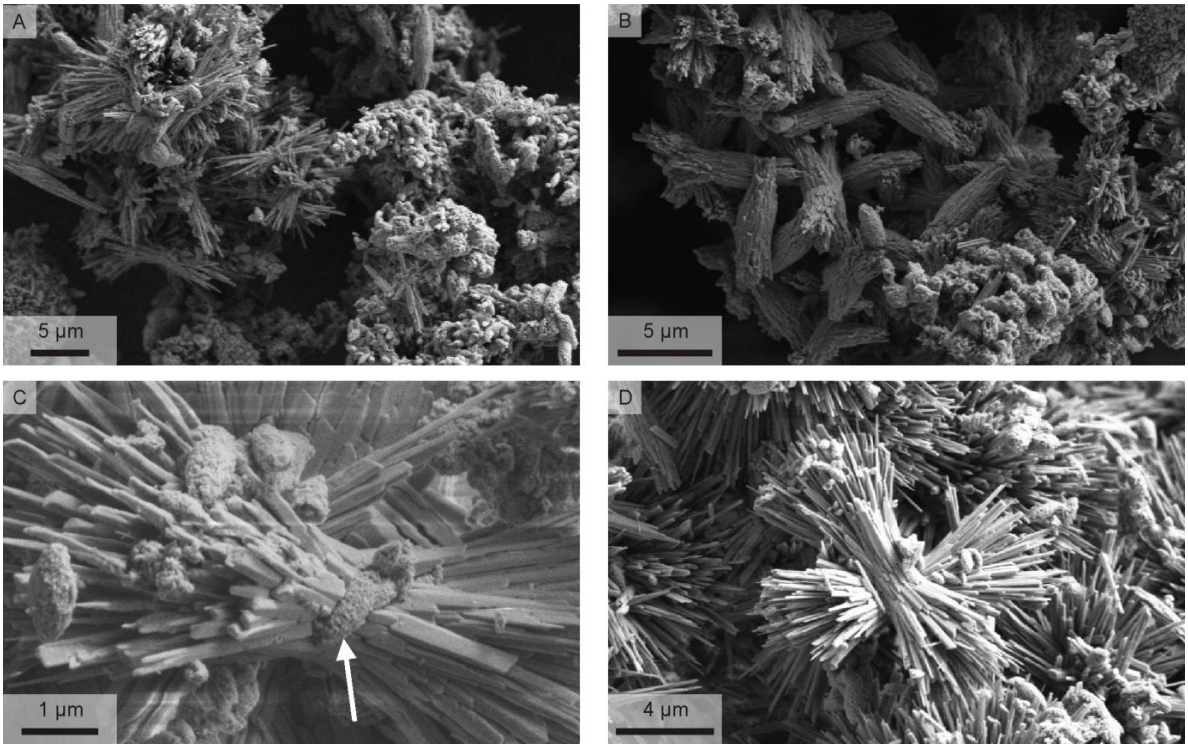

Figure 7.15 *Variations in needle-like morphologies present in carbonates produced by yellowfin mojarra and exposed to shallow porewater for 79 days following removal of organic coatings. Needle-like forms are present in approximately 70 % of all pellets examined, and where present are usually quite pervasive across visible areas (i.e., at least on pellet surfaces). Such pellets (A; top left) consequently differ markedly in appearance compared to those in which needles are scarce or absent (A; bottom right). In addition to individual needles like those shown in Fig. 7.14 H, variants of this form include: i) large (~ 5 µm in length) ellipsoids with frayed terminations that exhibit needle-like characteristics (B); and ii) dumbbell-shaped needle aggregates (C & D). The former suggest that some needle-like textures may begin to form following continued growth of pre-existing ellipsoids. However, in some cases needles appear to radiate from the surfaces of micron-scale ellipsoids (C; white arrow), suggesting that needles may also nucleate on pre-existing surfaces. It is worth pointing out that ellipsoids on the outer surfaces of needle-dumbbells appear to be resting on the surfaces rather than being intergrown with needles. Thus while there is evidence to suggest needles developed after at least some ellipsoids (e.g., ellipsoid at needle-dumbbell core; C), there is no evidence to suggest any ellipsoids formed after needles, and the assertion that needles formed after excretion therefore remains valid.*

7.3.2.3.2 Infrared analyses

ATR-FTIR analyses of carbonates produced by yellowfin mojarra further confirm the differences between control samples and those exposed to shallow porewater conditions (Fig 7.16). Samples at the point of excretion generate similar spectra to those obtained in previous studies (Chapter 3), indicating that these carbonates are predominantly poorly crystalline Mg calcite. The presence of a low intensity peak at 854 cm^{-1} indicates that aragonite probably occurs as a minor phase. Samples exposed to surface seawater for 12 days generate similar spectra, except that peaks generated by aragonite (at 1083, 854, and 700 cm^{-1}) are more intense, suggesting increased abundance of this

phase. Samples exposed to porewater (without pre-cleaning treatment) for a further 79 days generate almost identical carbonate vibrations. However, samples exposed to similar porewater conditions following pre-cleaning treatment generate considerably more intense vibrations assigned to aragonite (*e.g.*, note intensity of peak at 853 cm^{-1} in Fig. 7.16; bottom spectrum), suggesting that it occurs with the greatest abundance in these samples.

The increasing intensity of vibrational bands assigned to aragonite coincides with increasing abundance of needle-like forms and suggests that needles are aragonitic, which is not surprising given morphological similarities between many of these crystals and the fish-derived aragonite needles documented in Chapter 2 (Figs. 2.4 H and 2.9). This assertion is supported by EDX analyses, which show that needles have low magnesium concentrations and are enriched in strontium relative to ellipsoids (see next section).

Samples exposed to porewater further differ from control samples in that they consistently generate a weak broad band centred over ~1020 cm^{-1}, which is probably due to P–O stretching vibrations. The presence of phosphate in these samples only after exposure to porewater reveals a similar pattern of phosphate occurrence to that noted in samples produced by schoolmaster snapper (albeit at lower concentrations; see section 7.3.2.2), and supports the assertion that phosphate is somehow incorporated in these carbonates during seawater and/or porewater exposure on the order of months.

A further similarity with samples produced by schoolmaster snapper includes the lack of change in water stretching peaks (*i.e.*, peaks centred over ~3300 cm^{-1}; Fig. 7.16), which are weak and broad in all samples. Some control samples appear to contain small amounts of brucite, as indicated by clear sharp peaks at 3701 cm^{-1}, but, as with schoolmaster snapper samples, such peaks are never clearly discernable in exposed samples, suggesting that brucite may have dissolved following exposure. However, samples produced by this species commonly generate spectra that are noisy in the region where brucite O–H stretching peaks should occur, thus possibly causing brucite vibrations to be obscured.

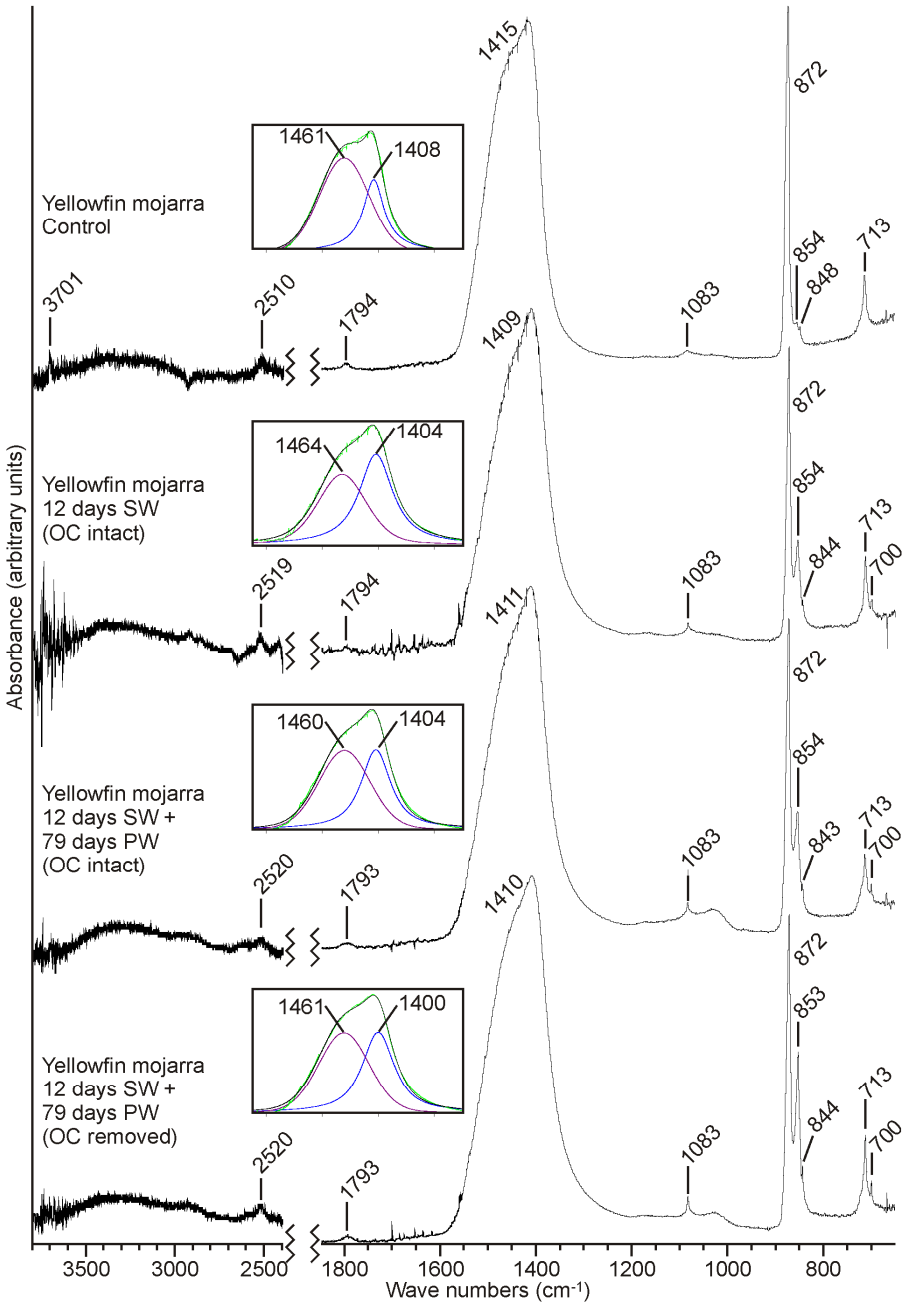

Figure 7.16 *ATR-FTIR absorbance patterns for carbonates produced by yellowfin mojarra, at various stages after excretion. Control samples generate a pattern typical for calcite, but a small shoulder at 854 cm^{-1} indicates the possible presence of minor aragonite. Samples left in seawater and porewater environments generate a similarly strong calcite signal, but also yield more intense vibrations associated with aragonite, suggesting the latter has actively grown in these conditions. Aragonite bands are most intense in samples buried in porewater environments without organic coatings. A broad, low intensity peak over the water stretching region suggests a partially hydrated phase is present and remains unchanged in all exposures, but a sharp peak at 3701 cm^{-1}, which may indicate the presence of a hydroxy phase, is only present in control samples and suggests this phase is rapidly removed after excretion.*

7.3.2.3.3 Compositional data

Monocrystalline ellipsoids show no significant variation in $MgCO_3$ content among control samples and all seawater and porewater exposures, with pellet averages in all sample sets typically ranging from approximately 9 to 13 mol%. It is worth noting, however, that these average values are considerably lower than those reported for monocrystalline ellipsoids produced by this species in Chapter 2, where the overall average $MgCO_3$ content was 22 mol% (*e.g.*, Fig. 2.12). The reasons for this difference are not known (sampling conditions and individual fish sizes were similar in both sample collection periods), but these data clearly demonstrate a previously unrecognised variability in $MgCO_3$ content of high-Mg calcite ellipsoids produced by this species.

Dumbbells and spheres, however, return values for $MgCO_3$ content that are within the range documented in previous studies (Chapter 2), with values typically between about 2 and 6 mol%. Average $SrCO_3$ contents in all samples are between 0.7 and 0.8 mol% (*i.e.*, higher than in ellipsoids, where the average is 0.3 mol%), indicating that at least some portion of these particles is aragonitic. As with ellipsoids, no compositional differences are observed in these morphotypes between control samples and seawater- and porewater-exposed samples.

Due to their absence or scarcity in control samples and samples exposed to seawater for 12 days, the compositions of needle-like forms were only obtained for porewater-exposed samples, and the tracking of potential compositional changes during exposure was therefore not possible. It is nevertheless worth mentioning that, where analysed, all needle-like forms returned low values for $MgCO_3$ content (up to 2.6 mol%, but typically <2 mol%), and high values for $SrCO_3$ content (0.6 mol% on average, compared with an average value of 0.3 mol% for monocrystalline ellipsoids), thus indicating that they are aragonitic and are therefore likely to be the source of aragonite bands shown in FTIR spectra.

Given the results of ATR-FTIR analyses (above), it was anticipated that samples exposed to porewater conditions would exhibit slightly higher phosphorus contents than control samples.

However, the atomic ratio of P/(Ca + Mg) is low for all crystals analysed in all sample sets, never exceeding 0.007. The origin of P–O stretching bands in FTIR spectra thus remains elusive.

7.3.2.4 Magnesium-rich amorphous carbonates and associated crystalline carbonates and hydroxides (produced by keeltail needlefish and bluehead wrasse)

7.3.2.4.1 Amorphous carbonate morphologies

Although previous studies have characterised the precipitation products of keeltail needlefish and bluehead wrasse as being quite different from each other (Salter *et al*., 2012), both species are known to excrete amorphous carbonates that are rich in magnesium (typically containing >95 mol% $MgCO_3$); these being the dominant phase of most pellets excreted by wrasse, and similarly dominant in some pellets excreted by needlefish. The results of seawater exposure experiments are therefore reported for both species in this section. As well as being compositionally similar, the amorphous phases produced by these species are characterised here and elsewhere (Chapter 2) by their lack of any definable shape at the point of excretion (*e.g.*, Fig. 7.19 A).

The most significant change that occurred in samples produced by both species following excretion was the rapid and visually obvious diminution of sample size when left in natural seawater, which is illustrated for samples produced by bluehead wrasse in Fig. 7.17. Visual examination of these samples using SEM reveals that the only precipitates remaining four days after excretion are crystalline phases (predominantly rhombohedra, spheres, ellipsoids; see next section); solid phases that lack definable form being completely absent (Figs. 7.18 & 7.19). These observations (which are further confirmed by FTIR analyses; see below) indicate that magnesium-rich amorphous carbonates (AMC) must have undergone pervasive dissolution within four days of excretion; the alternative possibility of wholescale crystallisation being ruled out by the large extent of sample volume reduction. Because this phase is the dominant precipitation product of bluehead wrasse (and at least two other species documented in this thesis; see Chapter 2) at the point of excretion,

this finding has potentially very important implications for the sedimentary significance of fish-derived carbonates (see discussion).

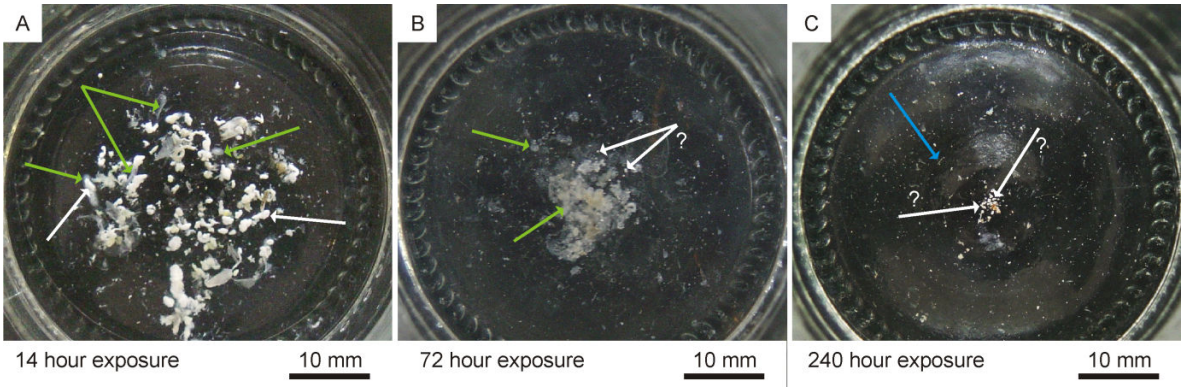

Figure 7.17 *Carbonate pellets produced by bluehead wrasse and held in aerated natural seawater. Photographs taken with samples held in seawater in experimental vessels. A) 14 hours after excretion: Abundant inorganic carbonate pellets (opaque white material; white arrows) within mucus coatings (translucent milky-white material; green arrows). B) 72 hours: Most visible material is organic mucus; inorganic carbonates having undergone large reduction in volume, with many that remain visible actually being skeletal particles that were presumably ingested and re-excreted by fish. C) 240 hours: Organic mucus is completely degraded, leaving inorganic carbonates (mostly skeletal) visible (white arrows). Numerous translucent off-white particles in this image (e.g., blue arrow) are insoluble calcium phosphate scales and fin rays that were ingested and excreted by fish that produced this sample.*

7.3.2.4.2 Crystalline carbonate morphologies

As well as amorphous carbonates, precipitation products excreted by needlefish and wrasse include crystalline carbonates; predominantly low- and high-Mg calcite (Salter *et al*., 2012). At the point of excretion, carbonate pellets produced by keeltail needlefish in this study fall into one of two categories with respect to their crystalline phases: 1) pellets that are dominated by admixed monocrystalline ellipsoids, rods, and small dumbbells, along with larger polycrystalline dumbbells and spheres (Fig. 7.18 A); and 2) pellets that comprise rhombohedra (with strong crystal habit; Fig. 7.18 B) evenly dispersed in a volumetrically more significant 'matrix' of AMC (lacking definable form) and platy forms, which are presumably brucite (see Chapter 3). Of the former pellet type, ellipsoids and rods are typically 1–2 µm in length, small dumbbells are up to 4 µm in length, and larger dumbbells and spheres are typically 5–30 µm in length. Ellipsoids and rods are typically slightly larger than those produced by schoolmaster snapper and, although some have similarly smooth surfaces, many further differ by having coarse surface textures and possibly showing signs

of becoming polycrystalline (shown clearly in rods at the top left of Fig. 7.18 F). These morphological characteristics are similar to those most commonly observed for products of this species in Chapter 2. In the second pellet type, which was less frequently observed in Chapter 2 as it is here (where it represents about 60 % of all excreted pellets), rhombohedra vary from 2–10 μm in length and are morphologically rather similar to those produced by bluehead wrasse (Chapter 2).

As described in the preceding section, all AMC was removed from these samples during a 12 day exposure to surface seawater. Further visual examination of the remaining precipitates also revealed the complete absence of brucite, which was presumably also lost to rapid dissolution. It is further evident from visual examination that rhombohedral forms are not obviously present in pellets retrieved following short seawater exposure. This is presumably a consequence of the typical occurrence of these forms within a 'matrix' of AMC and brucite; the dissolution of the latter phases resulting in liberation of rhombohedra as individual particles. Examination of material gently scraped from filter surfaces (as opposed to intact pellets) reveals that it contains abundant rhombohedra (Fig. 7.18 C), suggesting these morphotypes were indeed liberated from pellets. This finding supports the assertion that 'matrix' phases dissolved during seawater exposure; rhombohedra would presumably have been retained in pellets if these phases had (re)crystallised. Moreover, rhombohedra recovered in this manner are morphologically identical to those in control samples, exhibiting no textural evidence of extensive recrystallisation or dissolution.

The reasonably small amount of carbonate yielded by needlefish was sufficient for only one sample set to be exposed to porewater conditions; one that was not cleaned prior to sample burial. Rhombohedra were not recovered in pellets or as liberated crystals from the burial chamber used in this experiment. However, this is not necessarily an indication that these crystals dissolved during the porewater exposure period; in fact, given their large size and low $MgCO_3$ contents (relative to ellipsoids produced by schoolmaster snapper, for example), wholescale dissolution of this precipitation product during this short period of porewater exposure would be very surprising. It is perhaps more likely that, because of the small size of these crystals and the fact they had been

released from original pellets before porewater exposure, many were lost via holes that were necessarily made in burial chambers to facilitate porewater exchange.

With regard to other crystalline morphotypes, spheres, dumbbells, and ellipsoidal and rod-shaped particles are all commonly retained as components of intact pellets after both 12 day seawater exposures (Figs. 7.18 D–F) and longer (79 day) porewater exposures (Fig. 7.18 G–H); in all cases being similar to their control sample counterparts. Additional morphotypes that are reasonably common in these seawater-exposed pellets but are not observed in control samples are ellipsoid-, rod-, and dumbbell-shaped particles that are polycrystalline; individual crystals having sharply pointed terminations and being rather needle-like (Fig. 7.18 F). These particles are morphologically very similar to aragonitic forms identified in seawater- and porewater-exposed samples produced by yellowfin mojarra, and FTIR analyses (see below) indicate that they are probably this phase. Closer examination reveals that, in some cases, needle-like forms appear to emanate from a central core which has a similar coarse surface texture to many ellipsoids and rods in control samples; this suggesting that the latter morphotypes may have acted as precursors or nuclei to the growth of the former; the apparent absence of which from control samples perhaps indicating that this process took place after excretion. Note that, because pre-cleaned samples were not prepared and exposed to porewater conditions for this species, it is not possible to confirm the role of organic coatings that was proposed based on observations of samples produced by yellowfin mojarra.

It is interesting to note that similar needle-like morphotypes, although present, are much less common in porewater-exposed (79 days) samples than in seawater-exposed (12 days) samples, which is surprising given the former are a subset of the latter and should have been the same at the beginning of experiments. This observation could be explained by preferential dissolution of these aragonitic forms during porewater-exposure, although this would be surprising given that similar forms associated with carbonates produced by yellowfin mojarra are actually most abundant in porewater-exposed samples. Another possibility is that the difference between these sub-samples is due to a by-chance variation that occurred when the initial sample was divided.

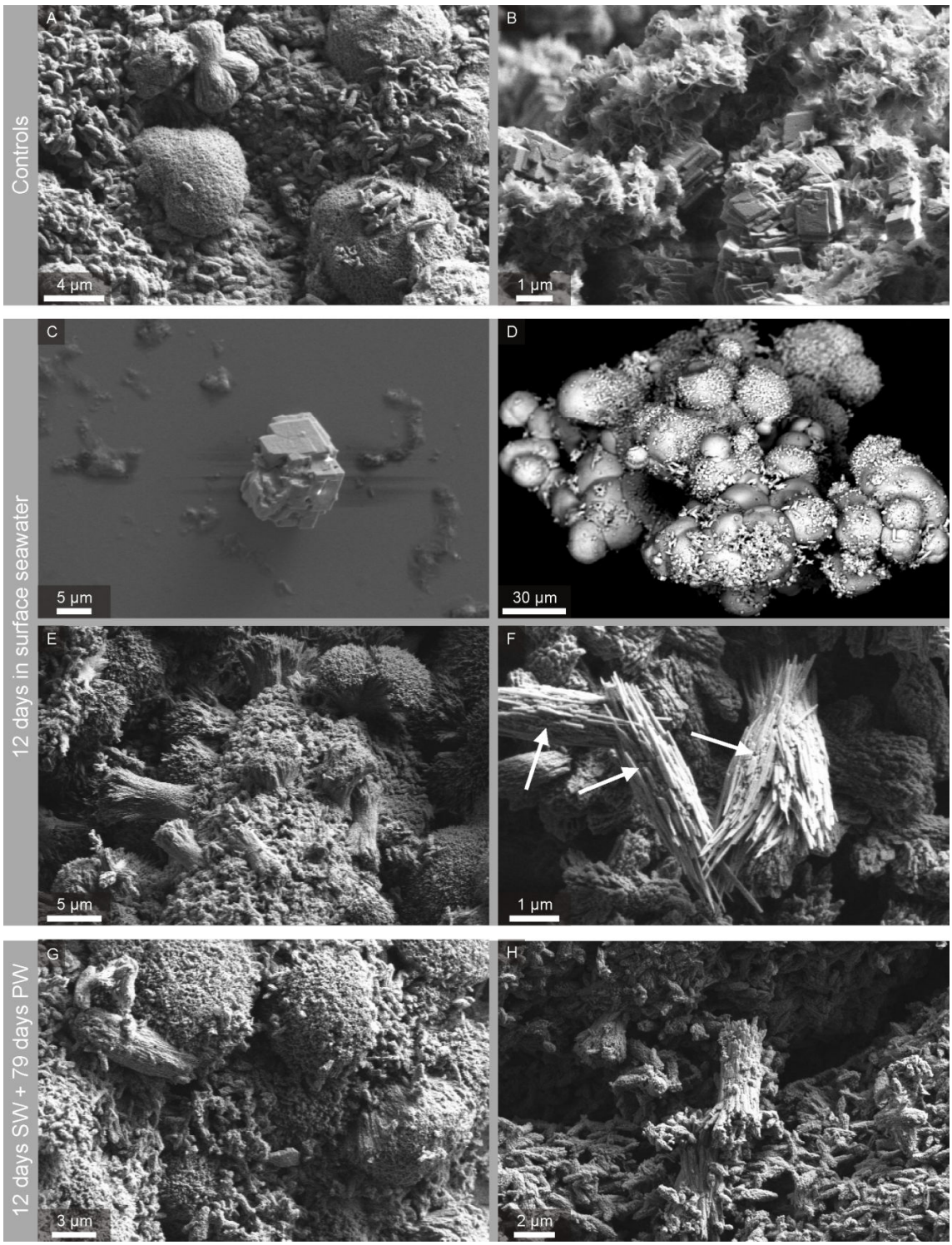

Figure 7.18 *Precipitates produced by keeltail needlefish. Control samples (i.e., at the point of excretion) typically contain mixed morphologies that include ellipsoids, dumbbells, rhombohedra, and platy forms (A & B); these being largely similar to previously described products (Chapter 2). Amorphous phases (not shown here) are also common at the point of excretion but, along with platy forms, these appear to dissolve within 12 days of seawater exposure (C–F). Associated rhombohedral crystals are consequently liberated from pellets and tend to occur as individual particles (C). All crystalline carbonate morphologies (i.e., ellipsoids, dumbbells, spheres, and rhombohedra) remain unaltered after exposure to seawater and porewater (C–H), but occasional needle-like forms in these samples (F) possibly represent as post-excretion precipitation product, perhaps nucleating on coarse surfaces of pre-existing rods and ellipsoids (white arrows).*

As described in the preceding section, amorphous carbonates that lack any readily definable form are the dominant precipitation product in carbonates excreted by bluehead wrasse, but they rapidly dissolve up on exposure to seawater. The carbonates that remain following this dissolution are barely discernable with the naked eye (intact pellets are very rare), and samples produced by this species were therefore considered to be impractical subjects for porewater exposure experiments, from which they would likely have been problematic to retrieve. As such, crystalline phases produced by this species were characterised only at the point of excretion and after 12 day seawater exposures.

At the point of excretion, crystalline phases are similar to those described from this species in previous studies (Salter *et al*., 2012), and also similar to many of those produced by needlefish; these comprising mostly rhombohedra and polycrystalline spheres and dumbbells, all of which typically range from 2–15 μm in length and tend to be thinly and sporadically distributed throughout a 'matrix' of AMC and, occasionally, plate-like brucite (Figs. 7.19 A–C). Parts of some pellets can be particularly crystal-rich, and in these areas spheres are commonly intergrown.

As mentioned above, intact pellets following seawater exposure are rare, and most preserved gut precipitates were retained as individual particles. However, several millimetre-scale pellets were retained; these comprising intergrown spheres each with diameters typically in the range 10–30 μm (but up to 100 μm; Figs. 7.19 D–E). Such pellets were not observed in control samples, although the spheres they consist of are morphologically and structurally similar to some of those dispersed in the 'matrix' material of pellets at the point of excretion. It is possible then that, following dissolution of 'matrix' phases, the only remaining intact pellets produced by this species are those that initially contained the greatest abundance of (intergrown) crystalline particles. A second possibility is that these pellets are the result of (re)crystallisation of initially excreted 'matrix' phases, but this is considered unlikely as it is difficult to explain why such a process would have occurred only in a few pellets.

Particles liberated from pellets following dissolution of 'matrix' phases were, in all cases (*i.e.*, rhombohedra, spheres, and dumbbells), preserved with textures identical those at the point of excretion, with spheres commonly occurring as intergrown clusters (Figs. 7.19 F–G).

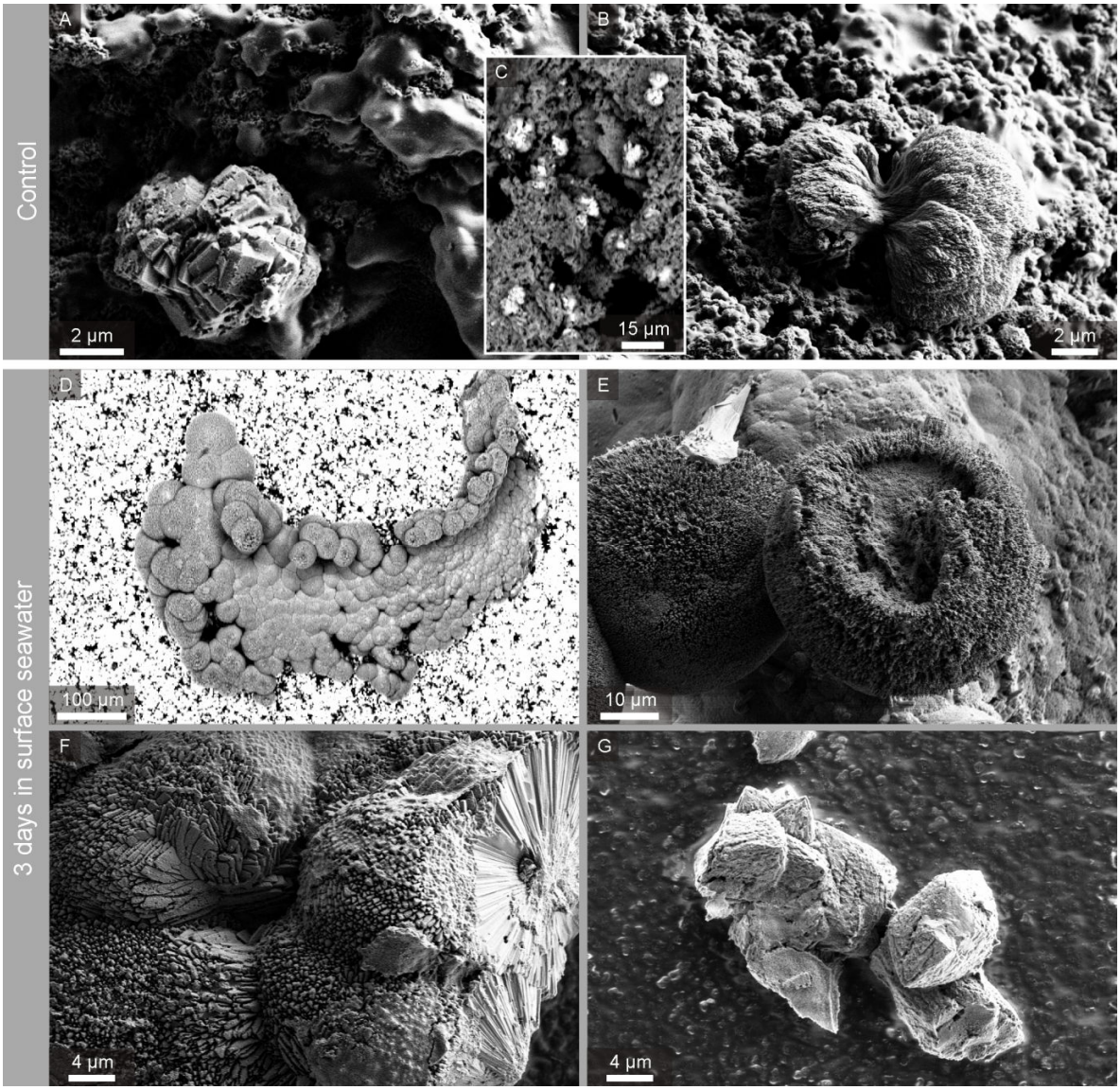

Figure 7.19 *Precipitates produced by bluehead wrasse. At the point of excretion, precipitates are dominated by amorphous magnesium carbonate in which individual (or sometimes clustered and intergrown) rhombohedral, dumbbell-shaped, or spherical crystals are evenly distributed (A–C). Backscatter electron (BSE) images (C) illustrate the sparse distribution of crystalline phases (pale areas) within the amorphous 'matrix' (dark areas). Most amorphous carbonates rapidly dissolve (i.e., within 3 days of excretion; note lack of dark areas in BSE image – D), leaving only crystalline phases that are morphologically identical to those at the point of excretion (D–G), and which either remain as intergrown clusters, or are liberated as individual particles.*

7.3.2.4.3 Infrared analyses

Infrared data generated by control samples produced by keeltail needlefish are similar to those collected in earlier studies for this species (Chapter 3), indicating the combined presence of calcite and a hydrated amorphous carbonate phase (Fig. 7.20); the former evidenced by the presence of a weak but well-defined peak at 713 cm^{-1}, and the latter evidenced by low intensity CO_3^{2-} ν_2 (874 cm^{-1}) and ν_4 (713 cm^{-1}) vibrations relative to the ν_3 (1414 cm^{-1}) vibration, and reasonably high intensity water stretching and bending bands at ~3320 and 1656 cm^{-1}, respectively. It is likely that amorphous carbonate is represented by precipitates that lack any definable form, whereas calcite is represented by ellipsoids, dumbbells, spheres, and rhombohedra. Due to observed textural variations among pellets (*i.e.*, the varying abundance of amorphous carbonate), the intensity of water stretching and bending vibrations is variable, but moderate to strong intensities as shown in Fig. 7.20 are common. In addition to these peaks, a weak shoulder at approximately 858 cm^{-1} and a possible very weak peak at 699 cm^{-1} may indicate the presence of a small amount of aragonite, although this is suggested only tentatively as the former could also be due to amorphous carbonate and the latter could be due to noise. A sharp peak at 3701 cm^{-1} is typical in spectra generated by pellets from this species at the point of excretion and is assigned to brucite.

A notable difference between spectra generated by control samples and spectra generated by all seawater- and porewater-exposed samples is the consistently lower intensity of water stretching and bending bands in the latter (Fig. 7.20). Because these peaks are assigned to the presence of a hydrous amorphous carbonate phase, this observation is consistent with the assertion (above) that such phases are no longer present in samples that have been exposed to seawater for a few days, and is further supported by the increased intensities of CO_3^{2-} ν_2 and ν_4 vibrations at 872 and 712 cm^{-1}, respectively; this being more typical of crystalline rather than amorphous phases. In addition, neither set of exposed samples generates a peak near 3700 cm^{-1}, indicating rapid removal or alteration of brucite; this being consistent with observations from samples produced by schoolmaster snapper and yellowfin mojarra.

With respect to crystalline carbonates, the main phase remaining after various exposures is calcite, which generates an intense peak at 872 cm^{-1}. A subsidiary phase in exposed samples is aragonite, which generates discrete peaks at 855 and 699 cm^{-1}, and also causes increased intensity of the peak at 1083 cm^{-1}. In all exposed samples the amount of aragonite appears to be greater than in control samples, suggesting that it formed after excretion. This pattern of occurrence is similar to that in samples produced by yellowfin mojarra; samples from both species suggesting that aragonite can form very quickly (within 12 days) following excretion. Based on morphological and compositional (see below) properties, aragonite is considered to be present mainly as needle-like forms. In support of this, infrared vibrations generated by aragonite are strongest in samples exposed to seawater for 12 days, which comprise the greatest abundance of needle-like forms. Aside from the apparent post-excretion development of aragonite, assessing changes to the calcite phase (*e.g.*, degree of crystallinity) is hampered owing to the fact that diagnostic peaks (CO_3^{2-} ν_2 and ν_4) are influenced by the presence of AMC in control samples and aragonite in exposed samples.

Samples excreted by bluehead wrasse were not analysed due to the small amount of retained sample material. However, given the results of visual observations (*i.e.*, rapid removal of amorphous and hydroxy phases, but preservation of rhombohedral and spherical crystals), it is likely that FTIR analyses would have yielded similar results to those for carbonates produced by needlefish.

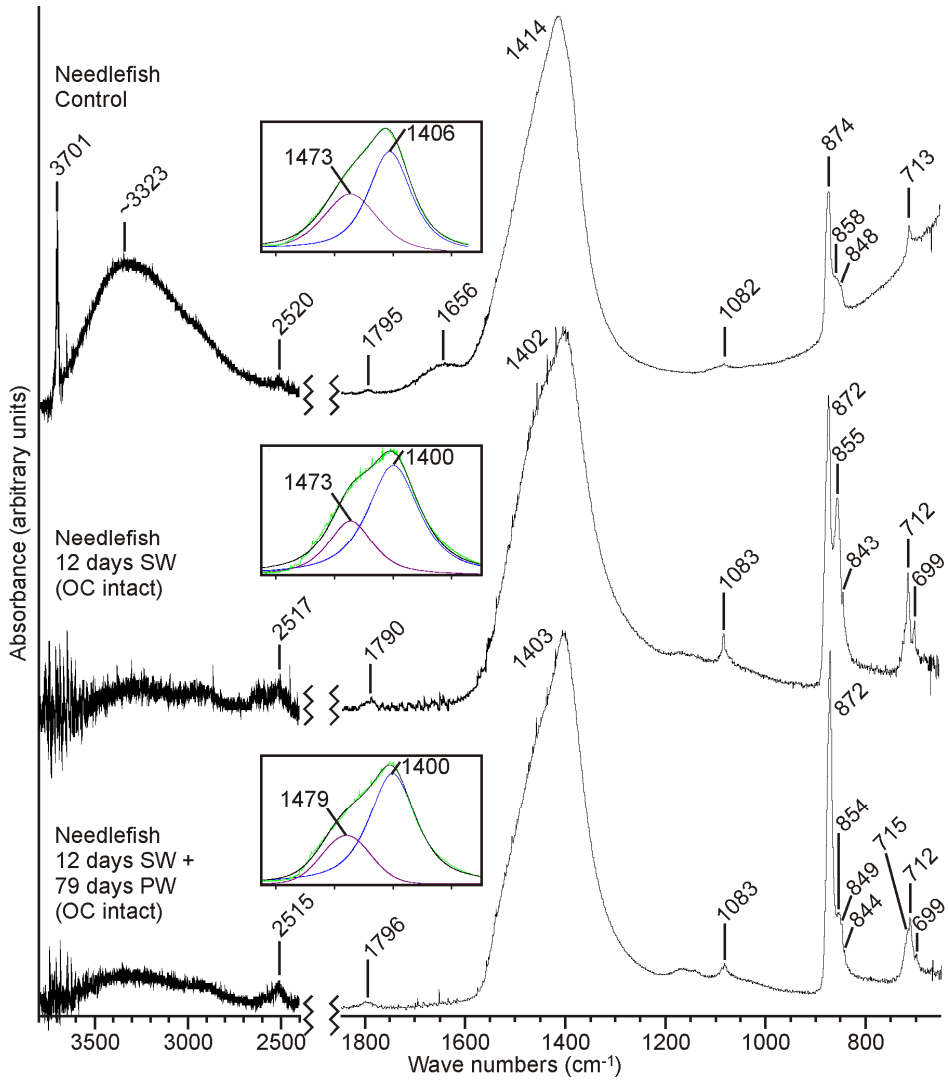

Figure 7.20 *ATR-FTIR spectra for samples produced by keeltail needlefish and exposed to various conditions following excretion: immediate cleaning (control); exposure in surface seawater for 12 days (organic coating intact); and exposure to porewater for 79 days (mucus coating intact). Note the rapid loss of brucite (disappearance of the sharp peak at 3701 cm^{-1}) and ACC (lower intensity of water stretch at ~3300 along with increased intensity of v_2 and v_4 peaks). Calcite is typically present in control pellets alongside ACC, and is preserved following exposure. Note that exposed samples also contain small amounts of aragonite; this phase being absent from, or only a very minor component of, control samples.*

7.3.2.4.4 Compositional analyses

At the point of excretion, precipitates produced by keeltail needlefish are compositionally varied. Ellipsoids and rods are compositionally consistent with high-Mg calcite, with $MgCO_3$ and $SrCO_3$ contents typically in the range 10–16 mol% and 0.3–0.4 mol%, respectively. Spheres and dumbbells are characterised by having lower $MgCO_3$ contents (0.6–5.2 mol%) and higher $SrCO_3$ contents (0.7–1.0 mol%), suggesting that these morphotypes comprise a mixture of Mg calcite and

aragonite. Following seawater and porewater exposures, compositions of these morphotypes remain within these ranges. Needle-like forms have similar $MgCO_3$ contents to spheres and dumbbells (in the range 0.8–3.2 mol%), but $SrCO_3$ contents tend to be slightly lower (in the range 0.5–0.7 mol%). Despite these lower $SrCO_3$ contents, values are considerably higher than in any high-Mg calcite, likely because needle-like forms are partially aragonitic. Crystals adjacent to needle-like forms (rod- and dumbbell-shaped particles with coarse surface textures) typically have higher magnesium contents (6.3–7.7 mol%) and lower $SrCO_3$ contents (0.2–0.3 mol%). The fact that needles appear to have grown from the surfaces of such crystals means that these compositional data are probably a result of mixed Mg calcite and aragonite signals, thus generating apparent $SrCO_3$ contents that are slightly lower than the actual $SrCO_3$ contents of aragonite needles. It is also possible that $SrCO_3$ contents differ due to different precipitating conditions; a similar difference is thought to occur in abiotic and biogenic aragonite from the Bahamas (Milliman, 1974).

Spheres and dumbbells produced by bluehead wrasse are similarly characterised by low $MgCO_3$ contents (in the range 1.9–8.2 mol%), but differ from needlefish-derived spheres by having lower $SrCO_3$ contents (0.1–0.2 mol%); these data indicating that aragonite is not present in these morphotypes, which are low- and high-Mg calcite (*i.e.*, as characterised in Chapters 2 and 3). Measured compositional ranges are similar in all exposures (up to 12 days in seawater), suggesting no rapid post-excretion changes in the compositions of excreted crystalline phases.

Rhombohedra and associated amorphous carbonates are compositionally similar among pellets produced by both species. Rhombohedra are difficult to analyse accurately in control pellets without interference from surrounding ‘matrix’ phases, but typically return values of 3.0–10.5 mol% $MgCO_3$. Compositional analyses from liberated crystals following seawater exposures (12 days) reveal $MgCO_3$ contents in the range 2.1–6.3 mol%; the smaller range and slightly lower values probably due to the absence of surrounding amorphia rather than actual compositional changes.

Owing to their absence from seawater-exposed samples, amorphous phases were only analysed in control samples, where they are compositionally similar to those described in previous studies (Salter *et al*., 2012), typically containing more than 95 mol% $MgCO_3$, having elevated sodium and chlorine concentrations relative to other phases, and also containing small amounts of silicon (typically 0.9 wt.%). In addition, it was noted that the amorphous forms present in one pellet produced by needlefish had a much lower $MgCO_3$ content (43.4–48.9 mol%) and correspondingly higher $CaCO_3$ content (51.1–56.6 mol%). This pellet also contained abundant micron-scale rod-shaped particles with $MgCO_3$ contents in the range 29.2–33.8 mol% and silicon concentrations similar to those of the surrounding amorphous phase, possibly indicating that they represent a stage of partial crystallisation from a precursor amorphous phase. Whatever the crystallisation process, neither amorphous phases, nor high-magnesium/high silicon rod-shaped particles, were found to be present in seawater exposed samples.

7.3.2.5 Polycrystalline spheres and associated amorphous carbonate phases (produced by bonefish)

7.3.2.5.1 Morphologies

At the point of excretion, precipitates produced by bonefish exhibit morphologies similar to those previously described (Salter *et al*., 2012). All fish (n = 3) produced pellets that are dominated by nano- to micron-scale spheres (typically less than 0.5 μm in diameter, but up to 2.0 μm; Fig. 7.21 A); these being morphologically identical to those identified as amorphous calcium carbonate (ACC) in earlier studies (Chapter 3). Many pellets dominated by nanospheres also comprise partially formed larger spheres (typically 10–20 μm in diameter; Fig. 7.21 B), many of which are structurally similar to polycrystalline spheres described in Chapter 2 (*i.e.*, they tend to comprise radially arranged fibres). Backscatter electron images of pellets containing these morphotypes render larger spheres a paler shade than nanospheres (Fig. 7.21 B), indicating that they comprise a greater abundance of heavier elements. Compositional analyses (see below) reveal that this is due

to lower magnesium contents in larger spheres, and these precipitates therefore fit a similar pattern to nanospheres and larger spheres from bonefish described in Chapter 2 (*e.g.*, Fig. 2.12).

Further to these two main forms of precipitation product, several textural features of large spheres are noted in control samples used in the present study that were not described in Chapter 2. These include: i) moulds of sub-micron spheres in the external surfaces of some larger polycrystalline spheres (Fig. 7.21 B; inset); and ii) rhombohedral crystals that commonly make up the external surfaces of polycrystalline spheres (Fig. 7.21 C) in place of the previously documented radially arranged fibrous crystals (Fig. 7.21 D), although the latter are also common in these samples. Rhombohedra typically occur as crystals that are less than 2.0 μm in length and less than 1.0 μm in width (although larger crystals also occur), and while most occur on sphere surfaces, some also occur as discrete crystals along with amorphous carbonates. In addition, the textural characteristics of several pellets are obscured by a coating of material that lacks any definable form and appears almost as a single continuous sheet draped over underlying spherical particles. This phase is somewhat similar in appearance to AMC produced by bluehead wrasse.

An interesting difference between the control samples described here and those described in Chapter 2 for bonefish is the relative abundance of ACC, which is easily the dominant phase in the present study, but is volumetrically subsidiary to large crystalline spheres in previously described samples. In contrast to control samples, precipitates exposed to seawater for 12 days are found herein to be dominated by polycrystalline spheres, with nano-scale ACC spheres being scarce (Fig. 7.21 E). It thus appears that, up on exposure to seawater, the relative abundance of polycrystalline spheres increased in samples used for this study, presumably due to dissolution or crystallisation of ACC nanospheres. This observation might also explain the difference between control samples characterised here and in Chapter 2; the latter study involved intervals of up to 24 hours between sample excretion and collection, as opposed to the two hour maximum intervals used here. The extra exposure time in the study documented in Chapter 2 may have been sufficient for substantial alteration of excreted ACC to take place.

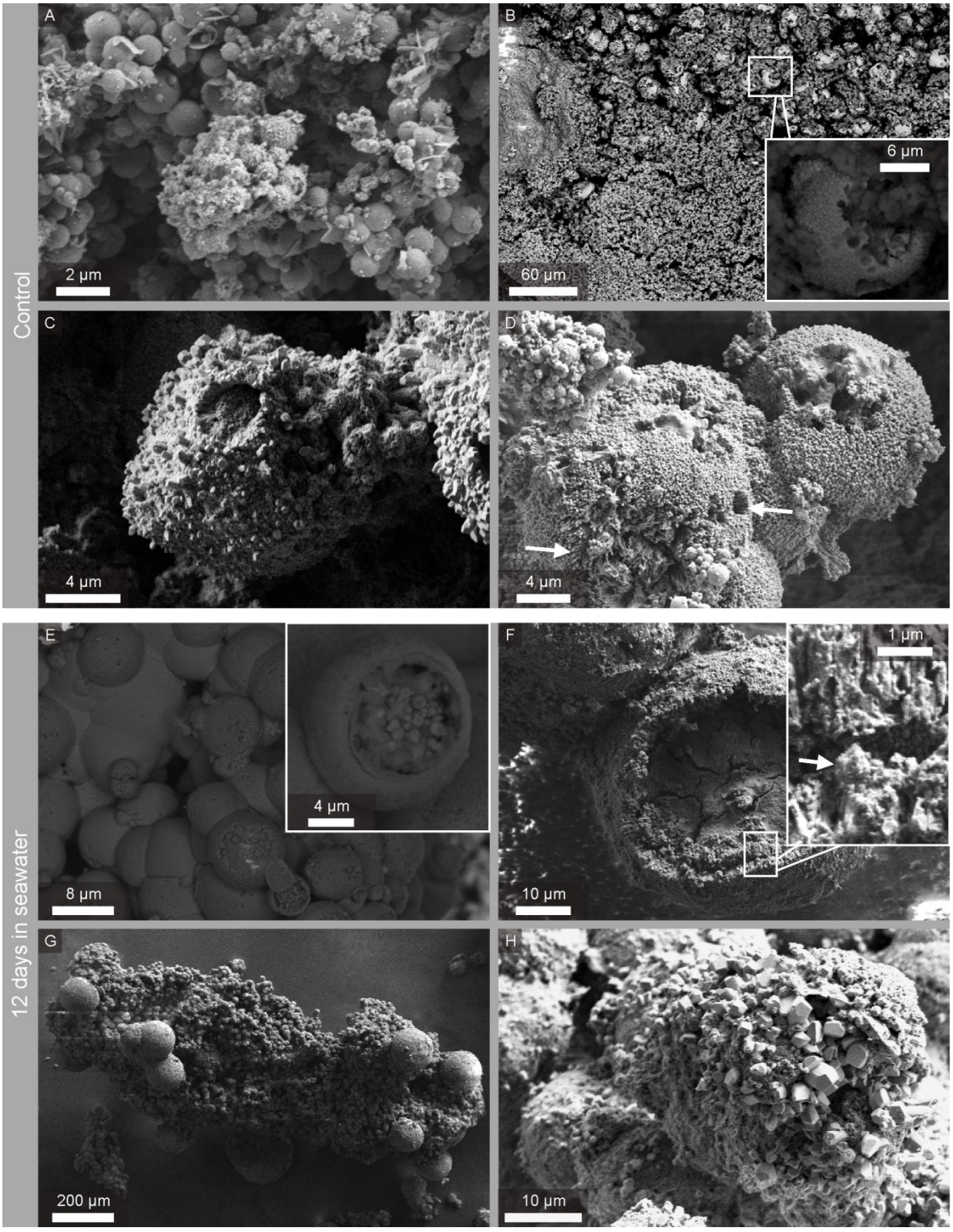

Figure 7.21 *Precipitates produced by bonefish at the point of excretion and after 12 days in seawater. Nanospheres make up the bulk of excreted precipitates (A–B; in the latter, which is a backscatter electron image, they appear darker than other morphotypes owing to their higher $MgCO_3$ contents), with larger polycrystalline spheres occurring as a common subsidiary morphotype (B–D). The latter are typically only partially formed when present amongst nanospheres (B, inset). Complete spheres are typically made up of rhombohedra (C) or radially arranged fibres (D). After 12 days in seawater, polycrystalline spheres are the dominant form (E–H), with nanospheres, although still present (E, inset; F, inset – arrow), being very rare. Spheres are texturally similar to those in control samples (E–H), but note the abundance of spheres greater than 50 µm in diameter (G); maximum sphere diameter in control samples never exceeds 50 µm.*

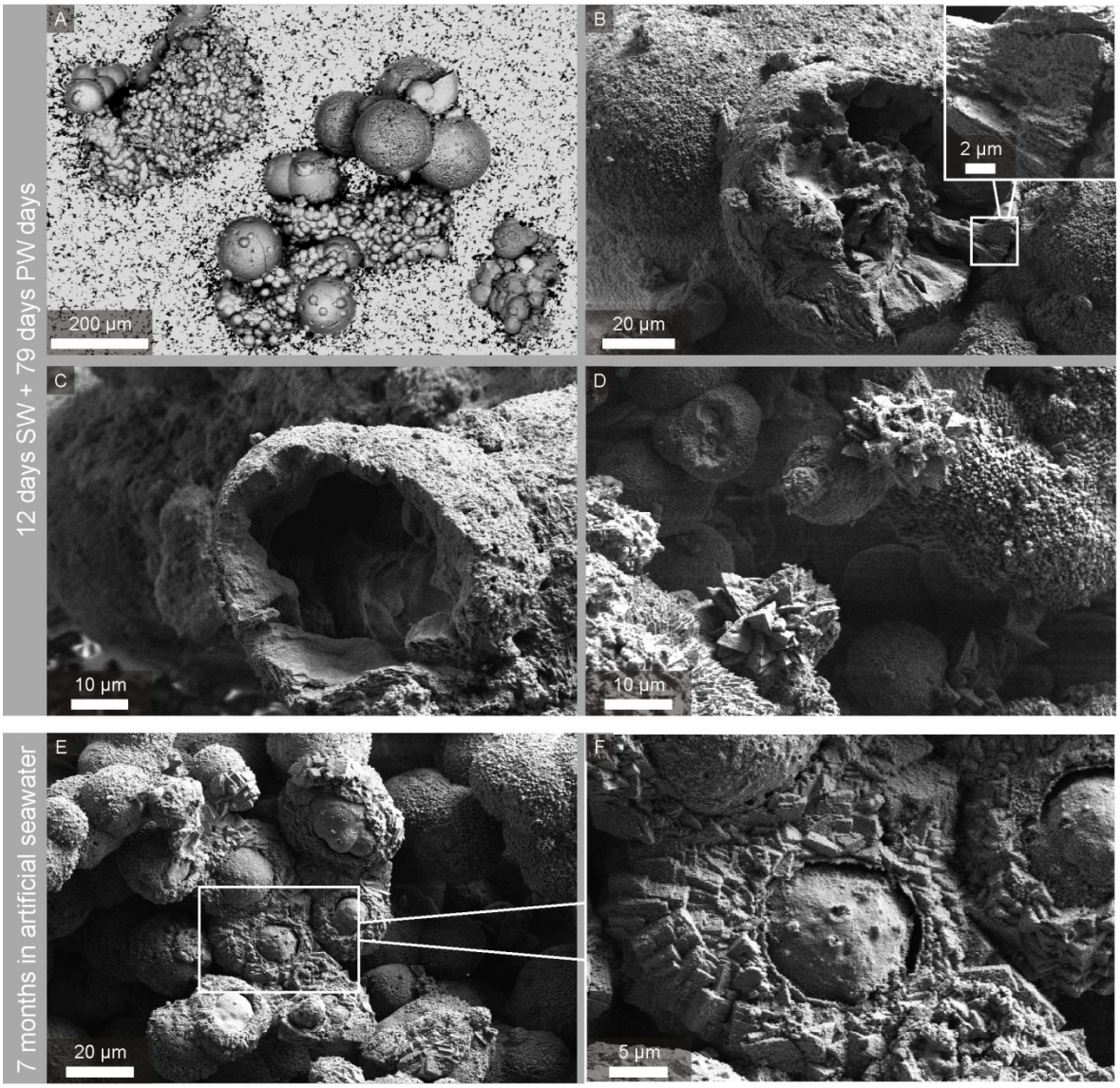

Figure 7.22 *Precipitates produced by bonefish and exposed to porewater conditions (top) and artificial seawater (bottom). Nanospheres are completely absent from both sample sets (A–F), which are instead dominated by larger polycrystalline spheres. The structures of these spheres are, in both cases, largely similar to those of control samples; the only major difference being the large number of spheres with diameters greater than 50 µm (A) – as is also observed after 12 days in seawater (Fig. 7.21). Other possible post-excretion alterations include: i) recrystallisation of original polycrystalline textures in some (scarce) porewater-exposed spheres to form massive textures (B–C); and ii) development of a range of rhombohedral morphologies (D–F; these morphologies not being observed in control samples).*

Several other factors are interesting with regard to the loss of ACC nanospheres from these samples. Firstly, although their disappearance is nearly complete after 12 days, some nanospheres (presumably ACC) are clearly retained (Fig. 7.21 E–F). In samples excreted by keeltail needlefish and bluehead wrasse, it is apparent that amorphous carbonates are completely removed after only a few days in seawater (see previous section), so this observation would appear to indicate that ACC nanospheres produced by bonefish are more stable than AMC produced by those species.

Nevertheless, no nanospheres are observed in samples exposed to porewater or artificial seawater for longer than three months (Fig 7.22), suggesting that all ACC is ultimately removed or altered. It is also worth pointing out that phases resembling AMC were not observed in any samples exposed to seawater for more than a few days and had presumably dissolved. Secondly, the loss of amorphous carbonate from precipitates produced by bonefish was accompanied by a visually obvious reduction in sample volume, but this volume change was not as striking as that observed in samples produced by needlefish and wrasse. Given the prevalence of ACC nanospheres in samples at the point of excretion, this observation makes it difficult to explain the loss of ACC as being due to dissolution alone. It is rather more likely that additional crystalline phases formed after excretion, due to either: i) dissolution of ACC and (re)precipitation as larger crystalline spheres; or ii) maturation and crystallisation of ACC to larger spheres.

Aside from the loss of ACC, the most striking difference between control samples and those exposed to seawater (for 12 days) and porewater conditions (for an additional 79 days) lies in the size of polycrystalline spheres (Figs. 7.21 G & 7.22 A). Measurement of more than 100 spheres in all samples indicates that many occur within similar size ranges (Fig. 7.23), with mean diameters (for all spheres of diameter <40 μm) of 15.0, 22.1 and 18.3 μm in control, seawater-exposed, and porewater-exposed samples, respectively. However, whereas the maximum diameter observed in control samples is 31 μm (maximum sphere diameter in all precipitates examined to-date from bonefish being about 50 μm at the point of excretion – see Chapter 6), maxima in seawater- and porewater-exposed samples are 225 and 205 μm, respectively. Not only are these diameters considerably larger than has been observed in precipitates at the point of excretion, but spheres with diameters greater than 50 μm (*i.e.*, larger than the largest spheres observed in any control sample to-date) account for approximately 40 % of the data points in both sample sets (Fig. 7.23), indicating that they are actually abundant. This observation suggests that spheres excreted along with ACC continue to grow following excretion, with the similar size distributions in samples exposed to seawater for a few days and in samples exposed to porewater conditions for a few

months indicating that most growth occurs in the very early stages after excretion and does not continue thereafter.

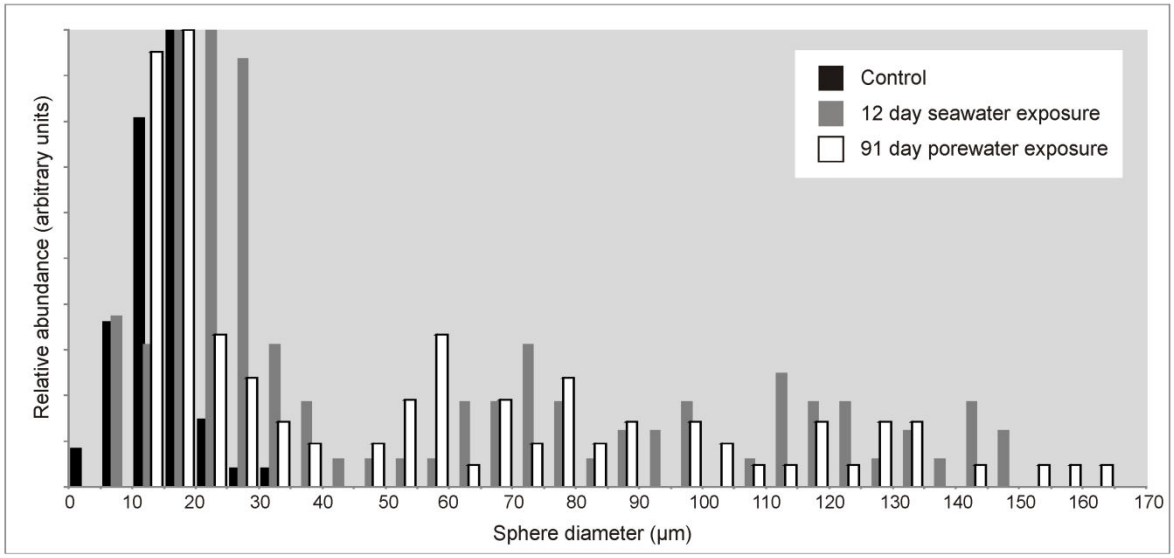

Figure 7.23 *Histograms showing size distributions of spheres in precipitates excreted by bonefish and exposed to a range of conditions (based on measurement of over 100 sphere diameters in each samples). All plots are normalised to the most frequently occurring particle diameter (the 15–20 µm interval in all cases). Note that the majority of spheres in each sample set have broadly similar size distributions (diameters in the range 5–30 µm). However, whereas spheres in control samples (i.e., those at the point of excretion) rarely exceed this size range, numerous spheres in both seawater- and porewater-exposed samples are considerably larger, with a secondary peak of occurrence at diameters of about 50–80 µm, and maxima of up to 225 µm (not shown here).*

These large polycrystalline spheres are texturally very similar to those in control samples (at least based on visual examination of their external surfaces), which suggests that post-excretion growth processes might have been similar to those that led to the formation of spheres in control samples (which presumably occurred before excretion). It has been proposed elsewhere (Chapter 3) that polycrystalline spheres might represent precipitates that formed via the maturation and crystallisation of ACC. The occurrence of partially formed spheres, some exhibiting nanosphere-shaped surface moulds (Fig. 7.21 B), within relatively large volumes of ACC nanospheres perhaps supports this idea, and it is conceivable that such crystallisation of ACC continued after excretion to result in the development of large spheres. This suggestion is further supported by the fact that sphere growth apparently occurred predominantly within 12 days of excretion, and did not appear to continue significantly thereafter (*i.e.*, when amorphous carbonates available for crystallisation processes had been largely exhausted).

Whatever the mechanism that results in the development of these large spheres, this finding suggests that a significant proportion of individual spheres released from pellets excreted by bonefish could ultimately be incorporated within the surface sediment as very fine (and even fine) sand-grade particles (*i.e.*, particle diameters in the range 63–250 μm), rather than just the fine to coarse silt fraction (*i.e.*, particle diameters in the range 10–63 μm) it was previously thought they might contribute to.

Further differences between control samples produced by bonefish and samples that were exposed to seawater and porewater conditions are difficult to assess properly owing to the large morphological variability of crystalline phases at the point of excretion. No further differences are evident in carbonates exposed to seawater for up to 12 days; all spheres in these samples comprising either radially arranged fibres (Fig. 7.21 E) or rhombohedra (Fig. 7.21 H) similar to those in control samples. Moreover, most precipitates retrieved after 79 days in porewater and after three and seven months in artificial seawater exhibit similar textures, suggesting that these crystalline phases are reasonably stable in post-excretion settings.

Textures in some spheres, however, are suggestive that recrystallisation might have taken place at local scales during porewater exposures. These spheres appear to have similar polycrystalline structures to spheres in control samples upon initial examination of their external surfaces, but internal surfaces (visible because spheres are broken or incomplete) reveal a texture that is rather massive (Figs. 7.22 B–C). Such textures have not previously been observed in spheres produced by bonefish (*e.g.*, see Fig 2.4), and it is possible that they formed during porewater exposure. In addition, rhombohedral crystals appear morphologically more varied in samples exposed to porewater and artificial seawater conditions (Figs. 7.22 D–F) than they do in control samples. Again, it is possible that these are textures that developed after excretion, perhaps due to crystallisation of ACC.

7.3.2.5.2 Infrared analyses

Due to the wide variety of precipitation products excreted by bonefish, it was instructive to perform numerous ATR-FTIR analyses using samples selected for their morphologies. Separation of morphotypes was aided by the relatively large size of spheres, their presence being discernable using an optical microscope. Control pellets were divided into those comprising spheres and those in which spheres appeared to be absent or rare (the latter being the most common), whereas seawater- and porewater-exposed carbonates, which typically comprise only larger polycrystalline spheres, were divided into intact pellets and liberated fines.

As in previous studies (Chapter 3), control pellets containing few obvious spheres are found to be dominated by a hydrated amorphous carbonate phase, whereas pellets that comprise abundant spheres appear to be dominated by monohydrocalcite (Fig. 7.24). Note that pellets dominated by ACC generate water stretching bands that are characterised by rounded peaks centred over about 3300 cm^{-1}, whereas equivalent bands generated by monohydrocalcite are characterised by more pointed peaks centred over about 3230 cm^{-1}. In addition to these phases, some pellets dominated by ACC contain a crystalline phase (indicated by a weak peak at 712 cm^{-1}, probably due to calcite), which presumably relates to polycrystalline spheres (a common subsidiary morphotype in these samples; see Fig. 7.21 B). Monohydrocalcite, which is identified by a characteristic split in the ν_3 peak at about 1450 cm^{-1} along with peaks at ~759 and 699 cm^{-1}, is also accompanied by calcite (as indicated by peaks at 712 cm^{-1}), whilst the reasonably low intensity of ν_2 peaks generated by these samples (*i.e.*, the peak centred over 871 cm^{-1}; compare top spectrum in Fig. 7.24 with bottom spectrum in Fig. 7.25) possibly indicates the presence of amorphous carbonate.

Pellets dominated by monohydrocalcite and ACC are both further characterised by the presence of phosphate, which generates broad bands centred over approximately 1040 cm^{-1}; peaks tending to be of strong intensity in association with monohydrocalcite, and ranging from moderate to strong in association with ACC (Fig. 7.24). In some cases, a weak peak at 965 cm^{-1} possibly indicates partial

crystallisation of a phosphate phase. Both pellet types also commonly contain brucite, the presence of which is indicated by sharp O–H stretching peaks at about 3700 cm^{-1}.

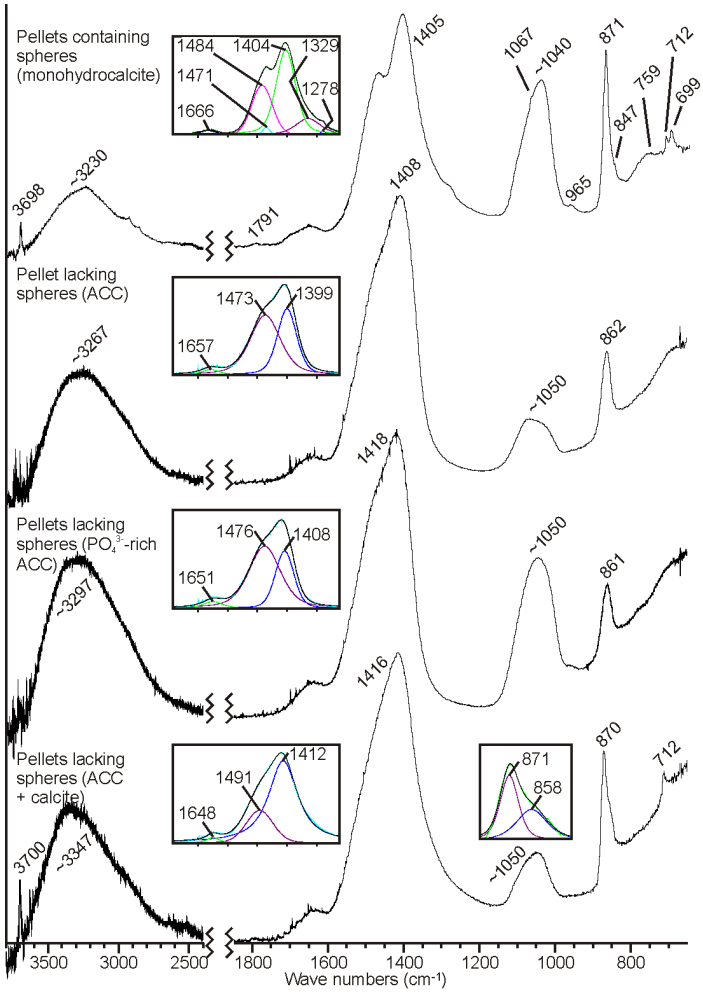

Figure 7.24 *Representative ATR-FTIR spectra for bonefish gut carbonates at the point of excretion. Inset boxes show results of deconvolution of adjacent peaks. The top spectrum is typical for pellets that comprise spheres. Carbonate peaks at or near 1484, 1404, 1067, 871, 759, and 699 cm^{-1} are assigned to monohydrocalcite, which also generates water stretching and bending peaks at 3230 and 1666 cm^{-1}. The three lower spectra are typical of pellets in which larger spheres are scarce; these being dominated by hydrated ACC. In comparison to spectra generated by crystalline phases, note the shortening and broadening of the ν_2 peak and its shift to 861 cm^{-1}, as well as the absence of a ν_4 peak near 713 cm^{-1}, and the presence of intense water stretching peaks at about 3300 cm^{-1}. Many pellets also contain calcite (note the presence of a weak peak at 712 cm^{-1} in top and bottom spectra). Broad peaks generated by all pellets at about 1040 cm^{-1} are assigned to phosphate, and a weak peak in some spectra at 965 cm^{-1} possibly indicates partial crystallisation of a phosphate phase. The presence of brucite in some pellets is indicated by sharp peaks at ~3700 cm^{-1}.*

Most pellets exposed to surface seawater for 12 days generate significantly different spectra to control samples, with higher intensity and sharper definition of carbonate ν_2 and ν_4 peaks at 872 and 713 cm^{-1}, respectively (Fig. 7.25), indicating calcite is the dominant phase; low ν_2/ν_4 intensity ratios (typically in the range 4.1–5.7) suggesting a higher degree of crystallinity than in other fish-

derived calcite (closer to skeletal Mg calcite from Bahamian surface sediments; see Chapter 3). Consistently lower intensities of water stretching and bending bands further indicate that these pellets contain less ACC than at the point of excretion, thus supporting the observed loss of nanospheres after a few days in seawater (see previous section). The fact that water stretching and bending peaks remain moderately intense in these samples is explained by the preservation of some ACC, which supports observations that ACC nanospheres remain as a scarce phase in these samples (Fig. 7.21 E). Because these spectra are generated by the majority of pellets analysed after 12 days in seawater, and because most pellets were dominated by ACC at the point of excretion, these data suggest that the calcite that dominates porewater-exposed samples is either: i) the only original precipitation product that remains following ACC dissolution; or ii) the phase that ACC crystallises to when left in seawater. Note that, if the latter is true, lower intensity phosphate vibrations generated by exposed samples suggest that phosphate associated with ACC is not retained during crystallisation to calcite.

Carbonates exposed to shallow porewater predominantly comprise intact pellets which generate similar spectra to those retrieved from seawater after 12 days (Fig. 7.25), with well crystallised calcite being the dominant phase. The presence of a water stretching band of similar intensity to that generated by samples exposed for 12 days is surprising given the apparent absence (based on visual examinations) of all amorphous carbonates from these samples. However, closer examination of this band reveals that it has a pointed peak centred over about 3230 cm^{-1}, which is more typical of monohydrocalcite than ACC. Indeed, at lower wavenumbers spectra commonly exhibit weak peaks that indicate the presence of this phase (*e.g.*, a broad hump at 760 cm^{-1}, and peaks at 700 and 1067 cm^{-1}). In contrast to intact pellets, peaks generated by liberated fine particles (which are predominantly spherical and account for approximately 5–10 % of samples by volume) indicate that monohydrocalcite is more abundant than it is in intact pellets, with calcite present as a minor phase. This indicates that not only is monohydrocalcite preserved after nearly three months in porewater conditions, but also that it shows no sign of beginning to convert to more stable

phases. As with monohydrocalcite in control samples, these liberated spheres are associated with high phosphate contents.

Carbonates exposed to artificial seawater were a subset of the control samples for which spectra are shown in Fig. 7.24; pellets being variously dominated by ACC and monohydrocalcite, with minor amounts of calcite. Material retrieved from experimental chambers after three and seven months were analysed using ATR-FTIR and revealed similar patterns as in porewater-exposed samples; complete loss of ACC, with samples instead dominated by well crystallised calcite (Fig. 7.25). An interesting difference between these carbonates and those exposed to natural porewater conditions is the absence of monohydrocalcite, with FTIR spectra consistently indicating that carbonates are almost completely anhydrous following exposure to artificial seawater (Fig. 7.25). These data suggest initial monohydrocalcite crystals were unstable in these solutions and underwent either: i) complete dissolution; or ii) complete neomorphism to calcite within three months. That being said, some samples generate very weak peaks at 700 cm^{-1}, which could be due to minor quantities of residual monohydrocalcite. However, it is not possible, based on these data, to rule out minor amounts of aragonite as the source of these peaks.

Brucite is generally rare in samples produced by bonefish, although its presence was detected in several control pellets and one pellet exposed to seawater for 12 days. Its absence from samples exposed for longer periods is in agreement with findings for pellets produced by other species, and supports the assertion that brucite dissolves or is altered quite rapidly following excretion.

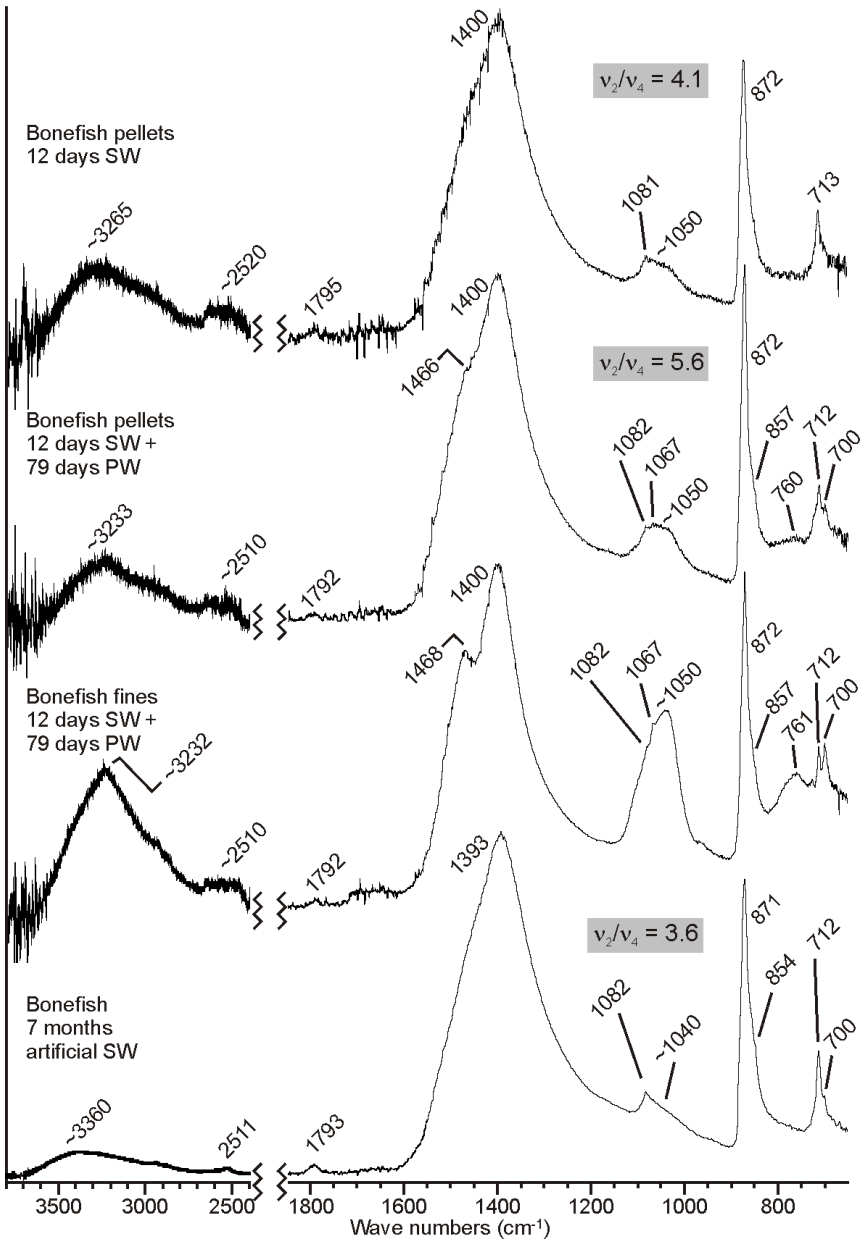

Figure 7.25 *Representative ATR-FTIR spectra generated by bonefish gut carbonates exposed to natural and artificial seawater (SW), and natural porewater (PW) conditions. Intact pellets after all exposures are dominated by calcite, as indicated by moderate intensity sharp peaks at 713 cm^{-1}. The ratio of peak intensity for peaks centred over about 872 and 713 cm^{-1} is typically less than 6, indicating this calcite is more strongly crystalline than that from other fish species (e.g., Chapter 3). Water stretching peaks (~3270 cm^{-1}) are of reduced intensity compared with control samples (Fig. 7.24) after 12 days in seawater, but their presence suggests some ACC remains. However, water stretching peaks in samples exposed to porewater are more characteristic of monohydrocalcite (note pointed peak over ~3230 cm^{-1}), the presence of which is confirmed by a weak hump at 760 cm^{-1} and a weak peak at 700 cm^{-1} (middle two spectra). Interestingly, this phase is more abundant in liberated spheres than in pellets, where calcite dominates. Spectra generated by all samples exposed for longer than 12 days (i.e., 3 to 7 month exposures) show no evidence for the presence of ACC, and also indicate that brucite has been lost during this time. Samples exposed to artificial seawater differ from those exposed to porewater in that monohydrocalcite is not detected (or is present as a very minor phase), suggesting it has either altered to calcite or dissolved.*

7.3.2.5.3 Compositional analyses

Compositional analyses of carbonates produced by bonefish indicate that, at the point of excretion, all morphotypes are compositionally similar to corresponding morphotypes described in Chapter 2. ACC nanospheres are magnesium-rich, typically containing between 30 and 37 mol% $MgCO_3$, while phosphorus concentrations are elevated relative to most other fish-derived carbonates, with the ratio of phosphorus to cations (Mg^{2+} and Ca^{2+}) being in the range 0.02–0.08 (compared with typical values of <0.008). Phosphorus presumably relates to phosphate detected using FTIR (see previous section) and, given suggestions that phosphate can act to stabilise ACC (*e.g.*, Raz *et al*., 2002), its presence here may be the reason that some ACC is preserved for longer than 12 days after excretion. In that case, these low, but elevated, phosphate concentrations may be an important factor controlling the apparent crystallisation of some ACC after excretion. ACC nanospheres are compositionally identical to those described above after 12 days in seawater.

Blanket-like features draped over spheres (described from SEM observations) are rare in control samples and absent from all other samples. Where analysed, they return $MgCO_3$ contents of 89–96 mol%, along with very low phosphorus contents (phosphorus to cation ratios are in the range 0.004–0.013). Given that this phase is morphologically and compositionally similar to AMC produced by bluehead wrasse, and appears to dissolve in the same manner as well, it is likely that it too is AMC.

Of the crystalline spherical forms, those that comprise radially arranged fibrous crystals occur with a wide range of $MgCO_3$ contents at the point of excretion, typically returning values between 8 and 19 mol%. Similar spheres (*i.e.*, all those with diameters less than about 50 μm) in seawater- and porewater-exposed samples show no compositional differences to those in control samples. However, larger spheres that seemingly developed after excretion (*i.e.*, those with diameters greater than about 50 μm; see preceding sections) have significantly lower $MgCO_3$ contents, returning an average value of 3.9 mol% (and not exceeding 8.6 mol%), which suggests that different factors may have influenced post-excretion formation of calcite. These typically coarse silt to fine sand-

grade particles are therefore likely to be incorporated within surface sediment as mostly low-Mg calcite alongside smaller spheres (fine to medium silt-grade) that are high-Mg calcite.

All rhombohedral forms in control samples (*i.e.*, those on sphere surfaces and those that occur as discrete particles) return $MgCO_3$ contents in the range 2.3–6.2 mol%, with a mean value of 4.6 mol%. Rhombohedra in exposed samples (including those with morphologies not observed in control samples; Figs. 7.22 D–F) have $MgCO_3$ contents that are within this range, with no significant differences noted.

7.3.2.5.4 Other observations

Samples exposed to artificial seawater were weighed before and after 7 month exposures, with both replicates found to have diminished greatly during experiments; losing 23 and 55 % of their initial masses. This mass reduction is probably a result of the loss of amorphous phases, and possibly monohydrocalcite, which FTIR analyses show to be present in control samples but absent in samples exposed to artificial seawater. It is not immediately clear whether mass was lost due to dissolution of these phases or due to their alteration to calcite and concomitant loss of water, although it is difficult to conceive that such large mass reductions could result from water loss alone. Indeed, studies of hydrated ACC of various other origins indicate that it usually contains one mole of H_2O for every mole of $CaCO_3$ (Levi-Kalisman *et al*., 2002), and if a similar situation is true here then loss of water during crystallisation of ACC would result in the crystallised phase having a mass that is about 15 % lower than the original ACC. Given that some precipitates excreted by bonefish are crystalline at the point of excretion (and presumably anhydrous), the total sample mass reduction caused by loss of water in this manner would likely be less than 15 %.

Solution monitoring during all artificial seawater experiments shows that, during the first week of exposure, pH increased in replicate chambers from 8.20 to 8.23 and 8.24 (NBS), whereas a stable pH was maintained in a blank seawater chamber and in seawater containing carbonates produced by schoolmaster snapper. Upon changing half of the seawater at the end of the first week, pH was

initially lowered to 8.22 before increasing again to 8.24 and 8.25 (NBS). Further solution changes were manipulated to ensure initial pH of refreshed seawater was always 8.20, which was necessary in order to prevent calcite and aragonite saturation states becoming too high. Seawater pH continued to increase for a few weeks (never going above 8.25), but it eventually stabilised in both replicate chambers during the fourth week of the experiment. The occurrence of these pH increases while all other seawater parameters (temperature, salinity, pressure, and pCO_2) remained stable is attributed to increases in the concentration of HCO_3^- and CO_3^{2-}, as indicated by calculations performed using CO2SYS (Pierrot *et al*., 2006). These changes must have been caused by the dissolution of solid phase carbonates, and this is presumably the process that resulted in sample mass reductions. Further to these findings, stabilisation of pH after 3–4 weeks indicates that dissolution largely ceased after this time, and that remaining solid phases (predominantly calcite) were stable in surface seawater conditions.

7.3.3 Stable isotope compositions: Carbon and oxygen

In Chapter 5 it was shown that ^{13}C and ^{18}O values of all fish-derived carbonates that were analysed were well outside the range of expected equilibrium values in Bahamian porewaters. Studies involving other carbonates (skeletal high-Mg calcite from fresh specimens of red algae) not in equilibrium with porewaters found that, after being exposed to porewaters for 500 days, they had begun to recrystallise and their stable isotope compositions had undergone a significant shift toward porewater equilibrium values (Patterson and Walter, 1994a). Although fish-derived carbonates in this study were exposed for a much shorter duration (91 days in total), their stable isotope compositions were determined in order to assess whether: i) they had undergone a significant shift towards porewater equilibrium; or ii) they had otherwise altered due to the preferential loss of some phases (*e.g.*, amorphous carbonates). The results are presented in Fig. 7.26.

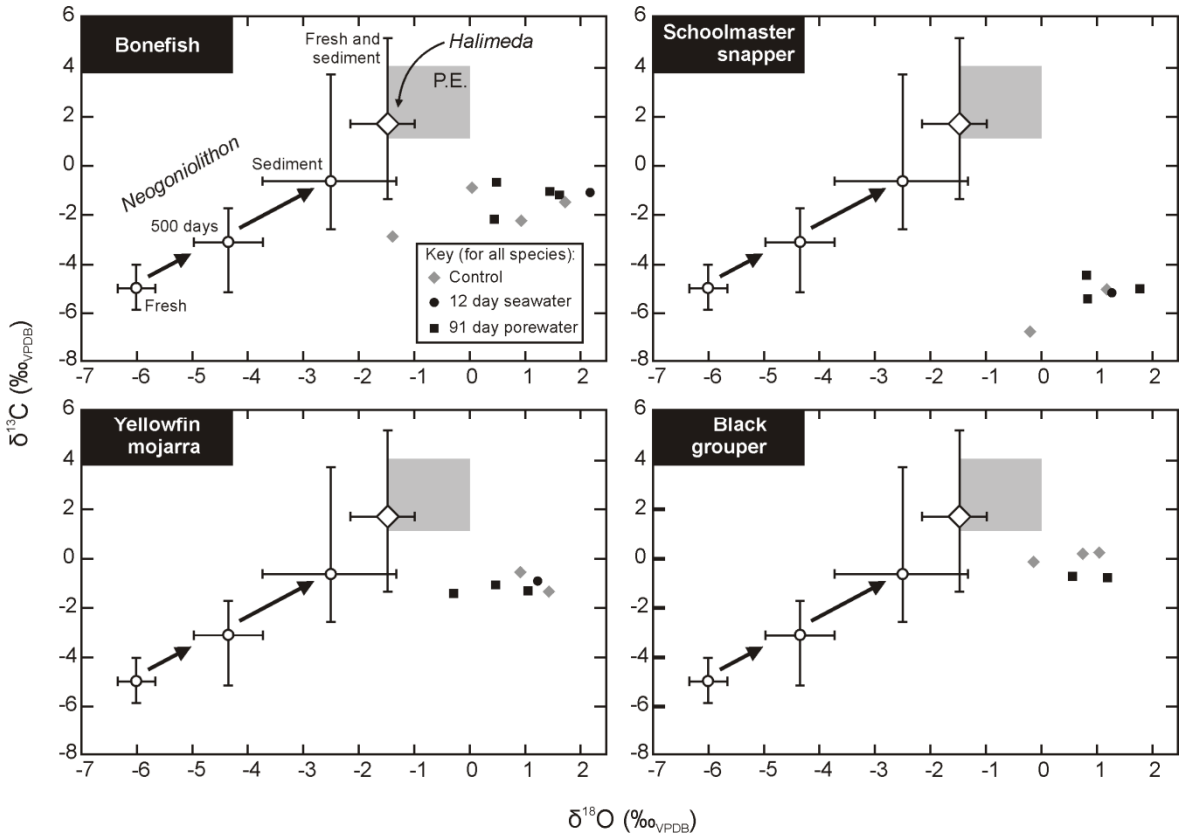

Figure 7.26 *Stable isotope compositions of bulk carbonate samples produced by four fish species. For each species, samples include those at the point of excretion (controls), those exposed to seawater for 12 days (except carbonates from black grouper), and those exposed to porewater for 79 days. Note that all samples produced by schoolmaster snapper are from fish that were fed a diet of sardines prior to sample production (and are thus depleted in ^{13}C; see Chapter 5). No obvious changes are noted in $\delta^{13}C$ or $\delta^{18}O$ values after exposure of samples produced by any species, despite the fact that dissolution and recrystallisation has occurred extensively in some (see text). The results of other studies are shown for comparison (these are the same in each plot): grey boxes (P.E.) show the predicted range of porewater equilibrium values (Walter et al., 1993); white diamonds/circles show average values for Halimeda algae and Neogoniolithon algae, respectively (Patterson and Walter, 1994a). Halimeda are close to equilibrium with porewater when fresh, with no changes observed in older particles. Neogoniolithon are well outside porewater equilibrium when fresh, but shift towards porewater equilibrium as they age.*

As in previous studies (Chapter 5), small sample volumes meant that only a small number of sub-samples could be analysed for each species, with insufficient sample sizes from keeltail needlefish and bluehead wrasse precluding analysis of carbonates produced by those species. However, it was possible to determine stable isotope compositions of at least two control sub-samples and two porewater-exposed samples from each of bonefish, schoolmaster snapper, yellowfin mojarra, and black grouper. Textural, mineralogical, and compositional data are not reported for the latter in the preceding sections, but results were generally similar to those reported for schoolmaster snapper.

In all cases, $\delta^{13}C$ values are within the ranges reported in Chapter 5, typically being between 0 and -2 $‰_{VPDB}$. However, note that schoolmaster snapper were fed a diet of sardines prior to sample production, so ^{13}C is more depleted here than it would be normally (see Chapter 5 for further details), with $\delta^{13}C$ values being between -4.41 and -6.71 $‰_{VPDB}$. Values for $\delta^{18}O$ are typically between 0 and 2 $‰_{VPDB}$ in all samples. Although this dataset is limited by the small number of samples, and interpretation of the results is hampered by the reasonably large spread of data at the point of excretion, no significant differences are noted between control samples and porewater-exposed samples for any species, and there is no indication of a shift towards porewater equilibrium.

For samples produced by bonefish, this result indicates that ACC, which is the dominant product in control samples and is not present at all in porewater-exposed samples, must be of isotopically similar composition to the calcite that remains after exposure. This result indicates that ACC and calcite either: i) precipitate with the same stable isotope fractionation factors in the piscine gut; or ii) precipitate with different stable isotope fractionation factors, but yield similar values here because calcite may have formed via crystallisation of ACC (see preceding sections) which, if involving a solid–solid transformation, may have imparted its stable isotope signature on calcite.

The lack of change in stable isotope composition in samples produced by schoolmaster snapper and black grouper is not unexpected. Although evidence was noted in the preceding sections that suggests recrystallisation and preferential dissolution of $MgCO_3$ might have occurred during porewater exposure (both of these processes having the potential to alter stable isotope compositions; *e.g.*, Patterson and Walter, 1994a; Jimenez-Lopez, 2006), the fact that this evidence was restricted to pellet surfaces, and that internal regions of pellets appeared to remain unaltered, suggests a volumetrically minor proportion of excreted carbonates would have been affected, and bulk stable isotope compositions are therefore likely to remain unchanged. Presumably more pervasive alteration occurring over longer exposure times might yield different stable isotope compositions.

Porewater-exposed samples produced by yellowfin mojarra, including one that was pre-cleaned, yield $\delta^{18}O$ and $\delta^{13}C$ values that are within the range of values measured in samples at the point of excretion from this and other species (Fig. 7.26; see also Chapter 5). Assuming the pre-cleaned porewater-exposed sample was representative of the sample-set it was taken from (pellets used for carbon and oxygen mass spectrometry were not examined using SEM prior to analysis), it should, at least at the pellet surface, have contained abundant aragonite needles (see previous sections). If, as the evidence appears to indicate, these needles grew after excretion (*i.e.*, under porewater conditions), they are predicted to have stable isotope ratios indicative of precipitation in equilibrium with porewaters. Assuming $\delta^{18}O$ and $\delta^{13}C$ values of porewater at the sample burial site do not differ greatly from those reported from elsewhere in the Bahamas by Walter *et al*. (1993), this means aragonite that grew after excretion should cause a shift in bulk sample $\delta^{18}O$ and $\delta^{13}C$ values towards porewater equilibrium. The fact that such a shift is not evident, albeit from a very limited number of data points (n = 1), indicates that aragonite needles are either: i) restricted to pellet surfaces and are actually a volumetrically minor phase; ii) developed via recrystallisation and/or neomorphism of excreted phases, from which they inherited the distinctive gut carbonate stable isotope signature; or iii) grown within the piscine gut. As pointed out in a previous section, the latter is highly improbable, and there is no textural evidence indicative of recrystallisation, so it appears likely that, after 3 months in porewater, newly precipitated aragonite is restricted to a visually striking, but proportionally limited, distribution at pellet surfaces.

7.4 PLATFORM-WIDE GUT CARBONATE PRODUCTION MODELLING

The rapid dissolution of excreted amorphous carbonate phases in seawater, together with the fact that several fish species investigated in this study produce substantial quantities of such phases (Chapters 2 and 3), means that a considerable proportion of gut carbonates excreted in the Bahamas may be of little or no sedimentary significance. The present section attempts to quantify the amount of carbonate lost to rapid dissolution based on estimates of relative volumetric abundances of different precipitate forms for each species documented in Chapter 2, measured production rates

from several of these fish species, and fish community structure in a range of habitats surveyed at various sites in the Bahamas[5]. Using these data, the relative abundance of amorphous carbonate excreted in various habitats in shallow waters surrounding eight Bahamian islands is estimated, and weighted means for each habitat across all islands surveyed are calculated and taken to be representative of platform-wide patterns of gut carbonate excretion (Table 7.6). Note that, because production rate data are calculated by weight, whereas relative abundances are estimated by volume, the results that follow are derived by necessarily assuming that abundance by weight and by volume are equivalent. Given that most precipitates are of closely related phases, their densities will be broadly similar and this assumption is therefore reasonable.

Because amorphous carbonate production varies according to producing species, and because fish community structure varies according to habitat, the results reveal large differences in the proportion of amorphous carbonate excreted according to specific environments. For example, it is estimated that, on average, fish communities inhabiting seagrass meadows produce carbonates that comprise 39.9 % amorphous phases, with the average value for each island surveyed always greater than 30.0 %. In contrast, fish that inhabit fringing mangroves are estimated to produce carbonates that comprise, on average, 1.4 % amorphous carbonates, with average values per island consistently below 3.0% (Table 7.6). These data therefore indicate that carbonates produced in seagrass and bare sand settings are of less sedimentary significance than previously thought (Perry *et al*., 2011), with about 35–40 % estimated to be lost to rapid dissolution. Conversely, reefs, hardgrounds, and fringing mangroves tend to host species that produce a greater proportion of crystalline forms, and platform-wide averages for production in those habitats typically involve <10 % amorphous carbonate (and as low as 1.4 %).

[5] Dr Alistair Harborne (University of Queensland) provided all fish community structure and habitat data, and also generated total excretion outputs based on production rates determined in this study.

Table 7.6 *Amorphous carbonate production as percent abundance (by volume) of total carbonates excreted in a range of platform settings (arranged by habitat and by island) within the Bahamas (see footnotes for further explanation).*

	Relative abundance (by volume) by island										
Habitat	Abaco	Andros	Bimini	Conception	Eleuthera	Exumas	Lee Stocking	San Salvador	All-island weighted average abundance	Total production (Mkg·yr^{-1})	Total dissolved [1, 2] (Mkg·yr^{-1})
Seagrass	**40.0**/8	**51.5**/6	**41.6**/9	n/d	n/d	n/d	**30.0**/6	**30.9**/3	39.9	2.11	0.84
Mangrove	**1.6**/3	**1.1**/2	**2.4**/3	n/d	n/d	n/d	**1.7**/3	**0.6**/4	1.4	0.98	0.01
Reef	**12.0**/7	**6.1**/18	**9.9**/1	**13.8**/4	**5.9**/4	**5.6**/7	**2.3**/6	**11.5**/15	8.2	0.90	0.07
Bare sand	n/d	**35.2**/2	n/d	n/d	n/d	n/d	n/d	n/d	35.5	0.04	0.01
Hardground	**6.6**/7	**11.0**/10	**12.8**/12	n/d	n/d	**8.6**/21	**8.6**/3	**14.5**/4	10.1	2.84	0.29
								Platform-wide totals	17.9	6.87	1.23

Data is entered in the following format: **(mean percent abundance)**/(number of sites from which data was obtained). Where no data was obtained, this is denoted by "n/d".

[1]Values for total dissolved carbonates relate to amorphous phases, which dissolve within weeks of excretion. These totals do not include dissolution of other gut-precipitated carbonates, which either do not dissolve, or do so over considerably longer time-scales.

[2]Different approaches to data generation dictate that total dissolved phases are calculated based on the assumption that volumetric and weight percent values are equivalent. Because abundance estimates are quite crude, and because phases are generally similar and probably have similar densities, this is probably a reasonable assumption.

The former two habitats, where losses to dissolution are large, represent more than 95 % of the total shallow platform area in the Bahamas (Perry *et al*., 2011), but they typically host a smaller fish biomass than other habitats, thus yielding lower production rates per unit area. Consequently, fish-derived carbonates excreted in these extensive habitats are estimated to account for less than a third of all carbonates excreted in shallow platform settings of the Bahamas, and the proportion of total excreted carbonates lost to dissolution across all habitats is therefore much lower than in these habitats. By combining the production rates determined in the present study with fish community structure data from numerous surveys, it was possible to estimate total carbonate production per year in the main habitat categories[6] (*i.e.*, those delineated by Perry *et al*., 2011). These production estimates are presented in Table 7.6, and, although yielding a total that is approximately 13 % higher, they are remarkably similar to the estimates of Perry *et al*. (2011). Applying all-island

[6] Dr Alistair. Harborne (University of Queensland) provided all fish community structure and habitat data, and also generated total excretion outputs based on production rates determined in this study.

weighted average abundance values, it is estimated that ~18 % of all excreted carbonates (or ~1.2 $Mkg \cdot yr^{-1}$) are amorphous and are therefore likely to be of little sedimentary significance as most will be lost to rapid dissolution.

It is worth mentioning, however, that these data represent only a crude estimate of the amount of carbonate lost to rapid dissolution. For example, estimated relative abundances (Appendix VIII) do not include amorphous phases for checkered puffer and redtail parrotfish because the presence of obviously amorphous carbonates was rarely confirmed by visual observations, making their quantification in these samples difficult (despite spectrographic evidence verifying their presence; Chapter 3). Estimates of ACC abundance in the products of bonefish may be similarly conservative given that a much larger proportion of excreted carbonate was identified as being amorphous in the present study than it was in Chapter 2, and it is further acknowledged that the unknown amount of bonefish-derived ACC that crystallises to calcite after excretion is not accounted for here. In addition, as stated in the methodology, applying these abundances across species not yet investigated with respect to gut carbonate production required that assumptions were made about which species produced which precipitation products (see Chapter 8). Moreover, it is not yet known what proportion of precipitates presumed to be crystalline in the abundance estimates used here would actually be amorphous in normal natural circumstances due to the effects of feeding, nor is the preservation potential of these phosphate-rich products known (see Chapter 4).

In contrast, platform-wide production of amorphous phases is likely to be overestimated because production data for reefal habitats (Perry *et al*., 2011) are conservative; they were calculated without taking into account the areal extent of patch reefs. If higher values for total production are used for reefal habitats, the relatively low estimated values for abundance of amorphous phases in these settings (Table 7.6) means percent loss to dissolution will be lower than estimated. Nevertheless, the available data indicate that amorphous carbonate represents a substantial proportion of total excreted carbonates, and should therefore be considered when assessments of the contribution of fish to carbonate sediments are being made.

In addition to amorphous carbonates, production data were used to estimate the platform-wide abundance of high-Mg calcite monocrystalline ellipsoids and rods excreted by fish. Using a similar series of calculations, estimates (shown in Table 7.7) indicate that these precipitation products account for approximately a quarter to a third of all excreted carbonates in bare sand and seagrass habitats, slightly more than a half in reefal habitats and hardgrounds, and more than 90 % in fringing mangroves. Consequently, an estimated 53 % of all gut carbonates excreted across Bahamian shallow platform settings is high-Mg calcite ellipsoids and rods. Data arising in this chapter indicate that these precipitation products are the least stable of excreted crystalline forms, and because they are estimated here to represent the largest fraction of excreted carbonates, their longer-term fate is of particular interest. This is discussed further in section 7.5.

Table 7.7 *High-Mg calcite ellipsoid production as percent abundance (by volume) of total carbonates excreted in a range of platform settings (arranged by habitat and by island) within the Bahamas (see footnotes for further explanation).*

	Relative abundance (by volume) by island										
Habitat	Abaco	Andros	Bimini	Conception	Eleuthera	Exumas	Lee Stocking	San Salvador	weighted average abundance	Total production (Mkg·yr^{-1})	Total ellipsoids /rods[1] (Mkg·yr^{-1})
Seagrass	**26.4**/8	**8.1**/6	**15.9**/9	n/d	n/d	n/d	**37.0**/6	**35.1**/3	22.8	2.11	0.48
Mangrove	**88.4**/3	**97.5**/2	**88.4**/3	n/d	n/d	n/d	**94.7**/3	**93.9**/4	92.3	0.98	0.90
Reef	**54.0**/7	**48.9**/18	**60.8**/1	**30.8**/4	**64.1**/4	**71.2**/7	**88.0**/6	**47.0**/15	55.3	0.90	0.50
Bare sand	n/d	**32.3**/2	n/d	n/d	n/d	n/d	n/d	n/d	32.3	0.04	0.01
Hardground	**64.9**/7	**52.6**/10	**63.4**/12	n/d	n/d	**66.0**/21	**60.2**/3	**43.1**/4	60.7	2.84	1.73
								Platform-wide totals	52.7	6.87	3.62

Data is entered in the following format: **(mean percent abundance)**/(number of sites from which data was obtained). Where no data was obtained, this is denoted by "n/d".

[1]Different approaches to data generation dictate that total excreted ellipsoids are calculated based on the assumption that volumetric and weight percent values are equivalent. Because abundance estimates are quite crude, and because phases are generally similar and probably have similar densities, this is probably a reasonable assumption.

Other crystalline forms, which the present chapter indicates are relatively stable in the short-term, represent approximately 30 % of total excreted carbonates across the Bahamian platform. However, the apparent post-excretion growth of aragonite needles associated with some fish-derived carbonates has not been quantified. If such needle growth is widely associated with the production

of fish-derived carbonates, and if these needles are assumed to be reasonably stable in shallow marine settings, the current best estimate for production of 'stable' (*i.e.*, not amorphous) forms by fish (5.7 Mkg·yr^{-1}; see Table 7.6) may be rather conservative.

7.5 DISCUSSION

7.5.1 Short-term fate of fish-derived carbonates

Data arising in the present study indicate that several important chemical changes occur in fish-derived carbonates within the first few months following their excretion; these changes broadly following the pattern of expected changes based on previous theoretical and experimental work (discussed in Chapter 1). Briefly, observed changes include: 1) loss of all amorphous carbonate phases, mostly to dissolution, although a proportion of ACC appears to crystallise to calcite; 2) loss of all brucite, probably to dissolution; 3) apparent preferential dissolution of the $MgCO_3$ component of Mg calcite ellipsoids that initially contain more than about 20 mol% $MgCO_3$, as well as possible concomitant recrystallisation of these phases; 4) apparent post-excretion development of mud-grade aragonite needles and related morphotypes in some samples; and 5) loss of monohydrocalcite, either to dissolution or recrystallisation to calcite, in certain situations. Of these changes, the first two typically proceed to completion within a few days of excretion, whereas the last three were most obvious after three months in porewater conditions and/or artificial seawater (and were either not observed, or had proceeded to a lesser degree, after 12 days in seawater). In some cases (*e.g.*, high-Mg calcite monocrystalline ellipsoids) these changes were apparently restricted to external regions of pellets, where interactions between solid phases and seawater solutions were presumably greatest, but it must be likely that longer exposure periods would result in more pervasive alteration. Some of the possible factors controlling these changes are shown schematically in Fig. 7.27, and are discussed in more detail below. Based on the results of this study, a hypothesis concerning the longer term fate of fish-derived carbonates as sedimentary particles is considered in Chapter 8.

These chemical changes also appear to have some influence on the grain size properties of some fish-derived carbonates. For example, rapid dissolution of amorphous magnesium carbonate (AMC) from pellets where it is the dominant phase results in the release of subsidiary rhombohedra and polycrystalline spheres as individual silt-grade particles and, in some cases, silt- to sand-grade clusters of intergrown particles; original pellets being obliterated. Dissolution of amorphous calcium carbonates (ACC) may result in a similar release of individual particles. Conversely, although apparent recrystallisation associated with high-Mg calcite ellipsoids is of limited extent and has little effect on pellet robustness in the first few months after exposure (*i.e.*, pellets still readily disaggregate), the potential for more pervasive recrystallisation to occur over longer periods suggests that pellet robustness could eventually increase as progressive recrystallisation acts to 'weld' component crystals together; this being a similar process to that proposed in Chapter 6. In addition, the apparent development of abundant low-Mg calcite spheres with diameters in the range 50–225 μm is tentatively attributed to post-excretion crystallisation of ACC; a process which appears to generate individual particles that are much larger (very fine to fine sand-grade) than any previously associated with fish-derived carbonates.

7.5.1.1 Influence of organic coatings

Although the changes documented herein clearly have the potential to influence the character and sedimentary significance of fish-derived carbonates – a point well illustrated by the fact that an estimated 18 % of all carbonate excreted by fish in the Bahamas is amorphous, and is thus likely to rapidly dissolve – it is worth considering which of these changes might actually occur under natural circumstances; *i.e.*, did any of the documented changes occur exclusively in carbonates that had been cleaned with sodium hypochlorite prior to exposure?

Several changes will evidently occur under normal natural circumstances; amorphous carbonates and brucite seemingly undergoing complete alteration in all samples prior to any cleaning having taken place. However, changes observed in samples produced by schoolmaster snapper were of considerably greater magnitude in pellets that had been cleaned (two replicates exposed to

porewater conditions and two exposed to artificial seawater) than they were in uncleaned pellets (two replicates exposed to porewater conditions). Specifically, these differences concern $MgCO_3$ contents, which were greatly reduced in many crystals in cleaned samples (values are commonly in the range 8–15 mol%) but were generally similar to those at the point of excretion in uncleaned samples (typically >15 mol%). Likewise, extensive development of aragonite needles in association with carbonates produced by yellowfin mojarra was noted in both replicate samples that were cleaned prior to porewater exposure, but similar crystals were much less common in samples that were not cleaned prior to exposure.

These observations indicate that the removal of organic matter prior to porewater and artificial seawater exposures may have been an important factor in the development of new textures after excretion. One explanation for this might be that uncleaned samples were protected from exposure to surrounding seawater and porewater solutions by a physical (mucosal) barrier, which would have been removed from samples that were cleaned. However, visual observations indicated that mucus coatings largely degraded within the first few days after excretion, and it is thus difficult (though not impossible) to conceive that all crystals would have been kept out of contact with seawater. Alternatively, the occurrence of phosphates, which can inhibit carbonate growth reactions (Morse, 1974), at elevated concentrations in porewater-exposed samples from both of these species raises the possibility that carbonate dissolution and growth were inhibited by its adsorption at crystal surfaces; a process which could have been promoted by the presence of residual organics in uncleaned samples. However, the fact that phosphate concentrations are elevated in cleaned and uncleaned samples exposed to porewater (and artificial seawater) appears to rule it out as the main reaction inhibitor in this case. A third possibility, discussed briefly in Chapter 1, concerns the surface adsorption of microbes and/or organic compounds; a process which is known to exert a considerable influence on carbonate reaction kinetics (Thomas *et al*., 1993; Reddy and Hoch, 2000; Lüttge and Conrad, 2004; Lin *et al*., 2005; Reddy, 2012). It is conceivable that the differences observed herein between cleaned and uncleaned samples could be due to the cleaning process preventing extensive adsorption of organic components at crystal surfaces. In contrast, organic

compounds and/or microbial cells could have been extensively adsorbed at crystal surfaces in uncleaned samples, thus inhibiting extensive dissolution or growth of carbonates upon exposure to porewaters.

Regardless of the mechanisms causing these differences, the data indicate that development of aragonite needles and lowering of $MgCO_3$ contents in high-Mg calcite probably occurred to a minor extent during porewater exposure of uncleaned samples, and it is possible that this was due to the inhibitory influence of organic coatings eventually being overcome. That being the case, it is possible that the changes observed here, although accelerated by the early removal of organic matter, are representative of what might actually occur under natural circumstances.

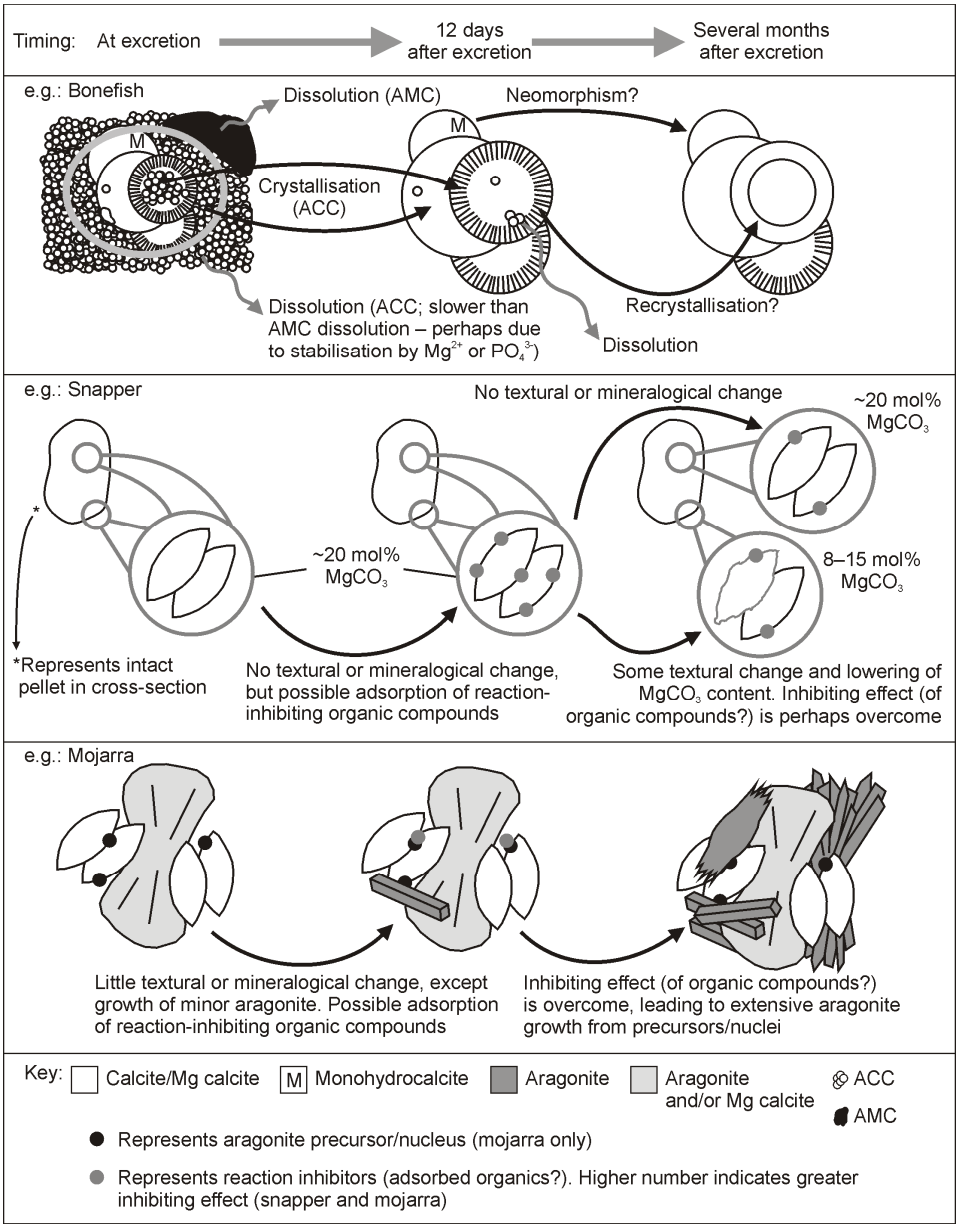

Figure 7.27 *Schematic diagrams showing some of the major changes that take place in fish-derived carbonates after excretion, the approximate timescales over which these occur, and factors that might exert some control on the rate of changes. In the example shown for bonefish gut precipitates, the oval highlights ACC that might crystallise; ACC outside of the oval is considered likely to dissolve. See main text for more details regarding these controls.*

7.5.1.2 Factors influencing the post-excretion formation of aragonite and calcite

An interesting feature regarding the aragonite formed in samples produced by yellowfin mojarra is its morphology. In many cases, aragonite that apparently formed after excretion exhibits a needle-like morphology with straight edges and blunt terminations. These crystals are of particular interest as they closely resemble needles that commonly occur in Bahamian surface sediments (*e.g.*, see Fig 6.11 B), and their formation here suggests that fish may represent a previously unrecognised source

of sedimentary aragonite needles along with traditionally cited sources such as calcareous green algae (Lowenstam and Epstein, 1957) and abiotic precipitation (MIlliman *et al*., 1993). Aragonite grows with similar needle-like morphology in several other situations in shallow sub-tropical marine settings (Loreau, 1982; Shinn *et al*., 1989; Morse *et al*., 2007), so the fact it develops with these morphologies in seawater solutions after excretion is not surprising.

However, the occurrence of several other needle morphologies (*e.g.*, dumbbell- and ellipsoid-shaped aggregates) that are seemingly unknown from Bahamian surface sediments requires further explanation. Such morphotypes are rarely or never described from modern marine surface sediments, and their formation here therefore suggests some control that does not affect other sources of marine aragonite; *i.e.*, a control that is seemingly unique to fish-derived carbonates. One possibility could be an organic control (*e.g.*, Van der Leeden and Van Rosmalen, 1987), but the fact that most of these crystals were observed in samples that had been cleaned prior to exposure should preclude this (however, note that organic molecules commonly occur with these carbonates even after cleaning – see Chapter 3). A second possibility is that these crystals grew from precursor particles or nuclei that dictated the final morphology. As discussed in Chapter 2, crystal growth inhibition can lead to the binding of sub-critical nuclei in order to facilitate continued crystal growth, with the result being that crystals grow as aggregates (Prieto *et al*., 1994), and it is reasonable to speculate that such a mechanism occurs with aragonite in fish. High Mg^{2+} concentrations in the intestinal fluids of marine teleosts (Wilson *et al*., 1996) should inhibit calcite growth and instead favour aragonite growth (Falini *et al*., 1994). However, the fact that Mg calcite is the dominant precipitation product perhaps suggests that aragonite growth is also inhibited in the piscine gut, and in some cases it is possible that this could lead to the binding of sub-critical aragonite nuclei that develop as aragonite needles after excretion.

An additional point worth discussing is the apparent crystallisation of some ACC to calcite after excretion. Data arising from this study clearly indicate that all AMC and a large proportion of ACC rapidly dissolve after excretion. A notable difference between the behaviour of these two phases,

however, is that the former appears to undergo complete dissolution within a few days, whereas dissolution of the latter is apparently not complete until a few weeks after excretion, and is apparently accompanied by partial crystallisation. In many cases documented in the existing literature, ACC is highly unstable and undergoes complete alteration (dissolution or crystallisation) within a few hours or days of its formation (Beniash *et al*., 1997; Radha *et al*., 2010). However, several workers propose that ACC might be stabilised by the presence of phosphate (Raz *et al*., 2002) and magnesium (Loste *et al*., 2003), and that such stabilisation might facilitate its crystallisation. Given that ACC nanospheres produced by bonefish contain both high concentrations of magnesium (typically 30–37 mol% $MgCO_3$) and elevated concentrations of phosphate (Fig. 7.24), it is possible that one or both of these properties acts to stabilise this phase after excretion, and that the resulting inhibition of dissolution allows some of it to crystallise as calcite. This being the case, it is possible that nanospheres produced by great barracuda might undergo similar transformations upon exposure to seawater, although this is somewhat uncertain given the substantially higher phosphorus contents of those precipitates measured in Chapter 2.

7.5.1.3 Implications in a wider range of porewater settings

An important caveat regarding interpretation of the results presented herein is that they are only relevant to porewater conditions at the sample burial site. This site was chosen on the basis that it represents a typical patch reef setting within Eleuthera Sound. Because patch reefs are focal points for high fish biomass, they should represent areas of abundant gut carbonate production, much of which should be retained locally given the quiescent conditions that are common around these habitats. Porewater conditions determined at this site are characterised as being of low pH and similar total alkalinity relative to overlying seawater (Fig. 7.28), and, while they are super-saturated with respect to most common carbonate minerals (including Mg calcite with more than 18 mol% $MgCO_3$ – so it is not surprising that many of the high-Mg calcite precipitates examined herein are well-preserved), they are consequently slightly less super-saturated than surface seawater. These data are in good agreement with those of Morse *et al*. (1985) for several coarse sediments

containing reasonably low amounts of organic matter (Fig. 7.28), and the results of the present study should therefore be relevant to fish-derived carbonate preservation where it is incorporated within sediments that have low organic contents and are well-connected with overlying waters.

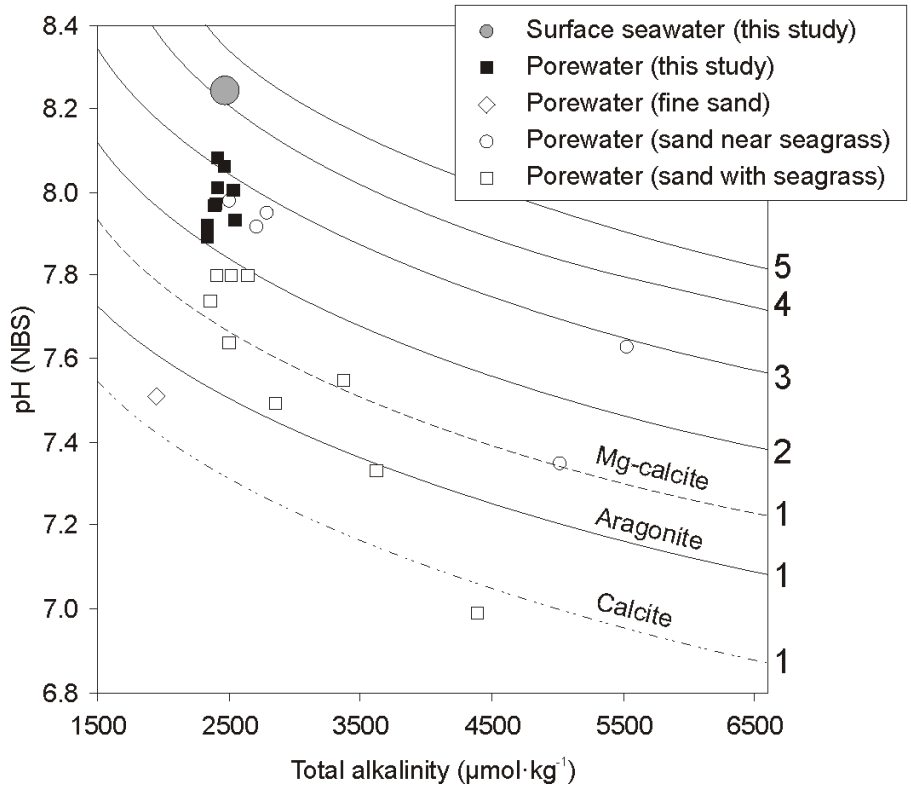

Figure 7.28 *Plot of pH against total alkalinity for seawater and porewater samples from shallow sites in the Bahamas (modified after Morse et al., 1985). Solid lines show aragonite saturation states (indicated at right of each line); dashed lines show calcite and Mg calcite (18 mol% $MgCO_3$) saturation states, as labelled. All curves plotted following calculations made using CO2SYS software, with the exception of Mg calcite which is based on the data of Morse et al. (1985). Porewater data from this study is for fine sand with sparse seagrass. Other porewater data is from Morse et al. (1985).*

However, the data of Morse *et al*. (1985) further indicate that conditions of undersaturation are common in some Bahamian porewaters, particularly those associated with organic-rich sands (*e.g.*, beneath seagrass beds; Fig. 7.28) and organic-poor fine sediments, where undersaturation is presumably caused by decomposition of organic matter via various aerobic and anaerobic pathways (see Chapter 1). It is common, at least in Eleuthera Sound, for substrates near patch reefs to be partially covered by seagrass of varying (but commonly high) density, and, due to the strong sediment baffling effect exerted by seagrass meadows (Scoffin, 1970), it is likely that some fish-derived carbonates produced in these areas will be deposited within these substrates, particularly in

cases where pellets disaggregate and release their component mud-grade particles (Chapter 6). This example serves to demonstrate that situations exist whereby fish-derived carbonates will be incorporated in surface sediments where porewater is likely to be characterised by considerably lower saturation states than those of the porewaters that carbonates were exposed to in the present study. It is therefore recommended that further work be conducted to assess the short-term fate of fish-derived carbonates in a wider range of depositional settings.

7.5.2 Implications of manganese precipitation in artificial seawater

Although elevated manganese concentrations and resultant interactions with fish-derived carbonates were accidental, with detailed information about its mode of precipitation being beyond the scope of this study, the observation that it precipitated more readily in the presence of fish-derived carbonates (at least those produced by schoolmaster snapper, black grouper, and bonefish) than in the presence of other common marine carbonates is interesting and merits further consideration. Moreover, manganese is known to exert great influence on the kinetics of calcite dissolution and precipitation in some scenarios (Vinson *et al*., 2007), and elevated concentrations in artificial seawater used in the present study must therefore raise questions about the applicability of findings arising from these experiments to events that take place in nature.

Numerous studies document various interactions between dissolved manganese and calcite in marine settings, where the former can either: i) be adsorbed at the calcite surface, frequently being resorbed as calcite dissolves (Martin and Knauer, 1983); ii) be adsorbed to the point of surface saturation, at which point precipitation of a discrete $MnCO_3$ phase may proceed (McBride, 1979); iii) form a solid solution with calcite, $Mn_xCa_{1-x}CO_3$ (Wartel *et al*., 1991); or iv) form a coating on existing minerals in the form of Mn(IV) oxides and oxyhydroxides (Mucci, 2004). The occurrence of manganese in the present study as a patchy orange-brown surface coating on pellets is remarkably similar to that described by Mucci (2004) in a similar experiment conducted in deionised water, which he considered to be a manganese oxide.

The oxidation of manganese requires a catalyst, and Boynton (1971) shows that calcite surfaces in inorganic oxic conditions (as was the case in artificial seawater experiments of the present study) can act as such. Loeppert and Hossner (1984) show that calcite similarly acts as a catalyst for the oxidation of Fe(II) in solution, and they suggest that two equivalents of $CaCO_3$ are dissolved per mole of Fe^{2+} neutralised, according to the following equations:

(1) $$4Fe^{2+} + O_2 + 2H_2O \rightarrow FeOOH + 8H^+$$ *equation* 7.8

(2) $$8H^+ + 4CaCO_3 \rightarrow 4Ca^{2+} + 4H_2O + 4CO_2$$ *equation* 7.9

where calcite is assumed to be the sink for liberated protons. A similar mechanism has also been described in deep marine settings, where calcite is thought to act as a surface that adsorbs Mn(II) and facilitates its oxidation to Mn(IV), thus nucleating manganese precipitation that eventually forms manganese crusts and nodules (Halbach, 1986; Konchisky and Halbach, 1995; Wang *et al*., 2009). If a similar reaction occurred in the present study to facilitate precipitation of a manganese oxide on calcite surfaces, it would suggest that fish-derived carbonates must exhibit a property that promotes higher reaction rates than other common marine carbonates. As the interactions described above require both the surface adsorption of metals, and the dissolution of calcite to occur, this result could be an indication of one or both of the following regarding fish-derived carbonates: i) they have a greater abundance of surface sites available for Mn(II) adsorption than other common marine carbonates; and ii) they are more soluble than other common marine carbonates. The latter would be in good agreement with available solubility data for fish-derived carbonates (high-Mg calcite ellipsoids) that demonstrate they can be highly soluble compared with aragonite (Woosley *et al*., 2012), and it is also in good agreement with the finding that high-Mg calcite ellipsoids appear to undergo partial dissolution within a few months when exposed to aragonite-supersaturated porewater. However, it is perhaps in less good agreement with findings that suggest calcite spheres produced by bonefish are reasonably stable in seawater (and theoretically should be more stable than aragonite given their low $MgCO_3$ contents in some cases). Nevertheless, manganese oxidation in samples produced by this species could occur via reactions with monohydrocalcite, or possibly via incorporation in calcite as it crystallised from ACC.

Because the manganese precipitates formed in this study have not been formally identified as Mn(IV) oxide surface coatings, it is prudent to consider other possibilities. These generally involve either surface adsorption of manganese on calcite or co-precipitation of $MnCO_3$ with $CaCO_3$ following partial dissolution of the former. In either case, the differences between fish-derived carbonates and other common marine carbonates that drive preferential precipitation of manganese in the presence of the former are likely to be the same as proposed above.

Although these findings may not be applicable in surface seawater in the Bahamas, where concentrations of manganese (and iron) are low, they may have implications for fish-derived carbonates incorporated within certain oxidising surface sediments where manganese (and iron) can occur at relatively high concentrations (Presley *et al*., 1967; Calvert and Price, 1972). In such settings it is possible that fish-derived carbonates could play an important role in fixing certain heavy metals. Furthermore, and relevant to Bahamian settings, if the capacity to promote precipitation of manganese oxides is due to greater availability of surface sites for its adsorption, this could mean fish-derived carbonates also have the potential to adsorb other chemical species, such as phosphate. This could explain the apparent phosphate increases in carbonates produced by schoolmaster snapper and yellowfin mojarra after their exposure to porewater, and because phosphate is known to inhibit calcite precipitation and dissolution in seawater (Morse, 1974), such a process could play an important role in stabilising these carbonates.

With regard to how elevated manganese concentrations might have affected the kinetics of calcite dissolution and/or precipitation during exposure experiments, Vinson *et al*. (2007) show that in high pH (>8.5) solutions with high carbonate (~0.1×10^{-3} molal; *i.e.*, the same order of magnitude as typical seawater concentrations) and manganese concentrations ($0.5–2.0 \times 10^{-6}$ molal), dissolution of calcite is inhibited (to almost complete arrest at the highest manganese concentrations), probably by the formation of $MnCO_3$ ion pairs at the calcite–water interface that act to stabilise reactive sites. However, those workers also show that the effect of manganese is strongly dependent on carbonate concentration, and that it may even enhance dissolution of calcite

in solutions where carbonate is absent. Whilst their findings demonstrate the potential that very low concentrations of dissolved manganese have to influence calcite stability, the solutions they use are unlike seawater and their results may not be applicable here. Indeed, Franklin and Morse (1983) find that surface adsorption of manganese on calcite, and subsequent nucleation of $MnCO_3$ precipitates, is inhibited in seawater, probably due to the presence of magnesium; a factor that was absent in the study by Vinson *et al*. (2007). Nevertheless, observations from the present study appear to suggest that manganese does interact with some (only fish-derived?) carbonates in some seawater solutions. The interactions of manganese with calcite in seawater are clearly complex and not well understood, but it appears they have the potential to exert strong influence on carbonate precipitation and dissolution kinetics. Thus, while the results obtained herein are generally similar for samples exposed to both natural porewater and Mn-rich artificial seawater, results from the latter are qualified as being obtained using a solution in which the kinetic effect of elevated manganese concentrations is not known. It is therefore particularly pertinent to exercise caution when considering the observation that monohydrocalcite underwent complete alteration in artificial seawater but not in porewater. Although this result is not surprising given the low stability of monohydrocalcite in seawater, it is possible that the disparity in results is caused by the presence of manganese.

To summarise the findings relating to elevated manganese in artificial seawater, although its presence may have had an unknown effect on the manner in which fish-derived carbonates exposed to artificial seawater were preserved, its preferential precipitation with fish-derived carbonates rather than other sedimentary carbonates is possibly indicative that the former have abundant surface sites available for adsorption of impurities. With many impurities having the potential to inhibit dissolution of the carbonates on which they are adsorbed (*e.g.*, Morse, 1974; Vinson, 2007), the preservation potential of fish-derived carbonates incorporated in surface sediments may depend not only on variations in sediment grain size and organic matter content (*i.e.*, factors that dictate porewater saturation states), but also on the concentration of heavy metals and nutrients available in interstitial waters for surface adsorption.

7.6 CONCLUSIONS

The results of the present study show that a significant proportion of fish-derived carbonates are unstable in surface seawater and shallow porewater of sub-tropical shallow carbonate settings, with several phases either undergoing complete dissolution within a few days, or undergoing partial dissolution and possible reprecipitation/recrystallisation within the first few months. However, other phases are preserved in their excreted forms after a few months, and are considered to represent stable forms in these settings. Moreover, precipitates produced by some species appear to act as nuclei for post-excretion development of aragonite needles that are texturally very similar to those observed in Bahamian surface sediments. The volume of needles produced via this process relative to the volume of excreted carbonate has not been quantified, but its observation here demands that further work be conducted in order to assess fish-derived carbonates as a potentially important source of aragonite needles in some sedimentary settings. An additional, and potentially important, finding arising from this work is that some of these processes appear to be inhibited when mucus coatings associated with excreted carbonates are left to degrade naturally. Post-excretion aragonite growth and high-Mg calcite dissolution is considerably more pronounced in samples that were cleaned prior to porewater exposure than in samples that were not cleaned, although the data suggest that such changes have nevertheless begun to occur in uncleaned samples, indicating that reaction-inhibiting processes might eventually be overcome.

The key post-excretion changes observed in the first three months, and their estimated platform-wide significance (where known) are as follows:

1. Complete dissolution of AMC and extensive dissolution of ACC within a few days of excretion, accounting for an estimated 18 % of total excreted carbonate.
2. Probable crystallisation of some ACC to calcite spheres, possibly promoted by presence of a stabilising phase (phosphate) in ACC at excretion.
3. Complete dissolution of brucite (a volumetrically minor phase).
4. Increased size of some calcite spheres, possibly as a result of ACC crystallisation.

5. Preferential dissolution of $MgCO_3$ from high-Mg calcite ellipsoids with more than about 20 mol% $MgCO_3$, possibly accompanied by recrystallisation. This process is apparently limited to surfaces of intact pellets, probably due to restricted exchange between solids and solutions in internal regions of pellets. However, it may be pervasive over longer periods, in which case an estimated 53 % of excreted carbonates might be altered in this manner.
6. Development of aragonite needles in samples that commonly contain small amounts of aragonite at excretion (volumetric significance not known).
7. With the exception of sphere enlargement, no mineralogical or compositional changes are observed in most low- and high-Mg calcite rhombohedra or polycrystalline spheres and dumbbells; these precipitation products are presumably stable in surface seawater and $CaCO_3$-supersaturated porewater. However, rare spheres exhibiting massive textures in porewater-exposed samples suggest some recrystallisation may occur in polycrystalline particles.

Finally, preferential precipitation of manganese in association with fish-derived carbonates over other sedimentary mud-grade carbonates possibly indicates that the former have a greater abundance of surface sites available for adsorption of impurities, some of which have the potential to inhibit crystal dissolution and/or growth processes. The preservation pathways of fish-derived carbonates may therefore depend not only on $CaCO_3$ saturation states of the fluids they are exposed to after excretion, but also on the chemical composition of those solutions and the availability of potential adsorbates.

Chapter 8: Summary of the present work and recommendations for the future

8.1 INTRODUCTION

This final chapter of this thesis is divided into two parts. The first of these provides a summary of the key findings reported in the preceding chapters regarding the production and short-term post-excretion fates of fish-derived carbonates in sub-tropical shallow marine carbonate platform settings. On the basis of these data, an attempt is also made to assess the likely longer-term preservation potential of these carbonates on the order of years to centuries. In addition to summarising the production and fate of fish-derived carbonates in modern sub-tropical marine settings, this section will also briefly consider (as a guide to possible areas of future research) their possible production and fate in comparable environmental settings over geological timescales.

The main aim of the second part of this summary is to provide a series of recommendations for future work. Most of these target questions arising in the present volume and are designed to elucidate additional characteristics of fish-derived carbonates and their significance as sedimentary particles in sub-tropical settings, at both local (*i.e.*, within the Bahamas) and global scales, thus extending and expanding the research themes of this thesis.

One of these recommendations highlights an issue that has come to be recognised as a fundamental point underlining the whole area of research regarding the production and sedimentary significance of fish-derived carbonates: the factors that result in different fish species producing different precipitation products. This among-species variation in precipitation products has implications for production modelling purposes, and understanding the mechanisms that cause this variation is crucial to facilitate proper determination of the relative proportions of each precipitation product

that enter sedimentary systems. However, it is acknowledged that these mechanisms are likely to be complex and, even if they can be understood, they may be difficult to apply across entire fish communities without studying each species separately. Such an eventuality would clearly be impractical, so an alternative approach is postulated here (and was utilised in Chapter 7): to assume that the different factors, whatever they may be, are shared at certain taxonomic levels, thus facilitating prediction of precipitation products across entire fish communities on the basis of existing data. Data gathered during the course of the present research afford the opportunity to begin to examine this idea, and the outcomes are presented here in the hope they will provide a valuable platform on which to base future work.

8.2 SUMMARY OF OUTCOMES OF PRESENT WORK

8.2.1 Characterisation

Prior to this study, knowledge of carbonate production by marine teleost fish in shallow sub-tropical settings was limited to 11 fish species, which were shown to excrete mostly high-Mg calcite (containing 18–39 mol% $MgCO_3$) and minor amounts of aragonite as mud-grade carbonates exhibiting morphologies that are seemingly unique in open marine environments (Perry *et al*., 2011). Measured production rates indicated that these crystals might make significant contributions to mud-grade carbonate sediments in certain platform-top settings, and examination of the finest fraction of surficial sediment from Eleuthera Sound, the Bahamas, revealed the presence of numerous particles that closely resemble fish-derived carbonates, thus supporting this assertion. However, the observations made by Perry *et al*. (2011) left several questions relevant to sediment production by marine fish unanswered, these including: i) had the full range of morphological, mineralogical, and compositional characteristics of fish-derived carbonates been documented?; ii) is crystal morphology specific to mineralogy?; iii) do other criteria exist that might aid confirmation of the presence of fish-derived carbonates in surface sediment samples?; iv) specifically, which sediment size fraction(s) do fish-derived carbonates contribute to?; and v) given

that the characteristics of gut precipitates are species-dependent, is it possible to determine specific controls on precipitation?

The first five data chapters in the thesis (Chapters 2–6) attempt to resolve these issues by: i) expanding the range of Caribbean fish species (to 22) for which gut carbonates have been characterised, and examining the full suite of precipitation products in greater detail (Chapter 2); ii) characterising, for the first time, carbonates excreted by recently fed fish as well as starved fish (Chapter 4); iii) utilising alternative analytical approaches (Fourier transform infrared spectroscopy and mass spectrometry) to determine the presence of previously unrecognised phases and to describe additional properties of already documented crystals (*e.g.*, degree of crystallinity and stable carbon and oxygen isotope compositions; Chapters 3 and 5); and iii) making detailed assessments of the size of excreted crystals using digital image analysis software (Chapter 6). Together, the results of these investigations are also used to assess whether or not fish body mass and/or dietary habits may influence the characteristics of excreted products.

Morphological, mineralogical, and compositional data arising from these studies are summarised in Fig. 8.1 for each of the main precipitate forms observed at the point of excretion, which are considerably more varied than previously thought (Perry *et al*., 2011). In addition to previously described ellipsoids, dumbbells, and spheres, it is shown that rhombohedral crystals are commonly excreted by some fish species, as are polycrystalline ellipsoids, needle-like and spherulitic crystals, nano-scale spheres, and platy crystals (commonly forming rosette-like structures). Further to these distinctive morphological forms, a dominant component of products excreted by some species (*e.g.*, bluehead wrasse) is one that lacks any clearly definable form.

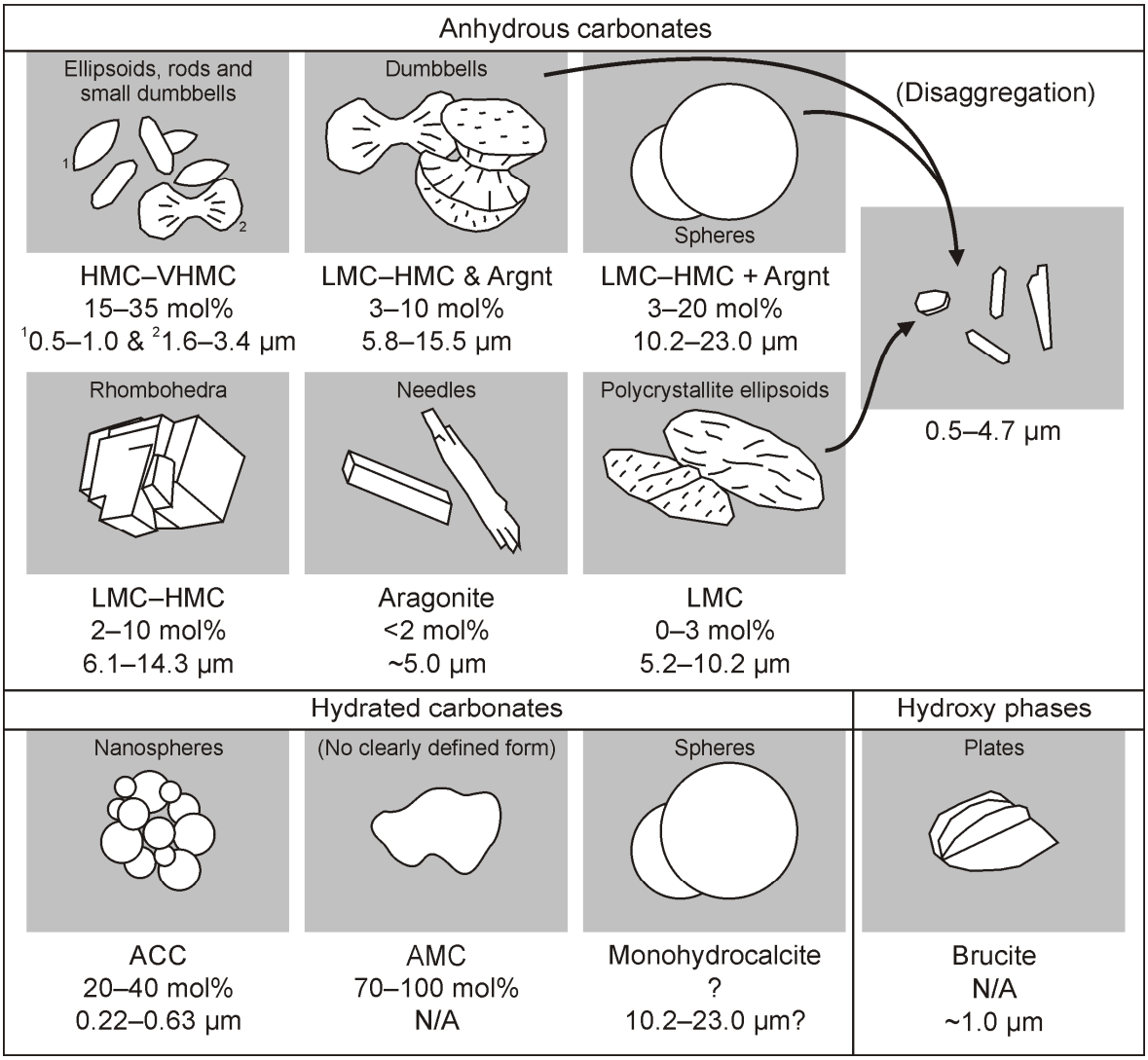

Figure 8.1 *Summary diagram showing morphological, mineralogical, and compositional properties of the main precipitate forms excreted by marine fish. Shown below each box are: phase, $MgCO_3$ content (where relevant and known), and length range of middle 80 % of measured crystals. LMC = low-Mg calcite (<5 mol% $MgCO_3$); HMC = high-Mg calcite (5–25 mol% $MgCO_3$); VHMC = very high-Mg calcite (>25 mol% $MgCO_3$); Argnt = aragonite; ACC = amorphous calcium carbonate; AMC = amorphous magnesium carbonate.*

The most commonly occurring phase in this investigation is Mg calcite, which takes the form of ellipsoids, spheres, dumbbells, and rhombohedra. Spectroscopic data show that this phase occurs over a considerably larger compositional range than previously thought, with the full extent of average $MgCO_3$ contents per species spanning ~0.5 to ~45 mol%, compared with a previously documented range of 18–39 mol% (Perry *et al.*, 2011). Furthermore, whereas the study by Perry *et al*. (2011) reported only the average $MgCO_3$ contents of Mg calcites produced by each species, it is shown here (Chapter 2) that $MgCO_3$ content varies not only with producing species, but also with crystal form. For example, polycrystalline dumbbells with ~5 mol% $MgCO_3$ are found to occur

alongside monocrystalline ellipsoids with ~20 mol% $MgCO_3$ in several samples. Infrared vibrations generated by these Mg-calcites show that many are poorly crystalline and contain a greater amount of water than is usual for sedimentary carbonates (although the state of its occurrence has not been determined). It is further shown that the 'minor' amounts of aragonite reported in previous studies can account for 0–27 wt% of excreted carbonates (~5–15 wt% is normal), with this phase being represented by needle-like forms and polycrystalline dumbbells and spheres. In addition to these anhydrous crystal phases, infrared spectroscopy reveals the presence (probably as polycrystalline spheres) of monohydrocalcite in some samples at the point of excretion, usually as a subsidiary phase, but in at least one case it was the dominant phase.

Further analysis of samples using Fourier transform infrared (FTIR) spectroscopy (Chapter 3) indicates the presence of abundant amorphous carbonate phases in many excreted pellets, with visual examinations and compositional analyses confirming that these occur as Mg-rich amorphous calcium carbonate (ACC) nanospheres and amorphous magnesium carbonate (ACM) that lacks any clearly definable form. Importantly, estimates of abundance of these phases in combination with modelling of platform-wide production (Chapter 6) suggests these amorphous phases account for about 18 % of the total carbonate excreted by fish (the sedimentary significance of this is discussed in the following section). Finally, plate-like precipitates are shown from a combination of infrared spectroscopy and compositional analyses to be brucite; a magnesium hydroxy phase that occurs as a minor component in many pellets of the point of excretion.

The above observations broadly confirm the assertion made by Perry *et al*. (2011) that fish-derived carbonates exhibit morphologies and compositions that are seemingly unique in most shallow sub-tropical marine settings, and should therefore be readily recognisable in bulk sediment samples. However, the new findings also identify some morphotypes that are less distinctive (*e.g.*, needle-like forms are similar to aragonite needles produced by some calcareous green algae – Loreau, 1982; Macintyre and Reid, 1995), and that the compositional range extends into the normal range of other Mg calcites occurring in shallow sub-tropical marine settings (*e.g.*, Chave, 1954; Bosence,

1985), indicating that a proportion of fish-derived carbonates may be difficult to assign to source with confidence when observed in bulk sediment samples. In light of this, stable carbon and oxygen isotope compositions were determined (Chapter 4) in order to provide additional characteristic information that might aid identification of fish-derived carbonates in bulk surface sediment samples. The results of this work confirmed a hypothesis that, because intestinal HCO_3^- is metabolically-derived (Wilson *et al*., 2002), and is thus diet-related, fish-derived carbonates are significantly depleted in ^{13}C with respect to sedimentary carbonates of most other common origins (*e.g.*, typical values are in the range -1 to -2 $‰_{VPDB}$, compared with values in the range +1 to +5 $‰_{VPDB}$ for other marine sedimentary carbonates), and are therefore isotopically distinct at the point of excretion. They also appear to be enriched in ^{18}O with respect to other sedimentary carbonates, although variability among samples is large and this may not be reliable as a distinguishing feature.

An additional aspect of the stable isotope work showed that carbonates produced by normally-fed fish are enriched in ^{13}C relative to those produced by fish of the same species that were fed a diet known to be depleted in ^{13}C. As well as confirming the metabolic origin of intestinal HCO_3^-, this result showed that the dietary influence on stable isotope compositions of intestinal HCO_3^- has no bearing on other crystal characteristics (*i.e.*, crystal morphology or $MgCO_3$ content). Further tests of potential controls on precipitation products (fish body mass and functional group; Chapter 2) also returned negative results, and factors that control the characteristics of precipitation products thus remain elusive. Other potential factors that are considered (but have not been tested) include: i) species-specific variations in gut microbial populations (indeed, many carbonates associated with bacteria exhibit similar morphologies to those described herein, illustrating the potential for a microbial influence on precipitation processes); ii) digestive strategies (*e.g.*, the utilisation of different digestive enzymes potentially influencing gut fluid pH, and thus saturation state); and iii) cation sequestration for physiological purposes, which has the potential to alter, for example, Mg^{2+}/Ca^{2+} ratios in gut fluids.

Finally, it is important to point out that these data are reported with the caveat that they relate to precipitation products formed in the guts of starved fish, and that the products of recently fed fish may be somewhat different. Evidence for such a difference is presented in Chapter 4, where it is shown that some of the carbonates produced by three species of recently fed piscivorous fish were dominated by phosphate- and magnesium-rich ACC, whereas the same individual animals produced phosphate-free crystalline phases when starved. These observations indicate that gut carbonates produced by fish under normal circumstances might comprise a proportionally greater volume of amorphous phases than most of the samples examined throughout this thesis. However, carbonates produced by several of the recently fed fish investigated in Chapter 4 comprised crystals that were identical to those produced by starved fish, suggesting that the effects of feeding are variable under normal natural circumstances. Similarly variable effects of feeding have been reported elsewhere in several temperate fish species (E.E. Reardon, *Pers. Comm.*), and, based on these findings, it is hypothesised herein that the effects of feeding may be most pronounced shortly after feeding events, diminishing thereafter as dietary phosphate levels in the gut decrease. Further work is needed test this hypothesis and to fully comprehend the extent of variations in precipitation products induced by feeding.

8.2.2 Short-term post-excretion fate (months)

Although Perry *et al*. (2011) find numerous particles that resemble fish-derived carbonates in the surface sediment of Eleuthera Sound, the Bahamas, various other investigations regarding carbonate mud sources in the Bahamas and contemporary settings (most recently, Gischler *et al*., 2013 – those authors being among the first to examine Bahamian carbonate muds whilst being aware of the potential contribution by fish-derived carbonates) have not reported similar crystals, and the sedimentary significance of these carbonates thus remains unclear. Chapters 6 and 7 attempt to elucidate the short-term fate of fish-derived carbonates following excretion in these settings by investigating: 1) the manner in which they break down mechanically; and 2) the crystallographic and compositional changes they undergo up on exposure to seawater and

porewater. Indeed, with regard to the latter, various findings of the characterisation work – such as the fact that: i) amorphous carbonates and monohydrocalcite can be abundant among excreted products; ii) Mg calcite commonly has very high $MgCO_3$ contents; and iii) Mg calcite can be poorly crystalline – are indicative that many precipitation products are metastable and may not persist for long periods in their excreted forms once exposed to seawater. The major outcomes of these studies are summarised in Fig. 8.2.

Prior to this study, Perry *et al*. (2011) and Salter *et al*. (2012) considered the sedimentary implications of fish-derived carbonates with respect to carbonate mud production, largely on the assumption that excreted pellets will rapidly disaggregate to release their component crystals as individual mud-grade particles, with specific size fractions as shown for each morphotype in Chapter 6. However, at the point of excretion these pellets are actually rather similar to faecal pellets and other muddy aggregates that characterise the surface sediment accumulating over large areas of Bahamian platform interiors, and as such their relevance to coarser fractions merits further consideration. Experiments in which pellets were placed in moderately agitated conditions for up to one month showed that approximately two thirds of the initial mass was lost to disaggregation, but that one third remained as intact pellets, albeit considerably smaller and more well-rounded than initial pellets. Morphologically, these partially disaggregated and reworked pellets are very similar to pellets found Bahamian in surface sediments (*e.g.*, Illing, 1954), and this result indicates that a significant proportion of fish-derived carbonates produced in shallow platform-top settings may be retained as fine and very fine sand-grade pellets. Furthermore, it is possible that an even larger proportion of pellets remain intact in quiescent settings that typify large areas of the Bahamian platform interior (although biologically-induced mechanical breakdown due to bioturbation, and/or mastication and ingestion may occur in such settings). Although it has not been demonstrated herein, it is speculated that the preservation of pellets as described above may be prolonged in certain platform settings by the development of cements.

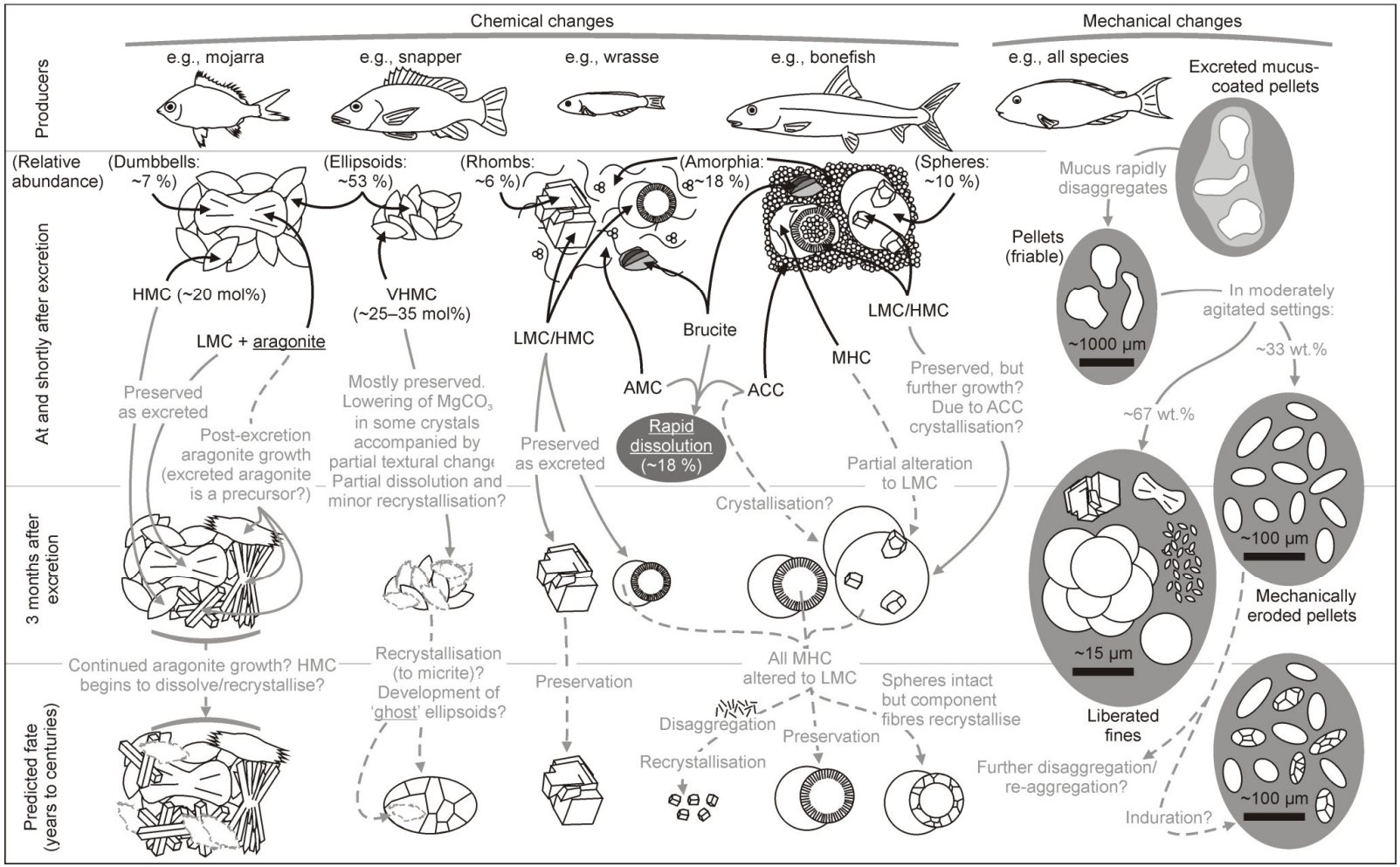

Figure 8.2 *Diagram showing the main carbonate products at the point of excretion, the chemical and mechanical changes they undergo during the first three months after excretion, and their hypothesised longer-term preservation potentials based on observed short-term changes. Abbreviations are as follows: ACC = amorphous calcium carbonate; AMC = amorphous calcium carbonate; LMC = low-Mg calcite (<5 mol% $MgCO_3$); HMC = high-Mg calcite (5–25 mol% $MgCO_3$); VHMC = very high-Mg calcite (>25 mol% $MgCO_3$); MHC = monohydrocalcite.*

Of the particles liberated from pellets, further investigation reveals that disaggregation proceeds by the release of most morphotypes as individual particles that retain their original morphologies, thus confirming assumptions made in earlier studies. However, two significant variations were also noted: 1) several morphotypes (mainly polycrystalline spheres and nano-scale spheres, but also some polycrystalline ellipsoids and rhombohedral crystals) can be intergrown, with cohesion being sufficiently strong that these intergrown forms behave as individual particles that are liberated from pellets as particle clusters (up to coarse silt and very fine sand grades) rather than individual mud-grade crystals; 2) polycrystalline precipitation products (spheres, dumbbells, and some ellipsoids) can further break down to release their component fibrous and plate-like crystals, these typically being <2 μm in length and lacking distinctive morphological features. Although promoted by quite vigorous agitation in the experimental work of Chapter 6, this second observation may also occur in nature due to mastication and/or prolonged periods of agitation, in which case the small size of resultant particles and their lack of distinguishing features may render them unrecognisable as fish-derived carbonates in surface sediment samples. Together, these results indicate that the mechanical breakdown of fish-derived carbonates can result not only in the generation of morphologically distinctive mud-grade particles, but also fine and very fine sand-grade particles (as intact pellets and particle clusters), and mud-grade particles that are perhaps not easily attributed to source.

The major implication of the mechanical processes described above is that not all excreted fish-derived carbonates will contribute to the mud-fraction, and that, consequently, investigations targeting only mud-grade sediments may overlook a significant contribution that fish-derived carbonates make to sedimentary budgets. This finding also means that the total contribution of fish-derived carbonate to the carbonate mud fraction that accumulates on Bahamian platforms is lower than previous production estimates suggest (Perry *et al*., 2011), and this effect may be further augmented by the very small size of some precipitation products (*e.g.*, monocrystalline ellipsoids); a significant proportion of which is likely to be exported off-platform to be deposited along with

platform-derived muds of other origins as periplatform carbonate ooze (in contrast, larger particles, such as spheres and rhombohedra, may be more likely to remain on-platform).

Reductions to estimates of fish-derived carbonate mud accumulation on Bahamian platform tops as outlined above are further increased when the results of seawater and porewater exposure experiments are taken into consideration. A major outcome of these investigations is that nearly all amorphous carbonate phases (estimated to account for approximately 18 % of the total excreted carbonate across the Bahamian platform), along with brucite (a comparatively minor component), rapidly dissolve within the first few days to weeks of excretion. It is postulated, however, that an unknown, but significant proportion of ACC produced by some species crystallises after excretion; a hypothesis motivated by the apparent post-excretion enlargement of polycrystalline spheres (in some case to more than 200 μm in diameter).

All other phases were largely retained during these experiments, with spheres, dumbbells, and rhombohedra undergoing few, if any, morphological, compositional, or mineralogical changes (excepting apparent sphere growth which, as mentioned above, may have been due to crystallisation of ACC). However, VHMC monocrystalline ellipsoids (and associated rods), which are estimated to be the most abundant precipitation products (modelling work suggests they account for ~53 % of all excreted products across the Bahamian platform), show a loss of clear definition at pellet surfaces accompanied in some cases by a substantial lowering of $MgCO_3$ contents (to values <6 mol%). These findings are interpreted as being an indication that VHMC crystals are beginning to dissolve (dissolution favouring their $MgCO_3$ components), with less clearly defined ellipsoids explained as being due to either: i) etching associated with dissolution; and/or ii) recrystallisation and formation of overgrowths (*e.g.*, see Fig. 1.8 B for comparable textures observed in other marine carbonates).

Recrystallisation textures might be expected to be accompanied by stable isotope values that are in equilibrium with the solutions in which they developed, yet stable isotope analysis of exposed carbonates reveals no significant difference between samples at the point of excretion and samples

exposed to porewater. Similarly, these textures might also be expected to exhibit a higher degree of crystallinity than initial fish-derived carbonates, but this is not observed. However, observations of broken pellet surfaces (*i.e.*, pellets broken *after* exposure experiments) indicate that dissolution and recrystallisation may only have proceeded at pellet surfaces in these experiments, presumably because these pellet regions were exposed to greater volumes of seawater/porewater. This being the case, the volumetrically minor proportion of recrystallised carbonates at pellet surfaces would probably not influence the bulk stable isotope composition of these samples.

One of the most intriguing findings of seawater and porewater exposure experiments is the apparent post-excretion development of aragonite needles in association with some fish-derived carbonates, which in some cases is abundant. These needles are morphologically similar to the needles described from Bahamian aragonite needle muds (*e.g.*, Shinn *et al*., 1989; Milliman *et al*., 1993), and they therefore represent a potential source of these sediments along with *Halimeda* algae. Textural evidence suggests that these needles developed via new growth rather than replacement or dissolution/reprecipitation reactions (*i.e.*, no intermediate textures were observed), and thus represent a post-excretion addition to (rather than replacement of) fish-derived carbonate bulk. However, this finding is complicated by the fact that the most extensive development of needles was associated with samples that were cleaned prior to porewater exposure, and that uncleaned carbonates from the same sample set contained only a few aragonite needles after exposure to similar porewater conditions. A similar phenomenon is also observed with VHMC ellipsoid alterations described above. These results suggest that aragonite growth (and other post-excretion alteration to fish-derived carbonates) is inhibited in uncleaned samples (*i.e.*, as in nature), possibly due to surface adsorption of reaction-inhibiting organic compounds (the adsorption of which may have been precluded by sample cleaning), thus raising the question of whether or not similar changes really occur in nature. Nevertheless, limited evidence for post-excretion alterations in uncleaned samples suggests the inhibiting factor might eventually be overcome, with longer seawater and porewater exposure thus predicted to result in more extensive changes. Further work is needed to better understand this process.

8.2.3 Longer-term preservation potential: A hypothesis

Although the findings of seawater and porewater exposure experiments demonstrate that an estimated 82 % of excreted gut carbonates persist in, or close to, their initial form for at least three months after they are produced, questions remain about their longer-term preservation potential and, consequently, about the full extent of their sedimentary significance. The findings of the exposure experiments presented in Chapter 7 of this thesis are therefore used as a starting point for hypothesising about the longer-term preservation potential of fish-derived carbonates here, as summarised in Fig. 8.2.

As stated above, an estimated 18 % of excreted precipitates (predominantly the amorphous carbonate phases) are predicted to dissolve rapidly in surface seawater and are not considered further here. In contrast, the short-term preservation of VHMC ellipsoids indicates that they have some preservation potential, although the fact they appear to undergo partial dissolution (and possibly recrystallisation) after only three months of porewater exposure suggests they are highly unstable. Based on this observation, is appears likely that these ellipsoids (and associated rods, and possibly small dumbbells, which are compositionally similar – see Chapter 2) will continue to dissolve and reprecipitate over longer timescales, eventually losing initial distinctive morphologies and high magnesium contents, and perhaps stabilising at a point where micritic textures have formed and $MgCO_3$ content is in the range 8–15 mol% (this range seems likely given the measured compositions after three months in porewater, and the magnesium content of bulk surface sediment samples in the Bahamas; *e.g.*, Bosence, 1985). It is difficult to estimate the timescale over which such alterations might occur, but the rapidity of changes observed herein suggests it could be on the order of years, probably being accelerated in cases where pellets disaggregate and thus fully expose the surfaces of all component particles to free flowing marine solutions.

If this hypothesis is correct, recrystallisation would presumably be accompanied by changes in carbon and oxygen stable isotope composition towards equilibrium with seawater or porewater; as documented to occur in other sedimentary high-Mg calcite (Patterson and Walter, 1994a). The

implication of this change, along with the loss of other distinguishing original features, is that the majority of excreted carbonates (an estimated 53 %) could be altered beyond easy recognition within a few years of production. In addition to the loss of amorphous phases, this means the sedimentary significance of an estimated ~70% of excreted products is either minimal (*e.g.*, amorphous phases), or likely to be difficult to confirm by identifying their presence in bulk sediment samples. Further studies may facilitate the tracking of post-excretion changes over longer timescales in these precipitation products, but if micritic textures are the result, the greatest potential for recognising these fish-derived carbonates may lie in the preservation of occasional ellipsoids (perhaps favouring larger crystals), or the formation of 'ghost' ellipsoids; *i.e.*, ellipsoid-shaped moulds that form as recrystallisation textures develop around intact (at the time) ellipsoids (Fig. 8.2). A similar situation to the latter is described from Pleistocene micrites by Lasemi and Sandberg (1984), who suggest that needle-shaped moulds are evidence of an aragonite needle precursor to recrystallisation textures.

Of the remaining ~30 % of excreted products, few changes were observed to occur in the short-term exposure study presented herein (the apparent growth of polycrystalline spheres and increased abundance of rhombohedral crystals in some samples is attributed to possible post-excretion crystallisation of excreted ACC, and is therefore not expected to continue over longer timescales). Accordingly, it is supposed that these crystals (polycrystalline spheres and dumbbells, rhombohedra, needles, and probably polycrystalline ellipsoids – although the short-term fate of the latter morphotype was not tested here), all of which have $MgCO_3$ contents typically lower 15 mol%, have good long-term preservation potential.

Theoretical considerations (see Chapter 1) indicate that rhombohedral precipitates, which are typically low-Mg calcite and in many cases occur as single crystals greater than 10 μm in length, should have good preservation potential in shallow settings. Indeed, on the basis of solubility studies (Morse and Mackenzie 1990; and references therein) they should be considerably more stable than many sedimentary carbonates (including aragonite needles) produced in Bahamian

platform-top settings. The same might also be true of polycrystalline precipitates, which are of similar size and typically have only slightly higher (and in some cases lower) $MgCO_3$ contents. However, the polycrystalline nature of these precipitates may influence the manner in which they are preserved. As shown in Chapter 6, the component crystals of these precipitates are typically very small (*e.g.*, fibres are typically <0.2 μm in width), and the associated high surface free energy (see Chapter 1) may influence their stability. In cases where these precipitates remain intact, this could result in recrystallisation such that original component crystals are replaced by micrite or microspar, but with overall morphologies being retained. Indeed, rare spheres exhibiting textures consistent with this hypothesis were observed in 3 month porewater exposures. Conversely, in higher energy environments, or in areas where mastication, ingestion, and re-excretion of carbonates is likely, original particle morphologies could be obliterated due to disaggregation, in which case liberated crystals might recrystallise, but resultant textures will probably make assigning these particles to source difficult. It is worth noting further that although monohydrocalcite spheres were not observed to undergo alteration in porewater during the first few months after excretion (alteration possibly being inhibited by the presence of adsorbed phosphate), this phase is considered to be unstable in sub-tropical surface marine settings and will likely alter to calcite over time. Indeed, it was no longer present in detectable amounts after exposure to artificial seawater, although confirmation that it altered to calcite is hampered by the possibility of dissolution.

Due to the considerable uncertainties regarding potential aragonite needle growth in association with fish-derived carbonates (see previous section), speculation over their longer-term significance is difficult. The observed properties of these crystals suggests they should follow similar preservation pathways as aragonite needles of other origins (*e.g.*, Macintyre and Reid, 1995; Reid and Macintyre, 1998), but a key question that remains concerns the extent to which they develop during and after the first few months following excretion. This can only begin to be understood with further work involving experiments over longer durations.

In summary, is it shown here that fish-derived carbonates produced in modern shallow sub-tropical marine settings in the Bahamas exhibit a wide array of mineralogical and morphological forms, but several of these (amorphous phases and brucite) rapidly dissolve following excretion. Monohydrocalcite is anticipated to alter to more stable forms, although it persists at least for a few months after excretion. Preserved phases are VHMC, HMC, LMC and aragonite. The latter two phases show no sign of alteration in the short-term, but the volumetrically more significant former phases (especially VHMC) show evidence of dissolution and possible recrystallisation within the first three months of excretion, suggesting they may ultimately undergo complete recrystallisation. An intriguing finding, the significance of which is yet to be fully understood, is that some excreted carbonates that contain aragonite appear to have the potential to induce further aragonite growth after excretion, these precipitates taking the form of needles that closely resemble the component crystals of aragonite needles muds that have previously been described from Bahamian surface sediments.

8.2.4 Geological implications

In the opening paragraphs of this thesis, the volumetric significance of carbonate mud in the geological record was discussed along with problems associated with assigning original mud-grade components to source due to grain obliteration during diagenesis. Because of this problem, it was stated that assignment of original grains to source requires that modern carbonate mud-forming processes are used as analogues. As indicated in the study by Perry *et al*. (2011), the finding that modern marine teleosts produce significant quantities of carbonate in certain sub-tropical shallow marine platform settings suggests that they should be included in considerations of mud production through geological time. The present study has documented various aspects of teleostal gut carbonate production and preservation in modern shallow sub-tropical marine environments, and the following paragraphs consider the potential significance of these findings in the geological record.

Before considering precipitation products and their potential sedimentary fates, it is first useful to establish the timescales over which fish can be assumed to have been producing gut carbonates. It is thought that the adaptation of alkaline, high HCO_3^- intestinal fluids (*i.e.*, the phenotype that results in gut carbonate precipitation) arose early in the evolution of vertebrates, because early chondrostean and chondrichthyan fishes (sturgeon and bamboo sharks) have been found to display this phenotype when experimentally manipulated to drink seawater by transfer to a hyperosmotic medium (Taylor and Grosell, 2006). These fishes are of phylogenetically lower lineages than teleosts (Fig. 8.3), and it is therefore assumed that all marine teleosts display the HCO_3^- phenotype and consequently produce gut carbonates (Taylor and Grosell, 2006; Wilson *et al*., 2009). This assumption is supported by the fact that nearly all teleosts investigated for this purpose to-date (including those in the present study) have produced gut precipitates; the non-appearance of carbonates from a small number of fish in this study (*e.g.*, white mullet and doctorfish; Chapter 2) possibly being due to factors other than these species not displaying the gut carbonate phenotype.

Modern marine teleosts are thought to have evolved from freshwater teleosts in the Jurassic (Finn *et al*., 2000), and, given the above assumptions, would most likely have excreted gut carbonates from this time onwards. Further questions concerning the sedimentary significance of these carbonates through geological time relate to the magnitude of teleost populations, and hence the total volume of carbonate produced. Marine teleosts underwent several major radiations that began in the Early Cretaceous, culminating in a particularly spectacular radiation during the Late Cretaceous (Benton, 2005; Finn and Kristoffersen, 2007). The volume of gut carbonates excreted by fish would therefore have risen throughout the Cretaceous, likely becoming an increasingly significant component of carbonate sedimentary systems during this period.

As an aside, although the present study focuses on carbonate production by teleosts, the findings of Taylor and Grosell (2006) show that chondrostean fishes (Siberian sturgeon, *Acipenser baerii*; the only member of that sub-class studied to-date with regard to intestinal HCO_3^-), as well as displaying the HCO_3^- phenotype, can produce and excrete gut carbonates when transferred to

hyperosmotic fluids. Other classes (*e.g.*, placodermi, which is extinct, and sarcopterygii) have not been studied with respect to intestinal HCO_3^- levels, but the fact that one of these (sarcopterygii; Fig. 8.3) arose later than the chondrichthyes (which display the HCO_3^- phenotype) suggests they might also produce gut carbonates. Indeed, there is strong evidence to suggest that even lower superclasses, such as agnatha (jawless fishes such as lamprey and hagfish), utilised intestinal HCO_3^- secretion (Taylor and Grosell, 2006; and references therein). That being the case, the geological significance of fish-derived carbonates could extend to periods much earlier than the Cretaceous – the radiation of teleosts prior to the Mesozoic is thought to have been restricted due to the fact that sarcopterygii and placodermi occupied most ecological niches during the Permian (Broughton *et al*., 2013), and those lineages could therefore have been an important source of carbonate prior to the emergence of teleosts. Further work is necessary to facilitate better understanding of fish-derived carbonate production in lower lineages than teleosts.

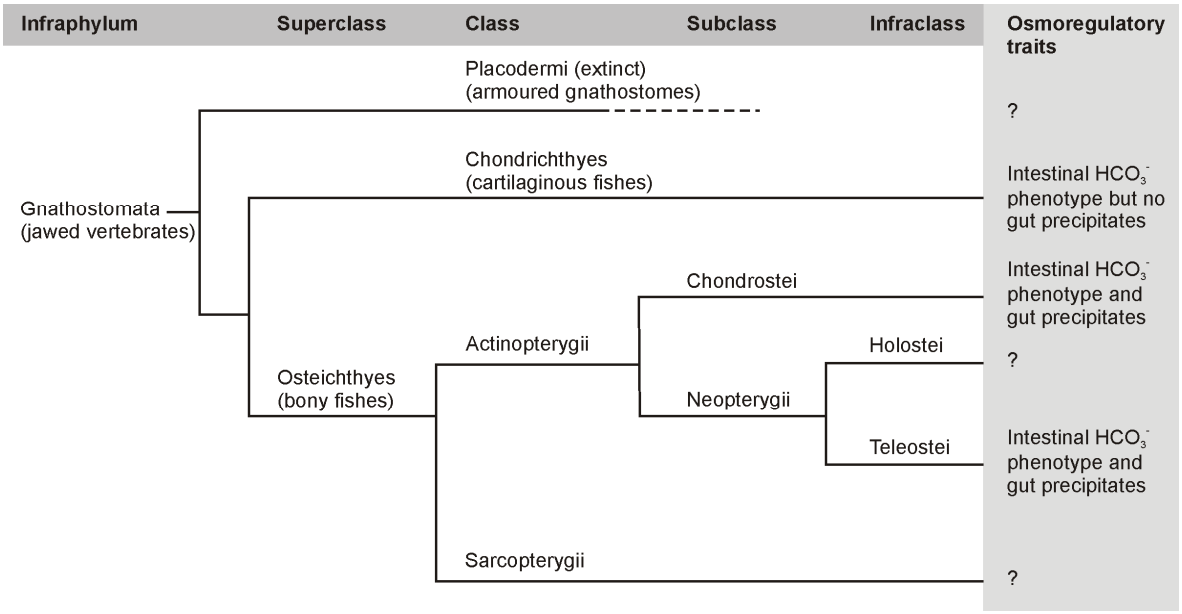

Figure 8.3 *Phylogenetic tree of the gnathostomata (adapted after Nelson, 2006). Numerous studies (cited in main text) report gut carbonate excretion by nearly all teleostei investigated to-date, and the only chondrostean fish studied in this regard has also been observed to produce carbonates when placed in hyperosmotic seawater. The intestinal bicarbonate phenotype has also been observed in lower classes (chondrichthyes), although gut carbonates have not been observed in these fishes. Other classes and infraclasses remain to be studied.*

Considering only carbonate production by marine teleosts, applying the results of the present study from the Cretaceous onwards is perhaps not appropriate given that seawater composition and

chemistry has been highly variable throughout this time (Hardie, 1996; Pearson *et al*., 2001; Horita *et al*., 2002; Tyrrell and Zeebe, 2004; Littler *et al*., 2011). For example, variations in Mg^{2+}/Ca^{2+} ratios from ~1 (Cretaceous seawater) to ~5 (modern seawater) have resulted in what have been termed 'calcite seas' (*i.e.*, where precipitation of calcite is favoured) and 'aragonite seas' (*i.e.*, where precipitation of aragonite and high-Mg calcite is favoured), respectively. During the Cretaceous, surface seawater conditions are thought to have been characterised by high pCO_2 (~2000 ppmv), low CO_3^{2-} (~50 μM), high Ca^{2+} (~25–35 mM), low Mg^{2+}/Ca^{2+} (~1), low pH (~7.6), and high temperatures (globally probably 6–12 °C higher than today) compared with modern surface seawater (Barrera and Johnson, 1999; Lowenstein *et al*., 2001; Horita *et al*., 2002; Tyrrell and Zeebe, 2004; Littler *et al*., 2011). With respect to gut carbonate production in fish, Wilson *et al*. (2009) show that high temperatures drive higher metabolic rates in ectothermic fishes, and thus higher rates of HCO_3^- secretion and gut carbonate precipitation. Furthermore, increased ambient pCO_2 in seawater is known to result in a corresponding increase of pCO_2 in the blood of fish (Seibel and Walsh, 2001), which has been shown to encourage higher rates of HCO_3^- secretion in the intestine (Grosell *et al*., 2005), and, based on these data, Wilson *et al*. (2009) surmise that the transfer of a fish from low pCO_2 to high pCO_2 seawater will likely result in increased rates of gut carbonate production. It is thus likely that teleosts inhabiting high temperature, high pCO_2 Cretaceous seas produced carbonates at greater rates than those living in modern seas – but note that tropical surface seawater temperature, or SST, during the Cretaceous was probably similar to tropical SST of today (Zeebe, 2001), in which case there should be little difference in production rates due to temperature differences alone when comparing Bahamian gut carbonate production rates with Cretaceous analogues. Nevertheless, preliminary results from ongoing studies in which fish are exposed to synthesised Cretaceous-like conditions indicate that carbonate production rates might have been five times higher than in modern seawater (R.W.Wilson, *Pers. Comm*).

In addition to these controls mentioned above, higher production rates in Cretaceous-like conditions may also be stimulated by lower magnesium concentrations than in modern seawater (*i.e.*, lessening the inhibitory effect of Mg^{2+} on calcite growth; Mucci and Morse, 1983) and higher

Ca^{2+} concentrations (*i.e.*, greater availability of Ca^{2+} for precipitation). These compositional factors may also have influenced the nature of precipitates produced during the Cretaceous. Reduced inhibition of calcite growth due to lower Mg^{2+} concentrations (Morse and Mackenzie, 1990) may mean that calcite phases were the dominant gut precipitation product, as is also typical of fish inhabiting modern seawater. However, the reduced availability of Mg^{2+} may have resulted in lower quantities of $MgCO_3$ being incorporated in these crystals compared to those documented for many fish species in the present study. Moreover, high Mg^{2+} concentrations in modern seawater may explain amorphous carbonate formation in the guts of several fish species examined in the present study; the high energy of hydration for Mg^{2+} (Lippmann, 1960) precluding its dehydration, and formation of hydrated amorphous phases thus being kinetically favoured. If this is true, the relatively low Mg^{2+} concentrations of Cretaceous seas may have favoured production of crystalline phases. Of course, these suggested differences between modern and Cretaceous gut carbonate properties (summarised in Fig. 8.4) are highly speculative, and further work is required to properly understand fish-derived carbonate formation throughout geological time, but if they are correct, it would appear that marine teleosts may have represented a significant source of carbonate during the Cretaceous, and that excreted products may have had better preservation potential (*i.e.*, calcite contained less $MgCO_3$ and was therefore more stable, and highly soluble amorphous phases represented a smaller proportion of total precipitates) than those produced in modern seawater.

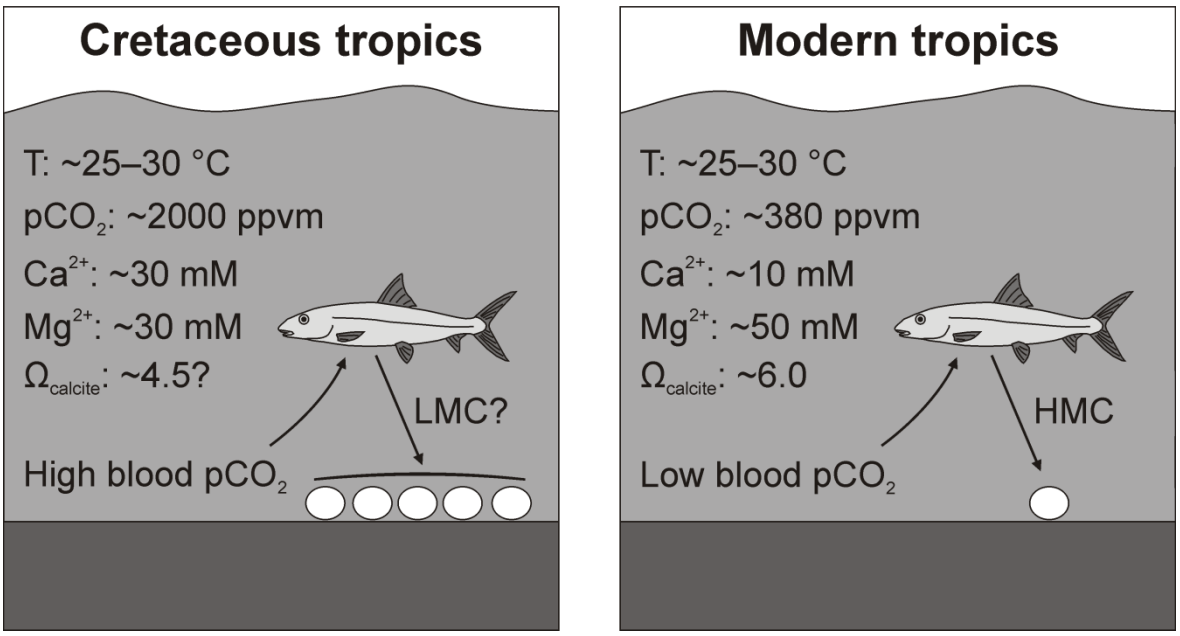

Figure 8.4 *Key differences between Cretaceous and modern seawater properties in tropical regions and the hypothesized effect on gut carbonate production.*

The point regarding preservation potential assumes that seawater saturation states with respect to carbonate minerals were similar during the Cretaceous to those of modern seawater. Despite large variations in DIC system parameters throughout geological time (*e.g.*, as described above), attempts at estimating changes in carbonate compensation depths during the last 100 million years have tended to yield results between 3.5 and 5.0 km as a global average, being slightly shallower during the Cretaceous (~3.5 km) than at present (~4.8 km) (Van Andel, 1975; Sclater *et al.*, 1977; Tyrrell and Zeebe, 2004). These results suggest that saturation states have varied little during this time, but were probably slightly lower during the Cretaceous than they are now. Thus, if fish-derived carbonates were produced as mostly (low?)-Mg calcite during the Cretaceous (as is speculated above), they probably represented a stable phase in shallow platform sedimentary settings. In contrast, if products were broadly similar to those described here (Chapter 2), amorphous phases would probably have dissolved and high-Mg calcite ellipsoids would, if anything, have been less stable than in modern seawater.

8.3 RECOMMENDATIONS FOR FUTURE WORK

Given the findings summarised in the previous section, numerous questions arise about the production of fish-derived carbonates and their significance as sedimentary components in shallow sub-tropical carbonate provinces. The questions outlined below are considered to be particularly important with regard to extending the research themes of the present volume, and the paragraphs that follow offer suggestions as to how these might be answered.

1. Have all precipitation products of the piscine gut (and associated short term preservation styles) been identified, both at regional (*i.e.*, in the Bahamas/Caribbean) and global scales?
2. Can the products documented in the present volume be applied across whole fish populations (*i.e.*, many additional species) in order to model platform-wide production rates of different precipitates, and thus to estimate the volume of excreted products that might be of sedimentary significance?
3. What is the full extent of the effects of feeding on gut carbonate production, and what are the implications of these effects – with particular focus on: i) the proportion of fish-derived carbonates influenced by feeding; ii) potential variations in the effects of feeding among fish species with different feeding habits; and iii) the post-excretion fate of feeding-induced phosphate-rich amorphous phases?
4. To what extent do carbonate production rates differ from those previously obtained for captive Caribbean fish species according to:
    a. Normal behaviour of fish in nature (*i.e.*, feeding and active swimming); and
    b. Metabolic rate variations among species (*e.g.*, high-activity pelagic fishes such as tuna and mackerel versus low-activity bottom-dwelling fishes such as flounder and toadfish)?
5. To what extent do aragonite needles grow in association with fish-derived carbonates after they are excreted?

6. What are the longer term (*i.e.*, years to millennia) fates and preservation textures of fish-derived carbonates?
7. Are fish-derived carbonates relevant with respect to pellet mud and peloid production in shallow sub-tropical platform settings?
8. How has the nature, rate, and preservation potential of piscine gut precipitates varied over geological timescales (*e.g.*, according to changes in seawater composition and temperature)?

The first three of these questions are fundamental with respect to understanding the characteristics of excreted products, and thus their preservation potential. With regard to the first question, the remarkable mineralogical and morphological variability of precipitation products documented from 22 fish species in the present volume, together with the fact that these species represent only 7 out of more than 40 extant teleost orders (Nelson, 2006), raises the possibility that many more precipitation products remain to be described. In addition, the precipitates documented herein are products of fish held exclusively in seawater drawn from Eleuthera Sound that is highly supersaturated with respect to aragonite. Although the HCO_3^- that drives intestinal precipitation is thought to be derived metabolically (Wilson et al., 2002), imbibed seawater must also have the potential to influence precipitation products due to variations in both salinity and alkalinity, as are known to occur at regional (*e.g.*, Morse et al., 1984; Morse et al., 2006) and global (*e.g.*, Lee et al., 2006) scales. Resolving these issues should be a key aim of future studies, and this can easily be achieved by expanding the range of fish species/orders investigated, and characterising their precipitation products in multiple locations of differing seawater properties.

Characterising the precipitation products of all marine teleost species, however, is clearly impractical, and in order to facilitate realistic platform-scale modelling of fish-derived carbonate products and their varying preservation potentials (*i.e.*, Question 2), it is necessary to be able to make reasonable assumptions about which species will produce which precipitate types. However, as discussed in the preceding section, factors that control the form and composition of precipitation

products are yet to be positively identified. There are two possible approaches to this problem. The first is to set out to demonstrate the nature of primary controls on precipitation products. If it is then possible to determine which of these controls operate in which species, this could enable modellers to make accurate predictions about the nature of precipitation products for any given fish. Such controls might be related to digestive strategies, gut microbial populations, fish activity levels, or sequestration of different ions to fulfil physiological requirements. For example, in the case of digestive strategies, certain digestive enzymes are known to operate most effectively at specific (mostly alkaline) pH levels, with the optimum pH for each varying according to fish species (Bone and Moore, 2008). This suggests that different fish species will have intestinal fluids of differing pH values according to the enzymes they utilise for digestive purposes, and this has the potential to might influence precipitation processes. Features such as these should be investigated in order to attempt to identify the factors that control precipitation products.

In the event that specific controls remain elusive, however, another possibility is to attempt to identify patterns in precipitation products among teleostal orders and/or families. For example, it is possible that factors controlling precipitation products are evolved, in which case it might be possible to predict crystal forms based on phylogenetic relationships (see section 8.4 for a short discussion). Another possibility is that controlling factors are common at the level of order or family. Indeed, it has been shown in the present volume that black grouper (family: Serranidae) consistently produce ellipsoidal and rod-shaped high-Mg calcite, as do all other Serranidae investigated to-date (Graysby grouper, Nassau grouper, and red hind), and, based on this observation, it is reasonable to assume that other Serranidae will produce similar crystal forms. Fewer species have been studied within other families thus far, and the robustness of this approach therefore remains uncertain, but if, following further studies involving other species/families/orders (*i.e.*, Question 1), meta-analyses confirm the existence of strong relationships within certain taxonomic levels, such an approach could represent a valuable tool for predicting the precipitation products of a given species (or individual fish), thus aiding platform- and global-scale modelling of fish-derived carbonate production.

Perhaps a more fundamental issue than those covered by the first two questions though, is that of precipitation products excreted in nature, and especially those influenced by processes associated with feeding. It is shown in Chapter 4 that the act of feeding in at least some fish species may induce changes in the properties of carbonates they excrete; namely the inhibition of carbonate crystallisation and the formation instead of phosphate-rich amorphous phases. A key question that remains to be answered regarding the species investigated in Chapter 4 is that of the longevity of feeding effects. If precipitation processes are only influenced for a short duration after a feeding event, it is likely that gut carbonates will rapidly revert to crystalline phases (as produced by starved fish in Chapter 2), and feeding-induced amorphia may only represent a small proportion of total excreted carbonates. However, it remains a possibility that the effects of feeding are more persistent, perhaps to the extent that they never completely diminish between feeding events under normal circumstances. In the latter scenario, the crystalline phases described in Chapter 2 could represent a less common form of gut carbonate than initially thought. Preliminary data presented in Chapter 4 indicate that the former scenario is most likely true. However, given the potential consequences of feeding-induced production of amorphous phases (*i.e.*, possible rapid dissolution after excretion), quantification of the proportion of gut carbonates influenced by feeding must be a priority for future studies in this field. By the same token, it is equally important that the effects of feeding are determined in species with different dietary habits.

Such issues can readily be assessed by using similar approaches to those employed in Chapter 4 of this thesis. However, proper quantification of the effects of feeding will require knowledge of what dietary items were ingested by fish, and precisely when this occurred relative to the precipitation and excretion of gut carbonates, while it would also be extremely useful to determine exactly how gut fluids change in response to feeding. The relevance of understanding the fate of feeding-induced amorphia after excretion will depend in part on the outcomes of these studies, and the matter can easily be addressed by conducting short-term preservation experiments similar to those described in Chapter 7.

Following the resolution of issues raised in the first three questions, future studies should also focus on production rates (Question 4). As mentioned in Chapter 1, the carbonate production rates of Caribbean fish species detailed by Perry *et al*. (2011) are probably conservative due to the fact that they were based on production by fish that were: a) held in restricted conditions (*i.e.*, precluding normal active swimming); and b) not actively feeding. Both of these factors would have reduced the metabolic rates of fish under investigation, and thus the rate at which HCO_3^- would have been secreted into the intestine (Wilson *et al*., 2002; Perry *et al*., 2011). Consequently, measured carbonate production rates were probably considerably lower than those in nature. In addition, the production rate curve determined by Perry *et al*. (2011) was based on a plot of production rate versus fish body mass for all species studied. Due to small sample sizes, they could not, however, attempt to separate these species based on their activity levels, and among-species variation in production rate according to species-specific metabolic rates is therefore not accounted for. Future studies could resolve some of these issues by measuring production rates from: a) fish held in larger tanks, where active swimming is more consistent with that in nature; b) fish that are being fed (note that diet would need to be controlled to preclude ingestion of $CaCO_3$ to ensure that measured $CaCO_3$ contents relate only to gut precipitates); and c) fish of differing activity levels (*e.g.*, bottom dwelling species versus fast-swimming pelagic species).

Questions 5, 6 and 7 refer to the preservation styles of fish-derived carbonates within Recent sediments. The first of these, regarding aragonite needle formation in association with fish-derived carbonates, has been discussed in section 8.2, and, in the first instance, the problem is probably best approached using seawater exposure experiments similar to those described in Chapter 7, but conducted over varying (and longer) timescales, and incorporating determinations of sample mass at the beginning and end of experiments to aid quantification of aragonite growth. The second, regarding assessment of longer-term preservation potential of fish-derived carbonates, may also be best achieved using similar experiments to those in Chapter 7, but over longer exposure periods. For example, Patterson and Walter (1994a) conducted similar experiments lasting 500 days, with results indicating significant changes had taken place in initial high-Mg calcite during this time. Of

course, there is a practical limit to the duration of such experiments, but initial outcomes could provide criteria for identifying (altered) fish-derived carbonates in surface and shallow subsurface sediments, thus informing assessments of longer-term preservation pathways (*i.e.*, on the order of millennia) based on examination of short sediment cores. Conducting exposure experiments in a wider range of porewater settings (*e.g.*, organic-rich mud-grade sediments through to organic-poor sand-grade sediments) may further reveal important differences in preservation style according to specific sedimentary settings.

With regard to the preservation of pellets, and the possible transformation of intact pellets to peloids, similar exposure experiment investigations to those described above (carried out in a range of differing environmental conditions) should be complimented by a systematic and exhaustive investigation of peloids (at various stages of cementation) and pellet muds collected from different platform environments (*e.g.*, highly supersaturated waters of moderate to high energy versus less highly supersaturated waters of low energy; see Chapter 6 for explanation of the relevance of these settings) in an attempt to identify their primary sources. Additional pellet agitation experiments run at varying degrees of agitation, over longer periods, and encompassing pellets comprising different crystal forms should also be carried out, and results should be compared with those of similar experiments involving pellet muds and/or faecal pellets (produced by other organisms) collected from surface sediments.

The above-described suggestions for future work have direct relevance for the production and preservation of fish-derived carbonates in modern sub-tropical shallow carbonate provinces. However, as considered in section 8.2.4, marine teleost fish may have represented an important source of carbonate since at least the Cretaceous, but direct evidence for this has yet to be documented. One approach to this would be to examine the rock record for crystals that resemble those described herein. However, in addition to the possibility that such studies will be hampered by obliteration of most original textures, a further problem discussed in section 8.2.4 is that variations in environmental conditions over geological time may be accompanied by temporal

variations in the characteristics of fish-derived carbonates, which raises the possibility that fish-derived carbonates produced in, for example, the Cretaceous might be completely different to those described herein, and could thus be overlooked. Therefore, it may first be necessary to simulate seawater conditions from different geological periods (*e.g.*, by manipulating Mg/Ca ratios and pCO_2 levels), and to characterise the carbonates excreted by fish held in these solutions.

8.4 PRECIPITATION PRODUCTS: AN OVERVIEW WITH RESPECT TO TELEOSTAL PHYLOGENIES

The precipitation products documented herein have been shown to vary according to producing species, but controls on morphological and mineralogical characteristics remain elusive. Whilst numerous possible controls (some of which are discussed in Chapter 2) can be hypothesised, and it may be possible for future studies to elucidate these, knowledge of precipitation product characteristics from at least 29 marine teleost species (in addition to 24 species investigated in the present volume, other data are available from: Humbert *et al*., 1989; Woosley *et al.,* 2012; Foran *et al*., 2013; and R.W.Wilson and E.E.Reardon, *Pers. Comm.*) presents the opportunity to analyse these with respect to phylogenetic relationships in order to investigate the possibility that crystal forms are associated with specific evolved traits. For example, unlike lower classes of fish such as sturgeon and lamprey, teleosts lack gluconolactone oxidase; an enzyme necessary in the formation of ascorbic acid (Fracalossi *et al*., 1998; Moreau and Dabrowski, 1998), the presence of which possibly influences uptake of metals within the intestine (Wood *et al*., 2011), thus demonstrating the potential for evolved traits to influence gut carbonate formation.

It is worth noting that, to-date, gut carbonate production has been found to occur in nearly all species investigated for this purpose (Humbert *et al*. 1989; Walsh *et al*., 1991; Wilson *et al*., 2009; Mekuchi *et al*., 2011; Perry *et al*., 2011; Salter *et al*., 2012; Woosley *et al*., 2012; Foran *et al*., 2013), covering at least 10 teleostal orders within two subdivisions (Fig. 8.5). Species belonging to other subdivisions (there are four extant subdivisions in total) have not yet been documented with respect to carbonate production, and only one order investigated (Mugiliformes) has not produced

gut carbonates under the experimental conditions described in Chapter 2, although this may be for a variety of reasons (see Chapter 2), and is not necessarily an indication that the species/order in question does not produce gut carbonates. As such, it is reasonably assumed that all teleosts produce gut carbonates (Wilson *et al*., 2009); an assertion supported by the findings of Taylor and Grosell (2006), who show that the phenotype for HCO_3^- production arose prior to the evolution of teleosts.

The phylogenetic relationships of teleosts for which precipitation products are known are presented in Fig. 8.5. However, the species studied to-date are phylogenetically limited, with 23 out of the 29 species belonging to the order Perciformes (Subdivision: Euteleostei; Superorder: Acanthopterygii), or orders that are considered by some workers (*e.g.*, Johnson and Patterson, 1993) to be sub-orders of Perciformes (*i.e.*, Pleuronectiformes, Tetraodontiformes, and Scorpaeniformes). Of the remaining six species, two belong to other orders within Acacnthopterygii, two belong to different superorders within Euteleostei, and only two belong to a more plesiomorphic subdivision (Elopomorpha). It is worth mentioning here that the study of teleost phylogeny is a rapidly evolving field, with conventional classification based on morphological traits being subject to many recent changes following the results of mitochondrial and molecular analyses – the reader is referred to Nelson (2006) for a full discussion. The phylogenetic relationships presented in Fig. 8.5 are therefore done so with the caveat that they may be subject to further changes as the field advances.

Based on the arrangement of precipitation products by phylogenetic relationships (Fig. 8.5), it is clear that polycrystalline spheres and dumbbells, rhombohedra, and amorphous phases (including nanospheres) are common to both Elopomorpha and Euteleostei, as is the precipitation of brucite and monohydrocalcite. The most commonly observed crystal form (high-Mg calcite monocrystalline ellipsoids) has yet to be described from species belonging to subdivisions outside Euteleostei, with the lowest level of documented occurrence being from Gulf toadfish (Subdivision: Euteostei; Superorder: Paracanthopterygii; Order: Batrachoidiformes). However,

only three species belonging to lower orders have so far been investigated, and only one of these (bonefish) in detail. Further work is clearly necessary to establish whether or not ellipsoidal Mg calcite crystals are produced by lower teleost orders, but these limited preliminary data do not reveal any obvious among-superorder or among-subdivision differences in excreted precipitation products.

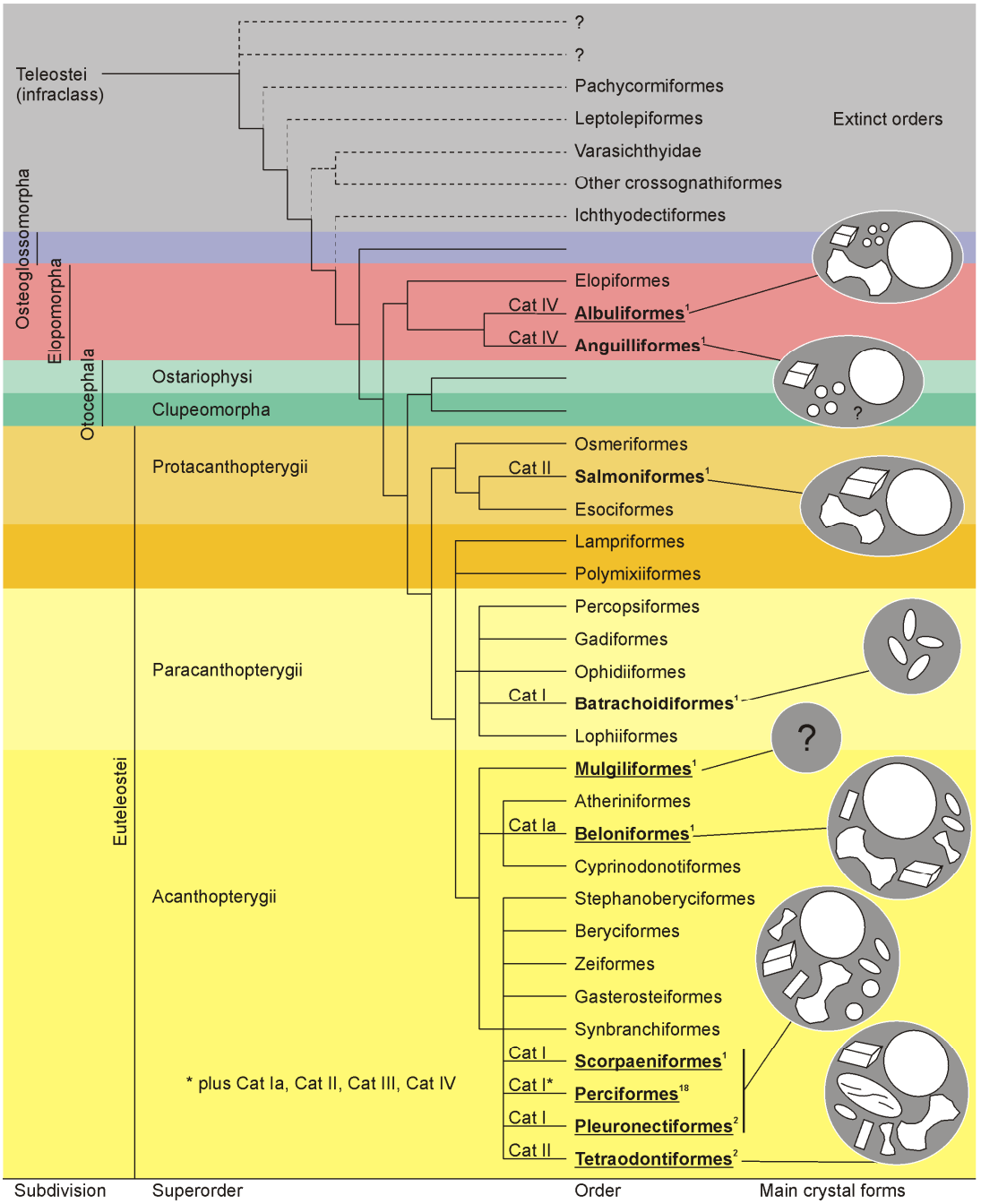

Albuliformes: bonefish **Anguilliformes**: silver eel (*Anguilla anguilla*; Humbert et al., 1986; 1989)
Salmoniformes: rainbow trout (*Oncorhynchus mykiss*; E.E. Reardon, *Pers. Comm*) **Beloniformes**: keeltail needlefish
Mugiliformes: white mullet (Mugiliformes) **Batrachoidiformes**: Gulf toadfish (*Opsanus beta*; Woosley et al., 2012)
Perciformes: grey angelfish, beaugregory, bluehead wrasse, slippery dick, french grunt, *Haemulon* sp., red hind, yellowfin mojarra, *Eucinostomus* sp., yellowtail snapper, schoolmaster snapper, black grouper, Nassau grouper, graysby grouper, redtail parrotfish, great barracuda, doctorfish, gilthead sea bream (*Sparus aurata*; Foran et al., 2013)
Pleuronectiformes: flounder sp. (Bahamas), European flounder (*Platichthys flesus*; E.E.Reardon, *Pers. Comm.*)
Tetraodontiformes: checkered puffer, scrawled cowfish **Scorpaeniformes**: red lionfish

Figure 8.5 *Phylogenetic relationships of selected Teleostean orders, and the main forms of gut carbonate produced within each. Orders for which data exist are shown in bold-type: underlined orders are those documented in the present volume. Numbers in superscript indicate the number of species documented within each, listed in full in the box below. Precipitate categories produced within each order are shown (Cat I – Cat IV; after Salter et al., 2012) along with diagrammatic representation of the main crystal forms. Phylogeny: subdivisions after Arratia, (2001) and Wang et al. (2003); Elopomorpha after Wang et al. (2003); Euteleostei superorders after Helfman et al. (2009); Protacanthopterygii after Zou et al. (2012); Paracanthopterygii and Acanthopterygii after Nelson (2006).*

Table 8.1 Dominant forms of gut carbonate produced by suborders and families of order Perciformes

Suborder	Family	No. of species	Dominant crystal forms	Other dominant crystal forms (if different among species)
Percoidei	Lutjanidae	2	HMC ellipsoids	
	Serranidae	4	HMC ellipsoids	
	Gerreidae	2	HMC ellipsoids/LMC dumbbells	HMC spheres/rhombs + AMC
	Haemulidae	2	HMC ellipsoids	HMC wheatsheafs
	Pomacanthidae	1	LMC(?) spheres/dumbbells	
	Sparidae	1	ACC nanospheres	
Labroidei	Labridae	2	AMC + LMC rhombs/spheres	
	Pomacentridae	1	AMC + LMC rhombs/spheres	
	Scaridae	1	AMC + LMC rhombs/spheres/ polycrystalline ellipsoids + aragonite needles	
Acanthuroidei	Acanthuridae	1	?	
Scrombroidei	Sphyraenidae	1	HMC small dumbbells	
Pleuronectiformes[1]	Pleuronectidae	1	HMC ellipsoids	
		1	HMC ellipsoids	
Tetraodontiformes[1]	Ostraciidae	1	LMC sph/dmbl/rhmb + AMC/ACC	
	Tetraodontidae	1	LMC sph/dmbl/rhmb + AMC/ACC	

[1]Included as suborders of Perciformes as proposed by Johnson and Patterson (1993)

Given that only one of order shown in Fig. 8.5 includes more than two species to have been investigated to-date (Perciformes, with a total of 18 species), it is perhaps more instructive to further divide that order by suborder and family. Table 8.1 shows that 12 species investigated within Perciformes belong to the suborder Percoidei, a further four to Labroidei, and one each to Acanthuroidei (doctorfish) and Scrombroidei (great barracuda). Of the Percoidei, eight species predominantly produce high-Mg calcite ellipsoids, and nine produce precipitates belonging to Category I and Ia (see Chapter 2 for assignment of categories). Other species produce Category II (n = 1), Category IV (n = 1), and uncategorised (nanospheres; n = 1) precipitates. By comparison, three of the four Labroidei species produce Category III precipitates that are predominantly AMC with subsidiary rhombohedra and spheres, whilst the other species (redtail parrotfish) produces similar precipitates, but these are typically dominated by crystalline phases which additionally include polycrystalline ellipsoids and aragonite needles. Although precipitates excreted by the latter

species are assigned to Category IV, the fact they can also contain substantial amounts of AMC (Chapter 3) suggests they may be closer to Category III, or perhaps intermediate between the two categories. Both species within Pleuronectiformes (possibly different families) produced high-Mg calcite ellipsoids (Category 1), and both species within Tetraodontoformes (different families) produced mainly low-Mg calcite spheres and rhombohedra (Category IV). Of species belonging to other suborders, doctorfish did not produce carbonates, and great barracuda produced high-Mg calcite small dumbbells (Category 1).

These data clearly indicate that precipitation products can vary considerably at the order level, but that species within a given suborder may tend to produce precipitates of similar character; a hypothesis that holds true for Pleuronectiformes, Tetraodontiformes, Labroidei, and most species within Percoidei. However, this assertion is based on a rather limited dataset, and it must be emphasised that, if valid, it appears only to represent a general tendency; it does not hold for all species within a suborder. Stricter rules may apply at the family level: out of four Percoidei families for which two or more species have been investigated (Table 8.1), all but one (Gerreidei) comprise species that produce precipitates belonging to the same category. Within Labroidei, precipitation products of the family Labridae (n = 2) are also consistent.

Further work is clearly necessary to identify and verify relationships between phylogenetic lineages and precipitation products, but the preliminary data compilation presented here offers some promise that such relationships do exist. As such, any modelling work based on the current understanding of fish-derived carbonate production can make reasonable assumptions that within-family products will be similar. For families in which no species have yet been studied, however, a best estimate is probably to assume an average of the products documented herein.

REFERENCES

Addadi, L., Raz, S., and **Weiner, S.** (2003) Taking advantage of disorder: Amorphous calcium carbonate and its roles in biomineralization. *Advanced Materials,* **15,** 959–970.

Adler, H.H. and **Kerr, P.F.** (1963) Infrared spectra, symmetry and structure relations of some carbonate minerals. *American Mineralogist,* **48,** 839–853.

Ahlrichs, J.L. (1968) Hydroxyl stretching frequencies of synthetic Ni-, Al-, and Mg-hydroxy interlayers in expanding clays. *Clays and Clay Minerals,* **16,** 63–71.

Aizenberg, J., Lambert, L., Addadi, L., and **Weiner, S.** (1996) Stabilization of amorphous calcium carbonate by specialized macromolecules in biological and synthetic precipitates. *Advanced Materials,* **8,** 222–226.

Ajikumar, P.A., Wong, L.G., Subramanyam, G., Lakshminarayanan, R., and **Valiyaveettil, S.** (2005) Synthesis and characterization of monodispersed spheres of amorphous calcium carbonate and calcite spherules. *Crystal Growth and Design,* **5,** 1129–1134.

Al-Jandal, N.J., Whittamore, J.M., Santos, E.M., and **Wilson, R.W.** (2011) The influence of 17 beta-estradiol on intestinal calcium carbonate precipitation and osmoregulation in seawater-acclimated rainbow trout (*Oncorhynchus mykiss*). *Journal of Experimental Biology*, **214,** 2791–2798.

Alongi, D.M., Tirendi, F., and **Clough, B.F.** (2000) Below ground decomposition of organic matter in forests of the mangrove *Rhizophorastylosa* and *Avicenia marina* along the arid coast of Western Australia. *Aquatic Botany,* **68,** 97–122.

Andersen, F.A. and **Brečević, L.** (1991) Infrared spectra of amorphous and crystalline calcium carbonate. *Acta Chemica Scandinavica,* **45,** 1018–1024.

Arratia, G. (2001) The sister-group of Teleostei: Consensus and disagreements. *Journal of Vertebrate Paleontology,* **21,** 767–773.

Banner, J.L. (1995) Application of the trace element and isotope geochemistry of strontium to studies of carbonate diagenesis. *Sedimentology,* **42,** 805–824.

Barrera, E. and **Johnson, C.C.** (1999) *Evolution of the Cretaceous Ocean-Climate System.* Geological Society of America Special Papers 332. Boulder, Colorado, 445 pp.

Barrera, E. and **Savin, S.M.** (1987) Effect of sample preparation on the δ^{18}O-value of fine-grained calcite. *Chemical Geology,* **66,** 301–305.

Bassinot, F., Mélières, F., Gehlen, M., Levi, C., and **Labeyrie, L.** (2004) Crystallinity of foraminifer shells: a proxy to reconstruct past bottom water $CO_3^{=}$ changes? *Geochemistry Geophysics Geosystems*, **5,** doi:10.1029/2003GC000668.

Batchelor, G.K. (1967) *An Introduction to Fluid Dynamics*. Cambridge University Press, 660 pp.

Bathurst, R.G.C. (1975) *Carbonate sediments and their diagenesis* (2nd Edition). Elsevier, New York, 658 pp.

Becker, A., Ziegler, A., and **Epple, M.** (2005) The mineral phase in the cuticles of two species of Crustacea consists of magnesium calcite, amorphous calcium carbonate, and amorphous calcium phosphate. *Dalton Transactions,* **10,** 1814–1820.

Beniash, E., Aizenberg, J., Addadi, L., and **Weiner, S.** (1997) Amorphous calcium carbonate transform into calcite during sea urchin larval spicule growth. *Proceedings of the Royal Society, London,* **264B,** 461–465.

Benton, M.J. (2005) *Vertebrate Palaeontology*. Blackwell Publishing, Oxford, 455 pp.

Bentov, S., Weil, S., Glazer, L., Saqi, A., and **Berman, A.** (2010) Stabilization of amorphous calcium carbonate by phosphate rich organic matrix proteins and by single phosphoamino acids. *Journal of Structural Biology,* **171,** 207–215.

Ben-Yaakov, S. (1973) pH buffering of pore water of recent anoxic marine sediment. *Limnology and Oceanography,* **18,** 86–94.

Berger, W.H. (1978) Deep-sea carbonate: pteropod distribution and the aragonite compensation depth. *Deep-Sea Research,* **25,** 447–452.

Berkeley, A., Perry, C.T., Smithers, S.G., Horton, B.P., and **Taylor, K.G.** (2007) A review of the ecological and taphonomic controls on foraminiferal assemblage development in intertidal environments. *Earth-Science reviews,* **83,** 205–230.

Berner, R.A. (1966) Chemical diagenesis of some modern carbonate sediments. *American Journal of Science,* **264,** 1–36.

Berner, R.A. and **Morse, J.W.** (1974) Dissolution kinetics of calcium carbonate in sea water IV. Theory of calcite dissolution. *American Journal of Science,* **274,** 1173–1186.

Berner, R.A., Scott, M.R., and **Thomlinson, C.** (1970) Carbonate alkalinity in the pore waters of anoxic marine sediments. *Limnology and Oceanography,* **15,** 544–549.

Bertram, M.A., Mackenzie, F.T., Bishop, F.C. and **Bischoff, W.D.** (1991) Influence of temperature on the stability of magnesian calcite. *American Mineralogist*, **76,** 1889–1896.

Bischoff, W.D., Bishop, F.C. and **Mackenzie, F.T.** (1983) Biogenically produced magnesian calcite: Inhomogeneities in chemical and physical properties; comparison with synthetic phases. *American Mineralogist*, **68,** 1183–1188.

Bischoff, W.D., Sharma, S.K., and **Mackenzie, F.T.** (1985) Carbonate ion disorder in synthetic and biogenic Mg-calcites: A Raman spectral study. *American Mineralogist,* **70,** 581–589.

Bischoff, W.D., Mackenzie, F.T. and **Bishop, F.C.** (1987) Stabilities of synthetic magnesian calcites in aqueous solution: comparison with biogenic materials. *Geochimica et Cosmochimica Acta*, **51,** 1413–1423.

Boardman, M.R. and **Carney, C.** (1991) Origin and accumulation of lime mud in ooid tidal channels, Bahamas. *Journal of Sedimentary Petrology*, **61,** 661–680.

Bode, A., Alvarez-Ossorio, M.T., Carrera, P., and **Lorenzo, J** (2004) Reconstruction of the trophic pathways between plankton and the North Iberian sardine (*Sardina pilchardus*) using stable isotopes. *Scientia Marina,* **68,** 165–178.

Boels, L., Wagterveld, R.M., Mayer, M.J., and **Witkamp, G.J.** (2010) Seeded calcite sonocrystallization. *Journal of Crystal Growth,* **312,** 961–966.

Bone, Q. and **Moore, R.H.** (2008) *Biology of Fishes* (3rd edition). Taylor and Francis, New York, 450 pp.

Bonneau, M.-C., Mélières, F., and **Vergnaud-Grazzini, C.** (1980) Variations isotopiques (oxygène et carbone) et cristallographiques chez les espèces actuelles de Foraminifères planctoniques en function de la profoundeur de dépôt. *Bulletin de la Société Géologique de France,* **7,** 791–793.

Bosence, D.W.J., Rowlands, R.J. and **Quine, M.L.** (1985) Sedimentology and budget of a Recent carbonate mound, Florida Keys. *Sedimentology*, **32,** 317–343.

Böttcher, M.E., Gehlken, P.-L., and **Steele, D.F.** (1997) Characterization of inorganic and biogenic magnesian calcites by Fourier Transform infrared spectroscopy. *Solid State Ionics,* **101–103,** 1379–1385.

Boudreau, B.P. (1991) Modelling the sulfide-oxygen reaction and associated pH gradients in porewaters. *Geochimica et Cosmochimica Acta,* **55,** 145–159.

Boynton, W.V. (1971) *An investigation of the thermodynamics of calcite–rhodochrisite solid solutions.* M.Sc. thesis, Carnegie-Melon University, 147 pp.

Brečević, L. and **Nielsen, A.E.** (1989) Solubility of amorphous calcium carbonate. *Journal of Crystal Growth,* **98,** 504–510.

Broecker, W.S. (1974) *Chemical Oceanography*. Harcourt Brace Jovanovich, New York, 214 pp.

Broecker, W.S. and **Takahashi, T.** (1966) Calcium carbonate precipitation on the Bahama Banks. *Journal of Geophysical Research*, **71,** 1575–1602.

Broecker, W.S., Sanyal, A. and **Takahashi, T.** (2000) The origin of Bahamian whitings revisited. *Geophysical Research Letters*, **27,** 3759–3760.

Broughton, R.E., Betancur-R., R., Li, C., Arratia, G., and **Ortí, G.** (2013) Multi-locus phylogenetic analysis reveals the pattern and tempo of bony fish evolution. *PLOS Currents Tree of Life* [last modified: 2013 May 9], Edition 1. doi: 10.1371/currents.tol.2ca8041495ffafd0c92756e75247483e.

Buczynski, C. and **Chafetz, H.S.** (1991) Habit of bacterially induced precipitates of calcium carbonate and the influence of medium viscosity on mineralogy. *Journal of Sedimentary Petrology*, **61,** 226–233.

Budd, D.A. and **Hiatt, E.E.** (1993) Mineralogical stabilization of high-magnesium calcite: geochemical evidence for intracrystal recrystalization within Holocene porcellaneous foraminifera. *Journal of Sedimentary Petrology,* **63,** 261–274.

Bullen, H.A., Oehrle, S.A., Bennett, A.F., Taylor, N.M., and **Barton, H.A.** (2008) Use of attenuated total reflectance Fourier transform infrared spectroscopy to identify microbial metabolic products on carbonate mineral surfaces. *Applied and Environmental Microbiology,* **74,** 4553–4559.

Burdige, D.J. and **Zimmerman, R.C.** (2002) Impact of seagrass density on carbonate dissolution in Bahamian sediments. *Limnology and Oceanography,* **47,** 1751–1763.

Burton, E.A. and **Walter, L.M.** (1990) The role of pH in phosphate inhibition of calcite and aragonite precipitation in seawater. *Geochimica et Cosmochimica Acta,* **54,** 797–808.

Busenberg, E. and **Plummer, L.N.** (1985) Kinetics and thermodynamic factors controlling the distribution of SO_4^{2-} and Na^+ in calcites and selected aragonites. *Geochimica et Cosmochimica Acta*, **49,** 713–725.

Busenberg, E. and **Plummer, L.N.** (1989) Thermodynamics of magnesian calcite solid solutions at 25 °C and 1 Atm total pressure. *Geochimica et Cosmochimica Acta*, **53,** 1189–1208.

Calvert, S.E. and **Price, N.B.** (1972) Diffusion and reaction profiles of dissolved manganese in the pore water of marine sediments. *Earth and Planetary Science Letters,* **16,** 245–249.

Carpenter, S.J. and **Lohmann, K.C.** (1992) Sr/Mg ratios of modern marine calcite: Empirical indicators of ocean chemistry and precipitation rate. *Geochimica et Cosmochimica Acta,* **56,** 1837–1849.

Chafetz, H.S. (1986) Marine peloids: a product of bacterially induced precipitation of calcite. *Journal of Sedimentary Research,* **56,** 812–817.

Chafetz, H.S. and **Buczynski, C.** (1992) Bacterially induced lithification of microbial mats. *Palaios*, **7,** 277–293.

Chafetz, H.S. and **Folk, R.L.** (1984) Travertines: depositional morphology and the bacterially constructed constituents. *Journal of Sedimentary Petrology,* **54,** 289–316.

Chave, K.E. (1954) Aspects of biogeochemistry of magnesium: 1. Calcareous marine organisms. *Journal of Geology*, **62,** 266–283.

Chave, K.E. (1962) Factors influencing the mineralogy of carbonate sediments. *Limnology and Oceanography*, **7,** 218–223.

Cheng, X., Varona, P.L., Olszta, M.J., and **Gower, L.B.** (2007) Biomimetic synthesis of calcite films by a polymer-induced liquid-precursor (PILP) process 1: Influence and incorporation of magnesium. *Journal of Crystal Growth,* **307,** 395–404.

Chu, V., Regev, L., Weiner, S., and **Boaretto, E.** (2008). Differentiating between anthropogenic calcite in plaster, ash and natural calcite using infrared spectroscopy: implication in archaeology. *Journal of Archaeological Sciences,* **35,** 905–911.

Clarkson, J.R., Price, T.J., and **Adams, C.J.** (1992) Role of metastable phases in the spontaneous precipitation of calcium carbonate. *Journal of the Chemical Society, Faraday Transactions,* **88,** 243–249.

Clifton, K.B. and **Motta, P.J.** (1998) Feeding morphology, diet, and ecomorphological relationships among five Caribbean labrids (Teleostei, Labridae). *Copeia*, **1998,** 953–966.

Cloud, P.E. (1962) Environment of calcium carbonate deposition west of Andros Island, Bahamas. *U.S. Geoogical Survey Professional Papers*, **350,** 1–138.

Coleyshaw, E.E., Crump, G., and **Griffith, W.P.** (2003) Vibrational spectra of the hydrated carbonate minerals ikaite, monohydrocalcite, lansfordite and nesquehonite. *Spectrochimica Acta A,* **59,** 2231–2239.

Combes, C. and **Rey, C.** (2010) Amorphous calcium phosphates: Synthesis, properties and uses in biomaterials. *Acta Biomaterialia,* **6,** 3362–3378.

Compere, E.L., Jr., and **Bates, J.M.** (1973) Determination of calcite:aragonite ratios in mollusc shells by infrared spectra. *Limnology and Oceanography,* **18,** 326–331.

Coplen, T.B. (1996) New guidelines for reporting stable hydrogen, carbon, and oxygen isotope-ratio data. *Geochimica et Cosmochimica Acta*, **60**, 3359-3360.

Craig, H. (1957) Isotopic standards for carbon and oxygen and correction factors for mass-spectrometric analysis of carbon dioxide. *Geochimica et Cosmochimica Acta*, **12**, 133-149.

Curran, H.A. and **Williams, A.B.** (1997) Ichnology of an intertidal carbonate sand flat: Pigeon Creek, San Salvador Island, Bahamas. In: *Proceedings of the Eighth Symposium on the Geology of The Bahamas and other carbonate regions: San Salvador* (Ed. J.L. Carew), pp. 33–46. Bahamian Field Station.

Dahl K. and **Buchardt, B.** (2006) Monohydrocalcite in the arctic Ikka Fjord, SW Greenland: First reported marine occurrence. *Journal of Sedimentary Research,* **76,** 460–471.

Davies, T.T. and **Hooper, P.R.** (1962) The determination of the calcite:aragonite ratio in mullusc shells by x-ray diffraction. *Mineralogical Magazine,* **33,** 608–612.

Debenay, J.P., André, J.P. and **Lesourd, M.** (1999) Production of lime mud by breakdown of foraminiferal tests. *Marine Geology*, **157,** 159–170.

Degens, E.T. and **Epstein, S.** (1964) Oxygen and carbon isotope ratios in coexisting calcites and dolomites from recent and ancient sediments. *Geochimica et Cosmochimica Acta,* **28,** 23–44.

Derrick, M.R., Stulik, D.C. and **Landry, J.M.** (1999) *Infrared Spectroscopy in Conservation Science*. The Getty Conservation Institute, Los Angeles, 235 pp.

Devery, D.M. and **Ehlmann, A.J.** (1981) Morphological changes in a series of synthetic Mg-calcites. *American Mineralogist*, **66,** 592–595.

Dickens, B. and **Brown, W.E.** (1970) The crystal structure of calcium carbonate hexahydrate at approximately -120 °C. *Inorganic Chemistry,* **9,** 480–486.

Dickson, A.G. (1990) Standard potential of the reaction: $AgCl(s) + 12H_2(g) = Ag(s) + HCl(aq)$, and the standard acidity constant of the ion HSO_4^- in synthetic sea water from 273.15 to 318.15 K. *Journal of Chemical Thermodynamics,* **22,** 113–127.

Dickson, A.G. (1993) ph buffers for sea water media based on the total hydrogen ion concentration scale. *Deep-Sea Research,* **40,** 107–118.

Dickson, A.G., and **Millero, F.J.** (1987) A comparison of the equilibrium constants for the dissociation of carbonic acid in seawater media. *Deep-Sea Research,* **34,** 1733–1743.

Dickson, A.G., Sabine, C.L., and Christian, J.R. (Eds.) (2007). *Guide to Best Practices for Ocean CO_2 measurements.* PICES Special Publication 3, 191 pp.

Dittmar, W. (1884) Report on researches into the composition of ocean water collected by H.M.S. Challenger during the years 1873–1876. In: *Voyage of the H.M.S. Challenger* (Ed. J. Murray). H.M. Station Office, London.

Dove, P.M. and **Hochella, M.F.** (1993) Calcite precipitation mechanisms and inhibition by orthophosphate: In-situ observations by scanning force microscopy. *Geochimica et Cosmochimica Acta,* **57,** 705–714.

Downs, R.T. (2006) The RRUFF Project: an integrated study of the chemistry, crystallography, Raman and infrared spectroscopy of minerals. *Program and Abstracts of the 19th General Meeting of the International Mineralogical Association***,** O03–13.

Dravis, J. (1979) Rapid and widespread generation of Recent oolitic hardgrounds on a high-energy Bahamian platform, Eleuthera Bank, Bahamas. *Journal of Sedimentary Petrology*, **49,** 195–207.

Droxler, A.W., Schlager, W., and **Whallon, C.C.** (1983) Quarternary aragonite cycles and oxygen-isotope record in Bahamian carbonate ooze. *Geology,* **11,** 235–239.

Droxler, A.W., Morse, J.W., and **Kornicker, W.A.** (1988) Conrols on carbonate mineral accumulation in Bahamas basins and adjacent Atlantic Ocean seidments. *Journal of Sedimentary Petrology,* **58,** 120–130.

Dupuis, T., Ducloux, J., Butel, P., and **Nahon, D.** (1984) Etude par spectrographie infrarouge d'un encroutement calcaires sous Galet. Mise en evidence et modelisation experimentale d'une suite minerale evolutive a partir de carbonate de calcium amorphe. *Clay Minerals,* **19,** 605–614.

Dye, A.H. and **Lasiak, T.A.** (1986) Microbenthos, meiobenthos and fiddler crabs: trophic interactions in a tropical mangrove sediment. *Marine Ecology – Progress Series,* **32,** 259–264.

Eardley, A.J. (1938) Sediments of Great Salt Lake, Utah. *Bulletin of the American Association of Petroleum Geologists,* **22,** 1305–1411.

Easley, R.A. and **Byrne, R.H.** (2012) Spectrophotometric calibration of pH electrodes in seawater using puried m-cresol purple. *Environmental Science and Technology,* **46,** 5018–5024.

Faggio, C., Torre, A., Lando, G., Sabatino, G., Trischitta, F. (2011) Carbonate precipitates and bicarbonate secretion in the intestine of sea bass, *Dicentrarchus labrax*. *Journal of Comparative Physiology B,* **181,** 517–525.

Fahraeus, L.E., Slatt, R.M., and Nowlan, G.S., 1974. Origin of carbonate pseudopellets. *Journal of Sedimentary Research,* **44,** 27–29.

Falini, G., Gazzano, M. and **Ripamonti, A.** (1994) Crystallization of calcium carbonate in presence of magnesium and polyelectrolytes. *Journal of Crystal Growth*, **137,** 577–584.

Falk, M. (1984) The frequency of the H-O-H bending fundamental in solids and liquids. *Spectrochimica Acta,* **40A,** 43–48.

Farmer, V.C. (1974) *Infra-red Spectra of Minerals* (Ed. V.C. Farmer), Mineralogical Society of America Monograph **4,** Mineralogical Society, London, 539 pp.

Feddern, H.A. (1965) The spawning, growth and general behaviour of the bluehead wrasse, *Thalassoma bifasciatum* (Pisces, Labridae). *Bulletin of Marine Science*, **15,** 896–941.

Fernández-Díaz, L., Putnis, A., Prieto, M. and **Putnis, C.V.** (1996) The role of magnesium in the crystallization of calcite and aragonite in a porous medium. *Journal of Sedimentary Research*, **66,** 482–491.

Finn, R.N. and **Kristoffersen, B.A.** (2007) Vertebrate vitellogenin gene duplication in relation to the "3R Hypothesis": Correlation to the pelagic egg and the oceanic radiation of teleosts. *Plos One*, **2,** e169.

Finn, R.N., Fyhn, H.J., Norberg, B., Munholland, J. and **Reith, M.** (2000) Oocyte hydration as a key feature in the adaptive evolution of teleost fishes to seawater. In: *6th International Symposium on Reproductive Physiology of Fish* (Eds. B. Norberg, O.S. Kjesbu, G.L. Taranger, E. Anderson and S.O. Stefansson), pp. 289–291, University of Bergen.

Flügel, E. (2004) *Microfacies of carbonate rocks: Analysis, Interpretation and Application*. Springer, Berlin Heidelberg New York, 976 pp.

Folk, R.L. (1965) Some aspects of recrystallization in ancient limestones. In: *Dolomitization and Limestone Diagenesis – A Symposium* (Eds. L.C. Pray and R.C. Murray). *Society of Economic Paleontologists and Mineralogists Special Publication,* **13,** 14–48.

Foran, E., Weiner, S., and **Fine, M.** (2013) Biogenic fish-gut calcium carbonate is a stable amorphous phase in the Gilt-head Seabream, *Sparus aurata*. *Nature Scientific Reports,* **3,** doi:10.1038/srep01700.

Fracalossi, D.M., Allen, M.E., Nichols, D.K., and **Oftedal, O.T.** (1998) Oscars, *Astronotus ocellatus*, have a dietary requirement for vitamin C. *Journal of Nutrition,* **128,** 1745–1751.

Franklin, M.L. and **Morse, J.W.** (1983) The interaction of manganese(II) with the surface of calcite in dilute solutions and seawater. *Marine Chemistry,* **12,** 241–254.

Froese, R. and **Pauly, D.** (2013) Fishbase. World wide web electronic publication – www.fishbase.org (version 10/2013). Accessed on 28th November 2013.

Frondel, C. and Bauer, L.H. (1955) Kutnahorite: a manganese dolomite, $CaMn(CO_3)_2$. *American Mineralogist,* **40,** 748–760.

Frost, R.L. and **Kloprogge, J.T.** (1999) Infrared emission spectroscopic study of brucite. *Spectrochimica Acta A,* **55,** 2195–2205.

Frost, R.L. and **Palmer, S.J.** (2011) Infrared and infrared emission spectroscopy of nesquehonite $Mg(OH)(HCO_3)\cdot 2H_2O$ – implications for the formula of nesquehonite. *Spectrochimica Acta A: Molecular and Biomolecular Spectroscopy,* **78,** 1255–1260.

Frost, R.L., Bahfenne, S., Graham, J., and **Reddy, B.J.** (2008) The structure of selected magnesium carbonate minerals – a near infrared and mid-infrared spectroscopic study. *Polyhedron,* **27,** 2069–2076.

Fry, B., Lutes, R., Northam, M., Parker, P.L., and **Ogden, J.** (1982) A $^{13}C/^{12}C$ comparison of food webs in Caribbean seagrass meadows and coral reefs. *Aquatic Botany,* **14,** 389–398.

Furukawa, K., Wolanski, E. and **Mueller, H.** (1997) Currents and sediment transport in mangrove forests. *Estuarine, Coastal and Shelf Science,* **44,** 301–310.

Fütterer, D.K. (1974) Significance of boring sponge Cliona for origin of fine-grained material of carbonate sediments. *Journal of Sedimentary Petrology*, **44,** 79–84.

Gaffey, S.J. (1995) H_2O and OH in echinoid calcite: A spectroscopic study. *American Mineralogist,* **80,** 947–959.

Gaffey, S.J. and **Bronnimann, C.E.** (1993) Effects of bleaching on organic and mineral phases in biogenic carbonates. *Journal of Sedimentary Petrology*, **63,** 752–754.

Gao, Y., Svec, R.A., and **Wallace, F.R.** (2012) Isotopic signatures of otoliths and the stock structure of canary rockfish along the Washington and Oregon coast. *Applied Geochemistry,* **32,** 70–75.

Garrels, R.M. and **Christ, C.L.** (1965) *Solutions, minerals, and equilibria*. Harper and Row, New York, 450 pp.

Gaudette, H.E. and **Lyons, W.B.** (1980) Phosphate geochemistry in nearshore carbonate sediments: a suggestion of apatite formation. In: *Marine Phosphorites* (Ed. Y.K. Bentor) *Society of Economic Paleotologists and Mineralogists Special Publication,* **29,** 215–225.

Gayathri, S., Lakshminarayanan, R., Weaver, J.C., Morse, D.E., Kini, R.M. and **Valiyaveettil, S.** (2007) In vitro study of magnesium-calcite biomineralization in the skeletal materials of the seastar *Pisaster giganteus*. *Chemistry-a European Journal*, **13,** 3262–3268.

Gehlen, M., Bassinot, F.C., Chou, L., and **McCorkle, D.** (2005) Reassessing the dissolution of marine carbonates: I. Solubility. *Deep-Sea Research I,* **52,** 1445–1460.

Genz, J., Taylor, J.R.and **Grosell, M.** (2008) Effects of salinity on intestinal bicarbonate secretion and compensatory regulation of acid–base balance in *Opsanus beta*. *Journal of Experimental Biology,* **211,** 2813–2827.

Gillet, P., McMillan, P., Schott, J., Badro, J., and **Grzechnik, A.** (1996) Thermodynamic properties and isotopic fractionation of calcite from vibrational spectroscopy of ^{18}O-substituted calcite. *Geochimica et Cosmochimica Acta,* **60,** 3471–3485.

Gillikin, D.P., Lorrain, A., Bouillon, S., Willenz, P., and **Dehairs, F.** (2006) Stable carbon isotopic composition of *Mytilus edulis* shells: relation to metabolism, salinity, $\delta^{13}C_{DIC}$ and phytoplankton. *Organic Geochemistry,* **37,** 1371–1382.

Ginsburg, R.N., Lloyd, R.M., McCallum, J.S., Stockman, K.W., and **Moody, R.A.** (1958) Surface sediments of the Great Bahama Bank, Shell Development Company, Houston, Texas, USA.

Ginsburg, R.N., Harris, P.M., Eberli, G.P., and Swart, P.K., 1991. The growth potential of a bypass margin, Great Bahama Bank. *Journal of Sedimentary Petrology,* **61,** 976–987.

Gischler, E. (2011) Sedimentary facies of Bora Bora, Darwin's Type barrier reef (Society Islands, South Pacific): The unexpected occurrence of non-skeletal grains. *Journal of Sedimentary Research*, **81,** 1–17.

Gischler, E. and **Zingeler, D.** (2002) The origin of carbonate mud in isolated carbonate platforms of Belize, Central America. *International Journal of Earth Sciences*, **91,** 1054–1070.

Gischler, E., Swart, P., and **Lomando, J.** (2009) Stable isotopes of carbon and oxygen in modern sediments of carbonate platforms, barrier reefs, atolls, and ramps: patterns and implications. In: *Perspectives in carbonate geology: A tribute to the career of Robert Nathan Ginsburg* (Eds. P.K Swart, G.P. Eberli, and J.A. McKenzie). *International Association of Sedimentologists Special Publication,* **41,** 61–74.

Gischler, E., Dietrich, S., Harris, D., Webster, J.M. and **Ginsburg, R.N.** (2013) A comparative study of modern carbonate mud in reefs and carbonate platforms: Mostly biogenic, some precipitated. *Sedimentary Geology,* **292,** 36–55.

Goldsmith, J.R., Graf, D.L. and **Heard, H.C.** (1961) Lattice constants of the calcium-magnesium carbonates. *American Mineralogist*, **46,** 453–457.

Golyshev, S.I., Padalko, N.L., and **Pechekin, S.A.** (1981) Fractionation of stable oxygen and carbon isotopes in carbonate systems. *Geokhimiya,* **10,** 1427–1441.

Gong, Y.U.T., Killian, C.E., Olson, I.C., Appathurai, N.P., Amasino, A.L., Martin, M.C., Holt, L.J., Wilt, F.H., and **Gilbert, P.U.P.A.** (2012) Phase transitions in biogenic amorphous calcium carbonate. *Proceedings of the National Academy of Sciences,* **109,** 6088–6093.

González-Muñoz, M.T., De Linares, C., Martínez-Ruiz, F., Morcillo, F., Martín-Ramos, D. and **Arias, J.M.** (2008) Ca-Mg kutnahorite and struvite production by Idiomarina strains at modern seawater salinities. *Chemosphere*, **72,** 465–472.

Google Earth 7.1.2.2041 (2013) *Eleuthera Bank and Exuma Sound, 24° 04' 02.66" N, 76° 16' 48.32" W, elevation -3 m (no data layers)*. Image created: 10th April 2013; Image accessed: 28th November 2013.

Grdadolnik, J. (2002) ATR-FTIR spectroscopy: Its advantages and limitations. *Acta Chimica Slovenica,* **49,** 631–642.

Greenfield, L.J. (1963) Metabolism and concentration of calcium and magnesium and precipitation of calcium carbonate by a marine bacterium. *Annals of the New York Academy of Sciences,* **109,** 23–45.

Grosell, M. (2006) Intestinal anion exchange in marine fish osmoregulation. *Journal of Experimental Biology*, **209,** 2813–2827.

Grosell M., Laliberte C.N., Wood S., Jensen F.B., and **Wood C.M.** (2001) Intestinal HCO_3^- secretion in marine teleost fish: evidence for an apical rather than a basolateral Cl^-/HCO_3^- exchanger. *Fish Physiology and Biochemistry,* **24,** 81–95.

Grosell, M., Wood, C.M., Wilson, R.W., Bury, N.R., Hogstrand, C., Rankin, C. and **Jensen, F.B.** (2005) Bicarbonate secretion plays a role in chloride and water absorption of the European flounder intestine. *American Journal of Physiology-Regulatory Integrative and Comparative Physiology*, **288,** R936–R946.

Grossman, E.T. and **Ku, T.L.** (1986) Oxygen and carbon isotope fractionation in biogenic aragonite: Temperature effects. *Chemical Geology,* **59,** 59–74.

Gulbrandsen, R.A., Roberson, C.E., and **Neil, S.T.** (1984) Time and the crystallization of apatite in seawater. *Geochimical et Cosmochimica Acta,* **48,** 213–218.

Gunnar, A., Blomqvist, S., and **Martinsson, C.** (2004) Inorganic formation of apatite in brackish seawater from the Baltic Sea: an experimental approach. *Marine Chemistry,* **91,** 15–26.

Gutjahr, A., Dabringhaus, H., and Lacmann, R. (1996) Studies of the growth and dissolution kinetics of the $CaCO_3$ polymorphs calcite and aragonite: II. The influence of divalent cation additives on the growth and dissolution rates. *Journal of Crystal Growth*, **158,** 310–315.

Halbach, P. (1986) Processes controlling the heavy metal distribution in Pacific ferromanganese nodules and crusts. *Geologische Rundschau,* **75,** 235–247.

Hardie, L.A. (1996) Secular variation in seawater chemistry: An explanation for the coupled secular variation in the mineralogies of marine limestones and potash evaporites over the past 600 my. *Geology*, **24,** 279–283.

Heath, K.C. and Mullins, H.T., 1984. Open-ocean off-bank transport of fine-grained carbonate sediment in the northern Bahamas. In: *Fine-grained Sediments: Deepwater processes and Facies* (Eds. D.A.V. Stow and D.J.W. Piper). *Geological Society of London Special Publications,* **15,** 199–208.

Helfman, G., Collette, B.B., Facey, D.E., and **Bowen, B.W.** (2009) *The Diversity of Fishes: Biology, Evolution, and Ecology*, 2nd edition. Wiley-Blackwell, New York, 736 pp.

Horita, J., Zimmermann, H. and **Holland, H.D.** (2002) Chemical evolution of seawater during the Phanerozoic: Implications from the record of marine evaporites. *Geochimica et Cosmochimica Acta*, **66,** 3733–3756.

Hover, V.C., Walter, L.M. and **Peacor, D.R.** (2001) Early marine diagenesis of biogenic aragonite and Mg-calcite: new constraints from high-resolution STEM and AEM analyses of modern platform carbonates. *Chemical Geology*, **175,** 221–248.

Hu, X. and **Burdige, D.J.** (2007) Enriched stable carbon isotopes in the pore waters of carbonate sediments dominated by seagrasses: Evidence for coupled carbonate dissolution and reprecipitation. *Geochimica et Cosmochimica Acta,* **71,** 129–144.

Huang C.K. and **Kerr P.F.** (1960) Infrared study of the carbonate minerals. *American Mineralogist,* **43,** 311–324.

Hull, H. and **Turnball, A.G.** (1973) A thermochemical study of monohydrocalcite. *Geochimica et Cosmochimica Acta,* **87,** 685–694.

Humbert, W., Kirsch, R. and **Simonneaux, V.** (1986) Is mucus involved in biocrystallization: study of the intestinal mucus of the sea-water eel, *Anguilla anguilla*. *Cell and Tissue Research*, **245,** 599–604.

Humbert, W., Voegel, J.C., Kirsch, R. and **Simonneaux, V.** (1989) Role of intestinal mucus in crystal biogenesis: an electron-microscopical, diffraction and X-ray microanalytical study. *Cell and Tissue Research*, **255,** 575–583.

Husseini, S.I. and **Matthews, R.K.** (1972) Distribution of high-magnesium calcite in lime muds of Great Bahama Bank: diagenetic implications. *Journal of Sedimentary Petrology*, **42,** 179–182.

Illing, L.V. (1954) Bahamian calcareous sands. *American Association of Petroleum Geologists Bulletin,* **38,** 1–95.

Ishikawa, M. and **Ichikuni, M.** (1981) Coprecipitation of phosphate with calcite. *Geochemical Journal,* **15,** 283–288.

Janet, C.M., Viswanathan, B., Viswanath, R.P., and **Varadarajan, T.K.** (2007) Characterization and photoluminescence properties of MgO microtubes synthesized from hydromagnesite flowers. *Journal of Physical Chemistry C,* **111,** 10267–10272.

JB Weld Co. (2012) MarineWeld resin and hardener [Material Safety Data Sheet]. Retrieved from: http://www.jbweld.com/wp-content/uploads/2012/08/J-B-Weld-MSDS-MarineWeld.pdf [22nd January 2013].

Jiménez-López, C., Caballero, E., Huertas, F.J., and **Romanek, C.S.** (2001) Chemical, mineralogical and isotope behaviour, and phase transformation during the precipitation of calcium carbonate minerals from intermediate ionic solution at 25 °C. *Geochimica et Cosmochimica Acta,* **65,** 3219–3231.

Jiménez-López, C., Romanek, C.S., and **Caballero, E.** (2006) Carbon isotope fractionation in synthetic magnesian calcite. *Geochimica et Cosmochimica Acta,* **70,** 1163–1171.

Johnson, G.D. and **Patterson, C.** (1993) Percomorph phylogeny: a survey of acanthomorphs and a new proposal. *Bulletin of Marine Science,* **52,** 554–626.

Kalish, J.M. (1991) ^{13}C and ^{18}O isotopic disequilibria in fish otoliths: metabolic and kinetic effects. *Marine Ecology Progress Series,* **75,** 191–203.

Kelley, D.S., Karson, J.A., Blackman, D.K., Früh-Green, G.L., Butterfield, D.A., Lilley, M.D., Olson, E.J., Schrenk, M.O., Roe, K.K., Lebon, G.T., and **Rivizzigno, P.** (2001) An off-axis hydrothermal vent field discovered near the Mid-Atlantic Ridge at 30° N. *Nature,* **412,** 150–157.

Kerr, S.R. (1982) Estimating the energy budgets of actively predatory fishes. *Canadian Journal of Fisheries and Aquatic Sciences,* **39,** 371–379.

Kibalczyc, W., Christoffersen, J., Christoffersen, M.R., Zielenkiewicz, A., and **Zielenkiewicz, W.** (1990) The effect of magnesium ions on the precipitation of calcium phosphates. *Journal of Crystal Growth,* **106,** 355–366.

Kieckbusch, D.K., Koch, M.S., Serafy, J.E., and **Anderson, W.T.** (2004) Trophic linkages among primary producers and consumers in fringing mangroves of subtropical lagoons. *Bulletin of Marine Science,* **74,** 271–285.

Kitano, Y., Tokuyama, A., and **Arakaki, T.** (1979) Magnesian calcite synthesis from calcium bicarbonate solution containing magnesium and barium ions. *Geochamical Journal,* **13,** 181–185.

Kloprogge, J.T., Martens, W.N., Nothdurft, L., Duong, L.V. and **Webb, G.E.** (2003) Low temperature synthesis and characterization of nesquehonite. *Journal of Materials Science Letters*, **22,** 825–829.

Konchisky, A. and **Halbach, P.** (1995) Sequential leaching of marine ferromanganese precipitates: Genetic implications. *Geochimica et Cosmochimica Acta,* **59,** 5113–5132.

Kontrovitz, M., Slack, J.M. and **Yuhong, Z.** (1991) On the use of some phosphates in the preparation of ostracod shells. *Journal of Micropalaeontology,* **10,** 121–126.

Kornicker, L.S. (1963) The Bahama banks: A "living" fossil environment. *Journal of Geological Education,* **11,** 17–25.

Kornicker, L.S. and Purdy, E.G., 1957. A Bahamian faecal-pellet sediment. *Journal of Sedimentary Research,* **27,** 126–128.

Kralj, D., Kontrec, J., Brecevic, L., Falini, G. and **Nothig-Laslo, V.** (2004) Effect of inorganic anions on the morphology and structure of magnesium calcite. *Chemistry-a European Journal*, **10,** 1647–1656.

Krauskopf, K.B. and **Bird, K.D.** (1995) *Introduction to Geochemistry* (3rd edition). McGraw-Hill, New York, 647 pp.

Krumbein, W.E. (1975) Biogenic monohydrocalcite spherules in lake sediments of Lake Kivu (Africa) and Solar Lake (Sinai). *Sedimentology,* **22,** 634–635.

Ku, T.C.W., Walter, L.M., Coleman, M.L., Blake, R.E., and **Martini, A.M.** (1999) Coupling between sulfur recycling and syndepositional carbonate dissolution: Evidence from pore water sulfate, South Florida Platform, U.S.A. *Geochimica et Cosmochimica Acta,* **63,** 2529–2546.

Labonne, M. and **Hillaire-Marcel, C.** (2000) Geochemical gradients within modern and fossil shells of *Conchlepas concholepas* from norther Chile: An insight into U–Th systematics and diagenetic/auhigenic isotopic imprints in mollusk shells. *Geochimica et Cosmochimica Acta,* **64,** 1523–1534.

Lafon, G.M. (1990). Reversed equilibrium solubility of a high-magnesian calcite. In: *Fluid-Mineral Interactions: A tribute to H.P. Eugster.* Special Publication 2 (Eds. R.J. Spencer and I-M. Chou). pp. 23–40. The Geochemical Society, San Antonio.

Lamb, K., Swart, P.K., and **Altabet, M.A.** (2012) Nitrogen and carbon isotopic systematics of the Florida reef tract. *Bulletin of Marine Science,* **88,** 119–146.

Land, L.S. (1967) Diagenesis of skeletal carbonates. *Journal of Sedimentary Petrology,* **37,** 914–930.

Lane, M.D. (1999) Midinfrared optical constants of calcite and their relationship to particle size effects in thermal emission spectra of granular calcite. *Journal of Geophysical Research: Planets,* **104,** 14099–14108.

Langmuir, D. (1997) *Aqueous Environmental Geochemistry*. Prentice Hall, New Jersey, 600 pp.

Lasemi, Z. and **Sandberg, P.** (1984) Transformation of aragonite-dominated lime muds to microcrystalline limestones. *Geology,* **12,** 420–423.

Layman, C.A. and **Silliman, B.R.** (2002) Preliminary survey and diet analysis of juvenile fishes of an estuarine creek on Andros Island, Bahamas. *Bulletin of Marine Science,* **70,** 199–210.

Lee, K., Tong, L.T., Millero, F.J., Sabine, C.L., Dickson, A.G., Goyet, C., Park, G-H., Wanninkhof, R., Feely, R.A. and **Key, R.M.** (2006) Global relationships of total alkalinity with salinity and temperature in surface waters of the world's oceans. *Geophysical Research Letters,* **33,** L19605, doi: 10.1029/2006GL027207.

Levi-Kalisman, Y., Raz, S., Weiner, S., Addadi, L., and **Sagi, I.** (2002) Structural differences between biogenic amorphous calcium carbonate phases using X-ray Absorption Spectroscopy. *Advanced Functional Materials,* **12,** 43–48.

Lin, Y.P., Singer, P.C., and **Aiken, G.R.** (2005) Inhibition of calcite precipitation by natural organic material: Kinetics, mechanisms and thermodynamics. *Environmental Science and Technology,* **39,** 6420–6428.

Lippmann, F. (1960) Versuch zur aufklarung der bildungsbedeingrengen von kalzit under aragonit. *Fortschritte der Mineralogie,* **38,** 156–161.

Littler, K., Robinson, S.A., Bown, P.R., Nederbragt, A.J. and **Pancost, R.D.** (2011) High sea-surface temperatures during the Early Cretaceous Epoch. *Nature Geoscience*, **4,** 169–172.

Llalier-Vergès, E., Perrussel, B.P., Disnar, J.-R., and **Baltzer, F.** (1998) The relationship between environmental conditions and the diagenetic evolution of organic matter derived from higher plants in a modern mangrove swamp system (Guadeloupe, French West Indies). *Organic Geochemistry,* **29,** 1663–1686.

Loeppert, R.H. and **Hossner, L.R.** (1984) Reactions of Fe^{2+} and Fe^{3+} with calcite. *Clays and Clay Minerals,* **32,** 213–222.

Long, X., Ma, Y. and **Qi, L.** (2011) In vitro synthesis of high Mg calcite under ambient conditions and its implication for biomineralization process. *Crystal Growth and Design,* **11,** 2866–2873.

Lopez, O., Zuddas, P. and **Faivre, D.** (2009) The influence of temperature and seawater composition on calcite crystal growth mechanisms and kinetics: implications for Mg incorporation in calcite lattice. *Geochimica et Cosmochimica Acta,* **73,** 337–347.

Loreau, J.P. (1982) *Sédiments aragonitiques et leur genèse*. Muséum National D'Histoire Naturelle, Paris. Mémoires, Série C 47, 300 pp.

Lorrain, A., Paulet, Y.-M., Chauvaud, L., Dunbar, R., Mucciarone, D., and **Fontugne, M.** (2004) $\delta^{13}C$ variation in scallop shells: increasing metabolic carbon contribution with body size? *Geochimica et Cosmochimica Acta,* **68,** 3509–3519.

Loste, E., Wilson, R.M., Seshadri, R., and **Meldrum, F.C.** (2003) The role of magnesium in stabilising amorphous calcium carbonate and controlling calcite morphologies. *Journal of Crystal Growth,* **254,** 206–218.

Love, K.M. and **Woronow, A.** (1991) Chemical changes induced in aragonite using treatments for the destruction of organic material. *Chemical Geology*, **93,** 291–301.

Lowenstam, H.A. (1954) Factors affecting the aragonite:calcite ratios in carbonate-secreting marine organisms. *Journal of Geology,* **62,** 284–322.

Lowenstam, H.A. and **Epstein, S.** (1957) On the origin of sedimentary aragonite needles of the Great Bahama Bank. *The Journal of Geology*, **65,** 364–375.

Lowenstein, T.K., Timofeeff, M.N., Brennan, S.T., Hardie, L.A., and **Demicco, R.V.** (2001) Oscillations in Phanerozoic seawater chemistry: Evidence from fluid inclusions. *Science,* **294,** 1086–1088.

Lüttge, A. and **Conrad, P.G.** (2004) Direct observation of microbial inhibition of calcite dissolution. *Applied Environmental Microbiology,* **70,** 1627–1632.

Luzinova, Y., Dobbs, G.T., Lapham, L., Chanton, J.P., and **Mizaikoff, B.** (2011) Detection of cold seep derived authigenic carbonates with infrared spectroscopy. *Marine Chemistry,* **125,** 8–18.

MacIntyre, I.G. and **Reid, R.P.** (1995) Crystal alteration in a living calcareous alga (*Halimeda*): implications for studies in skeletal diagenesis. *Journal of Sedimentary Research,* **65,** 143–153.

MacIntyre, I.G. and **Reid, R.P.** (1998) Recrystallization in living porcelaneous foraminifera (*Archaias angulatis*): Textural changes without mineralogic alteration. *Journal of Sedimentary Research*, **68,** 11–19.

Mackenzie, F.T., Bischoff, W.B., Bishop, F.C., Loijens, M., Schoonmaker, J. and **Wollast, R.** (1983) Magnesian calcites: low-temperature occurrence, solubility and solid-solution behaviour. In: *Carbonates, Mineralogy and Chemistry* (Ed. R.J. Reeder), pp. 97–144. Bookcrafters, Chelsea, Michigan.

Malone, M.J., Slowey, N.C., and **Henderson, G.M.** (2001) Early diagenesis of shallow-water periplatform carbonate sediments, leeward margin, Great Bahama Bank (Ocean Drilling Program Leg 166). *Geological Society of America Bulletin,* **113,** 881–894.

Marshall, W.S. and Grosell, M. (2005) Ion transport and osmoregulation in fish. In: *The Physiology of Fishes* (Ed. D. Evans). CRC Press, Boca Raton, Florida, pp. 177–230.

Martens, C.S. and **Harriss, R.C.** (1970) Inhibition of apatite precipitation in the marine environments by magnesium ions. *Geochimica et Cosmochimica Acta,* **34,** 621–625.

Martin, J.H. and **Knauer, G.A.** (1983) VERTEX: Manganese transport with $CaCO_3$. *Deep Sea Research Part A. Oceanographic Research Papers,* **30,** 411–425.

Mather, M.A., Vanni, M.J., Wissing, T.E., Davis, S.A., and **Schaus, M.H.** (1995) Regeneration of nitrogen and phosphorus by bluegill and gizzard shad: Effect of feeding history. *Canadian Journal of Fisheries and Aquatic Sciences,* **52,** 2327–2338.

Matthews, R.K. (1966) Genesis of recent lime mud in Southern British Honduras. *Journal of Sedimentary Petrology*, **36,** 428–454.

McBride, M.B. (1979) Chemisorption and precipitation of Mn^{2+} at $CaCO_3$ surfaces. *Soil Science Society of America Journal,* **43,** 693–698.

McConnaughey, T.A., Burdett, J., Whelan, J.F., and **Paull, C.K.** (1997) Carbon isotopes in biological carbonates: respiration and photosynthesis. *Geochimica et Cosmochimca Acta,* **61,** 611–622.

McCrea, J.M. (1950) On the isotopic chemistry of carbonates and a paleotemperature scale. *Journal of Chemical Physics*, **18**, 849-857.

McKee, E.D. and Gutschick, R.C., 1969. *History of the Redwall Limestone of Northern Arizona*. Geological Society of America, 726 pp.

Mehrbach, C., Culberson, C.H., Hawley, J.E., and **Pytkowicz, R.M.** (1973) Measurement of the apparent dissociation constants of carbonic acid in seawater at atmospheric pressure. *Limnology and Oceanography,* **18,** 897–907.

Mekuchi, M., Hatta, T. and **Kaneko, T.** (2010) Mg-calcite, a carbonate mineral, constitutes Ca precipitates produced as a byproduct of osmoregulation in the intestine of seawater-acclimated Japanese eel *Anguilla japonica*. *Fisheries Science*, **76,** 199–205.

Meldrum, F.C. and **Hyde, S.T.** (2001) Morphological influence of magnesium and organic additives on the precipitation of calcite. *Journal of Crystal Growth*, **231,** 544–558.

Melim, L.A., and **Spilde, M.N.** (2011) Rapid growth and recrystallization of cave pearls in an underground limestone mine. *Journal of Sedimentary Research,* **81,** 775–786.

Millero, F.J. (1996) *Chemical Oceanography*. CRC Press, Boca Raton, Florida, 469 pp.

Millero, F.J., Milne, P.J., and **Thurmond, V.L.** (1984) The solubility of calcite, strontianite and witherite in NaCl solutions at 25 °C. *Geochimica et Cosmochimica Acta,* **48,** 1141–1143.

Milliman, J.D., Gastner, M., and **Muller, J.** (1971) Utilization of magnesium in coralline algae. *Geological Society of America Bulletin,* **82,** 573–580.

Milliman, J.D. (1974) *Marine Carbonates*. Springer-Verlag, Heidelberg, 375 pp.

Milliman, J.D., Freile, D., Steinen, R.P. and **Wilber, R.J.** (1993) Great Bahama Bank aragonitic muds; mostly inorganically precipitated, mostly exported. *Journal of Sedimentary Petrology*, **63,** 589–595.

Mitchell, S. (1987) Sedimentology of Pigeon Creek, San Salvador Island, Bahamas. In: *Proceedings of the Third Symposium on the Geology of The Bahamas: Fort Lauderdale, Florida, CCFL* (Ed. H.A. Curran), pp. 215–230. Bahamian Field Station.

Moreau, R. and **Dabrowski, K.** (1998) Fish acquired ascorbic acid synthesis prior to terrestrial vertebrate emergence. *Free Radical Biology and Medicine,* **25,** 989–990.

Morrow, J.E. and **Mauro, A.** (1950) Body temperatures of some marine fishes. *Copeia,* **1950,** 108–116.

Morse, J.W. (1974) Dissolution kinetics of calcium carbonate in seawater: V. Effects of natural inhibitors and the position of the chemical lysocline. *American Journal of Science*, **274,** 638–647.

Morse J.W. and **Arvidson, R.S.** (2002) The dissolution kinetics of major sedimentary carbonate minerals. *Earth-Science Reviews,* **58,** 51–84.

Morse, J.W. and **Mackenzie, F.T.** (1990) *Geochemistry of Sedimentary Carbonates*. Elsevier, Amsterdam, 707 pp.

Morse, J.W., deKanel, J., and **Harris, J.** (1979) Dissolution kinetics of calcium carbonate in seawater: VII. The dissolution kinetics of synthetic aragonite and pteropod tests. *American Journal of Science,* **279,** 482–502.

Morse, J.W., Millero, F.J., Thurmond, V., Brown, E., and **Ostlund, H.G.** (1984) The carbonate chemistry of Grand Bahama Bank waters: after 18 years another look. *Journal of Geophysical Research*, **89,** 622–628.

Morse, J.W., Zullig, J.J., Lawrence, D.B., Millero, F.J., Milne, P., Mucci, A. and **Choppin, G.R.** (1985) Chemistry of calcium carbonate-rich shallow water sediments in the Bahamas. *American Journal of Science,* **285,** 147–185.

Morse, J.W., Wang, Q.W. and **Tsio, M.Y.** (1997) Influences of temperature and Mg:Ca ratio on CaCO3 precipitates from seawater. *Geology*, **25,** 85–87.

Morse, J.W., Gledhill, D.K., and **Millero, F.J.** (2003) $CaCO_3$ precipitation kinetics in waters from the Great Bahama Bank: Implications for the relationship between Bank hydrochemistry and whitings. *Geochimica et Cosmochimica Acta,* **67,** 2819–2826.

Morse, J.W., Andersson, A.J. and **Mackenzie, F.T.** (2006) Initial responses of carbonate-rich shelf sediments to rising atmospheric pCO(2) and "ocean acidification": Role of high Mg-calcites. *Geochimica et Cosmochimica Acta*, **70,** 5814–5830.

Morse, J.W., Arvidson, R.S., and Lüttge, A. (2007) Calcium carbonate formation and dissolution. *Chemical Reviews,* **107,** 342–381.

Moulin, E.A., Jordens, A., and **Wollast, R.** (1985) Influence of the aerobic bacerial respiration on the early dissolution of carbonates in coastal sediments. *Proceedings in Progress in Belgian Oceanographic Research, Brussels,* 196–205.

Mucci, A. (2004) The behaviour of mixed Ca–Mn carbonates in water and seawater: Controls of manganese concentrations in marine porewaters. *Aquatic Geochemistry,* **10,** 139–169.

Mucci, A. and **Morse, J.W.** (1983) The incorporation of Mg^{2+} and Sr^{2+} into calcite overgrowths: influences of growth-rate and solution composition. *Geochimica et Cosmochimica Acta*, **47,** 217–233.

Mucci, A. and **Morse, J.W.** (1984) The solubility of calcite in seawater solutions of various magnesium concentration, I_t = 0.697 m at 25 °C and one atmosphere total pressure. *Geochimica et Cosmochimica Acta*, **48,** 815–822.

Mucci, A., Morse, J.W. and **Kaminsky, M.S.** (1985) Auger-spectroscopy analysis of magnesian calcite overgrowths precipitated from seawater and solutions of similar composition. *American Journal of Science*, **285,** 289–305.

Mullins, H.T. (1983) Modern carbonate slopes and basins of the Bahamas. In: *Platform margin and deep water carbonates* (Eds. H.E. Cook and H.T. Mullins) *Society for Economic Paleontologists and Mineralogists Short Course,* **12,** p. 4-1–4-138.

Mullins, H.T., Heath, K.C., and **Van Buren, H.M.** (1984) Anatomy of a modern open ocean carbonate slope: northern Little Bahama Bank. *Sedimentology,* **31,** 141–168.

Multer, H.G. (1988) Growth-rate, ultrastructure and sediment contribution of *Halimeda incrassata* and *Halimeda monile*, Nonsuch and Falmouth Bays, Antigua, WI. *Coral Reefs*, **6,** 179–186.

Nakamoto, K., Fujita, J., Tanaka, S., and **Kobayashi, M.** (1957) Infrared spectra of metallic complexes. IV. Comparison of the infrared spectra of unidentate and bidentate metallic complexes. *Journal of the American Chemical Society,* **79,** 4904–4908.

Nelson, J.S. (2006) *Fishes of the World*, 4th edition. John Wiley and Sons, 624 pp.

Neumann, A.C. and **Land, L.S.** (1975) Lime mud deposition and calcareous algae in Bight of Abaco, Bahamas: a budget. *Journal of Sedimentary Petrology*, **45,** 763–786.

Neumann, M. and **Epple, M.** (2007) Monohydrocalcite and its relationship to hydrated amorphous calcium carbonate in biominerals. *European Journal of Inorganic Chemistry,* **2007,** 1953–1957.

Newell, N.D., Imbrie, J., Purdy, E.G., and **Thurber, D.L.** (1959) Organism communities and bottom facies, Great Bahama Bank. *Bulletin of the American Museum of Natural History,* **117,** 177–228.

Newman, M.J.H., Paredes, G.A., Sala, E. and **Jackson, J.B.C.** (2006) Structure of Caribbean coral reef communities across a large gradient of fish biomass. *Ecology Letters*, **9,** 1216–1227.

Nothdurft, L.D., Webb, G.E., Buster, N.A., Holmes, C.W., Sorauf, J.E., and **Kloprogge, J.E.** (2005) Brucite microbialites in living coral skeletons: Indicators of extreme microenvironments in shallow-marine settings. *Geology,* **33,** 169–172.

Patterson, W.P. and **Walter, L.M.** (1994a) Syndepositional diagenesis of modern platform carbonates: Evidence from isotopic and minor element data. *Geology,* **22,** 127–130.

Patterson, W.P. and **Walter, L.M.** (1994b) Depletion of ^{13}C in seawater ΣCO_2 on modern carbonate platforms: Significance for the carbon isotopic record of carbonates. *Geology,* **22,** 885–888.

Pearson, P.N., Ditchfield, P.W., Singano, J., Harcourt-Brown, K.G., Nicholas, C.J., Olsson, R.K., Shackleton, N.J. and **Hall, M.A.** (2001) Warm tropical sea surface temperatures in the Late Cretaceous and Eocene epochs. *Nature*, **413,** 481–487.

Peckol, P.M., Curran, H.A., Greenstein, B.J., Floyd, E.Y., and **Robbart, M.L.** (2003) Assessment of coral reefs off San Salvador Island, Bahamas (stony corals, algae and fish populations). In: *Status of coral reefs in the Western Atlantic: Results of initial surveys, Atlantic and Gulf rapid reef assessment (AGRRA) program* (Ed. J.C. Lang). *Atoll Research Bulletin,* **496,** pp. 124–144.

Pedley, M., Rogerson, M. and **Middleton, R.** (2009) Freshwater calcite precipitates from *in vitro* mesocosm flume experiments: a case for biomediation of tufas. *Sedimentology,* **56,** 511–527.

Perry, C.T. (2000) Factors controlling sediment preservation on a north Jamaican fringing reef: a process based approach to microfacies analysis. *Journal of Sedimentary Research,* **70,** 633–648.

Perry, C.T. and **Taylor, K.G.** (2007) *Environmental Sedimentology*. Blackwell Publishing, Oxford, 441 pp.

Perry, C.T., Berkeley, A., and **Smithers, S.G.** (2008) Microfacies characteristics of a tropical, mangrove-fringed shoreline, Cleveland Bay, Queensland, Australia: Sedimentary and taphonomic controls on mangrove facies development. *Journal of Sedimentary Research,* **78,** 77–97.

Perry, C.T., Salter, M.A., Harborne, A.R., Crowley, S.F., Jelks, H.L. and **Wilson, R.W.** (2011) Fish as major carbonate mud producers and missing components of the tropical carbonate factory. *Proceedings of the National Academy of Sciences*, **108,** 3865–3869.

Pierrot, D., Lewis, E., and **Wallace, D.W.R.** (2006) MS Excel program developed for CO_2 system calculations. ORNL/CDIAC–105a. Carbon Dioxide Information Analysis Centre, Oak Ridge National Laboratory, U.S. Depertment of Energy, Oak Ridge, Tennessee. doi: 10.3334/CDIAC/otg.CO2SYS_XLS_CDIAC105a.

Pilskaln, C.H., Neumann, S.C., and **Bane, J.M.** (1989) Periplatform flux in the northern Bahamas. *Deep-Sea Research,* **36,** 1391–1406.

Pingitore Jr., N.E., Lytle, F.W., Davies, B.M., Eastman, M.P., Eller, P.G. and **Larson E.M.** (1992) Mode of incorporation of Sr^{2+} in calcite: determination by X-ray absorption spectroscopy. *Geochimica et Cosmochimica Acta,* **56,** 1531–1538.

Plaziat, J.-C. (1995) Modern and fossil mangroves and mangals: their climatic and biogeographic variability. In: *Marine Palaeoenvironmental Analysis from Fossils* (Eds. D.W.J. Bosence and P.A. Allison). *Geological Society Special Publication,* **83**, 73–96.

Plummer, L.N. and **Busenberg, E.** (1982) The solubilities of calcite, aragonite, and vaterite in CO_2–H_2O solutions between 0 and 90 °C, and an evaluation of the aqueous model for the system $CaCO_3$–CO_2–H_2O. *Geochimica et Cosmochimica Acta,* **46,** 1011–1040.

Plummer, L.N. and **Mackenzie, F.T.** (1974) Predicting mineral solubility from rate data; application to dissolution of magnesian calcites. *American Journal of Science*, **274,** 61–83.

Politi, Y., Arad, T., Klein, E., Weiner, S., and **Addadi, L.** (2004) Sea urchin spine calcite forms via a transient amorphous calcium carbonate phase. *Science,* **306,** 1161–1164.

Pomar, L. and **Hallock, P.** (2008) Carbonate factories: A conundrum in sedimentary geology. *Earth Science Reviews*, **87,** 134–169.

Power, I.M., Wilson, S.A., Thom, J.M., Dipple, G.M. and **Southam, G.** (2007) Biologically induced mineralization of dypingite by cyanobacteria from an alkaline wetland near Atlin, British Columbia, Canada. *Geochemical Transactions*, **8:13.**

Presley, B.J., Brooks, R.R., and **Kaplan, I.R.** (1967) Manganese and related elements in the interstitial water of marine sediments. *Science*, **17,** 906–910.

Prieto, M., Putnis, A., Fernández-Díaz, L. and **López-Andrés, S.** (1994) Metastability in diffusing-reacting systems. *Journal of Crystal Growth*, **142,** 225–235.

Purdy, E.G. (1963) Recent calcium carbonate facies of the Great Bahama Bank. 2. Sedimentary facies. *Journal of Geology,* **71,** 472–497.

Purdy, E.G. (1968) Carbonate diagenesis: An environmental survey. *Geologica Romana,* **7,** 183–228.

Purdy, E.G. and **Gischler, E.** (2003) The Belize margin revisited: 1. Holocene marine facies. *International Journal of Earth Sciences*, **92,** 532–551.

Ramasamy, V., Ponnusamy, V., Sabari, S., Anishia, S.R., and **Gomathi, S.S.** (2009) Effect of grinding on the crystal structure of recently excavated dolomite. *Indian Journal of Pure and Applied Physics,* **47,** 586–591.

Radha, A.V., Forbes, T.Z., Killian, C.E., Gilbert, P.U.P.A, and **Navrotsky, A.** (2010) Transformation and crystallization energetics of synthetic and biogenic amorphous calcium carbonate. *Proceedings of the National Academy of Sciences*, **107,** 16438–16443.

Randall, J.E. (1967) Food habits of reef fishes of the West Indies. *Studies in Tropical Oceanography*, **5,** 665–847.

Rankey, E.C. and **Doolittle, D.F.** (2012) Geomorphology of carbonate platform-marginal uppermost slopes: Insights from a Holocene analogue, Little Bahama Bank, Bahamas. *Sedimentology,* **59,** 2146–2171.

Rankey, E.C., and **Reeder, S.L.** (2010) Controls on platform-scale patterns of surface sediments, shallow Holocene platforms, Bahamas. *Sedimentology,* **57,** 1545–1565.

Raz, S., Testeniere, O., Hecker, A.,Weiner, S., and **Luquet, G.** (2002) Stable amorphous calcium carbonate is the main component of the calcium storage structures of the crustacean *Orchestia cavimana*. *The Biological Bulletin,* **203,** 269–274.

Reddy, M.M. (2012) Calcite growth-rate inhibition by fulvic acid and magnesium ion – possible influence on biogenic calcite formation. *Journal of Crystal Growth,* **352,** 151–154.

Reddy, M.M. and **Hoch, A.R.** (2002) Calcite crystal growth rate inhibition by aquatic humic substances. In: *Advances in Crystal Growth Inhibition Technologies* (Ed. Z. Amjad). Kluwer Academic/Plenum Publishers, New York, 107–121.

Reddy, M.M. and **Wang, K.K.** (1980) Crystallization of calcium carbonate in the presence of metal ions: 1. Inhibition by magnesium ion at pH 8.8 and 25 °C. *Journal of Crystal Growth*, **50,** 470–480.

Redfield, A.C., Ketchum, B.H., and **Rickard, F.A.** (1963) The influence of organisms on the composition of seawater. In: *The Sea*, Vol. 2 (Ed. M.M. Hill). John Wiley and Sons, New York, pp. 27–77.

Reid, R.P. and **MacIntyre, I.G.** (1998) Carbonate recrystallization in shallow marine environments: A widespread diagenetic process forming micritized grains. *Journal of Sedimentary Research*, **68,** 928–946.

Reid, R.P., MacIntyre, I.G. and **Post, J.E.** (1992) Micritized skeletal grains in Northern Belize lagoon: a major source of Mg-calcite mud. *Journal of Sedimentary Petrology*, **62,** 145–156.

Regev, L., Poduska, K.M., Addadi, L., Weiner, S., and **Boaretto, E.** (2010) Differentiating between calcites formed by different mechanisms using infrared spectrometry: Archaeological applications. *Journal of Archaeological Science,* **37,** 3022–3029.

Reijmer, J.J.G., Swart, P.K., Bauch, T., Otto, R., Reuning, L., Roth, S., and **Zechel, S.** (2009) A re-evaluation of facies on Great Bahama Bank I: new facies maps of western Great Bahama Bank. In: *Perspectives in carbonate geology: A tribute to the career of Robert Nathan Ginsburg* (Eds. P.K Swart, G.P. Eberli, and J.A. McKenzie). *International Association of Sedimentologists Special Publication,* **41,** 29–46.

Riebesell, U., Fabry, V.J., Hansson, L., and **Gattuso, J.-P.** (2010) *Guide to best practices for ocean acidification research and data reporting*. Publications office of the European Union, Luxembourg. 260 pp.

Rivadeneyra, M.A., Delgado, R., Parraga, J., Ramos-Cormenzana, A. and **Delgado, G.** (2006) Precipitation of minerals by 22 species of moderately halophilic bacteria in artificial marine salts media: Influence of salt concentration. *Folia Microbiologica*, **51,** 445–453.

Robbins, L.L. and **Blackwelder, P.L.** (1992) Biochemical and ultrastructural evidence for the origin of whitings: a biologically induced calcium carbonate precipitation mechanism. *Geology*, **20,** 464–468.

Rodriguez-Blanco, J.D., Shaw, S., Bots, P., Roncal-Herrero, T. and **Benning, L.G.** (2012) The mechanism of monohydrocalcite formation. European Mineralogical Conference, Vol. 1. EMC2012-397.

Rodríguez-Clemente, R. and **Gómez-Morales, J.** (1996) Microwave precipitation of $CaCO_3$ from homogeneous solutions. *Journal of Crystal Growth,* **169,** 339–346.

Roduit, N. (2008) JMicroVision: Image analysis toolbox for measuring and quantifying components of high definition images. Version 1.2.7. Software available for free download at http://www.jmicrovision.com/ Accessed January 2010.

Rosenthal, J.K. (1979) Interstitial water and sediment chemistry of two cores from Florida Bay. *Journal of Sedimentary Petrology,* **49,** 989–994.

Rubinson, M. and **Clayton, R.N.** (1969) Carbon-13 fractionation between aragonite and calcite. *Geochimica et Cosmochimica Acta,* **33,** 997–1002.

Rude, P.D. and **Aller, R.C.** (1991) Flourine mobility during early diagenesis of carbonate sediment: an indicator of mineral transformations. *Geochemica et Cosmochimica Acta,* **55,** 2491–2509.

Salimi, M.H., Heughebaert, J.C., and **Nancollas, G.H.** (1985) Crystal growth of calcium phosphates in the presence of magnesium ions. *Langmuir,* **1,** 119–122.

Salter, M.A., Perry, C.T., and **Wilson, R.W.** (2012) Production of mud-grade carbonates by marine fish: Crystalline products and their sedimentary significance. *Sedimentology,* **59,** 2172–2198.

Samankassou, E., Tresch, J., and Strasser, A. (2005) Origin of peloids in Early Cretaceous deposits, Dorset, South England. *Facies,* **51,** 264–273.

Sánchez-Román, M., Rivadeneyra, M.A., Vasconcelos, C. and **McKenzie, J.A.** (2007) Biomineralization of carbonate and phosphate by moderately halophilic bacteria. *Fems Microbiology Ecology*, **61,** 273–284.

Sanders, D. (2003) Syndepositional dissolution of calcium carbonate in neritic carbonate environments: Geological recognition, processes, potential significance. *Journal of African Earth Sciences,* **36,** 99–134.

Sass, E., Morse, J.W., and **Millero, F.J.** (1983) Dependence of the values of calcite and aragonite thermodynamic solubility products on ionic models. *American Journal of Science,* **283,** 218–229.

Sato, M. and **Matsuda, S.** (1969) Structure of vaterite and infrared spectra. *Zeitschrift für Kristallographie,* **129,** 405–410.

Sawada, K. (1997) The mechanisms of crystallization and transformation of calcium carbonates. *Pure and Applied Chemistry,* **69,** 921–928.

Sawada, K., Ogino, T. and **Suzuki, T.** (1990) The distribution coefficients of Mg^{2+} ion between $CaCO_3$ polymorphs and solution and the effects on the formation and transformation of $CaCO_3$ in water. *Journal of Crystal Growth*, **106,** 393–399.

Schlager, W. (2003) Benthic carbonate factories of the Phanerozoic. *International Journal of Earth Sciences,* **92,** 445–464.

Schmalz, R.F. (1965) Brucite in carbonate secreted by the red alga *goniolithon* sp. *Science,* **149,** 993–996.

Schmalz, R.F. (1967) Kinetics and diagenesis of carbonate sediments. *Journal of Sedimentary Research*, **37,** 60–67.

Schroeder, P.A. (2002) Infrared spectroscopy in clay science. In: *Teaching in Clay Science,* CMS Workshop Lectures, 11 (Eds. A. Rule and S. Guggenheim). The Clay Mineral Society, Aurora, CO, 181–206.

Sclater, J.G., Abbott, D. and **Thiede, J.** (1977) Paleobathymetry and sediments of the Indian Ocean. In: *Indian Ocean Geology and Biostratigraphy* (Eds. J.R. Heirtzler, H.M Bolli, T.A. Davies, J.B. Saunders, and J.G. Sclater). American Geophysical Union, 25–60.

Scoffin, T.P. (1970) The trapping and binding of subtidal carbonate sediments by marine vegetation in Bimini Lagoon, Bahamas. *Journal of Sedimentary Petrology,* **40,** 249–273.

Seibel, B.A. and **Walsh, P.J.** (2001) Potential impacts of CO_2 injection on deep-sea biota. *Science,* **294,** 319–320.

Sepulcre, S., Durand, N., and **Bard, E.** (2009) Mineralogical determination of reef and periplatform carbonates:Calibration and implications for paleoceanography and radiochronology. *Global and Planetary Change,* **66,** 1–9.

Sharqawy, M.H., Lienhard V, J.H. and Zubair, S.M. (2010) Thermophysical properties of seawater: A review of existing correlations and data. *Desalination and Water Treatment,* **16,** 354–380.

Shehadeh, Z.H. and **Gordon, M.S.** (1969) The role of the intestine in salinity adaptation of the rainbow trout, *Salmo gairdneri*. *Comparative Biochemistry and Physiology*, **21,** 7711–7717.

Shinn, E.A., Steinen, R.P., Lidz, B.H. and **Swart, P.K.** (1989) Whitings, a sedimentologic dilemma. *Journal of Sedimentary Petrology*, **59,** 147–161.

Sjöberg, E.L. (1978) *Kinetics and mechanism of calcite dissolution in aqueous solutions at low termperatures*. Stockholm Contributions in Geology 32, Almqvist and Wiskell, Stockholm, 92 pp.

Skrtic, D., Antonucci, J.M., and **Eanes, E.D.** (2003) Amorphous calcium phosphate-based bioactive polymeric composites for mineralized tissue regeneration. *Journal of Research of NIST,* **108,** 167–182.

Smith, S.V. (1972) Production of calcium carbonate on the mainland shelf of Southern California. *Limnology and Oceanography*, **17,** 28–41.

Speer, J.A. (1983) Crystal chemistry and phase relations of orthorhombic carbonates. In: *Carbonates: Mineralogy and Chemistry* (Ed. R.J. Reeder). *Mineralogical Society of America, Reviews in Mineralogy,* **44,** 145–189.

Sterzel, W. (1969) Der Einfluß der kristallstruktur auf die kopplung der v_2-schwingung von carbonationen. *Journal of Inorganic ad General Chemistry,* **368,** 308–316.

Stieglitz, R.D. (1972) Scanning electron microscopy of the fine fraction of recent carbonate sediments from Bimini, Bahamas. *Journal of Sedimentary Petrology*, **42,** 411–426.

Stockman, K.W., Ginsburg, R.N. and **Shinn, E.A.** (1967) The production of lime mud by algae in South Florida. *Journal of Sedimentary Petrology*, **37,** 633–648.

Swart, P.K., Burns, S.J. and **Leder, J.J.** (1991) Fractionation of the stable isotopes of oxygen and carbon in carbon-dioxide during reaction of calcite with phosphoric acid as a function of temperature and technique. *Chemical Geology*, **52**, 365-374.

Swart, P.K., Reijmer, J.J.G., and **Otto, R.** (2009) A re-evaluation of facies on Greta Bahama Bank II: variations in the $\delta^{13}C$, $\delta^{18}O$ and mineralogy of surface sediments. In: *Perspectives in carbonate geology: A tribute to the career of Robert Nathan Ginsburg* (Eds. P.K Swart, G.P. Eberli, and J.A. McKenzie). *International Association of Sedimentologists Special Publication,* **41,** 47–59.

Taft, W.H. and **Harbaugh, J.W.** (1964) *Modern carbonate sediments of southern Florida, Bahamas, and Espiritu Santo island, Baja, California: a comparison of their mineralogy and chemistry*. Stanford University Press, 133 pp.

Tarutani , T., Clayton, R.N., and **Mayeda, T.K.** (1969) The effect of polymorphism and magnesium substitution on oxygen isotope fractionation between calcium carbonate and water. *Geochimica et Cosmochimica Acta,* **33,** 987–996.

Taylor, G.F. (1975) The occurrence of monohydrocalcite in two small lakes in the southeast of South Australia. *American Mineralogist,* **60,** 690–697.

Taylor, J.R., and **Grosell, M.** (2006) Evolutionary aspects of intestinal bicarbonate secretion in fish. *Comparative Biochemistry and Physiology – Part A: Molecular & Integrative Physiology,* **143,** 523–529.

Taylor, M.G., Simkiss, K., Greaves, G. N., Okasaki, M., and **Mann, S.** (1993) An X-ray absorption spectroscopy study of the structure and transformation of amorphous calcium carbonate from plant cystoliths. *Proceedings of the Royal Society of London B,* **252,** 75–80.

Thayer, G.W., Govoni, J.J., and **Connally, D.W.** (1983) Stable carbon isotope ratios of the planktonic food web in the Northern Gulf of Mexico. *Bulletin of Marine Science,* **33,** 247–256.

Thomas, M.M., Clouse, J.A., and **Longo, J.M.** (1993) Adsorption of organic compounds on carbonate minerals: 1. Model compounds and their influence on mineral wettability. *Chemical Geology,* **109,** 201–213.

Thorstenson, D.C. and **Mackenzie, F.T.** (1974) Time variability of pore water chemistry in recent carbonate sediments, Devil's Hole, Harrington Sound, Bermuda. *Geochimica et Cosmochimica Acta,* **38,** 1–19.

Thorstenson, D.C. and **Plummer, L.N.** (1977) Equilibrium cruteria for two component solids reacting with fixed composition in an aqueous phase-example: the magnesian calcites. *American Journal of Science,* **277,** 1203–1233.

Tlili, M.M., Ben Amor, M., Gabriellie, C., Joiret, S., Maurin, G., and **Rousseau, P.** (2001) Characterization of $CaCO_3$ hydrates by micro-Raman spectroscopy. *Journal of Raman Spectroscopy,* **33,** 10–16.

Towe, K.M. and **Hemleben, C.** (1976) Diagenesis of magnesian calcite: evidence from miliolacean foraminifera. *Geology,* **4,** 337–339.

Tucker, M.E. and **Wright, V.P.** (1990) *Carbonate Sedimentology*. Blackwell Scientific Publications, Oxford, 496 pp.

Turekian, K.K. (1968) *Oceans*. Prentice Hall, 120 pp.

Turner, J.V. (1982) Kinetic fractionation of carbon-13 during calcium carbonate precipitation. *Geochimica et Cosmochimica Acta,* **46,** 1183–1191.

Tyrrell, T. and **Zeebe, R.E.** (2004) History of carbonate ion concentration over the past 100 million years. *Geochimica et Cosmochimica Acta,* **68,** 3521–3530.

van Andel, T.H. (1975) Mesozoic/Cenozoic calcite compensation depth and the global distribution of calcareous sediments. *Earth and Planetary Science Letters,* **26,** 187–194.

Van Cappellen, P. and **Berner, R.A.** (1991) Fluorapatite crystal growth from modified seawater solutions. *Geochimica et Cosmochimica Acta,* **55,** 1219–1234.

Van der Leeden, M.C. and **Van Rosmalen, G.M.** (1987) Aspects of additives in precipitation processes: performance of polycarboxylates in gypsum growth prevention. *Desalination*, **66,** 185–200.

Veizer, J. (1983) Trace elements and isotopes in sedimentary carbonates. *Reviews in Mineralogy and Geochemistry,* **11,** 265–299.

Vinson, M.D., Arvidson, R.S., and **Lüttge, A.** (2007) Kinetic inhibition of calcite (1 0 4) dissolution by aqueous manganese(II). *Journal of Crystal Growth,* **307,** 116–125.

Walsh, P.J., Blackwelder, P., Gill, K.A., Danulat, E. and **Mommsen, T.P.** (1991) Carbonate deposits in marine fish intestines: a new source of biomineralization. *Limnology and Oceanography*, **36,** 1227–1232.

Walter, L.M. and **Burton, E.A.** (1986) The effect of orthophosphate on carbonate mineral dissolution rates in seawater. *Chemical Geology,* **56,** 313–323.

Walter, L.M. and **Burton, E.A.** (1990) Dissolution of recent platform carbonate sediments in marine pore fluids. *American Journal of Science,* **290,** 601–643.

Walter, L.M. and **Morse, J.W.** (1984) Magnesian calcite stabilities: a re-evaluation. *Geochimica et Cosmochimica Acta*, **48,** 1059–1069.

Walter, L.M., Bischof, S.A., Patterson, W.P. and **Lyons, T.W.** (1993) Dissolution and recrystallization in modern shelf carbonates: Evidence from porewater and solid-phase chemistry. *Philosophical Transactions of the Royal Society of London Series a-Mathematical Physical and Engineering Sciences*, **344,** 27–36.

Wang, C., Kuo, C., Mok, H., and **Lee, S.** (2003) Molecular phylogeny of elopomorph fishes inferred from mitochondrial 12S ribosomal RNA sequences. *Zoologica Scripta,* **32,** 231–241.

Wang, X., Schlossmacher, U., Natalio, F., Schröder, H.C., Wolf, S.E., Tremel, W., and **Müller, W.E.G.** (2009) Evidence for biogenic processes during formation of ferromanganese crusts from the Pacific Ocean: Implication for biologically induced mineralization. *Micron,* **40,** 526–535.

Wartel, M., Skiker, M., Auger, Y., Boughriet, A., Puskaric, E., and **Guegueniat, P.** (1991) Seasonal variation of Mn^{2+} adsorption on to calcareous surfaces in the English Channel, and its implication on the manganese distribution coefficient. *Marine Chemistry,* **36,** 85–105.

Weir, C.E. and **Lippincott, E.R.** (1961) Infrared studies of aragonite, calcite, and vaterite type structures in the borates, carbonates, and nitrates. *Journal of Research of NBS – A: Physics and Chemistry,* **65A,** 173–183.

White, J.W. and **Samhouri, J.F.** (2011) Oceanographic coupling across three trophic levels shapes source-sink dynamics in marine metacommunities. *Oikos*, **120,** 1151–1164.

White, W.B. (1971) Infrared characterization of water and hydroxyl ion in the basic magnesium carbonate minerals. *American Mineralogist,* **56,** 46–53.

White, W.B. (1974) The carbonate minerals. In: *The Infra-red Spectra of Minerals* (Ed. V.C. Farmer), pp. 227–284, Mineralogical Society of America Monograph **4,** Mineralogical Society, London.

Wilber, R.J., Milliman, J.D., and **Halley, R.B.** (1990) Accumulation of bank-top sediment on the western slope of Great Bahama Bank: rapid progradation of a carbonate megabank. *Geology*, **18,** 970–974.

Wilson, R.W. and **Grosell, M.** (2003) Intestinal bicarbonate secretion by marine teleost fish—source of bicarbonate, pH sensitivity, and consequences for whole animal acid–base and calcium homeostasis. *Biochimica et Biophysica Acta,* **1618,** 163–174.

Wilson, R.W., Gilmour, K.M., Henry, R.P. and **Wood, C.M.** (1996) Intestinal base excretion in the seawater-adapted rainbow trout: A role in acid-base balance? *Journal of Experimental Biology*, **199,** 2331–2343.

Wilson, R.W., Wilson, J.M. and **Grosell, M.** (2002) Intestinal bicarbonate secretion by marine teleost fish – why and how? *Biochimica Et Biophysica Acta-Biomembranes*, **1566,** 182–193.

Wilson, R.W., Millero, F.J., Taylor, J.R., Walsh, P.J., Christensen, V., Jennings, S. and **Grosell, M.** (2009) Contribution of fish to the marine inorganic carbon cycle. *Science*, **323,** 359–362.

Wolanski, E. (1992) Hydrodynamics of mangrove swamps and their coastal waters. *Hydrobiologia,* **247,** 141–161.

Wood., C.M., Farrell, A.P., and **Brauner, C.J.** (2011) *Fish physiology: homeostasis and toxicology of essential metals.* Academic Press, 520 pp.

Woosley, R.J., Millero, F.J., and **Grosell, M.** (2012) The solubility of fish-produced high magnesium calcite in seawater. *Journal of Geophysical Research*, **117,** C04018.

Yagi, S. and **Fukushi, K.** (2011) Phosphate sorption on monohydrocalcite. *Journal of Mineralogical and Petrological Sciences,* **106,** 109–113.

Yeager, L.A. and **Layman, C.A.** (2011) Energy flow to two abundant consumers in a subtropical oyster reef food web. *Aquatic Ecology,* **45,** 267–277.

Zeebe, R.E. (2001) Seawater pH and isotopic paleotemperatures of Cretaceous oceans. *Palaeogeography, Palaeoclimatology, Palaeoecology,* **170,** 49–57.

Zhang, F.F., Xu, H.F., Konishi, H. and **Roden, E.E.** (2010) A relationship between d(104) value and composition in the calcite-disordered dolomite solid-solution series. *American Mineralogist*, **95,** 1650–1656.

Zou, M., Guo, B., Tao, W., Arratia, G., and **He, S.** (2012) Integrating multi-origin expression data improves the resolution of deep phylogeny of ray-finned fish (Actinopterygii). *Scientifc Reports,* **2,** 1–7.

Appendix I – X-ray diffraction data

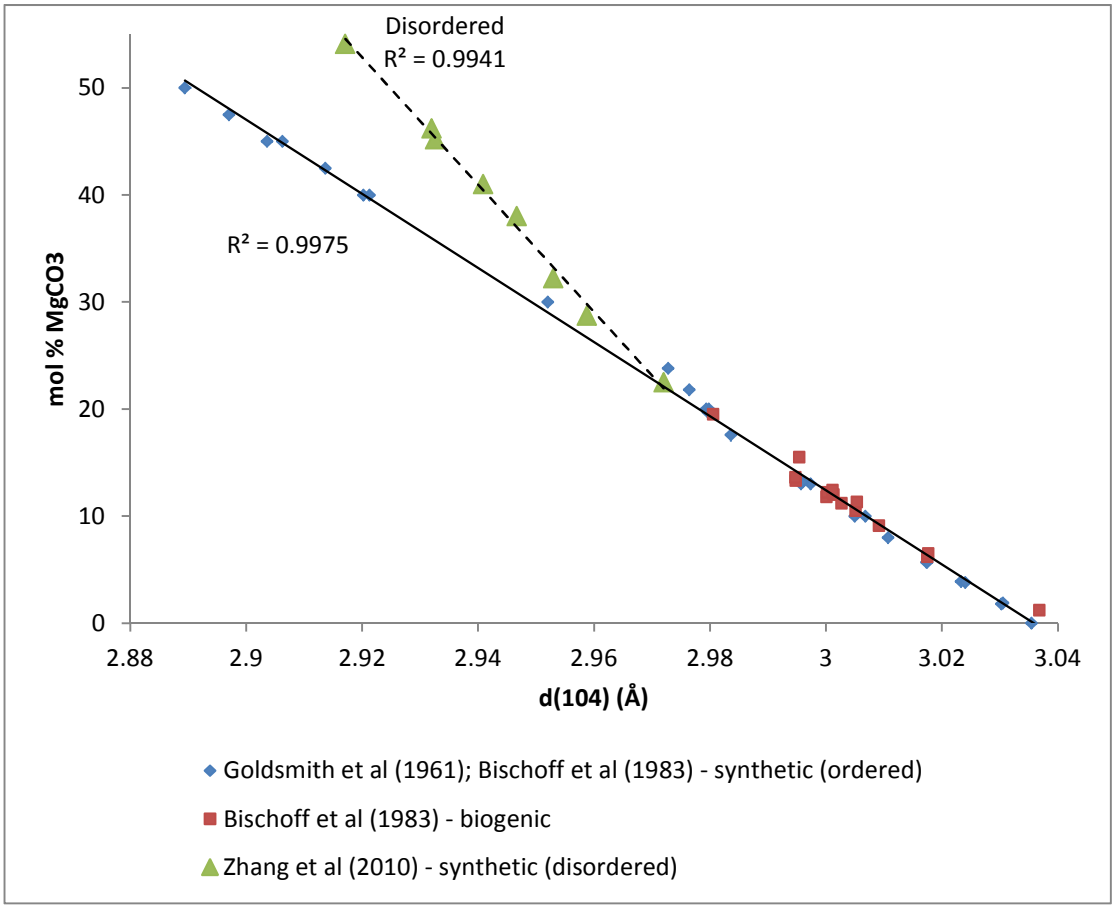

Figure AI 1 *Relationships between D_{104}-spacing and magnesium content in calcite and Mg-calcite (based on data in Table AII 1). Note that the data of Zhang et al (2010) are only relevant where calcite contains more than about 20 mol% $MgCO_3$. Based on these curves, the position of the d_{104} diffraction peak for calcite can be used as a proxy for magnesium content using the following formulae:*

$$\text{(ordered calcite) mol\% } MgCO_3 = -347.84(d_{104}) + 1055.8$$

$$\text{(disordered calcite) mol\% } MgCO_3 = -594.39(d_{104}) + 1788.5$$

For ordered calcite this formula is calculated using only the data for synthetic crystals in Goldsmith et al. (1961) and Bischoff et al. (1983). Data for biogenic crystals in the latter are in good agreement with this relationship up to about 20 mol% $MgCO_3$, but they have not been determined for calcites with higher magnesium contents. Because the degree of order is not known in the biogenic calcites used in that study, the data arising from them are omitted in the construction of the relationship used for the present study.

Table AI 1 *Unit cell parameters of calcite and Mg-calcite as determined in existing literature from XRD data obtained for synthetic, biogenic, and disordered phases. Corresponding magnesium contents were determined using direct methods of compositional analysis (such as electron dispersive X-ray spectroscopy). Relationships between d_{104}-spacing and magnesium content in calcite are determined from these data (see Fig. AI 3).*

Author/ sample	a	c	h	k	l	d-spacing (Angstroms)	mol% MgCO3	Key
1	4.949	16.876	1	0	4	3.0068	10.0	1 - Goldsmith et al. (1961)
1	4.947	16.863	1	0	4	3.0050	10.0	(synthetic)
1	4.913	16.699	1	0	4	2.9798	20.0	2 - Bischoff et al. (1983)
1	4.912	16.698	1	0	4	2.9793	20.0	(synthetic)
1	4.876	16.514	1	0	4	2.9520	30.0	3 - Bischoff et al. (1983)
1	4.841	16.291	1	0	4	2.9213	40.0	(biogenic)
1	4.843	16.274	1	0	4	2.9202	40.0	4 - Zhang et al. (2010)
1	4.833	16.235	1	0	4	2.9137	42.5	(disordered)
1	4.826	16.178	1	0	4	2.9063	45.0	
1	4.823	16.156	1	0	4	2.9036	45.0	
1	4.815	16.111	1	0	4	2.8971	47.5	
1	4.805	16.061	1	0	4	2.8894	50.0	
2	4.989	17.062	1	0	4	3.0355	0.0	
2	4.982	17.028	1	0	4	3.0303	1.8	
2	4.982	17.031	1	0	4	3.0306	1.9	
2	4.972	16.984	1	0	4	3.0233	3.9	
2	4.973	16.988	1	0	4	3.0240	3.8	
2	4.964	16.944	1	0	4	3.0173	5.7	
2	4.964	16.945	1	0	4	3.0175	5.7	
2	4.954	16.903	1	0	4	3.0107	8.0	
2	4.934	16.806	1	0	4	2.9957	13.0	
2	4.937	16.813	1	0	4	2.9974	13.0	
2	4.935	16.805	1	0	4	2.9960	13.2	
2	4.918	16.724	1	0	4	2.9836	17.6	
2	4.918	16.680	1	0	4	2.9796	19.7	
2	4.914	16.658	1	0	4	2.9764	21.8	
2	4.904	16.649	1	0	4	2.9728	23.8	
3	4.979	17.111	1	0	4	3.0368	1.2	
3	4.965	16.944	1	0	4	3.0175	6.2	
3	4.964	16.950	1	0	4	3.0177	6.5	
3	4.949	16.904	1	0	4	3.0092	9.1	
3	4.946	16.869	1	0	4	3.0051	10.5	
3	4.943	16.854	1	0	4	3.0027	11.2	
3	4.946	16.871	1	0	4	3.0054	11.3	
3	4.940	16.834	1	0	4	3.0001	11.8	
3	4.942	16.840	1	0	4	3.0014	12.0	
3	4.939	16.837	1	0	4	3.0002	12.2	
3	4.940	16.846	1	0	4	3.0012	12.4	
3	4.932	16.800	1	0	4	2.9948	13.3	
3	4.931	16.803	1	0	4	2.9947	13.6	
3	4.932	16.809	1	0	4	2.9954	15.5	
3	4.914	16.704	1	0	4	2.9806	19.5	
4	-	-	-	-	-	2.9720	22.5	
4	-	-	-	-	-	2.9588	28.7	
4	-	-	-	-	-	2.9530	32.2	
4	-	-	-	-	-	2.9467	38.0	
4	-	-	-	-	-	2.9409	41.0	
4	-	-	-	-	-	2.9326	45.2	
4	-	-	-	-	-	2.9320	46.2	
4	-	-	-	-	-	2.9171	54.1	

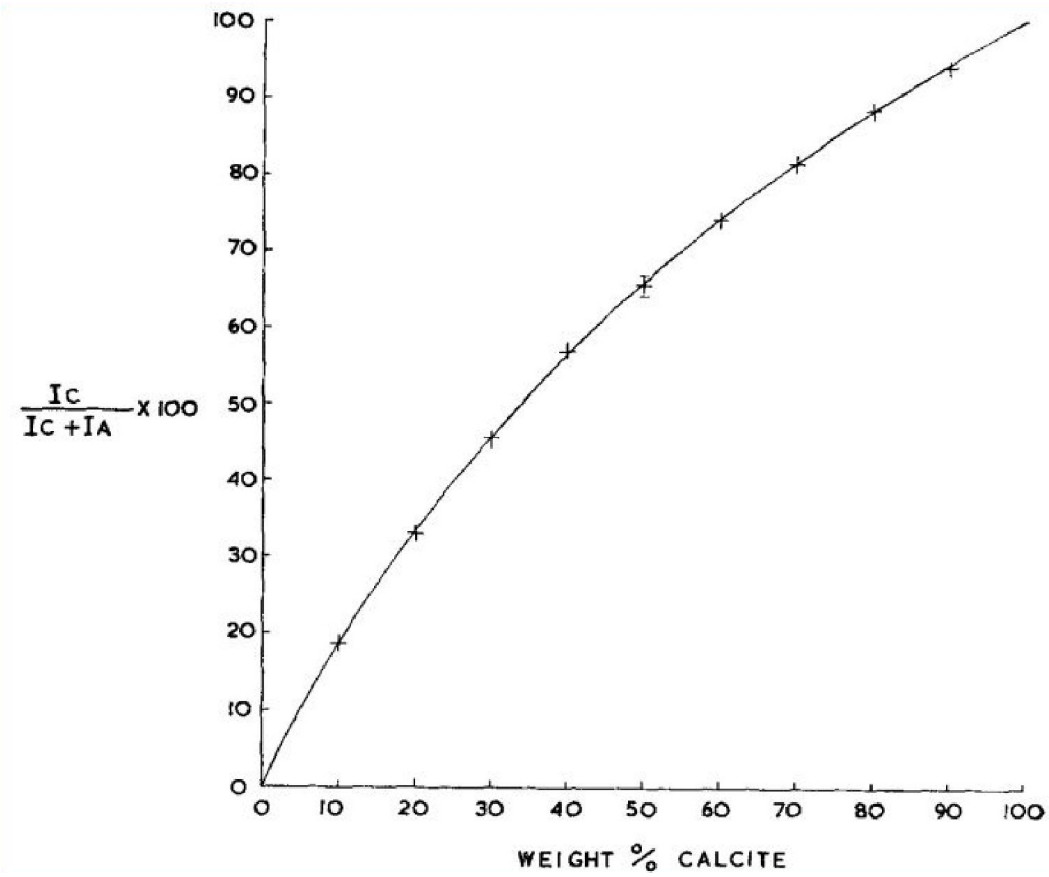

Figure AI 2 *Calibration curve for estimating the relative abundances of calcite and aragonite in a sample based on XRD patterns, where I_C = integral of the d_{104} peak for calcite, and I_A = combined integrals of the d_{111} and d_{021} peaks for aragonite. After Davies and Hooper (1962).*

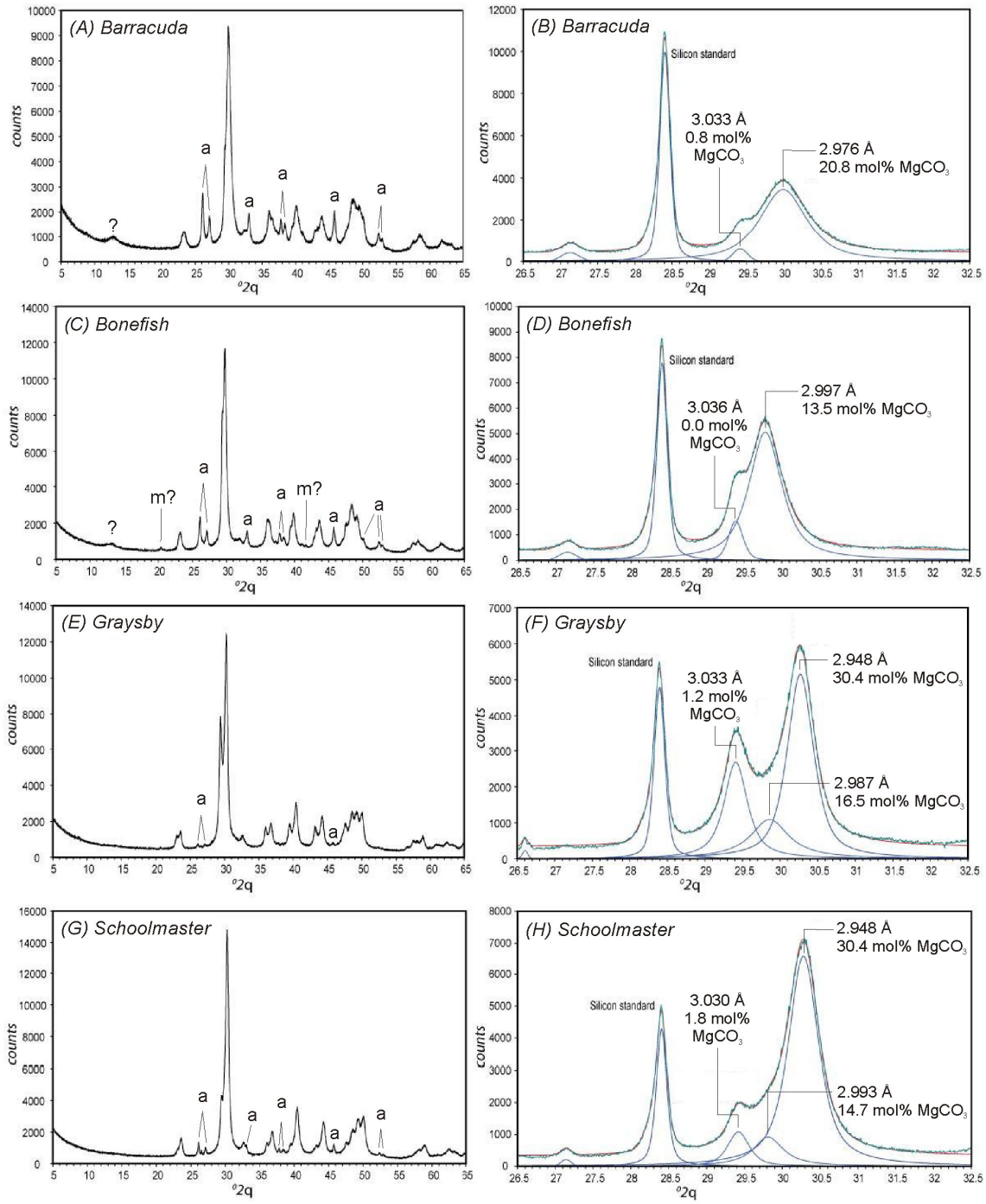

Figure AI 3 *X-ray diffraction patterns used for assessing the relative abundances of aragonite and calcite (wt%) in carbonates produced by four different fish species. All peaks are generated by calcite or Mg calcite unless otherwise stated (i.e., a = aragonite; m = monohydrocalcite). Peaks used for estimating relative abundances are those at 26.3 and 27.3 °2ϑ for aragonite, and that at about 30.0 °2ϑ for calcite. Original spectra from Perry et al. (2011).*

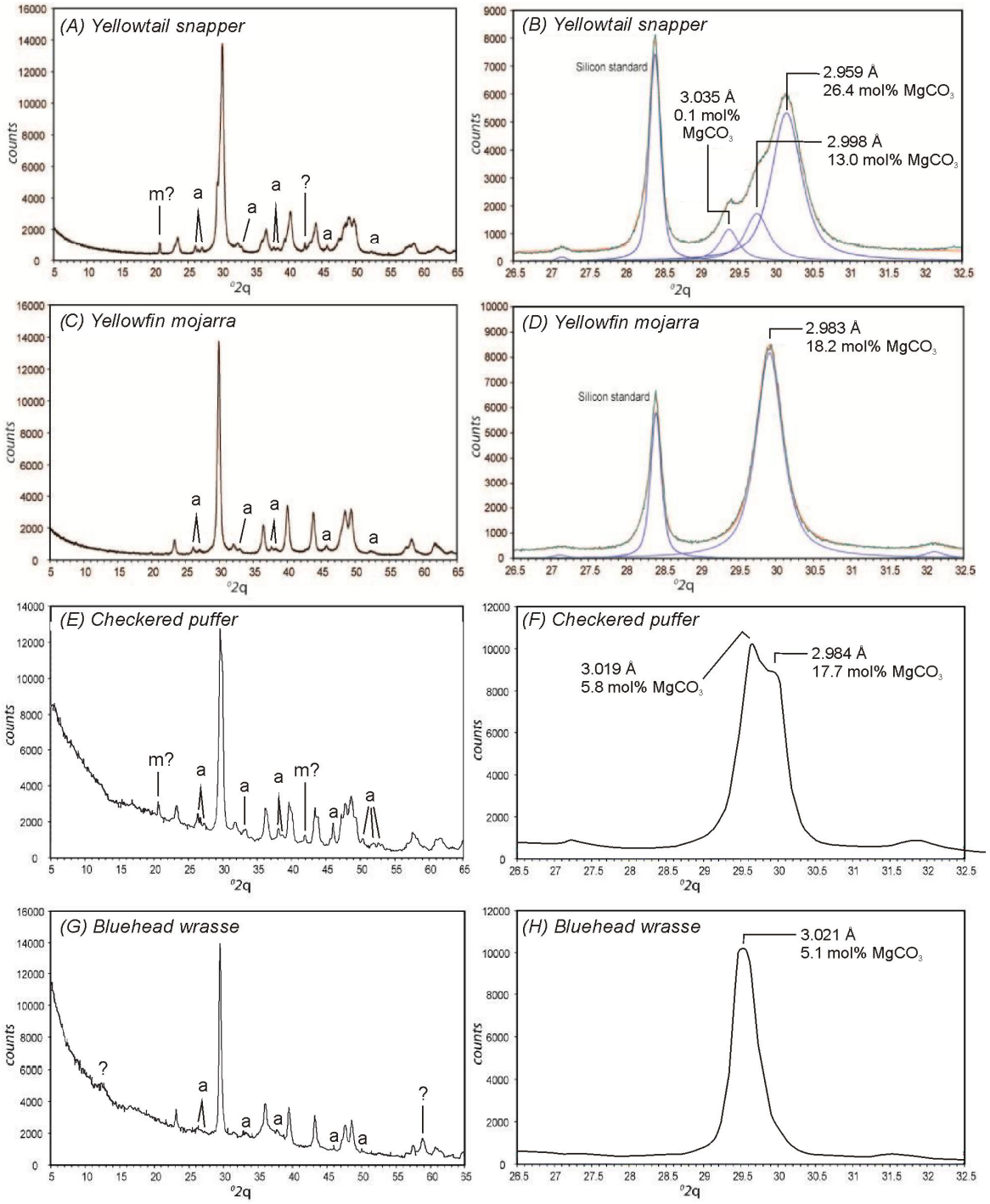

Figure AI 4 *X-ray diffraction patterns used for assessing the relative abundances of aragonite and calcite (wt%) in carbonates produced by four different fish species. All peaks are generated by calcite or Mg calcite unless otherwise stated (i.e., a = aragonite; m = monohydrocalcite). Peaks used for estimating relative abundances are those at 26.3 and 27.3 °2ϑ for aragonite, and that at about 30.0 °2ϑ for calcite. Original spectra from Perry et al. (2011) for yellowtail snapper and yellowfin mojarra. Spectra for checkered puffer and bluehead wrasse are from the present study.*

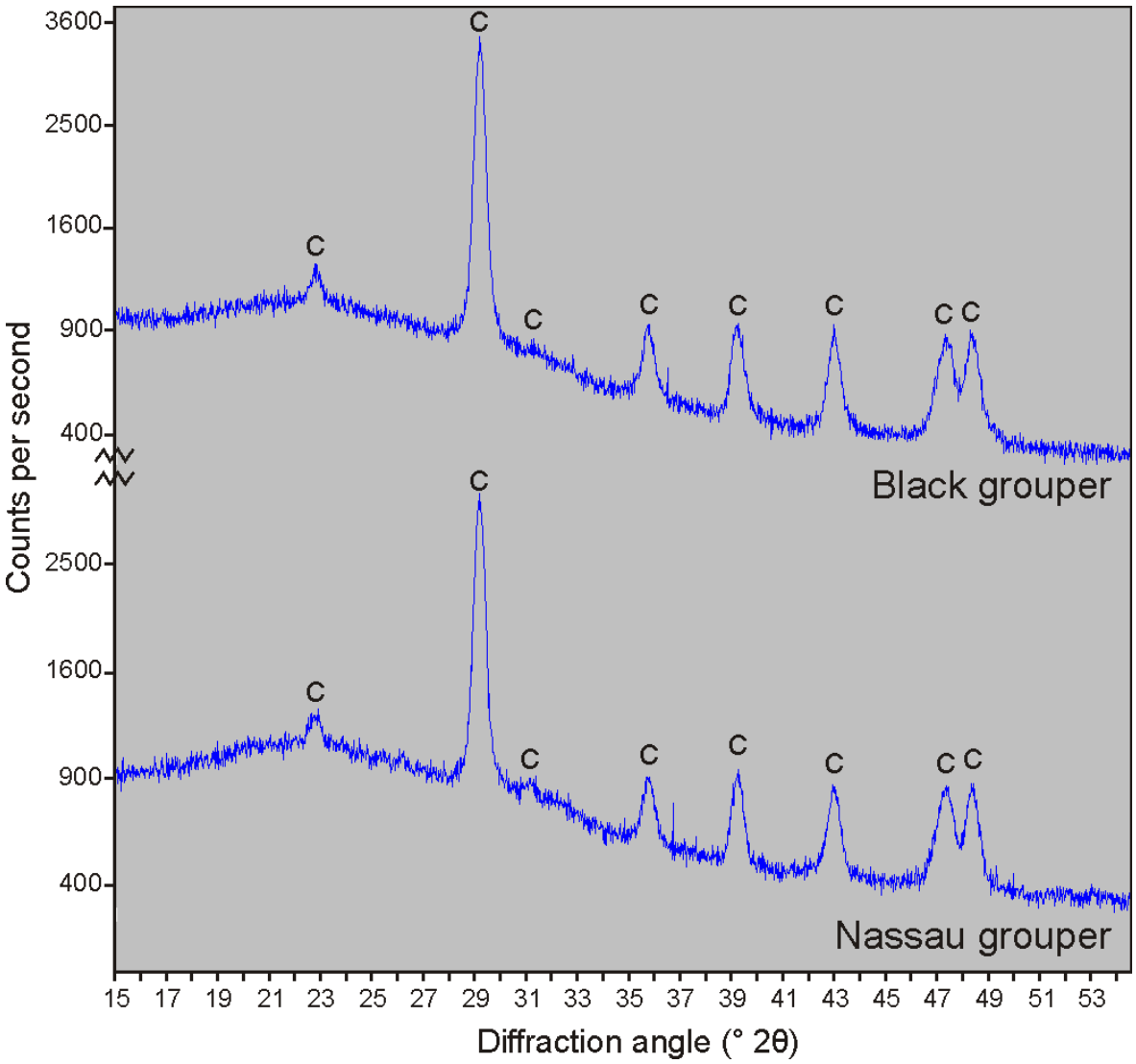

Figure AI 5 *X-ray diffraction patterns for carbonates produced by black grouper and Nassau grouper (at the point of excretion), showing peaks consistent with high-Mg calcite. Note the absence of peaks at 26.3 and 27.3 °2θ, suggesting no aragonite is present in these samples.*

Appendix II – chemical composition of fish derived carbonates determined by energy-dispersive X-ray spectroscopy

At least 30 (and in most cases at least 50) compositional analyses were performed on carbonates produced by numerous Bahamian fish species using energy-dispersive X-ray spectroscopy (EDX), as described in the main text (Chapter 2). In many cases data were obtained from at least five pellets in a single carbonate sample (i.e. collected from a single fish/group of fish on the same day). In other cases, numerous pellets were analysed from several different samples. In all cases, separate data were collected for each crystal form present in a given sample. Data presented in the following tables are organised by sample, pellet, and crystal form, thus facilitating the assessment of variability among each. A key to the crystal codes is shown in Table AII 1.

Table AII 1 Key to crystal codes used in all tables in Appendix II

Crystal code	Description
ME	Monocrystalline ellipsoid (includes similar-sized monocrystalline rods)
PE	Polycrystalline ellipsoid
Rhomb	Rhombohedron (includes discrete rhombohedral crystals and spheres and dumbbells made up of micron-scale rhombohedra)
Amorph	Material that lacks any definable form
Sphere	Polycrystalline sphere (radially fibrous); some discrete, some intergrown and forming lobate structures.
Dmbl	Dumbbell (typically >4 m in length; radially fibrous). Dumbbells include a range of forms from rod-like to hemi-spherical. Differentiation of spheres and dumbbells is not always easy and in many cases where differentiation was not possible crystal form is given as Dmbl/Sph.
Sml dmbl	Small dumbbell (<4 µm in length; radially fibrous)
Whtsf	Wheatsheaf. Similar to above but more rod-like (smaller degree of splay)
Needle	Needle-shaped or acicular crystals
Sphl/Nee	Spherulitic forms (usually comprising needles)
Nanosph	Nanoscale spherical forms

Calcium and magnesium are the main elemental components. Additionally, strontium, sodium, chlorine, sulphur, and phosphorus are also commonly detected, although values for these trace elements were not always obtained. As such, blank cells in the following data tables should be taken to mean ‘value not reported’ rather than ‘element not detected’.

Magnesium presumably substitutes for calcium in the $CaCO_3$ crystal lattice, and values for mol% $MgCO_3$ are reported here. Strontium is also assumed to substitute for calcium, and two columns are therefore added to the tables below to show values for: i) mol% $MgCO_3$ when strontium is taken into account (these values are typically within 0.2 mol% of $MgCO_3$ values calculated when strontium is ignored); and ii) mol% $SrCO_3$.

The mode of incorporation of other trace elements is not known. Finally, small concentrations of silicon were detected in most phases lacking definable form. Although no strontium peaks were observed for the same materials, it is possible they are obscured by the overlapping silicon peak.

Table AII 2 EDX data for samples produced by schoolmaster snapper (all elemental data reported as atomic %)

Sample	Pellet	Crystal form	Ca	Mg	Sr	Na	Cl	S	P	Si	$MgCO_3$ (mol%)	$MgCO_3$ (mol%)	$SrCO_3$ (mol%)
1	1	ME	22.69	5.53							19.6		
		ME	30.22	5.99							16.5		
		ME	18.12	6.38							26.0		
		ME	21.6	5.48							20.2		
		ME	20.18	5.8							22.3		
		ME	19.95	4.62							18.8		
		ME	20.71	5.98							22.4		
		ME	20.7	5.26							20.3		
		ME	17.64	4.56							20.5		
	2	ME	18.75	6.92							27.0		
		ME	19.34	5.45							22.0		
		ME	19.16	6.2							24.4		
2	3	ME	8.69	8.88							50.5		
		ME	9.33	6.81							42.2		
		ME	9.14	6.79							42.6		
		ME	10.08	10.06							50.0		
		ME	9.13	8.29							47.6		
		ME	11.4	8.46							42.6		
		ME	16.41	7.52							31.4		
		ME	9.22	6.25							40.4		
		ME	9.49	6.83							41.9		
		ME	8.17	5.21							38.9		
	4	ME	17.4	6.38							26.8		
		ME	15.84	3.51							18.1		
		ME	12.69	3.99							23.9		
		ME	10.16	3.83							27.4		
		ME	10.55	4.1							28.0		
		ME	9.02	4.13							31.4		
		ME	10.47	4.19							28.6		
		ME	12.19	4.3							26.1		
		ME	11.97	4.39							26.8		
		ME	10.47	3.94							27.3		
	5	ME	10.61	6.13							36.6		
		ME	8.06	6.44							44.4		
		ME	8.36	6.29							42.9		
		ME	7.03	6.71							48.8		
		ME	8.61	6.86							44.3		
		ME	8.45	6.61							43.9		
		ME	9.83	7.41							43.0		
		ME	10.14	8.44							45.4		
		ME	7.03	5.11							42.1		
		ME	7.74	5.23							40.3		
	6	ME	10.76	6.23							36.7		
		ME	11.69	6.8							36.8		
		ME	10.09	6.11							37.7		
		ME	10.05	6.12							37.8		
		ME	13.55	7.45							35.5		

Sample	Pellet	Crystal form	Ca	Mg	Sr	Na	Cl	S	P	Si	$MgCO_3$ (mol%)	$MgCO_3$ (mol%)	$SrCO_3$ (mol%)
2	6	ME	9.54	5.55							36.8		
		ME	12.74	6.32							33.2		
		ME	9.55	5.63							37.1		
		ME	9.16	5.09							35.7		
		ME	9.31	5.51							37.2		
	7	ME	12.84	6.92							35.0		
		ME	9.58	6.86							41.7		
		ME	9.47	5.69							37.5		
		ME	12.23	6.33							34.1		
		ME	11.99	6.55							35.3		
		ME	12.1	6.92							36.4		
		ME	7.93	6.67							45.7		
		ME	12.76	7.5							37.0		
		ME	12.59	6.38							33.6		
		ME	10.25	5.35							34.3		
3	8	ME	13.01	3.40	0.08	0.46	0.14	0.06	0.10		20.7	20.62	0.49
		ME	13.29	3.50	0.07	0.47	0.15	0.05	0.07		20.8	20.76	0.42
		ME	16.20	3.54	0.08	0.45	0.18	0.08	0.11		17.9	17.86	0.40
		ME	14.76	3.48	0.07	0.49	0.12	0.05	0.08		19.1	19.01	0.38
		ME	13.11	3.36	0.07	0.45	0.13	0.05	0.08		20.4	20.31	0.42
		ME	11.69	3.14	0.07	0.42	0.13	0.05	0.07		21.2	21.07	0.47
		ME	14.98	4.57	0.06	0.54	0.35	0.05	0.09		23.4	23.30	0.31
		ME	15.07	4.20	0.08	0.53	0.29	0.04	0.11		21.8	21.71	0.41
		ME	13.97	3.47	0.07	0.51	0.21	0.70	0.10		19.9	19.82	0.40
	9	ME	17.54	3.46	0.07	0.44	0.20	0.00	0.05		16.5	16.42	0.33
		ME	15.28	3.30	0.08	0.50	0.18	0.02	0.06		17.8	17.68	0.43
		ME	17.33	3.52	0.08	0.50	0.21	0.02	0.05		16.9	16.82	0.38
		ME	14.16	3.21	0.08	0.46	0.13	0.04	0.07		18.5	18.40	0.46
		ME	16.93	3.59	0.09	0.54	0.21	0.01	0.04		17.5	17.42	0.44
		ME	16.09	3.97	0.08	0.59	0.23	0.01	0.04		19.8	19.71	0.40
		ME	13.70	3.40	0.07	0.51	0.16	0.07	0.08		19.9	19.80	0.41
		ME	15.61	3.45	0.08	0.69	0.36	0.08	0.11		18.1	18.03	0.42
	10	ME	14.99	3.57	0.08	0.46	0.16	0.07	0.06		19.2	19.15	0.43
		ME	15.85	4.28	0.08	0.58	0.23	0.05	0.10		21.3	21.18	0.40
		ME	15.90	4.19	0.10	0.50	0.19	0.06	0.10		20.9	20.75	0.50
		ME	14.53	3.55	0.07	0.48	0.16	0.06	0.07		19.6	19.56	0.39
		ME	15.64	3.82	0.07	0.50	0.20	0.05	0.09		19.6	19.56	0.36
		ME	15.55	4.51	0.10	0.49	0.24	0.04	0.12		22.5	22.37	0.50
	11	ME	17.45	4.07	0.09	0.43	0.28	0.02	0.07		18.9	18.83	0.42
		ME	16.19	3.86	0.06	0.46	0.26	0.02	0.03		19.3	19.19	0.30
		ME	17.54	4.07	0.10	0.46	0.28	0.03	0.05		18.8	18.75	0.46
		ME	17.79	4.26	0.10	0.45	0.29	0.03	0.05		19.3	19.23	0.45
		ME	15.75	2.65	0.09	0.49	0.17	0.02	0.06		14.4	14.33	0.49
		ME	15.87	3.42	0.08	0.52	0.20	0.03	0.06		17.7	17.66	0.41

Table AII 3 EDX data for samples produced by yellowtail snapper (all elemental data reported as atomic %)

Sample	Pellet	Crystal form	Ca	Mg	Sr	Na	Cl	S	P	Si	$MgCO_3$ (mol%)	$MgCO_3$ (mol%)	$SrCO_3$ (mol%)
1	1	ME	12.15	7.83							39.2		
		ME	10.38	6.88							39.9		
		ME	10.24	6.91							40.3		
		ME	7.69	4.28							35.8		
		ME	8.30	4.79							36.6		
		ME	9.47	4.76							33.5		
		ME	9.96	5.14							34.0		
		ME	11.96	6.92							36.7		
		ME	11.11	6.07							35.3		
		ME	12.07	7.33							37.8		
	2	ME	8.21	5.21							38.8		
		ME	11.01	6.43							36.9		
		ME	7.69	4.99							39.4		
		ME	8.98	5.69							38.8		
		ME	10.92	6.76							38.2		
		ME	10.99	6.76							38.1		
		ME	11.31	7.00							38.2		
		ME	10.00	6.69							40.1		
		ME	10.53	6.76							39.1		
		ME	10.23	6.82							40.0		
	3	ME	12.64	5.78							31.4		
		ME	11.45	5.32							31.7		
		ME	11.34	5.62							33.1		
		ME	12.79	5.79							31.2		
		ME	10.36	5.21							33.5		
		ME	10.43	5.82							35.8		
		ME	11.80	5.59							32.1		
		ME	12.46	5.90							32.1		
		ME	11.31	5.77							33.8		
		ME	11.66	6.04							34.1		
	4	ME	14.77	7.30							33.1		
		ME	11.94	6.68							35.9		
		ME	13.49	6.68							33.1		
		ME	12.90	5.15							28.5		
		ME	12.72	5.63							30.7		
		ME	12.27	6.12							33.3		
		ME	12.90	6.73							34.3		
		ME	13.44	7.25							35.0		
		ME	11.34	6.29							35.7		
		ME	11.33	6.13							35.1		
	5	ME	10.99	5.04							31.4		
		ME	10.89	4.90							31.0		
		ME	13.51	5.55							29.1		
		ME	11.48	5.15							31.0		
		ME	12.18	5.21							30.0		
		ME	11.29	4.88							30.2		
		ME	11.89	4.92							29.3		

Sample	Pellet	Crystal form	Ca	Mg	Sr	Na	Cl	S	P	Si	$MgCO_3$ (mol%)	$MgCO_3$ (mol%)	$SrCO_3$ (mol%)
1	5	ME	11.54	4.81							29.4		
		ME	9.45	4.35							31.5		
		ME	9.28	4.31							31.7		
2	6	ME	11.68	5.87							33.4		
		ME	11.53	5.85							33.7		
		ME	10.11	4.94							32.8		
		ME	11.34	4.80							29.7		
		ME	11.13	4.99							31.0		
		ME	12.10	6.26							34.1		
		ME	11.15	6.19							35.7		
		ME	15.64	7.11							31.3		
		ME	19.56	6.94							26.2		
		ME	11.80	6.47							35.4		
3	7	ME	9.41	5.66							37.6		
		ME	9.85	7.77							44.1		
		ME	10.44	5.59							34.9		
		ME	8.94	5.77							39.2		

Table AII 4 EDX data for samples produced by yellowfin mojarra (all elemental data reported as atomic %)

Sample	Pellet	Crystal form	Ca	Mg	Sr	Na	Cl	S	P	Si	$MgCO_3$ (mol%)	$MgCO_3$ (mol%)	$SrCO_3$ (mol%)
1	1	ME	18.02	3.76	0.09	0.47	0.03	0.08	0.10		17.3	17.19	0.41
		ME	22.68	4.32	0.08	0.34	0.06	0.12	0.11		16.0	15.95	0.30
		ME	21.02	3.94	0.06	0.30	0.08	0.11	0.11		15.8	15.75	0.24
		ME	19.97	4.02	0.07	0.55	0.01	0.10	0.07		16.8	16.71	0.29
		ME	17.24	3.67	0.05	0.52	0.02	0.07	0.09		17.6	17.51	0.24
	2	ME	18.85	3.23	0.06	0.44	0.07	0.06	0.08		14.6	14.59	0.27
		ME	17.89	3.24	0.06	0.44	0.01	0.06	0.08		15.3	15.29	0.28
		ME	17.91	2.74	0.06	0.51	0.00	0.06	0.05		13.3	13.23	0.29
		ME	18.86	2.77	0.05	0.43	0.01	0.08	0.07		12.8	12.78	0.23
	3	ME	14.74	3.74	0.07	0.53	0.02	0.05	0.06		20.2	20.16	0.38
		ME	19.34	3.73	0.08	0.45	0.07	0.08	0.08		16.2	16.11	0.35
2	4	ME	22.30	3.70	0.08	0.46	0.15	0.02			14.2	14.19	0.31
		ME	20.16	3.00	0.09	0.43	0.12	0.00			13.0	12.90	0.39
		ME	18.42	3.25	0.07	0.46	0.10	0.00			15.0	14.95	0.32
		ME	15.84	3.58	0.07	0.40	0.11	0.01			18.4	18.37	0.36
		ME	17.60	3.51	0.09	0.41	0.13	0.01			16.6	16.56	0.42
		ME	17.93	4.56	0.08	0.53	0.14	0.02			20.3	20.20	0.35
		ME	20.76	3.28	0.18	0.50	0.14	0.02			13.6	13.54	0.74
		ME	21.33	4.36	0.08	0.42	0.17	0.03			17.0	16.92	0.31
		ME	16.98	3.65	0.06	0.38	0.11	0.00			17.7	17.64	0.29
	5	ME	22.30	3.99	0.07	0.51	0.11	0.02			15.2	15.14	0.27
		ME	24.85	5.16	0.12	0.49	0.15	0.02			17.2	17.13	0.40
3	6	ME	13.15	3.80							22.4		
		ME	11.18	3.62							24.5		
		ME	9.87	3.45							25.9		
		ME	10.73	3.69							25.6		
		ME	9.19	3.30							26.4		
		ME	11.15	3.70							24.9		
		ME	10.20	3.57							25.9		
		ME	12.63	3.76							22.9		
		ME	12.62	3.84							23.3		
	7	ME	11.23	2.82							20.1		
		ME	13.39	3.84							22.3		
		ME	10.19	3.10							23.3		
		ME	10.85	2.83							20.7		
		ME	14.85	3.15							17.5		
		ME	11.60	2.77							19.3		
		ME	9.60	3.28							25.5		
		ME	9.72	2.41							19.9		
		ME	10.05	2.41							19.3		
		ME	10.41	2.58							19.9		
	8	ME	14.90	4.08							21.5		
		ME	14.33	4.00							21.8		
		ME	12.24	3.73							23.4		
		ME	12.05	3.67							23.3		
		ME	12.84	3.82							22.9		
		ME	13.02	4.07							23.8		

Sample	Pellet	Crystal form	Ca	Mg	Sr	Na	Cl	S	P	Si	$MgCO_3$ (mol%)	$MgCO_3$ (mol%)	$SrCO_3$ (mol%)
3	8	ME	12.35	3.54							22.3		
		ME	11.77	3.62							23.5		
		ME	12.26	3.66							23.0		
		ME	12.03	3.77							23.9		
	9	ME	22.41	5.05	0.23						18.4	18.24	0.83
		ME	12.06	3.46	0.13						22.3	22.11	0.83
		ME	11.91	3.12	0.11						20.8	20.61	0.73
		ME	10.57	2.94	0.12						21.8	21.57	0.88
		ME	10.22	2.84	0.10						21.7	21.58	0.76
		ME	11.60	2.18	0.18						15.8	15.62	1.29
	10	ME	10.50	2.55	0.09						19.5	19.41	0.68
		ME	9.37	3.44	0.06						26.9	26.73	0.47
		ME	12.43	4.14	0.08						25.0	24.86	0.48
		ME	10.66	3.66	0.08						25.6	25.42	0.56
		ME	13.05	3.91	0.08						23.1	22.95	0.47
		ME	10.54	3.15	0.13						23.0	22.79	0.94
4	11	ME	17.08	2.14	0.08	0.28	0.05	0.05	0.12		11.1	11.09	0.41
		ME	15.27	1.42	0.06	0.27	0.02	0.03	0.08		8.5	8.48	0.36
		ME	17.87	2.20	0.07	0.32	0.06	0.08	0.08		11.0	10.92	0.35
		ME	14.75	2.09	0.05	0.30	0.02	0.03	0.06		12.4	12.37	0.30
	12	ME	16.14	1.88	0.07	0.36	0.05	0.13	0.05		10.4	10.39	0.39
		ME	10.45	1.05	0.07	0.42	0.00	0.00	0.02		9.1	9.08	0.61
	13	ME	16.78	2.99	0.03	0.57	0.15	0.02	0.07		15.1	15.10	0.15
		ME	15.84	2.14	0.06	0.28	0.06	0.02	0.10		11.9	11.86	0.33
		ME	14.62	2.44	0.04	0.29	0.06	0.01	0.11		14.3	14.27	0.23
		ME	16.54	2.01	0.05	0.31	0.05	0.02	0.10		10.8	10.81	0.27
		ME	15.80	2.25	0.04	0.30	0.07	0.02	0.11		12.5	12.44	0.22
		ME	14.93	2.67	0.04	0.31	0.08	0.01	0.05		15.2	15.14	0.23
		ME	16.08	2.92	0.05	0.28	0.10	0.02	0.08		15.4	15.33	0.26
	14	ME	17.68	2.06	0.05	0.41	0.06	0.07	0.07		10.4	10.41	0.25
		ME	15.38	1.94	0.04	0.32	0.02	0.06	0.04		11.2	11.18	0.23
		ME	17.49	1.77	0.04	0.38	0.06	0.09	0.09		9.2	9.17	0.21
	15	ME	19.04	2.42	0.05	0.35	0.08	0.04	0.04		11.3	11.25	0.23
		ME	16.56	1.77	0.07	0.33	0.06	0.05	0.09		9.7	9.62	0.38
		ME	16.91	2.38	0.07	0.35	0.05	0.04	0.06		12.3	12.29	0.36
1	16	Dmbl/Sph	20.15	0.79	0.17	0.49	0.01	0.05	0.09		3.8	3.74	0.81
		Dmbl/Sph	19.81	1.04	0.18	0.49	0.00	0.02	0.09		5.0	4.95	0.86
		Dmbl/Sph	20.52	0.65	0.21	0.46	0.01	0.04	0.14		3.1	3.04	0.98
		Dmbl/Sph	22.39	0.31	0.23	0.49	0.04	0.04	0.14		1.4	1.35	1.00
	17	Dmbl/Sph	25.14	0.94	0.29	0.48	0.08	0.03	0.20		3.6	3.56	1.10
		Dmbl/Sph	20.42	0.68	0.21	0.57	0.00	0.00	0.14		3.2	3.19	0.99
		Dmbl/Sph	23.96	0.82	0.24	0.56	0.01	0.01	0.13		3.3	3.28	0.96
	18	Dmbl/Sph	24.37	0.57	0.25	0.56	0.01	0.03	0.11		2.3	2.26	0.99
		Dmbl/Sph	20.15	0.51	0.21	0.48	0.01	0.04	0.07		2.5	2.44	1.01
		Dmbl/Sph	22.16	0.33	0.22	0.46	0.05	0.05	0.13		1.5	1.45	0.97
3	19	Dmbl/Sph	13.28	1.36	0.21						9.3	9.16	1.41
		Dmbl/Sph	13.06	0.98	0.25						7.0	6.86	1.75
		Dmbl/Sph	14.18	1.00	0.25						6.6	6.48	1.62

Sample	Pellet	Crystal form	Ca	Mg	Sr	Na	Cl	S	P	Si	$MgCO_3$ (mol%)	$MgCO_3$ (mol%)	$SrCO_3$ (mol%)
3	19	Dmbl/Sph	11.31	1.30	0.20						10.3	10.15	1.56
	20	Dmbl/Sph	13.30	1.32	0.25						9.0	8.88	1.68
		Dmbl/Sph	10.97	1.21	0.21						9.9	9.77	1.69
		Dmbl/Sph	13.01	1.38	0.23						9.6	9.44	1.57
		Dmbl/Sph	12.61	1.16	0.23						8.4	8.29	1.64
4	21	Dmbl/Sph	20.46	0.78	0.23	0.35	0.01	0.02	0.12		3.7	3.63	1.07
		Dmbl/Sph	20.51	0.82	0.22	0.38	0.04	0.03	0.13		3.8	3.81	1.02
		Dmbl/Sph	17.79	0.94	0.20	0.33	0.05	0.02	0.09		5.0	4.97	1.06
		Dmbl/Sph	22.42	0.57	0.23	0.35	0.05	0.05	0.11		2.5	2.45	0.99
		Dmbl/Sph	21.72	0.54	0.23	0.34	0.03	0.03	0.12		2.4	2.40	1.02
		Dmbl/Sph	16.79	0.74	0.15	0.41	0.02	0.02	0.06		4.2	4.19	0.85
		Dmbl/Sph	16.18	0.76	0.15	0.40	0.03	0.02	0.08		4.5	4.45	0.88
	22	Dmbl/Sph	17.18	0.31	0.16	0.43	0.02	0.05	0.06		1.8	1.76	0.91
		Dmbl/Sph	18.61	0.46	0.17	0.35	0.03	0.04	0.08		2.4	2.39	0.88
		Dmbl/Sph	15.54	0.42	0.13	0.41	0.02	0.03	0.04		2.6	2.61	0.81
		Dmbl/Sph	16.14	0.32	0.14	0.44	0.04	0.03	0.04		1.9	1.93	0.84
	23	Dmbl/Sph	15.16	1.47	0.16	0.40	0.06	0.02	0.09		8.8	8.76	0.95
		Dmbl/Sph	16.27	1.34	0.17	0.41	0.04	0.01	0.08		7.6	7.54	0.96

Table AII 5 EDX data for samples produced by *Eucinostomus* sp. (all elemental data reported as atomic %)

Sample	Pellet	Crystal form	Ca	Mg	Sr	Na	Cl	S	P	Si	$MgCO_3$ (mol%)	$MgCO_3$ (mol%)	$SrCO_3$ (mol%)
1	1	Sphere	14.89	3.31	0.08						18.2	18.11	0.44
		Sphere	12.25	2.95	0.06						19.4	19.33	0.39
		Sphere	11.83	2.72	0.05						18.7	18.63	0.34
		Sphere	15.12	3.02	0.05						16.6	16.60	0.27
		Sphere	13.41	3.11	0.06						18.8	18.76	0.36
		Sphere	12.1	2.95	0.08						19.6	19.50	0.53
		Sphere	10.78	2.92	0.05						21.3	21.24	0.36
		Sphere	10.36	2.73	0.05						20.9	20.78	0.38
		Sphere	10.94	2.9	0.06						21.0	20.86	0.43
		Sphere	14	3.2	0.07						18.6	18.53	0.41
	2	Sphere	11.1	2.11	0.06						16.0	15.90	0.45
		Sphere	12.27	2.37	0.08						16.2	16.10	0.54
		Sphere	11.35	2.35	0.07						17.2	17.07	0.51
		Sphere	15.06	2.15	0.06						12.5	12.45	0.35
		Sphere	13.77	2.07	0.07						13.1	13.01	0.44
		Sphere	9.89	2.09	0.05						17.4	17.37	0.42
		Sphere	11.96	3.92	0.1						24.7	24.53	0.63
		Sphere	11.59	3.24	0.06						21.8	21.76	0.40
		Sphere	12.64	3.18	0.08						20.1	20.00	0.50
		Sphere	9.95	2.13	0.05						17.6	17.56	0.41
	3	Sphere	14.74	3.16	0.18						17.7	17.48	1.00
		Sphere	12.12	2.36	0.11						16.3	16.18	0.75
		Sphere	9.86	2.31	0.08						19.0	18.86	0.65
		Sphere	11.5	2.7	0.11						19.0	18.87	0.77
		Sphere	11.13	2.64	0.07						19.2	19.08	0.51
		Sphere	12.37	2.81	0.08						18.5	18.41	0.52
		Sphere	10.72	2.37	0.07						18.1	18.01	0.53
		Sphere	10.69	2.6	0.09						19.6	19.43	0.67
		Sphere	10.06	2.47	0.07						19.7	19.60	0.56
		Sphere	10.17	2.24	0.04						18.0	17.99	0.32
	4	Sphere	9.37	2.03	0.04						17.8	17.74	0.35
		Sphere	10.42	2.33	0.07						18.3	18.17	0.55
		Sphere	10.96	2.3	0.08						17.3	17.24	0.60
		Sphere	7.72	1.75	0.06						18.5	18.36	0.63
		Sphere	10.1	1.91	0.06						15.9	15.82	0.50
		Sphere	10.68	2.02	0.06						15.9	15.83	0.47
		Sphere	10.97	2.32	0.08						17.5	17.35	0.60
		Sphere	12.35	2.61	0.1						17.4	17.33	0.66
		Sphere	10.13	2.31	0.08						18.6	18.45	0.64
		Sphere	10.48	2.29	0.08						17.9	17.82	0.62
	5	Sphere	7.33	2.42	0.06						24.8	24.67	0.61
		Sphere	10.98	2.45	0.08						18.2	18.13	0.59
		Sphere	10.58	2.14	0.08						16.8	16.72	0.63
		Sphere	7.26	2.51	0.07						25.7	25.51	0.71
		Sphere	8.57	2.81	0.06						24.7	24.56	0.52
		Sphere	8.25	2.72	0.06						24.8	24.66	0.54
		Sphere	11.04	3.13	0.09						22.1	21.95	0.63
		Sphere	11.37	2.49	0.07						18.0	17.88	0.50
		Sphere	12.27	3.01	0.07						19.7	19.61	0.46
		Sphere	10.22	2.62	0.09						20.4	20.26	0.70

Table AII 6 EDX data for samples produced by black grouper (all elemental data reported as atomic %)

Sample	Pellet	Crystal form	Ca	Mg	Sr	Na	Cl	S	P	Si	$MgCO_3$ (mol%)	$MgCO_3$ (mol%)	$SrCO_3$ (mol%)
1	1	ME	15.36	8.06	0.10						34.4	34.27	0.43
		ME	20.94	7.44	0.16						26.2	26.07	0.56
		ME	12.68	5.62	0.10						30.7	30.54	0.54
		ME	15.09	5.54	0.20						26.9	26.60	0.96
		ME	8.00	3.96	0.03						33.1	33.03	0.25
		ME	13.29	5.93	0.14						30.9	30.63	0.72
		ME	10.52	4.34	0.07						29.2	29.07	0.47
		ME	10.95	5.94	0.13						35.2	34.90	0.76
		ME	12.36	8.09	0.12						39.6	39.33	0.58
		ME	9.43	4.82	0.07						33.8	33.66	0.49
	2	ME	11.22	5.02	0.14						30.9	30.65	0.85
		ME	16.33	6.67	0.21						29.0	28.74	0.90
		ME	18.10	5.56	0.36						23.5	23.15	1.50
		ME	17.21	7.44	0.10						30.2	30.06	0.40
		ME	17.06	10.42	0.22						37.9	37.62	0.79
		ME	17.96	9.05	0.25						33.5	33.20	0.92
		ME	15.87	5.26	0.18						24.9	24.68	0.84
		ME	15.06	6.31	0.18						29.5	29.28	0.84
		ME	19.26	5.92	0.61						23.5	22.95	2.37
		ME	13.87	4.25	0.10						23.5	23.33	0.55
	3	ME	9.53	4.76	0.07						33.3	33.15	0.49
		ME	11.36	6.46	0.13						36.3	35.99	0.72
		ME	10.69	6.01	0.09						36.0	35.80	0.54
		ME	14.71	6.39	0.12						30.3	30.11	0.57
		ME	11.69	5.73	0.13						32.9	32.65	0.74
		ME	14.21	5.33	0.17						27.3	27.04	0.86
		ME	11.72	4.88	0.11						29.4	29.20	0.66
		ME	12.18	5.29	0.08						30.3	30.14	0.46
		ME	9.34	5.79	0.10						38.3	38.02	0.66
		ME	12.13	7.39	0.16						37.9	37.55	0.81
	4	ME	9.88	7.17	0.10						42.1	41.81	0.58
		ME	14.54	5.12	0.09						26.0	25.92	0.46
		ME	14.01	4.93	0.13						26.0	25.85	0.68
		ME	10.54	5.05	0.11						32.4	32.17	0.70
		ME	13.95	5.18	0.15						27.1	26.87	0.78
		ME	14.53	7.68	0.18						34.6	34.30	0.80
		ME	14.86	6.18	0.16						29.4	29.15	0.75
		ME	10.98	5.72	0.13						34.3	33.99	0.77
		ME	12.22	4.98	0.05						29.0	28.87	0.29
		ME	11.96	6.33	0.16						34.6	34.31	0.87
	5	ME	14.01	3.52	0.13						20.1	19.93	0.74
		ME	10.98	5.58	0.10						33.7	33.49	0.60
		ME	8.53	5.52	0.05						39.3	39.15	0.35
		ME	9.17	5.17	0.08						36.1	35.85	0.55
		ME	9.63	5.35	0.09						35.7	35.50	0.60
		ME	10.61	4.95	0.07						31.8	31.67	0.45
		ME	5.55	3.90	0.03						41.3	41.14	0.32
		ME	6.19	4.21	0.05						40.5	40.29	0.48
		ME	6.71	3.66	N/r						35.3		
		ME	11.28	2.54	0.08						18.4	18.27	0.58

Sample	Pellet	Crystal form	Ca	Mg	Sr	Na	Cl	S	P	Si	$MgCO_3$ (mol%)	$MgCO_3$ (mol%)	$SrCO_3$ (mol%)
2	6	ME	16.86	3.36	0.08	0.43	0.07	0.00	0.15		16.6	16.55	0.39
		ME	19.14	5.80	0.08	0.29	0.20	0.00	0.21		23.3	23.18	0.32
		ME	17.60	5.46	0.08	0.30	0.13	0.00	0.16		23.7	23.60	0.35
		ME	17.64	4.98	0.06	0.37	0.11	0.00	0.17		22.0	21.96	0.26
		ME	19.07	4.31	0.07	0.29	0.08	0.00	0.22		18.4	18.38	0.30
		ME	20.38	4.22	0.09	0.31	0.10	0.00	0.25		17.2	17.09	0.36
		ME	22.65	4.61	0.09	0.33	0.12	0.00	0.24		16.9	16.86	0.33
	7	ME	20.82	3.72	0.09	0.36	0.12	0.00	0.28		15.2	15.10	0.37
		ME	21.39	3.69	0.08	0.35	0.08	0.00	0.25		14.7	14.67	0.32
		ME	18.10	3.01	0.09	0.33	0.07	0.00	0.22		14.3	14.20	0.42
		ME	22.24	3.64	0.09	0.39	0.08	0.00	0.22		14.1	14.02	0.35
		ME	20.29	3.90	0.10	0.39	0.11	0.00	0.32		16.1	16.06	0.41
		ME	17.74	3.27	0.07	0.40	0.06	0.00	0.15		15.6	15.51	0.33
		ME	17.98	3.47	0.07	0.37	0.06	0.00	0.17		16.2	16.12	0.33
	8	ME	18.87	3.52	0.08	0.36	0.07	0.00	0.27		15.7	15.67	0.36
		ME	17.93	6.63	0.07	0.39	0.18	0.00	0.44		27.0	26.92	0.28
		ME	18.93	5.26	0.08	0.38	0.16	0.00	0.36		21.7	21.67	0.33
		ME	19.22	8.67	0.07	0.43	0.33	0.00	0.58		31.1	31.01	0.25
		ME	17.34	6.65	0.07	0.44	0.28	0.00	0.49		27.7	27.64	0.29
		ME	19.17	7.36	0.11	0.38	0.34	0.00	0.63		27.7	27.63	0.41
		ME	19.87	4.00	0.07	0.36	0.12	0.00	0.30		16.8	16.71	0.29
		ME	19.44	4.22	0.07	0.35	0.10	0.00	0.31		17.8	17.78	0.29
	9	ME	17.53	4.49	0.07	0.34	0.10	0.00	0.21		20.4	20.33	0.32
		ME	15.50	3.29	0.07	0.36	0.02	0.00	0.15		17.5	17.44	0.37
		ME	14.63	4.29	0.06	0.36	0.05	0.00	0.17		22.7	22.60	0.32
		ME	17.65	3.82	0.08	0.35	0.06	0.00	0.21		17.8	17.73	0.37
		ME	17.65	3.81	0.08	0.36	0.08	0.00	0.20		17.8	17.69	0.37
		ME	17.73	3.93	0.07	0.36	0.03	0.00	0.20		18.1	18.09	0.32
3	10	ME	14.83	6.26							29.7		
		ME	15.20	5.95							28.1		
		ME	14.87	6.00							28.8		
		ME	15.04	5.89							28.1		
		ME	11.86	2.58							17.9		
		ME	16.31	2.51							13.3		
		ME	17.69	2.74							13.4		
		ME	13.73	6.08							30.7		
		ME	14.61	6.41							30.5		
		ME	15.17	5.64							27.1		
		ME	15.44	5.91							27.7		
	11	ME	17.28	6.31	0.08	0.37	0.17	0.00	0.13		26.7	26.66	0.34
		ME	15.05	5.19	0.09	0.39	0.10	0.00	0.12		25.6	25.53	0.44
		ME	12.47	5.18	0.06	0.36	0.08	0.00	0.08		29.3	29.25	0.34
	12	ME	12.68	7.26	0.07	0.35	0.18	0.00	0.47		36.4	36.28	0.35
		ME	12.49	6.54	0.07	0.35	0.17	0.00	0.28		34.4	34.24	0.37
		ME	15.38	6.78	0.09	0.26	0.12	0.00	0.23		30.6	30.47	0.40
3	13	ME	12.13	4.72	0.06	0.34	0.14	0.00	0.05		28.0	27.91	0.35
		ME	11.27	4.50	0.06	0.29	0.15	0.01	0.05		28.5	28.43	0.38
		ME	15.03	5.84	0.07	0.37	0.10	0.00	0.05		28.0	27.89	0.33
	14	ME	12.32	6.22	0.05	0.34	0.11	0.00	0.15		33.5	33.46	0.27
		ME	15.12	6.11	0.08	0.26	0.13	0.00	0.13		28.8	28.67	0.38
		ME	17.56	7.22	0.09	0.39	0.19	0.00	0.19		29.1	29.03	0.36

Sample	Pellet	Crystal form	Ca	Mg	Sr	Na	Cl	S	P	Si	$MgCO_3$ (mol%)	$MgCO_3$ (mol%)	$SrCO_3$ (mol%)
	15	ME	14.54	6.92	0.07	0.41	0.18	0.00	0.18		32.2	32.14	0.33
		ME	12.60	7.08	0.06	0.31	0.21	0.00	0.30		36.0	35.87	0.30
		ME	13.23	7.22	0.07	0.38	0.18	0.00	0.33		35.3	35.19	0.34
		ME	17.77	5.13	0.07	0.45	0.12	0.00	0.12		22.4	22.33	0.30
4	16	ME	17.19	4.99	0.06	0.51	0.10	0.00	0.10		22.5	22.44	0.27
		ME	18.05	4.98	0.06	0.48	0.20	0.04	0.18		21.6	21.57	0.26
		ME	16.99	5.52	0.07	0.49	0.13	0.04	0.12		24.5	24.45	0.31
		ME	19.60	5.88	0.09	0.33	0.13	0.04	0.23		23.1	23.00	0.35
		ME	17.13	6.13	0.08	0.48	0.22	0.02	0.23		26.4	26.26	0.34
2	6	Dmbl/Sph	19.18	3.59	0.10	0.32	0.12	0.00	0.15		15.8	15.70	0.44
		Dmbl/Sph	16.73	2.47	0.06	0.48	0.07	0.00	0.21		12.9	12.82	0.31
4	16	Dmbl/Sph	18.66	2.35	0.08	0.57	0.07	0.00	0.22		11.2	11.14	0.38
		Dmbl/Sph	18.11	2.48	0.10	0.42	0.05	0.45	0.06		12.0	11.99	0.48
		Dmbl/Sph	20.04	1.41	0.09	0.71	0.04	0.00	0.23		6.6	6.55	0.42
4	16	Amorph	21.26	6.39	0.08	0.34	0.13	0.00	0.13		23.1	23.04	0.29
		Amorph	14.20	6.85	0.08	0.37	0.12	0.00	0.11		32.5	32.42	0.38
		Amorph	15.41	6.79	0.08	0.30	0.12	0.00	0.26		30.6	30.48	0.36
		Amorph	19.85	6.30	0.08	0.36	0.20	0.00	0.31		24.1	24.02	0.30
		Amorph	16.33	8.60	0.08	0.33	0.18	0.00	0.23		34.5	34.39	0.32

Table AII 7 EDX data for samples produced by Graysby grouper (all elemental data reported as atomic %)

Sample	Pellet	Crystal form	Ca	Mg	Sr	Na	Cl	S	P	Si	$MgCO_3$ (mol%)	$MgCO_3$ (mol%)	$SrCO_3$ (mol%)
1	1	ME	12.31	4.6	0.12						27.2	27.01	0.70
		ME	8.65	6.65	0.11						43.5	43.15	0.71
		ME	11.39	6.48	0.16						36.3	35.94	0.89
		ME	11.48	6.52	0.13						36.2	35.96	0.72
		ME	13.25	6.51	0.1						32.9	32.78	0.50
		ME	13.7	5.54	0.1						28.8	28.65	0.52
		ME	14.68	7.32	0.12						33.3	33.09	0.54
		ME	13.4	6.62	0.1						33.1	32.90	0.50
		ME	11.47	7.15	0.11						38.4	38.17	0.59
		ME	12.82	6.89	0.11						35.0	34.76	0.55
	2	ME	8.54	6.38	0.11						42.8	42.45	0.73
		ME	11.36	6.42	0.15						36.1	35.81	0.84
		ME	11.02	6.8	0.14						38.2	37.86	0.78
		ME	9.91	6.76	0.11						40.6	40.29	0.66
		ME	10.01	6.72	0.12						40.2	39.88	0.71
		ME	10.87	6.2	0.13						38.3	36.05	0.76
		ME	14.29	6.23	0.14						32.0	30.15	0.68
		ME	12.46	5.98	0.1						33.2	32.25	0.54
		ME	12.07	6.09	0.12						33.5	33.32	0.66
		ME	13.49	6.5	0.13						32.5	32.31	0.65
	3	ME	12.21	3.75	0.11						23.5	23.34	0.68
		ME	10.52	5.67	0.11						35.0	34.79	0.67
		ME	9.39	5.91	0.1						38.6	38.38	0.65
		ME	12.35	6.36	0.11						34.0	33.79	0.58
		ME	13.36	6.88	0.12						34.0	33.79	0.59
		ME	11.94	6.41	0.13						34.9	34.69	0.70
		ME	13.24	6.46	0.12						32.8	32.59	0.61
		ME	11.99	6.32	0.13						34.5	34.27	0.70
		ME	11.92	5.65	0.12						32.2	31.94	0.68
		ME	12.91	6.04	0.13						31.9	31.66	0.68
	4	ME	12.03	7.39	0.13						38.1	37.80	0.66
		ME	13.78	7.49	0.13						35.2	35.00	0.61
		ME	12.92	7.77	0.13						37.6	37.32	0.62
		ME	11.41	7.11	0.12						38.4	38.14	0.64
		ME	13.38	7.45	0.13						35.8	35.54	0.62
		ME	10.4	6.91	0.11						39.9	39.67	0.63
		ME	12.59	6.94	0.12						35.5	35.32	0.61
		ME	12.81	6.62	0.12						34.1	33.86	0.61
		ME	12.66	7.42	0.12						37.0	36.73	0.59
		ME	12.47	7.3	0.13						36.9	36.68	0.65
	5	ME	9.24	3.83	0.08						29.3	29.13	0.61
		ME	9.92	3.77	0.09						27.5	27.36	0.65
		ME	12	4.46	0.12						27.1	26.90	0.72
		ME	9.92	3.78	0.11						27.6	27.37	0.80
		ME	9.52	4.17	0.1						30.5	30.24	0.73
		ME	10.16	3.74	0.12						26.9	26.68	0.86
		ME	9.87	3.57	0.11						26.6	26.35	0.81
		ME	9.46	3.15	0.08						25.0	24.82	0.63
		ME	8.48	3.55	0.08						29.5	29.31	0.66
		ME	11.16	3.73	0.12						25.1	24.85	0.80

Table AII 8 EDX data for samples produced by red hind (all elemental data reported as atomic %)

Sample	Pellet	Crystal form	Ca	Mg	Sr	Na	Cl	S	P	Si	$MgCO_3$ (mol%)	$MgCO_3$ (mol%)	$SrCO_3$ (mol%)
1	1	ME	14.96	8.07	0.15						35.04	34.81	0.65
		ME	15.28	7.88	0.19						34.02	33.75	0.81
		ME	14.39	9.02	0.20						38.53	38.20	0.85
		ME	16.94	8.64	0.24						33.78	33.46	0.93
		ME	12.01	5.72	0.17						32.26	31.96	0.95
		ME	9.01	6.08	0.11						40.29	40.00	0.72
		ME	10.3	6.38	0.11						38.25	38.00	0.66
		ME	9.36	6.22	0.12						39.92	39.62	0.76
		ME	10.03	6.35	0.11						38.77	38.51	0.67
		ME	10.67	6.55	0.14						38.04	37.73	0.81
	2	ME	10.32	8.08	0.13						43.91	43.60	0.70
		ME	10.03	8.44	0.12						45.70	45.40	0.65
		ME	10.25	8.12	0.11						44.20	43.94	0.60
		ME	9.32	8.24	0.13						46.92	46.58	0.73
		ME	10.01	7.98	0.12						44.36	44.06	0.66
		ME	8.64	7.65	0.12						46.96	46.62	0.73
		ME	7.3	6.51	0.11						47.14	46.77	0.79
		ME	7.96	7.1	0.11						49.01	46.80	0.73
		ME	8.53	8	0.12						43.28	48.05	0.72
		ME	7.39	6.58	0.09						47.10	46.80	0.64
	3	ME	11.52	8.79	0.11						43.28	43.05	0.54
		ME	9.03	8.01	0.11						47.01	46.71	0.64
		ME	12.34	7.23	0.10						36.94	36.76	0.51
		ME	9.45	5.86	0.11						38.28	38.00	0.71
		ME	9.41	4.9	0.12						34.24	33.96	0.83
		ME	12.37	6.21	0.13						33.42	33.19	0.69
		ME	11.57	8.54	0.12						42.47	42.21	0.59
		ME	9.42	7.6	0.13						44.65	44.31	0.76
		ME	11.59	7.68	0.12						39.85	39.61	0.62
		ME	12.37	4.74	0.13						27.70	27.49	0.75
	4	ME	12.14	7.66	0.13						38.69	38.43	0.65
		ME	13.67	7.57	0.13						35.64	35.42	0.61
		ME	12.88	6.2	0.13						32.49	32.27	0.68
		ME	7.48	7.59	0.12						50.36	49.97	0.79
		ME	8.18	6.79	0.13						45.36	44.97	0.86
		ME	11.53	6.72	0.11						36.82	36.60	0.60
		ME	11.34	7.63	0.12						40.22	39.97	0.63
		ME	10.65	7.63	0.12						41.74	41.47	0.65
		ME	8.57	6.54	0.11						43.28	42.97	0.72
		ME	7.15	5.93	0.07						45.34	45.10	0.53
	5	ME	11.15	5.26	0.14						32.05	31.78	0.85
		ME	11.48	5.52	0.11						32.47	32.26	0.64
		ME	13.26	4.85	0.13						26.78	26.59	0.71
		ME	14.15	5.74	0.16						28.86	28.63	0.80
		ME	15.6	6.54	0.13						29.54	29.37	0.58
		ME	12.36	5.75	0.11						31.75	31.56	0.60
		ME	12.11	5.82	0.12						32.46	32.24	0.66
		ME	13.61	5.49	0.14						28.74	28.53	0.73
		ME	14.43	5.66	0.12						28.17	28.01	0.59
		ME	10.86	5.79	0.13						34.77	34.51	0.77

Table AII 9 EDX data for samples produced by bonefish (all elemental data reported as atomic %)

Sample	Pellet	Crystal form	Ca	Mg	Sr	Na	Cl	S	P	Si	$MgCO_3$ (mol%)	$MgCO_3$ (mol%)	$SrCO_3$ (mol%)
1	1	Sphere	11.73	2.82							19.4		
		Sphere	11.56	3.00							20.6		
		Sphere	16.23	3.09							16.0		
		Sphere	11.50	3.12							21.3		
		Sphere	14.14	3.28							18.8		
		Sphere	11.74	2.51							17.6		
		Sphere	13.60	3.25							19.3		
		Sphere	11.59	2.71							19.0		
		Sphere	11.11	2.70							19.6		
		Sphere	10.47	2.27							17.8		
	2	Sphere	14.46	2.08							12.6		
		Sphere	19.06	3.72							16.3		
		Sphere	12.92	4.25							24.8		
		Sphere	16.01	4.28							21.1		
		Sphere	11.47	4.20							26.8		
		Sphere	10.16	4.67							29.6		
		Sphere	11.28	3.65							27.1		
		Sphere	10.83	3.19							30.1		
		Sphere	12.26	3.54							22.4		
		Sphere	12.67	3.12							19.8		
	3	Sphere	13.58	3.41							20.1		
		Sphere	14.72	3.75							20.3		
		Sphere	11.67	3.68							24.0		
		Sphere	10.73	4.04							27.4		
		Sphere	11.48	3.85							25.1		
		Sphere	11.97	3.83							24.2		
		Sphere	11.68	4.02							25.6		
		Sphere	10.67	3.61							25.3		
		Sphere	12.51	3.78							23.2		
		Sphere	10.73	3.05							22.1		
	4	Sphere	13.24	4.48							25.3		
		Sphere	11.60	4.13							26.3		
		Sphere	11.12	4.91							30.6		
		Sphere	14.70	4.73							24.3		
		Sphere	12.00	4.50							27.3		
		Sphere	9.73	4.47							31.5		
		Sphere	13.62	0.65							4.6		
		Sphere	12.44	4.27							25.6		
		Sphere	11.40	3.77							24.9		
	5	Sphere	12.31	5.54							31.0		
		Sphere	12.34	4.14							25.1		
		Sphere	12.98	3.48							21.1		
		Sphere	12.79	4.05							24.0		
		Sphere	13.62	3.66							21.2		
		Sphere	11.77	3.35							22.2		
		Sphere	12.54	3.92							23.8		
		Sphere	11.95	3.70							23.6		
		Sphere	12.10	3.31							21.5		
		Sphere	12.82	3.55							21.7		

Sample	Pellet	Crystal form	Ca	Mg	Sr	Na	Cl	S	P	Si	$MgCO_3$ (mol%)	$MgCO_3$ (mol%)	$SrCO_3$ (mol%)
2	6	Sphere	15.96	5.55	0.08	0.33	0.33	0.00	0.35		25.8	25.71	0.37
		Sphere	15.50	5.00	0.08	0.32	0.30	0.00	0.11		24.4	24.30	0.39
		Sphere	16.84	5.35	0.08	0.38	0.28	0.00	0.10		24.1	24.02	0.36
		Sphere	20.22	3.33	0.05	0.46	0.23	0.00	0.35		14.1	14.11	0.21
		Sphere	20.96	4.46	0.34	0.28	0.41	0.00	0.74		17.5	17.31	1.32
		Sphere	19.48	2.16	0.07	0.62	0.13	0.00	0.31		10.0	9.95	0.32
		Sphere	19.22	5.31	0.03	0.43	0.33	0.00	0.43		21.6	21.62	0.12
3	7	Sphere	23.27	5.16	0.38	1.21	0.60		0.39		18.1	17.91	1.32
		Sphere	19.18	4.74	0.29	1.12	0.42		0.33		19.8	19.58	1.20
		Sphere	22.22	3.17	0.17	1.13	0.47		0.29		12.5	12.40	0.67
		Sphere	20.78	2.73	0.20	0.87	0.25		0.30		11.6	11.51	0.84
		Sphere	22.33	3.02	0.21	0.76	0.28		0.31		11.9	11.82	0.82
	8	Sphere	21.68	3.33	0.08	0.46	0.33		0.24		13.3	13.27	0.32
		Sphere	22.29	2.43	0.08	0.71	0.41		0.28		9.8	9.80	0.32
		Sphere	25.76	3.45	0.08	0.50	0.30		0.28		11.8	11.78	0.27
		Sphere	22.51	4.16	0.08	0.47	0.48		0.23		15.6	15.55	0.30
2	9	Nanosph	14.14	6.28	0.07	0.30	0.16	0.06	0.22		30.8	30.65	0.34
		Nanosph	12.21	6.83	0.09	0.41	0.15	0.05	0.56		35.9	35.70	0.47
		Nanosph	13.44	7.13	0.06	0.39	0.18	0.07	0.59		34.7	34.56	0.29
		Nanosph	13.26	6.81	0.06	0.29	0.22	0.03	0.33		33.9	33.83	0.30
		Nanosph	13.30	6.46	0.06	0.35	0.18	0.06	0.25		32.7	32.59	0.30
		Nanosph	11.88	6.22	0.06	0.30	0.23	0.06	0.24		34.4	34.25	0.33
		Nanosph	9.92	6.35	0.06	0.20	0.25	0.06	0.08		39.0	38.89	0.37
		Nanosph	9.41	5.60	0.04	0.22	0.29	0.00	0.12		37.3	37.21	0.27
3	10	Nanosph	11.44	19.55	0.04	0.88	1.54		2.35	0.22	63.1	63.00	0.13
		Nanosph	10.83	15.29	0.06	0.85	1.28		2.10	0.21	58.5	58.40	0.23
		Nanosph	13.34	21.74	0.16	0.89	1.83		2.99	0.21	62.0	61.69	0.45
		Nanosph	13.02	17.12	0.17	0.96	0.90		3.11	0.25	56.8	56.48	0.56
		Nanosph	14.91	13.60	0.20	1.06	0.97		3.45	0.18	47.7	47.37	0.70
3	10	Amorph	2.78	22.95		0.90	2.13		0.11	0.43	89.2		
		Amorph	2.87	27.99		0.53	3.69		0.12	0.5	90.7		
		Amorph	2.52	26.09		0.50	3.63		0.12	0.54	91.2		
		Amorph	2.27	28.01		0.55	3.44		0.44	0.56	92.5		
3	11	Rhomb	25.66	2.19	0.05	0.57	0.14		0.26		7.9	7.85	0.18
		Rhomb	24.49	1.57	0.09	0.61	0.11		0.23		6.0	6.00	0.34
		Rhomb	25.46	1.38	0.06	0.68	0.12		0.23		5.1	5.13	0.22
		Rhomb	25.93	0.79	0.08	0.63	0.07		0.16		3.0	2.95	0.30
		Rhomb	23.04	0.92	0.07	0.60	0.06		0.10		3.8	3.83	0.29
		Rhomb	21.64	1.38	0.07	0.74	0.07		0.15		6.0	5.98	0.30
		Rhomb	22.43	0.70	0.08	0.68	0.08		0.13		3.0	3.02	0.34
	12	Rhomb	23.68	0.74	0.09	0.56	0.12		0.25		3.0	3.02	0.37
		Rhomb	28.64	1.46	0.10	0.73	0.15		0.19		4.9	4.83	0.33
		Rhomb	27.27	0.75	0.09	0.56	0.08		0.33		2.7	2.67	0.32
		Rhomb	25.26	1.67	0.09	0.56	0.24		0.28		6.2	6.18	0.33
		Rhomb	24.75	0.75	0.09	0.64	0.09		0.17		2.9	2.93	0.35
		Rhomb	25.82	0.32	0.09	0.59	0.07		0.14		1.2	1.22	0.34
		Rhomb	21.70	1.92	0.09	0.64	0.23		0.24		8.1	8.10	0.38

Table AII 10 EDX data for samples produced by checkered puffer (all elemental data reported as atomic %)

Sample	Pellet	Crystal form	Ca	Mg	Sr	Na	Cl	S	P	Si	$MgCO_3$ (mol%)	$MgCO_3$ (mol%)	$SrCO_3$ (mol%)
1	1	Sphere	25.87	0.59	0.21						2.2	2.21	0.79
		Sphere	17.90	0.39	0.25						2.1	2.10	1.35
		Sphere	16.89	0.88	0.25						5.0	4.88	1.39
		Sphere	20.00	0.93	0.23						4.4	4.40	1.09
		Sphere	17.90	0.42	0.2						2.3	2.27	1.08
		Sphere	17.51	0.50	0.13						2.8	2.76	0.72
		Sphere	19.37	0.36	0.11						1.8	1.81	0.55
		Sphere	21.61	0.24	0.12						1.1	1.09	0.55
		Sphere	21.41	0.34	0.1						1.6	1.56	0.46
		Sphere	16.70	1.23	0.18						6.9	6.79	0.99
	2	Sphere	21.53	0.81	0.25						3.6	3.59	1.11
		Sphere	18.27	0.64	0.09						3.4	3.37	0.47
		Sphere	18.67	0.51	0.08						2.7	2.65	0.42
		Sphere	14.45	0.26	0.08						1.8	1.76	0.54
		Sphere	18.03	0.53	0.23						2.9	2.82	1.22
		Sphere	16.58	0.45	0.23						2.6	2.61	1.33
		Sphere	10.64	0.38	0.13						3.4	3.41	1.17
2	3	Sphere	17.54	0.19	0.02	0.27	0.01	0.03	0.04		1.1	1.07	0.11
		Sphere	20.91	0.23	0.03	0.27	0.00	0.02	0.06		1.1	1.09	0.14
3	4	Sphere	17.58	0.14		0.31		0.05			0.8		
		Sphere	22.30	0.24		0.34		0.05			1.1		
		Sphere	18.40	0.15		0.34		0.07			0.8		
		Sphere	17.48	0.15		0.32		0.04			0.9		
		Sphere	17.95	0.17		0.33		0.03			0.9		
		Sphere	18.82	0.39		0.31		0.02			2.0		
4	5	Sphere	10.25	0.41	0.05						3.8	3.83	0.47
		Sphere	23.46	0.37	0.19						1.6	1.54	0.79
		Sphere	8.77	0.47	0.06						5.1	5.05	0.65
		Sphere	22.43	0.32	0.10						1.4	1.40	0.44
		Sphere	11.33	0.33	0.07						2.8	2.81	0.60
		Sphere	22.55	0.49	0.11						2.1	2.12	0.48
3	6	PE	18.00	0.10		0.24		0.03			0.6		
		PE	20.19	0.13		0.24		0.01			0.6		
		PE	20.16	0.16		0.22		0.03			0.8		
	7	PE	24.64	0.10		0.20		0.04			0.4		
		PE	21.50	0.20		0.26		0.04			0.9		
		PE	20.94	0.18		0.20		0.03			0.9		
		PE	19.39	0.19		0.20		0.04			1.0		
		PE	15.54	0.13		0.27		0.04			0.8		
4	5	PE	11.80	0.31	0.06						2.6		
		PE	12.04	0.30	0.06						2.4		
		PE	12.80	0.30	0.06						2.3		
2	3	Rhomb	20.72	0.24	0.03	0.27	0.00	0.03	0.07		1.1	1.14	0.14
		Rhomb	20.45	0.19	0.02	0.20	0.00	0.00	0.04		0.9	0.92	0.10
		Rhomb	19.95	0.48	0.02	0.28	0.01	0.01	0.09		2.3	2.35	0.10
5	8	ME	25.62	4.39	0.09	0.45	0.07	0.00			14.6	14.58	0.30
		ME	23.94	4.05	0.10	0.43	0.12	0.03			14.5	14.42	0.36
		ME	22.41	3.40	0.10	0.38	0.17	0.04			13.2	13.12	0.39
	9	ME	23.10	5.17	0.08	0.39	0.12	0.00			18.3	18.24	0.28
		ME	24.60	5.69	0.08	0.42	0.09	0.01			18.8	18.74	0.26

Sample	Pellet	Crystal form	Ca	Mg	Sr	Na	Cl	S	P	Si	$MgCO_3$ (mol%)	$MgCO_3$ (mol%)	$SrCO_3$ (mol%)
5	8	ME	24.93	4.53	0.07	0.40	0.04	0.00			15.4	15.34	0.24
		ME	24.14	4.56	0.08	0.44	0.09	0.00			15.9	15.84	0.28
		ME	20.26	5.10	0.08	0.48	0.09	0.00			20.1	20.05	0.31
		ME	26.53	5.11	0.10	0.45	0.21	0.03			16.2	16.10	0.32
		ME	23.13	4.18	0.07	0.40	0.09	0.03			15.3	15.27	0.26
		ME	22.57	5.55		0.44	0.11	0.00	0.04		19.7		
	10	ME	24.42	3.47	0.12	0.45	0.10	0.04	0.06		12.4	12.39	0.43
		ME	24.10	5.32	0.09	0.47	0.15	0.00	0.08		18.1	18.03	0.30
		ME	26.60	4.36	0.08	0.38	0.13	0.01	0.06		14.1	14.05	0.26
		ME	26.61	5.12	0.09	0.33	0.21	0.02	0.05		16.1	16.09	0.28
		ME	25.93	5.13	0.07	0.47	0.19	0.00	0.05		16.5	16.48	0.22
		ME	26.19	5.43	0.08	0.39	0.26	0.01	0.07		17.2	17.13	0.25
		ME	32.31	4.74	0.08	0.39	0.23	0.02	0.07		12.8	12.77	0.22
		ME	19.83	3.85	0.06	0.30	0.10	0.00	0.04		16.3	16.22	0.25
2	3	Dmbl	19.49	1.83	0.04	0.67	0.12	0.00	0.19		8.6	8.57	0.19
		Dmbl	18.64	2.05	0.04	0.74	0.10	0.00	0.16		9.9	9.89	0.19
5	8	Dmbl	28.85	3.04	0.29	0.52	0.13	0.04	0.02		9.5	9.45	0.90
	9	Dmbl	32.05	0.72	0.32	0.43	0.02	0.01	0.08		2.2	2.18	0.97
		Dmbl	22.44	1.27	0.20	0.45	0.04	0.03	0.02		5.4	5.31	0.84
		Dmbl	23.96	1.42	0.20	0.52	0.07	0.08	0.04		5.6	5.55	0.78
		Dmbl	24.06	1.46	0.23	0.49	0.02	0.06	0.06		5.7	5.67	0.89
6	11	Dmbl	13.88	1.88		0.61	0.09		0.03		11.9		
		Dmbl	24.44	3.05		0.25	0.02	0.08			11.1		
		Dmbl	15.99	2.68		0.27	0.03	0.02			14.4		
		Dmbl	18.98	2.15		0.11	0.01	0.05			10.2		

Table AII 11 EDX data for samples produced by scrawled cowfish (all elemental data reported as atomic %)

Sample	Pellet	Crystal form	Ca	Mg	Sr	Na	Cl	S	P	Si	$MgCO_3$ (mol%)	$MgCO_3$ (mol%)	$SrCO_3$ (mol%)
1	1	Sphere	10.06	0.54	0.03						5.1	5.08	0.28
		Sphere	13.45	0.72	0.04						5.1	5.07	0.28
		Sphere	13.87	0.61	0.03						4.2	4.20	0.21
		Sphere	14.84	0.67	0.03						4.3	4.31	0.19
		Sphere	11.54	0.59	0.02						4.9	4.86	0.16
		Sphere	13.42	0.43	0.01						3.1	3.10	0.07
		Sphere	14.01	0.40	0.01						2.8	2.77	0.07
		Sphere	15.73	1.04	0.03						6.2	6.19	0.18
		Sphere	13.90	0.97	0.03						6.5	6.51	0.20
		Sphere	13.06	0.75	0.03						5.4	5.42	0.22
	2	Sphere	15.99	0.52	0.03						3.1	3.14	0.18
		Sphere	16.21	0.43	0.02						2.6	2.58	0.12
		Sphere	16.18	0.94	0.04						5.5	5.48	0.23
		Sphere	14.35	0.89	0.04						5.8	5.82	0.26
		Sphere	15.55	1.01	0.04						6.1	6.08	0.24
		Sphere	15.63	1.26	0.04						7.5	7.44	0.24
		Sphere	14.88	1.17	0.05						7.3	7.27	0.31
		Sphere	16.42	0.26	0.02						1.6	1.56	0.12
		Sphere	16.07	0.57	0.02						3.4	3.42	0.12
		Sphere	16.37	0.53	0.02						3.1	3.13	0.12
	3	Sphere	13.94	1.24	0.04						8.2	8.15	0.26
		Sphere	14.11	1.08	0.04						7.1	7.09	0.26
		Sphere	17.41	1.34	0.04						7.1	7.13	0.21
		Sphere	14.22	1.00	0.04						6.6	6.55	0.26
		Sphere	14.39	0.89	0.03						5.8	5.81	0.20
		Sphere	14.2	0.92	0.03						6.1	6.07	0.20
		Sphere	14.08	0.91	0.04						6.1	6.05	0.27
		Sphere	16.18	1.09	0.04						6.3	6.30	0.23
		Sphere	15.77	1.31	0.05						7.7	7.65	0.29
		Sphere	15.64	1.30	0.05						7.7	7.65	0.29
	4	Sphere	14.02	0.27	0.01						1.9	1.89	0.07
		Sphere	14.36	0.31	0.02						2.1	2.11	0.14
		Sphere	16.15	0.56	0.02						3.4	3.35	0.12
		Sphere	15.98	0.45	0.02						2.7	2.74	0.12
		Sphere	15.42	0.32	0.02						2.0	2.03	0.13
		Sphere	15.45	0.40	0.02						2.5	2.52	0.13
		Sphere	15.02	0.87	0.03						5.5	5.46	0.19
		Sphere	15.09	0.99	0.04						6.2	6.14	0.25
		Sphere	15	0.64	0.03						4.1	4.08	0.19
		Sphere	15.78	1.03	0.03						6.1	6.12	0.18

Table AII 12 EDX data for samples produced by grey angelfish (all elemental data reported as atomic %)

Sample	Pellet	Crystal form	Ca	Mg	Sr	Na	Cl	S	P	Si	$MgCO_3$ (mol%)	$MgCO_3$ (mol%)	$SrCO_3$ (mol%)
1	1	Dmbl	18.20	0.44	0.06	0.15		0.02			2.36	2.35	0.32
		Dmbl	17.20	0.41	0.07	0.15		0.00			2.33	2.32	0.40
		Dmbl	18.34	0.35	0.06	0.15	0.00	0.00			1.87	1.87	0.32
		Dmbl	22.10	0.85	0.06	0.13	0.03	0.11			3.70	3.69	0.26
		Dmbl	23.69	0.73	0.06	0.14	0.03	0.13			2.99	2.98	0.25
		Dmbl	23.86	0.35	0.07	0.17	0.00	0.04	0.12		1.45	1.44	0.29
		Dmbl	27.00	0.40	0.05	0.19	0.00	0.03			1.46	1.46	0.18
		Dmbl	23.55	0.34	0.07	0.09	0.03	0.03	0.09		1.42	1.42	0.29
		Dmbl	19.80	0.36	0.06	0.14	0.00	0.00	0.07		1.79	1.78	0.30
	2	Dmbl	20.80	0.33	0.06	0.10	0.02	0.03			1.56	1.56	0.28
		Dmbl	20.46	0.36	0.06	0.20	0.02	0.04	0.08		1.73	1.72	0.29
		Dmbl	18.63	0.37	0.06	0.12	0.00	0.02	0.07		1.95	1.94	0.31
		Dmbl	21.29	0.42	0.07	0.14	0.01	0.01	0.07		1.93	1.93	0.32
		Dmbl	21.43	0.36	0.07	0.16	0.00	0.00	0.07		1.65	1.65	0.32
		Dmbl	19.14	0.32	0.06	0.17	0.00	0.02	0.06		1.64	1.64	0.31
		Dmbl	24.08	0.39	0.09	0.13	0.02	0.05	0.11		1.59	1.59	0.37
		Dmbl	19.14	0.40	0.05	0.16	0.01	0.04	0.08		2.05	2.04	0.26
		Dmbl	20.11	0.34	0.05	0.18	0.02	0.03	0.07		1.66	1.66	0.24
		Dmbl	19.00	0.37	0.05	0.11	0.00	0.03	0.07		1.91	1.91	0.26
		Dmbl	23.76	0.44	0.07	0.13	0.03	0.03	0.10		1.82	1.81	0.29
	1	Sphere	22.28	0.45	0.07	0.11	0.00	0.00	0.09		1.98	1.97	0.31
		Sphere	20.22	0.48	0.06	0.16	0.00	0.00	0.08		2.32	2.31	0.29
		Sphere	20.63	0.52	0.07	0.13	0.00	0.01	0.09		2.46	2.45	0.33
		Sphere	22.56	0.51	0.07	0.22	0.00	0.05	0.12		2.21	2.20	0.30
		Sphere	21.36	0.42	0.07	0.18	0.02	0.01	0.09		1.93	1.92	0.32
	2	Sphere	14.28	0.61	0.06	0.13		0.03			4.10	4.08	0.40
		Sphere	18.38	0.41	0.05	0.16	0.00	0.02			2.18	2.18	0.27
		Sphere	17.87	0.38	0.06	0.12	0.01	0.04	0.11		2.08	2.08	0.33
		Sphere	15.99	0.38	0.06	0.17	0.01	0.02	0.07		2.32	2.31	0.37
		Sphere	15.90	0.41	0.06	0.14	0.00	0.01	0.06		2.51	2.50	0.37

Table AII 13 EDX data for samples produced by keeltail needlefish (all elemental data reported as atomic %)

Sample	Pellet	Crystal form	Ca	Mg	Sr	Na	Cl	S	P	Si	$MgCO_3$ (mol%)	$MgCO_3$ (mol%)	$SrCO_3$ (mol%)
1	1	Sml Dmbl	17.64	2.09	0.03	0.34	0.00	0.06	0.09		10.6	10.58	0.15
		Sml Dmbl	15.60	2.35	0.04	0.40	0.00	0.06	0.09		13.1	13.06	0.22
		Sml Dmbl	24.29	3.76	0.06	0.20	0.03	0.05	0.13		13.4	13.38	0.21
		Sml Dmbl	16.75	2.71	0.05	0.40	0.00	0.04	0.09		13.9	13.89	0.26
2	5	Sml Dmbl	21.32	4.58	0.06	0.47	0.00	0.04	0.10		17.7	17.64	0.23
1	1	ME	16.42	2.67	0.05	0.33	0.00	0.01	0.09		14.0	13.95	0.26
		ME	20.02	2.24	0.08	0.43	0.01	0.09	0.12		10.1	10.03	0.36
	2	ME	21.64	2.66	0.07	0.46	0.01	0.15	0.10		10.9	10.92	0.29
		ME	19.32	2.95	0.06	0.43	0.02	0.12	0.09		13.2	13.21	0.27
		ME	19.16	2.93	0.05	0.40	0.00	0.07	0.07		13.3	13.23	0.23
	3	ME	24.73	3.73	0.08	0.40	0.04	0.08	0.12		13.1	13.07	0.28
2	4	ME	20.91	2.36	0.05	0.33	0.01	0.06	0.06		10.1	10.12	0.21
		ME	23.36	2.49	0.05	0.27	0.05	0.08	0.08		9.6	9.61	0.19
	5	ME	19.99	4.41	0.07	0.49	0.03	0.04	0.10		18.1	18.02	0.29
		ME	16.15	4.25	0.06	0.47	0.02	0.04	0.11		20.8	20.77	0.29
		ME	17.81	4.06	0.06	0.38	0.01	0.04	0.09		18.6	18.51	0.27
		ME	18.91	3.99	0.06	0.42	0.01	0.05	0.11		17.4	17.38	0.26
		ME	18.45	3.99	0.07	0.52	0.00	0.05	0.05		17.8	17.73	0.31
		ME	18.51	4.12	0.07	0.58	0.00	0.05	0.06		18.2	18.15	0.31
3	6	ME	13.60	2.03	0.05	0.42	0.00	0.08	0.07		13.0	12.95	0.32
		ME	20.04	2.46	0.08	0.47	0.00	0.12	0.10		10.9	10.89	0.35
		ME	16.54	2.35	0.07	0.47	0.01	0.10	0.10		12.4	12.39	0.37
		ME	17.97	2.44	0.08	0.48	0.00	0.08	0.09		12.0	11.91	0.39
	7	ME	17.36	2.65	0.06	0.39	0.00	0.06	0.07		13.2	13.20	0.30
		ME	15.43	2.62	0.05	0.46	0.00	0.07	0.08		14.5	14.48	0.28
	8	ME	16.91	2.74	0.06	0.46	0.00	0.07	0.07		13.9	13.90	0.30
		ME	21.29	3.42	0.08	0.44	0.01	0.08	0.13		13.8	13.80	0.32
4	9	ME	20.35	2.00	0.08	0.34	0.06	0.01	0.04		8.9	8.92	0.36
		ME	19.37	2.82	0.07	0.37	0.09	0.01	0.04		12.7	12.67	0.31
	10	ME	17.96	3.70	0.07	0.35	0.09	0.01	0.04		17.1	17.03	0.32
		ME	19.30	5.26	0.08	0.31	0.13	0.02	0.04		21.4	21.35	0.32
	11	ME	21.19	3.07	0.09	0.30	0.07	0.04	0.05		12.7	12.61	0.37
		ME	18.56	3.29	0.07	0.44	0.07	0.07	0.07		15.1	15.01	0.32
5	12	ME	41.12	3.06	0.10	-	-	0.20	-		6.9	6.91	0.23
		ME	17.81	2.69	0.05	-	-	0.06	-		13.1	13.09	0.24
		ME	32.53	3.17	0.10	-	-	0.18	-		8.9	8.85	0.28
		ME	27.13	3.25	0.07	-	-	0.12	-		10.7	10.67	0.23
		ME	22.23	2.78	0.05	-	-	0.11	-		11.1	11.09	0.20
		ME	21.91	3.00	0.07	-	-	0.08	-		12.0	12.01	0.28
		ME	24.60	2.55	0.04	-	-	0.08	-		9.4	9.38	0.15
		ME	22.57	2.82	0.04	-	-	0.09	-		11.1	11.09	0.16
		ME	17.50	2.41	0.06	-	-	0.11	-		12.1	12.07	0.30
		ME	20.62	2.29	0.10	-	-	0.07	-		10.0	9.95	0.43
		ME	26.71	3.17	0.08	-	-	0.13	-		10.6	10.58	0.27
		ME	18.40	2.75	0.05	-	-	0.10	-		13.0	12.97	0.24
1	1	Dmbl/Sph	19.77	0.40	0.14	0.55	0.00	0.03	0.06		2.0	1.97	0.69
		Dmbl/Sph	18.88	0.67	0.18	0.44	0.00	0.00	0.09		3.4	3.40	0.91
		Dmbl/Sph	20.59	1.23	0.15	0.49	0.00	0.02	0.07		5.6	5.60	0.68
	3	Dmbl/Sph	22.02	0.93	0.16	0.51	0.00	0.04	0.09		4.1	4.02	0.69
		Dmbl/Sph	25.04	0.71	0.18	0.43	0.00	0.05	0.07		2.8	2.74	0.69

Sample	Pellet	Crystal form	Ca	Mg	Sr	Na	Cl	S	P	Si	$MgCO_3$ (mol%)	$MgCO_3$ (mol%)	$SrCO_3$ (mol%)
1	3	Dmbl/Sph	18.53	0.51	0.15	0.49	0.00	0.05	0.05		2.7	2.66	0.78
		Dmbl/Sph	15.21	0.45	0.11	0.41	0.00	0.04	0.03		2.9	2.85	0.70
2	4	Dmbl/Sph	25.55	0.64	-	0.28	0.00	0.02	0.05		2.4		
		Dmbl/Sph	18.55	1.01	0.21	0.50	0.05	0.00	0.16		5.2	5.11	1.06
	5	Dmbl/Sph	21.50	0.74	0.16	0.58	0.00	0.00	0.15		3.3	3.30	0.71
		Dmbl/Sph	23.23	0.62	0.17	0.53	0.00	0.01	0.09		2.6	2.58	0.71
4	10	Dmbl/Sph	17.25	1.86	0.12	0.47	0.02	0.02	0.02		9.7	9.67	0.62
5	12	Dmbl/Sph	25.67	0.38	0.21	-	-	0.06	-		1.5	1.45	0.80
		Dmbl/Sph	24.49	0.72	0.18	-	-	0.05	-		2.9	2.84	0.71
		Dmbl/Sph	24.69	0.43	0.19	-	-	0.09	-		1.7	1.70	0.75
		Dmbl/Sph	27.68	0.34	0.22	-	-	0.06	-		1.2	1.20	0.78
		Dmbl/Sph	15.76	0.39	0.11	-	-	0.07	-		2.4	2.40	0.68
		Dmbl/Sph	24.34	0.29	0.20	-	-	0.10	-		1.2	1.17	0.81
		Dmbl/Sph	26.11	0.77	0.20	-	-	0.05	-		2.9	2.84	0.74
		Dmbl/Sph	23.93	0.22	0.18	-	-	0.10	-		0.9	0.90	0.74
		Dmbl/Sph	21.96	0.49	0.19	-	-	0.07	-		2.2	2.16	0.84
		Dmbl/Sph	19.55	0.31	0.16	-	-	0.06	-		1.6	1.55	0.80
2	4	Amorph	3.50	18.43		0.74	0.50	-	0.04	0.	84.0		
		Amorph	5.53	17.30		0.59	0.50	-	0.05	0.	75.8		
		Amorph	1.93	17.15		0.46	0.46	-	0.04	0.	89.9		
		Amorph	5.20	20.78		0.56	0.70	-	0.07	0.	80.0		
	5	Amorph	0.67	26.84		0.61	1.22	0.00	0.08	0.	97.6		
		Amorph	0.65	22.36		0.57	0.93	0.00	0.06	0.	97.2		
		Amorph	0.85	23.63		0.50	0.99	0.00	0.07	0.	96.5		
2	4	Rhomb	21.13	1.92	0.12	0.67	0.09	-	0.07		8.3	8.29	0.52
		Rhomb	21.19	1.64	0.11	0.86	0.03	-	0.05		7.2	7.15	0.48
		Rhomb	20.99	2.38	0.12	0.92	0.11	-	0.07		10.2	10.13	0.51
		Rhomb	18.68	2.02	0.11	0.82	0.07	-	0.07		9.8	9.71	0.53
		Rhomb	16.45	1.62	0.09	0.74	0.06	-	0.05		9.0	8.92	0.50
		Rhomb	20.72	0.88	0.11	0.71	0.08	-	0.08		4.1	4.05	0.51
		Rhomb	16.91	1.00	0.09	0.68	0.05	-	0.08		5.6	5.56	0.50
		Rhomb	18.44	1.24	0.10	0.59	0.03	-	0.07		6.3	6.27	0.51
		Rhomb	18.76	0.85	0.10	0.59	0.03		0.07		4.3	4.31	0.51
		Rhomb	21.69	0.73	0.12	0.62	0.06	-	0.07		3.3	3.24	0.53
	5	Rhomb	21.35	1.81	0.12	0.58	0.11	0.00	0.25		7.8	7.77	0.52
		Rhomb	24.45	2.54	0.14	0.54	0.15	0.00	0.30		9.4	9.36	0.52
		Rhomb	19.08	0.80	0.12	0.67	0.03	0.00	0.15		4.0	4.00	0.60

Table AII 14 EDX data for samples produced by redtail parrotfish (all elemental data reported as atomic %)

Sample	Pellet	Crystal form	Ca	Mg	Sr	Na	Cl	S	P	Si	$MgCO_3$ (mol%)	$MgCO_3$ (mol%)	$SrCO_3$ (mol%)
1	1	PE	30.02	0.29	0.00	0.16					1.0	0.96	0.00
		PE	18.66	0.25	0.00	0.17					1.3	1.32	0.00
		PE	23.15	0.27	0.00	0.15					1.2	1.15	0.00
		PE	24.89	0.31	0.00	0.13					1.2	1.23	0.00
	2	PE	24.65	0.27	0.00	0.16					1.1	1.08	0.00
		PE	23.56	0.24	0.00	0.14					1.0	1.01	0.00
		PE	25.67	0.18	0.00	0.13					0.7	0.70	0.00
		PE	27.74	0.27	0.00	0.11					1.0	0.96	0.00
		PE	28.30	0.42	0.00	0.19					1.5	1.46	0.00
	3	PE	21.18	0.22	0.06	0.15					1.0	1.03	0.28
		PE	22.24	0.18	0.03	0.15					0.8	0.80	0.13
	4	PE	24.97	0.27	0.00	0.14					1.1	1.07	0.00
		PE	16.75	0.26	0.00	0.22					1.5	1.53	0.00
		PE	17.42	0.37	0.00	0.16					2.1	2.08	0.00
		PE	18.34	0.34	0.00	0.23					1.8	1.82	0.00
		PE	21.33	0.33	0.00	0.20					1.5	1.52	0.00
		PE	21.82	0.19	0.00	0.20					0.9	0.86	0.00
		PE	22.42	0.28	0.00	0.17					1.2	1.23	0.00
		PE	25.68	0.19	0.00	0.13					0.7	0.73	0.00
		PE	19.00	0.31	0.00	0.16					1.6	1.61	0.00
	5	PE	23.87	0.31	0.00	0.15					1.3	1.28	0.00
		PE	18.41	0.26	0.00	0.18					1.4	1.39	0.00
		PE	25.88	0.34	0.00	0.14					1.3	1.30	0.00
		PE	20.79	0.27	0.00	0.16					1.3	1.28	0.00
		PE	23.74	0.23	0.00	0.13					1.0	0.96	0.00
		PE	26.38	0.44	0.00	0.14					1.6	1.64	0.00
		PE	19.94	0.23	0.00	0.20					1.1	1.14	0.00
		PE	18.76	0.43	0.00	0.23					2.2	2.24	0.00
		PE	20.64	0.26	0.00	0.17					1.2	1.24	0.00
	6	PE	19.10	0.20	0.03						1.0	1.03	0.16
		PE	11.89	0.20	0.03						1.7	1.65	0.25
1	3	Sphl/Nee	29.03	0.37	0.17	0.30					1.3	1.25	0.57
		Sphl/Nee	27.95	0.30	0.17	0.24					1.1	1.06	0.60
		Sphl/Nee	23.10	0.32	0.15	0.27					1.4	1.36	0.64
		Sphl/Nee	18.70	0.47	0.15	0.38					2.5	2.43	0.78
		Sphl/Nee	22.60	0.27	0.15	0.31					1.2	1.17	0.65
		Sphl/Nee	21.63	0.46	0.20	0.40					2.1	2.06	0.90
		Sphl/Nee	29.18	0.64	0.21	0.33					2.1	2.13	0.70
	7	Sphl/Nee	22.01	0.11	0.13	0.28					0.5	0.49	0.58
		Sphl/Nee	17.23	0.12	0.08	0.25					0.7	0.69	0.46
		Sphl/Nee	19.26	0.79	0.09	0.25					3.9	3.92	0.45
		Sphl/Nee	22.32	0.66	0.12	0.24					2.9	2.86	0.52
		Sphl/Nee	25.82	0.28	0.12	0.22					1.1	1.07	0.46
		Sphl/Nee	26.05	0.32	0.23	0.37					1.2	1.20	0.86
		Sphl/Nee	26.42	0.28	0.23	0.35					1.0	1.04	0.85
		Sphl/Nee	19.62	0.32	0.14						1.6	1.59	0.70
1	8	Needle	21.55	0.41	0.05						1.9	1.86	0.23
		Needle	19.62	0.24	0.05						1.2	1.21	0.25
		Needle	19.90	0.15	0.06						0.7	0.75	0.30
		Needle	15.27	0.14	0.06						0.9	0.90	0.39

Sample	Pellet	Crystal form	Ca	Mg	Sr	Na	Cl	S	P	Si	$MgCO_3$ (mol%)	$MgCO_3$ (mol%)	$SrCO_3$ (mol%)
1	1	Rhomb	26.12	0.30	0.00	0.15					1.1	1.14	0.00
		Rhomb	28.64	0.39	0.00	0.14					1.3	1.34	0.00
		Rhomb	21.78	0.33	0.00	0.16					1.5	1.49	0.00
	2	Rhomb	26.41	0.42	0.00	0.11					1.6	1.57	0.00
		Rhomb	19.87	0.47	0.00	0.16					2.3	2.31	0.00
	4	Rhomb	22.72	0.19	0.00	0.17					0.8	0.83	0.00
	5	Rhomb	22.77	0.47	0.00	0.18					2.0	2.02	0.00
	6	Rhomb	15.54	0.71	0.00						4.4	4.37	0.00
		Rhomb	13.12	0.74	0.00						5.3	5.34	0.00
1	9	Sphere	23.99	0.29	0.00	0.11					1.2	1.19	0.00
		Sphere	16.74	0.73	0.18	0.53					4.2	4.14	1.02
		Sphere	17.20	0.61	0.18	0.42					3.4	3.39	1.00
		Sphere	20.13	0.38	0.19	0.22					1.9	1.84	0.92
		Sphere	20.78	0.41	0.18	0.37					1.9	1.92	0.84
1	1	Amorph	32.87	0.50	0.20	0.32					1.5	1.49	0.60
		Amorph	24.28	0.34	0.18	0.21					1.4	1.37	0.73
	2	Amorph*	23.44	0.26	0.00	0.16					1.1	1.10	0.00
		Amorph*	15.28	0.19	0.00	0.17					1.2	1.23	0.00
		Amorph	17.06	0.31	0.11	0.46					1.8	1.77	0.63

Most amorphous material occurs as a discrete coating covering whole pellets, but its occurrence is rare.
Material indicated with "*" is more closely associated with polycrystalline dumbbells

Table AII 15 EDX data for samples produced by French grunt (all elemental data reported as atomic %)

Sample	Pellet	Crystal form	Ca	Mg	Sr	Na	Cl	S	P	Si	$MgCO_3$ (mol%)	$MgCO_3$ (mol%)	$SrCO_3$ (mol%)
1	1	ME	22.92	4.85	0.08			0.07			17.5	17.41	0.29
		ME	20.04	5.14	0.09			0.06			20.4	20.34	0.36
		ME	27.21	5.92	0.09			0.08			17.9	17.82	0.27
		ME	29.16	6.74	0.12			0.10			18.8	18.71	0.33
		ME	19.73	5.20	0.08			0.07			20.9	20.79	0.32
		ME	19.31	5.38	0.07			0.05			21.8	21.73	0.28
		ME	17.81	5.11	0.07			0.06			22.3	22.23	0.30
		ME	14.16	4.99	0.06			0.03			26.1	25.98	0.31
		ME	18.13	5.08	0.08			0.07			21.9	21.81	0.34
	2	ME	22.24	3.25	0.07			0.08			12.8	12.72	0.27
		ME	23.24	3.10	0.07			0.06			11.8	11.74	0.27
		ME	24.30	4.79	0.09			0.11			16.5	16.42	0.31
		ME	18.89	4.16	0.08			0.11			18.0	17.99	0.35
		ME	20.50	4.30	0.09			0.12			17.3	17.28	0.36
		ME	18.78	4.13	0.08			0.10			18.0	17.96	0.35
		ME	21.73	4.48	0.08			0.10			17.1	17.04	0.30
		ME	15.24	3.69	0.06			0.11			19.5	19.43	0.32
		ME	20.99	3.68	0.07			0.06			14.9	14.87	0.28
	3	ME	24.72	3.66	0.07			0.06			12.9	12.86	0.25
		ME	19.01	5.51	0.08			0.07			22.5	22.40	0.33
		ME	16.03	4.61	0.08			0.07			22.3	22.25	0.39
		ME	15.60	4.22	0.09			0.08			21.3	21.20	0.45
		ME	16.67	4.45	0.07			0.07			21.1	21.00	0.33
		ME	19.50	4.99	0.11			0.08			20.4	20.28	0.45
		ME	14.01	4.10	0.07			0.08			22.6	22.55	0.39
		ME	15.23	4.54	0.07			0.08			23.0	22.88	0.35
		ME	22.11	5.13	0.10			0.10			18.8	18.76	0.37
		ME	18.67	4.73	0.09			0.10			20.2	20.14	0.38
	4	ME	17.09	4.38	0.08			0.05			20.4	20.32	0.37
		ME	14.36	3.86	0.07			0.03			21.2	21.10	0.38
		ME	14.07	3.83	0.07			0.05			21.4	21.31	0.39
		ME	14.22	3.75	0.06			0.05			20.9	20.80	0.33
		ME	14.97	3.58	0.06			0.07			19.3	19.24	0.32
		ME	15.28	3.60	0.05			0.06			19.1	19.02	0.26
		ME	17.36	4.16	0.06			0.06			19.3	19.28	0.28
		ME	15.28	3.69	0.06			0.07			19.5	19.39	0.32
		ME	17.27	4.29	0.07			0.07			19.9	19.83	0.32
		ME	14.22	3.73	0.07			0.07			20.8	20.70	0.39
	5	ME	15.66	3.96	0.07			0.04			20.2	20.11	0.36
		ME	15.72	3.85	0.06			0.04			19.7	19.61	0.31
		ME	14.41	3.59	0.06			0.06			19.9	19.88	0.33
		ME	15.73	3.99	0.06			0.08			20.2	20.17	0.30
		ME	15.27	4.47	0.07			0.03			22.6	22.56	0.35
		ME	14.83	4.48	0.06			0.04			23.2	23.13	0.31
		ME	14.74	4.35	0.07			0.04			22.8	22.70	0.37
		ME	13.65	4.58	0.06			0.04			25.1	25.04	0.33
		ME	14.06	4.68	0.06			0.06			25.0	24.89	0.32
		ME	14.45	4.38	0.06			0.02			23.3	23.19	0.32
2	6	ME	15.76	4.38							21.7		
		ME	17.03	3.77							18.1		

Sample	Pellet	Crystal form	Ca	Mg	Sr	Na	Cl	S	P	Si	$MgCO_3$ (mol%)	$MgCO_3$ (mol%)	$SrCO_3$ (mol%)
2	6	ME	17.15	3.84							18.3		
		ME	15.38	3.71							19.4		
1	1	Dmbl	20.75	1.32	0.22			0.00			6.0	5.92	0.99
	2	Dmbl	23.67	1.53	0.23			0.00			6.1	6.02	0.90

Table AII 16 EDX data for samples produced by *Haemulon* sp. (all elemental data reported as atomic %)

Sample	Pellet	Crystal form	Ca	Mg	Sr	Na	Cl	S	P	Si	$MgCO_3$ (mol%)	$MgCO_3$ (mol%)	$SrCO_3$ (mol%)
1	1	Whtsf	11.84	5.41							31.4		
		Whtsf	9.71	5.05							34.2		
		Whtsf	10.47	4.99							32.3		
		Whtsf	9.48	4.61							32.7		
		Whtsf	10.64	5.14							32.6		
		Whtsf	10.43	5.32							33.8		
		Whtsf	12.35	4.87							28.3		
		Whtsf	11.88	5.68							32.3		
		Whtsf	10.99	5.50							33.4		
		Whtsf	12.58	7.74							38.1		
	2	Whtsf	11.27	3.96							26.0		
		Whtsf	15.34	4.97							24.5		
		Whtsf	10.51	4.48							29.9		
		Whtsf	8.73	4.89							35.9		
		Whtsf	11.33	4.23							27.2		
		Whtsf	11.24	4.55							28.8		
		Whtsf	10.28	4.44							30.2		
		Whtsf	8.33	3.37							28.8		
		Whtsf	10.09	4.34							30.1		
		Whtsf	11.13	4.71							29.7		
	3	Whtsf	10.57	4.33							29.1		
		Whtsf	9.83	4.07							29.3		
		Whtsf	10.32	4.09							28.4		
		Whtsf	9.38	4.22							31.0		
		Whtsf	10.19	5.20							33.8		
		Whtsf	11.46	5.53							32.5		
		Whtsf	9.82	3.15							24.3		
		Whtsf	9.58	3.32							25.7		
		Whtsf	9.27	3.07							24.9		
		Whtsf	9.32	4.95							34.7		
	4	Whtsf	9.24	4.43							32.4		
		Whtsf	10.07	4.54							31.1		
		Whtsf	11.17	4.92							30.6		
		Whtsf	10.03	4.76							32.2		
		Whtsf	10.64	4.82							31.2		
		Whtsf	8.53	4.25							33.3		
		Whtsf	9.65	4.95							33.9		
		Whtsf	10.02	4.92							32.9		
		Whtsf	7.97	5.49							40.8		
		Whtsf	8.41	4.61							35.4		
	5	Whtsf	10.28	2.67							20.6		
		Whtsf	9.56	2.62							21.5		
		Whtsf	9.24	2.24							19.5		
		Whtsf	9.75	2.42							19.9		
		Whtsf	9.01	2.54							22.0		
		Whtsf	9.60	2.53							20.9		
		Whtsf	10.59	2.55							19.4		
		Whtsf	9.06	2.21							19.6		
		Whtsf	9.75	2.63							21.2		
		Whtsf	9.62	2.38							19.8		

Table AII 17 EDX data for samples produced by bluehead wrasse (all elemental data reported as atomic %)

Sample	Pellet	Crystal form	Ca	Mg	Sr	Na	Cl	S	P	Si	$MgCO_3$ (mol%)	$MgCO_3$ (mol%)	$SrCO_3$ (mol%)
1	1	Rhomb	25.90	1.28	0.14	0.68	0.11		0.03		4.7	4.69	0.51
		Rhomb	20.91	1.06	0.11	0.86	0.13		0.05		4.8	4.80	0.50
		Rhomb	17.04	1.57	0.10	0.84	0.20		0.12		8.4	8.39	0.53
		Rhomb	20.48	1.49	0.11	0.76	0.18		0.12		6.8	6.75	0.50
		Rhomb	17.10	3.65	0.10	0.89	0.55		0.11		17.6	17.51	0.48
		Rhomb	15.31	3.34	0.09	0.75	0.52		0.09		17.9	17.82	0.48
	2	Rhomb	18.26	0.88	0.09	0.75	0.24		0.12		4.6	4.58	0.47
		Rhomb	19.61	1.73	0.11	0.59	0.21		0.17		8.1	8.07	0.51
		Rhomb	20.61	0.59	0.09	0.62	0.16		0.08		2.8	2.77	0.42
		Rhomb	23.54	1.17	0.07	0.66	0.18		0.26		4.7	4.72	0.28
	3	Rhomb	17.63	1.36	0.12	0.68	0.27		0.05		7.2	7.12	0.63
		Rhomb	16.53	1.02	0.11	0.74	0.13		0.05		5.8	5.78	0.62
		Rhomb	19.77	1.31	0.12	0.50	0.17		0.06		6.2	6.18	0.57
		Rhomb	18.48	1.15	0.09	0.61	0.24		0.03		5.9	5.83	0.46
		Rhomb	18.68	0.60	0.13	0.64	0.08		0.06		3.1	3.09	0.67
		Rhomb	19.38	1.16	0.10	0.67	0.22		0.06		5.6	5.62	0.48
		Rhomb	12.92	2.59	0.09	0.72	0.39		0.03		16.7	16.60	0.58
		Rhomb	18.32	1.05	0.11	0.56	0.21		0.09		5.4	5.39	0.56
	5	Rhomb	20.66	4.96	0.09	0.48	0.62		0.23		19.4	19.29	0.35
		Rhomb	19.02	0.71	0.12	0.47	0.13		0.10		3.6	3.58	0.60
	6	Rhomb	12.84	0.81	0.06	0.62	0.19		0.06		5.9	5.91	0.44
		Rhomb	14.91	0.43	0.09	0.72	0.07		0.11		2.8	2.79	0.58
	7	Rhomb	15.95	2.51	0.08	0.67	0.30		0.20		13.6	13.54	0.43
		Rhomb	14.93	5.95	0.09	0.57	0.67		0.11		28.5	28.37	0.43
	8	Rhomb	17.54	0.69	0.08	0.66	0.18		0.21		3.8	3.77	0.44
		Rhomb	18.68	1.36	0.12	0.66	0.22		0.10		6.8	6.75	0.60
		Rhomb	17.67	1.28	0.10	0.57	0.14		0.07		6.8	6.72	0.52
		Rhomb	23.71	1.93	0.13	0.70	0.25		0.14		7.5	7.49	0.50
2	9	Rhomb	13.85	2.67	0.17						16.2		
		Rhomb	15.28	6.91	0.17						31.1		
3	10	Rhomb	21.51	1.45	0.13	0.83	0.12		0.11		6.3	6.28	0.56
		Rhomb	24.89	1.37	0.17	0.74	0.15		0.18		5.2	5.18	0.64
		Rhomb	18.28	5.03	0.13	0.71	0.42		0.31		21.6	21.46	0.55
		Rhomb	17.28	2.50	0.12	0.76	0.13		0.20		12.6	12.56	0.60
		Rhomb	16.42	4.98	0.11	0.71	0.53		0.26		23.3	23.15	0.51
		Rhomb	19.26	0.78	0.14	0.79	0.17		0.34		3.9	3.87	0.69
		Rhomb	22.83	1.20	0.15	0.71	0.21		0.13		5.0	4.96	0.62
1	1	Amorph	6.82	23.92		0.61	6.34		0.11	0.38	77.8		
		Amorph	0.92	19.60		0.52	4.30		0.06	0.53	95.5		
		Amorph	0.60	18.72		0.61	3.71		0.08	0.49	96.9		
		Amorph	1.16	22.20		0.53	5.41		0.05	0.55	95.0		
	2	Amorph	0.41	20.76		0.57	3.57		0.06		98.1		
	3	Amorph	0.73	16.90		0.35	2.45		0.01	0.28	95.9		
		Amorph	2.69	15.94		0.52	1.85		0.02	0.23	85.6		
		Amorph	0.21	19.24		0.40	2.42		0.06	0.34	98.9		
	4	Amorph	0.11	13.55		0.41	1.15		0.03	0.26	99.2		
		Amorph	0.51	13.22		0.43	1.31		0.06	0.20	96.3		
		Amorph	0.06	12.62		0.46	1.12		0.04	0.27	99.5		
	5	Amorph	0.19	18.09		0.32	2.32		0.07	0.38	99.0		
		Amorph	0.10	17.06		0.29	2.10		0.04	0.29	99.4		

Sample	Pellet	Crystal form	Ca	Mg	Sr	Na	Cl	S	P	Si	$MgCO_3$ (mol%)	$MgCO_3$ (mol%)	$SrCO_3$ (mol%)
1	6	Amorph	0.60	15.64		0.54	2.24		0.03	0.35	96.3		
	7	Amorph	0.77	15.17		0.53	2.40		0.02	0.32	95.2		
2	9	Amorph	0.17	15.48		0.34	1.10			0.30	98.9		
		Amorph	0.13	17.69			1.45			0.32	99.3		
		Amorph	0.15	19.81			1.69			0.28	99.2		
3	10	Amorph	3.11	24.56		0.63	2.17		0.64	0.34	88.8		
		Amorph	0.40	24.20		0.55	3.05		0.11	0.53	98.4		
1	4	Needle	20.81	0.90	0.21	0.20	0.10		0.04		4.1	4.11	0.96
		Needle	18.93	2.43	0.21	0.25	0.26		0.04		11.4	11.27	0.97
		Needle	17.42	1.66	0.19	0.24	0.17		0.05		8.7	8.61	0.99
		Needle	14.12	1.85	0.16	0.23	0.21		0.02		11.6	11.47	0.99
1	2	Dmbl	19.49	2.30	0.10	0.64	0.29		0.10		10.6	10.51	0.46
1	8	Dmbl	24.23	1.39	0.13	0.56	0.18		0.23		5.4	5.40	0.50

Table AII 18 EDX data for samples produced by beaugregory (all elemental data reported as atomic %)

Sample	Pellet	Crystal form	Ca	Mg	Sr	Na	Cl	S	P	Si	$MgCO_3$ (mol%)	$MgCO_3$ (mol%)	$SrCO_3$ (mol%)
1	1	Rhomb	20.17	0.96							4.5		
		Rhomb	22.34	0.91							3.9		
		Rhomb	20.03	0.66							3.2		
		Rhomb	23.23	0.74							3.1		
		Rhomb	19.97	1.30							6.1		
	2	Rhomb	20.47	1.17							5.4		
		Rhomb	23.28	1.00							4.1		
		Rhomb	20.83	2.81							11.9		
		Rhomb	20.14	1.18							5.5		
	3	Rhomb	24.70	0.90							3.5		
		Rhomb	23.58	3.88							14.1		
		Rhomb	19.52	0.87							4.3		
		Rhomb	20.14	0.76							3.6		
		Rhomb	21.42	1.07							4.8		
		Rhomb	24.19	0.77							3.1		
		Rhomb	23.67	0.76							3.1		
		Rhomb	21.25	1.21							5.4		
		Rhomb	21.93	1.15							5.0		
	4	Rhomb	23.06	1.26							5.2		
		Rhomb	22.39	0.81							3.5		
		Rhomb	24.38	0.64							2.6		
		Rhomb	22.35	0.61							2.7		
		Rhomb	21.11	3.73							15.0		
		Rhomb	21.98	0.66							2.9		
		Rhomb	23.51	5.10							17.8		
		Rhomb	19.34	1.09							5.3		
	5	Rhomb	22.14	0.76							3.3		
		Rhomb	22.54	0.74							3.2		
		Rhomb	21.89	0.64							2.8		
		Rhomb	21.89	1.34							5.8		
		Rhomb	19.35	0.73							3.6		
		Rhomb	19.96	1.78							8.2		
1	1	Amorph	1.02	22.56							95.7		
		Amorph	0.58	17.54							96.8		
		Amorph	0.87	22.84							96.3		
		Amorph	0.48	20.34							97.7		
		Amorph	1.08	19.14							94.7		
	2	Amorph	0.19	21.06							99.1		
		Amorph	0.75	17.33							95.9		
		Amorph	0.82	19.63							96.0		
		Amorph	0.35	19.77							98.3		
		Amorph	1.59	19.67							92.5		
		Amorph	0.29	20.61							98.6		
	3	Amorph	0.95	17.75							94.9		
	4	Amorph	0.40	22.82							98.3		
		Amorph	0.35	18.22							98.1		
	5	Amorph	0.88	19.14							95.6		
		Amorph	0.36	22.89							98.5		
		Amorph	0.45	17.19							97.4		
		Amorph	2.32	19.17							89.2		

Table AII 19 EDX data for samples produced by slippery dick (all elemental data reported as atomic %)

Sample	Pellet	Crystal form	Ca	Mg	Sr	Na	Cl	S	P	Si	$MgCO_3$ (mol%)	$MgCO_3$ (mol%)	$SrCO_3$ (mol%)
1	1	Rhomb	10.07	1.18							10.5		
		Rhomb	10.22	0.67							6.2		
		Rhomb	10.36	0.36							3.4		
		Rhomb	18.45	1.02							5.2		
		Rhomb	16.07	1.08							6.3		
	2	Rhomb	21.52	1.95							8.3		
		Rhomb	21.55	0.53							2.4		
		Rhomb	21.24	1.22							5.4		
		Rhomb	21.46	1.74							7.5		
		Rhomb	15.98	0.56							3.4		
		Rhomb	17.69	1.75							9.0		
		Rhomb	16.43	3.30							16.7		
		Rhomb	16.40	0.50							3.0		
	3	Rhomb	15.32	0.87							5.4		
		Rhomb	21.04	0.75							3.4		
		Rhomb	21.53	0.98							4.4		
		Rhomb	19.70	1.90							8.8		
		Rhomb	19.50	1.44							6.9		
	4	Rhomb	20.25	1.23							5.7		
		Rhomb	14.78	0.33							2.2		
		Rhomb	16.68	2.53							13.2		
		Rhomb	14.57	1.23							7.8		
		Rhomb	15.12	0.64							4.1		
		Rhomb	15.32	0.45							2.9		
		Rhomb	21.67	1.28							5.6		
		Rhomb	17.99	2.06							10.3		
		Rhomb	15.02	2.11							12.3		
	5	Rhomb	15.12	1.13							7.0		
		Rhomb	19.37	0.50							2.5		
		Rhomb	18.23	1.41							7.2		
		Rhomb	18.67	0.92							4.7		
		Rhomb	16.40	0.55							3.2		
		Rhomb	14.74	2.91							16.5		
		Rhomb	16.21	2.80							14.7		
		Rhomb	19.38	1.17							5.7		
		Rhomb	18.44	2.59							12.3		
1	1	Amorph	0.07	9.40							99.3		
		Amorph	0.11	14.15							99.2		
		Amorph	0.19	16.00							98.8		
		Amorph	0.39	20.62							98.1		
	2	Amorph	0.33	14.40							97.8		
		Amorph	0.80	16.41							95.4		
		Amorph	0.24	15.64							98.5		
		Amorph	0.41	18.32							97.8		
		Amorph	0.13	19.98							99.4		
		Amorph	0.94	19.56							95.4		
		Amorph	0.39	20.91							98.2		
		Amorph	0.38	20.03							98.1		
	3	Amorph	0.91	18.44							95.3		
		Amorph	0.82	15.56							95.0		

Sample	Pellet	Crystal form	Ca	Mg	Sr	Na	Cl	S	P	Si	$MgCO_3$ (mol%)	$MgCO_3$ (mol%)	$SrCO_3$ (mol%)
1	3	Amorph	0.83	19.93							96.0		
		Amorph	1.85	15.79							89.5		
	4	Amorph	0.41	14.83							97.3		
		Amorph	0.30	14.21							97.9		
		Amorph	0.96	19.95							95.4		
		Amorph	0.10	13.01							99.2		
		Amorph	0.24	16.51							98.6		
		Amorph	0.14	11.46							98.8		
		Amorph	0.24	17.27							98.6		
		Amorph	1.19	8.55							87.8		
	5	Amorph	0.78	20.08							96.3		
		Amorph	1.27	20.63							94.2		
		Amorph	0.62	16.29							96.3		
		Amorph	0.53	17.07							97.0		
		Amorph	0.69	15.93							95.8		
		Amorph	0.47	19.84							97.7		

Table AII 20 EDX data for samples produced by red lionfish (all elemental data reported as atomic %)

Sample	Pellet	Crystal form	Ca	Mg	Sr	Na	Cl	S	P	Si	$MgCO_3$ (mol%)	$MgCO_3$ (mol%)	$SrCO_3$ (mol%)
1	1	ME	12.32	7.09	0.11						36.5	36.32	0.56
		ME	12.60	7.12	0.11						36.1	35.91	0.55
		ME	13.82	7.45	0.14						35.0	34.80	0.65
		ME	11.04	6.77	0.12						38.0	37.76	0.67
		ME	13.26	7.44	0.12						35.9	35.73	0.58
		ME	10.47	6.76	0.10						39.2	39.01	0.58
		ME	11.70	7.32	0.13						38.5	38.22	0.68
		ME	11.23	6.61	0.11						37.1	36.82	0.61
		ME	11.18	7.09	0.10						38.8	38.60	0.54
		ME	10.52	6.18	0.11						37.0	36.76	0.65
	2	ME	11.42	6.28	0.10						35.5	35.28	0.56
		ME	12.19	6.46	0.11						34.6	34.43	0.59
		ME	10.28	4.27	0.11						29.3	29.13	0.75
		ME	10.32	4.90	0.08						32.2	32.03	0.52
		ME	11.55	6.65	0.10						36.5	36.34	0.55
		ME	12.56	4.79	0.12						27.6	27.42	0.69
		ME	12.67	5.10	0.13						28.7	28.49	0.73
		ME	9.63	5.36	0.10						35.8	35.52	0.66
		ME	10.53	5.34	0.11						33.6	33.42	0.69
		ME	12.92	4.77	0.12						27.0	26.78	0.67
	3	ME	12.52	6.73	0.15						35.0	34.69	0.77
		ME	12.69	6.91	0.14						35.3	35.01	0.71
		ME	10.90	6.07	0.13						35.8	35.50	0.76
		ME	11.83	5.23	0.12						30.7	30.44	0.70
		ME	10.50	3.68	0.11						26.0	25.75	0.77
		ME	9.82	2.72	0.10						21.7	21.52	0.79
		ME	13.23	7.18	0.14						35.2	34.94	0.68
		ME	12.53	5.99	0.14						32.3	32.10	0.75
		ME	11.06	3.65	0.13						24.8	24.60	0.88
		ME	11.27	3.90	0.13						25.7	25.49	0.85
	4	ME	9.12	5.92	0.08						39.4	39.15	0.53
		ME	9.51	5.15	0.11						35.1	34.87	0.74
		ME	7.91	5.42	0.08						40.7	40.42	0.60
		ME	8.88	6.35	0.09						41.7	41.45	0.59
		ME	9.15	5.48	0.11						37.5	37.18	0.75
		ME	8.75	5.32	0.08						37.8	37.60	0.57
		ME	9.33	6.01	0.09						39.2	38.95	0.58
		ME	8.09	5.39	0.07						40.0	39.78	0.52
		ME	10.04	5.45	0.12						35.2	34.91	0.77
		ME	10.41	6.01	0.11						36.6	36.36	0.67
	5	ME	10.60	6.63	0.11						38.5	38.24	0.63
		ME	9.19	6.98	0.08						43.2	42.95	0.49
		ME	11.66	7.12	0.10						37.9	37.71	0.53
		ME	9.68	6.12	0.10						38.7	38.49	0.63
		ME	11.26	6.36	0.10						36.1	35.89	0.56
		ME	11.15	5.35	0.11						32.4	32.21	0.66
		ME	11.57	5.81	0.11						33.4	33.22	0.63
		ME	10.77	7.08	0.11						39.7	39.42	0.61
		ME	10.92	4.39	0.08						28.7	28.53	0.52
		ME	11.75	4.96	0.10						29.7	29.51	0.59

Table AII 21 EDX data for samples produced by a flounder sp. (all elemental data reported as atomic %)

Sample	Pellet	Crystal form	Ca	Mg	Sr	Na	Cl	S	P	Si	$MgCO_3$ (mol%)	$MgCO_3$ (mol%)	$SrCO_3$ (mol%)
1	1	ME	11.98	2.58							17.7		
		ME	10.09	5.18							33.9		
		ME	9.21	5.09							35.6		
		ME	12.69	5.32							29.5		
		ME	11.18	5.91							34.6		
		ME	10.93	5.82							34.7		
		ME	9.40	5.56							37.2		
		ME	12.33	6.00							32.7		
		ME	11.37	5.59							33.0		
		ME	12.61	4.52							26.4		
	2	ME	11.50	5.96							34.1		
		ME	12.83	6.12							32.3		
		ME	12.35	6.46							34.3		
		ME	10.91	5.13							32.0		
		ME	12.78	6.51							33.7		
		ME	11.34	6.16							31.1		
		ME	12.32	5.85							34.6		
		ME	12.60	6.53							32.8		
		ME	14.36	6.65							31.7		
		ME	10.15	5.82							36.4		
	3	ME	9.80	5.89							37.5		
		ME	10.10	5.75							36.3		
		ME	10.23	5.90							36.6		
		ME	9.02	5.41							37.5		
		ME	9.56	5.87							38.0		
		ME	11.63	6.02							34.1		
		ME	10.49	5.56							34.6		
		ME	7.39	4.85							39.6		
		ME	10.13	5.89							36.8		
		ME	9.62	5.70							37.2		
	4	ME	10.75	7.43							40.9		
		ME	10.46	6.19							37.2		
		ME	11.75	7.80							39.9		
		ME	10.12	7.32							42.0		
		ME	11.76	6.92							37.0		
		ME	10.60	7.22							40.5		
		ME	9.17	6.30							40.7		
		ME	10.63	6.39							37.5		
		ME	12.17	7.34							37.6		
		ME	10.68	6.69							38.5		
	5	ME	8.86	6.03							40.5		
		ME	9.99	5.88							37.1		
		ME	9.43	5.38							36.3		
		ME	7.74	5.97							43.5		
		ME	6.66	5.44							45.0		
		ME	8.06	6.10							43.1		
		ME	7.77	5.37							40.9		
		ME	7.95	5.46							40.7		
		ME	9.07	6.06							40.1		
		ME	7.81	5.71							42.2		

Table AII 22 EDX data for samples produced by a great barracuda (all elemental data reported as atomic %)

Sample	Pellet	Crystal form	Ca	Mg	Sr	Na	Cl	S	P	Si	$MgCO_3$ (mol%)	$MgCO_3$ (mol%)	$SrCO_3$ (mol%)
1	1	Sml dmbl	12.90	6.12							32.2		
		Sml dmbl	13.75	6.70							32.8		
		Sml dmbl	14.06	6.72							32.3		
		Sml dmbl	11.47	6.47							36.1		
		Sml dmbl	16.18	7.63							32.0		
		Sml dmbl	13.39	6.53							32.8		
		Sml dmbl	9.78	6.67							40.5		
		Sml dmbl	10.34	6.28							37.8		
		Sml dmbl	11.08	6.18							35.8		
		Sml dmbl	9.74	5.66							36.8		
	2	Sml dmbl	9.52	5.75							37.7		
		Sml dmbl	8.39	4.62							35.5		
		Sml dmbl	10.04	5.53							35.5		
		Sml dmbl	8.51	4.63							35.2		
		Sml dmbl	7.98	4.56							36.4		
		Sml dmbl	8.26	5.08							38.1		
		Sml dmbl	8.29	5.29							39.0		
		Sml dmbl	11.79	6.68							36.2		
		Sml dmbl	10.37	5.48							34.6		
		Sml dmbl	8.18	4.95							37.7		
	3	Sml dmbl	7.37	6.56							47.1		
		Sml dmbl	7.47	6.99							48.3		
		Sml dmbl	7.30	7.01							49.0		
		Sml dmbl	7.33	6.57							47.3		
		Sml dmbl	10.12	7.49							42.5		
		Sml dmbl	10.29	8.67							45.7		
		Sml dmbl	8.89	7.23							44.9		
		Sml dmbl	10.78	8.12							43.0		
		Sml dmbl	7.32	6.41							46.7		
		Sml dmbl	8.31	7.24							46.6		
	4	Sml dmbl	9.88	4.76							32.5		
		Sml dmbl	12.17	4.93							28.8		
		Sml dmbl	14.52	6.85							32.1		
		Sml dmbl	11.20	5.45							32.7		
		Sml dmbl	11.68	5.24							31.0		
		Sml dmbl	9.58	4.74							33.1		
		Sml dmbl	10.01	5.05							33.5		
		Sml dmbl	11.79	5.25							30.8		
		Sml dmbl	10.55	4.14							28.2		
		Sml dmbl	9.53	4.87							33.8		
	5	Sml dmbl	13.14	7.62							36.7		
		Sml dmbl	15.29	8.48							35.7		
		Sml dmbl	12.67	6.33							33.3		
		Sml dmbl	10.54	6.26							37.3		
		Sml dmbl	13.97	6.96							33.3		
		Sml dmbl	8.06	5.15							39.0		
		Sml dmbl	10.50	7.77							42.5		
		Sml dmbl	11.55	6.67							36.6		
		Sml dmbl	12.91	6.34							32.9		
		Sml dmbl	9.85	5.64							36.4		

Sample	Pellet	Crystal form	Ca	Mg	Sr	Na	Cl	S	P	Si	$MgCO_3$ (mol%)	$MgCO_3$ (mol%)	$SrCO_3$ (mol%)
2		Sml dmbl	12.42	5.68	0.06	0.65	0.09		0.08		31.4	31.28	0.33
		Sml dmbl	14.28	5.30	0.08	0.59	0.11		0.11		27.1	26.96	0.41
		Sml dmbl	18.06	7.72	0.05	0.46	0.30		0.73		29.9	29.89	0.19
		Sml dmbl	17.90	7.33	0.08	0.42	0.17		0.15		29.1	28.96	0.32
		Sml dmbl	11.74	6.53	0.04	0.50	0.16		0.13		35.7	35.66	0.22
		Sml dmbl	19.34	9.21	0.06	0.48	0.22		0.20		32.3	32.19	0.21
		Sml dmbl	20.97	9.29	0.04	0.27	0.07		0.24		30.7	30.66	0.13
		Sml dmbl	12.63	7.47	0.05	0.49	0.20		0.17		37.2	37.07	0.25
		Sml dmbl	22.47	5.61	0.08	0.33	0.07		0.09		20.0	19.92	0.28
		Sml dmbl	32.13	7.01	0.07	0.18	0.02		0.12		17.9	17.88	0.18
		Sml dmbl	14.89	4.00	0.06	0.54	0.08		0.05		21.2	21.11	0.32
2		Nanosph	25.65	7.27		0.42	1.15		6.32		22.1		
		Nanosph	13.34	7.58		0.58	1.01		4.98		36.2		
		Nanosph	17.12	5.21		0.47	0.61		6.02		23.3		
		Nanosph	14.62	6.52		0.59	0.80		5.66		30.8		
		Nanosph	15.98	6.23		0.62	0.82		5.80		28.1		
		Nanosph	16.63	4.53		0.73	0.66		6.01		21.4		
		Nanosph	15.59	4.20		0.59	0.54		5.58		21.2		
		Nanosph	17.05	5.01		0.78	0.87		6.27		22.7		
		Nanosph	17.23	4.76		0.82	0.75		6.16		21.6		
		Nanosph	16.08	4.68		0.73	0.77		6.09		22.5		
		Nanosph	16.75	5.12		0.79	0.89		6.80		23.4		
		Nanosph	15.19	4.46		0.31	0.46		4.94		22.7		
		Nanosph	12.70	4.10		0.33	0.44		5.24		24.4		
		Nanosph	12.94	4.17		0.31	0.44		5.38		24.4		
2		Dmbl	24.90	0.43	0.21	0.45	0.04		0.06		1.7	1.68	0.82
		Dmbl	26.59	0.50	0.20	0.47	0.04	0.06			1.8	1.83	0.73
		Dmbl	22.07	1.06	0.18	0.49	0.02	0.04			4.6	4.55	0.77
		Dmbl	17.78	0.89	0.20	0.66	0.07	0.04	0.10		4.8	4.72	1.06

Appendix III: liquid ion chromatography data for fish-derived carbonates

Fish-derived carbonate samples weighing approximately 10–100 mg, each typically comprising 5–30 individual pellets, were dissolved in preparation for liquid ion chromatography to determine the concentration of various cations and anions. The analytical method is described in detail in the main text (Chapter 2). Specifically, pellets were placed in 20 mL of Ultrapure™ water and dissolved by slowly adding a 0.02 M solution of HCl until no crystals remained and solution pH was lower than 4.00. The preparation stage was also used to determine the mass of $CaCO_3$ present in each sample using a double titration approach (see main text of Chapter 5 for further details), and it was thus necessary to bring the solution containing dissolved carbonates back to its initial pH by adding a 0.02 M solution of NaOH. The final stage prior to analysis by liquid ion chromatography was to re-acidify the solution to a pH <4.00 (by adding a small volume of 0.02 M HCl) to ensure no reprecipitation of dissolved ions would take place.

The full data sets generated by liquid ion chromatography analysis are presented in Tables AIII 1 and 2. Data presented in Table AIII 1 were generated at the University of Exeter by Dr. R.W. Wilson and Dr. J. Whittamore using fish carbonate samples collected in the Bahamas during November and December 2009. Data in Table AIII 2 were generated using the same approach at that in Table AIII 1, but analyses were performed at the University of Exeter by M.A. Salter and Dr. E.E. Reardon using samples collected in the Bahamas during July 2010.

Where measured, sodium and chloride are present at varying concentrations in all samples due to addition of HCl and NaOH during sample preparation, and the concentrations determined here do not reflect sample concentrations. All other cation and anion concentrations determined using this approach are representative of concentrations in dissolved samples, although in most cases only calcium and magnesium are present in significant concentrations. It is worth pointing out, however, that some samples also appear to contain low, but significant, concentrations of phosphate.

Table AIII 1 Liquid ion chromatography results and calculated mol% $MgCO_3$ for fish-derived carbonates collected in the Bahamas in November and December 2009. Analyses performed at the University of Exeter by Dr. R.W. Wilson and Dr. J. Whittamore; results published in Perry et al. (2011) and Salter et al. (2012).

Sample	Sample Name	Na^+ (uM)	K^+ (uM)	Mg^{2+} (uM)	Ca^{2+} (uM)	Dilution	Cl^- (uM)	PO_4^{3-} (uM)	SO_4^{2-} (uM)	Dilution	Na^+ (mM)	K^+ (mM)	Mg^{2+} (mM)	Ca^{2+} (mM)	Cl^- (mM)	PO_4^{3-} (mM)	SO_4^{2-} (mM)	MgCO3 (mol%)
1	Std1			0.0	0.0	1							0.00	0.00				
2	Std2			41.2	24.6	1000							41.18	24.58				
3	Std3			83.8	49.7	500							41.92	24.86				
4	Std4			209.7	125.3	200							41.95	25.07				
5	Std5			419.4	248.5	100							41.94	24.85				
6	Std6			837.0	497.6	50							41.85	24.88				
7	Std7			1636.2	999.0	25							40.90	24.97				
8	Std4 check			207.8	122.9	200							41.56	24.58				
9	Schoolmaster snapper			142.1	271.1	101							14.36	27.38				34.4
10	Graysby grouper			349.8	779.1	11							3.85	8.57				31.0
11	Graysby grouper			310.5	673.7	11							3.42	7.41				31.6
12	Graysby grouper			352.4	812.6	11							3.88	8.94				30.2
13	Graysby grouper			64.8	149.9	101							6.54	15.13				30.2
14	Graysby grouper			49.9	139.5	101							5.04	14.09				26.3
15	Graysby grouper			47.1	142.6	101							4.76	14.40				24.8
16	Red lionfish			236.7	498.1	11							2.60	5.48				32.2
17	Red lionfish			131.0	279.8	11							1.44	3.08				31.9
18	Std4 check			210.9	124.4	200							42.18	24.87				
19	Red lionfish			117.8	245.5	11							1.30	2.70				32.4
20	Red lionfish			56.3	182.8	11							0.62	2.01				23.6
21	Red lionfish			3.3	4.8	11							0.04	0.05				40.8
22	Red lionfish			83.0	204.1	11							0.91	2.24				28.9
23	Yellowtail snapper			73.2	201.8	101							7.39	20.38				26.6
24	Yellowtail snapper			38.7	106.0	101							3.91	10.71				26.7
25	Yellowtail snapper			54.9	143.3	101							5.55	14.47				27.7
26	Yellowtail snapper			164.1	683.7	11							1.80	7.52				19.4
27	Yellowtail snapper			105.6	281.7	11							1.16	3.10				27.3

Table AIII 1 cont.

Sample	Sample Name	Na^+ (uM)	K^+ (uM)	Mg^{2+} (uM)	Ca^{2+} (uM)	Dilution	Cl^- (uM)	PO_4^{3-} (uM)	SO_4^{2-} (uM)	Dilution	Na^+ (mM)	K^+ (mM)	Mg^{2+} (mM)	Ca^{2+} (mM)	Cl^- (mM)	PO_4^{3-} (mM)	SO_4^{2-} (mM)	MgCO3 (mol%)
28	Std4 check			211.9	123.6	200							42.37	24.71				
29	Yellowtail snapper			194.6	460.5	11							2.14	5.07				29.7
30	Yellowtail snapper			80.0	163.3	101							8.08	16.50				32.9
31	Yellowtail snapper			122.7	431.4	101							12.40	43.57				22.2
32	*Haemulon* sp.			229.2	448.4	11							2.52	4.93				33.8
33	White mullet (dirty?)			55.5	275.9	11							0.61	3.03				16.7
35	Red hind			290.3	537.6	11							3.19	5.91				35.1
36	Schoolmaster snapper			76.5	178.1	101							7.73	17.99				30.1
37	Schoolmaster snapper			104.4	217.8	101							10.55	22.00				32.4
38	Std4 check			212.1	123.4	200							42.43	24.68				
39	Schoolmaster snapper			184.1	739.4	11							2.02	8.13				19.9
40	Schoolmaster snapper			43.3	113.2	101							4.37	11.43				27.7
41	Schoolmaster snapper			34.1	98.1	101							3.45	9.91				25.8
42	Schoolmaster snapper			52.0	124.4	101							5.25	12.57				29.5
43	Schoolmaster snapper			71.4	170.5	101							7.21	17.22				29.5
44	Schoolmaster snapper			60.2	141.5	101							6.08	14.29				29.8
45	Schoolmaster snapper			113.3	234.1	101							11.45	23.64				32.6
46	Great barracuda			117.5	239.4	101							11.87	24.18				32.9
47	Great barracuda			339.4	330.4	11							3.73	3.63				50.7
48	Std4 check			211.0	122.3	200							42.19	24.47				
49	Great barracuda			63.4	85.8	11							0.70	0.94				42.5
50	Great barracuda			29.5	103.0	11							0.32	1.13				22.2
51	Great barracuda			41.9	61.9	11							0.46	0.68				40.4
52	Great barracuda			111.1	293.1	101							11.22	29.61				27.5
53	Great barracuda			242.0	550.9	101							24.44	55.64				30.5
54	Yellowfin mojarra			53.3	218.5	101							5.38	22.07				19.6
55	Bonefish			134.9	371.7	101							13.63	37.54				26.6
56	Bonefish			113.2	191.3	101							11.43	19.32				37.2

Table AIII 1 cont.

Sample	Sample Name	Na^+ (uM)	K^+ (uM)	Mg^{2+} (uM)	Ca^{2+} (uM)	Dilution	Cl^- (uM)	PO_4^{3-} (uM)	SO_4^{2-} (uM)	Dilution	Na^+ (mM)	K^+ (mM)	Mg^{2+} (mM)	Ca^{2+} (mM)	Cl^- (mM)	PO_4^{3-} (mM)	SO_4^{2-} (mM)	MgCO3 (mol%)
57	Bonefish			204.4	374.6	101							20.64	37.83				35.3
58	Std4 check			211.7	123.1	200							42.34	24.61				

Standard 4 statistics	Mg^{2+} (uM)	Ca^{2+} (uM)
Mean	**210.9**	**123.3**
SD	**1.58**	**0.68**
SE	**0.65**	**0.28**
N	**6**	**6**

Table AIII 2 Liquid ion chromatography results and calculated mol% $MgCO_3$ for fish-derived carbonates collected in the Bahamas in July 2010. Analyses performed at the University of Exeter by M.A. Salter and Dr. E.E. Reardon; results published in Salter et al. (2012).

Sample	Sample Name	Na^+ (uM)	K^+ (uM)	Mg^{2+} (uM)	Ca^{2+} (uM)	Dilution	Cl^- (uM)	PO_4^{3-} (uM)	SO_4^{2-} (uM)	Dilution	Na^+ (mM)	K^+ (mM)	Mg^{2+} (mM)	Ca^{2+} (mM)	Cl^- (mM)	PO_4^{3-} (mM)	SO_4^{2-} (mM)	MgCO3 (mol%)
2	Std2	56.4	24.0	29.8	21.7	1000	41.0	17.9	17.9	500	56.4	24.0	29.8	21.7	20.5	8.9	9.0	
3	Std3	216.5	123.4	184.1	123.1	500	105.7	45.5	44.9	200	108.2	61.7	92.1	61.6	21.1	9.1	9.0	
4	Std4	219.8	124.9	190.2	126.1	200	219.0	92.9	90.7	100	44.0	25.0	38.0	25.2	21.9	9.3	9.1	
5	Std5	435.9	254.1	394.9	245.1	100	472.6	194.3	187.9	50	43.6	25.4	39.5	24.5	23.6	9.7	9.4	
6	Std6	870.9	511.1	820.6	496.7	50	1050.2	403.9	394.8	25	43.5	25.6	41.0	24.8	26.3	10.1	9.9	
7	Std7	1738.5	1024.1	1653.3	1000.3	25	2328.9	857.2	850.8	13	43.5	25.6	41.3	25.0	29.1	10.7	10.6	
8	Std 4	218.8	126.5	181.7	120.0	200	219.2	93.2	90.8	100	43.8	25.3	36.3	24.0	21.9	9.3	9.1	
9	Yellowfin mojarra (B)	1079.3	80.0	194.6	481.6	1	2581.0	4.0	1.8	1	1.08	0.08	0.19	0.48	2.58	0.00	0.00	28.78
10	Yellowfin mojarra (C)	401.1	2.5	96.7	407.0	1	1362.8	9.8	6.4	1	0.40	0.00	0.10	0.41	1.36	0.01	0.01	19.19
11	French grunt (C/D)	578.2	17.8	279.2	903.0	1	3073.5	3.6	12.9	1	0.58	0.02	0.28	0.90	3.07	0.00	0.01	23.62
12	*Eucinostomus* sp. (D/E)	667.3	21.4	167.4	609.7	1	2272.1	5.9	4.2	1	0.67	0.02	0.17	0.61	2.27	0.01	0.00	21.54
13	Beaugregory (A)	641.7	8.8	18.3	45.1	1	780.7	0.9	4.0	1	0.64	0.01	0.02	0.05	0.78	0.00	0.00	28.90
14	Beaugregory (A)	555.5	2.3	47.6	66.4	1	767.6	4.5	0.7	1	0.56	0.00	0.05	0.07	0.77	0.00	0.00	41.77
15	Beaugregory (B/C/D)	629.0	22.9	455.7	216.3	1	2019.7	21.5	2.0	1	0.63	0.02	0.46	0.22	2.02	0.02	0.00	67.82
16	Beaugregory (B/C/D)	601.3	1.7	28.3	50.0	1	631.7	7.1	4.3	1	0.60	0.00	0.03	0.05	0.63	0.01	0.00	36.14
17	Beaugregory (B/C/D)	665.8	2.6	33.3	59.7	1	843.8	5.1	2.0	1	0.67	0.00	0.03	0.06	0.84	0.01	0.00	35.82
18	Beaugregory (E/F/G)	939.8	4.0	151.1	494.0	1	1982.5	246.7	0.9	1	0.94	0.00	0.15	0.49	1.98	0.25	0.00	23.43
19	Keeltail needlefish (C)	373.8	3.4	134.0	688.4	1	2038.2	3.3	1.1	1	0.37	0.00	0.13	0.69	2.04	0.00	0.00	16.29
20	Checkered puffer (A)	804.5	12.6	54.8	511.7	1	1933.5	1.7	3.0	1	0.80	0.01	0.05	0.51	1.93	0.00	0.00	9.68
21	Bluehead wrasse (A/B)	1021.0	3.3	195.0	105.2	1	1636.9	5.5	0.7	1	1.02	0.00	0.19	0.11	1.64	0.01	0.00	64.96
22	Bluehead wrasse (I/J/K)	988.8	4.2	236.1	175.0	1	1802.1	18.6	3.2	1	0.99	0.00	0.24	0.18	1.80	0.02	0.00	57.43
23	Bluehead wrasse (L/M)	939.6	8.1	691.0	338.3	1	3160.2	10.2	2.0	1	0.94	0.01	0.69	0.34	3.16	0.01	0.00	67.13
24	Std 4	219.5	126.7	184.3	125.4	200	219.5	94.0	90.9	100	43.91	25.34	36.85	25.08	21.95	9.40	9.09	
25	Yellowfin mojarra (A)	341.8	2.6	122.0	774.2	4	2169.4	0.6	3.2	4	1.37	0.01	0.49	3.10	8.68	0.00	0.01	13.61
26	Yellowfin mojarra (C)	450.2	2.8	165.8	523.3	2	1812.4	3.9	6.5	2	0.90	0.01	0.33	1.05	3.62	0.01	0.01	24.07
27	Black grouper (A)	180.6	2.8	164.4	524.6	10	1471.4	3.7	1.7	10	1.81	0.03	1.64	5.25	14.71	0.04	0.02	23.87
28	Black grouper (B)	258.4	2.2	229.3	461.9	10	1563.8	9.9	0.8	10	2.58	0.02	2.29	4.62	15.64	0.10	0.01	33.17
29	Black grouper (C)	241.1	4.1	380.6	712.0	10	2406.4	11.1	1.7	10	2.41	0.04	3.81	7.12	24.06	0.11	0.02	34.83

Table AIII 2 cont.

Sample	Sample Name	Na^+ (uM)	K^+ (uM)	Mg^{2+} (uM)	Ca^{2+} (uM)	Dilution	Cl^- (uM)	PO_4^{3-} (uM)	SO_4^{2-} (uM)	Dilution	Na^+ (mM)	K^+ (mM)	Mg^{2+} (mM)	Ca^{2+} (mM)	Cl^- (mM)	PO_4^{3-} (mM)	SO_4^{2-} (mM)	MgCO3 (mol%)
30	Black grouper (D)	102.2	2.3	222.3	481.1	20	1475.9	5.0	2.3	20	2.04	0.05	4.45	9.62	29.52	0.10	0.05	31.61
31	Black grouper (E)	165.7	3.5	260.6	600.9	20	1754.8	10.3	2.0	20	3.31	0.07	5.21	12.02	35.10	0.21	0.04	30.25
32	Checkered puffer (A)	396.3	5.9	25.9	662.6	2	1662.7	1.7	6.1	2	0.79	0.01	0.05	1.33	3.33	0.00	0.01	3.77
33	Checkered puffer (B)	263.4	2.6	24.3	711.1	4	1611.7	1.4	0.9	4	1.05	0.01	0.10	2.84	6.45	0.01	0.00	3.31
34	Checkered puffer (C)	359.3	4.2	45.7	797.3	2	1975.0	1.3	2.2	2	0.72	0.01	0.09	1.59	3.95	0.00	0.00	5.43
35	Checkered puffer (E)	863.2	8.4	28.8	850.3	2	2190.2	14.5	3.0	2	1.73	0.02	0.06	1.70	4.38	0.03	0.01	3.27
36	Keeltail needlefish (G)	184.1	5.9	381.6	468.4	4	1818.2	7.0	2.4	4	0.74	0.02	1.53	1.87	7.27	0.03	0.01	44.90
37	Keeltail needlefish (D)	179.5	2.1	135.7	473.7	2	1318.7	3.1	2.3	2	0.36	0.00	0.27	0.95	2.64	0.01	0.00	22.27
38	French grunt (A/B)	196.8	7.4	167.7	588.2	3	1670.3	3.2	1.7	3	0.59	0.02	0.50	1.76	5.01	0.01	0.01	22.18
39	std 4	219.6	127.3	179.4	122.0	200	219.2	95.5	91.5	100	43.92	25.45	35.88	24.40	21.92	9.55	9.15	

Standard 4 statistics	Mg^{2+} (uM)	Ca^{2+} (uM)
Mean	**181.8**	**122.5**
SD	**2.42**	**2.74**
SE	**1.40**	**1.58**
N	**3**	**3**

Appendix IV – representative ATR-FTIR spectra

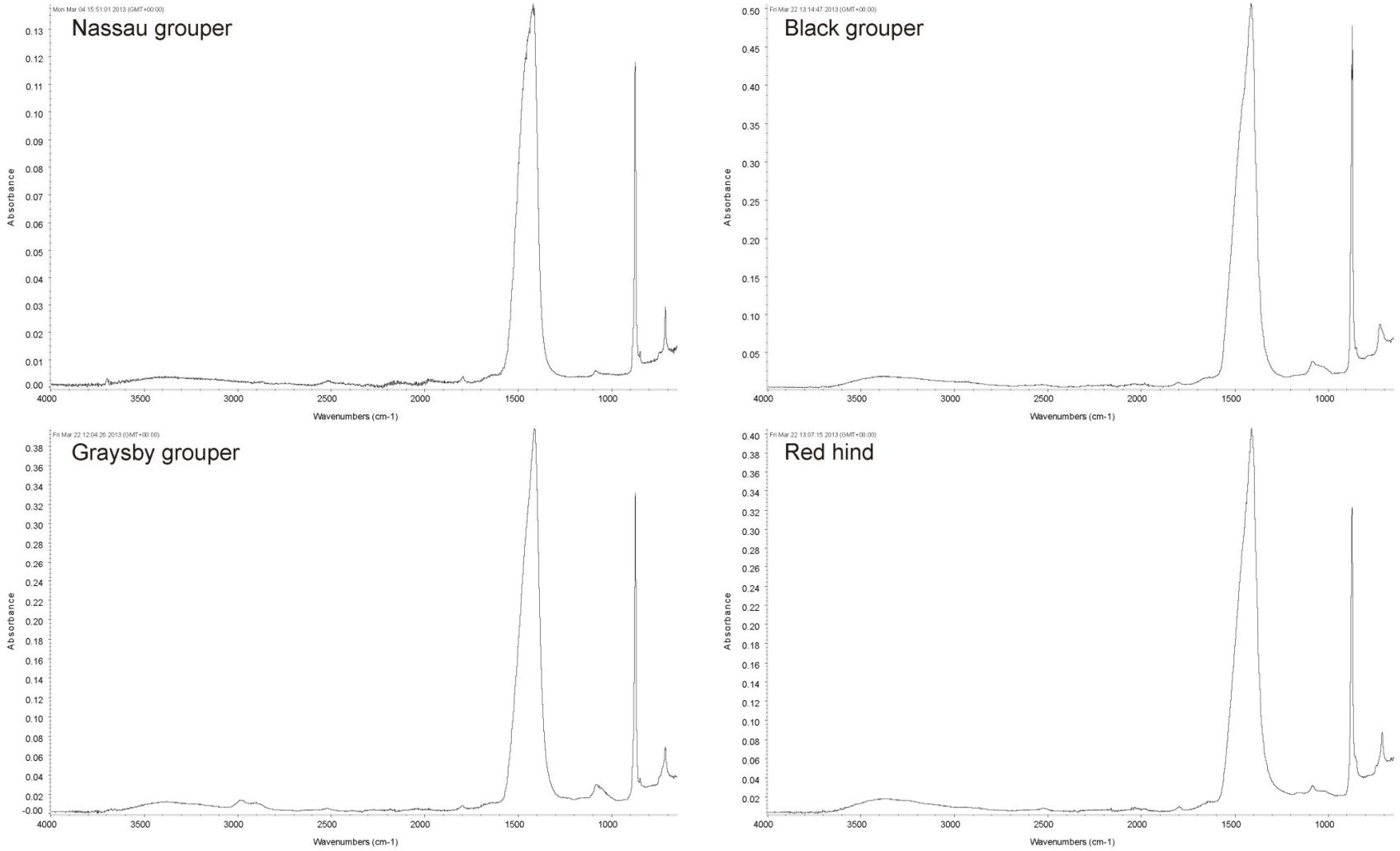

Figure AIV 1 *Representative ATR-FTIR spectra for carbonates excreted by four fish species. All samples are dominated by monocrystalline ellipsoids and related morphotypes.*

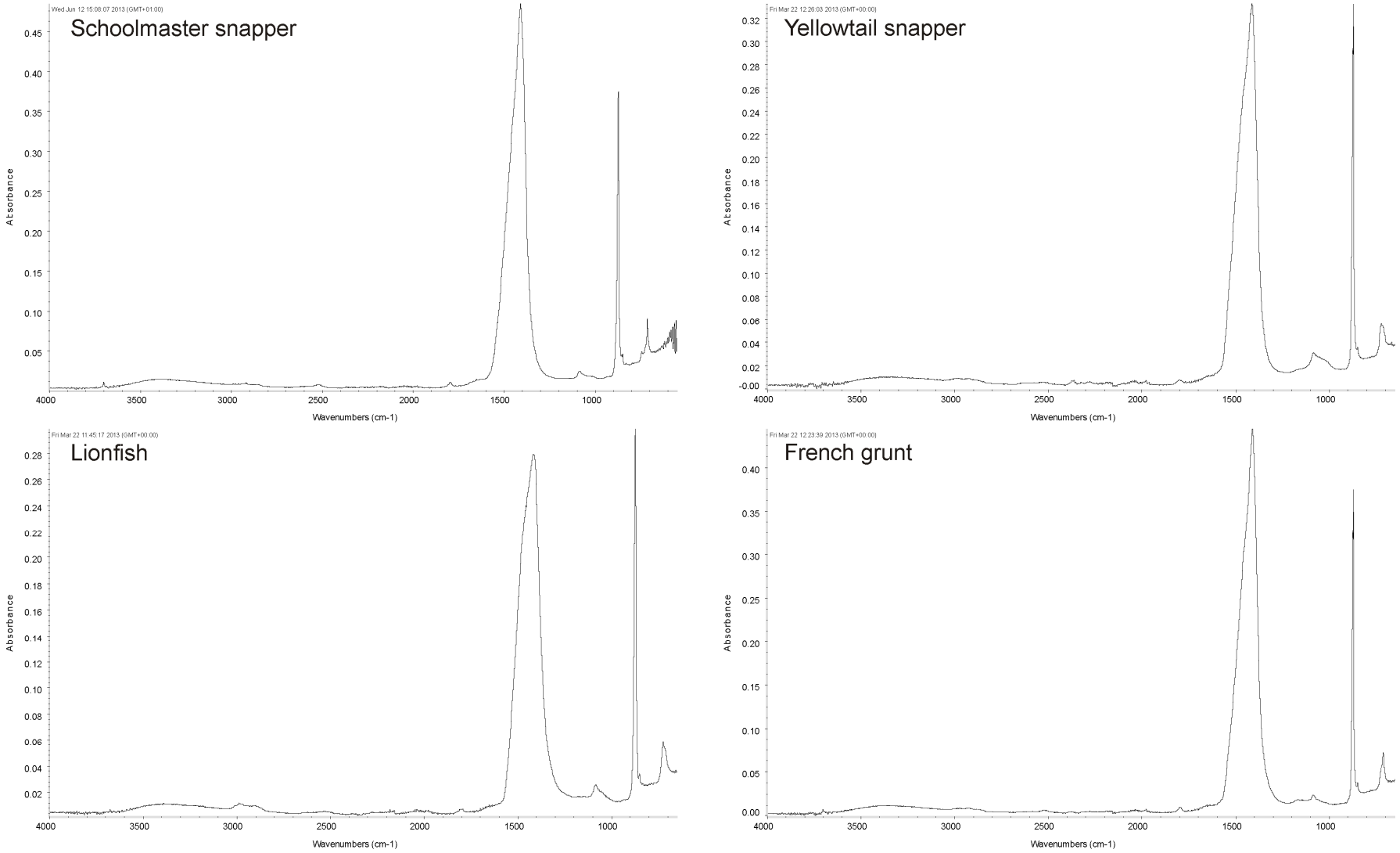

Figure AIV 2 *Representative ATR-FTIR spectra for carbonates excreted by four fish species. All samples are dominated by monocrystalline ellipsoids and related morphotypes.*

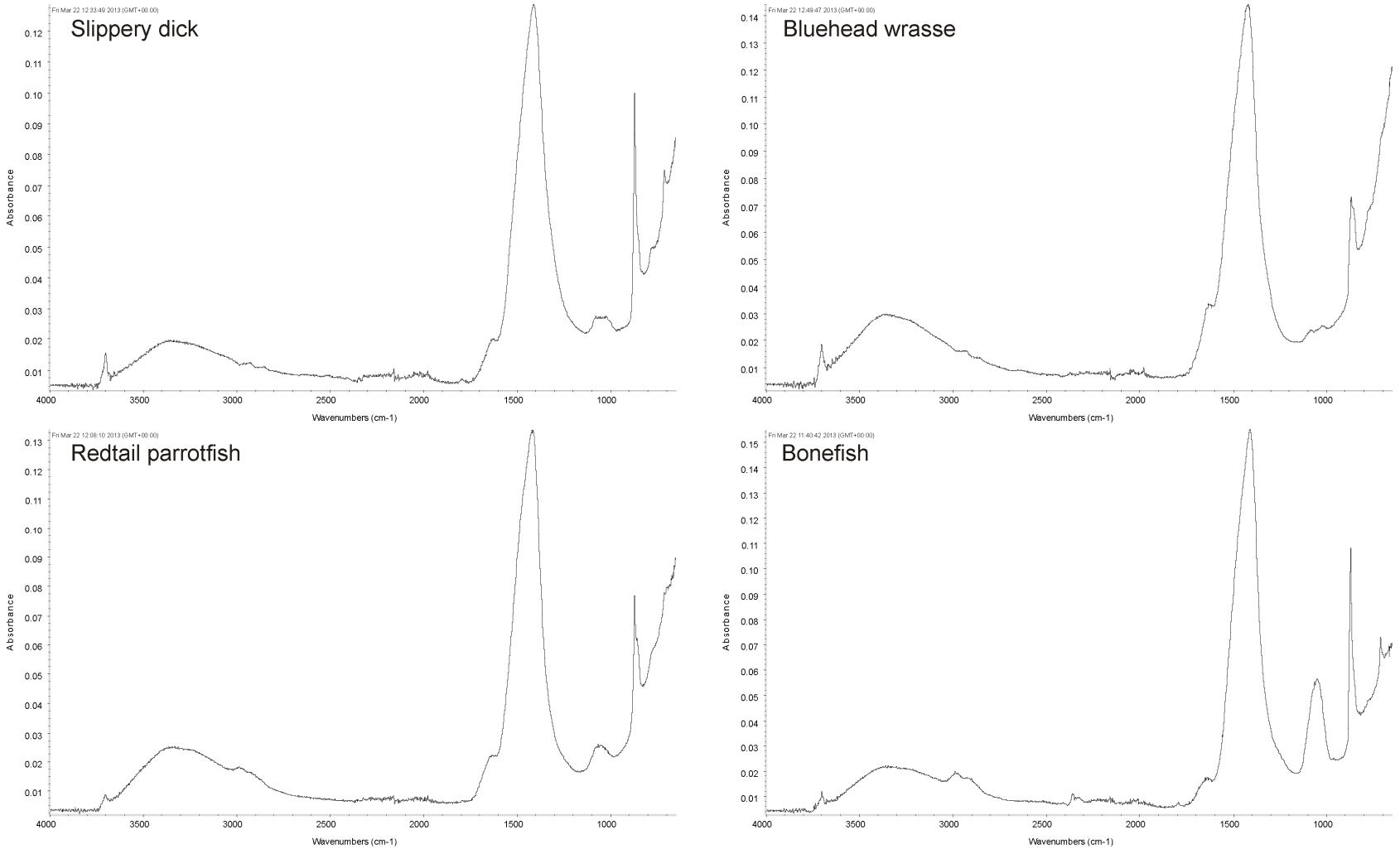

Figure AIV 3 *Representative ATR-FTIR spectra for carbonates excreted by four fish species. Samples are dominated by AMC and calcite rhombohedra (top two spectra), or ACC and calcite spheres (bonefish). Samples produced by redtail parrotfish are dominated by calcite spheres and ellipsoids, although spectra typically indicate the presence of amorphous carbonate as well.*

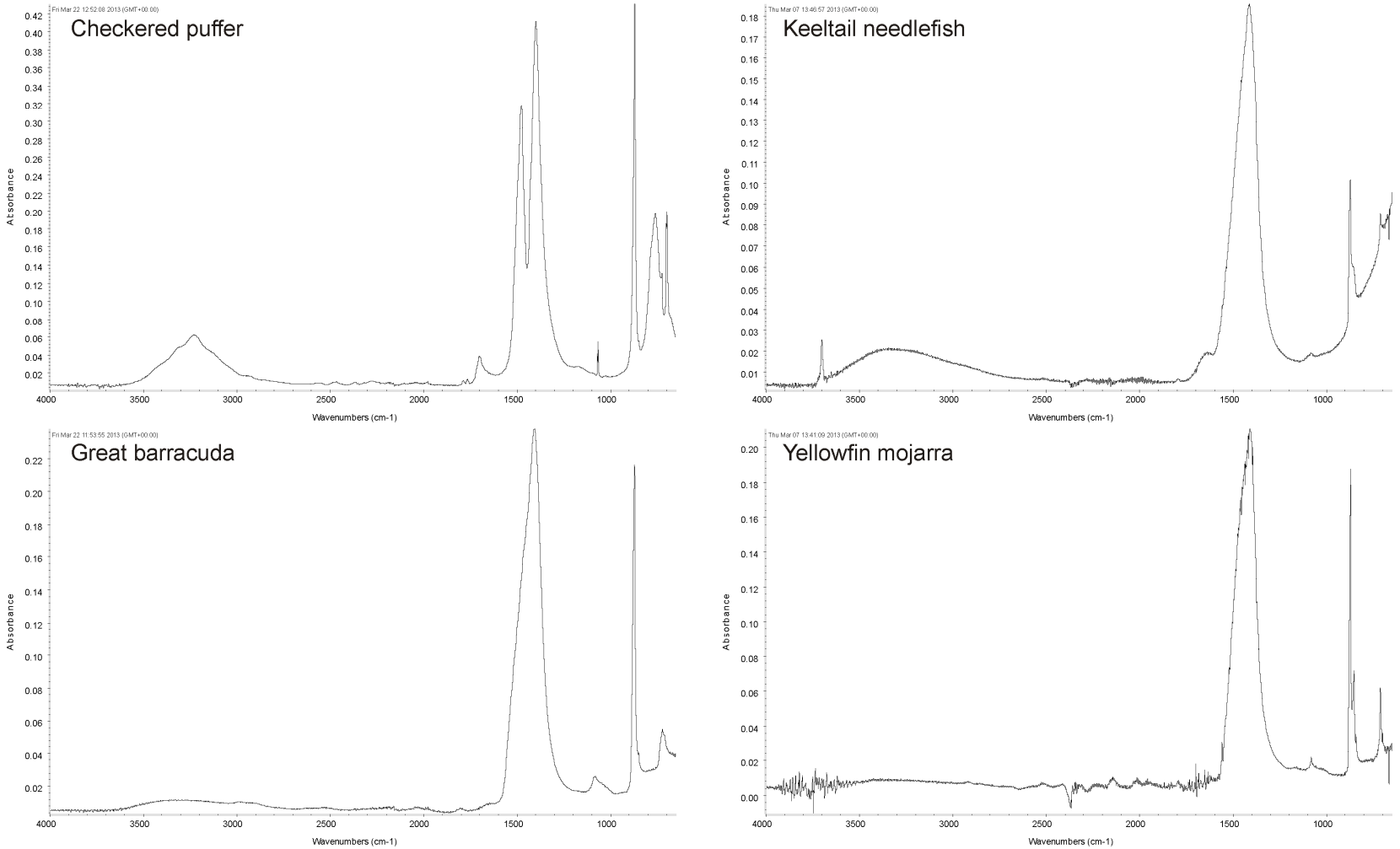

Figure AIV 4 *Representative ATR-FTIR spectra for carbonates excreted by four fish species. Checkered puffer – monohydrocalcite spheres (spectra can also reveal calcite and amorphous carbonate as the dominant phases – see main text); keeltail needlefish – AMC, calcite (ellipsoids and dumbbells), and brucite; great barracuda – calcite (small dumbbells); yellowfin mojarra – calcite (ellipsoids, spheres, dumbbells) is dominant, but also minor aragonite (needles, spheres, dumbbells).*

Appendix V – Stable isotope data – carbon and oxygen

Table AV 1 *Full data set for stable isotope analyses of selected fish-derived carbonates.*

Species	Lab[1]	Notes[2, 3, 4, 5]	Rinses[6]	$10^3\delta^{13}C_{VPDB}$	$10^3\delta^{18}O_{VPDB}$
Black grouper	Liverpool	Point of excretion	1	0.26	1.08
	Liverpool	Point of excretion	1	0.20	0.77
	UEA	Point of excretion	1	-0.12	-0.14
	UEA	12 days in seawater	1	-0.72	0.58
	Liverpool	12 days in seawater	1	-0.77	1.23
Graysby grouper	Liverpool	Point of excretion	1	-0.33	1.23
Schoolmaster	Liverpool	Point of excretion	1	-1.10	1.38
snapper	Liverpool	Point of excretion	1	-1.16	1.57
	Liverpool	Point of excretion	1	-1.17	2.08
	Liverpool	Point of excretion	2	-0.95	1.99
	Liverpool	Point of excretion	2	-1.25	1.86
	Liverpool	Point of excretion - emitted pink gas	2	-1.28	1.18
	Liverpool	Point of excretion	4	-1.36	1.61
	Liverpool	Point of excretion	4	-1.44	1.20
	Liverpool	Point of excretion	4	-1.48	1.14
	Liverpool	Point of excretion - sample size <3 mg	6	-1.77	1.80
	Liverpool	Point of excretion	6	-1.70	1.46
	Liverpool	Point of excretion - sample size <3 mg	6	-1.69	1.83
	Liverpool	Point of excretion	1	-2.17	0.95
	UEA	Point of excretion	1	-1.48	0.57
	UEA	Point of excretion - **fed sardines**	1	-6.71	-0.20
	Liverpool	8 days in seawater	1	-1.78	1.16
	Liverpool	8 days in seawater - **fed sardines**	1	-5.12	1.29
	UEA	3 months in porewater (u) - **fed sardines**	1	-5.38	0.85
	Liverpool	3 months in porewater (u) - **fed sardines**	1	-4.95	1.79
	Liverpool	3 months in porewater (p) - **fed sardines**	1	-4.41	0.82
Bonefish	Liverpool	Point of excretion - **fed sardines**	1	-2.19	0.90
	Liverpool	Point of excretion - **fed sardines**	1	-1.46	1.69
	Liverpool	Point of excretion - **fed sardines**	1	-0.91	0.02
	UEA	Point of excretion - **fed sardines**	1	-2.81	-1.42
	Liverpool	Point of excretion	1	2.55	1.65
	Liverpool	12 days in seawater - **fed sardines**	1	-1.07	2.14
	Liverpool	3 months in porewater (u) - **fed sardines**	1	-1.00	1.41
	UEA	3 months in porewater(u) - **fed sardines**	1	-2.11	0.42

Table AV 1 *cont.*

Species	Lab[1]	Notes	Rinses[2]	$10^3 \delta^{13}C_{VPDB}$	$10^3 \delta^{18}O_{VPDB}$
Bonefish (cont.)	Liverpool	3 months in porewater (p) - **fed sardines**	1	-1.16	1.59
	UEA	3 months in porewater - (sph) - **fed sardines**	1	-0.67	0.45
Yellowfin mojarra	Liverpool	Point of excretion	1	-0.58	0.90
	Liverpool	Point of excretion	1	-1.22	-0.33
	Liverpool	12 days in seawater	1	-0.92	1.20
	Liverpool	3 months in porewater (u)	1	-1.05	0.45
	Liverpool	3 months in porewater (p) - sample size <3 mg	1	-1.41	-0.31
Barracuda	Liverpool	Point of excretion	1	-1.28	0.82
	Liverpool	Point of excretion	1	-3.35	-0.26
	Liverpool	Point of excretion	1	-1.36	1.41
Checkered puffer	Liverpool	Point of excretion - **fed sardines**	1	-5.71	1.17
Yellowtail snapper	Liverpool	Point of excretion	1	-1.92	0.65

[1] Analyses were performed in two laboratories:

UEA – Dr Paul Dennis, University of East Anglia

Liverpool – Dr Stephen Crowley, University of Liverpool

[2] All samples are from fish that were starved immediately after capture from the wild, with the exception of those that are denoted as having been fed a diet of sardines prior to being starved.

[3] u = uncleaned samples

[4] p = pre-cleaned samples

[5] sph = spheres only

[6] All samples were analysed following preparation following the methodology outlined in Chapter 2, with the exception of several samples produced by schoolmaster snapper; these were bleached, rinsed, and dried over multiple cycles to test the effect of preparation on stable isotope composition

Appendix VI: Pellet and crystal size variations

The dimensions of fish-derived carbonate pellets and crystals were measured using optical and electron microscope images within calibrated image analysis software (JMicroVision, v.1.2.7). The full methodology is described in the main text (Chapter 5). In most cases, reported values correspond with the longest a- and b- axes. However, for spheres only the diameter is reported, and for dumbbells values are reported at the widest and narrowest points. Data in the tables that follow are separated by sample, and accompanying tables show among-sample variability as well as overall statistics for value ranges and averages.

Table AVI 1 *Crystal codes used in this appendix and brief descriptions of the crystal forms they refer to.*

Crystal code	Crystal form
M. Ellip	Monocrystalline ellipsoid
P. Ellip	Polycrystalline ellipsoid
N/sphere	Nanoscale sphere
N/sphere dbl	Nanosphere doublet (comprising two intergrown nanospheres)
N/sphere clust	Cluster of intergrown nanospheres
Lrg dmbl	Dumbbell-shaped crystal typically >4 µm in length
Sml dmbl	Dumbbell-shaped crystal typically <4 µm in length
Rhomb	Any crystal displaying clear rhombohedral faces
Fib/nee	Crystal with fibrous or acicular form, probably released from polycrystalline particles (spheres/dumbbells) during disaggregation
Sph/nee	Spherulitic particle comprising needle-like crystals
Sphere	Polycrystalline sphere
Sph clust	Cluster of intergrown polycrystalline spheres
Rosette	Rosette of interlocking plates (probably brucite)

Table AVI 2 *Dimensional data for small dumbbells produced by great barracuda. All dimensions are in micrometers. Shading scheme differentiates between data from different samples (see footnote for key).*

length	width (centre)	width (at widest)	length	width (centre)	width (at widest)	length	width (centre)	width (at widest)	length	width (centre)	width (at widest)	length	width (centre)	width (at widest)
2.38	0.49	1.33	2.63	0.68	1.24	3.43	0.91	2.34	1.76	0.48	1.12	1.88	0.21	0.47
3.16	0.36	0.85	3.21	0.71	2.22	3.38	0.86	1.77	1.73	0.58	1.21	3.03	0.64	1.86
2.99	0.49	1.16	3.63	0.71	2.05	2.99	0.58	1.27	1.71	0.29	0.46	1.77	0.34	0.68
3.13	0.62	1.35	1.85	0.45	0.77	2.76	0.51	1.25	3.63	0.57	1.68	2.35	0.49	1.16
2.44	0.54	1.07	1.85	0.42	0.84	3.73	0.76	1.78	2.35	0.47	0.91	3.18	0.51	1.51
3.16	0.55	1.24	1.41	0.24	0.42	2.52	0.47	0.93	2.32	0.44	1.14	1.40	0.34	0.62
2.26	0.48	0.80	3.40	0.82	2.11	2.48	0.71	1.39	2.62	0.73	1.60	2.20	0.40	0.84
2.82	0.70	1.38	3.54	0.73	1.97	1.59	0.32	0.41	2.24	0.61	1.25	1.51	0.41	0.88
2.94	0.63	1.41	1.83	0.53	0.83	3.27	0.86	1.57	2.90	0.74	1.71	1.21	0.33	0.59
2.79	0.56	1.37	1.48	0.42	0.60	3.44	0.80	1.71	1.79	0.60	1.17	3.12	0.59	1.86
2.15	0.36	0.83	1.51	0.48	0.86	3.07	0.58	1.42	2.27	0.60	1.31	2.58	0.68	1.45
1.84	0.28	0.53	1.79	0.50	0.96	3.34	0.62	1.51	2.24	0.49	1.03	1.87	0.47	0.90
2.18	0.51	0.83	2.74	0.69	1.50	2.14	0.62	1.07	4.05	0.57	2.10	1.84	0.67	1.46
2.11	0.31	0.56	2.95	0.70	1.82	3.91	0.95	2.08	3.05	0.60	1.61	1.85	0.31	0.69
2.68	0.64	1.52	2.10	0.57	1.17	1.92	0.32	0.70	3.25	0.58	1.45	2.64	0.57	1.76
2.88	0.61	1.48	2.76	0.60	1.39	2.94	0.75	1.27	1.75	0.46	0.90	1.82	0.36	0.77
3.28	0.64	1.91	1.39	0.48	0.75	2.26	0.47	1.20	1.94	0.39	0.80	2.62	0.60	1.55
1.53	0.40	0.75	2.49	0.67	1.83	2.97	0.58	1.09	1.73	0.42	0.82	3.65	0.67	2.13
3.15	0.59	1.74	1.56	0.39	0.82	2.64	0.64	1.23	2.39	0.64	1.53	1.73	0.37	0.69
2.57	0.62	1.31	1.73	0.48	0.88	2.33	0.44	0.97	2.68	0.73	1.79	3.40	0.60	1.84
2.56	0.80	1.78	3.39	0.79	1.84	3.44	0.67	1.54	2.78	0.60	1.75	2.91	0.39	1.11
1.92	0.63	1.22	2.63	0.73	1.42	2.20	0.52	1.07	3.95	0.86	2.48	0.94	0.29	0.48
3.64	0.67	1.99	3.03	0.70	1.50	2.56			2.57	0.54	1.25	2.18	0.49	0.85
3.38	0.63	1.65	1.43	0.35	0.84	2.52	0.53	1.13	2.13	0.53	1.18	1.46	0.39	0.56
2.08	0.42	0.80	2.43	0.57	1.52	2.64	0.62	1.04	3.09	0.68	1.72	2.64	0.42	1.30
1.71	0.44	0.97	3.32	0.65	2.00	1.94	0.53	0.82	2.87	0.68	1.54	2.67	0.43	1.28
1.43	0.41	0.67	3.52	0.60	1.84	3.26	0.65	1.58	2.43	0.50	1.10	2.41	0.55	1.20
1.53	0.35	0.75	3.61	0.82	1.99	3.08	0.55	1.17	3.07	0.63	1.45	2.62	0.52	1.30
3.44	0.73	1.98	3.63	0.89	2.30	2.16	0.26	0.63	1.45	0.36	0.69	1.59	0.37	0.63
1.79	0.30	0.76	2.99	0.61	1.52	3.07	0.65	1.90	3.28	0.72	2.17	1.69	0.37	0.69
2.57	0.50	1.31	3.44	0.75	1.74	1.85	0.33	0.64	3.50	0.63	2.32	1.84	0.43	0.67
2.01	0.46	0.79	3.85	0.86	1.98	2.25	0.58	0.91	2.15	0.54	1.12	2.00	0.47	0.88
1.65	0.31	0.64	1.98	0.59	1.38	1.97	0.43	0.81	2.98	0.68	1.47	2.57	0.56	1.58
1.67	0.55	1.14	3.62	0.70	2.33	2.99	0.62	0.97	1.42	0.35	0.74	2.76	0.55	1.42
2.41	0.51	1.53	1.57	0.41	0.82	1.59	0.51	1.03	2.92	0.75	1.23	2.47	0.44	1.28
2.83	0.75	1.88	2.62	0.68	2.00	1.30	0.39	0.60	2.43	0.57	1.11	2.02	0.47	0.72
2.52	0.67	1.72	3.58	0.79	2.09	3.07	0.62	1.57	3.08	0.64	1.71	2.25	0.63	1.28
1.78	0.36	0.56	3.41	0.69	1.56	1.53	0.55	1.07	2.86	0.54	1.42	2.58	0.42	1.22
1.67	0.49	0.92	1.90	0.52	0.91	1.24	0.28	0.46	3.27	0.58	1.55	2.16	0.52	1.13
2.63	0.47	1.29	4.43			3.72	0.68	1.79	3.58	0.66	2.26	2.37	0.56	1.29
1.25	0.25	0.55	1.89	0.59	1.01	1.65	0.46	0.81	3.14	0.56	1.66	1.81	0.45	0.68
2.39	0.36	1.17	4.07	0.94	1.97	2.43	0.51	1.19	2.19	0.55	1.26	3.54	0.81	1.11
2.25	0.58	1.17	3.75	0.89	1.77	1.81	0.66	1.15	3.45	0.62	1.81	3.24	0.58	1.33
2.71	0.53	1.32	2.98	0.72	1.68	2.50	0.71	1.68	2.85	0.45	1.05	2.35	0.47	0.98
3.23	0.58	1.66	2.86	0.65	1.33	2.98	0.70	1.40	2.81	0.52	1.41	3.63	0.63	1.71
1.80	0.35	0.62	1.99	0.47	1.10	1.96	0.64	1.05	2.87	0.52	1.33	2.91	0.62	1.77
3.43	0.63	2.01	3.17	0.78	1.93	2.63	0.71	1.72	3.09	0.59	1.25	1.97	0.55	1.25
2.71	0.63	1.88	3.17	0.71	1.79	2.49	0.67	1.38	2.55	0.50	1.01	2.00	0.54	1.14

Shading scheme identifies sample codes: CEI-28 | Sample #10 | Sample # 46 | Sample #76 | CEI-D-11

Table AVI 3 *Dimensional data for nanospheres produced by great barracuda. All dimensions are in micrometers. Shading scheme differentiates between data from different samples (see footnote for key).*

diameter	diameter	diameter	diameter	diameter	diameter
1.35	1.12	0.88	0.74	1.06	0.72
0.57	1.10	1.72	0.74	0.78	0.90
0.85	0.67	1.15	1.45	1.01	0.92
0.85	0.66	0.88	1.08	0.99	1.06
0.90	1.38	1.01	0.78	0.50	1.25
0.96	2.16	0.86	0.75	1.14	0.87
0.95	0.93	0.92	0.68	0.69	1.08
1.08	0.94	1.21	1.45	0.81	0.96
1.42	1.15	0.92	0.77	0.77	0.85
0.80	1.20	0.94	1.04	0.60	0.86
0.92	1.06	0.98	1.14	0.39	1.15
0.80	0.87	1.56	0.99	0.66	1.28
1.01	1.18	1.15	1.07	0.81	1.41
0.89	1.06	1.10	0.72	0.45	1.11
0.61	0.94	0.95	0.85	0.55	1.37
0.51	0.66	0.81	1.07	0.96	1.01
0.73	0.67	1.25	0.85	0.97	0.79
0.76	0.90	1.05	0.96	1.01	1.56
0.73	1.00	0.93	0.96	0.93	0.82
0.88	1.36	1.45	0.74	0.86	1.26
0.76	1.10	0.81	0.93	1.07	1.00
0.71	0.74	1.28	0.73	0.97	0.95
0.74	0.74	1.05	0.81	0.80	0.85
0.72	0.88	1.18	1.17	0.76	1.16
0.75	0.84	0.88	1.02	0.92	0.89
1.34	1.01	1.18	0.96	0.81	0.55
0.93	2.38	1.11	0.71	0.90	1.36
1.18	1.23	0.83	0.68	0.81	0.85
0.96	0.73	1.24	1.03	0.55	0.78
0.90	0.57	1.13	0.87	0.87	1.30
0.71	1.34	1.13	0.83	0.84	
1.28	1.04	1.11	1.23	0.64	
0.90	0.90	0.61	0.74	0.61	
0.76	1.13	0.81	0.72	0.98	
1.04	1.04	0.88	0.76	0.61	
1.14	0.65	0.94	0.57	0.46	
0.75	1.04	1.46	0.89	0.54	
0.92	0.84	0.62	1.03	0.73	
1.34	1.09	1.34	0.80	0.82	
1.15	0.77	0.92	1.06	0.98	
1.01	0.90	1.15	1.14	0.57	
1.22	0.74	0.95	1.11	0.89	
0.90	1.11	0.82	0.61	0.85	
0.95	1.09	0.67	0.75	0.96	
0.98	0.98	0.90	0.56	1.04	
1.16	0.95	0.83	0.90	0.67	
1.31	1.55	0.67	0.90	1.01	
0.81	1.11	0.71	0.86	0.78	

Shading scheme identifies sample codes: CEI-28 | Sample #10 | Sample # 46 | Sample #76 | CEI-D-11

Table AVI 4 *Dimensional data for subsidiary crystal forms produced by great barracuda. All dimensions are in micrometers. Shading scheme differentiates between data from different samples (see footnote for key).*

Fib/nee			Lrg dmbl			N/sphere dbl	Rhomb	M. ellip			Rosette
length	width	aspect ratio	length	width (centre)	width (at widest)	length	length	length	width	aspect ratio	diameter
1.46	0.38	3.81	16.73	5.85	13.91	2.04	2.08	0.51	0.28	1.84	1.30
1.46	0.37	3.95	16.94	3.90	11.44	1.89		0.51	0.31	1.63	1.04
1.43	0.31	4.55	15.34	3.86	9.67	2.25		0.97	0.44	2.19	1.03
1.75	0.50	3.49	14.10	5.04	12.03	1.87		0.61	0.31	2.00	1.11
1.23	0.34	3.66	14.13	4.76	12.32	2.11		0.85	0.36	2.34	0.95
1.11	0.23	4.93	16.07			2.13		1.00	0.44	2.28	1.44
2.91	0.81	3.57	15.99	5.85	12.81	1.45		0.97	0.45	2.17	1.08
1.82	0.57	3.20	8.39	2.41	5.70	1.81		1.07	0.38	2.81	0.92
2.39	1.00	2.38	14.53	3.82	8.44	2.15		1.37	0.53	2.59	1.01
1.09	0.24	4.47	14.80	4.16	9.63	1.74		1.59	0.66	2.41	1.13
1.07	0.26	4.19				1.60		1.59	0.60	2.65	0.99
0.70	0.20	3.57				2.25		1.31	0.51	2.57	1.45
0.83	0.18	4.73				1.62		1.68	0.69	2.43	0.95
0.78	0.19	4.06				1.98		1.48	0.57	2.60	4.62
0.80	0.18	4.35				1.25		1.14	0.45	2.53	2.56
0.68	0.18	3.74				1.99		1.53	0.64	2.39	4.01
0.68	0.17	4.08				1.82		1.87	0.64	2.92	3.10
1.02	0.21	4.88				1.77		0.73	0.34	2.15	
0.77	0.18	4.24				2.49		1.54	0.55	2.80	
0.71	0.17	4.15				1.62		1.67	0.59	2.83	
0.81	0.12	6.77				2.02		1.49	0.51	2.92	
0.85	0.10	8.39				2.07		1.05	0.41	2.56	
1.09	0.26	4.14				1.61		1.01	0.42	2.40	
0.81	0.16	5.05				2.42		1.31	0.53	2.47	
0.76	0.18	4.11				2.14		1.48	0.51	2.90	
0.84	0.20	4.17				1.35		1.53	0.59	2.59	
0.80	0.21	3.84				1.73		1.36	0.56	2.43	
1.11	0.31	3.58				2.20		1.24	0.52	2.38	
1.02	0.25	4.12				1.86		1.89	0.68	2.78	
0.88	0.15	5.91				1.12		0.96	0.40	2.40	
0.87	0.21	4.24				1.63		0.99	0.40	2.48	
0.98	0.17	5.71				1.41		1.34	0.58	2.31	
0.65	0.17	3.82				1.54		1.15	0.45	2.56	
1.19	0.33	3.62				2.15		1.43	0.62	2.31	
0.88	0.16	5.36				1.49		1.62	0.59	2.75	
0.74	0.16	4.75				1.56		1.72	0.67	2.57	
0.55	0.10	5.73				2.95		0.72	0.30	2.42	
0.62	0.10	6.42				1.82					
1.08	0.14	7.95				2.43					
0.72	0.12	6.16				2.63					
1.11	0.14	8.14				2.52					
1.04	0.18	5.89				1.54					
0.90	0.08	11.54				2.00					
0.63	0.13	4.79				2.30					
						2.18					
						2.19					
						2.08					

Shading scheme identifies sample codes: CEI-28 | Sample #10 | Sample # 46 | Sample #76 | CEI-D-11

Table AVI 5 *Dimensional data for pellets produced by great barracuda. All dimensions are in millimetres.*

Length	Width	Aspect ratio	Length	Width	Aspect ratio	Length	Width	Aspect ratio	Length	Width	Aspect ratio
0.63	0.39	1.60	0.15	0.11	1.40	0.20	0.14	1.39	0.61	0.29	2.08
1.02	0.64	1.59	0.20	0.16	1.23	0.51	0.29	1.79	0.36	0.22	1.66
0.55	0.32	1.72	0.23	0.21	1.11	0.41	0.24	1.67	0.76	0.18	4.30
0.50	0.30	1.65	0.62	0.20	3.14	0.44	0.33	1.31	0.34	0.22	1.57
0.64	0.56	1.14	0.17	0.13	1.30	0.25	0.21	1.20	0.83	0.46	1.78
0.77	0.41	1.89	0.12	0.08	1.55	0.32	0.29	1.09	0.51	0.30	1.67
0.42	0.24	1.75	0.22	0.16	1.36	0.26	0.16	1.63	0.19	0.12	1.67
0.45	0.35	1.28	0.24	0.22	1.13	0.21	0.13	1.59	0.18	0.16	1.13
0.23	0.15	1.53	0.06	0.04	1.55	0.41	0.35	1.19	0.29	0.27	1.09
0.06	0.03	1.99	0.18	0.11	1.63	0.22	0.15	1.44	0.24	0.18	1.35
0.28	0.20	1.43	0.27	0.12	2.16	0.48	0.36	1.34	0.38	0.32	1.18
0.05	0.03	1.57	0.15	0.13	1.16	0.62	0.42	1.47	0.32	0.16	1.94
0.51	0.26	1.97	0.38	0.22	1.75	0.49	0.44	1.13	0.29	0.14	2.05
0.53	0.34	1.56	0.18	0.15	1.17	0.21	0.10	2.03	0.43	0.33	1.29
0.33	0.26	1.25	0.35	0.29	1.21	0.21	0.18	1.21	0.17	0.11	1.59
0.58	0.36	1.60	0.13	0.10	1.27	0.13	0.11	1.17	0.22	0.17	1.26
0.06	0.04	1.44	0.22	0.13	1.68	0.32	0.26	1.21	0.15	0.14	1.09
0.25	0.16	1.54	0.14	0.11	1.32	0.23	0.17	1.31	0.59	0.46	1.30
0.17	0.11	1.45	0.29	0.20	1.48	0.47	0.31	1.54	0.29	0.24	1.20
0.60	0.38	1.57	0.17	0.12	1.43	0.26	0.22	1.22	0.45	0.38	1.20
0.07	0.05	1.33	0.28	0.24	1.18	0.44	0.26	1.71	0.60	0.30	1.99
0.91	0.43	2.12	0.47	0.33	1.41	0.68	0.55	1.24	0.60	0.39	1.53
0.48	0.33	1.46	0.29	0.20	1.46	0.51	0.35	1.46	0.33	0.22	1.50
0.52	0.34	1.54	0.18	0.12	1.49	0.14	0.10	1.34	0.31	0.21	1.47
0.75	0.48	1.55	0.95	0.47	2.01	0.21	0.15	1.44	0.54	0.24	2.27
0.57	0.53	1.09	0.67	0.35	1.94	0.27	0.19	1.42	0.15	0.14	1.12
0.55	0.36	1.52	0.64	0.36	1.77	0.51	0.33	1.54	0.21	0.15	1.35
0.32	0.21	1.49	0.69	0.33	2.09	0.26	0.22	1.16	0.95	0.24	3.90
0.23	0.15	1.56	0.34	0.24	1.44	0.33	0.20	1.65	0.40	0.28	1.45
0.97	0.56	1.73	0.52	0.25	2.09	0.18	0.13	1.35	0.38	0.25	1.53
0.44	0.33	1.33	0.51	0.19	2.67	0.36	0.23	1.58	0.26	0.12	2.09
0.64	0.52	1.23	0.27	0.23	1.14	0.20	0.13	1.59	0.81	0.54	1.50
0.42	0.27	1.54	0.20	0.18	1.09	0.34	0.11	3.07	0.24	0.12	1.91
0.23	0.17	1.39	0.35	0.19	1.91	0.74	0.30	2.44	0.43	0.23	1.87
0.43	0.19	2.27	0.44	0.34	1.29	0.61	0.41	1.48	0.31	0.21	1.44
0.74	0.24	3.12	0.28	0.14	2.02	0.12	0.10	1.23	0.70	0.48	1.46
0.22	0.19	1.14	0.15	0.06	2.32	0.17	0.10	1.76	0.45	0.44	1.01
1.13	0.56	2.02	0.31	0.22	1.39	0.98	0.53	1.83	0.70	0.59	1.18
0.40	0.14	2.83	0.10	0.08	1.23	0.11	0.10	1.19	0.25	0.23	1.08
0.19	0.18	1.08	0.37	0.15	2.47	0.76	0.52	1.46	0.39	0.20	1.98
0.49	0.36	1.34	0.18	0.12	1.54	0.71	0.35	2.01	0.27	0.19	1.44
0.52	0.27	1.90	0.51	0.39	1.30	0.14	0.14	1.02	0.46	0.20	2.26
0.38	0.26	1.43	0.11	0.09	1.21	0.20	0.13	1.52	0.25	0.15	1.60
0.18	0.12	1.49	0.25	0.14	1.72	0.32	0.27	1.19	0.81	0.65	1.25
0.12	0.12	1.08	0.59	0.26	2.22	0.39	0.18	2.19	0.55	0.37	1.50
0.30	0.21	1.42	0.59	0.31	1.94	0.15	0.13	1.20	0.68	0.38	1.76
0.82	0.52	1.58	0.58	0.31	1.85	0.73	0.44	1.68	0.59	0.38	1.56
0.48	0.25	1.93	0.28	0.21	1.32	0.31	0.25	1.25	0.06	0.05	1.33
0.73	0.36	2.02	0.19	0.18	1.10	0.25	0.20	1.23	0.31	0.18	1.78
0.22	0.16	1.32	0.70	0.50	1.40	0.52	0.44	1.18	1.03	0.39	2.61
0.44	0.27	1.60	0.42	0.29	1.42	0.26	0.17	1.49	0.99	0.58	1.71

Table AVI 5 *cont.*

Length	Width	Aspect ratio	Length	Width	Aspect ratio	Length	Width	Aspect ratio	Length	Width	Aspect ratio
0.38	0.34	1.11	0.64	0.40	1.61	0.60	0.39	1.52	0.28	0.17	1.58
0.45	0.43	1.03	0.42	0.26	1.61	0.53	0.30	1.79	0.55	0.43	1.29
0.38	0.12	3.16	0.48	0.41	1.15	0.48	0.33	1.45	0.20	0.17	1.22
0.52	0.35	1.48	0.26	0.18	1.48	0.26	0.25	1.05	0.17	0.14	1.20
0.24	0.12	2.01	0.62	0.29	2.13	0.69	0.39	1.75	0.27	0.16	1.69
0.51	0.43	1.18	0.44	0.29	1.49	0.53	0.26	2.02	0.20	0.15	1.34
0.14	0.12	1.16	0.39	0.27	1.44	0.68	0.47	1.45	0.14	0.11	1.34
0.56	0.50	1.13	0.49	0.34	1.41	0.34	0.26	1.33	0.17	0.11	1.57
0.57	0.30	1.90	0.39	0.36	1.08	0.40	0.26	1.58	0.21	0.10	2.04
0.35	0.29	1.24	1.57	0.89	1.76	0.27	0.17	1.61	0.28	0.24	1.19
0.28	0.12	2.23	0.44	0.30	1.47	0.52	0.41	1.26	0.50	0.44	1.13
0.28	0.21	1.34	0.77	0.49	1.55	1.12	0.59	1.90	0.27	0.20	1.36
0.88	0.46	1.90	0.34	0.30	1.15	0.61	0.38	1.59	0.11	0.08	1.42
0.64	0.32	2.04	0.91	0.54	1.70	0.34	0.23	1.50	0.14	0.12	1.18
0.63	0.36	1.73	0.30	0.25	1.22	0.47	0.26	1.80	0.11	0.07	1.63
0.55	0.36	1.52	0.48	0.37	1.29	0.27	0.19	1.44	0.19	0.14	1.36
0.42	0.19	2.22	0.45	0.28	1.65	0.48	0.29	1.67	0.17	0.16	1.09
0.27	0.24	1.11	0.51	0.44	1.17	0.35	0.24	1.51	0.19	0.12	1.65
0.68	0.48	1.41	0.40	0.25	1.56	0.47	0.25	1.90	0.28	0.15	1.87
0.49	0.27	1.79	0.41	0.20	2.05	0.30	0.18	1.63	0.13	0.08	1.67
0.25	0.16	1.52	0.42	0.26	1.62	0.86	0.55	1.56	0.10	0.10	1.01
0.26	0.18	1.47	0.60	0.39	1.53	0.76	0.35	2.14	0.29	0.22	1.32
0.57	0.24	2.38	0.57	0.49	1.16	0.49	0.36	1.36	0.18	0.16	1.12
0.20	0.13	1.60	0.59	0.40	1.49	0.30	0.19	1.58	0.16	0.10	1.58
0.25	0.18	1.35	1.37	0.45	3.03	0.37	0.20	1.88	0.07	0.06	1.27
0.56	0.24	2.31	0.61	0.34	1.80	0.53	0.35	1.53	0.40	0.21	1.87
0.46	0.21	2.16	0.50	0.30	1.69	0.30	0.22	1.36	0.17	0.10	1.64
0.55	0.34	1.60	0.42	0.32	1.31	0.25	0.17	1.44	0.06	0.04	1.35
0.43	0.24	1.80	0.89	0.41	2.18	0.13	0.10	1.35	0.20	0.14	1.39
0.16	0.11	1.49	0.64	0.33	1.94	1.14	0.57	1.98	0.28	0.11	2.54
0.72	0.48	1.51	0.46	0.29	1.58	0.82	0.47	1.74	0.17	0.15	1.17
0.23	0.18	1.26	0.44	0.37	1.21	0.42	0.28	1.53	0.07	0.07	1.10
0.34	0.24	1.43	0.65	0.52	1.25	0.73	0.38	1.94	0.24	0.18	1.38
0.32	0.24	1.35	0.40	0.28	1.46	0.74	0.35	2.12	0.13	0.10	1.29
0.60	0.48	1.26	0.24	0.22	1.08	0.44	0.29	1.52	0.17	0.10	1.58
0.28	0.18	1.59	0.49	0.29	1.72	0.35	0.30	1.15	0.18	0.09	1.86
0.40	0.26	1.56	0.11	0.08	1.33	0.32	0.31	1.05	0.30	0.19	1.56
0.56	0.24	2.33	0.21	0.16	1.29	0.63	0.28	2.24	0.17	0.13	1.29
0.61	0.37	1.62	0.96	0.76	1.26	0.42	0.28	1.48	0.43	0.22	1.94
0.70	0.26	2.70	0.14	0.11	1.29	0.55	0.24	2.36	0.21	0.13	1.65
0.90	0.65	1.37	0.11	0.10	1.15	0.35	0.21	1.67	0.65	0.34	1.92
0.93	0.35	2.67	0.13	0.09	1.47	0.50	0.36	1.39	0.18	0.17	1.06
0.53	0.32	1.68	0.46	0.37	1.26	0.21	0.11	1.80	0.20	0.13	1.55
1.26	0.74	1.70	0.27	0.17	1.65	0.36	0.33	1.10	0.47	0.31	1.48
0.15	0.11	1.35	0.13	0.10	1.28	0.53	0.34	1.59	0.14	0.11	1.26
0.51	0.31	1.64	0.05	0.03	1.71	0.49	0.21	2.29	0.20	0.17	1.14
0.42	0.31	1.36	0.20	0.16	1.29	0.42	0.18	2.30	0.28	0.16	1.74
0.56	0.42	1.33	0.25	0.18	1.35	0.28	0.24	1.14	0.23	0.17	1.35
0.81	0.54	1.49	0.29	0.22	1.36	0.36	0.26	1.37	0.47	0.25	1.84
0.40	0.21	1.94	0.34	0.22	1.52	0.28	0.25	1.13	0.34	0.28	1.19
0.64	0.40	1.60	0.43	0.31	1.41	0.30	0.22	1.38	0.22	0.17	1.27

Table AVI 5 *cont.*

Length	Width	Aspect ratio	Length	Width	Aspect ratio
0.22	0.16	1.41	0.39	0.36	1.07
0.85	0.45	1.87	0.64	0.24	2.62
0.18	0.12	1.50	0.32	0.25	1.25
0.61	0.27	2.22	0.44	0.25	1.72
0.24	0.17	1.42	0.28	0.21	1.36
0.17	0.10	1.73	0.83	0.44	1.89
0.13	0.09	1.47	0.99	0.60	1.64
0.81	0.30	2.72	0.83	0.47	1.76
0.52	0.42	1.22	0.71	0.44	1.63
0.38	0.20	1.86	1.09	0.41	2.66
0.15	0.12	1.31	1.09	0.32	3.39
0.34	0.28	1.22	0.78	0.52	1.50
0.25	0.17	1.51	0.87	0.42	2.09
0.38	0.24	1.59	0.82	0.52	1.59
0.25	0.14	1.78	0.29	0.12	2.46
0.28	0.20	1.40	0.90	0.38	2.38
0.29	0.19	1.53	1.74	0.61	2.84
0.51	0.37	1.35	0.88	0.49	1.81
0.26	0.22	1.17	0.66	0.58	1.14
0.19	0.13	1.50	0.74	0.36	2.04
0.21	0.12	1.76	0.59	0.32	1.83
0.19	0.18	1.06	0.50	0.40	1.26
0.14	0.12	1.13	0.10	0.07	1.49
0.35	0.18	2.01	0.62	0.43	1.43
0.18	0.13	1.42	0.50	0.27	1.83
0.29	0.23	1.27	0.68	0.34	2.03
0.26	0.18	1.47	0.25	0.19	1.37
0.13	0.12	1.15	0.96	0.44	2.20
0.35	0.18	1.91	0.14	0.12	1.14
0.34	0.19	1.82	0.67	0.49	1.36
0.29	0.22	1.32	0.61	0.36	1.67
0.15	0.14	1.12	0.16	0.13	1.26
0.32	0.27	1.17	0.61	0.34	1.82
0.23	0.13	1.82	0.54	0.45	1.22
0.38	0.30	1.25	0.40	0.28	1.42
0.32	0.27	1.19	0.70	0.34	2.07
0.39	0.29	1.35	0.30	0.24	1.24
0.29	0.19	1.52	0.49	0.26	1.90
0.27	0.21	1.32	0.64	0.48	1.32
0.33	0.29	1.13	0.25	0.16	1.55
0.50	0.29	1.70	0.32	0.25	1.28
0.49	0.31	1.59	0.12	0.10	1.24
0.29	0.25	1.18			
0.45	0.34	1.32			
0.61	0.54	1.13			
0.54	0.41	1.31			
0.76	0.46	1.65			
0.64	0.37	1.73			
1.27	0.79	1.61			
0.47	0.28	1.66			
0.51	0.43	1.19			

Table AVI 6 *Summary statistics for all pellets and crystal forms produced by great barracuda. All values are given in micrometers and refer to the longest axes unless specified otherwise.*

	Pellet length	Pellet width	Sml dmbl	Fib/nee	Lrg dmbl	N/sphere	N/sphere dbl	Rhomb	M. ellip	Rosette
count	501	501	240	44	10	270	47	1	37	17
min	50	30	0.94	0.55	8.39	0.39	1.12	2.08	0.51	0.92
d10	**150**	**110**	**1.64**	**0.68**	**13.53**	**0.67**	**1.47**	**2.08**	**0.73**	**0.95**
Median	***380***	***240***	***2.56***	***0.88***	***15.07***	***0.92***	***1.98***	***2.08***	***1.31***	***1.11***
d90	**740**	**460**	**3.44**	**1.46**	**16.75**	**1.25**	**2.42**	**2.08**	**1.67**	**3.47**
max	590	350	4.43	2.91	16.94	2.38	2.95	2.08	1.89	4.62
d90-d10	1740	890	1.80	0.78	3.22	0.58	0.95	0.00	0.95	2.52
Mean	421	266	2.54	1.04	14.70	0.95	1.93	2.08	1.25	1.69
SD	248	138	0.70	0.46	2.44	0.25	0.38	N/a	0.37	1.16
SE of mean	11	6	0.05	0.07	0.77	0.02	0.06	N/a	0.06	0.28

Table AVI 7 *Dimensional data for rhombohedral crystal forms produced by bluehead wrasse. All dimensions are in micrometers. Shading scheme differentiates between data from different samples (see footnote for key).*

Rhomb (length)	Rhomb (length)	Rhomb (length)	Rhomb (length)	Rhomb (length)	Rhomb (length)	Rhomb (length)
0.97	14.63	6.68	18.05	8.94	10.98	16.49
0.85	9.35	5.79	10.92	9.12	10.85	11.37
7.85	10.95	3.89	9.50	13.07	5.58	13.55
4.02	9.17	10.85	12.58	4.73	13.61	10.90
12.45	10.53	14.20	12.76	9.33	7.01	9.17
6.67	6.27	7.41	4.72	10.29	7.16	15.11
8.06	6.83	17.12	8.78	11.79	4.05	12.51
8.83	7.20	6.96	5.16	9.85	7.86	12.64
10.45	6.37	10.88	9.89	10.80	11.84	9.30
10.96	7.64	12.00	10.30	10.09	9.48	11.77
11.96	7.89	10.55	7.90	11.63	8.13	6.10
8.94	9.96	12.01	11.08	11.66	8.68	11.05
7.81	5.95	17.11	8.87	7.59	8.41	10.98
8.09	7.32	9.87	8.86	12.53	12.66	6.69
11.17	6.54	6.50	6.07	10.71	8.50	13.23
4.77	6.20	15.78	12.55	7.26	9.56	14.20
8.46	5.95	14.99	16.59	8.76	4.41	6.32
11.91	4.37	14.56	13.40	6.93	12.18	12.39
10.41	7.08	15.79	9.74	8.01	7.43	13.46
8.92	5.61	13.24	9.36	10.95	9.49	
6.35	6.19	17.85	9.34	8.30	5.76	
14.24	9.98	7.95	9.46	11.10	3.67	
13.25	6.10	15.76	7.89	9.37	10.37	
8.54	11.73	18.44	13.27	11.45	12.25	
6.65	12.30	13.46	8.64	15.10	8.59	
7.39	14.09	10.45	6.54	11.23	9.01	
10.46	8.83	14.87	12.07	13.17	8.64	
7.73	5.98	21.09	13.34	9.38	8.80	
14.44	5.05	5.42	7.41	10.06	8.51	
13.30	6.37	13.18	6.12	9.24	9.03	
10.00	7.45	16.63	10.89	13.13	14.05	
13.70	6.46	12.50	11.13	9.58	8.68	
10.90	11.60	14.78	8.46	10.25	6.18	
12.10	12.47	12.01	16.69	10.83	19.77	
10.90	6.22	17.83	9.13	10.50	10.06	
7.30	15.42	8.87	13.78	9.88	8.11	
11.40	12.33	14.48	9.51	15.92	10.59	
12.70	10.71	9.98	8.95	8.87	9.64	
12.60	7.80	9.66	8.61	12.40	5.28	
11.30	11.33	7.70	5.87	10.36	11.72	
9.80	15.78	8.01	11.30	9.76	9.07	
8.10	4.05	17.07	8.53	14.59	14.77	
10.30	5.44	3.41	10.92	11.20	7.09	
11.50	5.94	6.30	3.72	12.19	10.68	
10.90	5.58	13.31	8.50	10.85	12.45	
9.20	5.27	12.39	8.59	11.67	16.41	
10.30	10.70	10.71	10.14	12.49	8.74	
9.70	5.75	13.73	9.72	14.94	11.37	
10.10	5.05	7.33	10.30	10.54	9.26	
6.10	9.57	11.08	11.17	9.07	13.92	

Shading scheme identifies sample codes: CE-10-1 | CE-10-2 | CE-10-21 | CE-10-22 | CE-10-27

Table AVI 8 *Dimensional data for subsidiary crystal forms and particle clusters produced by bluehead wrasse. All dimensions are in micrometers. Shading scheme differentiates between data from different samples (see footnote for key).*

Lrg dmbl (length)	Sphere (diameter)	Sphere (diameter)	Particle cluster (length)
11.58	18.59	14.77	47.10
4.40	13.32	6.49	24.60
5.69	10.07	12.23	23.40
5.01	16.53	11.26	37.30
9.37	18.88	10.38	46.20
11.41	18.02	11.90	16.50
7.51	8.98	11.86	24.80
9.93	8.25	9.46	15.25
13.99	11.96	18.71	14.00
18.12	13.22	24.29	17.40
16.10	13.69	28.45	25.50
17.77	12.38	19.31	18.80
11.50	13.40	8.87	15.80
8.90	12.51	14.82	34.00
10.00	15.28	10.23	14.83
7.08	8.90	12.74	9.10
13.01	12.50	12.21	8.28
5.89	6.33	9.61	33.10
7.11	12.90	14.56	16.38
6.47	17.33	24.52	16.55
11.74	11.00	15.60	17.20
11.95	8.43	13.67	41.10
11.58	9.00	12.57	29.73
8.59	18.06	25.33	34.37
	6.39	15.56	73.00
	9.86	9.42	39.70
	15.46	17.58	17.76
	16.06	22.86	22.68
	15.82	19.23	25.12
	7.50	14.03	37.13
	9.90	14.73	29.49
	10.50	19.21	24.51
	12.16	19.25	19.93
	13.99	13.35	36.19
	13.69		30.48
	14.09		28.20
	11.88		52.32
	12.30		29.54
	7.74		38.43
	13.94		14.84
	12.72		49.50
	11.41		23.99
	8.74		18.18
	10.50		8.29

Shading scheme identifies sample codes: CE-10-1 | CE-10-2 | CE-10-21 | CE-10-22 | CE-10-27

Table AVI 9 *Dimensional data for pellets produced by bluehead wrasse. All dimensions are in millimetres.*

Length	Width	Aspect ratio	Length	Width	Aspect ratio	Length	Width	Aspect ratio	Length	Width	Aspect ratio
0.74	0.27	2.78	0.11	0.08	1.33	0.54	0.44	1.24	0.41	0.30	1.34
0.43	0.29	1.50	0.09	0.08	1.06	0.60	0.41	1.47	0.78	0.63	1.24
0.62	0.43	1.43	0.39	0.28	1.38	0.55	0.40	1.37	0.40	0.28	1.42
0.58	0.42	1.35	0.38	0.31	1.22	0.67	0.58	1.15	0.18	0.11	1.61
0.57	0.42	1.36	0.60	0.39	1.53	0.43	0.32	1.32	0.78	0.52	1.51
0.44	0.27	1.63	0.39	0.27	1.45	0.44	0.36	1.23	0.40	0.35	1.13
1.02	0.72	1.41	0.11	0.07	1.52	0.83	0.74	1.13	0.34	0.28	1.22
0.64	0.34	1.87	0.13	0.08	1.60	0.34	0.29	1.17	0.29	0.22	1.33
0.60	0.39	1.54	0.27	0.19	1.45	0.55	0.44	1.23	0.13	0.06	2.16
0.46	0.36	1.28	0.11	0.09	1.17	0.62	0.39	1.58	0.90	0.53	1.68
0.81	0.42	1.93	0.38	0.30	1.28	0.76	0.30	2.56	0.69	0.47	1.48
0.96	0.39	2.47	0.09	0.06	1.50	1.31	0.77	1.70	0.32	0.30	1.07
0.87	0.44	1.98	0.89	0.69	1.28	0.80	0.46	1.74	1.29	0.73	1.75
0.75	0.59	1.26	0.55	0.32	1.70	0.60	0.48	1.27	0.74	0.48	1.53
0.68	0.62	1.10	0.43	0.42	1.01	0.75	0.53	1.42	0.56	0.39	1.44
1.27	0.62	2.07	0.41	0.33	1.26	0.72	0.59	1.24	0.13	0.12	1.09
0.86	0.65	1.33	0.52	0.26	2.01	0.55	0.38	1.44	0.45	0.26	1.74
0.33	0.29	1.11	0.14	0.05	3.06	0.38	0.25	1.50	0.17	0.15	1.15
0.18	0.14	1.26	0.33	0.27	1.23	0.66	0.55	1.21	0.15	0.07	2.12
0.67	0.52	1.28	1.02	0.58	1.75	0.12	0.08	1.47	0.23	0.20	1.15
0.34	0.30	1.12	0.14	0.13	1.03	0.28	0.16	1.74	0.34	0.27	1.29
0.64	0.37	1.74	0.25	0.19	1.36	0.36	0.24	1.49	0.12	0.11	1.11
0.31	0.25	1.24	0.09	0.08	1.16	0.11	0.08	1.36	0.78	0.60	1.30
0.72	0.43	1.67	0.09	0.06	1.46	1.08	0.47	2.33	1.10	0.51	2.15
0.54	0.40	1.33	0.20	0.18	1.16	1.11	0.64	1.72	0.82	0.49	1.68
0.94	0.41	2.29	0.47	0.22	2.11	1.17	0.41	2.88	0.85	0.59	1.44
1.02	0.46	2.20	0.30	0.28	1.09	0.83	0.69	1.22	0.33	0.25	1.30
0.83	0.49	1.70	0.57	0.42	1.34	1.04	0.43	2.39	0.40	0.35	1.16
1.19	0.87	1.37	0.16	0.13	1.19	1.05	0.58	1.81	0.19	0.16	1.23
0.91	0.68	1.33	0.45	0.37	1.21	0.22	0.16	1.40	0.36	0.29	1.21
0.50	0.42	1.18	0.89	0.58	1.54	0.31	0.30	1.01	0.36	0.28	1.29
0.75	0.69	1.08	0.08	0.06	1.22	0.40	0.35	1.15	0.43	0.34	1.26
0.07	0.05	1.27	0.76	0.57	1.35	1.15	0.60	1.92	0.39	0.34	1.14
0.43	0.36	1.20	0.55	0.46	1.18	0.57	0.45	1.25	0.40	0.28	1.47
0.82	0.42	1.94	1.99	0.66	3.02	0.29	0.23	1.27	0.10	0.08	1.34
0.54	0.35	1.54	0.07	0.05	1.43	0.63	0.39	1.60	0.55	0.28	1.96
0.61	0.51	1.20	0.74	0.40	1.87	0.50	0.35	1.45	0.88	0.67	1.31
0.48	0.43	1.12	0.38	0.35	1.11	0.75	0.31	2.40	0.70	0.38	1.83
0.65	0.42	1.54	0.76	0.74	1.03	0.88	0.39	2.23	0.82	0.50	1.65
0.29	0.20	1.45	0.41	0.31	1.31	0.48	0.30	1.59	0.90	0.77	1.18
0.15	0.08	1.80	0.77	0.50	1.54	1.44	0.68	2.11	0.43	0.31	1.39
0.09	0.07	1.20	0.74	0.34	2.18	0.59	0.39	1.52	0.79	0.53	1.48
0.23	0.15	1.55	0.54	0.35	1.56	0.48	0.40	1.18	0.71	0.37	1.92
0.10	0.06	1.72	0.71	0.46	1.55	0.64	0.38	1.68	0.69	0.43	1.63
0.28	0.25	1.09	0.49	0.29	1.72	0.48	0.28	1.73	0.81	0.72	1.13
0.77	0.45	1.71	0.30	0.22	1.35	0.33	0.24	1.35	0.68	0.48	1.42
0.14	0.08	1.70	0.10	0.08	1.31	0.90	0.66	1.36	0.70	0.45	1.56
0.57	0.41	1.38	0.37	0.22	1.70	0.49	0.36	1.35	0.44	0.28	1.57
0.54	0.44	1.24	0.36	0.17	2.12	0.62	0.48	1.29	1.02	0.58	1.75
0.11	0.09	1.21	0.28	0.22	1.25	0.20	0.19	1.05	0.72	0.52	1.39
0.09	0.07	1.34	0.61	0.36	1.69	0.67	0.54	1.24	0.82	0.55	1.49

Table AVI 9 *cont.*

Length	Width	Aspect ratio	Length	Width	Aspect ratio	Length	Width	Aspect ratio
0.41	0.34	1.19	0.36	0.32	1.13	0.70	0.70	1.01
0.45	0.37	1.24	0.79	0.61	1.30	0.99	0.46	2.16
0.57	0.54	1.06	1.00	0.63	1.59	0.58	0.48	1.21
0.12	0.07	1.74	0.52	0.40	1.29	0.71	0.61	1.17
0.80	0.54	1.47	0.36	0.33	1.07	0.86	0.59	1.44
0.95	0.42	2.27	0.36	0.32	1.13	0.86	0.40	2.14
0.67	0.48	1.41	0.74	0.36	2.09	1.20	0.67	1.80
0.37	0.31	1.19	0.22	0.16	1.42	1.10	0.59	1.87
0.76	0.50	1.52	0.47	0.32	1.46	0.51	0.41	1.23
0.48	0.24	1.99	0.52	0.42	1.24	0.36	0.27	1.36
0.86	0.53	1.60	0.59	0.35	1.68	0.42	0.30	1.40
0.55	0.39	1.40	0.50	0.34	1.47	0.21	0.19	1.14
0.76	0.47	1.61	1.06	0.45	2.35	0.44	0.25	1.77
0.86	0.71	1.20	1.35	0.63	2.15	0.38	0.35	1.10
0.75	0.51	1.48	1.02	0.69	1.47	0.35	0.31	1.12
0.59	0.36	1.64	0.70	0.46	1.53	0.53	0.47	1.13
0.31	0.28	1.08	0.23	0.10	2.25	0.45	0.35	1.27
0.12	0.11	1.12	0.34	0.21	1.60	0.86	0.70	1.23
0.83	0.40	2.08	0.67	0.46	1.44	0.76	0.65	1.17
0.41	0.27	1.50	0.53	0.46	1.14	0.32	0.26	1.22
0.32	0.27	1.20	0.43	0.33	1.30	0.26	0.17	1.55
0.41	0.31	1.30	0.68	0.50	1.36	0.38	0.23	1.65
0.40	0.29	1.39	0.46	0.35	1.30	0.08	0.08	1.10
0.32	0.23	1.41	0.49	0.33	1.47	0.61	0.34	1.82
0.78	0.48	1.62	0.67	0.34	1.99	0.49	0.36	1.38
0.41	0.24	1.70	0.44	0.38	1.14	0.23	0.22	1.04
0.51	0.24	2.09	0.41	0.31	1.32	0.35	0.20	1.73
0.42	0.23	1.78	0.39	0.28	1.43	0.53	0.29	1.86
0.40	0.26	1.56	1.17	0.83	1.41	0.75	0.47	1.59
0.10	0.08	1.25	1.27	0.97	1.31	0.93	0.42	2.24
0.75	0.60	1.25	1.64	0.82	2.00	0.20	0.08	2.37
0.42	0.37	1.13	1.13	0.55	2.06	0.18	0.08	2.30

Table AVI 10 *Summary statistics for all pellets and crystal forms produced by bluehead wrasse. All values are given in micrometers and refer to the longest axes unless specified otherwise.*

	Pellet length	Pellet width	Rhomb	Lrg dmbl	Sphere	Particle cluster
count	300	300	319	24	78	44
min	70	50	0.85	4.40	6.33	8.28
d10	**150**	**109**	**6.05**	**5.75**	**8.83**	**14.83**
Median	***520***	***360***	***9.98***	***9.96***	***12.82***	***24.70***
d90	**941**	**621**	**14.28**	**15.46**	**19.22**	**44.67**
max	1990	970	21.09	18.12	28.45	73.00
d90-d10	791	512	8.22	9.71	10.39	29.84
Mean	558	371	10.06	10.19	13.63	27.29
SD	308	182	3.27	3.81	4.50	13.30
SE of mean	18	10	0.18	0.78	0.51	2.00

Table AVI 11 *Dimensional data for nanospheres produced by bonefish. All dimensions are in micrometers. Shading scheme differentiates between data from different samples (see footnote for key).*

N/spheres	N/spheres	N/spheres	N/spheres	N/spheres	N/spheres	N/spheres	N/spheres	N/spheres	N/spheres
0.92	0.35	0.45	0.16	0.25	0.55	0.19	0.51	0.32	0.44
0.31	0.36	0.55	0.35	0.17	0.25	0.31	0.24	0.28	0.34
0.65	0.90	0.44	0.22	0.29	0.45	0.27	0.23	0.29	0.42
0.38	0.55	0.24	0.77	0.25	0.37	0.34	0.42	0.30	0.31
0.24	0.50	0.27	0.33	0.31	0.34	0.31	0.29	0.23	0.17
0.34	1.00	0.30	0.22	0.45	0.49	0.25	0.28	0.33	0.47
0.92	0.32	0.28	0.68	0.37	0.50	0.30	0.44	0.25	0.31
0.72	0.34	0.32	0.22	0.46	0.39	0.17	0.20	0.22	0.36
0.46	0.44	0.31	0.41	0.41	0.34	0.17	0.40	0.21	0.25
0.38	0.58	0.30	0.34	0.49	0.53	0.43	0.32	0.44	0.31
0.34	0.44	0.22	0.28	0.22	0.26	0.21	0.27	0.20	0.30
0.42	0.46	0.20	0.20	0.53	0.25	0.22	0.30	0.30	0.28
0.45	0.31	0.72	0.22	0.62	0.88	0.29	0.26	0.28	0.24
0.51	0.73	0.30	0.17	0.36	0.25	0.31	0.22	0.21	0.50
0.49	0.61	0.38	0.17	0.41	0.57	0.23	0.26	0.23	0.23
0.37	0.23	0.29	0.32	0.40	0.63	0.17	0.85	0.22	0.23
0.33	1.17	0.27	0.29	0.38	0.91	0.17	1.00	0.50	0.25
0.25	0.20	0.19	0.23	0.36	0.48	0.41	0.98	0.31	0.32
0.44	0.31	0.36	0.41	0.48	0.55	0.55	0.72	0.18	0.28
0.60	0.77	0.27	0.28	0.46	0.63	0.30	0.59	0.43	0.37
0.47	0.20	0.38	0.27	0.58	0.31	0.48	0.73	0.26	0.28
0.53	0.17	0.80	0.20	0.33	0.28	0.32	0.68	0.22	0.38
0.36	0.74	0.32	0.28	0.24	0.23	0.41	0.86	0.24	0.23
0.24	0.29	0.39	0.21	0.35	0.33	0.25	0.45	0.34	0.32
0.37	0.48	0.87	0.16	0.63	0.33	0.34	0.20	0.30	0.26
0.22	0.31	0.70	0.10	0.56	0.48	0.29	0.89	0.23	0.28
0.31	0.64	0.81	0.31	0.26	0.25	0.29	0.29	0.32	0.35
0.38	0.61	0.87	0.21	0.95	0.50	0.30	0.26	0.30	0.34
0.48	0.23	0.60	0.58	0.32	0.88	0.26	0.37	0.39	
0.24	0.27	0.34	0.59	0.39	0.40	0.28	0.39	0.22	
0.25	0.31	0.40	0.22	0.37	0.67	0.51	0.35	0.29	
0.47	0.22	0.40	0.19	0.42	0.33	0.44	0.42	0.26	
0.88	0.26	0.26	0.18	0.84	0.25	0.31	0.53	0.34	
0.60	0.35	0.33	0.24	0.59	0.35	0.25	0.45	0.25	
0.48	0.32	0.76	0.30	0.85	0.26	0.19	0.33	0.36	
0.63	0.33	0.38	0.45	0.24	0.23	0.23	0.26	0.39	
0.50	0.25	0.39	0.19	0.46	0.41	0.64	0.35	0.39	
0.36	0.48	0.38	0.67	0.22	0.34	0.18	0.43	0.29	
0.57	0.22	0.78	0.39	0.36	0.24	0.35	0.49	0.33	
0.55	0.85	0.34	0.12	0.39	0.17	0.22	0.30	0.31	
0.37	0.19	0.27	0.87	0.24	0.23	0.33	0.26	0.42	
0.40	0.34	0.24	0.48	0.28	0.19	0.27	0.33	0.28	
0.24	0.32	0.25	0.29	0.45	0.24	0.20	0.32	0.29	
0.24	0.43	0.35	0.17	0.53	0.20	0.24	0.32	0.32	
0.59	0.37	0.35	0.33	0.33	0.36	0.28	0.36	0.32	
0.69	0.32	0.32	0.46	0.26	0.47	0.33	0.23	0.25	
0.92	0.35	0.18	0.34	0.79	0.29	0.26	0.18	0.40	

Shading scheme identifies sample codes: Bon-D68, CEI-D7, CEI-D4, CE Sample #48, Bon-ST68, Bon-1-11, Bon-2-11, Bon-3-11

Table AVI 12 *Dimensional data for spheres produced by bonefish. All dimensions are in micrometers. Shading scheme differentiates between data from different samples (see footnote for key).*

Sphere	Sphere	Sphere	Sphere	Sphere	Sphere	Sphere
10.80	18.01	22.04	12.62	9.74	15.70	16.05
10.19	23.43	14.71	9.07	14.65	17.95	15.81
12.69	23.08	17.93	12.01	19.17	14.12	14.31
14.01	10.52	16.33	11.72	14.57	17.03	8.29
11.03	8.46	19.51	15.46	15.69	18.60	18.12
21.30	12.75	20.70	11.62	15.55	7.51	18.60
26.51	7.97	18.57	13.98	17.38	12.52	20.88
16.82	15.30	18.62	15.34	24.22	12.46	17.04
19.44	15.34	17.45	14.66	18.74	17.58	22.24
18.46	11.12	17.34	14.71	12.58	15.73	22.89
22.82	13.50	17.93	13.44	24.10	16.61	20.60
19.87	11.50	16.13	12.17	19.23	16.63	15.08
18.84	8.60	20.78	16.11	16.84	11.02	16.73
26.47	7.49	19.76	14.06	12.53	20.08	15.59
23.99	19.82	15.32	16.69	16.32	8.97	14.31
26.93	13.24	19.42	21.32	10.18	18.09	16.36
9.72	8.63	14.67	18.04	45.33	16.21	12.40
10.29	16.21	15.48	21.71	32.41	15.50	18.32
8.37	14.18	14.29	19.17	35.07	14.62	5.70
7.75	16.42	17.33	19.14	26.00	15.49	6.40
7.30	6.43	20.12	21.96	21.68	12.67	4.80
11.72	5.44	17.78	20.29	11.91	13.65	17.17
9.36	5.44	28.30	15.54	33.93	22.48	19.84
12.02	5.27	19.40	20.32	41.98	23.70	16.82
9.85	6.84	19.91	19.37	38.53	16.20	16.57
30.65	6.82	17.26	14.71	38.26	28.73	17.75
18.78	6.20	16.14	12.91	23.18	17.45	18.93
12.40	6.12	18.59	13.75	27.84	12.32	19.91
13.93	4.53	20.36	18.38	27.23	12.44	16.67
11.90	12.55	19.02	16.44	25.16	15.00	19.60
16.35	16.07	10.20	17.96	23.26	12.32	15.63
16.64	17.10	16.92	18.93	30.50	12.40	
20.06	12.67	16.29	17.27	34.18	13.61	
12.40	10.26	15.27	15.92	11.71	15.19	
12.40	14.10	17.46	15.85	16.31	15.36	
16.64	15.41	17.55	23.60	30.42	12.27	
22.03	11.00	13.52	15.21	17.48	17.91	
15.69	17.83	16.42	18.93	17.47	13.29	
12.02	14.76	18.74	18.38	20.62	14.09	
12.40	13.90	20.13	16.23	17.55	11.98	
19.70	12.92	16.55	19.92	13.94	12.38	
13.15	12.66	18.35	17.27	19.09	12.00	
20.70	11.19	16.43	16.55	18.96	15.75	
13.76	8.58	17.56	20.79	17.04	23.78	
16.35	17.91	15.76	15.94	14.30	26.38	
14.51	9.60	16.07	12.70	19.73	16.69	
29.19	9.64	20.69	14.02	16.35	18.27	

Shading scheme identifies sample codes:

Bon-D68	CEI-D7	CEI-D4	CE Sample #48	Bon-ST68
Bon-1-11	Bon-2-11	Bon-3-11		

Table AVI 13 *Dimensional data for subsidiary crystal forms produced by bonefish. All dimensions are in micrometers. Shading scheme differentiates between data from different samples (see footnote for key).*

Sph clust	Sph clust	N/sphere clust	N/sphere clust	N/sphere clust	Fib/nee	Fib/nee	Fib/nee
26.21	31.20	21.52	4.00	6.20	1.14	0.58	5.02
38.94	112.90	13.09	3.60	15.61	1.97	0.54	3.28
61.58	41.80	5.15	3.90	2.64	0.81	1.42	3.19
45.51	25.40	4.17	1.60	3.11	0.69	0.49	2.93
26.43	37.90	5.19	2.00	2.43	0.75	0.62	2.89
11.66	58.10	0.62	5.40	4.53	0.88	0.63	5.21
25.15	78.80	14.90	2.20	2.46	1.11	1.02	6.05
36.50	23.20	8.40	5.10	4.82	0.68	1.17	4.38
46.13	19.90	1.70	7.70	4.41	0.56	0.66	3.83
45.64	23.70	9.10	6.60	5.06	0.39	1.51	3.39
98.86	39.90	2.73	10.30	6.76	0.73	0.99	3.23
121.40	176.60	3.10	0.95	10.97	0.88	0.56	2.64
96.01	106.10	2.38	2.90	11.39	1.03	0.62	3.25
82.80	100.70	2.00	15.60	16.04	1.15	3.83	2.89
80.30	28.80	15.40	0.80		2.22	4.11	4.42
93	39.70	24.00	2.10		0.86	4.48	4.86
59.80	135.60	3.24	2.00		1.40	5.06	3.75
41.10		4.61	6.00		0.67	2.23	4.70
67.20		3.90	5.00		1.52	2.90	6.16
85.91		1.20	3.00		1.70	3.00	4.59
82.40		3.12	2.60		0.82	5.75	1.97
74.91		1.12	2.20		0.59	3.80	2.72
33.00		1.50	1.20		0.48	3.53	4.51
28.10		6.40	4.00		1.23	6.34	2.51
18.90		0.40	4.30		0.47	3.02	2.38
28.00		4.20	7.90		0.67	2.60	
38.70		2.70	3.10		0.24	2.19	
17.80		4.30	5.20		0.61	6.24	
31.90		3.90	12.30		0.77	2.64	
22.30		2.05	1.80		0.51	2.17	
42.10		2.60	3.50		0.49	2.22	
72.80		4.10	2.80		0.49	4.01	
23.93		10.10	0.30		0.70	8.75	
12.60		2.90	0.20		0.54	3.16	
86.70		1.03	0.90		0.68	4.03	
121.90		1.20	9.80		0.48	6.59	
74.50		1.81	5.80		1.32	2.97	
81.20		0.90	2.10		0.60	1.95	
102.40		6.90	2.40		0.29	2.40	
44.80		3.90	1.20		0.36	3.44	
102.20		2.00	2.00		0.88	2.95	
35.86		1.90	2.30		0.79	3.04	
49.60		2.10	0.70		0.67	4.33	
57.15		3.40	6.50		1.58	1.98	
29.20		3.20	1.50		0.74	5.13	
31.60		11.30	2.60		1.44	3.53	
70.30		4.10	2.40		0.70	4.35	

Shading scheme identifies sample codes:

Bon-D68	CEI-D7	CEI-D4	CE Sample #48	Bon-ST68
Bon-1-11	Bon-2-11	Bon-3-11		

Table AVI 14 *Dimensional data for pellets produced by bonefish. All dimensions are in millimetres.*

Length	Width	Aspect ratio	Length	Width	Aspect ratio	Length	Width	Aspect ratio	Length	Width	Aspect ratio
1.79	1.60	1.12	2.04	1.38	1.48	0.58	0.41	1.41	0.87	0.73	1.19
1.07	0.81	1.32	1.55	1.16	1.34	0.26	0.20	1.33	0.16	0.07	2.24
2.10	1.32	1.59	1.70	1.16	1.46	0.20	0.17	1.20	0.66	0.48	1.38
1.48	1.13	1.31	0.83	0.64	1.30	0.28	0.22	1.31	0.48	0.34	1.42
2.07	1.07	1.93	0.52	0.45	1.14	0.28	0.18	1.59	0.31	0.27	1.15
1.49	1.00	1.49	0.18	0.11	1.65	0.43	0.23	1.85	0.66	0.47	1.40
2.45	1.55	1.58	0.49	0.30	1.66	0.46	0.38	1.22	0.86	0.80	1.07
0.99	0.94	1.05	1.16	0.82	1.42	0.30	0.19	1.64	1.11	0.80	1.39
1.29	1.06	1.22	1.87	1.48	1.26	0.16	0.10	1.66	0.29	0.25	1.15
1.22	0.97	1.26	1.02	0.64	1.61	0.54	0.43	1.24	0.16	0.09	1.77
0.97	0.57	1.70	0.14	0.12	1.13	0.16	0.13	1.20	1.00	0.61	1.63
1.50	1.09	1.37	0.62	0.47	1.32	0.11	0.08	1.41	1.02	0.79	1.28
1.36	1.04	1.31	0.22	0.19	1.18	0.09	0.07	1.23	1.00	0.78	1.28
0.84	0.60	1.39	0.41	0.28	1.48	0.65	0.57	1.14	1.09	0.84	1.29
1.23	0.70	1.75	0.45	0.33	1.37	0.31	0.17	1.80	1.02	0.63	1.63
0.11	0.08	1.37	0.40	0.31	1.30	0.27	0.15	1.73	1.09	0.86	1.26
1.10	0.85	1.29	0.12	0.10	1.14	0.21	0.19	1.14	1.58	1.09	1.44
0.42	0.37	1.12	0.19	0.16	1.16	0.41	0.32	1.28	1.57	1.18	1.33
1.06	0.87	1.22	0.16	0.10	1.57	0.23	0.16	1.45	1.50	1.12	1.34
0.67	0.45	1.50	0.21	0.16	1.38	0.09	0.07	1.25	0.28	0.18	1.55
0.94	0.62	1.51	0.12	0.09	1.28	0.16	0.11	1.39	0.45	0.28	1.60
0.58	0.54	1.08	0.28	0.23	1.23	0.17	0.10	1.67	1.00	0.83	1.20
0.42	0.26	1.59	0.37	0.27	1.36	0.35	0.31	1.14	0.48	0.27	1.75
0.22	0.10	2.19	0.19	0.15	1.24	0.29	0.23	1.23	0.85	0.81	1.05
0.41	0.22	1.87	0.18	0.12	1.46	0.45	0.40	1.13	1.10	0.74	1.49
0.11	0.06	1.72	0.45	0.25	1.79	0.16	0.09	1.78	0.93	0.55	1.70
1.09	0.80	1.36	0.58	0.51	1.14	0.12	0.08	1.44	0.80	0.58	1.40
1.25	0.91	1.37	0.55	0.55	1.01	0.13	0.12	1.08	1.49	1.04	1.44
0.57	0.40	1.43	0.87	0.60	1.45	0.20	0.17	1.19	1.82	1.05	1.74
0.51	0.40	1.27	0.26	0.20	1.29	0.22	0.15	1.45	1.07	0.69	1.55
0.97	0.79	1.23	0.42	0.33	1.27	0.27	0.17	1.58	0.70	0.50	1.40
1.83	1.41	1.30	0.29	0.25	1.18	0.11	0.05	2.20	0.45	0.37	1.20
0.24	0.16	1.47	0.15	0.09	1.57	0.12	0.10	1.22	1.32	1.14	1.15
0.16	0.08	1.96	0.17	0.11	1.56	0.18	0.14	1.27	0.35	0.31	1.11
0.52	0.42	1.25	0.13	0.11	1.23	0.39	0.35	1.11	0.50	0.38	1.33
0.27	0.23	1.20	0.28	0.24	1.18	0.45	0.34	1.30	0.50	0.28	1.76
0.44	0.30	1.48	0.43	0.36	1.19	1.46	1.11	1.32	1.03	0.87	1.18
0.56	0.46	1.21	0.36	0.21	1.74	1.36	1.11	1.23	0.48	0.27	1.77
0.72	0.50	1.43	0.36	0.32	1.12	0.75	0.53	1.42	0.80	0.57	1.42
0.78	0.60	1.29	0.12	0.12	1.05	0.50	0.40	1.24	0.19	0.17	1.13
0.47	0.36	1.30	0.37	0.26	1.45	2.00	1.31	1.52	0.90	0.52	1.74
0.56	0.36	1.56	0.43	0.22	1.98	1.71	1.18	1.45	0.58	0.39	1.50
0.34	0.15	2.30	0.10	0.09	1.14	0.39	0.25	1.59	0.60	0.34	1.76
0.11	0.07	1.48	0.27	0.26	1.03	0.86	0.74	1.17	0.34	0.22	1.50
0.24	0.16	1.56	0.53	0.42	1.26	2.05	1.80	1.14	0.86	0.70	1.23
0.09	0.08	1.25	0.25	0.22	1.14	0.89	0.60	1.48	1.32	0.66	2.00
0.56	0.40	1.38	0.28	0.26	1.11	1.44	1.25	1.15	0.34	0.31	1.09
0.80	0.53	1.51	0.25	0.17	1.49	0.96	0.66	1.46	0.92	0.58	1.60
0.61	0.46	1.32	0.48	0.32	1.53	2.20	1.69	1.30	0.36	0.26	1.42
0.58	0.35	1.68	0.65	0.50	1.29	0.58	0.38	1.51	0.36	0.34	1.06
1.45	0.87	1.66	0.43	0.22	1.95	1.99	1.09	1.82	0.11	0.09	1.16

Table AVI 14 *cont.*

Length	Width	Aspect ratio	Length	Width	Aspect ratio	Length	Width	Aspect ratio	Length	Width	Aspect ratio
0.26	0.20	1.28	0.74	0.49	1.51	1.06	0.47	2.26	0.81	0.68	1.19
0.30	0.29	1.03	0.48	0.43	1.12	0.83	0.41	2.03	2.14	0.91	2.35
0.15	0.12	1.20	0.52	0.37	1.43	0.60	0.54	1.11	0.88	0.45	1.96
0.15	0.11	1.33	0.45	0.24	1.91	1.48	0.49	3.01	0.99	0.59	1.69
0.23	0.19	1.21	0.76	0.35	2.17	0.74	0.43	1.71	0.61	0.49	1.23
0.39	0.29	1.34	0.63	0.47	1.35	1.02	0.50	2.06	0.63	0.43	1.46
0.57	0.47	1.22	0.89	0.67	1.32	0.97	0.52	1.89	0.93	0.52	1.78
0.48	0.33	1.47	0.35	0.21	1.63	1.08	0.53	2.03	0.10	0.08	1.30
0.68	0.52	1.32	0.39	0.36	1.09	1.27	0.82	1.54	0.56	0.32	1.73
1.35	1.05	1.29	0.47	0.38	1.24	1.61	0.93	1.74	1.23	0.73	1.68
0.26	0.17	1.51	0.45	0.36	1.24	0.89	0.54	1.64	0.65	0.53	1.22
0.53	0.48	1.09	0.54	0.33	1.62	0.76	0.52	1.45	1.46	0.75	1.93
1.37	0.82	1.67	0.58	0.38	1.52	0.66	0.50	1.32	0.15	0.13	1.15
0.81	0.46	1.75	0.68	0.43	1.59	0.78	0.72	1.09	1.15	0.60	1.91
0.44	0.31	1.39	0.49	0.38	1.30	0.51	0.39	1.30	1.02	0.55	1.86
0.44	0.39	1.12	0.63	0.44	1.45	1.84	0.71	2.60	3.32	1.27	2.61
0.35	0.31	1.15	0.65	0.62	1.04	1.84	0.81	2.26	2.27	2.07	1.10
0.40	0.31	1.31	0.47	0.33	1.43	1.15	0.59	1.95	2.59	1.48	1.75
0.80	0.65	1.24	0.45	0.23	1.96	1.81	0.74	2.46	1.65	1.37	1.20
0.65	0.48	1.34	0.46	0.40	1.16	2.21	1.00	2.20	2.57	1.16	2.21
0.70	0.53	1.33	0.71	0.47	1.51	1.40	0.53	2.63	2.15	1.69	1.27
0.61	0.50	1.22	1.44	1.04	1.38	1.60	0.69	2.31	2.70	1.83	1.48
0.34	0.30	1.12	0.63	0.53	1.20	1.78	0.78	2.28	3.63	2.11	1.72
0.77	0.77	1.00	0.22	0.15	1.46	1.12	0.67	1.66	2.93	1.16	2.52
0.27	0.23	1.18	0.82	0.45	1.81	0.11	0.09	1.20	1.46	1.08	1.35
0.54	0.46	1.17	0.44	0.41	1.07	1.27	0.76	1.69	1.96	1.53	1.28
0.58	0.43	1.35	1.73	0.75	2.30	1.54	0.85	1.81	1.54	1.45	1.06
0.68	0.47	1.43	0.61	0.53	1.14	0.66	0.46	1.45	1.75	1.31	1.34
0.79	0.53	1.48	1.55	1.04	1.48	0.42	0.28	1.52	2.20	1.32	1.67
0.55	0.41	1.36	0.62	0.53	1.17	1.02	0.62	1.66	2.09	1.32	1.58
0.72	0.46	1.56	0.76	0.53	1.44	0.57	0.37	1.55	1.41	1.22	1.16
0.49	0.30	1.63	0.37	0.29	1.28	0.91	0.48	1.89	1.25	0.98	1.28
0.55	0.34	1.64	0.38	0.26	1.44	0.82	0.49	1.67	1.83	1.17	1.57
1.18	0.65	1.83	0.76	0.72	1.06	0.97	0.45	2.15	2.27	1.45	1.57
0.41	0.33	1.27	0.36	0.28	1.29	0.96	0.70	1.38	1.84	0.84	2.18
0.50	0.40	1.25	1.24	0.56	2.22	2.12	0.91	2.32	1.72	1.01	1.71
0.47	0.32	1.48	0.87	0.59	1.47	1.24	0.69	1.80	1.12	0.88	1.26
0.38	0.31	1.20	1.30	0.57	2.28	1.32	0.59	2.22	1.05	0.80	1.31
0.30	0.17	1.79	0.89	0.62	1.43	1.55	0.50	3.08	1.18	0.82	1.44
0.52	0.37	1.42	0.62	0.53	1.16	0.91	0.51	1.80	2.08	1.11	1.87
0.26	0.20	1.32	0.88	0.72	1.22	1.13	0.80	1.40	2.05	1.32	1.56
0.37	0.29	1.26	1.14	0.50	2.27	0.37	0.21	1.75	1.24	1.13	1.10
0.48	0.34	1.41	1.58	0.79	2.01	0.79	0.52	1.54	1.64	1.17	1.40
0.80	0.62	1.29	1.59	0.92	1.72	1.53	0.69	2.23	1.63	0.86	1.89
0.43	0.32	1.35	1.04	0.74	1.41	1.07	0.49	2.20	1.55	1.22	1.27
0.46	0.36	1.27	1.30	0.89	1.47	2.01	0.70	2.86	1.64	1.04	1.57
0.36	0.20	1.78	0.61	0.53	1.15	1.50	0.56	2.70	1.52	0.91	1.67
0.25	0.21	1.18	0.95	0.48	1.98	1.34	0.58	2.32	1.93	1.68	1.15
0.24	0.22	1.06	0.51	0.41	1.25	1.05	0.52	2.01	1.55	1.52	1.02
0.62	0.43	1.45	0.56	0.46	1.22	1.16	0.51	2.26	1.83	1.51	1.21
0.38	0.23	1.63	0.43	0.31	1.37	1.48	0.49	3.03	1.85	1.43	1.30

Table AVI 14 *cont.*

Length	Width	Aspect ratio	Length	Width	Aspect ratio	Length	Width	Aspect ratio	Length	Width	Aspect ratio
2.08	1.39	1.50	2.54	1.40	1.81	0.46	0.29	1.60	0.16	0.11	1.51
1.87	1.18	1.58	0.56	0.51	1.11	0.70	0.45	1.58	0.26	0.18	1.42
1.21	1.19	1.02	2.63	1.75	1.51	1.14	0.64	1.77	0.16	0.10	1.61
1.15	0.95	1.20	2.19	1.28	1.71	0.65	0.50	1.32	0.18	0.18	1.01
0.28	0.24	1.18	1.16	0.77	1.52	0.78	0.48	1.64	0.18	0.13	1.34
1.07	0.76	1.41	1.44	1.18	1.22	1.07	0.46	2.34	0.12	0.08	1.36
1.29	1.05	1.23	1.96	1.25	1.57	0.40	0.23	1.73	0.13	0.13	1.06
1.27	1.08	1.17	1.23	0.81	1.51	0.39	0.24	1.58	0.11	0.09	1.18
1.28	1.01	1.27	0.45	0.32	1.41	0.48	0.28	1.74	0.20	0.13	1.49
1.26	0.85	1.49	1.21	0.78	1.55	0.43	0.33	1.32	0.40	0.19	2.09
1.62	1.23	1.31	0.80	0.48	1.66	1.20	0.79	1.51	0.49	0.21	2.33
0.34	0.30	1.14	0.50	0.39	1.28	1.20	0.97	1.24	0.15	0.10	1.54
1.46	0.96	1.51	1.32	0.85	1.56	0.87	0.62	1.40	0.24	0.13	1.83
1.83	0.96	1.91	0.60	0.27	2.28	0.65	0.47	1.40	0.24	0.17	1.39
1.15	0.73	1.57	0.46	0.30	1.52	0.29	0.21	1.35	0.12	0.06	1.90
1.85	0.94	1.96	0.66	0.39	1.66	1.14	0.98	1.16	0.19	0.09	2.04
1.45	1.17	1.25	1.45	0.92	1.58	0.21	0.16	1.30	0.51	0.42	1.20
1.43	1.02	1.39	0.67	0.35	1.92	0.24	0.21	1.17	0.21	0.16	1.31
1.07	0.77	1.39	0.79	0.35	2.28	0.19	0.12	1.64	0.26	0.14	1.85
1.10	0.80	1.38	0.76	0.52	1.48	0.27	0.21	1.28	0.41	0.25	1.67
0.83	0.59	1.41	1.65	1.43	1.15	0.37	0.28	1.31	0.29	0.21	1.40
0.93	0.75	1.24	0.72	0.50	1.44	0.18	0.16	1.12	0.43	0.27	1.57
0.83	0.56	1.49	0.30	0.29	1.05	0.21	0.19	1.11	0.78	0.44	1.77
1.02	0.80	1.27	1.19	1.10	1.08	0.14	0.11	1.29	0.26	0.18	1.45
1.22	0.88	1.39	2.37	1.38	1.72	0.38	0.35	1.07	0.75	0.53	1.42
1.02	0.70	1.46	0.79	0.31	2.58	0.93	0.35	2.64	0.25	0.15	1.69
1.17	0.69	1.69	2.09	0.92	2.28	0.22	0.13	1.67	0.21	0.15	1.42
1.35	0.64	2.12	0.60	0.31	1.92	0.51	0.29	1.77	0.11	0.09	1.31
0.80	0.61	1.31	1.73	1.29	1.34	0.32	0.23	1.40	0.37	0.36	1.03
0.78	0.61	1.29	1.40	0.54	2.59	0.16	0.10	1.68	0.33	0.29	1.12
1.11	0.95	1.17	1.14	0.74	1.55	0.75	0.40	1.88	0.16	0.12	1.35
0.87	0.52	1.67	1.99	1.52	1.31	0.22	0.10	2.36	0.18	0.10	1.85
1.17	0.99	1.19	2.50	2.20	1.14	0.17	0.14	1.24	0.29	0.17	1.67
0.92	0.79	1.15	2.08	1.36	1.53	0.25	0.18	1.44	0.23	0.12	1.94
1.02	0.96	1.06	0.44	0.33	1.35	0.16	0.12	1.36	0.26	0.18	1.41
0.99	0.77	1.29	0.42	0.34	1.24	0.18	0.14	1.29	0.28	0.21	1.34
0.54	0.44	1.23	0.22	0.21	1.06	0.23	0.20	1.17	0.44	0.31	1.41
0.77	0.52	1.47	0.18	0.11	1.57	0.10	0.08	1.17	0.23	0.22	1.08
1.34	0.72	1.87	1.13	0.59	1.92	0.25	0.14	1.81	0.22	0.19	1.19
0.49	0.48	1.02	0.16	0.10	1.60	0.19	0.13	1.51	0.86	0.55	1.57
0.63	0.56	1.12	0.66	0.42	1.55	0.34	0.20	1.69	0.22	0.11	2.06
0.97	0.62	1.58	0.55	0.36	1.52	0.17	0.09	1.88	0.29	0.22	1.29
0.78	0.76	1.03	0.32	0.25	1.29	0.21	0.13	1.66	0.84	0.52	1.61
0.85	0.51	1.66	1.15	0.68	1.70	0.18	0.13	1.32	0.30	0.27	1.13
0.80	0.69	1.17	0.47	0.38	1.25	0.13	0.09	1.56	0.33	0.21	1.54
1.38	1.32	1.05	0.73	0.64	1.14	0.21	0.11	1.95	0.32	0.15	2.15
1.83	0.96	1.91	1.61	0.63	2.57	0.14	0.13	1.07	0.21	0.14	1.43
1.81	0.68	2.65	0.66	0.46	1.43	0.32	0.25	1.31	0.55	0.23	2.39
2.38	0.82	2.89	0.73	0.46	1.56	0.17	0.15	1.16	0.42	0.27	1.56
1.34	0.80	1.69	0.72	0.30	2.42	0.19	0.13	1.43	0.69	0.55	1.25
1.29	0.90	1.43	0.60	0.41	1.49	0.24	0.11	2.25	0.61	0.35	1.72

Table AVI 14 *cont.*

Length	Width	Aspect ratio	Length	Width	Aspect ratio	Length	Width	Aspect ratio	Length	Width	Aspect ratio
0.17	0.11	1.63	0.78	0.59	1.31	0.37	0.31	1.19	1.12	0.60	1.88
0.71	0.35	2.05	0.53	0.33	1.60	0.21	0.21	1.00	0.57	0.49	1.17
0.29	0.25	1.16	1.00	0.60	1.67	1.45	0.75	1.93	0.57	0.29	1.99
0.97	0.54	1.81	1.11	0.67	1.66	0.62	0.34	1.81	0.50	0.28	1.77
0.48	0.39	1.21	0.68	0.45	1.52	0.57	0.35	1.62	1.39	1.05	1.33
0.40	0.32	1.24	0.89	0.61	1.46	0.17	0.09	1.80	1.76	0.65	2.69
0.20	0.12	1.64	0.25	0.15	1.67	0.22	0.16	1.37	1.38	0.58	2.41
0.20	0.18	1.11	0.77	0.67	1.15	0.70	0.51	1.38	1.27	0.42	3.05
0.13	0.10	1.32	0.86	0.41	2.08	0.42	0.27	1.54	2.55	0.88	2.89
0.30	0.15	2.04	0.40	0.33	1.22	0.41	0.28	1.50	0.59	0.41	1.43
0.37	0.21	1.72	0.20	0.14	1.48	0.74	0.43	1.72	1.74	1.03	1.69
0.27	0.17	1.59	0.46	0.24	1.90	0.49	0.32	1.53	0.46	0.28	1.62
0.26	0.18	1.45	0.25	0.16	1.50	1.05	0.59	1.78	1.01	0.78	1.29
0.46	0.37	1.22	0.26	0.11	2.29	0.69	0.37	1.86	1.57	0.59	2.65
0.37	0.22	1.72	0.19	0.12	1.57	0.44	0.22	2.01	0.81	0.50	1.63
0.33	0.25	1.34	0.44	0.27	1.60	0.36	0.23	1.53	0.23	0.17	1.40
0.51	0.38	1.34	0.24	0.23	1.03	0.34	0.21	1.63	0.91	0.61	1.49
0.53	0.49	1.08	0.27	0.18	1.46	0.62	0.60	1.03	0.55	0.30	1.81
0.65	0.33	1.98	0.18	0.15	1.23	0.73	0.43	1.71	0.29	0.24	1.22
1.11	0.66	1.69	0.25	0.17	1.47	0.83	0.76	1.09	1.07	0.75	1.43
0.60	0.44	1.39	0.21	0.19	1.13	0.39	0.31	1.27	0.20	0.15	1.34
0.58	0.30	1.94	0.26	0.17	1.51	0.83	0.59	1.41	0.15	0.09	1.58
0.53	0.35	1.50	0.09	0.07	1.16	0.90	0.47	1.89	0.74	0.57	1.30
0.19	0.12	1.62	0.28	0.11	2.44	0.58	0.45	1.29	0.39	0.27	1.46
0.64	0.45	1.43	0.32	0.17	1.95	0.53	0.32	1.64	0.89	0.56	1.58
0.39	0.36	1.07	0.52	0.32	1.64	0.99	0.37	2.66	0.16	0.13	1.24
0.89	0.46	1.92	0.14	0.09	1.66	0.61	0.58	1.04	0.56	0.27	2.07
0.64	0.21	3.02	0.23	0.18	1.28	0.50	0.34	1.45	0.18	0.13	1.35
0.72	0.64	1.13	0.17	0.11	1.64	0.68	0.37	1.85	0.59	0.35	1.70
0.37	0.25	1.44	0.51	0.33	1.57	0.43	0.22	1.98	0.48	0.33	1.45
0.35	0.30	1.17	0.10	0.09	1.18	0.34	0.23	1.48	0.20	0.18	1.10
0.23	0.18	1.27	0.36	0.24	1.47	0.77	0.34	2.26	1.80	0.67	2.69
0.58	0.39	1.50	0.17	0.11	1.52	0.90	0.45	2.01	1.34	0.81	1.65
0.24	0.19	1.23	0.17	0.11	1.51	0.41	0.28	1.45	1.21	0.78	1.55
0.30	0.18	1.69	0.14	0.10	1.34	0.57	0.39	1.47	2.54	0.97	2.62
0.37	0.26	1.44	0.45	0.32	1.40	0.86	0.32	2.68	0.48	0.29	1.68
0.54	0.47	1.16	0.14	0.10	1.40	0.80	0.61	1.30	0.76	0.37	2.07
1.45	1.20	1.21	0.24	0.17	1.42	0.22	0.22	1.02	1.01	0.76	1.33
0.68	0.48	1.42	0.15	0.10	1.43	1.28	0.71	1.81	0.72	0.56	1.30
0.40	0.33	1.23	0.17	0.14	1.22	0.58	0.46	1.26	0.38	0.35	1.09
0.44	0.32	1.38	0.51	0.38	1.35	0.73	0.60	1.23	0.41	0.32	1.29
0.36	0.22	1.62	0.71	0.35	2.01	0.59	0.38	1.52	1.01	0.80	1.27
0.81	0.63	1.30	0.24	0.15	1.63	0.34	0.26	1.28	0.89	0.45	1.97
0.32	0.27	1.20	0.27	0.21	1.27	0.40	0.32	1.24	0.46	0.31	1.47
1.15	0.54	2.14	0.43	0.31	1.37	0.72	0.58	1.26	1.63	0.88	1.86
1.90	0.97	1.96	0.10	0.09	1.19	0.57	0.39	1.46	0.48	0.36	1.33
0.40	0.36	1.09	0.23	0.16	1.47	0.63	0.44	1.42	1.00	0.65	1.53
1.70	0.77	2.20	0.21	0.15	1.38	0.84	0.61	1.38	0.75	0.60	1.23
0.53	0.40	1.32	0.18	0.12	1.43	0.53	0.36	1.49	0.86	0.64	1.35
0.66	0.47	1.40	0.11	0.08	1.29	0.62	0.50	1.25	0.93	0.71	1.31
0.62	0.41	1.51	0.28	0.19	1.50	0.50	0.34	1.47	0.67	0.62	1.08

Table AVI 14 *cont.*

Length	Width	Aspect ratio	Length	Width	Aspect ratio	Length	Width	Aspect ratio	Length	Width	Aspect ratio
0.51	0.30	1.68	0.41	0.33	1.24	0.47	0.23	2.00	0.09	0.06	1.71
0.79	0.59	1.33	0.57	0.45	1.25	0.75	0.53	1.41	0.07	0.05	1.35
0.67	0.47	1.44	0.39	0.29	1.38	0.33	0.27	1.21	0.42	0.25	1.66
0.92	0.70	1.32	0.67	0.40	1.66	0.38	0.37	1.04	0.66	0.54	1.22
1.53	1.09	1.41	0.67	0.49	1.36	0.31	0.21	1.43	0.19	0.11	1.71
1.07	0.83	1.30	0.74	0.50	1.47	0.39	0.30	1.30	0.18	0.13	1.37
0.62	0.45	1.36	0.52	0.32	1.63	0.48	0.40	1.20	0.12	0.10	1.20
0.35	0.24	1.44	0.30	0.25	1.20	1.15	0.69	1.66	0.33	0.20	1.63
1.62	0.91	1.78	0.52	0.35	1.50	0.09	0.06	1.37			
0.69	0.44	1.58	0.74	0.42	1.77	0.14	0.08	1.90			
0.49	0.31	1.55	1.23	0.82	1.49	0.07	0.06	1.18			
0.76	0.54	1.40	0.84	0.55	1.53	0.27	0.22	1.22			
0.18	0.11	1.73	0.59	0.41	1.43	0.35	0.20	1.79			
0.64	0.43	1.50	0.23	0.23	1.04	0.75	0.52	1.45			
0.72	0.53	1.36	0.50	0.39	1.28	0.18	0.16	1.13			
0.60	0.45	1.33	1.18	0.90	1.32	0.20	0.14	1.48			
0.49	0.39	1.26	0.59	0.53	1.12	0.23	0.21	1.07			
0.69	0.53	1.29	0.50	0.36	1.37	0.99	0.55	1.80			
0.58	0.37	1.57	0.50	0.34	1.46	0.33	0.24	1.33			
0.64	0.59	1.08	0.61	0.61	1.00	0.74	0.58	1.28			
0.90	0.52	1.71	0.68	0.62	1.09	1.02	0.85	1.19			
0.23	0.14	1.64	0.39	0.30	1.32	0.16	0.08	1.87			
0.28	0.18	1.58	0.77	0.49	1.56	0.34	0.23	1.47			
0.59	0.53	1.12	0.53	0.44	1.20	0.35	0.27	1.33			
0.25	0.21	1.16	0.51	0.37	1.37	0.51	0.26	1.99			
0.47	0.35	1.35	0.31	0.25	1.21	0.27	0.17	1.56			
0.84	0.52	1.61	0.76	0.58	1.31	0.32	0.19	1.67			
0.64	0.46	1.38	0.57	0.43	1.35	0.39	0.17	2.31			
0.47	0.28	1.67	0.85	0.60	1.40	0.28	0.18	1.52			
0.19	0.17	1.08	0.58	0.39	1.48	0.46	0.27	1.71			
0.27	0.19	1.44	1.00	0.68	1.48	0.08	0.06	1.42			
0.36	0.24	1.52	0.49	0.41	1.20	0.14	0.08	1.69			
0.09	0.08	1.05	0.79	0.54	1.47	0.07	0.06	1.17			
1.30	0.84	1.55	0.75	0.53	1.40	0.07	0.05	1.32			
0.88	0.67	1.31	0.55	0.28	2.01	0.22	0.16	1.38			
0.14	0.11	1.34	1.06	0.63	1.68	0.20	0.14	1.48			
0.31	0.28	1.12	0.34	0.30	1.12	0.55	0.37	1.49			
0.77	0.49	1.58	1.10	0.87	1.26	0.09	0.07	1.37			
0.54	0.46	1.18	0.85	0.53	1.60	0.07	0.05	1.20			
0.65	0.62	1.06	0.85	0.58	1.48	1.18	0.69	1.72			
0.54	0.42	1.30	1.25	0.84	1.49	0.08	0.06	1.32			
0.90	0.62	1.46	0.89	0.56	1.59	0.78	0.56	1.39			
0.77	0.46	1.67	0.72	0.40	1.79	0.63	0.62	1.01			
0.60	0.30	1.97	0.24	0.23	1.05	0.44	0.30	1.47			
0.86	0.54	1.60	0.49	0.34	1.44	0.33	0.18	1.85			
0.44	0.29	1.52	0.27	0.26	1.04	0.52	0.32	1.63			
0.27	0.20	1.32	0.52	0.38	1.38	0.66	0.39	1.70			
0.74	0.49	1.53	0.33	0.22	1.51	0.69	0.48	1.44			
0.64	0.32	2.05	1.02	0.48	2.14	0.23	0.17	1.36			
1.08	0.75	1.43	0.37	0.25	1.49	0.31	0.14	2.13			
0.27	0.19	1.42	0.68	0.47	1.44	0.09	0.05	1.63			

Table AVI 15 *Summary statistics for pellets and crystal forms produced by bonefish. All values are given in micrometers and refer to the longest axes unless specified otherwise.*

	Pellet length	Pellet width	N/spheres	Sphere	Sph clust	N/sphere clust	Fib/nee
count	977	977	451	313	64	108	119
min	70	50	0.10	4.53	11.66	0.20	0.24
d10	**180**	**120**	**0.22**	**10.18**	**23.35**	**1.18**	**0.54**
Median	***570***	***390***	***0.33***	***16.31***	***45.16***	***3.22***	***1.97***
d90	**1490**	**954**	**0.63**	**23.04**	**102.3**	**11.07**	**4.73**
max	3630	2200	1.17	45.33	177	24.00	8.75
d90-d10	1310	834	0.42	12.86	78.95	9.89	4.19
Mean	719	478	0.38	16.62	57.59	4.80	2.31
SD	541	344	0.18	5.88	34.99	4.45	1.79
SE of mean	17	11	0.01	0.33	4.37	0.43	0.16

Table AVI 16 *Dimensional data for rhombohedra, spheres, and related particle clusters produced by checkered puffer. All dimensions are in micrometers. Shading scheme differentiates between data from different samples (see footnote for key).*

Rhomb	Rhomb	Rhomb	Rhomb	Rhomb clust.	Sphere	Sphere	Sph clust.
9.00	2.90	5.20	2.20	71.30	19.20	15.50	36.70
12.90	1.90	2.90		8.50	21.00	36.80	55.10
4.90	6.40	2.10		10.50	12.20	53.90	54.10
5.10	5.60	3.00		8.90	17.30	34.60	109.80
4.60	3.70	2.40		9.50	9.90	40.00	54.20
2.90	3.10	2.30		19.00	11.10	45.40	76.10
3.80	2.90	8.90		6.40	8.50	23.60	72.30
4.40	2.50	7.00		3.80	13.90	35.90	70.80
2.00	3.50	7.80		6.70	34.80	33.30	64.30
2.80	2.30	8.50		14.10	9.10	29.80	47.10
2.60	3.10	6.50		8.20	22.30	33.80	30.50
3.40	6.30	5.10		8.20	7.30	29.60	75.00
2.40	2.50	4.40		6.00	14.60	13.60	49.40
3.50	4.10	4.90		8.20	13.40	14.20	67.00
2.50	6.40	3.20		13.00	15.90	11.70	90.60
2.70	2.70	2.90		6.20	15.20	19.40	90.20
2.50	3.20	3.10		7.70	9.00	18.00	58.80
2.10	5.20	2.90		7.60	9.40	18.50	112.60
2.00	3.50	4.90		8.10	16.60	14.70	63.30
2.40	4.70	4.30		8.40	18.10	18.60	57.70
2.50	4.50	3.70		8.90	9.90	25.90	58.00
2.40	4.00	4.10			26.40	25.00	44.70
5.30	3.70	3.40			26.30	20.50	85.00
2.20	4.10	3.20			11.50	21.40	33.40
4.80	4.90	2.70			7.60	27.50	62.90
3.10	3.30	3.40			7.90	22.20	70.00
3.30	3.50	3.10			9.30	19.60	31.20
2.80	4.10	3.60			14.10	25.70	
3.40	4.40	2.70			25.90	28.40	
5.50	4.20	3.90			19.00	23.10	
4.80	2.80	2.50			15.60	30.20	
5.20	2.10	3.60			10.70	35.60	
2.40	2.30	2.90			26.20	33.00	
2.40	3.80	3.10			23.50	11.80	
2.70	5.20	4.00			29.20	13.10	
3.40	5.20	3.40			45.70	38.80	
3.00	9.10	3.60			29.20	33.80	
2.80	2.10	4.10			28.60	25.40	
1.70	3.00	3.60			40.70	12.50	
3.80	2.90	3.20			40.70	32.60	
3.20	4.30	3.40			35.50	23.00	
2.10	4.40	2.90			27.30		
3.30	3.00	2.80			29.40		
3.80	4.20	2.70			28.20		
3.00	3.00	3.10			28.20		
3.90	4.60	2.80			12.30		
3.40	2.80	3.00			20.00		

Shading scheme identifies sample codes: CE-10-43 | CE-10-26 | CE-10-3 | CE-10-25

Table AVI 17 *Dimensional data for polycrystalline ellipsoids, unclassified grains, and related particle clusters produced by checkered puffer. All dimensions are in micrometers. Shading scheme differentiates between data from different samples (see footnote for key).*

P Ellip	P Ellip	P Ellip clust.	Unclassified grain clust.	Unclassified grain clust.	Unclassified grain clust.	Unclassified grain
7.50	10.50	27.00	37.10	8.70	8.50	1.50
6.60	9.60	13.40	26.00	13.10	11.00	1.50
8.40	4.40	46.90	74.80	48.90	9.90	2.00
7.30	9.10	47.10	3.70	33.20	52.70	2.20
6.50	6.10	74.10	10.70	17.60	59.10	1.40
14.80	7.60	106.80	8.50	26.90	26.70	1.80
10.80	7.60	81.40	11.70	8.70	54.60	2.30
8.00	7.60	64.20	5.70	13.30	14.80	2.40
8.00	5.60	81.10	13.60	6.60	4.80	1.90
7.80	4.90	66.70	20.80	10.80	18.90	1.50
7.70	5.70	6.90	20.40	12.10	2.70	2.00
6.70	6.50	10.00	56.20	5.70	4.90	1.60
8.80	7.60	10.60	35.10	2.70	3.70	1.10
7.30	6.40	9.00	77.80	6.40	3.10	2.60
6.60	7.40	149.90	17.20	7.30	1.50	3.30
7.60	5.00	83.20	12.70	4.70	5.10	2.60
6.00	5.90	59.30	7.90	9.20	2.90	0.80
7.60	11.00	73.00	51.60	10.80	4.40	1.90
6.40	10.20		114.60	13.70	1.40	2.40
6.10	12.30		43.40	4.50	5.40	1.60
7.60	10.60		19.50	5.20	6.70	1.70
7.90	9.00		30.90	18.50	4.20	1.30
8.20	7.60		16.10	6.30	9.50	1.10
7.40	9.10		8.70	17.50	3.60	59.50
5.40	10.40		42.40	44.80	1.90	
9.00	8.70		17.20	19.40	2.70	
8.80			10.70	11.70	10.30	
5.20			7.10	9.00	8.50	
3.30			13.80	4.70		
4.80			41.10	16.10		
6.80			13.50	6.40		
9.90			30.40	6.80		
6.00			10.60	9.90		
6.80			64.70	8.70		
7.20			25.60	5.10		
6.20			50.00	12.70		
5.70			12.30	3.00		
6.30			9.50	4.30		
5.80			11.20	5.40		
5.20			28.60	3.60		
5.10			9.70	4.50		
4.80			12.00	4.70		
5.30			10.20	3.80		
9.50			11.40	4.70		
10.00			9.60	7.80		
7.90			10.10	6.60		
7.90			6.50	3.40		

Shading scheme identifies sample codes: CE-10-43 | CE-10-26 | CE-10-3 | CE-10-25

Table AVI 18 *Dimensional data for pellets produced by checkered puffer. All dimensions are in millimetres.*

Length	Width	Aspect ratio	Length	Width	Aspect ratio	Length	Width	Aspect ratio	Length	Width	Aspect ratio
0.21	0.10	2.09	0.14	0.13	1.11	0.24	0.15	1.64	0.34	0.31	1.08
0.26	0.22	1.17	0.27	0.17	1.54	0.21	0.18	1.18	0.17	0.11	1.53
0.13	0.10	1.33	0.23	0.13	1.87	0.20	0.18	1.10	0.32	0.20	1.55
0.19	0.15	1.27	0.25	0.17	1.46	0.20	0.16	1.29	0.20	0.19	1.07
0.18	0.17	1.07	0.30	0.18	1.67	0.33	0.23	1.43	0.29	0.26	1.12
0.36	0.32	1.14	0.16	0.10	1.66	0.15	0.11	1.38	0.27	0.14	1.85
0.17	0.12	1.47	0.15	0.12	1.22	0.15	0.12	1.18	0.12	0.07	1.73
0.35	0.32	1.11	0.16	0.11	1.46	0.27	0.24	1.13	0.19	0.18	1.08
0.13	0.09	1.39	0.23	0.18	1.28	0.21	0.10	2.05	0.18	0.12	1.53
0.33	0.28	1.19	0.24	0.14	1.66	0.14	0.10	1.32	0.35	0.21	1.68
0.19	0.13	1.51	0.25	0.12	2.08	0.21	0.16	1.34	0.45	0.17	2.65
0.16	0.10	1.62	0.14	0.13	1.09	0.31	0.22	1.39	0.42	0.31	1.34
0.20	0.10	1.91	0.15	0.11	1.44	0.20	0.14	1.43	0.28	0.13	2.10
0.28	0.20	1.41	0.13	0.08	1.66	0.22	0.16	1.42	0.17	0.11	1.56
0.21	0.13	1.59	0.19	0.13	1.47	0.14	0.13	1.08	0.22	0.11	2.02
0.16	0.12	1.32	0.16	0.13	1.21	0.14	0.10	1.45	0.47	0.29	1.65
0.12	0.09	1.23	0.17	0.13	1.35	0.15	0.14	1.07	0.25	0.17	1.48
0.21	0.14	1.45	0.21	0.11	1.97	0.18	0.14	1.31	0.35	0.23	1.51
0.30	0.15	1.97	0.21	0.18	1.19	0.20	0.17	1.20	0.24	0.18	1.37
0.18	0.16	1.15	0.24	0.13	1.87	0.18	0.11	1.63	0.26	0.18	1.43
0.22	0.15	1.47	0.20	0.14	1.46	0.21	0.12	1.71	0.16	0.11	1.54
0.22	0.17	1.29	0.34	0.16	2.09	0.17	0.11	1.60	0.34	0.18	1.95
0.14	0.13	1.11	0.24	0.21	1.15	0.20	0.15	1.38	0.35	0.27	1.30
0.14	0.07	1.94	0.23	0.12	1.84	0.17	0.16	1.07	0.30	0.14	2.15
0.26	0.15	1.67	0.18	0.14	1.32	0.19	0.14	1.32	0.30	0.17	1.80
0.18	0.15	1.20	0.19	0.11	1.77	0.20	0.15	1.37	0.16	0.09	1.74
0.16	0.11	1.39	0.22	0.20	1.13	0.29	0.23	1.25	0.18	0.11	1.70
0.27	0.18	1.52	0.27	0.18	1.50	0.16	0.12	1.30	0.32	0.17	1.93
0.19	0.09	2.02	0.27	0.15	1.77	0.21	0.17	1.22	0.11	0.10	1.10
0.23	0.18	1.28	0.18	0.09	2.02	0.29	0.19	1.52	0.16	0.12	1.40
0.22	0.20	1.11	0.25	0.16	1.54	0.37	0.23	1.60	0.14	0.11	1.25
0.27	0.18	1.52	0.20	0.16	1.27	0.18	0.16	1.15	0.15	0.13	1.23
0.23	0.21	1.08	0.10	0.06	1.62	0.28	0.20	1.39	0.32	0.29	1.11
0.27	0.18	1.55	0.14	0.10	1.45	0.21	0.19	1.08	0.16	0.09	1.79
0.15	0.10	1.54	0.33	0.17	1.87	0.25	0.23	1.12	0.17	0.11	1.51
0.18	0.14	1.26	0.20	0.17	1.19	0.26	0.21	1.21	0.17	0.16	1.11
0.14	0.13	1.12	0.16	0.13	1.21	0.23	0.13	1.70	0.16	0.13	1.20
0.22	0.14	1.57	0.29	0.18	1.60	0.32	0.22	1.44	0.11	0.08	1.38
0.15	0.13	1.21	0.16	0.10	1.58	0.39	0.29	1.33	0.32	0.18	1.79
0.29	0.14	2.08	0.14	0.08	1.72	0.24	0.13	1.82	0.18	0.11	1.68
0.16	0.09	1.81	0.18	0.15	1.16	0.20	0.11	1.85	0.23	0.14	1.61
0.12	0.09	1.33	0.22	0.13	1.65	0.16	0.11	1.51	0.30	0.22	1.36
0.25	0.23	1.09	0.18	0.13	1.40	0.28	0.18	1.62	0.23	0.17	1.36
0.20	0.14	1.46	0.13	0.08	1.55	0.26	0.19	1.39	0.10	0.08	1.25
0.32	0.18	1.75	0.17	0.15	1.15	0.20	0.11	1.80	0.22	0.10	2.11
0.18	0.14	1.25	0.26	0.18	1.45	0.28	0.19	1.49	0.24	0.19	1.25
0.23	0.16	1.51	0.25	0.21	1.17	0.26	0.16	1.67	0.15	0.11	1.35
0.38	0.25	1.48	0.32	0.16	2.03	0.38	0.16	2.34	0.28	0.20	1.35
0.11	0.09	1.16	0.20	0.14	1.41	0.32	0.23	1.38	0.14	0.10	1.36
0.30	0.25	1.19	0.29	0.21	1.39	0.18	0.13	1.38	0.14	0.13	1.09
0.35	0.19	1.86	0.26	0.14	1.81	0.20	0.14	1.45	0.17	0.12	1.43

Table AVI 18 *cont.*

Length	Width	Aspect ratio	Length	Width	Aspect ratio	Length	Width	Aspect ratio	Length	Width	Aspect ratio
0.11	0.06	1.76	0.15	0.14	1.14	0.30	0.24	1.26	0.23	0.18	1.22
0.07	0.04	1.59	0.08	0.07	1.07	0.21	0.16	1.35	0.27	0.18	1.50
0.24	0.15	1.61	0.09	0.05	1.63	0.22	0.16	1.43	0.08	0.06	1.35
0.13	0.09	1.33	0.08	0.06	1.32	0.31	0.21	1.51	0.21	0.14	1.48
0.15	0.14	1.05	0.09	0.07	1.36	0.12	0.09	1.35	0.24	0.23	1.08
0.15	0.13	1.23	0.05	0.04	1.35	0.13	0.10	1.34	0.25	0.16	1.62
0.20	0.12	1.65	0.10	0.06	1.56	0.20	0.12	1.70	0.06	0.05	1.15
0.13	0.12	1.12	0.13	0.09	1.39	0.03	0.02	1.32	0.13	0.13	1.07
0.15	0.11	1.39	0.10	0.06	1.51	0.11	0.06	1.79	0.13	0.10	1.31
0.09	0.06	1.48	0.07	0.06	1.08	0.20	0.15	1.38	0.16	0.10	1.61
0.27	0.16	1.64	0.21	0.13	1.64	0.11	0.07	1.53	0.21	0.15	1.45
0.21	0.10	2.03	0.08	0.06	1.31	0.21	0.12	1.72	0.43	0.27	1.59
0.24	0.19	1.24	0.14	0.10	1.33	0.10	0.08	1.13	0.25	0.19	1.33
0.15	0.09	1.64	0.05	0.04	1.30	0.21	0.10	2.12	0.12	0.10	1.21
0.26	0.16	1.63	0.08	0.04	2.01	0.12	0.10	1.20	0.16	0.13	1.22
0.22	0.16	1.38	0.11	0.06	1.83	0.14	0.08	1.82	0.18	0.15	1.22
0.14	0.07	1.97	0.09	0.08	1.16	0.12	0.11	1.11	0.17	0.15	1.10
0.23	0.11	2.09	0.09	0.06	1.63	0.34	0.20	1.69	0.17	0.12	1.37
0.07	0.06	1.06	0.07	0.05	1.39	0.13	0.12	1.09	0.21	0.18	1.16
0.29	0.18	1.58	0.23	0.13	1.79	0.20	0.16	1.21	0.19	0.14	1.40
0.16	0.14	1.15	0.12	0.07	1.64	0.10	0.07	1.37	0.16	0.14	1.14
0.09	0.07	1.35	0.05	0.03	1.72	0.13	0.10	1.24	0.23	0.15	1.51
0.19	0.11	1.78	0.04	0.03	1.37	0.18	0.12	1.54	0.12	0.10	1.22
0.10	0.07	1.54	0.10	0.06	1.76	0.09	0.07	1.43	0.34	0.22	1.57
0.21	0.18	1.14	0.19	0.15	1.25	0.17	0.12	1.37	0.30	0.23	1.27
0.15	0.14	1.12	0.06	0.03	1.80	0.11	0.09	1.24	0.17	0.11	1.53
0.12	0.09	1.24	0.05	0.04	1.20	0.11	0.08	1.37	0.19	0.14	1.36
0.17	0.11	1.48	0.25	0.19	1.29	0.09	0.07	1.24	0.17	0.11	1.47
0.18	0.14	1.24	0.18	0.10	1.75	0.09	0.07	1.35	0.13	0.11	1.25
0.12	0.11	1.10	0.09	0.05	1.86	0.46	0.21	2.17	0.37	0.16	2.31
0.08	0.06	1.28	0.22	0.12	1.79	0.28	0.16	1.79	0.36	0.17	2.14
0.18	0.10	1.75	0.12	0.09	1.31	0.29	0.24	1.21	0.17	0.12	1.45
0.20	0.15	1.40	0.09	0.07	1.23	0.19	0.14	1.31	0.20	0.15	1.31
0.16	0.10	1.64	0.16	0.13	1.20	0.27	0.26	1.05	0.27	0.23	1.17
0.28	0.13	2.20	0.23	0.12	1.91	0.20	0.10	1.91	0.94	0.30	3.14
0.23	0.19	1.20	0.09	0.09	1.07	0.24	0.18	1.32	0.20	0.17	1.18
0.13	0.08	1.60	0.09	0.07	1.32	0.27	0.21	1.27	0.37	0.19	1.92
0.08	0.07	1.21	0.24	0.10	2.47	0.37	0.35	1.06	0.17	0.12	1.39
0.07	0.07	1.13	0.27	0.23	1.20	0.44	0.38	1.15	0.26	0.26	1.03
0.16	0.12	1.27	0.23	0.13	1.70	0.38	0.27	1.40	0.25	0.14	1.73
0.11	0.09	1.20	0.20	0.18	1.11	0.58	0.35	1.64	0.19	0.13	1.45
0.10	0.06	1.68	0.07	0.05	1.24	0.11	0.08	1.42	0.39	0.24	1.63
0.14	0.11	1.24	0.22	0.15	1.45	0.26	0.15	1.74	0.31	0.20	1.54
0.09	0.07	1.32	0.43	0.40	1.07	0.35	0.25	1.39	0.33	0.18	1.80
0.16	0.09	1.89	0.14	0.11	1.29	0.45	0.38	1.18	0.27	0.20	1.36
0.09	0.08	1.11	0.38	0.28	1.34	0.16	0.12	1.34	0.19	0.15	1.26
0.07	0.06	1.30	0.13	0.09	1.38	0.32	0.26	1.23	0.22	0.14	1.65
0.19	0.13	1.51	0.09	0.06	1.49	0.16	0.12	1.31	0.14	0.11	1.32
0.28	0.18	1.61	0.32	0.21	1.52	0.17	0.15	1.15	0.15	0.14	1.12
0.10	0.06	1.77	0.15	0.10	1.57	0.43	0.30	1.41	0.11	0.10	1.20
0.18	0.11	1.67	0.12	0.09	1.28	0.35	0.24	1.45	0.19	0.16	1.19

Table AVI 18 *cont.*

Length	Width	Aspect ratio	Length	Width	Aspect ratio	Length	Width	Aspect ratio	Length	Width	Aspect ratio
0.26	0.22	1.18	0.23	0.15	1.51	0.12	0.10	1.15	0.17	0.12	1.42
0.39	0.21	1.85	0.22	0.11	1.93	0.14	0.11	1.32	0.43	0.30	1.42
0.30	0.27	1.12	0.15	0.13	1.17	0.11	0.10	1.09	0.42	0.33	1.28
0.13	0.11	1.15	0.12	0.08	1.52	0.16	0.11	1.44	0.13	0.09	1.45
0.12	0.11	1.04	0.32	0.18	1.79	0.12	0.08	1.54	0.59	0.54	1.08
0.19	0.14	1.40	0.44	0.28	1.57	0.15	0.10	1.47	0.39	0.27	1.41
0.09	0.08	1.20	0.22	0.17	1.33	0.10	0.10	1.03	0.10	0.07	1.36
0.12	0.08	1.44	0.14	0.09	1.45	0.15	0.10	1.50	0.10	0.07	1.50
0.39	0.28	1.36	0.11	0.08	1.47	0.13	0.07	1.77	0.09	0.06	1.50
0.11	0.06	1.71	0.54	0.41	1.30	0.13	0.11	1.24	0.10	0.07	1.47
0.12	0.08	1.55	0.21	0.16	1.32	0.11	0.08	1.33	0.53	0.41	1.30
0.12	0.10	1.27	0.10	0.06	1.49	0.08	0.05	1.54	0.55	0.22	2.48
0.11	0.10	1.15	0.11	0.06	1.77	0.09	0.07	1.28	0.44	0.24	1.80
0.18	0.14	1.31	0.10	0.09	1.10	0.07	0.06	1.15	0.14	0.12	1.15
0.13	0.10	1.31	0.25	0.17	1.47	0.08	0.05	1.48	0.06	0.05	1.21
0.15	0.09	1.55	0.18	0.15	1.20	0.12	0.08	1.52	0.19	0.19	1.04
0.17	0.12	1.42	0.12	0.10	1.21	0.22	0.20	1.13	0.07	0.06	1.18
0.14	0.08	1.64	0.16	0.14	1.14	0.15	0.07	2.06	0.07	0.04	1.99
0.08	0.07	1.16	0.35	0.17	2.00	0.08	0.05	1.62	0.09	0.06	1.36
0.24	0.12	1.97	0.21	0.16	1.30	0.10	0.06	1.57	0.31	0.20	1.58
0.10	0.07	1.33	0.22	0.17	1.26	0.09	0.07	1.37	0.61	0.19	3.30
0.11	0.08	1.30	0.31	0.22	1.39	0.17	0.11	1.54	0.28	0.19	1.49
0.12	0.09	1.32	0.10	0.08	1.35	0.10	0.06	1.48	1.04	0.82	1.28
0.32	0.31	1.05	0.15	0.08	1.88	0.10	0.08	1.22	0.21	0.15	1.38
0.14	0.11	1.30	0.15	0.12	1.23	0.06	0.03	1.69	0.16	0.11	1.50
0.13	0.10	1.33	0.13	0.09	1.49	0.10	0.05	1.99	0.13	0.07	1.79
0.12	0.11	1.06	0.32	0.17	1.93	0.14	0.10	1.34	0.14	0.11	1.24
0.16	0.07	2.31	0.11	0.07	1.47	0.08	0.06	1.30	0.23	0.21	1.12
0.17	0.13	1.24	0.52	0.36	1.45	0.05	0.04	1.15	0.20	0.16	1.22
0.11	0.07	1.53	0.11	0.08	1.40	0.09	0.08	1.19	0.11	0.09	1.14
0.12	0.08	1.48	0.11	0.07	1.46	0.08	0.08	1.03	1.01	0.84	1.20
0.26	0.14	1.90	0.11	0.08	1.29	0.33	0.32	1.04			
0.12	0.09	1.42	0.11	0.07	1.68	0.14	0.11	1.30			
0.12	0.11	1.16	0.27	0.18	1.48	0.10	0.07	1.51			
0.12	0.08	1.55	0.08	0.06	1.33	0.07	0.06	1.24			
0.16	0.13	1.17	0.21	0.13	1.65	0.16	0.13	1.26			
0.12	0.10	1.31	0.37	0.33	1.14	0.19	0.12	1.58			
0.29	0.22	1.35	0.14	0.10	1.41	0.05	0.03	1.52			
0.22	0.21	1.09	0.11	0.08	1.35	0.06	0.06	1.11			
0.18	0.16	1.13	0.13	0.09	1.34	0.06	0.06	1.03			
0.25	0.16	1.60	0.08	0.04	1.97	0.11	0.10	1.15			
0.15	0.11	1.36	0.10	0.06	1.65	0.08	0.06	1.33			
0.14	0.12	1.18	0.45	0.29	1.54	0.15	0.09	1.59			
0.10	0.08	1.38	0.09	0.07	1.38	0.26	0.15	1.76			
0.18	0.15	1.20	0.29	0.20	1.45	0.09	0.08	1.09			
0.27	0.17	1.57	0.15	0.13	1.19	0.17	0.09	1.87			
0.25	0.18	1.33	0.13	0.09	1.39	0.14	0.10	1.38			
0.12	0.11	1.11	0.12	0.09	1.36	0.09	0.07	1.21			
0.12	0.10	1.23	0.11	0.06	1.88	0.12	0.07	1.58			
0.23	0.12	1.93	0.15	0.12	1.24	0.18	0.13	1.40			
0.50	0.39	1.30	0.10	0.10	1.04	0.16	0.10	1.59			

Table AVI 19 *Summary statistics for pellets and crystals produced by checkered puffer. All values are given in micrometers and refer to the longest axes unless specified otherwise.*

	Pellet length	Pellet width	Rhomb	Rhomb clust.	Sphere	Sph clust.	Dmbl	P Ellip	P Ellip clust.	Unclassified grain clust.	Unclassified grain	Combined rhomb clust. and unclassified grain clust.	Combined sph clust. and P ellip clust.
count	592	592	142	21	88	27	18	73	18	122	24	143	45
min	30	20	1.70	3.80	7.30	30.50	5.40	3.30	6.90	1.40	0.80	1.40	6.90
d10	**90**	**61**	**2.40**	**6.20**	**9.90**	**35.38**	**5.87**	**5.20**	**9.70**	**3.70**	**1.16**	**3.80**	**18.84**
median	***180***	***120***	***3.35***	***8.20***	***21.80***	***62.90***	***8.45***	***7.50***	***61.75***	***10.15***	***1.85***	***9.50***	***62.90***
d90	**320**	**229**	**5.20**	**14.10**	**35.69**	**90.36**	**18.71**	**10.16**	**90.28**	**43.30**	**2.60**	**42.14**	**90.44**
max	1040	840	12.90	71.30	53.90	112.60	21.10	14.80	149.90	114.60	59.50	114.60	149.90
d90-d10	230	168	2.80	7.90	25.79	54.98	12.84	4.96	80.58	39.60	1.44	38.34	71.60
mean	199	140	3.76	11.87	22.70	63.73	10.78	7.49	56.14	16.77	4.25	16.05	60.70
SD	112	80	1.62	13.99	10.31	21.35	5.38	1.99	38.98	18.45	11.78	17.91	29.51
SE of mean	5	3	0.14	3.05	1.10	4.11	1.27	0.23	9.19	1.67	2.40	1.50	4.40

Table AVI 20 *Dimensional data for monocrystalline ellipsoids produced by schoolmaster snapper. All dimensions are in micrometers. Shading scheme differentiates between data from different samples (see footnote for key).*

length	width	aspect ratio	length	width	aspect ratio	length	width	aspect ratio	length	width	aspect ratio
0.68	0.24	2.79	0.59	0.26	2.32	0.39	0.19	2.00	0.38	0.18	2.15
1.07	0.50	2.13	0.53	0.23	2.31	0.73	0.31	2.36	1.02	0.50	2.03
0.76	0.35	2.18	0.51	0.26	1.98	0.38	0.17	2.20	0.84	0.38	2.20
0.43	0.17	2.57	0.28	0.12	2.38	1.04	0.49	2.12	0.63	0.29	2.20
0.56	0.26	2.15	0.63	0.26	2.48	0.51	0.23	2.23	0.79	0.38	2.06
0.84	0.37	2.26	0.63	0.29	2.17	0.65	0.26	2.49	0.95	0.42	2.24
0.79	0.33	2.39	0.63	0.31	2.00	0.73	0.31	2.37	0.59	0.25	2.38
0.38	0.15	2.56	0.63	0.29	2.16	0.54	0.23	2.37	0.57	0.26	2.23
1.04	0.49	2.13	0.93	0.41	2.26	1.16	0.46	2.50	0.77	0.36	2.12
0.41	0.14	2.90	0.78	0.35	2.19	0.41	0.20	2.10	0.67	0.31	2.19
0.72	0.28	2.58	0.47	0.23	2.03	0.37	0.16	2.27	0.75	0.38	1.96
0.64	0.30	2.18	0.74	0.34	2.16	0.46	0.18	2.48	0.85	0.36	2.36
0.42	0.21	2.00	0.45	0.22	2.08	0.33	0.16	2.04	0.96	0.36	2.62
0.59	0.25	2.38	0.40	0.18	2.28	0.58	0.23	2.56	0.66	0.30	2.22
0.54	0.25	2.22	0.57	0.26	2.22	0.68	0.27	2.54	0.90	0.38	2.40
0.57	0.24	2.33	0.71	0.26	2.70	0.76	0.32	2.41	1.18	0.46	2.57
0.42	0.19	2.16	0.58	0.30	1.94	0.81	0.39	2.10	0.63	0.27	2.36
0.55	0.25	2.21	0.65	0.28	2.37	0.45	0.23	1.99	0.69	0.27	2.57
0.90	0.40	2.26	0.92	0.39	2.38	0.83	0.38	2.16	0.76	0.30	2.54
0.48	0.22	2.25	0.44	0.21	2.12	0.56	0.27	2.08	1.04	0.49	2.14
0.44	0.19	2.36	0.57	0.28	2.05	0.71	0.33	2.20	0.68	0.30	2.27
0.49	0.21	2.32	0.59	0.28	2.07	0.60	0.26	2.29	0.75	0.32	2.37
0.39	0.19	2.05	0.71	0.25	2.85	0.41	0.20	2.11	0.51	0.23	2.24
0.38	0.17	2.22	0.59	0.27	2.21	0.34	0.15	2.32	0.84	0.38	2.24
0.66	0.30	2.19	0.49	0.25	2.00	0.80	0.35	2.30	0.69	0.31	2.25
0.55	0.24	2.30	0.70	0.35	2.04	0.44	0.22	1.97	0.83	0.36	2.31
0.52	0.26	2.03	0.83	0.40	2.09	0.43	0.21	2.06	0.78	0.34	2.27
0.78	0.31	2.50	0.54	0.24	2.24	0.47	0.21	2.25	0.64	0.28	2.25
0.49	0.21	2.39	0.53	0.26	2.05	0.47	0.20	2.35	0.50	0.23	2.21
0.50	0.21	2.45	0.45	0.21	2.15	0.54	0.22	2.45	0.86	0.37	2.30
0.53	0.25	2.09	0.65	0.30	2.13	1.24	0.48	2.57	0.72	0.29	2.44
0.57	0.23	2.50	0.52	0.25	2.11	0.49	0.22	2.21	0.61	0.29	2.09
1.13	0.47	2.41	0.75	0.33	2.29	0.53	0.25	2.15	0.48	0.23	2.10
0.74	0.29	2.54	0.85	0.41	2.08	0.81	0.36	2.26	0.86	0.36	2.39
0.94	0.41	2.31	0.94	0.39	2.40	0.48	0.22	2.20	0.63	0.31	2.06
0.40	0.19	2.06	0.38	0.17	2.20	0.40	0.20	1.98	0.73	0.27	2.72
0.63	0.27	2.38	0.74	0.33	2.28	0.32	0.15	2.13	0.79	0.36	2.22
0.48	0.21	2.32	0.51	0.20	2.50	0.51	0.26	2.00	0.73	0.29	2.49
0.56	0.26	2.16	0.65	0.28	2.35	0.68	0.31	2.23	0.88	0.35	2.49
0.68	0.27	2.47	0.70	0.29	2.39	0.74	0.27	2.71	0.62	0.28	2.25
0.78	0.31	2.52	0.60	0.24	2.46	0.60	0.26	2.28	0.56	0.28	2.05
0.51	0.22	2.31	0.51	0.24	2.16	0.74	0.26	2.84	0.72	0.33	2.21
0.44	0.18	2.44	0.35	0.16	2.18	0.69	0.32	2.17	0.66	0.31	2.12
0.69	0.30	2.26	0.46	0.23	2.00	0.79	0.34	2.36	0.84	0.35	2.38
0.36	0.18	2.01	0.87	0.38	2.32	0.91	0.38	2.39	0.93	0.36	2.60
0.54	0.26	2.08	0.54	0.26	2.04	0.72	0.28	2.62	0.62	0.27	2.29
0.89	0.42	2.12	0.43	0.20	2.23	0.73	0.31	2.38	0.53	0.24	2.25
0.93	0.44	2.12	0.53	0.23	2.36	0.58	0.28	2.07	0.70	0.33	2.12
0.56	0.29	1.96	0.56	0.28	2.00	0.61	0.31	1.94	0.50	0.24	2.07

Shading scheme identifies sample codes: CEI-ST-0 | CEI-D1 | CE Sample #50 | CE Sample #3 | CE Sample #72 | CE Sample #52 | CEI-31

Table AVI 20 *cont.*

length	width	aspect ratio	length	width	aspect ratio	length	width	aspect ratio	length	width	aspect ratio
0.66	0.29	2.25	0.54	0.27	2.03	0.62	0.27	2.32	0.85	0.38	2.24
0.89	0.44	2.00	0.75	0.35	2.17	0.40	0.17	2.42	0.70	0.31	2.28
0.61	0.26	2.34	0.40	0.22	1.84	0.61	0.26	2.32	0.68	0.32	2.10
0.63	0.27	2.31	0.72	0.33	2.19	0.96	0.40	2.38	0.70	0.32	2.22
0.79	0.31	2.55	1.08	0.44	2.43	0.60	0.31	1.92	0.73	0.32	2.26
0.60	0.33	1.83	0.67	0.30	2.23	0.76	0.34	2.26	0.47	0.24	2.00
0.35	0.18	1.95	0.71	0.29	2.49	0.53	0.22	2.48	0.41	0.20	2.00
0.73	0.31	2.36	0.79	0.33	2.41	0.80	0.36	2.19	0.72	0.36	2.04
0.55	0.25	2.22	0.68	0.33	2.06	0.73	0.29	2.49	0.90	0.42	2.17
0.56	0.27	2.07	0.56	0.26	2.17	0.84	0.33	2.54	0.65	0.29	2.28
0.64	0.28	2.24	0.51	0.25	2.02	0.54	0.26	2.06	0.74	0.35	2.13
0.39	0.18	2.14	0.83	0.39	2.15	0.47	0.24	1.98	0.73	0.32	2.31
0.69	0.35	2.00	0.85	0.33	2.59	0.46	0.21	2.18	0.64	0.27	2.40
0.64	0.28	2.24	0.48	0.26	1.84	0.72	0.34	2.09	0.75	0.33	2.31
0.90	0.42	2.14	0.47	0.18	2.57	0.35	0.18	1.91	0.59	0.29	2.05
0.68	0.36	1.92	0.53	0.23	2.29	0.80	0.36	2.25	0.72	0.31	2.33
0.67	0.23	2.90	0.47	0.23	2.08	1.02	0.47	2.20	0.64	0.27	2.38
0.62	0.32	1.97	0.48	0.22	2.18	0.69	0.34	2.05	0.62	0.29	2.14
0.54	0.19	2.81	0.75	0.40	1.90	0.79	0.33	2.39	0.57	0.26	2.16
0.41	0.16	2.48	0.46	0.22	2.12	0.62	0.25	2.46	0.84	0.37	2.24
0.42	0.17	2.45	0.53	0.25	2.10	1.03	0.49	2.10	0.81	0.37	2.17
0.60	0.22	2.75	0.60	0.29	2.03	0.87	0.40	2.20	0.93	0.39	2.42
0.51	0.26	1.97	0.61	0.29	2.11	0.59	0.25	2.36	0.59	0.25	2.40
0.68	0.27	2.49	0.48	0.24	1.98	0.93	0.45	2.05	0.82	0.32	2.61
1.01	0.40	2.55	0.62	0.25	2.46	0.72	0.34	2.13	0.84	0.38	2.20
0.62	0.26	2.41	0.84	0.41	2.03	0.80	0.37	2.19	0.63	0.32	1.97
0.99	0.45	2.18	0.68	0.32	2.12	0.56	0.26	2.15	1.06	0.51	2.10
0.84	0.41	2.03	0.56	0.25	2.23	0.87	0.38	2.30	0.78	0.37	2.09
0.41	0.20	2.10	0.52	0.24	2.18	1.05	0.48	2.18	0.76	0.30	2.54
0.71	0.30	2.34	0.79	0.35	2.27	0.69	0.35	1.95	0.72	0.32	2.22
0.42	0.22	1.89	0.89	0.43	2.06	0.89	0.36	2.45	0.72	0.32	2.26
0.71	0.34	2.05	0.75	0.35	2.17	0.50	0.25	2.00	0.76	0.34	2.26
0.53	0.22	2.46	1.00	0.48	2.07	0.55	0.25	2.18	1.07	0.42	2.55
0.76	0.29	2.63	0.51	0.23	2.16	0.69	0.35	1.95	0.57	0.27	2.15
0.52	0.24	2.18	0.93	0.40	2.30	0.70	0.31	2.25	1.10	0.51	2.15
0.59	0.25	2.39	0.60	0.29	2.10	0.58	0.27	2.10	0.72	0.30	2.42
0.57	0.23	2.45	0.93	0.42	2.21	0.51	0.25	2.04	0.55	0.23	2.43
0.71	0.31	2.31	0.51	0.24	2.16	0.73	0.33	2.21	0.48	0.21	2.26
0.78	0.35	2.21	0.60	0.25	2.38	0.64	0.32	2.00	0.60	0.25	2.36
0.90	0.39	2.30	0.49	0.26	1.85	0.77	0.35	2.20	0.77	0.26	2.90
0.56	0.26	2.15	0.53	0.26	2.05	0.38	0.18	2.12	0.67	0.24	2.80
0.49	0.27	1.84	0.62	0.29	2.12	0.53	0.25	2.13	0.76	0.34	2.25
0.65	0.28	2.36	0.53	0.26	2.05	0.52	0.23	2.30	0.77	0.29	2.69
0.62	0.28	2.20	0.42	0.20	2.12	0.95	0.39	2.47	0.66	0.23	2.90
0.66	0.27	2.48	0.48	0.22	2.18	0.79	0.37	2.13	0.47	0.21	2.26
0.54	0.26	2.05	0.71	0.30	2.37	0.89	0.39	2.25	0.73	0.29	2.49
0.99	0.42	2.37	0.80	0.36	2.22	0.46	0.21	2.17	0.44	0.21	2.15
0.57	0.26	2.20	1.19	0.52	2.28	0.92	0.43	2.14	0.49	0.24	2.10
0.42	0.19	2.20	0.76	0.37	2.06	0.81	0.38	2.15	0.62	0.24	2.59

Shading scheme identifies sample codes:

CEI-ST-0	CEI-D1	CE Sample #50	CE Sample #3	CE Sample #72
CE Sample #52	CEI-31			

Table AVI 20 *cont.*

length	width	aspect ratio	length	width	aspect ratio	length	width	aspect ratio	length	width	aspect ratio
0.60	0.25	2.37	0.71	0.33	2.13	0.58	0.30	1.95	0.40	0.19	2.11
0.46	0.20	2.32	0.42	0.19	2.22	0.55	0.25	2.17	1.03	0.33	3.09
0.62	0.29	2.12	0.79	0.27	2.87	0.45	0.21	2.15	0.55	0.19	2.91
0.57	0.19	3.02	0.56	0.23	2.47	0.35	0.19	1.86	0.59	0.27	2.17
0.49	0.20	2.44	0.78	0.31	2.52	0.32	0.14	2.30	0.69	0.25	2.72
0.69	0.31	2.24	0.52	0.22	2.40	0.53	0.24	2.23	0.56	0.23	2.42
0.76	0.28	2.67	0.48	0.16	2.95	0.55	0.21	2.67	0.71	0.29	2.44
0.60	0.22	2.70	0.70	0.27	2.59	0.48	0.20	2.37	0.51	0.24	2.14
0.41	0.16	2.57	0.65	0.29	2.26	0.71	0.29	2.49	0.36	0.15	2.37
1.29	0.51	2.52	0.42	0.12	3.49	0.36	0.16	2.27	0.48	0.21	2.23
0.77	0.36	2.12	0.44	0.18	2.41	0.64	0.27	2.39	0.46	0.18	2.61
0.54	0.24	2.26	0.45	0.19	2.36	0.56	0.25	2.22	0.41	0.17	2.49
0.55	0.24	2.31	0.74	0.32	2.35	0.40	0.19	2.11	0.83	0.27	3.15
0.43	0.19	2.30	0.53	0.24	2.26	0.53	0.20	2.65	0.70	0.22	3.16
0.50	0.25	2.00	0.69	0.26	2.61	0.54	0.25	2.19	0.64	0.26	2.52
0.56	0.22	2.57	0.67	0.21	3.25	0.59	0.23	2.53	0.46	0.19	2.40
0.52	0.24	2.19	1.00	0.33	3.07	0.51	0.22	2.29	0.74	0.26	2.89
0.53	0.24	2.22	0.43	0.18	2.35	0.66	0.31	2.11	0.57	0.21	2.75
0.47	0.23	2.08	0.79	0.28	2.81	0.87	0.33	2.66	0.44	0.23	1.93
0.65	0.31	2.09	0.62	0.26	2.36	0.62	0.23	2.64	0.30	0.10	2.97
0.96	0.36	2.62	0.64	0.27	2.40	0.63	0.23	2.76	0.43	0.20	2.18
0.24	0.11	2.18	0.50	0.19	2.69	0.73	0.34	2.14	0.29	0.11	2.66
0.77	0.29	2.64	1.05	0.38	2.77	0.52	0.27	1.94	0.53	0.22	2.42
0.45	0.18	2.46	0.68	0.24	2.81	0.48	0.21	2.23	0.75	0.31	2.41
0.47	0.21	2.22	0.60	0.25	2.43	0.45	0.20	2.27	0.73	0.31	2.37
0.63	0.26	2.40	0.50	0.21	2.43	0.85	0.30	2.85	0.54	0.19	2.84
0.50	0.22	2.21	0.43	0.17	2.58	0.54	0.21	2.63	0.68	0.27	2.50
0.64	0.30	2.12	0.52	0.20	2.61	0.83	0.36	2.28	0.70	0.28	2.48
0.52	0.21	2.46	0.83	0.24	3.51	0.68	0.28	2.45	0.56	0.22	2.56
0.59	0.30	2.00	0.69	0.27	2.51	0.50	0.19	2.63	0.65	0.28	2.34
0.71	0.28	2.52	0.87	0.36	2.41	0.48	0.21	2.31	0.47	0.19	2.52
0.64	0.24	2.73	0.50	0.22	2.30	0.45	0.22	2.06	0.75	0.29	2.62
0.47	0.21	2.29	0.39	0.17	2.30	0.73	0.27	2.73	0.37	0.16	2.28
0.46	0.22	2.15	0.35	0.15	2.30	0.46	0.22	2.10	0.55	0.22	2.46
0.51	0.22	2.33	0.44	0.17	2.55	0.51	0.21	2.39	0.47	0.23	2.07
0.95	0.41	2.31	0.50	0.22	2.30	0.98	0.32	3.08	0.58	0.21	2.71
0.55	0.21	2.56	0.40	0.20	2.00	0.67	0.26	2.59	0.80	0.31	2.56
0.51	0.22	2.32	0.76	0.27	2.78	2.09	0.91	2.29	0.68	0.24	2.89
0.63	0.26	2.45	0.31	0.13	2.37	0.83	0.36	2.31	0.49	0.22	2.19
1.07	0.53	2.02	0.83	0.28	2.92	0.52	0.19	2.83	0.78	0.29	2.68
0.44	0.18	2.43	0.62	0.20	3.15	0.52	0.27	1.92	0.81	0.29	2.79
0.68	0.29	2.35	0.60	0.22	2.69	0.49	0.19	2.66	0.52	0.24	2.14
0.77	0.28	2.73	0.73	0.29	2.52	0.58	0.20	2.89	0.82	0.28	3.00
0.48	0.21	2.27	0.61	0.23	2.72	0.84	0.31	2.76	0.66	0.25	2.66
0.59	0.26	2.29	0.56	0.24	2.40	0.56	0.21	2.61	0.46	0.17	2.64
0.83	0.26	3.14	0.55	0.24	2.32	0.44	0.18	2.47	0.71	0.32	2.19
0.57	0.23	2.48	0.57	0.24	2.38	0.37	0.17	2.12	1.11	0.50	2.22
0.59	0.26	2.26	0.47	0.18	2.69	0.65	0.28	2.34	0.55	0.25	2.18
0.55	0.25	2.19	0.77	0.26	3.02	0.39	0.18	2.20	0.84	0.35	2.43

Shading scheme identifies sample codes: CEI-ST-0; CEI-D1; CE Sample #50; CE Sample #3; CE Sample #72; CE Sample #52; CEI-31

Table AVI 20 *cont.*

length	width	aspect ratio	length	width	aspect ratio	length	width	aspect ratio	length	width	aspect ratio
0.52	0.23	2.26	0.42	0.18	2.38	0.50	0.23	2.21	0.65	0.32	2.00
0.67	0.29	2.28	0.46	0.22	2.10	0.61	0.28	2.21	0.66	0.36	1.83
0.36	0.18	2.03	0.55	0.18	2.99	0.65	0.34	1.89	1.11	0.53	2.12
0.60	0.22	2.68	0.40	0.15	2.65	0.55	0.29	1.86	0.81	0.35	2.31
0.56	0.25	2.26	0.60	0.21	2.93	0.62	0.29	2.12	0.61	0.25	2.40
0.91	0.31	2.98	0.38	0.17	2.28	1.07	0.55	1.93	0.97	0.52	1.86
0.62	0.28	2.27	1.03	0.35	2.97	0.74	0.34	2.14	0.95	0.50	1.91
0.53	0.23	2.28	0.45	0.19	2.33	1.05	0.51	2.06	0.39	0.22	1.74
0.46	0.19	2.44	0.49	0.17	2.92	0.82	0.41	1.98	0.48	0.25	1.89
0.67	0.28	2.41	0.61	0.20	3.03	0.82	0.32	2.61	0.62	0.28	2.19
0.41	0.20	2.08	0.72	0.27	2.70	0.72	0.34	2.11	0.88	0.48	1.82
0.48	0.18	2.61	0.92	0.33	2.75	1.41	0.58	2.45	0.73	0.36	2.04
0.59	0.24	2.50	0.72	0.32	2.23	0.65	0.31	2.05	0.99	0.49	2.00
0.69	0.28	2.47	0.72	0.25	2.85	0.76	0.37	2.07	0.85	0.42	2.04
0.62	0.26	2.40	0.72	0.34	2.09	0.66	0.32	2.06	0.55	0.27	2.06
0.62	0.26	2.37	1.17	0.61	1.93	1.20	0.60	2.01	1.02	0.47	2.18
0.58	0.24	2.48	0.63	0.33	1.88	0.65	0.29	2.24	1.09	0.52	2.09
0.56	0.21	2.66	0.88	0.47	1.90	0.84	0.44	1.90	0.77	0.37	2.08
0.57	0.27	2.15	1.06	0.51	2.08	1.21	0.62	1.96	0.66	0.33	2.00
0.67	0.26	2.59	1.34	0.64	2.11	0.69	0.33	2.06	0.74	0.38	1.97
0.54	0.25	2.17	1.03	0.51	2.02	0.83	0.41	2.05	0.70	0.37	1.91
0.60	0.25	2.38	0.79	0.38	2.10	0.53	0.27	2.00	0.77	0.39	2.00
0.71	0.30	2.39	0.98	0.47	2.07	0.81	0.37	2.21	0.85	0.41	2.09
0.52	0.21	2.43	0.75	0.32	2.37	0.35	0.17	2.01	0.65	0.33	1.96
0.59	0.23	2.61	1.07	0.53	2.00	0.78	0.39	1.98	0.68	0.36	1.89
0.73	0.29	2.55	1.03	0.50	2.06	0.70	0.36	1.94	0.44	0.23	1.86
0.62	0.26	2.36	1.36	0.65	2.09	1.09	0.58	1.87	0.89	0.41	2.15
0.53	0.25	2.13	0.75	0.37	2.00	0.70	0.36	1.93	0.83	0.43	1.95
0.64	0.26	2.43	0.76	0.38	2.02	0.73	0.37	2.00	1.46	0.68	2.15
0.58	0.21	2.71	0.95	0.47	2.04	0.45	0.22	2.06	1.24	0.59	2.11
0.69	0.33	2.05	1.01	0.56	1.80	1.42	0.65	2.19	0.43	0.21	2.03
0.51	0.22	2.30	0.90	0.43	2.09	0.70	0.34	2.07	0.82	0.39	2.14
0.44	0.20	2.21	0.74	0.35	2.10	0.70	0.35	1.97	0.83	0.41	2.04
0.72	0.32	2.23	0.88	0.46	1.90	0.74	0.35	2.11	0.50	0.25	2.00
0.48	0.21	2.26	0.54	0.25	2.17	0.88	0.38	2.32	1.14	0.60	1.89
0.61	0.28	2.17	1.35	0.65	2.08	0.77	0.34	2.28	0.67	0.32	2.11
0.74	0.26	2.87	1.05	0.47	2.25	0.77	0.39	1.95	0.75	0.33	2.26
1.06	0.34	3.14	1.31	0.60	2.18	0.92	0.45	2.02	0.50	0.25	1.98
0.71	0.28	2.53	0.67	0.33	2.00	1.26	0.61	2.08	0.48	0.25	1.95
0.62	0.23	2.65	0.98	0.50	1.94	1.36	0.64	2.13	0.64	0.31	2.05
0.85	0.34	2.51	0.67	0.28	2.40	0.85	0.39	2.18	0.98	0.46	2.11
0.63	0.21	2.93	0.87	0.34	2.58	0.71	0.33	2.15	0.54	0.28	1.95
0.52	0.21	2.41	0.89	0.44	2.01	1.16	0.60	1.93	0.65	0.31	2.11
0.82	0.36	2.28	1.08	0.53	2.04	0.46	0.23	2.05	0.46	0.22	2.09
0.36	0.17	2.13	1.08	0.57	1.89	1.00	0.42	2.37	1.18	0.56	2.11
0.76	0.29	2.61	1.05	0.50	2.10	0.79	0.38	2.11	1.01	0.46	2.18
0.44	0.20	2.22	1.02	0.49	2.09	0.62	0.30	2.04	0.60	0.29	2.05
0.76	0.32	2.39	0.63	0.35	1.80	0.83	0.45	1.85	1.07	0.52	2.06
0.53	0.22	2.47	0.68	0.30	2.24	0.67	0.35	1.93	0.90	0.40	2.27

Shading scheme identifies sample codes: CEI-ST-0; CEI-D1; CE Sample #50; CE Sample #3; CE Sample #72; CE Sample #52; CEI-31

Table AVI 20 *cont.*

length	width	aspect ratio	length	width	aspect ratio	length	width	aspect ratio	length	width	aspect ratio
0.79	0.39	2.04	0.45	0.21	2.15	0.77	0.35	2.21	0.90	0.47	1.92
0.54	0.25	2.13	0.84	0.38	2.24	1.20	0.56	2.14	0.79	0.37	2.15
0.67	0.33	2.00	0.56	0.27	2.07	0.90	0.43	2.09	0.72	0.34	2.11
0.28	0.14	2.01	0.88	0.43	2.03	0.98	0.48	2.04	0.70	0.33	2.11
0.78	0.39	1.99	0.60	0.29	2.05	0.65	0.31	2.10	0.55	0.25	2.15
0.72	0.34	2.13	0.49	0.25	1.98	0.83	0.43	1.96	0.57	0.24	2.32
0.52	0.27	1.93	0.61	0.34	1.83	1.08	0.48	2.24	0.46	0.24	1.95
0.80	0.37	2.15	0.79	0.35	2.24	1.11	0.46	2.44	0.57	0.27	2.10
1.05	0.52	2.01	0.73	0.34	2.15	0.99	0.48	2.07	0.54	0.27	1.97
0.67	0.32	2.10	0.69	0.36	1.94	0.64	0.29	2.18	0.63	0.30	2.09
0.90	0.45	2.00	0.57	0.27	2.10	0.66	0.32	2.07	1.34	0.62	2.16
0.48	0.23	2.07	0.35	0.17	2.10	0.68	0.36	1.89	0.88	0.43	2.06
0.61	0.33	1.86	0.63	0.30	2.11	0.62	0.27	2.28	1.02	0.54	1.88
0.87	0.45	1.93	0.95	0.43	2.18	0.50	0.24	2.08	1.14	0.57	1.99
0.70	0.35	2.01	1.45	0.68	2.14	0.84	0.42	2.00	0.76	0.36	2.11
0.65	0.31	2.12	1.00	0.47	2.15	0.87	0.36	2.41	0.38	0.16	2.30
0.93	0.46	2.00	0.55	0.25	2.21	0.47	0.25	1.92	0.86	0.38	2.23
0.63	0.27	2.31	0.55	0.26	2.15	0.86	0.37	2.31	0.87	0.40	2.18
0.81	0.40	2.03	0.48	0.21	2.32	0.73	0.35	2.09	0.73	0.35	2.11
1.73	0.67	2.57	0.64	0.27	2.38	0.82	0.39	2.10	1.04	0.49	2.11
0.85	0.43	1.96	0.62	0.28	2.21	0.90	0.36	2.50	1.11	0.50	2.22
0.37	0.18	2.05	0.94	0.44	2.14	2.20	0.90	2.44	0.92	0.38	2.44
0.36	0.14	2.53	0.49	0.24	2.08	2.12	0.84	2.51	0.91	0.38	2.37
0.54	0.26	2.09	0.51	0.22	2.30	0.93	0.44	2.10	0.65	0.29	2.20
0.61	0.31	1.97	0.61	0.27	2.25	1.36	0.56	2.43	0.55	0.25	2.21
0.90	0.45	2.02	0.35	0.16	2.11	0.55	0.29	1.92	0.60	0.29	2.04
0.53	0.25	2.13	0.68	0.35	1.93	0.62	0.33	1.86	0.77	0.32	2.44
0.84	0.38	2.18	0.99	0.44	2.23	0.51	0.23	2.25	0.93	0.42	2.22
0.70	0.37	1.91	0.65	0.31	2.06	0.74	0.32	2.35	0.86	0.37	2.31
1.21	0.62	1.97	0.64	0.31	2.05	0.56	0.23	2.43	0.72	0.36	2.03
0.91	0.46	1.96	0.79	0.34	2.32	0.67	0.32	2.12	1.22	0.55	2.24
0.88	0.44	2.00	0.61	0.26	2.33	0.88	0.42	2.11	0.89	0.39	2.30
0.40	0.20	2.03	0.66	0.31	2.10	1.58	0.63	2.50	0.71	0.34	2.07
0.91	0.42	2.15	0.55	0.26	2.10	1.51	0.66	2.30	0.69	0.33	2.13
0.42	0.20	2.08	1.42	0.65	2.20	1.35	0.53	2.54	0.64	0.30	2.12
0.64	0.30	2.14	0.51	0.22	2.32	1.22	0.63	1.93	1.12	0.50	2.26
0.74	0.38	1.94	0.57	0.28	2.07	0.42	0.21	1.96	1.18	0.56	2.11
0.81	0.38	2.14	0.87	0.42	2.07	0.46	0.24	1.91	0.57	0.26	2.21
0.65	0.33	1.95	1.14	0.54	2.14	0.97	0.43	2.26	0.59	0.26	2.29
0.77	0.34	2.24	0.66	0.33	1.99	0.50	0.23	2.14	0.55	0.27	2.00
0.70	0.35	2.00	0.82	0.42	1.96	0.57	0.30	1.88	0.80	0.38	2.12
0.71	0.31	2.29	0.66	0.32	2.07	0.91	0.38	2.37	1.11	0.48	2.32
0.69	0.30	2.31	0.60	0.27	2.21	0.84	0.38	2.19	0.71	0.40	1.76
0.78	0.31	2.47	0.65	0.30	2.18	1.70	0.70	2.41	0.99	0.45	2.20
0.60	0.27	2.18	0.66	0.29	2.25	0.53	0.22	2.39	0.79	0.38	2.06
0.73	0.32	2.28	0.67	0.35	1.91	0.65	0.29	2.25	0.78	0.38	2.07
0.42	0.20	2.11	0.68	0.33	2.05	0.67	0.31	2.15	0.82	0.39	2.11
0.71	0.34	2.13	0.50	0.28	1.77	0.66	0.31	2.16	0.64	0.29	2.22
0.63	0.30	2.13	0.51	0.26	2.00	1.36	0.63	2.16	0.74	0.35	2.13

Shading scheme identifies sample codes:

CEI-ST-0	CEI-D1	CE Sample #50	CE Sample #3	CE Sample #72
CE Sample #52	CEI-31			

Table AVI 20 *cont.*

length	width	aspect ratio	length	width	aspect ratio	length	width	aspect ratio
0.62	0.30	2.08	0.79	0.36	2.20	0.58	0.27	2.16
0.60	0.28	2.15	0.74	0.32	2.30	1.23	0.46	2.68
1.20	0.53	2.25	0.63	0.29	2.18	0.85	0.38	2.27
0.96	0.47	2.06	0.76	0.36	2.11	0.68	0.31	2.16
0.67	0.32	2.09	0.84	0.36	2.31	0.78	0.36	2.17
0.53	0.25	2.17	1.04	0.43	2.41	0.66	0.31	2.09
1.04	0.44	2.34	0.92	0.46	1.99	1.07	0.50	2.15
0.50	0.27	1.88	0.68	0.31	2.15	0.52	0.25	2.06
0.35	0.19	1.87	0.44	0.22	2.05	0.71	0.29	2.41
1.37	0.63	2.16	1.78	0.77	2.30	0.60	0.26	2.35
0.79	0.33	2.39	0.65	0.29	2.24	0.70	0.34	2.07
1.25	0.61	2.05	1.01	0.41	2.46	0.65	0.31	2.08
1.01	0.43	2.35	0.77	0.38	2.04	0.60	0.29	2.08
0.64	0.34	1.87	0.77	0.38	2.02	0.60	0.28	2.11
0.67	0.32	2.07	0.70	0.31	2.27	1.38	0.54	2.58
0.89	0.40	2.20	0.85	0.36	2.34	0.83	0.44	1.88
0.61	0.31	2.00	0.72	0.31	2.31	0.67	0.31	2.14
1.16	0.50	2.31	1.11	0.46	2.44	0.77	0.40	1.93
0.60	0.29	2.05	0.64	0.35	1.86	0.47	0.21	2.26
0.72	0.36	1.99	0.53	0.26	2.06			
0.75	0.36	2.06	0.70	0.35	2.00			
0.58	0.25	2.30	0.71	0.42	1.71			
0.67	0.33	2.03	0.68	0.35	1.97			
0.78	0.38	2.03	0.56	0.29	1.89			
0.68	0.27	2.47	0.78	0.41	1.91			
0.92	0.49	1.89	1.25	0.63	2.00			
0.96	0.52	1.87	0.91	0.47	1.94			
0.78	0.42	1.83	0.62	0.29	2.13			
1.02	0.50	2.04	0.75	0.34	2.20			
0.65	0.30	2.16	0.90	0.43	2.06			
0.66	0.32	2.06	0.96	0.46	2.10			
0.60	0.26	2.34	0.63	0.32	1.94			
0.54	0.26	2.05	1.65	0.75	2.19			
0.59	0.30	1.96	0.77	0.32	2.37			
0.73	0.33	2.19	0.50	0.24	2.06			
0.73	0.32	2.26	0.51	0.24	2.11			
0.61	0.30	2.07	0.62	0.31	2.03			
0.81	0.37	2.21	0.85	0.41	2.05			
0.49	0.24	2.07	0.71	0.37	1.93			
0.62	0.29	2.16	0.75	0.36	2.07			
0.70	0.26	2.66	1.11	0.53	2.09			
0.46	0.20	2.26	0.89	0.41	2.18			
0.75	0.35	2.15	0.70	0.29	2.36			
0.69	0.32	2.16	0.66	0.28	2.32			
0.56	0.27	2.05	0.75	0.38	2.00			
0.72	0.35	2.05	0.80	0.40	2.00			
0.61	0.29	2.10	1.30	0.60	2.18			
0.61	0.30	2.04	0.64	0.28	2.31			
0.79	0.40	1.99	0.62	0.30	2.08			

Shading scheme identifies sample codes:

CEI-ST-0	CEI-D1	CE Sample #50	CE Sample #3	CE Sample #72
CE Sample #52	CEI-31			

Table AVI 21 *Dimensional data for rod-shaped crystals produced by schoolmaster snapper. All dimensions are in micrometers. Shading scheme differentiates between data from different samples (see footnote for key).*

length	width	aspect ratio
1.03	0.22	4.64
0.70	0.15	4.72
0.62	0.21	2.99
0.87	0.27	3.19
0.96	0.23	4.13
0.72	0.21	3.44
0.97	0.26	3.67
0.95	0.26	3.72
0.80	0.20	4.08
0.55	0.14	4.02
0.91	0.24	3.86
0.91	0.19	4.77
0.87	0.21	4.22
0.72	0.16	4.36
0.76	0.18	4.23
0.58	0.15	3.75
1.01	0.27	3.76
0.65	0.09	6.94
0.69	0.22	3.11
0.65	0.14	4.61
1.13	0.14	8.06
0.56	0.11	5.22
0.67	0.22	3.05
0.61	0.16	3.83
0.73	0.14	5.05
0.74	0.19	3.97
0.83	0.17	4.92
0.85	0.17	5.04
0.98	0.27	3.60
0.91	0.28	3.23
0.76	0.18	4.17
0.77	0.16	4.79

Shading scheme identifies sample codes:

CEI-ST-0	CEI-D1	CE Sample #50	CE Sample #3	CE Sample #72
CE Sample #52	CEI-31			

Table AVI 22 *Dimensional data for pellets produced by schoolmaster snapper. All dimensions are in millimetres.*

Length	Width	Aspect ratio	Length	Width	Aspect ratio	Length	Width	Aspect ratio	Length	Width	Aspect ratio
0.68	0.53	1.28	0.85	0.73	1.16	0.26	0.18	1.44	0.62	0.52	1.19
0.40	0.26	1.54	1.11	0.71	1.56	0.50	0.36	1.39	0.13	0.09	1.44
0.57	0.29	1.97	1.62	0.86	1.88	0.37	0.20	1.85	0.15	0.14	1.07
1.39	0.65	2.14	0.91	0.57	1.60	0.17	0.16	1.06	0.25	0.25	1.00
0.37	0.32	1.16	1.42	0.93	1.53	0.14	0.08	1.75	0.08	0.08	1.00
0.39	0.35	1.11	0.32	0.26	1.23	1.20	0.70	1.71	0.19	0.18	1.06
0.40	0.24	1.67	0.60	0.42	1.43	1.18	0.79	1.49	0.13	0.11	1.18
0.28	0.20	1.40	0.22	0.15	1.47	0.57	0.51	1.12	0.18	0.11	1.64
0.24	0.16	1.50	0.17	0.08	2.13	0.16	0.13	1.23	0.22	0.15	1.47
1.90	1.14	1.67	0.61	0.54	1.13	0.23	0.17	1.35	0.28	0.12	2.33
1.59	1.09	1.46	0.91	0.56	1.63	0.80	0.74	1.08	0.19	0.19	1.00
2.24	1.08	2.07	0.10	0.08	1.25	0.33	0.26	1.27	0.11	0.09	1.22
1.71	1.16	1.47	0.65	0.41	1.59	0.30	0.27	1.11	0.18	0.17	1.06
1.86	1.00	1.86	0.73	0.47	1.55	0.85	0.53	1.60	0.10	0.06	1.67
1.07	0.63	1.70	1.57	0.87	1.80	0.69	0.47	1.47	0.22	0.16	1.38
1.45	1.06	1.37	0.47	0.33	1.42	1.04	0.50	2.08	0.11	0.09	1.22
2.04	1.28	1.59	0.44	0.33	1.33	0.33	0.22	1.50	0.19	0.12	1.58
1.18	1.02	1.16	0.65	0.47	1.38	0.20	0.15	1.33	0.09	0.07	1.29
0.92	0.50	1.84	1.18	0.73	1.62	0.28	0.17	1.65	0.11	0.08	1.38
0.39	0.23	1.70	0.93	0.73	1.27	0.92	0.30	3.07	0.09	0.08	1.13
0.81	0.55	1.47	1.09	0.53	2.06	0.57	0.32	1.78	0.21	0.16	1.31
1.28	1.04	1.23	1.73	0.83	2.08	0.34	0.18	1.89	0.20	0.17	1.18
1.86	0.97	1.92	1.73	0.92	1.88	0.55	0.36	1.53	0.17	0.13	1.31
0.51	0.35	1.46	1.51	0.95	1.59	0.23	0.18	1.28	0.09	0.08	1.13
1.40	0.98	1.43	0.68	0.37	1.84	0.51	0.26	1.96	0.28	0.19	1.47
0.35	0.29	1.21	0.58	0.37	1.57	1.22	0.61	2.00	0.12	0.08	1.50
1.69	1.35	1.25	0.84	0.43	1.95	0.36	0.29	1.24	0.11	0.06	1.83
0.42	0.32	1.31	0.44	0.36	1.22	0.19	0.14	1.36	0.12	0.09	1.33
0.87	0.71	1.23	1.34	0.91	1.47	0.15	0.13	1.15	0.85	0.61	1.39
1.62	0.94	1.72	0.94	0.81	1.16	0.78	0.68	1.15	0.37	0.25	1.48
0.47	0.25	1.88	1.39	1.11	1.25	0.20	0.18	1.11	0.13	0.12	1.08
0.65	0.52	1.25	1.86	1.02	1.82	0.84	0.46	1.83	0.16	0.10	1.60
1.30	0.75	1.73	0.63	0.51	1.24	1.10	0.59	1.86	0.30	0.23	1.30
0.14	0.09	1.56	0.33	0.31	1.06	1.41	0.86	1.64	0.12	0.09	1.33
0.21	0.15	1.40	0.22	0.20	1.10	0.78	0.38	2.05	0.11	0.10	1.10
0.46	0.27	1.70	0.59	0.28	2.11	1.43	1.01	1.42	0.21	0.13	1.62
1.21	0.57	2.12	1.57	1.01	1.55	0.61	0.49	1.24	0.14	0.12	1.17
1.17	0.71	1.65	1.06	0.83	1.28	0.50	0.33	1.52	0.17	0.12	1.42
0.42	0.35	1.20	1.49	0.71	2.10	0.65	0.47	1.38	0.22	0.15	1.47
0.33	0.30	1.10	0.28	0.23	1.22	0.70	0.43	1.63	0.10	0.07	1.43
1.06	0.81	1.31	0.46	0.41	1.12	0.21	0.18	1.17	0.09	0.07	1.29
0.16	0.12	1.33	0.50	0.34	1.47	1.40	1.05	1.33	0.09	0.08	1.13
0.56	0.36	1.56	0.86	0.50	1.72	1.13	1.01	1.12	0.12	0.09	1.33
1.04	0.54	1.93	0.68	0.49	1.39	0.50	0.43	1.16	0.31	0.26	1.19
0.98	0.48	2.04	0.30	0.26	1.15	0.12	0.08	1.50	0.09	0.09	1.00
1.09	0.65	1.68	0.11	0.10	1.10	0.10	0.08	1.25	0.13	0.11	1.18
0.24	0.17	1.41	0.43	0.29	1.48	0.14	0.13	1.08	0.21	0.19	1.11
0.73	0.59	1.24	0.31	0.28	1.11	0.25	0.14	1.79	0.19	0.13	1.46
0.60	0.48	1.25	0.35	0.24	1.46	0.09	0.09	1.00	0.15	0.09	1.67
0.80	0.53	1.51	0.22	0.14	1.57	0.16	0.11	1.45	0.15	0.08	1.88
1.74	1.00	1.74	0.18	0.13	1.38	0.50	0.42	1.19	0.11	0.09	1.22
0.29	0.15	1.93	0.31	0.19	1.63	0.19	0.14	1.36	0.10	0.08	1.25

Table AVI 22 *cont.*

Length	Width	Aspect ratio	Length	Width	Aspect ratio	Length	Width	Aspect ratio	Length	Width	Aspect ratio
0.15	0.11	1.36	0.26	0.22	1.18	0.95	0.68	1.40	0.17	0.14	1.21
0.30	0.15	2.00	0.13	0.11	1.18	0.25	0.22	1.14	0.10	0.07	1.43
0.11	0.07	1.57	0.16	0.09	1.78	0.28	0.20	1.40	1.01	0.72	1.40
0.26	0.25	1.04	0.58	0.49	1.18	0.86	0.67	1.28	0.45	0.23	1.96
0.16	0.13	1.23	1.07	0.75	1.43	0.49	0.45	1.09	0.16	0.10	1.60
0.22	0.12	1.83	0.44	0.26	1.69	0.27	0.15	1.80	0.35	0.30	1.17
0.10	0.09	1.11	0.20	0.12	1.67	0.30	0.21	1.43	0.18	0.16	1.13
0.11	0.07	1.57	0.17	0.15	1.13	0.48	0.31	1.55	0.22	0.13	1.69
0.57	0.54	1.06	0.16	0.14	1.14	1.38	0.64	2.16	0.19	0.10	1.90
0.78	0.47	1.66	0.48	0.25	1.92	0.33	0.28	1.18	0.44	0.41	1.07
0.30	0.19	1.58	0.15	0.11	1.36	0.22	0.16	1.38	0.18	0.16	1.13
0.09	0.07	1.29	0.38	0.31	1.23	0.22	0.14	1.57	0.13	0.07	1.86
0.21	0.15	1.40	0.19	0.17	1.12	0.36	0.20	1.80	0.28	0.21	1.33
0.10	0.08	1.25	0.17	0.13	1.31	0.37	0.23	1.61	0.12	0.07	1.71
0.09	0.07	1.29	0.09	0.08	1.13	1.40	0.83	1.69	0.32	0.25	1.28
0.35	0.16	2.19	0.13	0.09	1.44	1.08	0.54	2.00	0.32	0.22	1.45
1.20	0.78	1.54	0.29	0.14	2.07	0.44	0.25	1.76	0.57	0.44	1.30
0.11	0.11	1.00	0.14	0.14	1.00	0.48	0.32	1.50	0.81	0.71	1.14
0.10	0.07	1.43	0.25	0.24	1.04	0.26	0.22	1.18	1.07	0.58	1.84
0.09	0.09	1.00	0.18	0.10	1.80	1.20	1.13	1.06	1.56	0.83	1.88
0.16	0.10	1.60	0.09	0.07	1.29	0.28	0.25	1.12	1.20	0.79	1.52
0.16	0.12	1.33	0.41	0.16	2.56	0.98	0.61	1.61	2.03	0.79	2.57
0.08	0.07	1.14	0.20	0.18	1.11	1.03	0.69	1.49	0.92	0.75	1.23
0.28	0.13	2.15	0.12	0.07	1.71	1.25	1.02	1.23	1.61	0.85	1.89
0.22	0.16	1.38	0.22	0.16	1.38	0.78	0.39	2.00	1.53	0.81	1.89
0.17	0.16	1.06	0.28	0.14	2.00	1.88	1.82	1.03	1.18	0.77	1.53
0.14	0.09	1.56	0.15	0.14	1.07	1.57	0.86	1.83	0.20	0.12	1.67
0.37	0.22	1.68	0.39	0.28	1.39	0.87	0.74	1.18	1.21	0.89	1.36
0.18	0.16	1.13	0.33	0.23	1.43	0.13	0.08	1.63	0.44	0.20	2.20
0.94	0.63	1.49	0.17	0.13	1.31	1.20	0.81	1.48	0.25	0.25	1.00
0.35	0.22	1.59	0.68	0.56	1.21	0.14	0.08	1.75	1.24	0.55	2.25
0.28	0.15	1.87	0.13	0.08	1.63	0.10	0.07	1.43	0.26	0.23	1.13
0.31	0.17	1.82	0.11	0.08	1.38	2.04	1.43	1.43	2.04	0.80	2.55
0.17	0.10	1.70	0.15	0.13	1.15	1.00	0.76	1.32	0.81	0.54	1.50
0.28	0.14	2.00	0.22	0.11	2.00	1.94	0.95	2.04	0.65	0.45	1.44
0.64	0.35	1.83	0.11	0.06	1.83	0.86	0.74	1.16	1.51	0.78	1.94
0.13	0.10	1.30	0.12	0.09	1.33	1.20	0.86	1.40	0.54	0.47	1.15
0.13	0.09	1.44	0.86	0.61	1.41	0.45	0.21	2.14	0.49	0.36	1.36
0.43	0.27	1.59	0.09	0.08	1.13	0.19	0.12	1.58	2.20	1.09	2.02
0.69	0.46	1.50	0.27	0.14	1.93	0.23	0.10	2.30	0.13	0.09	1.44
0.53	0.37	1.43	1.15	0.67	1.72	0.13	0.09	1.44	0.49	0.33	1.48
0.43	0.35	1.23	0.10	0.07	1.43	0.20	0.16	1.25	0.18	0.12	1.50
0.22	0.18	1.22	0.49	0.42	1.17	0.25	0.16	1.56	0.34	0.25	1.36
0.25	0.15	1.67	0.09	0.08	1.13	0.36	0.27	1.33	0.41	0.23	1.78
0.13	0.08	1.63	0.12	0.08	1.50	0.21	0.12	1.75	0.10	0.10	1.00
0.21	0.14	1.50	0.20	0.17	1.18	0.09	0.08	1.13	0.16	0.13	1.23
0.26	0.14	1.86	0.14	0.11	1.27	0.10	0.06	1.67	0.10	0.10	1.00
0.18	0.15	1.20	0.21	0.11	1.91	0.17	0.12	1.42	0.18	0.12	1.50
0.39	0.26	1.50	0.16	0.13	1.23	1.10	0.56	1.96	0.12	0.10	1.20
0.22	0.13	1.69	0.38	0.29	1.31	0.13	0.10	1.30	0.09	0.08	1.13
1.86	0.71	2.62	0.29	0.19	1.53	0.20	0.14	1.43	0.26	0.15	1.73
0.19	0.13	1.46	1.21	0.84	1.44	0.18	0.16	1.13	0.21	0.13	1.62

Table AVI 22 *cont.*

Length	Width	Aspect ratio	Length	Width	Aspect ratio	Length	Width	Aspect ratio	Length	Width	Aspect ratio
0.15	0.10	1.50	0.44	0.36	1.22	0.29	0.23	1.26	0.74	0.53	1.40
0.35	0.21	1.67	0.52	0.37	1.41	1.20	0.76	1.58	0.66	0.41	1.61
0.15	0.11	1.36	0.34	0.14	2.43	0.79	0.43	1.84	1.03	0.91	1.13
1.23	0.75	1.64	1.09	0.79	1.38	0.40	0.32	1.25	0.49	0.46	1.07
0.12	0.10	1.20	0.19	0.17	1.12	0.34	0.20	1.70	0.72	0.54	1.33
0.16	0.14	1.14	0.20	0.09	2.22	0.29	0.23	1.26	0.14	0.10	1.40
0.16	0.12	1.33	0.41	0.24	1.71	2.78	1.39	2.00	0.14	0.11	1.27
0.13	0.07	1.86	0.12	0.11	1.09	0.41	0.34	1.21	0.28	0.18	1.56
0.26	0.12	2.17	0.09	0.08	1.13	1.79	1.32	1.36	0.11	0.10	1.10
0.25	0.18	1.39	1.24	1.01	1.23	0.17	0.14	1.21	0.19	0.15	1.27
0.10	0.07	1.43	0.17	0.13	1.31	1.72	1.00	1.72	0.37	0.31	1.19
0.13	0.12	1.08	0.60	0.55	1.09	0.24	0.17	1.41	0.37	0.29	1.28
0.20	0.12	1.67	0.15	0.13	1.15	0.65	0.54	1.20	0.15	0.10	1.50
0.42	0.28	1.50	0.76	0.42	1.81	0.32	0.30	1.07	0.25	0.20	1.25
0.12	0.07	1.71	1.41	1.05	1.34	0.95	0.73	1.30	0.63	0.34	1.85
0.22	0.17	1.29	2.19	1.83	1.20	0.50	0.27	1.85	0.15	0.13	1.15
0.28	0.26	1.08	0.26	0.16	1.63	0.11	0.10	1.10	0.44	0.35	1.26
0.19	0.14	1.36	0.79	0.49	1.61	1.41	1.12	1.26	0.10	0.08	1.25
0.25	0.17	1.47	0.29	0.24	1.21	1.69	1.03	1.64	0.28	0.23	1.22
0.13	0.11	1.18	0.45	0.39	1.15	0.45	0.38	1.18	0.12	0.10	1.20
0.23	0.23	1.00	0.13	0.12	1.08	1.42	1.30	1.09	0.27	0.23	1.17
0.09	0.08	1.13	0.55	0.30	1.83	1.63	1.34	1.22	0.21	0.13	1.62
0.23	0.16	1.44	0.10	0.06	1.67	1.38	1.05	1.31	0.31	0.26	1.19
0.27	0.20	1.35	0.12	0.08	1.50	0.36	0.30	1.20	0.42	0.29	1.45
0.26	0.23	1.13	0.17	0.11	1.55	1.24	0.70	1.77	0.43	0.29	1.48
0.11	0.10	1.10	0.32	0.22	1.45	2.02	1.43	1.41	0.64	0.44	1.45
0.10	0.07	1.43	0.11	0.08	1.38	1.28	0.74	1.73	0.39	0.28	1.39
0.10	0.08	1.25	0.11	0.07	1.57	0.21	0.15	1.40	0.36	0.22	1.64
0.12	0.10	1.20	0.42	0.34	1.24	0.55	0.46	1.20	0.16	0.12	1.33
0.14	0.10	1.40	0.17	0.16	1.06	0.12	0.11	1.09	0.35	0.31	1.13
0.10	0.07	1.43	0.40	0.33	1.21	1.67	1.04	1.61	0.13	0.10	1.30
0.40	0.22	1.82	0.44	0.36	1.22	1.04	0.72	1.44	0.63	0.61	1.03
0.11	0.09	1.22	1.02	0.60	1.70	0.98	0.49	2.00	1.03	0.55	1.87
0.45	0.37	1.22	0.15	0.09	1.67	0.40	0.31	1.29	0.37	0.28	1.32
0.15	0.12	1.25	0.13	0.11	1.18	0.45	0.38	1.18	0.38	0.26	1.46
0.11	0.08	1.38	0.09	0.07	1.29	1.23	0.69	1.78	0.19	0.12	1.58
0.09	0.08	1.13	0.11	0.09	1.22	0.45	0.27	1.67	0.21	0.19	1.11
0.18	0.12	1.50	0.20	0.17	1.18	0.79	0.57	1.39	0.33	0.23	1.43
0.19	0.14	1.36	0.13	0.08	1.63	1.40	0.68	2.06	1.30	0.72	1.81
0.17	0.12	1.42	0.70	0.59	1.19	0.14	0.11	1.27	0.70	0.64	1.09
0.16	0.15	1.07	0.28	0.15	1.87	0.41	0.27	1.52	0.43	0.31	1.39
0.27	0.20	1.35	0.17	0.16	1.06	0.13	0.10	1.30	0.87	0.72	1.21
0.11	0.09	1.22	0.32	0.20	1.60	0.30	0.22	1.36	0.25	0.17	1.47
0.09	0.08	1.13	0.45	0.23	1.96	1.09	0.48	2.27	0.60	0.57	1.05
0.18	0.13	1.38	0.15	0.12	1.25	1.05	0.62	1.69	0.47	0.41	1.15
1.16	0.61	1.90	0.28	0.25	1.12	0.72	0.56	1.29	0.19	0.07	2.71
0.92	0.74	1.24	0.20	0.12	1.67	0.78	0.64	1.22	0.50	0.47	1.06
1.41	0.92	1.53	0.24	0.21	1.14	0.53	0.40	1.33	0.17	0.12	1.42
0.22	0.19	1.16	1.17	0.93	1.26	0.16	0.12	1.33	0.18	0.08	2.25
0.26	0.24	1.08	0.17	0.11	1.55	0.46	0.39	1.18	0.19	0.14	1.36
0.18	0.14	1.29	0.24	0.12	2.00	0.44	0.22	2.00	0.11	0.06	1.83
0.26	0.19	1.37	1.48	0.92	1.61	0.41	0.35	1.17	0.33	0.31	1.06

Table AVI 22 *cont.*

Length	Width	Aspect ratio	Length	Width	Aspect ratio	Length	Width	Aspect ratio	Length	Width	Aspect ratio
0.30	0.13	2.31	0.21	0.16	1.31	0.33	0.24	1.38	0.14	0.12	1.17
0.12	0.08	1.50	0.12	0.08	1.50	0.10	0.08	1.25	0.09	0.08	1.13
0.09	0.07	1.29	0.22	0.15	1.47	0.28	0.20	1.40	0.86	0.79	1.09
1.25	0.78	1.60	0.40	0.35	1.14	0.17	0.10	1.70	0.19	0.12	1.58
0.31	0.15	2.07	0.14	0.12	1.17	0.46	0.29	1.59	0.75	0.68	1.10
0.17	0.11	1.55	0.37	0.19	1.95	0.16	0.14	1.14	0.77	0.60	1.28
0.18	0.11	1.64	0.30	0.18	1.67	0.34	0.29	1.17	0.43	0.34	1.26
1.08	0.64	1.69	0.52	0.28	1.86	0.53	0.41	1.29	0.42	0.38	1.11
0.20	0.16	1.25	0.15	0.09	1.67	0.10	0.09	1.11	1.16	0.67	1.73
0.15	0.09	1.67	0.12	0.08	1.50	0.16	0.13	1.23	1.01	0.65	1.55
0.62	0.35	1.77	0.15	0.11	1.36	0.29	0.24	1.21	0.49	0.39	1.26
0.28	0.21	1.33	0.12	0.09	1.33	0.70	0.60	1.17	0.34	0.29	1.17
0.17	0.12	1.42	0.20	0.08	2.50	0.30	0.25	1.20	0.29	0.19	1.53
0.25	0.19	1.32	0.30	0.21	1.43	0.24	0.22	1.09	0.39	0.27	1.44
0.10	0.07	1.43	0.24	0.23	1.04	0.57	0.50	1.14	0.20	0.12	1.67
0.12	0.06	2.00	0.20	0.15	1.33	1.77	1.07	1.65	1.04	0.69	1.51
0.19	0.14	1.36	1.35	0.99	1.36	0.68	0.52	1.31	0.11	0.09	1.22
0.26	0.23	1.13	0.13	0.13	1.00	0.33	0.25	1.32	0.18	0.14	1.29
0.69	0.52	1.33	0.21	0.14	1.50	0.34	0.19	1.79	0.12	0.09	1.33
0.08	0.07	1.14	0.22	0.14	1.57	0.74	0.53	1.40	0.18	0.13	1.38
0.14	0.09	1.56	0.20	0.17	1.18	0.14	0.10	1.40	0.26	0.25	1.04
0.27	0.18	1.50	1.37	0.63	2.17	0.72	0.62	1.16	0.23	0.13	1.77
0.13	0.08	1.63	0.26	0.23	1.13	0.17	0.11	1.55	0.24	0.16	1.50
0.25	0.22	1.14	0.26	0.19	1.37	1.36	0.60	2.27	0.20	0.13	1.54
0.13	0.10	1.30	1.40	0.89	1.57	0.95	0.77	1.23	0.25	0.20	1.25
0.17	0.11	1.55	0.19	0.16	1.19	0.94	0.69	1.36	0.24	0.22	1.09
0.12	0.10	1.20	0.27	0.18	1.50	0.12	0.09	1.33	0.24	0.16	1.50
0.16	0.10	1.60	0.34	0.23	1.48	0.10	0.09	1.11	0.25	0.23	1.09
0.19	0.12	1.58	0.23	0.12	1.92	0.31	0.23	1.35	0.19	0.15	1.27
0.23	0.14	1.64	0.26	0.21	1.24	0.47	0.27	1.74	0.28	0.16	1.75
0.15	0.15	1.00	0.40	0.32	1.25	0.10	0.07	1.43	0.34	0.23	1.48
0.13	0.07	1.86	0.13	0.09	1.44	0.11	0.08	1.38	0.14	0.09	1.56
0.12	0.07	1.71	0.41	0.27	1.52	0.15	0.12	1.25	0.18	0.11	1.64
0.18	0.14	1.29	0.12	0.08	1.50	0.13	0.11	1.18	0.16	0.11	1.45
0.15	0.11	1.36	0.09	0.07	1.29	0.11	0.08	1.38	0.12	0.09	1.33
0.17	0.10	1.70	0.09	0.06	1.50	0.10	0.07	1.43	0.11	0.07	1.57
0.10	0.08	1.25	0.13	0.11	1.18	0.34	0.27	1.26	0.28	0.21	1.33
0.13	0.11	1.18	0.18	0.12	1.50	0.45	0.37	1.22	0.11	0.09	1.22
0.12	0.09	1.33	0.16	0.10	1.60	1.16	0.75	1.55	0.22	0.13	1.69
0.32	0.29	1.10	0.20	0.18	1.11	0.15	0.09	1.67	0.16	0.11	1.45
0.13	0.10	1.30	0.15	0.08	1.88	0.12	0.08	1.50	0.14	0.13	1.08
0.28	0.26	1.08	0.08	0.08	1.00	0.14	0.11	1.27	0.11	0.05	2.20
0.17	0.14	1.21	0.10	0.09	1.11	0.12	0.12	1.00	0.12	0.10	1.20
0.15	0.10	1.50	0.72	0.52	1.38	0.44	0.36	1.22	0.09	0.08	1.13
0.12	0.07	1.71	0.57	0.33	1.73	0.61	0.49	1.24	0.16	0.14	1.14
0.52	0.30	1.73	0.21	0.14	1.50	0.13	0.08	1.63	0.31	0.16	1.94
0.26	0.16	1.63	0.47	0.43	1.09	0.09	0.07	1.29	0.21	0.18	1.17
0.50	0.30	1.67	0.14	0.12	1.17	0.51	0.46	1.11	0.23	0.14	1.64
0.45	0.37	1.22	0.11	0.11	1.00	0.11	0.06	1.83	0.14	0.13	1.08
0.11	0.09	1.22	0.15	0.10	1.50	0.13	0.08	1.63	0.28	0.25	1.12
0.13	0.10	1.30	0.13	0.10	1.30	0.15	0.09	1.67	0.18	0.15	1.20
0.15	0.15	1.00	0.16	0.12	1.33	0.11	0.10	1.10	0.20	0.17	1.18

Table AVI 22 *cont.*

Length	Width	Aspect ratio	Length	Width	Aspect ratio	Length	Width	Aspect ratio	Length	Width	Aspect ratio
0.19	0.15	1.27	0.60	0.56	1.07	0.19	0.18	1.06	0.28	0.21	1.33
0.32	0.20	1.60	0.21	0.12	1.75	0.62	0.39	1.59	0.17	0.16	1.06
0.77	0.62	1.24	0.17	0.09	1.89	1.45	0.82	1.77	0.13	0.08	1.63
0.20	0.18	1.11	0.25	0.22	1.14	0.68	0.44	1.55	0.14	0.12	1.17
0.29	0.18	1.61	0.32	0.22	1.45	0.23	0.16	1.44	0.44	0.37	1.19
0.18	0.12	1.50	0.19	0.13	1.46	0.34	0.23	1.48	0.56	0.20	2.80
0.16	0.12	1.33	0.23	0.15	1.53	0.58	0.50	1.16	0.16	0.15	1.07
0.10	0.07	1.43	0.92	0.73	1.26	0.15	0.13	1.15	0.24	0.18	1.33
0.76	0.62	1.23	0.22	0.15	1.47	0.76	0.56	1.36	0.15	0.10	1.50
0.09	0.07	1.29	0.20	0.12	1.67	0.37	0.33	1.12	1.24	0.95	1.31
0.12	0.08	1.50	0.13	0.11	1.18	0.50	0.28	1.79	0.36	0.28	1.29
0.17	0.16	1.06	0.16	0.10	1.60	0.40	0.34	1.18	0.76	0.46	1.65
0.19	0.17	1.12	0.14	0.07	2.00	0.29	0.21	1.38	0.31	0.20	1.55
0.33	0.26	1.27	0.91	0.63	1.44	0.12	0.08	1.50	0.28	0.25	1.12
0.09	0.06	1.50	0.58	0.41	1.41	0.24	0.17	1.41	0.94	0.85	1.11
0.27	0.16	1.69	0.11	0.07	1.57	0.18	0.14	1.29	0.35	0.15	2.33
0.44	0.26	1.69	0.20	0.13	1.54	0.23	0.17	1.35	0.35	0.27	1.30
0.16	0.13	1.23	0.17	0.14	1.21	0.21	0.18	1.17	0.25	0.24	1.04
0.16	0.10	1.60	0.24	0.12	2.00	0.14	0.10	1.40	0.11	0.10	1.10
0.15	0.13	1.15	0.15	0.12	1.25	0.13	0.07	1.86	0.30	0.23	1.30
0.14	0.12	1.17	0.21	0.14	1.50	0.57	0.41	1.39	0.16	0.11	1.45
0.13	0.11	1.18	0.23	0.15	1.53	0.14	0.09	1.56	0.43	0.24	1.79
0.13	0.12	1.08	0.32	0.25	1.28	1.46	0.90	1.62	1.60	1.18	1.36
0.14	0.11	1.27	0.26	0.18	1.44	0.36	0.21	1.71	2.07	1.11	1.86
0.46	0.31	1.48	0.40	0.24	1.67	0.17	0.12	1.42	0.22	0.14	1.57
0.12	0.11	1.09	0.29	0.17	1.71	0.30	0.21	1.43	0.45	0.33	1.36
0.09	0.07	1.29	0.27	0.19	1.42	0.29	0.20	1.45	0.48	0.27	1.78
0.29	0.21	1.38	0.82	0.70	1.17	0.15	0.13	1.15	0.14	0.14	1.00
0.16	0.15	1.07	0.92	0.63	1.46	0.19	0.15	1.27	0.29	0.23	1.26
0.38	0.21	1.81	0.20	0.11	1.82	0.16	0.12	1.33	0.15	0.14	1.07
0.13	0.11	1.18	0.10	0.08	1.25	0.15	0.10	1.50	0.18	0.10	1.80
0.15	0.12	1.25	0.22	0.18	1.22	0.10	0.06	1.67	0.63	0.37	1.70
0.11	0.07	1.57	0.22	0.13	1.69	0.27	0.23	1.17	0.16	0.14	1.14
0.13	0.11	1.18	0.44	0.33	1.33	0.37	0.27	1.37	0.87	0.62	1.40
0.14	0.10	1.40	0.22	0.14	1.57	0.09	0.07	1.29	0.12	0.08	1.50
0.09	0.07	1.29	0.24	0.19	1.26	0.10	0.08	1.25	0.39	0.26	1.50
0.12	0.09	1.33	0.52	0.50	1.04	0.38	0.22	1.73	0.09	0.05	1.80
0.11	0.06	1.83	0.38	0.23	1.65	0.13	0.09	1.44	0.55	0.50	1.10
0.13	0.10	1.30	0.35	0.26	1.35	0.11	0.09	1.22	0.38	0.22	1.73
0.18	0.17	1.06	0.28	0.22	1.27	0.28	0.18	1.56	0.13	0.11	1.18
0.27	0.18	1.50	0.26	0.21	1.24	0.51	0.37	1.38	1.63	1.23	1.33
0.38	0.27	1.41	0.21	0.21	1.00	0.19	0.10	1.90	0.14	0.08	1.75
0.15	0.13	1.15	0.13	0.11	1.18	0.63	0.56	1.13	1.70	0.74	2.30
0.30	0.19	1.58	0.13	0.09	1.44	0.26	0.25	1.04	0.36	0.28	1.29
0.34	0.20	1.70	0.42	0.34	1.24	0.53	0.31	1.71	1.37	1.04	1.32
0.18	0.15	1.20	0.97	0.48	2.02	0.10	0.08	1.25	0.14	0.10	1.40
0.28	0.22	1.27	0.58	0.33	1.76	0.09	0.07	1.29	2.27	1.31	1.73
0.17	0.10	1.70	0.18	0.11	1.64	0.16	0.13	1.23	0.15	0.09	1.67
0.20	0.11	1.82	0.29	0.26	1.12	0.16	0.16	1.00	0.10	0.08	1.25
0.11	0.07	1.57	1.98	1.08	1.83	0.72	0.33	2.18	0.15	0.10	1.50
0.19	0.16	1.19	0.24	0.21	1.14	0.57	0.30	1.90	0.24	0.22	1.09
0.18	0.17	1.06	0.28	0.22	1.27	0.30	0.15	2.00	0.36	0.27	1.33

Table AVI 22 *cont.*

Length	Width	Aspect ratio	Length	Width	Aspect ratio	Length	Width	Aspect ratio
0.90	0.65	1.38	2.12	0.80	2.65	0.11	0.06	1.83
0.11	0.05	2.20	1.08	0.64	1.69	0.31	0.21	1.48
0.28	0.18	1.56	0.73	0.40	1.83	0.12	0.07	1.71
0.53	0.45	1.18	0.32	0.28	1.14	0.18	0.09	2.00
0.33	0.26	1.27	0.55	0.40	1.38	0.23	0.13	1.77
0.35	0.24	1.46	0.32	0.28	1.14	0.12	0.08	1.50
0.13	0.09	1.44	0.15	0.11	1.36	0.20	0.11	1.82
0.21	0.18	1.17	0.27	0.20	1.35	0.13	0.09	1.44
0.16	0.15	1.07	0.53	0.33	1.61	0.20	0.15	1.33
0.13	0.08	1.63	0.19	0.17	1.12	0.24	0.21	1.14
0.17	0.07	2.43	0.34	0.18	1.89	0.14	0.11	1.27
0.21	0.18	1.17	1.36	1.10	1.24	0.10	0.08	1.25
0.13	0.08	1.63	1.80	0.75	2.40	0.13	0.12	1.08
0.10	0.08	1.25	0.24	0.18	1.33	0.10	0.09	1.11
0.16	0.13	1.23	0.76	0.45	1.69	0.10	0.08	1.25
0.11	0.08	1.38	0.27	0.18	1.50	0.15	0.14	1.07
0.13	0.12	1.08	0.42	0.36	1.17	0.11	0.09	1.22
0.13	0.12	1.08	1.07	0.67	1.60	0.84	0.83	1.01
0.18	0.14	1.29	0.10	0.06	1.67	1.11	0.75	1.48
0.15	0.13	1.15	0.28	0.21	1.33	0.88	0.69	1.28
0.52	0.46	1.13	0.79	0.62	1.27	0.29	0.14	2.07
0.30	0.23	1.30	0.46	0.22	2.09	0.66	0.36	1.83
0.16	0.15	1.07	0.53	0.46	1.15	1.35	0.61	2.21
0.14	0.11	1.27	2.14	0.94	2.28	1.92	0.84	2.29
0.14	0.10	1.40	0.32	0.27	1.19	0.28	0.25	1.12
0.28	0.17	1.65	0.31	0.22	1.41	0.24	0.13	1.85
0.14	0.09	1.56	0.15	0.12	1.25	0.26	0.17	1.53
0.09	0.07	1.29	0.37	0.15	2.47	0.12	0.11	1.09
0.15	0.10	1.50	0.16	0.13	1.23	0.20	0.13	1.54
0.28	0.23	1.22	0.55	0.34	1.62	0.15	0.07	2.14
0.10	0.09	1.11	0.15	0.14	1.07	0.97	0.45	2.16
0.40	0.25	1.60	0.56	0.42	1.33	1.05	0.75	1.40
0.12	0.07	1.71	0.19	0.16	1.19	0.42	0.23	1.83
0.09	0.06	1.50	0.24	0.15	1.60	0.31	0.24	1.29
0.12	0.10	1.20	0.17	0.10	1.70	0.24	0.20	1.20
0.36	0.20	1.80	0.45	0.28	1.61	0.70	0.42	1.67
0.08	0.08	1.00	0.25	0.18	1.39	1.16	0.89	1.30
0.13	0.10	1.30	0.16	0.12	1.33	0.19	0.13	1.46
0.99	0.46	2.15	1.45	1.13	1.28	1.29	0.82	1.57
1.17	0.80	1.46	0.59	0.40	1.48	0.35	0.25	1.40
1.04	0.93	1.12	0.25	0.20	1.25	0.28	0.22	1.27
0.14	0.09	1.56	0.10	0.08	1.25	0.19	0.16	1.19
0.15	0.11	1.36	0.10	0.07	1.43	0.17	0.13	1.31
0.20	0.12	1.67	0.11	0.06	1.83	0.98	0.49	2.00
0.10	0.10	1.00	0.10	0.10	1.00	1.69	0.93	1.82
0.76	0.57	1.33	0.52	0.41	1.27			
0.35	0.26	1.35	0.18	0.08	2.25			
0.54	0.41	1.32	0.11	0.08	1.38			
0.60	0.36	1.67	0.69	0.35	1.97			
0.54	0.28	1.93	0.17	0.12	1.42			
0.24	0.16	1.50	0.17	0.11	1.55			
0.36	0.22	1.64	0.71	0.53	1.34			

Table AVI 23 *Summary statistics for pellets and crystals produced by schoolmaster snapper. All values are given in micrometers and refer to the longest axes unless specified otherwise.*

	Pellet length	Pellet width	Monocrystalline ellipsoid	Rod
count	1189	1189	1097	32
min	80	50	0.24	0.55
d10	**110**	**80**	**0.46**	**0.61**
median	***260***	***180***	***0.66***	***0.77***
d90	**1092**	**722**	**0.99**	**0.97**
max	2780	1830	2.20	1.13
d90-d10	982	642	0.53	0.36
mean	437	297	0.70	0.80
SD	437	275	0.23	0.15
SE of mean	13	8	0.01	0.03

Table AVI 24 *Dimensional data for monocrystalline ellipsoids produced by black grouper. All dimensions are in micrometers. Shading scheme differentiates between data from different samples (see footnote for key).*

Length	Length	Length	Length	Length	Length	Length	Length	Length	Length
1.04	0.83	0.91	0.65	0.77	1.40	0.73	1.26	0.71	0.93
1.18	1.12	1.10	1.02	0.74	1.01	1.06	1.02	0.88	1.02
0.88	1.18	1.30	1.22	0.50	0.59	0.59	1.18	1.22	0.45
0.49	0.84	1.06	0.76	0.60	1.04	1.49	1.25	1.08	1.04
0.63	0.74	1.30	0.92	0.90	0.96	0.94	0.85	0.87	0.82
0.55	1.02	0.84	0.87	1.14	1.14	0.79	1.16	1.29	1.52
0.65	1.74	0.72	1.28	0.93	1.16	0.68	1.65	0.67	0.84
1.04	0.73	1.04	1.39	0.49	0.79	0.85	1.01	0.99	1.41
0.60	0.95	1.38	0.89	0.76	1.09	1.50	1.32	0.97	0.96
0.83	0.59	0.88	0.74	0.71	1.39	1.12	0.85	0.93	0.80
1.46	0.56	1.26	0.91	0.90	1.12	1.07	0.94	1.80	1.09
0.94	0.79	0.99	1.03	0.93	0.80	0.89	0.76	0.95	1.14
0.87	0.67	0.74	1.37	1.12	1.02	0.88	0.73	1.08	0.81
0.96	1.09	1.36	1.02	0.47	0.61	0.86	1.05	1.13	1.42
1.30	1.17	0.82	0.74	1.18	0.49	1.14	0.63	0.56	0.87
0.96	1.25	1.02	0.49	0.94	0.53	0.94	0.66	0.76	0.85
1.13	1.07	1.02	0.82	0.81	1.43	0.97	0.73	1.23	1.00
1.17	1.04	1.12	1.37	0.88	0.52	1.02	0.51	1.42	1.21
1.00	1.58	2.06	1.23	0.53	0.60	0.87	0.83	1.18	0.95
1.51	1.02	0.85	0.89	1.19	0.32	0.95	0.72	0.54	0.93
0.91	1.17	0.75	1.52	0.78	0.72	1.17	1.07	1.02	0.80
1.08	0.77	0.57	1.13	0.59	1.13	1.12	1.01	0.94	1.12
1.04	0.99	1.12	0.98	1.08	1.10	0.52	1.05	1.16	1.10
0.66	0.46	0.80	1.19	1.22	1.36	0.36	1.23	0.77	1.37
0.94	0.57	0.63	0.83	0.99	1.57	0.78	1.28	0.70	1.37
0.85	0.85	0.68	0.58	1.04	0.96	1.31	0.74	1.28	1.51
0.74	0.90	1.14	0.45	1.03	1.42	0.59	0.49	0.93	1.30
0.72	0.75	1.14	1.02	1.45	1.38	1.09	0.70	1.18	1.17
1.06	0.68	1.12	0.89	0.53	0.70	1.01	0.79	1.37	1.53
0.77	1.21	0.37	0.61	0.81	0.94	1.52	0.83	0.94	0.95
1.17	0.61	0.58	1.30	1.43	0.98	1.07	1.75	1.01	0.65
0.93	0.87	0.84	0.90	1.29	0.82	1.06	1.00	1.14	0.60
0.76	0.85	0.83	1.12	0.80	1.06	0.96	0.46	0.78	1.12
0.82	1.09	0.36	0.69	0.66	1.47	1.29	1.86	0.99	0.57
0.56	0.83	0.69	0.73	0.93	0.68	1.09	1.17	0.96	0.85
1.39	1.01	0.85	1.21	1.06	1.03	1.38	0.89	0.65	0.64
0.69	0.62	0.81	0.90	0.54	1.07	1.07	1.43	0.62	0.70
0.93	1.06	0.81	0.67	0.61	1.41	0.91	1.02	1.15	0.68
1.43	1.36	0.98	0.91	1.42	0.78	0.62	1.15	1.09	1.14
1.15	1.39	0.94	0.49	1.53	0.80	0.71	1.40	0.41	0.73
1.06	1.18	1.29	1.26	0.66	0.63	0.59	0.70	0.50	1.27
1.09	1.26	0.88	1.28	1.17	1.57	0.62	1.17	1.37	1.33
0.81	0.69	0.85	1.39	0.73	1.01	0.49	1.06	0.59	0.84
1.14	0.81	0.89	1.14	1.45	1.07	0.87	0.71	1.27	1.03
0.82	1.03	1.27	1.06	0.86	1.31	1.05	1.04	0.53	0.69
0.54	0.99	1.00	0.48	0.78	0.74	0.57	0.97	0.96	0.56
0.92	1.05	0.58	0.57	1.10	1.45	0.56	1.19	1.45	0.99
0.68	0.59	1.65	0.63	0.70	1.30	1.38	0.63	0.62	0.61
0.87	1.03	1.21	1.17	0.44	0.95	0.90	1.15	0.59	1.20
0.90	1.25	0.97	1.07	0.73	1.26	0.70	0.69	1.08	0.79

Shading scheme identifies sample codes: CEI-BG-D1 | CEI-BG-D2 | CEI-BG-D3

Table AVI 24 *cont.*

Length	Length	Length	Length	Length	Length	Length	Length	Length	Length
1.11	0.91	0.98	0.50	0.54	1.14	1.43	1.01	0.65	0.87
0.86	0.65	1.28	1.09	1.28	1.27	0.84	0.60	0.90	0.83
1.37	0.83	0.43	1.06	0.86	1.24	1.26	0.83	0.92	0.95
1.24	0.69	1.48	1.32	1.37	1.16	0.83	0.64	1.61	1.56
1.44	0.76	1.44	1.33	0.53	1.71	0.86	0.62	0.99	0.95
0.62	0.57	1.54	1.21	1.13	0.39	0.81	0.96	1.25	1.18
0.95	1.16	1.21	1.12	1.22	0.65	1.03	1.03	1.12	0.96
1.06	0.61	1.03	0.77	0.91	1.04	1.46	1.02	0.93	0.85
1.04	1.13	1.54	0.91	0.67	1.32	0.69	0.47	1.19	0.78
0.71	0.51	1.01	0.61	0.84	0.62	0.79	1.07	0.75	0.86
0.83	0.79	0.59	1.20	0.69	1.17	1.89	0.75	1.16	0.94
1.16	1.08	0.95	1.01	1.30	1.09	0.54	0.84	0.91	1.17
0.89	0.89	0.67	0.77	1.08	0.84	1.11	0.65	0.69	1.45
0.78	1.21	0.55	0.50	0.71	0.71	1.04	1.15	0.83	0.77
0.71	0.91	1.50	0.76	0.68	0.91	0.87	0.53	1.80	0.78
1.06	1.28	1.60	0.79	0.86	0.82	1.12	1.25	1.63	1.02
1.13	1.35	0.95	0.99	0.85	1.64	0.52	0.79	1.08	1.08
0.60	0.80	1.22	0.69	1.25	1.29	1.50	0.78	1.06	0.64
1.13	1.53	0.41	0.78	1.45	0.93	1.23	0.86	1.00	1.00
0.65	0.94	0.89	1.20	0.93	1.55	0.59	0.67	0.70	1.14
1.30	1.08	0.78	1.21	1.61	0.48	0.88	0.74	1.23	1.38
1.49	0.43	0.64	0.90	1.22	1.87	1.20	0.69	0.85	1.60
0.97	1.17	0.66	0.95	1.28	1.25	1.22	0.79	1.00	1.46
1.22	0.76	1.16	0.95	0.88	1.21	0.79	1.51	1.30	0.78
0.78	0.97	0.72	0.70	1.00	0.73	1.47	0.64	0.65	0.88
1.35	1.06	1.16	0.62	0.59	1.39	1.09	1.10	1.24	1.93
0.74	0.71	0.82	1.81	1.36	1.11	1.45	1.01	1.63	0.76
0.50	1.02	1.23	0.54	0.84	1.18	1.14	0.87	1.66	0.85
0.91	0.92	1.26	1.02	1.02	0.94	1.12	1.64	0.68	0.95
1.18	1.10	1.29	1.20	1.10	0.76	0.62	0.98	1.60	0.63
1.59	0.91	1.46	0.58	1.13	0.37	0.75	1.26	1.28	0.87
1.17	1.23	1.45	1.01	0.95	0.89	0.77	1.06	0.53	1.66
1.17	1.46	0.82	0.99	1.23	0.69	1.45	0.52	0.70	1.05
0.93	2.22	1.73	0.91	1.05	1.05	0.75	0.96	0.86	1.35
0.78	1.15	1.00	1.25	1.23	1.12	0.95	0.93	0.77	0.77
1.14	0.91	1.47	1.07	1.16	1.27	1.09	1.00	0.86	1.22
0.53	1.57	1.12	1.04	1.04	1.01	1.14	1.41	1.31	1.28
0.91	0.84	0.88	1.31	0.92	1.06	1.03	1.24	0.55	1.23
0.94	0.73	0.92	1.22	1.49	1.11	1.96	1.18	0.53	1.00
0.85	1.48	0.99	0.57	0.79	1.00	1.64	0.62	0.83	0.59
1.22	1.53	0.92	0.68	1.26	1.14	0.89	0.98	1.27	1.13
0.70	0.93	0.76	0.98	1.23	1.10	1.27	0.92	0.94	0.82
1.18	1.19	0.90	0.95	1.17	0.75	0.74	1.07	0.57	0.83
0.74	1.40	0.65	0.93	1.02	1.35	0.96	1.37	1.03	1.02
0.93	1.37	0.88	1.43	0.92	1.12	0.88	0.75	0.90	0.63
1.08	0.95	1.18	0.47	1.38	0.77	0.71	0.66	0.84	1.14
1.06	1.11	0.88	0.93	1.00	1.07	0.77	0.67	0.99	0.73
0.87	1.65	0.99	0.71	0.89	1.18	0.87	0.98	0.84	0.81
0.65	0.76	0.95	0.89	1.47	1.15	0.99	0.84	1.12	0.68
1.00	1.21	1.24	0.42	1.02	0.39	1.21	1.00	1.48	0.83
0.78	0.75	1.23	1.09	1.29	0.75	0.97	0.72	0.74	1.56

Shading scheme identifies sample codes: CEI-BG-D1 CEI-BG-D2 CEI-BG-D3

Table AVI 24 *cont.*

Length	Length	Length	Length	Length	Length	Length	Length	Length	Length	Length
1.36	0.98	1.02	1.35	1.09	1.42	1.07	0.98	0.97	0.86	0.99
1.41	0.73	2.04	1.05	1.09	1.56	1.12	0.77	1.08	0.61	0.83
1.17	1.04	0.71	1.37	1.00	0.51	0.72	0.79	0.54	0.83	1.02
1.05	0.84	0.82	1.68	1.36	1.39	0.29	1.16	1.01	0.74	0.85
1.17	0.92	1.02	0.74	0.47	1.31	1.35	1.29	0.63	0.99	1.12
0.80	0.86	1.27	1.42	0.47	0.81	0.68	0.72	0.88	0.73	0.70
1.16	0.99	1.17	1.08	0.64	0.41	1.28	0.90	1.62	0.95	1.39
1.24	0.82	1.19	1.40	1.29	2.00	1.22	0.92	1.00	1.29	1.04
1.08	1.32	0.61	1.16	1.63	1.70	1.11	0.93	1.03	0.39	1.79
1.20	0.58	0.77	0.96	0.68	0.67	1.21	0.96	1.19	1.01	1.40
1.11	1.00	0.87	0.82	0.80	1.80	1.08	0.88	1.08	0.65	0.56
0.86	1.11	1.05	0.80	1.58	1.18	0.84	0.42	0.62	1.23	1.25
0.66	1.20	1.37	0.98	1.12	1.56	0.79	0.81	1.27	0.97	0.61
1.20	1.59	0.95	1.27	1.25	1.56	0.74	0.42	0.87	1.06	0.64
1.27	0.97	1.32	1.08	1.01	1.13	1.13	1.21	0.92	1.19	1.12
1.12	1.14	1.11	0.69	0.92	1.54	1.06	0.89	0.91	1.03	0.90
0.75	1.25	1.06	1.10	1.00	0.62	1.07	0.99	0.78	1.06	0.76
0.83	0.50	1.49	0.89	1.52	1.14	0.70	0.67	0.66	1.11	0.77
1.21	0.78	1.07	0.95	0.88	0.91	0.51	0.79	1.08	1.11	1.08
0.92	0.99	1.51	1.36	0.84	1.02	1.01	1.28	0.67	0.79	0.52
0.87	1.56	0.84	0.81	0.94	0.97	0.87	1.14	1.03	0.71	0.87
0.90	1.41	1.55	0.96	0.87	1.18	0.81	0.91	1.31	0.97	1.10
1.06	0.81	1.36	1.07	1.14	1.24	0.78	1.13	0.87	0.71	0.95
1.00	0.93	1.91	0.55	1.49	0.82	1.27	0.69	0.62	0.81	0.73
1.38	0.72	1.39	1.18	1.53	1.00	1.17	1.28	0.88	0.89	0.91
1.28	0.83	1.26	0.91	0.90	1.45	1.37	0.97	0.59	1.29	0.81
0.44	0.75	0.77	1.14	0.72	0.91	1.38	1.38	1.01	0.86	1.11
0.95	0.61	1.10	2.10	1.14	0.66	0.67	0.77	0.98	0.79	0.97
1.36	0.85	0.79	1.76	1.84	1.29	0.88	1.05	0.41	0.93	0.66
0.73	0.95	1.71	1.41	1.46	1.59	0.83	0.79	1.32	0.72	0.85
0.93	0.79	0.81	1.29	0.91	0.74	0.95	1.13	0.69	0.89	0.89
0.93	0.64	0.88	1.17	1.61	0.85	0.59	1.20	0.48	0.91	0.94
0.96	1.14	0.87	0.70	1.11	1.27	0.60	0.98	0.63	1.35	1.10
0.85	1.00	1.21	1.89	0.81	1.14	1.03	1.00	1.16	0.75	0.92
0.95	0.63	0.96	1.94	1.14	1.33	0.89	0.75	0.81	1.35	0.87
0.81	1.36	1.36	1.14	0.97	1.19	1.11	1.09	0.94	1.12	1.03
0.81	1.68	0.95	0.85	0.89	1.16	0.77	0.73	1.51	0.78	1.14
1.17	0.89	1.32	0.82	1.13	0.81	1.42	0.70	0.81	1.21	0.93
0.99	1.06	1.22	0.75	1.58	1.03	1.04	0.80	0.64	0.74	0.76
1.39	0.74	1.01	1.02	1.43	1.06	1.03	1.29	1.68	0.97	0.87
0.85	1.07	0.99	1.14	1.57	1.12	0.82	0.75	1.14	0.75	0.78
1.19	0.73	1.14	1.37	0.75	1.10	0.94	0.83	0.52	0.89	0.83
0.86	0.84	1.21	0.64	1.21	1.03	0.69	0.90	0.55	1.45	
0.88	0.86	1.41	0.83	1.49	1.50	0.80	1.00	0.83	0.97	
1.49	0.83	1.51	1.04	1.13	1.26	0.67	1.36	0.82	0.70	
1.12	0.78	1.21	2.12	0.80	1.22	0.79	1.00	1.01	0.84	
1.17	0.89	1.25	0.80	1.93	1.67	1.14	1.08	1.19	0.73	
1.42	1.25	1.19	0.94	0.95	1.12	1.03	0.88	1.15	1.19	
1.59	1.15	1.42	0.75	1.40	0.60	0.69	1.24	0.98	0.83	
0.83	0.96	0.94	1.04	0.61	1.55	0.98	1.22	0.76	0.98	
1.22	0.93	1.41	1.16	0.99	1.10	1.00	0.71	0.97	0.99	

Shading scheme identifies sample codes: CEI-BG-D1 | CEI-BG-D2 | CEI-BG-D3

Table AVI 25 *Dimensional data for rod-shaped crystals produced by black grouper. All dimensions are in micrometers. Shading scheme differentiates between data from different samples (see footnote for key).*

Length	Length	Length	Length	Length	Length	Length	Length	Length	Length
1.05	1.11	0.92	1.51	1.03	1.56	0.59	1.20	1.26	1.30
1.16	1.15	1.10	1.36	1.30	0.83	1.35	1.13	1.62	1.15
1.49	1.68	1.50	0.81	1.59	1.04	0.57	0.97	1.25	1.91
0.50	1.39	1.34	1.20	1.68	1.22	0.60	1.09	0.90	1.11
0.91	1.14	1.05	1.02	0.76	1.00	1.22	1.05	0.93	1.26
1.17	1.20	0.95	1.24	1.07	1.44	0.65	1.21	1.55	1.42
0.96	0.86	1.13	0.72	1.66	1.18	1.06	1.22	0.62	1.09
1.34	0.88	1.35	1.66	1.47	1.05	0.69	0.70	0.43	1.36
1.32	0.64	1.48	1.18	1.23	1.67	0.79	0.91	0.55	1.00
0.95	1.02	1.81	0.75	1.19	1.28	0.90	0.74	1.04	0.69
1.36	1.17	1.38	0.90	1.64	1.05	0.87	1.33	1.08	1.49
1.21	0.84	0.96	0.91	1.41	1.24	0.89	1.79	0.99	1.09
1.42	0.95	1.45	1.92	1.29	1.03	1.34	1.33	0.87	1.34
0.79	1.33	1.44	1.67	1.37	1.12	1.00	1.23	0.91	0.80
1.29	1.08	1.38	1.45	1.64	1.14	0.99	1.56	1.66	1.07
1.11	1.18	1.13	2.10	1.50	0.85	1.05	1.35	1.98	0.83
1.17	1.26	1.42	2.09	1.50	1.80	1.15	0.97	1.03	0.82
0.96	1.05	1.47	0.79	1.20	0.76	1.14	1.07	2.06	1.19
1.06	0.46	1.44	1.21	0.80	1.38	0.94	0.90	1.11	1.10
1.57	0.48	1.30	1.20	1.12	1.68	0.75	1.46	1.24	1.04
1.12	1.19	1.25	1.17	0.61	1.39	0.97	1.09	1.30	1.60
0.66	1.37	2.04	1.46	1.07	0.97	1.22	1.51	1.27	1.10
1.49	0.84	1.37	0.75	1.36	1.13	0.99	1.39	0.71	0.87
1.18	0.71	0.97	1.11	1.43	2.02	1.33	1.07	1.06	1.13
1.21	0.98	1.45	1.18	1.09	0.88	0.92	0.63	0.93	0.63
1.68	1.17	0.90	1.24	1.40	1.29	1.34	1.12	0.92	0.95
0.65	1.07	1.45	1.86	1.25	1.20	1.31	1.49	0.98	1.05
1.29	1.03	1.02	0.74	0.76	1.24	1.86	0.90	0.74	1.09
0.91	0.97	1.12	0.59	0.87	1.27	1.39	0.86	1.13	1.15
1.11	0.61	0.35	1.02	1.07	1.36	1.37	1.12	1.04	1.18
1.28	1.25	1.50	0.82	1.13	0.89	0.66	1.04	0.98	0.96
0.95	1.12	1.41	0.58	0.73	0.83	1.10	1.31	1.35	1.18
1.10	0.74	1.04	0.92	1.58	1.13	1.14	0.71	1.20	1.20
0.26	1.43	0.99	1.54	1.31	1.45	0.89	0.52	1.42	1.15
1.11	0.61	1.32	0.70	0.74	1.17	1.18	1.38	1.38	0.90
1.29	1.57	1.56	1.33	1.34	1.46	1.51	1.21	1.23	0.93
1.50	1.23	1.25	1.50	1.17	0.66	1.61	1.92	0.80	1.17
1.39	1.41	1.52	0.71	1.15	1.14	1.28	1.14	1.51	1.25
1.26	0.96	0.78	1.00	0.85	0.71	1.37	1.45	0.54	1.40
1.40	1.36	0.73	0.96	0.83	0.81	1.59	0.89	1.11	1.75
1.49	1.30	1.63	0.61	0.92	1.04	1.17	1.29	1.49	0.91
1.30	1.46	0.89	0.76	0.94	1.19	1.08	0.73	1.17	0.86
1.66	1.40	0.58	1.37	1.39	0.89	1.40	1.47	1.24	1.30
1.52	1.59	0.75	1.32	0.75	0.86	0.71	0.86	1.06	1.26
0.80	1.36	1.02	1.14	0.80	0.97	0.83	1.60	1.53	0.96
0.92	1.42	0.93	1.00	1.61	0.70	1.14	1.11	1.40	1.63
1.54	1.47	1.88	1.10	1.32	1.87	1.02	0.65	1.03	1.44
1.65	0.27	1.34	1.32	1.20	0.77	1.31	1.25	0.91	1.51
1.18	1.29	1.22	1.18	1.17	0.78	1.30	0.96	0.86	1.21
1.11	1.65	0.97	1.28	1.73	0.68	1.61	0.78	1.03	1.05
0.50	1.04	0.77	1.13	1.21	0.63	1.56	1.21	1.01	1.19

Shading scheme identifies sample codes: CEI-BG-D1 | CEI-BG-D2 | CEI-BG-D3

Table AVI 25 *cont.*

Length	Length	Length	Length	Length	Length	Length	Length
0.57	1.58	0.52	1.01	1.13	1.12	0.82	0.80
1.10	1.04	0.75	0.88	1.24	1.69	0.97	0.48
1.04	0.88	1.42	0.80	1.17	0.86	1.05	1.08
1.10	0.82	0.93	1.41	1.07	1.34	1.85	1.24
1.14	1.47	0.80	1.30	0.83	1.90	0.95	0.84
0.84	0.73	1.24	0.64	0.85	1.22	0.66	0.97
1.36	1.08	0.95	0.79	1.26	1.58	0.81	0.53
1.04	1.01	1.80	0.87	1.17	0.95	1.04	1.33
0.64	1.09	1.32	0.90	0.49	1.36	0.87	1.25
1.06	0.98	1.14	0.45	0.77	1.05	1.44	1.65
0.89	1.23	0.79	1.83	1.06	1.26	1.20	1.80
1.25	1.24	1.10	1.35	1.38	1.13	0.90	1.44
1.17	0.91	1.04	1.74	1.85	1.04	0.76	1.15
1.22	1.10	1.21	0.77	1.39	0.70	1.53	1.44
1.30	1.55	1.48	1.25	1.22	0.90	1.05	1.37
1.44	1.08	0.98	1.32	1.15	1.35	0.76	1.03
1.56	0.99	0.96	1.01	1.11	1.81	1.30	1.53
0.88	0.97	1.48	0.70	0.65	1.24	1.13	1.11
0.76	0.70	0.76	1.12	0.97	1.13	0.66	1.32
1.23	0.72	0.92	1.06	1.30	1.01	0.52	1.01
1.66	1.26	1.29	1.22	1.49	0.80	1.06	1.50
1.52	1.03	1.40	1.01	1.05	0.75	0.97	
1.13	1.01	0.88	1.12	0.94	1.09	0.42	
1.47	1.85	0.77	1.06	1.06	0.78	0.86	
1.23	1.31	0.88	1.24	1.21	0.62	0.90	
1.28	1.34	1.09	0.91	1.26	0.98	0.87	
1.26	1.33	1.32	0.94	0.82	1.05	0.85	
1.25	0.93	0.71	1.48	1.18	1.60	1.11	
1.80	1.44	1.23	1.21	1.02	1.28	1.04	
0.95	1.14	1.31	1.09	0.78	0.66	0.89	
0.84	0.75	1.50	1.30	0.83	1.21	1.04	
0.88	1.10	0.79	0.98	1.33	0.90	0.99	
0.99	0.64	0.94	0.78	0.81	1.21	1.21	
1.36	1.19	1.22	1.01	1.00	1.09	0.75	
1.09	0.86	0.91	1.20	0.63	1.32	1.08	
1.37	1.39	0.98	0.99	1.11	0.91	1.29	
1.40	1.29	0.98	1.05	0.99	0.79	1.22	
1.28	0.91	0.92	0.67	1.14	0.87	1.49	
1.02	1.03	1.47	1.80	1.00	1.15	0.99	
1.11	0.81	0.91	1.54	1.05	1.50	0.54	
1.28	0.97	1.44	0.93	1.37	1.25	0.88	
0.90	1.66	1.11	1.21	1.20	1.31	1.29	
1.29	0.85	0.80	1.56	0.79	1.10	1.02	
0.56	0.80	1.37	0.88	1.00	1.11	0.56	
0.95	1.01	1.23	1.06	0.95	0.45	1.10	
0.98	1.30	1.01	0.96	0.87	1.30	0.66	
1.21	1.02	0.96	1.50	0.88	1.09	0.71	
1.66	1.15	0.87	1.24	1.03	0.94	0.72	
0.76	1.57	1.23	1.44	1.11	1.28	0.75	
0.87	1.03	0.89	0.99	0.97	0.88	0.87	
1.47	0.93	1.14	1.11	1.48	1.30	0.74	

Shading scheme identifies sample codes: CEI-BG-D1 | CEI-BG-D2 | CEI-BG-D3

Table AVI 26 *Dimensional data for subsidiary crystal forms produced by black grouper. All dimensions are in micrometers. Shading scheme differentiates between data from different samples (see footnote for key).*

Rhomb	Rhomb	Rhomb	Sml dmbl	Sml dmbl	Sml dmbl
0.38	0.91	0.69	1.13	1.00	0.44
0.90	0.31	0.65	1.35	1.28	1.31
0.61	0.27	0.80	0.95	1.09	0.92
0.35	0.35	0.82	1.09	1.53	0.98
0.42	1.33	1.11	1.21	1.14	0.76
0.36	0.97	0.81	1.45	0.93	1.01
0.41	0.75	0.73	1.54	1.03	1.33
0.51	0.46	1.72	1.70	0.92	
0.41	0.34	1.16	0.92	1.32	
0.41	0.30	0.38	1.48	1.26	
0.38	0.64		1.22	1.10	

Shading scheme identifies sample codes: CEI-BG-D1 | CEI-BG-D2 | CEI-BG-D3

Table AVI 27 *Dimensional data for pellets produced by black grouper. All dimensions are in millimetres.*

Length	Width	Aspect ratio	Length	Width	Aspect ratio	Length	Width	Aspect ratio	Length	Width	Aspect ratio
0.87	0.76	1.14	1.34	0.87	1.54	1.17	0.80	1.46	0.82	0.62	1.32
0.92	0.60	1.53	0.60	0.56	1.07	1.01	0.76	1.33	1.01	0.75	1.35
0.81	0.68	1.19	0.82	0.73	1.12	0.93	0.74	1.26	0.32	0.20	1.60
0.88	0.76	1.16	0.97	0.94	1.03	0.68	0.60	1.13	0.89	0.53	1.68
1.23	1.00	1.23	1.33	0.82	1.62	1.09	0.74	1.47	0.89	0.73	1.22
0.83	0.57	1.46	0.91	0.66	1.38	1.34	1.08	1.24	0.49	0.32	1.53
0.94	0.55	1.71	1.58	0.70	2.26	0.95	0.75	1.27	0.18	0.12	1.50
1.00	0.66	1.52	0.89	0.64	1.39	1.54	1.32	1.17	0.76	0.49	1.55
0.71	0.62	1.15	0.79	0.62	1.27	1.82	1.22	1.49	0.93	0.61	1.52
0.81	0.55	1.47	0.77	0.53	1.45	1.43	1.17	1.22	0.17	0.10	1.70
0.72	0.56	1.29	1.12	0.77	1.45	1.58	1.29	1.22	0.13	0.11	1.18
0.76	0.56	1.36	0.90	0.80	1.13	1.91	1.13	1.69	0.13	0.12	1.08
0.88	0.59	1.49	1.30	0.65	2.00	1.05	0.59	1.78	0.33	0.27	1.22
0.22	0.18	1.22	1.24	0.94	1.32	0.35	0.16	2.19	0.71	0.64	1.11
1.02	0.65	1.57	0.45	0.24	1.88	2.19	1.13	1.94	1.01	0.77	1.31
1.25	0.47	2.66	1.22	0.89	1.37	1.59	1.20	1.33	0.29	0.22	1.32
0.73	0.52	1.40	1.23	0.86	1.43	1.73	1.29	1.34	0.77	0.70	1.10
0.73	0.50	1.46	1.17	0.70	1.67	2.60	1.49	1.74	0.82	0.66	1.24
0.40	0.23	1.74	0.89	0.77	1.16	2.13	1.49	1.43	0.89	0.53	1.68
0.70	0.60	1.17	0.18	0.13	1.38	0.85	0.76	1.12	1.05	0.80	1.31
1.31	0.64	2.05	0.22	0.15	1.47	1.33	0.95	1.40	1.27	0.98	1.30
0.15	0.10	1.50	0.25	0.17	1.47	1.36	0.85	1.60	1.32	0.82	1.61
0.26	0.18	1.44	0.57	0.38	1.50	1.28	0.96	1.33	1.11	0.81	1.37
0.33	0.22	1.50	1.12	0.77	1.45	0.34	0.25	1.36	0.93	0.78	1.19
1.11	0.74	1.50	0.83	0.62	1.34	1.31	1.05	1.25	1.30	0.78	1.67
0.72	0.65	1.11	1.34	1.08	1.24	1.34	0.82	1.63	1.09	1.08	1.01
0.69	0.66	1.05	1.24	1.05	1.18	1.69	1.30	1.30	1.37	1.08	1.27
0.72	0.54	1.33	0.84	0.68	1.24	1.05	0.73	1.44	0.88	0.77	1.14
0.63	0.49	1.29	1.13	0.71	1.59	1.22	0.82	1.49	0.70	0.54	1.30
0.75	0.56	1.34	0.42	0.40	1.05	0.85	0.57	1.49	1.33	1.16	1.15
0.11	0.09	1.22	1.48	0.99	1.49	0.83	0.56	1.48	0.84	0.74	1.14
0.63	0.48	1.31	1.14	0.77	1.48	2.24	1.34	1.67	0.27	0.20	1.35
0.18	0.13	1.38	0.63	0.44	1.43	0.22	0.18	1.22	1.23	0.94	1.31
0.20	0.11	1.82	0.68	0.50	1.36	0.18	0.15	1.20	1.47	1.33	1.11
0.70	0.58	1.21	0.61	0.53	1.15	1.84	1.36	1.35	0.93	0.73	1.27
0.93	0.53	1.75	0.31	0.20	1.55	1.09	0.81	1.35	1.16	0.91	1.27
0.22	0.09	2.44	0.66	0.48	1.38	0.26	0.16	1.63	0.67	0.52	1.29
0.14	0.10	1.40	0.70	0.50	1.40	1.01	0.69	1.46	1.18	0.89	1.33
0.89	0.53	1.68	0.61	0.41	1.49	0.76	0.58	1.31	1.25	1.03	1.21
0.25	0.19	1.32	0.64	0.46	1.39	0.98	0.56	1.75	1.10	0.77	1.43
0.24	0.12	2.00	0.36	0.23	1.57	0.97	0.51	1.90	0.23	0.19	1.21
0.71	0.53	1.34	0.93	0.80	1.16	0.76	0.73	1.04	1.14	0.75	1.52
0.09	0.08	1.13	0.64	0.49	1.31	0.86	0.68	1.26	1.22	0.90	1.36
0.92	0.71	1.30	0.73	0.55	1.33	0.97	0.81	1.20	1.30	0.78	1.67
0.21	0.13	1.62	0.12	0.11	1.09	0.97	0.73	1.33	0.91	0.58	1.57
0.54	0.44	1.23	0.19	0.10	1.90	1.12	0.89	1.26	0.80	0.50	1.60
1.20	0.65	1.85	0.91	0.43	2.12	1.10	1.06	1.04	0.51	0.47	1.09
1.42	0.97	1.46	0.84	0.59	1.42	1.03	0.72	1.43	1.17	0.59	1.98
0.93	0.65	1.43	0.26	0.16	1.63	1.13	0.64	1.77	0.82	0.66	1.24
1.05	0.67	1.57	0.87	0.66	1.32	0.77	0.63	1.22	0.26	0.14	1.86
1.30	1.10	1.18	0.23	0.17	1.35	1.25	0.71	1.76	0.99	0.60	1.65

Table AVI 27 *cont.*

Length	Width	Aspect ratio	Length	Width	Aspect ratio	Length	Width	Aspect ratio	Length	Width	Aspect ratio
0.67	0.56	1.20	0.19	0.15	1.27	1.41	1.25	1.13	0.98	0.88	1.11
0.81	0.69	1.17	0.33	0.24	1.38	1.17	0.61	1.92	0.45	0.24	1.88
0.69	0.63	1.10	0.57	0.41	1.39	1.11	0.63	1.76	0.27	0.20	1.35
1.15	1.13	1.02	0.94	0.66	1.42	1.18	0.67	1.76	0.26	0.18	1.44
0.94	0.72	1.31	0.99	0.67	1.48	0.91	0.64	1.42	0.26	0.09	2.89
0.24	0.19	1.26	0.93	0.82	1.13	1.37	0.83	1.65	0.21	0.14	1.50
0.96	0.65	1.48	0.14	0.12	1.17	0.94	0.47	2.00	0.24	0.19	1.26
0.86	0.68	1.26	0.15	0.13	1.15	0.74	0.64	1.16	0.64	0.58	1.10
0.71	0.61	1.16	0.34	0.25	1.36	1.22	1.01	1.21	1.02	0.83	1.23
1.36	1.20	1.13	1.09	0.71	1.54	0.79	0.51	1.55	1.23	0.62	1.98
1.22	0.60	2.03	1.13	0.92	1.23	0.72	0.51	1.41	1.05	0.75	1.40
1.11	0.87	1.28	0.45	0.23	1.96	0.25	0.16	1.56	0.29	0.24	1.21
1.12	0.93	1.20	0.76	0.75	1.01	1.01	0.75	1.35	1.26	0.76	1.66
0.63	0.51	1.24	0.27	0.23	1.17	1.02	0.83	1.23	0.18	0.17	1.06
0.82	0.67	1.22	0.14	0.10	1.40	1.66	1.09	1.52	0.81	0.71	1.14
0.98	0.83	1.18	0.19	0.14	1.36	0.96	0.53	1.81	0.87	0.60	1.45
1.30	1.05	1.24	1.15	0.86	1.34	1.10	0.80	1.38	0.93	0.55	1.69
1.08	0.78	1.38	0.57	0.46	1.24	0.54	0.27	2.00	0.68	0.63	1.08
1.54	1.29	1.19	0.76	0.66	1.15	1.14	0.95	1.20	1.06	0.80	1.33
1.22	0.66	1.85	0.85	0.65	1.31	0.31	0.22	1.41	0.73	0.64	1.14
1.32	0.89	1.48	0.80	0.65	1.23	0.24	0.17	1.41	0.85	0.64	1.33
0.85	0.47	1.81	1.13	1.05	1.08	1.12	1.07	1.05	0.78	0.56	1.39
1.47	0.94	1.56	0.24	0.20	1.20	0.78	0.56	1.39	0.70	0.63	1.11
0.96	0.64	1.50	0.20	0.12	1.67	0.31	0.17	1.82	1.47	0.73	2.01
0.76	0.69	1.10	0.89	0.74	1.20	0.27	0.19	1.42	0.88	0.51	1.73
0.86	0.75	1.15	0.23	0.16	1.44	0.20	0.13	1.54	0.16	0.09	1.78
0.77	0.65	1.18	0.16	0.08	2.00	0.85	0.71	1.20	0.23	0.13	1.77
0.99	0.85	1.16	0.29	0.22	1.32	0.90	0.64	1.41	1.20	1.18	1.02
0.89	0.63	1.41	0.40	0.29	1.38	0.74	0.52	1.42	0.92	0.51	1.80
0.78	0.71	1.10	0.76	0.57	1.33	1.14	0.69	1.65	1.17	0.75	1.56
0.17	0.11	1.55	0.19	0.16	1.19	0.71	0.71	1.00	1.15	0.64	1.80
0.95	0.89	1.07	1.24	0.85	1.46	0.91	0.68	1.34			

Table AVI 28 *Summary statistics for pellets and crystals produced by black grouper. All values are given in micrometers and refer to the longest axes unless specified otherwise.*

	Pellet length	Pellet width	Monocrystalline ellipsoid	Rod	Rhombohedron	Small dumbbell
count	331	331	1562	888	32	29
min	90	80	0.29	0.26	0.27	0.44
d10	**230**	**160**	**0.64**	**0.75**	**0.34**	**0.92**
Median	***870***	***640***	***0.98***	***1.11***	***0.56***	***1.13***
d90	**1320**	**1010**	**1.39**	**1.50**	**1.10**	**1.49**
max	2600	1490	2.22	2.10	1.72	1.70
d90-d10	1090	850	0.75	0.76	0.75	0.57
Mean	845	613	1.00	1.12	0.64	1.15
SD	425	309	0.30	0.30	0.34	0.27
SE of mean	23	17	0.01	0.01	0.06	0.05

Appendix VII: Pellet size data before and after wave agitation experiments

Pellets comprising monocrystalline ellipsoids (produced by black grouper) were placed in artificial seawater and moderately agitated for one week and then a further three weeks. Images collected before the experiment, after one week, and four weeks were analysed using calibrated software (JMicroVision, v.1.2.7.) to obtain size data in order to establish the rate of pellet breakdown due to purely physical processes. The full details of this experiment are described in the main text (Chapter 5). Complete size data are presented in the following tables.

Table AVII 1 *Pellet dimensions before agitation experiments (all dimension values are given in micrometers).*

Length	Width	Aspect ratio	Length	Width	Aspect ratio	Length	Width	Aspect ratio
860	760	1.13	800	670	1.19	990	840	1.18
130	90	1.44	770	600	1.28	940	590	1.59
140	110	1.27	710	420	1.69	740	450	1.64
880	660	1.33	370	320	1.16	870	600	1.45
120	70	1.71	90	80	1.13	710	590	1.20
870	670	1.30	150	50	3.00	840	510	1.65
90	80	1.13	90	80	1.13	860	620	1.39
690	520	1.33	160	120	1.33	1060	900	1.18
140	80	1.75	700	630	1.11	730	720	1.01
140	80	1.75	950	560	1.70	1090	610	1.79
160	80	2.00	1140	730	1.56	540	520	1.04
900	710	1.27	1020	820	1.24	1020	760	1.34
300	240	1.25	230	170	1.35	910	670	1.36
720	570	1.26	150	120	1.25	1160	960	1.21
120	60	2.00	550	400	1.38	1160	910	1.27
110	60	1.83	180	140	1.29	1020	660	1.55
180	140	1.29	380	300	1.27	300	270	1.11
740	560	1.32	720	530	1.36	890	760	1.17
110	80	1.38	740	500	1.48	890	680	1.31
850	560	1.52	600	490	1.22	100	90	1.11
340	220	1.55	610	370	1.65	180	70	2.57
1630	830	1.96	360	240	1.50	100	80	1.25
1280	790	1.62	510	460	1.11	940	750	1.25
230	130	1.77	910	760	1.20	810	690	1.17
1110	670	1.66	210	190	1.11	100	70	1.43
760	580	1.31	410	300	1.37	450	320	1.41
940	640	1.47	1160	920	1.26	800	720	1.11
840	630	1.33	730	690	1.06	770	560	1.38
750	630	1.19	970	890	1.09	1130	1040	1.09
740	610	1.21	560	550	1.02	500	370	1.35

Table AVII 1 *cont.*

Length	Width	Aspect ratio	Length	Width	Aspect ratio	Length	Width	Aspect ratio	Length	Width	Aspect ratio
1090	750	1.45	90	30	3.00	1050	680	1.54	1070	520	2.06
120	110	1.09	70	30	2.33	1470	1010	1.46	120	80	1.50
90	40	2.25	80	70	1.14	1270	790	1.61	470	320	1.47
60	40	1.50	100	50	2.00	950	580	1.64	270	160	1.69
80	40	2.00	80	60	1.33	960	630	1.52	110	70	1.57
1130	860	1.31	690	460	1.50	110	80	1.38	850	620	1.37
80	60	1.33	140	100	1.40	1300	630	2.06	750	590	1.27
100	70	1.43	210	120	1.75	1260	580	2.17	1180	810	1.46
970	760	1.28	990	760	1.30	1240	900	1.38	810	530	1.53
290	220	1.32	1090	690	1.58	100	80	1.25	810	540	1.50
250	220	1.14	230	190	1.21	840	550	1.53	660	550	1.20
90	80	1.13	510	460	1.11	910	720	1.26	730	370	1.97
290	190	1.53	100	60	1.67	720	570	1.26	430	330	1.30
330	150	2.20	630	580	1.09	1070	770	1.39	470	400	1.18
340	230	1.48	140	90	1.56	1430	910	1.57	450	410	1.10
130	60	2.17	70	60	1.17	840	630	1.33	590	590	1.00
130	120	1.08	560	440	1.27	940	520	1.81	890	420	2.12
60	40	1.50	100	60	1.67	640	580	1.10	710	440	1.61
860	560	1.54	230	160	1.44	840	750	1.12	200	140	1.43
180	90	2.00	140	90	1.56	990	550	1.80	960	800	1.20
820	540	1.52	890	420	2.12	820	510	1.61	720	550	1.31
800	640	1.25	830	750	1.11	880	690	1.28	890	700	1.27
210	140	1.50	120	80	1.50	610	510	1.20	730	410	1.78
330	160	2.06	110	90	1.22	570	400	1.43	100	60	1.67
610	430	1.42	120	70	1.71	720	580	1.24	780	550	1.42
940	610	1.54	70	50	1.40	770	550	1.40	550	440	1.25
70	60	1.17	170	90	1.89	660	440	1.50	90	80	1.13
880	450	1.96	50	30	1.67	650	580	1.12	140	120	1.17
190	120	1.58	750	460	1.63	330	250	1.32	560	540	1.04
160	130	1.23	100	70	1.43	720	670	1.07	170	90	1.89
1080	740	1.46	1230	670	1.84	880	720	1.22	180	100	1.80
300	170	1.76	1340	950	1.41	830	690	1.20	690	540	1.28
110	50	2.20	890	810	1.10	990	950	1.04	440	370	1.19
130	90	1.44	1650	720	2.29	110	70	1.57	540	430	1.26
920	610	1.51	1120	690	1.62	730	610	1.20	570	520	1.10
70	60	1.17	1360	810	1.68	860	670	1.28	280	240	1.17
90	60	1.50	1150	820	1.40	820	590	1.39	160	150	1.07
240	210	1.14	1020	650	1.57	150	130	1.15	760	540	1.41
180	120	1.50	1140	790	1.44	670	520	1.29	540	420	1.29
200	130	1.54	800	580	1.38	1260	540	2.33	110	80	1.38
60	50	1.20	1340	780	1.72	820	490	1.67	660	450	1.47
60	40	1.50	1030	980	1.05	980	560	1.75	150	80	1.88
110	50	2.20	1000	660	1.52	140	100	1.40	120	90	1.33
70	50	1.40	1100	950	1.16	140	80	1.75	110	100	1.10
80	50	1.60	100	90	1.11	1050	600	1.75	520	440	1.18
80	40	2.00	1240	610	2.03	940	440	2.14	270	230	1.17
1170	880	1.33	1120	700	1.60	870	620	1.40	420	320	1.31
230	220	1.05	930	840	1.11	220	150	1.47	610	410	1.49
120	100	1.20	1300	870	1.49	830	550	1.51	1130	730	1.55
770	600	1.28	1160	770	1.51	820	470	1.74	750	570	1.32
270	170	1.59	1050	510	2.06	140	70	2.00	800	650	1.23
130	90	1.44	810	520	1.56	110	80	1.38	260	170	1.53

Table AVII 1 *cont.*

Length	Width	Aspect ratio	Length	Width	Aspect ratio	Length	Width	Aspect ratio	Length	Width	Aspect ratio
750	730	1.03	710	600	1.18	1090	770	1.42	940	720	1.31
1070	640	1.67	800	560	1.43	170	90	1.89	920	600	1.53
980	510	1.92	990	750	1.32	190	160	1.19	1090	660	1.65
960	780	1.23	370	260	1.42	950	710	1.34	770	710	1.08
1250	650	1.92	610	340	1.79	130	70	1.86	890	710	1.25
750	680	1.10	550	320	1.72	1010	750	1.35	1310	1090	1.20
700	590	1.19	130	100	1.30	200	170	1.18	860	560	1.54
690	640	1.08	630	530	1.19	780	600	1.30	870	600	1.45
820	640	1.28	100	60	1.67	1290	1050	1.23	1050	760	1.38
810	650	1.25	830	670	1.24	160	140	1.14	920	700	1.31
720	680	1.06	150	90	1.67	890	750	1.19	1120	890	1.26
640	460	1.39	110	70	1.57	870	750	1.16	1010	710	1.42
750	730	1.03	940	600	1.57	400	220	1.82	880	790	1.11
120	90	1.33	640	480	1.33	140	120	1.17	860	710	1.21
140	110	1.27	1110	780	1.42	240	180	1.33	170	140	1.21
110	80	1.38	100	70	1.43	820	550	1.49	900	730	1.23
130	80	1.63	950	630	1.51	220	180	1.22	120	90	1.33
110	90	1.22	140	100	1.40	740	640	1.16	940	580	1.62
200	100	2.00	580	500	1.16	640	490	1.31	1400	1070	1.31
350	220	1.59	270	150	1.80	640	500	1.28	230	170	1.35
1210	610	1.98	140	110	1.27	760	600	1.27	100	70	1.43
100	80	1.25	940	720	1.31	970	550	1.76	1290	960	1.34
760	440	1.73	790	740	1.07	800	560	1.43	840	700	1.20
150	80	1.88	720	670	1.07	920	640	1.44	960	530	1.81
770	530	1.45	1040	740	1.41	740	530	1.40	100	70	1.43
570	510	1.12	910	690	1.32	680	660	1.03	770	750	1.03
100	70	1.43	130	120	1.08	810	730	1.11	1000	850	1.18
820	610	1.34	640	540	1.19	1250	540	2.31	160	130	1.23
910	560	1.63	1360	1100	1.24	970	690	1.41	1160	600	1.93
980	630	1.56	1640	620	2.65	880	650	1.35	1130	900	1.26
100	70	1.43	1270	790	1.61	660	500	1.32	750	680	1.10
690	640	1.08	1540	1260	1.22	980	760	1.29	1080	690	1.57
690	470	1.47	920	660	1.39	710	530	1.34	1420	820	1.73
760	520	1.46	1310	910	1.44	640	570	1.12	970	550	1.76
180	80	2.25	1330	1160	1.15	690	440	1.57	800	660	1.21
950	590	1.61	540	460	1.17	690	630	1.10	620	450	1.38
90	80	1.13	1090	820	1.33	550	520	1.06	400	160	2.50
160	70	2.29	1330	990	1.34	90	80	1.13	890	750	1.19
230	150	1.53	820	560	1.46	100	70	1.43	960	540	1.78
580	440	1.32	1300	1080	1.20	780	440	1.77	1240	660	1.88
600	500	1.20	840	730	1.15	710	540	1.31	1380	750	1.84
870	850	1.02	870	730	1.19	890	810	1.10	1290	980	1.32
740	590	1.25	1100	730	1.51	1190	590	2.02	740	400	1.85
690	540	1.28	110	90	1.22	810	620	1.31	1080	760	1.42
320	190	1.68	170	70	2.43	80	70	1.14	790	560	1.41
1000	830	1.20	130	110	1.18	770	560	1.38	1210	730	1.66
1040	760	1.37	180	120	1.50	920	660	1.39	700	690	1.01
890	540	1.65	680	570	1.19	130	90	1.44	900	740	1.22
840	690	1.22	1060	860	1.23	750	510	1.47	700	600	1.17
770	720	1.07	100	60	1.67	820	610	1.34	700	510	1.37
1000	690	1.45	1130	1050	1.08	820	660	1.24	120	70	1.71
730	600	1.22	660	620	1.06	1080	580	1.86	790	510	1.55

Table AVII 2 *Pellet dimensions after one week of moderate agitation (all dimension values are given in micrometers).*

Length	Width	Aspect ratio	Length	Width	Aspect ratio	Length	Width	Aspect ratio	Length	Width	Aspect ratio
1070	760	1.41	200	100	2.00	190	80	2.38	400	370	1.08
640	440	1.45	330	190	1.74	140	70	2.00	410	390	1.05
460	330	1.39	600	530	1.13	380	320	1.19	620	460	1.35
390	270	1.44	250	90	2.78	310	290	1.07	380	350	1.09
580	420	1.38	130	90	1.44	420	180	2.33	310	120	2.58
190	120	1.58	120	110	1.09	740	510	1.45	610	420	1.45
170	120	1.42	90	70	1.29	730	460	1.59	620	390	1.59
850	740	1.15	120	70	1.71	1280	520	2.46	280	220	1.27
170	110	1.55	720	340	2.12	530	410	1.29	590	390	1.51
190	120	1.58	210	130	1.62	470	280	1.68	810	290	2.79
470	360	1.31	190	130	1.46	860	350	2.46	610	510	1.20
180	70	2.57	110	50	2.20	650	510	1.27	600	350	1.71
130	100	1.30	140	70	2.00	370	250	1.48	920	330	2.79
110	60	1.83	120	100	1.20	490	350	1.40	790	490	1.61
640	530	1.21	140	50	2.80	440	350	1.26	570	450	1.27
440	310	1.42	150	90	1.67	600	390	1.54	730	610	1.20
480	270	1.78	200	110	1.82	380	290	1.31	410	290	1.41
440	250	1.76	220	130	1.69	590	340	1.74	340	240	1.42
220	100	2.20	190	70	2.71	560	420	1.33	140	130	1.08
430	340	1.26	280	130	2.15	400	270	1.48	240	130	1.85
200	120	1.67	680	510	1.33	1050	350	3.00	110	80	1.38
170	150	1.13	160	140	1.14	520	210	2.48	340	160	2.13
110	60	1.83	190	100	1.90	460	270	1.70	130	100	1.30
70	50	1.40	170	100	1.70	880	490	1.80	440	270	1.63
220	80	2.75	550	450	1.22	640	430	1.49	710	310	2.29
770	390	1.97	170	90	1.89	400	330	1.21	500	310	1.61
580	350	1.66	670	470	1.43	350	320	1.09	450	300	1.50
170	100	1.70	210	110	1.91	550	360	1.53	330	230	1.43
170	70	2.43	410	250	1.64	650	450	1.44	430	360	1.19
100	70	1.43	950	340	2.79	570	330	1.73	250	180	1.39
100	60	1.67	580	470	1.23	320	190	1.68	510	200	2.55
80	70	1.14	140	100	1.40	810	470	1.72	390	250	1.56
170	140	1.21	130	90	1.44	650	340	1.91	810	710	1.14
350	160	2.19	610	480	1.27	520	420	1.24	660	430	1.53
100	70	1.43	420	190	2.21	650	210	3.10	500	310	1.61
810	390	2.08	320	300	1.07	360	230	1.57	510	390	1.31
90	60	1.50	450	230	1.96	290	210	1.38	210	170	1.24
320	250	1.28	680	410	1.66	310	230	1.35	570	300	1.90
450	230	1.96	190	150	1.27	470	240	1.96	250	180	1.39
150	100	1.50	160	120	1.33	350	320	1.09	350	200	1.75
490	450	1.09	280	180	1.56	910	360	2.53	290	170	1.71
140	90	1.56	420	270	1.56	480	260	1.85	410	340	1.21
180	90	2.00	290	180	1.61	470	380	1.24	260	180	1.44
770	340	2.26	150	90	1.67	450	400	1.13	200	150	1.33
130	90	1.44	180	140	1.29	540	460	1.17	880	330	2.67
100	80	1.25	130	100	1.30	330	200	1.65	260	150	1.73
120	100	1.20	580	290	2.00	460	320	1.44	370	220	1.68
190	160	1.19	200	150	1.33	840	540	1.56	600	440	1.36
100	60	1.67	440	320	1.38	240	140	1.71	520	300	1.73
260	110	2.36	280	240	1.17	380	140	2.71	820	360	2.28
100	90	1.11	270	190	1.42	580	370	1.57	390	270	1.44
230	90	2.56	290	190	1.53	390	170	2.29	790	290	2.72

Table AVII 2 *cont.*

Length	Width	Aspect ratio	Length	Width	Aspect ratio	Length	Width	Aspect ratio	Length	Width	Aspect ratio
840	330	2.55	540	370	1.46	300	230	1.30	450	330	1.36
540	500	1.08	450	300	1.50	260	170	1.53	550	220	2.50
790	240	3.29	210	130	1.62	200	160	1.25	720	390	1.85
350	240	1.46	410	170	2.41	440	390	1.13	490	190	2.58
300	160	1.88	470	460	1.02	230	150	1.53	670	300	2.23
420	200	2.10	570	550	1.04	230	160	1.44	110	70	1.57
850	300	2.83	770	400	1.93	690	320	2.16	110	70	1.57
420	370	1.14	450	320	1.41	330	150	2.20	90	70	1.29
280	110	2.55	750	520	1.44	270	240	1.13	390	200	1.95
500	350	1.43	430	290	1.48	410	360	1.14	380	300	1.27
310	250	1.24	170	160	1.06	310	110	2.82	800	380	2.11
390	190	2.05	280	220	1.27	210	150	1.40	740	430	1.72
270	230	1.17	640	490	1.31	140	100	1.40	380	260	1.46
530	380	1.39	250	160	1.56	200	200	1.00	910	410	2.22
420	400	1.05	360	290	1.24	200	150	1.33	380	270	1.41
880	510	1.73	650	580	1.12	330	230	1.43	400	250	1.60
480	260	1.85	220	170	1.29	130	80	1.63	420	340	1.24
570	330	1.73	320	160	2.00	220	180	1.22	390	200	1.95
350	320	1.09	480	360	1.33	310	200	1.55	340	290	1.17
800	400	2.00	300	270	1.11	420	350	1.20	740	320	2.31
300	200	1.50	190	140	1.36	570	440	1.30	780	360	2.17
310	210	1.48	530	280	1.89	220	140	1.57	270	140	1.93
550	240	2.29	210	130	1.62	270	190	1.42	560	270	2.07
400	340	1.18	210	190	1.11	320	160	2.00	460	310	1.48
590	500	1.18	200	190	1.05	250	150	1.67	450	270	1.67
420	390	1.08	260	190	1.37	270	160	1.69	340	150	2.27
390	360	1.08	340	170	2.00	190	130	1.46	280	190	1.47
120	60	2.00	200	140	1.43	620	380	1.63	1040	550	1.89
400	360	1.11	220	140	1.57	320	240	1.33	200	140	1.43
650	430	1.51	740	520	1.42	250	190	1.32	280	180	1.56
560	300	1.87	210	180	1.17	850	390	2.18	230	210	1.10
390	340	1.15	720	490	1.47	240	140	1.71	280	150	1.87
600	290	2.07	220	140	1.57	270	130	2.08	300	160	1.88
400	310	1.29	380	170	2.24	260	250	1.04	1290	450	2.87
360	200	1.80	210	100	2.10	470	300	1.57	390	170	2.29
270	220	1.23	230	180	1.28	200	160	1.25	510	420	1.21
410	200	2.05	430	380	1.13	400	290	1.38	150	70	2.14
430	260	1.65	270	170	1.59	340	210	1.62	590	470	1.26
1000	410	2.44	410	270	1.52	190	130	1.46	100	70	1.43
250	180	1.39	740	370	2.00	380	170	2.24	630	600	1.05
280	130	2.15	240	140	1.71	290	220	1.32	490	350	1.40
150	120	1.25	450	300	1.50	210	170	1.24	410	320	1.28
560	330	1.70	300	230	1.30	770	510	1.51	380	380	1.00
410	330	1.24	370	190	1.95	270	180	1.50	380	270	1.41
390	360	1.08	230	130	1.77	600	470	1.28	370	190	1.95
330	270	1.22	210	130	1.62	770	380	2.03	270	180	1.50
550	350	1.57	220	180	1.22	560	260	2.15	260	160	1.63
340	240	1.42	320	230	1.39	410	310	1.32	160	100	1.60
340	230	1.48	240	170	1.41	350	290	1.21	330	280	1.18
560	280	2.00	390	210	1.86	590	490	1.20	600	280	2.14
500	270	1.85	190	140	1.36	400	330	1.21	420	240	1.75
150	130	1.15	220	100	2.20	310	280	1.11	210	120	1.75

Table AVII 2 *cont.*

Length	Width	Aspect ratio	Length	Width	Aspect ratio	Length	Width	Aspect ratio	Length	Width	Aspect ratio
230	110	2.09	140	120	1.17	130	80	1.63	150	90	1.67
390	100	3.90	160	80	2.00	140	70	2.00	90	50	1.80
1010	290	3.48	90	70	1.29	90	70	1.29	90	70	1.29
580	470	1.23	110	70	1.57	170	110	1.55	210	100	2.10
490	250	1.96	190	120	1.58	180	60	3.00	150	120	1.25
840	410	2.05	150	90	1.67	180	90	2.00	120	80	1.50
310	150	2.07	120	80	1.50	170	120	1.42	120	110	1.09
220	110	2.00	170	110	1.55	190	70	2.71	160	130	1.23
410	300	1.37	110	100	1.10	90	80	1.13	80	70	1.14
150	70	2.14	240	100	2.40	110	80	1.38	200	110	1.82
160	110	1.45	130	100	1.30	170	110	1.55	180	90	2.00
520	360	1.44	140	110	1.27	90	70	1.29	110	100	1.10
410	230	1.78	200	160	1.25	120	70	1.71	140	100	1.40
250	230	1.09	160	130	1.23	270	160	1.69	140	110	1.27
130	70	1.86	180	110	1.64	260	70	3.71	120	110	1.09
170	130	1.31	160	90	1.78	140	100	1.40	90	60	1.50
190	180	1.06	140	110	1.27	130	80	1.63	110	60	1.83
240	200	1.20	150	100	1.50	140	90	1.56	220	130	1.69
400	320	1.25	210	130	1.62	150	80	1.88	120	60	2.00
130	120	1.08	130	70	1.86	140	100	1.40	120	60	2.00
120	110	1.09	160	90	1.78	130	110	1.18	170	140	1.21
130	110	1.18	130	110	1.18	130	80	1.63	140	90	1.56
320	250	1.28	120	100	1.20	160	120	1.33	130	80	1.63
430	230	1.87	200	150	1.33	70	60	1.17	100	90	1.11
290	240	1.21	120	120	1.00	190	170	1.12	100	50	2.00
880	440	2.00	410	330	1.24	160	100	1.60	140	110	1.27
260	140	1.86	140	80	1.75	170	130	1.31	70	60	1.17
370	260	1.42	310	220	1.41	140	90	1.56	290	150	1.93
100	80	1.25	200	110	1.82	70	40	1.75	160	110	1.45
170	90	1.89	240	130	1.85	70	50	1.40	180	110	1.64
160	100	1.60	120	100	1.20	90	60	1.50	220	150	1.47
330	160	2.06	70	40	1.75	80	60	1.33	110	80	1.38
190	90	2.11	180	110	1.64	110	60	1.83	200	90	2.22
110	80	1.38	150	100	1.50	130	80	1.63	220	130	1.69
170	90	1.89	250	140	1.79	170	80	2.13	170	100	1.70
170	90	1.89	160	110	1.45	120	50	2.40	200	130	1.54
90	80	1.13	120	90	1.33	80	60	1.33	100	100	1.00
170	100	1.70	170	80	2.13	190	100	1.90	160	100	1.60
90	80	1.13	160	110	1.45	100	80	1.25	100	70	1.43
100	80	1.25	220	160	1.38	120	60	2.00	160	90	1.78
100	90	1.11	110	80	1.38	110	80	1.38	150	110	1.36
170	110	1.55	160	100	1.60	130	90	1.44	110	50	2.20
180	170	1.06	130	80	1.63	330	160	2.06	190	110	1.73
180	90	2.00	110	80	1.38	170	120	1.42	130	100	1.30
140	110	1.27	100	90	1.11	150	110	1.36	90	60	1.50
160	90	1.78	120	90	1.33	310	290	1.07	150	110	1.36
150	90	1.67	160	100	1.60	210	100	2.10	140	80	1.75
190	70	2.71	70	50	1.40	220	140	1.57	110	80	1.38
140	110	1.27	160	90	1.78	150	90	1.67	140	70	2.00
110	70	1.57	160	90	1.78	100	60	1.67	260	160	1.63
310	200	1.55	110	60	1.83	180	110	1.64	180	90	2.00
240	140	1.71	210	90	2.33	260	150	1.73	160	110	1.45

Table AVII 2 *cont.*

Length	Width	Aspect ratio	Length	Width	Aspect ratio	Length	Width	Aspect ratio	Length	Width	Aspect ratio
110	80	1.38	140	70	2.00	110	70	1.57	140	100	1.40
250	100	2.50	90	70	1.29	160	120	1.33	210	120	1.75
80	60	1.33	110	100	1.10	80	60	1.33	140	90	1.56
90	60	1.50	120	80	1.50	80	50	1.60	290	170	1.71
120	70	1.71	450	290	1.55	260	120	2.17	100	90	1.11
130	100	1.30	220	160	1.38	160	130	1.23	200	120	1.67
200	110	1.82	210	110	1.91	150	90	1.67	150	110	1.36
180	90	2.00	180	80	2.25	120	70	1.71	100	40	2.50
120	90	1.33	150	110	1.36	190	110	1.73	150	110	1.36
140	100	1.40	110	70	1.57	120	80	1.50	100	60	1.67
170	90	1.89	160	90	1.78	140	90	1.56	180	140	1.29
120	80	1.50	160	110	1.45	180	120	1.50	120	110	1.09
210	90	2.33	290	160	1.81	220	90	2.44	190	100	1.90
130	80	1.63	180	130	1.38	160	60	2.67	220	130	1.69
110	70	1.57	180	100	1.80	170	90	1.89	110	100	1.10
140	100	1.40	90	60	1.50	120	90	1.33	140	90	1.56
170	70	2.43	170	110	1.55	120	50	2.40	180	130	1.38
80	80	1.00	120	80	1.50	80	70	1.14	190	100	1.90
100	80	1.25	160	140	1.14	70	60	1.17	230	140	1.64
90	70	1.29	160	90	1.78	110	60	1.83	120	70	1.71
250	120	2.08	120	90	1.33	160	100	1.60	140	90	1.56
140	70	2.00	140	80	1.75	100	90	1.11	150	50	3.00
220	130	1.69	180	100	1.80	160	110	1.45	100	60	1.67
70	70	1.00	220	90	2.44	110	80	1.38	130	110	1.18
180	90	2.00	130	70	1.86	180	140	1.29	230	120	1.92
170	50	3.40	130	90	1.44	110	50	2.20	160	90	1.78
180	70	2.57	140	60	2.33	130	120	1.08	270	130	2.08
110	90	1.22	130	80	1.63	90	70	1.29	190	110	1.73
160	90	1.78	60	50	1.20	70	50	1.40	160	90	1.78
120	80	1.50	190	120	1.58	150	120	1.25	180	110	1.64
150	110	1.36	140	130	1.08	150	70	2.14	170	110	1.55
140	80	1.75	100	80	1.25	140	110	1.27	120	90	1.33
150	70	2.14	100	60	1.67	190	100	1.90	160	80	2.00
190	60	3.17	170	130	1.31	210	90	2.33	150	80	1.88
190	100	1.90	200	110	1.82	160	90	1.78	170	100	1.70
80	50	1.60	140	110	1.27	160	70	2.29	200	90	2.22
130	90	1.44	190	100	1.90	120	40	3.00	200	100	2.00
140	80	1.75	120	60	2.00	170	150	1.13	200	140	1.43
250	120	2.08	150	70	2.14	110	90	1.22	210	120	1.75
210	80	2.63	410	240	1.71	130	60	2.17	150	80	1.88
150	100	1.50	170	90	1.89	250	140	1.79	90	70	1.29
110	70	1.57	190	160	1.19	80	60	1.33	460	210	2.19
210	120	1.75	130	100	1.30	180	120	1.50	110	90	1.22
160	120	1.33	160	90	1.78	150	90	1.67	80	60	1.33
180	120	1.50	110	100	1.10	140	70	2.00	80	70	1.14
190	120	1.58	150	110	1.36	170	130	1.31	170	90	1.89
140	60	2.33	130	90	1.44	230	150	1.53	190	140	1.36
120	70	1.71	120	60	2.00	220	120	1.83	120	70	1.71
110	70	1.57	130	90	1.44	110	100	1.10	140	90	1.56
190	100	1.90	150	100	1.50	230	110	2.09	100	80	1.25
130	90	1.44	130	130	1.00	160	110	1.45	200	70	2.86
120	120	1.00	100	80	1.25	220	110	2.00	60	40	1.50

Table AVII 2 *cont.*

Length	Width	Aspect ratio	Length	Width	Aspect ratio	Length	Width	Aspect ratio
80	60	1.33	160	80	2.00	150	120	1.25
130	100	1.30	460	260	1.77	150	110	1.36
80	70	1.14	190	80	2.38	120	70	1.71
160	110	1.45	100	70	1.43	130	90	1.44
90	60	1.50	120	50	2.40	130	70	1.86
130	100	1.30	130	60	2.17	310	120	2.58
70	70	1.00	160	100	1.60	300	110	2.73
90	60	1.50	100	70	1.43	230	80	2.88
210	100	2.10	90	60	1.50	90	70	1.29
160	140	1.14	220	170	1.29	200	110	1.82
120	100	1.20	200	120	1.67	110	50	2.20
80	60	1.33	170	120	1.42	500	270	1.85
190	90	2.11	130	90	1.44	110	80	1.38
190	80	2.38	150	50	3.00	130	70	1.86
120	80	1.50	170	80	2.13	140	80	1.75
80	60	1.33	240	120	2.00	130	60	2.17
70	60	1.17	200	90	2.22	110	90	1.22
80	70	1.14	80	70	1.14	130	80	1.63
120	70	1.71	160	140	1.14	160	50	3.20
110	100	1.10	90	60	1.50	150	90	1.67
110	60	1.83	140	90	1.56	210	100	2.10
130	60	2.17	110	80	1.38	120	80	1.50
170	120	1.42	110	50	2.20	120	80	1.50
100	80	1.25	120	70	1.71	90	70	1.29
80	60	1.33	170	80	2.13	100	90	1.11
80	60	1.33	60	40	1.50	130	70	1.86
250	90	2.78	240	130	1.85	120	80	1.50
190	80	2.38	100	100	1.00	130	110	1.18
140	90	1.56	200	100	2.00	80	70	1.14
70	60	1.17	100	70	1.43	100	70	1.43
90	60	1.50	90	80	1.13	280	180	1.56
200	80	2.50	140	120	1.17	320	140	2.29
200	110	1.82	130	120	1.08			
140	90	1.56	120	110	1.09			
120	80	1.50	130	70	1.86			
280	130	2.15	180	100	1.80			
80	60	1.33	150	100	1.50			
180	100	1.80	170	70	2.43			
150	90	1.67	210	130	1.62			
110	80	1.38	110	90	1.22			
90	50	1.80	130	80	1.63			
90	60	1.50	70	60	1.17			
120	80	1.50	320	220	1.45			
150	110	1.36	190	110	1.73			
120	80	1.50	210	110	1.91			
140	100	1.40	200	100	2.00			
180	140	1.29	210	110	1.91			
320	150	2.13	160	90	1.78			
120	80	1.50	140	90	1.56			
180	120	1.50	80	50	1.60			
150	80	1.88	70	40	1.75			
230	90	2.56	140	70	2.00			

Table AVII 3 *Pellet dimensions after one week of moderate agitation (all dimension values are given in micrometers).*

Length	Width	Aspect ratio	Length	Width	Aspect ratio	Length	Width	Aspect ratio	Length	Width	Aspect ratio
160	100	1.60	330	190	1.74	460	170	2.71	80	50	1.60
130	100	1.30	330	250	1.32	180	140	1.29	80	40	2.00
80	50	1.60	70	50	1.40	500	340	1.47	100	60	1.67
70	50	1.40	90	50	1.80	130	90	1.44	140	70	2.00
80	70	1.14	170	120	1.42	120	50	2.40	170	90	1.89
80	50	1.60	210	130	1.62	200	130	1.54	220	90	2.44
120	90	1.33	80	50	1.60	200	110	1.82	120	100	1.20
170	110	1.55	100	60	1.67	510	270	1.89	260	120	2.17
150	90	1.67	90	60	1.50	320	190	1.68	380	130	2.92
130	110	1.18	130	90	1.44	130	100	1.30	180	100	1.80
120	90	1.33	90	80	1.13	180	100	1.80	150	130	1.15
140	80	1.75	180	130	1.38	260	180	1.44	120	90	1.33
230	160	1.44	130	90	1.44	150	120	1.25	100	50	2.00
70	70	1.00	200	140	1.43	110	60	1.83	60	50	1.20
130	110	1.18	120	70	1.71	220	110	2.00	80	50	1.60
90	70	1.29	140	110	1.27	460	250	1.84	160	110	1.45
90	60	1.50	160	110	1.45	80	70	1.14	140	90	1.56
460	220	2.09	120	80	1.50	480	320	1.50	140	70	2.00
560	360	1.56	120	80	1.50	150	60	2.50	100	80	1.25
290	190	1.53	90	70	1.29	350	200	1.75	90	80	1.13
320	120	2.67	70	60	1.17	130	80	1.63	90	60	1.50
130	70	1.86	440	260	1.69	190	110	1.73	80	60	1.33
270	140	1.93	220	120	1.83	130	80	1.63	90	80	1.13
280	260	1.08	80	50	1.60	70	50	1.40	120	90	1.33
190	100	1.90	130	70	1.86	140	110	1.27	240	170	1.41
300	130	2.31	230	140	1.64	410	270	1.52	100	90	1.11
130	70	1.86	140	100	1.40	150	50	3.00	70	50	1.40
150	90	1.67	80	60	1.33	70	40	1.75	100	60	1.67
260	100	2.60	110	60	1.83	180	70	2.57	210	100	2.10
110	50	2.20	70	60	1.17	110	80	1.38	230	210	1.10
150	130	1.15	90	70	1.29	150	100	1.50	180	60	3.00
110	70	1.57	110	100	1.10	110	60	1.83	550	490	1.12
200	110	1.82	130	100	1.30	150	120	1.25	750	390	1.92
210	100	2.10	290	170	1.71	90	70	1.29	340	270	1.26
90	60	1.50	130	100	1.30	50	50	1.00	200	160	1.25
100	70	1.43	90	70	1.29	60	50	1.20	80	70	1.14
110	70	1.57	170	110	1.55	130	80	1.63	90	50	1.80
60	50	1.20	190	80	2.38	70	70	1.00	100	70	1.43
110	70	1.57	240	120	2.00	110	70	1.57	180	130	1.38
120	90	1.33	550	400	1.38	90	70	1.29	100	70	1.43
170	130	1.31	590	460	1.28	80	50	1.60	90	80	1.13
70	50	1.40	210	160	1.31	240	220	1.09	210	100	2.10
150	110	1.36	250	200	1.25	280	110	2.55	150	70	2.14
290	150	1.93	110	70	1.57	170	100	1.70	190	160	1.19
70	70	1.00	260	160	1.63	70	40	1.75	110	90	1.22
80	70	1.14	170	80	2.13	70	40	1.75	100	60	1.67
250	140	1.79	250	160	1.56	310	250	1.24	100	70	1.43
180	100	1.80	100	60	1.67	150	100	1.50	200	90	2.22
80	60	1.33	180	120	1.50	140	80	1.75	380	220	1.73
110	60	1.83	60	40	1.50	240	110	2.18	310	210	1.48
70	60	1.17	80	40	2.00	120	70	1.71	100	80	1.25
490	370	1.32	410	370	1.11	120	100	1.20	130	100	1.30

Table AVII 3 *cont.*

Length	Width	Aspect ratio	Length	Width	Aspect ratio	Length	Width	Aspect ratio	Length	Width	Aspect ratio
180	80	2.25	80	60	1.33	70	50	1.40	110	70	1.57
200	80	2.50	160	100	1.60	90	60	1.50	190	100	1.90
70	50	1.40	120	90	1.33	200	120	1.67	100	80	1.25
130	80	1.63	210	130	1.62	140	50	2.80	120	70	1.71
90	50	1.80	190	100	1.90	170	110	1.55	120	80	1.50
130	70	1.86	150	100	1.50	190	70	2.71	120	90	1.33
150	130	1.15	190	80	2.38	210	130	1.62	80	70	1.14
90	60	1.50	70	50	1.40	100	60	1.67	130	60	2.17
340	280	1.21	190	80	2.38	250	90	2.78	100	70	1.43
120	70	1.71	140	80	1.75	230	120	1.92	260	90	2.89
150	80	1.88	110	70	1.57	140	80	1.75	140	60	2.33
200	80	2.50	60	60	1.00	180	140	1.29	110	60	1.83
90	60	1.50	210	110	1.91	140	80	1.75	380	270	1.41
70	40	1.75	200	110	1.82	160	130	1.23	130	60	2.17
150	90	1.67	80	70	1.14	230	160	1.44	110	100	1.10
390	200	1.95	120	60	2.00	170	80	2.13	210	70	3.00
170	130	1.31	160	100	1.60	270	150	1.80	120	60	2.00
110	80	1.38	170	120	1.42	180	110	1.64	270	190	1.42
130	80	1.63	180	120	1.50	150	90	1.67	180	100	1.80
110	60	1.83	110	70	1.57	110	100	1.10	90	60	1.50
310	160	1.94	170	80	2.13	120	100	1.20	80	50	1.60
800	320	2.50	100	60	1.67	110	80	1.38	90	60	1.50
160	100	1.60	100	70	1.43	250	190	1.32	70	50	1.40
80	50	1.60	140	90	1.56	100	70	1.43	100	80	1.25
200	110	1.82	140	120	1.17	110	90	1.22	190	140	1.36
130	70	1.86	170	130	1.31	160	90	1.78	100	70	1.43
90	60	1.50	170	90	1.89	80	70	1.14	50	40	1.25
80	50	1.60	110	90	1.22	130	50	2.60	60	50	1.20
240	170	1.41	70	60	1.17	150	100	1.50	170	70	2.43
80	70	1.14	160	100	1.60	260	220	1.18	180	160	1.13
70	50	1.40	330	170	1.94	290	170	1.71	140	90	1.56
110	70	1.57	150	100	1.50	180	100	1.80	240	100	2.40
120	90	1.33	200	110	1.82	90	60	1.50	90	80	1.13
130	60	2.17	270	170	1.59	160	80	2.00	100	60	1.67
100	60	1.67	150	80	1.88	140	100	1.40	140	70	2.00
120	90	1.33	150	130	1.15	130	70	1.86	90	70	1.29
190	100	1.90	360	200	1.80	110	80	1.38	120	70	1.71
100	70	1.43	190	140	1.36	180	130	1.38	110	60	1.83
350	140	2.50	160	80	2.00	140	80	1.75	200	60	3.33
140	120	1.17	200	130	1.54	390	170	2.29	100	60	1.67
100	90	1.11	220	150	1.47	220	130	1.69	80	50	1.60
90	80	1.13	120	100	1.20	300	160	1.88	160	140	1.14
80	80	1.00	200	100	2.00	160	120	1.33	100	40	2.50
130	70	1.86	160	110	1.45	110	70	1.57	90	60	1.50
270	160	1.69	130	90	1.44	170	100	1.70	310	210	1.48
120	70	1.71	80	50	1.60	130	100	1.30	60	50	1.20
180	70	2.57	70	60	1.17	200	60	3.33	120	70	1.71
220	190	1.16	170	130	1.31	130	100	1.30	230	80	2.88
110	70	1.57	100	80	1.25	90	70	1.29	150	90	1.67
390	150	2.60	180	150	1.20	90	70	1.29	90	50	1.80
100	70	1.43	90	60	1.50	60	50	1.20	140	80	1.75
450	230	1.96	150	140	1.07	120	50	2.40	90	50	1.80

Table AVII 3 *cont.*

Length	Width	Aspect ratio	Length	Width	Aspect ratio	Length	Width	Aspect ratio	Length	Width	Aspect ratio
220	110	2.00	110	40	2.75	120	70	1.71	170	130	1.31
110	80	1.38	80	70	1.14	220	120	1.83	110	70	1.57
120	70	1.71	70	60	1.17	130	80	1.63	80	60	1.33
140	110	1.27	140	90	1.56	90	60	1.50	120	90	1.33
140	90	1.56	120	70	1.71	100	60	1.67	140	70	2.00
140	50	2.80	120	70	1.71	50	50	1.00	120	60	2.00
110	70	1.57	120	50	2.40	210	120	1.75	110	100	1.10
70	50	1.40	110	80	1.38	70	60	1.17	90	70	1.29
110	50	2.20	80	50	1.60	140	110	1.27	190	90	2.11
130	110	1.18	240	140	1.71	150	70	2.14	120	70	1.71
240	110	2.18	120	80	1.50	80	70	1.14	130	50	2.60
230	140	1.64	120	80	1.50	180	90	2.00	90	60	1.50
230	100	2.30	110	80	1.38	80	50	1.60	120	60	2.00
120	80	1.50	160	130	1.23	60	50	1.20	70	40	1.75
330	300	1.10	210	80	2.63	100	70	1.43	70	60	1.17
160	80	2.00	120	50	2.40	130	90	1.44	80	50	1.60
200	120	1.67	160	90	1.78	110	40	2.75	100	60	1.67
130	110	1.18	70	70	1.00	220	90	2.44	150	90	1.67
140	80	1.75	80	60	1.33	110	70	1.57	90	60	1.50
280	200	1.40	110	80	1.38	130	60	2.17	100	90	1.11
220	150	1.47	190	130	1.46	80	60	1.33	230	110	2.09
90	80	1.13	80	50	1.60	60	40	1.50	80	60	1.33
120	90	1.33	140	60	2.33	60	40	1.50	120	60	2.00
140	110	1.27	110	100	1.10	90	60	1.50	90	60	1.50
70	60	1.17	130	110	1.18	90	50	1.80	110	70	1.57
60	50	1.20	60	40	1.50	120	50	2.40	120	90	1.33
120	90	1.33	90	50	1.80	140	90	1.56	60	50	1.20
100	100	1.00	270	100	2.70	140	130	1.08	100	80	1.25
190	110	1.73	180	80	2.25	110	80	1.38	80	60	1.33
90	60	1.50	180	100	1.80	90	70	1.29	90	70	1.29
150	100	1.50	80	80	1.00	80	60	1.33	80	60	1.33
100	60	1.67	140	70	2.00	100	90	1.11	140	70	2.00
140	110	1.27	130	90	1.44	150	80	1.88	120	70	1.71
110	100	1.10	120	80	1.50	110	90	1.22	110	100	1.10
150	80	1.88	70	60	1.17	110	80	1.38	130	90	1.44
130	70	1.86	70	60	1.17	140	110	1.27	100	70	1.43
220	110	2.00	70	40	1.75	60	40	1.50	70	70	1.00
150	80	1.88	90	60	1.50	90	50	1.80	70	60	1.17
240	130	1.85	190	100	1.90	50	30	1.67	100	60	1.67
190	100	1.90	120	110	1.09	80	60	1.33	60	50	1.20
180	100	1.80	100	40	2.50	70	40	1.75	60	40	1.50
170	90	1.89	90	50	1.80	70	60	1.17	110	70	1.57
130	80	1.63	150	90	1.67	130	90	1.44	110	60	1.83
150	90	1.67	80	70	1.14	110	80	1.38	130	70	1.86
120	100	1.20	110	90	1.22	170	110	1.55	60	40	1.50
250	120	2.08	240	80	3.00	80	60	1.33	80	80	1.00
140	50	2.80	140	130	1.08	170	100	1.70	150	110	1.36
140	50	2.80	120	110	1.09	70	50	1.40	100	80	1.25
270	150	1.80	110	70	1.57	100	60	1.67	100	80	1.25
130	100	1.30	80	60	1.33	150	90	1.67	90	70	1.29
100	60	1.67	150	80	1.88	160	110	1.45	100	90	1.11
100	50	2.00	200	80	2.50	250	120	2.08	150	100	1.50

Table AVII 3 *cont.*

Length	Width	Aspect ratio	Length	Width	Aspect ratio	Length	Width	Aspect ratio	Length	Width	Aspect ratio
150	100	1.50	150	110	1.36	110	90	1.22	110	80	1.38
60	50	1.20	100	60	1.67	120	90	1.33	150	90	1.67
80	80	1.00	130	90	1.44	220	90	2.44	170	80	2.13
60	50	1.20	190	100	1.90	180	90	2.00	160	80	2.00
120	50	2.40	120	80	1.50	190	140	1.36	180	100	1.80
100	70	1.43	170	90	1.89	190	120	1.58	90	70	1.29
80	60	1.33	150	70	2.14	110	90	1.22	150	90	1.67
130	100	1.30	160	100	1.60	120	90	1.33	140	80	1.75
240	130	1.85	390	220	1.77	110	70	1.57	120	70	1.71
150	90	1.67	90	80	1.13	140	80	1.75	110	50	2.20
100	70	1.43	60	40	1.50	190	80	2.38	110	40	2.75
80	70	1.14	90	80	1.13	100	60	1.67	90	60	1.50
100	80	1.25	140	120	1.17	80	40	2.00	180	100	1.80
130	80	1.63	130	110	1.18	50	40	1.25	170	100	1.70
120	70	1.71	90	60	1.50	290	180	1.61	140	70	2.00
260	220	1.18	120	60	2.00	130	100	1.30	80	40	2.00
130	100	1.30	110	80	1.38	130	100	1.30	160	120	1.33
160	90	1.78	140	60	2.33	80	60	1.33	100	70	1.43
110	60	1.83	160	90	1.78	140	110	1.27	150	100	1.50
70	50	1.40	140	70	2.00	130	110	1.18	90	80	1.13
60	40	1.50	70	60	1.17	170	80	2.13	230	120	1.92
200	110	1.82	60	40	1.50	120	60	2.00	100	60	1.67
160	120	1.33	70	50	1.40	250	110	2.27	260	100	2.60
80	60	1.33	110	90	1.22	100	40	2.50	120	80	1.50
110	70	1.57	60	50	1.20	260	120	2.17	110	70	1.57
130	40	3.25	70	50	1.40	90	70	1.29	160	110	1.45
110	90	1.22	190	100	1.90	140	90	1.56	220	110	2.00
80	70	1.14	100	70	1.43	280	110	2.55	160	80	2.00
140	90	1.56	80	60	1.33	180	90	2.00	100	60	1.67
180	100	1.80	210	130	1.62	80	60	1.33	170	100	1.70
120	70	1.71	70	40	1.75	180	100	1.80	150	100	1.50
130	60	2.17	140	80	1.75	150	60	2.50	120	120	1.00
70	60	1.17	120	100	1.20	100	60	1.67	110	70	1.57
120	90	1.33	280	130	2.15	80	50	1.60	210	130	1.62
90	80	1.13	140	80	1.75	80	60	1.33	170	100	1.70
70	50	1.40	200	110	1.82	100	70	1.43	160	110	1.45
70	70	1.00	180	130	1.38	110	60	1.83	100	80	1.25
110	100	1.10	140	90	1.56	110	60	1.83	140	120	1.17
70	50	1.40	250	160	1.56	110	60	1.83	130	60	2.17
100	70	1.43	160	100	1.60	70	60	1.17	160	90	1.78
210	160	1.31	130	70	1.86	140	90	1.56	110	80	1.38
70	60	1.17	210	70	3.00	70	50	1.40	90	60	1.50
190	90	2.11	80	70	1.14	120	90	1.33	170	110	1.55
80	60	1.33	240	180	1.33	310	110	2.82	180	110	1.64
160	80	2.00	130	70	1.86	130	90	1.44	150	130	1.15
70	50	1.40	100	70	1.43	130	80	1.63	80	60	1.33
120	80	1.50	140	90	1.56	80	70	1.14	150	90	1.67
120	90	1.33	160	80	2.00	90	70	1.29	300	200	1.50
210	190	1.11	150	80	1.88	130	90	1.44	80	50	1.60
180	110	1.64	90	70	1.29	180	130	1.38	60	50	1.20
140	70	2.00	310	210	1.48	170	80	2.13	170	90	1.89
270	70	3.86	80	60	1.33	220	110	2.00	290	120	2.42

Table AVII 3 *cont.*

Length	Width	Aspect ratio	Length	Width	Aspect ratio	Length	Width	Aspect ratio	Length	Width	Aspect ratio
60	60	1.00	220	140	1.57	120	70	1.71	110	50	2.20
260	140	1.86	300	160	1.88	50	50	1.00	290	240	1.21
140	90	1.56	110	70	1.57	300	230	1.30	310	260	1.19
130	100	1.30	390	210	1.86	200	120	1.67	220	170	1.29
540	210	2.57	180	120	1.50	830	300	2.77	100	90	1.11
130	80	1.63	110	80	1.38	580	390	1.49	200	120	1.67
110	50	2.20	130	90	1.44	230	200	1.15	110	50	2.20
90	50	1.80	130	80	1.63	150	100	1.50	90	50	1.80
130	90	1.44	100	70	1.43	330	280	1.18	390	210	1.86
130	70	1.86	290	190	1.53	130	80	1.63	220	100	2.20
80	70	1.14	100	50	2.00	110	80	1.38	130	70	1.86
310	150	2.07	430	340	1.26	370	350	1.06	210	120	1.75
160	110	1.45	290	210	1.38	550	360	1.53	170	80	2.13
140	90	1.56	210	80	2.63	190	110	1.73	80	70	1.14
160	90	1.78	370	110	3.36	110	90	1.22	110	50	2.20
210	90	2.33	310	220	1.41	730	520	1.40	90	50	1.80
150	90	1.67	310	280	1.11	430	310	1.39	710	250	2.84
100	80	1.25	600	380	1.58	130	40	3.25	360	270	1.33
280	100	2.80	350	100	3.50	160	90	1.78	420	220	1.91
170	110	1.55	330	300	1.10	110	70	1.57	410	260	1.58
140	60	2.33	230	110	2.09	200	110	1.82	250	190	1.32
100	80	1.25	720	320	2.25	270	120	2.25	80	50	1.60
230	90	2.56	350	270	1.30	540	430	1.26	90	70	1.29
230	210	1.10	110	90	1.22	410	270	1.52	130	90	1.44
230	110	2.09	160	130	1.23	400	270	1.48	390	210	1.86
230	170	1.35	550	330	1.67	800	420	1.90	280	160	1.75
130	80	1.63	280	160	1.75	270	230	1.17	100	80	1.25
90	50	1.80	130	70	1.86	350	60	5.83	150	120	1.25
100	90	1.11	170	110	1.55	140	110	1.27	140	90	1.56
90	80	1.13	390	310	1.26	150	120	1.25	130	70	1.86
80	60	1.33	400	270	1.48	130	90	1.44	110	70	1.57
100	70	1.43	120	60	2.00	100	70	1.43	290	180	1.61
70	50	1.40	120	60	2.00	170	110	1.55	90	70	1.29
110	70	1.57	110	80	1.38	100	60	1.67	140	100	1.40
100	70	1.43	70	40	1.75	150	110	1.36	460	240	1.92
80	70	1.14	130	100	1.30	870	290	3.00	100	60	1.67
270	210	1.29	570	360	1.58	300	270	1.11	390	320	1.22
170	110	1.55	170	160	1.06	280	130	2.15	290	200	1.45
210	90	2.33	150	80	1.88	730	370	1.97	380	360	1.06
130	90	1.44	500	310	1.61	200	180	1.11	520	360	1.44
140	140	1.00	290	210	1.38	800	310	2.58	110	90	1.22
300	150	2.00	380	210	1.81	70	50	1.40	520	420	1.24
140	140	1.00	150	50	3.00	380	260	1.46	340	220	1.55
120	80	1.50	210	80	2.63	440	300	1.47	110	80	1.38
300	170	1.76	670	410	1.63	430	200	2.15	190	150	1.27
230	130	1.77	170	120	1.42	580	470	1.23	730	360	2.03
160	110	1.45	240	90	2.67	150	70	2.14	400	380	1.05
160	70	2.29	150	110	1.36	200	140	1.43	330	130	2.54
270	150	1.80	800	380	2.11	140	60	2.33	390	290	1.34
180	120	1.50	160	90	1.78	90	70	1.29	580	490	1.18
190	110	1.73	310	250	1.24	220	130	1.69	540	260	2.08
140	120	1.17	180	90	2.00	150	120	1.25	470	260	1.81

Table AVII 3 *cont.*

Length	Width	Aspect ratio	Length	Width	Aspect ratio	Length	Width	Aspect ratio	Length	Width	Aspect ratio
500	360	1.39	260	230	1.13	140	100	1.40	210	120	1.75
100	70	1.43	170	110	1.55	140	80	1.75	180	80	2.25
370	290	1.28	90	70	1.29	180	80	2.25	220	130	1.69
440	170	2.59	140	80	1.75	110	70	1.57	120	50	2.40
390	250	1.56	460	220	2.09	190	160	1.19	160	110	1.45
380	220	1.73	330	270	1.22	310	70	4.43	160	100	1.60
400	120	3.33	190	80	2.38	120	90	1.33	140	110	1.27
300	150	2.00	280	130	2.15	140	100	1.40	160	100	1.60
230	160	1.44	630	500	1.26	280	220	1.27	200	180	1.11
100	70	1.43	150	90	1.67	260	120	2.17	220	90	2.44
350	180	1.94	370	190	1.95	130	80	1.63	130	70	1.86
210	90	2.33	150	80	1.88	120	70	1.71	90	60	1.50
330	280	1.18	110	80	1.38	210	100	2.10	290	130	2.23
230	110	2.09	90	50	1.80	180	80	2.25	120	70	1.71
130	90	1.44	170	90	1.89	90	50	1.80	230	170	1.35
140	110	1.27	210	170	1.24	150	90	1.67	200	110	1.82
590	290	2.03	220	110	2.00	80	50	1.60	100	70	1.43
360	210	1.71	230	110	2.09	120	80	1.50	180	140	1.29
170	100	1.70	160	110	1.45	150	100	1.50	250	140	1.79
320	270	1.19	130	110	1.18	100	70	1.43	200	140	1.43
340	250	1.36	120	90	1.33	120	70	1.71	290	210	1.38
200	150	1.33	320	250	1.28	140	110	1.27	190	80	2.38
190	120	1.58	220	130	1.69	150	80	1.88	550	220	2.50
170	110	1.55	170	80	2.13	270	130	2.08	260	160	1.63
210	140	1.50	110	80	1.38	120	80	1.50	100	90	1.11
140	110	1.27	130	60	2.17	200	100	2.00	210	110	1.91
340	270	1.26	180	130	1.38	140	90	1.56	380	190	2.00
430	220	1.95	230	140	1.64	140	80	1.75	190	110	1.73
230	160	1.44	100	80	1.25	90	70	1.29	120	50	2.40
630	330	1.91	270	160	1.69	130	80	1.63	110	40	2.75
440	270	1.63	150	120	1.25	80	50	1.60	220	120	1.83
250	200	1.25	180	110	1.64	270	160	1.69	160	110	1.45
170	80	2.13	100	60	1.67	100	70	1.43	140	130	1.08
390	190	2.05	80	50	1.60	110	100	1.10	130	60	2.17
350	200	1.75	140	70	2.00	150	60	2.50	230	160	1.44
360	130	2.77	210	120	1.75	100	90	1.11	120	80	1.50
180	100	1.80	270	190	1.42	160	80	2.00	110	90	1.22
160	50	3.20	180	110	1.64	120	50	2.40	150	90	1.67
230	140	1.64	400	250	1.60	170	100	1.70	310	140	2.21
290	180	1.61	80	70	1.14	170	50	3.40	70	60	1.17
200	130	1.54	330	140	2.36	140	100	1.40	210	140	1.50
190	100	1.90	310	180	1.72	120	80	1.50	150	110	1.36
290	170	1.71	450	330	1.36	90	70	1.29	120	100	1.20
450	300	1.50	170	80	2.13	100	60	1.67	150	110	1.36
270	180	1.50	480	210	2.29	110	110	1.00	90	50	1.80
90	70	1.29	450	380	1.18	120	90	1.33	250	130	1.92
140	50	2.80	270	150	1.80	130	90	1.44	490	390	1.26
170	150	1.13	150	110	1.36	160	90	1.78	150	140	1.07
300	210	1.43	130	80	1.63	120	90	1.33	150	80	1.88
200	130	1.54	200	140	1.43	90	60	1.50	140	80	1.75
160	110	1.45	310	170	1.82	160	90	1.78	150	100	1.50
120	90	1.33	200	100	2.00	130	120	1.08	150	70	2.14

Table AVII 3 *cont.*

Length	Width	Aspect ratio	Length	Width	Aspect ratio	Length	Width	Aspect ratio
150	100	1.50	210	100	2.10	110	80	1.38
130	80	1.63	150	70	2.14	180	130	1.38
150	90	1.67	140	80	1.75	170	100	1.70
170	80	2.13	130	110	1.18	170	140	1.21
190	160	1.19	350	260	1.35	130	100	1.30
130	90	1.44	140	50	2.80	1080	430	2.51
100	70	1.43	300	200	1.50	170	110	1.55
120	70	1.71	110	70	1.57	230	100	2.30
190	140	1.36	180	100	1.80	200	180	1.11
190	80	2.38	340	150	2.27	220	90	2.44
160	100	1.60	210	90	2.33	170	90	1.89
110	70	1.57	200	140	1.43			
90	50	1.80	140	90	1.56			

Table AVII 4 *Summary statistics for all stages of the agitation experiment. Dimensional values are given in micrometers.*

	Before			1 week			4 week		
	Length	Width	Aspect ratio	Length	Width	Aspect ratio	Length	Width	Aspect ratio
count	506	506	506	968	968	968	1285	1285	1285
min	50	30	1.00	60	40	1.00	50	30	1.00
d10	**110**	**70**	**1.11**	**100**	**70**	**1.17**	**80**	**50**	**1.17**
median	***725***	***540***	***1.38***	***190***	***110***	***1.55***	***140***	***90***	***1.56***
d90	**1130**	**785**	**1.85**	**563**	**360**	**2.20**	**310**	**200**	**2.20**
max	1650	1260	3.00	1290	760	3.90	1080	520	5.83
d90-d10	1020	715	0.73	463	290	1.03	230	150	1.03
mean	641.5	463.1	1.44	266.9	168.1	1.63	177.1	110.1	1.64
SD	394.1	285.0	0.31	198.5	122.6	0.44	118.9	71.8	0.45
SE of mean	17.5	12.7	0.01	6.4	3.9	0.01	3.3	2.0	0.01

Appendix VIII – Estimated relative volumetric abundances of precipitation products

Table AVIII 1 *Estimated relative volumetric abundances of the main precipitation products identified for each species studied in Chapter 2 of this study, based on observations made using scanning electron microscopy.*

	Precipitation products (estimated relative volumetric % produced by each species) [1, 2]								
Species	Ellipsoid (mono)	Ellipsoid (poly)	Rod/Small dumbbell/ wheatsheaf [3]	Dumbbell	Sphere	Needle	Amorphous carbonate	Rhomb	**Sum**
Schoolmaster snapper	100								**100**
Yellowtail snapper	100								**100**
Graysby grouper	100								**100**
Black grouper	65		31				2	2	**100**
French grunt	100								**100**
Grunt sp.			100						**100**
Flounder sp.	100								**100**
Red hind	95							5	**100**
Red lionfish	90						10		**100**
Great barracuda	1		73		1		23	2	**100**
Yellowfin mojarra	70			15	15				**100**
Mojarra sp.				60	40				**100**
Keeltail needlefish	40		25	10	20		5		**100**
Grey angelfish				80	20				**100**
Scrawled cowfish				5	95				**100**
Checkered puffer		15		10	70		?	5	**100**
Redtail parrotfish		45			45	5	?	5	**100**
Bluehead wrasse				15			65	20	**100**
Slippery dick				15			65	20	**100**
Beaugregory				15			65	20	**100**
Bonefish				4	71		24	1	**100**

[1] Based on either counts of crystal morphologies within disaggregated individual pellets (where crystal volumes are similar), or

estimates based on analysis of complete pellets

[2] Where counts or estimates indicate individual precipitation products contribute <1% of the total excreted volume

these have been discarded from the analysis

[3] Crystal forms grouped together as part of a gradational sequence

Appendix IX – Carbonate production rates

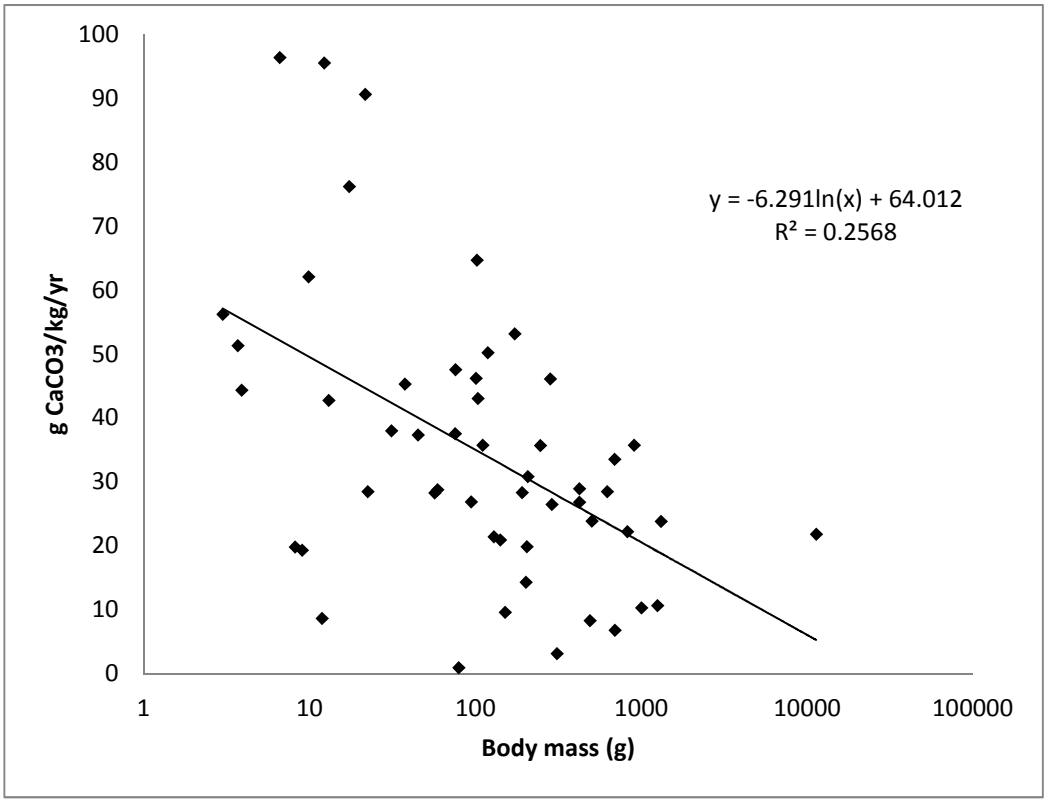

Figure AIX 1 *Relationship between fish mass and carbonate excretion rate, based on measured production rates from 18 different fish species that are common in the Bahamas.*

Table AIX 1 *Annual carbonate production rates by various fish species common to the Bahamas – measured in November 2009 (see footnotes for details regarding data collection)*

Species	number of fish in tank	individual fish body mass (g)				Mean body mass (g)	Production rate (g CaCO3/kg/yr)[2]	Value used for production rate curves (g CaCO3/kg/yr)[3]
Schoolmaster snapper	3					247	35.7	35.7
Schoolmaster snapper	3	261	286	322		290	21.9	**26.5**
Schoolmaster snapper	3	261	286	322		290	31.1	
Schoolmaster snapper	3	90	95	126		104	33.0	**43.1**
Schoolmaster snapper	3	90	95	126		104	50.2	
Schoolmaster snapper	3	90	95	126		104	46.1	
Schoolmaster snapper	13	4.6	to	13.9		9.9	39.4	**62.1**
Schoolmaster snapper	13	4.6	to	13.9		9.9	78.5	
Schoolmaster snapper	13	4.6	to	13.9		9.9	68.5	
Schoolmaster snapper	4					119	50.2	50.2
Graysby grouper	3	62	88	134		95	28.7	**26.9**
Graysby grouper	3	62	88	134		95	25.1	
Graysby grouper	4	78	141	162	185	142	13.9	**20.9**
Graysby grouper	4	78	141	162	185	142	28.0	
Graysby grouper	4	59	58	91	95	76	43.0	**37.6**
Graysby grouper	4	59	58	91	95	76	32.1	
Lionfish	2	241	381			311	3.2	3.2
Lionfish	1	57				57	28.3	28.3
Lionfish	3	25	30	39		31	54.6	**38.0**
Lionfish	3	25	30	39		31	31.3	
Lionfish	3	25	30	39		31	28.1	
Yellowtail snapper	5					695	6.8	6.8
Yellowtail snapper	4	60	75	83	86	76	57.9	**47.6**
Yellowtail snapper	4	60	75	83	86	76	32.8	
Yellowtail snapper	4	60	75	83	86	76	52.0	
Yellowtail snapper	6	13.4	to	31.7		22.6	37.3	**28.5**
Yellowtail snapper	6	13.4	to	31.7		22.6	14.1	
Yellowtail snapper	6	13.4	to	31.7		22.6	34.0	
Yellowtail snapper	10					45	37.3	37.3
Grunt (*Haemulon*) sp.	1					101	46.2	46.2
Red Hind	1					205	13.9	**19.9**
Red Hind	1					205	25.9	
Mojarra (*Eucinostomus*) sp.	2					173	53.2	53.2
Barracuda	1					11364	21.8	21.8
Barracuda	1					1259	10.7	10.7
Barracuda	1					691	33.5	33.5
Barracuda	1					491	8.3	8.3

Table AIX 1 *cont.*

Species	number of fish in tank	individual fish body mass (g)			Mean body mass (g)	Production rate (g $CaCO_3$/kg/yr)[2]	Value used for production rate curves (g $CaCO_3$/kg/yr)[3]
Barracuda	5	41	to	118	80	1.4	**1.0**
Barracuda	5	41	to	118	80	0.9	
Barracuda	5	41	to	118	80	0.6	
Bonefish	5				1006	10.5	**10.3**
Bonefish	5				1006	10.1	
Mullet	9				3	56.3	56.3

[1] Data for the November 2009 sampling period are those used for construction of the production rate curve by Perry *et al*. (2011). Data for the July 2010 sampling period are new data arising from the present study.

[2] Data are based on measured production rates over (typically) 24 hour intervals. Mass of excreted carbonates based either on the double titration method (see main text) or direct weighing of cleaned and dried samples.

[3] Values in the right-hand column are those used to construct the production rate curve (Fig. AIX 1); values in bold type are the average of multiple data points from groups of similar sized fish. This was necessary in some cases due to the highly variable output over 24 hours (e.g., compare two data points for beaugregory B/C/D)

Table AIX 2 *Annual carbonate production rates by various fish species common to the Bahamas – measured in July 2010 (see footnotes to Table AIX 1 for details regarding data collection)*

Species	number of fish in tank	individual fish body mass (g)	Mean body mass (g)	Production rate (g $CaCO_3$/kg/yr)[2]	Value used for production rate curves (g $CaCO_3$/kg/yr)[3]
Yellowfin mojarra A	1	107	**111**	83.0	**35.8**
Yellowfin mojarra B	1	113		10.7	
Yellowfin mojarra C	1	113		21.1	
Yellowfin mojarra C	1	113		5.9	
Yellowfin mojarra	3		59.3	28.8	28.8
Yellowfin mojarra	3		192.0	28.4	28.4
Black grouper A	1	424	424	26.8	26.8
Black grouper B	1	426	426	28.9	28.9
Black grouper C	1	505	505	23.9	23.9
Black grouper D	1	626	626	43.8	**28.5**
Black grouper D	1	626	626	13.1	
Black grouper F	1	827	827	22.2	22.2
Black grouper E	1	908	908	35.8	35.8
French grunt	2		21.7	90.7	90.7
French grunt	2		17.4	76.2	76.2
Mojarra (*Eucinostomus*) sp.	2		13.1	42.8	42.8
Beaugregory A	1	11.9	11.9	6.0	**8.7**
Beaugregory A	1	11.9	11.9	11.4	
Beaugregory B/C/D	3		8.2	32.3	**19.8**
Beaugregory B/C/D	3		8.2	7.4	
Beaugregory E/F/G	3		9.1	19.3	19.3
Needlefish C	1		12.3	95.5	95.5
Needlefish D	1		37.7	45.3	45.3
Checkered puffer A	1	152	152	13.8	**9.6**
Checkered puffer A	1	152	152	5.4	
Checkered puffer B	1	208	208	30.8	30.8
Checkered puffer C	1	129	129	21.4	21.4
Checkered puffer D	1	203	203	14.3	14.3
Bluehead wrasse A/B	2	3.7	3.7	51.3	51.3
Bluehead wrasse I/J/K	3	3.9	3.9	44.3	44.3
Bluehead wrasse L/M	2	6.6	6.6	96.4	96.4
Nassau grouper	1	1318	1318	23.9	23.9
Schoolmaster snapper	3		102	64.7	64.7
Schoolmaster snapper	3		284	46.1	46.1

SEDIMENTOLOGY the journal of the International Association of Sedimentologists

Sedimentology (2012) doi: 10.1111/j.1365-3091.2012.01339.x

Production of mud-grade carbonates by marine fish: Crystalline products and their sedimentary significance

MICHAEL A. SALTER*, CHRISTOPHER T. PERRY† and ROD W. WILSON‡
**School of Science and the Environment, Manchester Metropolitan University, John Dalton Building, Chester Road, Manchester, M1 5GD, UK (E-mail: michael.a.salter@stu.mmu.ac.uk)*
†Department of Geography, College of Life and Environmental Sciences, University of Exeter, Amory Building, Rennes Drive, Exeter, EX4 4RJ, UK
‡Department of Biosciences, College of Life and Environmental Sciences, University of Exeter, Geoffrey Pope Building, Stocker Road, Exeter, EX4 4QD, UK

Associate Editor – Bernhard Riegl

ABSTRACT

Recent work has established that marine teleost (bony) fish represent a prolific source of mud grade, mainly high-Mg calcite, carbonate sediment by means of primary precipitation within the intestine. Previously documented crystalline products display a diverse array of morphologies, many unique in shallow tropical marine settings, and have a wide range of magnesium contents (from 18 to 39 mol% $MgCO_3$). This study utilizes scanning electron microscopy, energy-dispersive X-ray spectroscopy, X-ray diffraction and liquid ion chromatography to provide a more extensive and expansive morphological, mineralogical and chemical characterization of the crystalline forms produced by a wider range of piscine functional groups (covering 21 different fish species common in The Bahamas). Several crystal morphologies not previously described in fish-derived carbonates are documented, and chemical composition is found to be more variable than previously reported: in addition to high-Mg calcites with >18 mol% $MgCO_3$, high-Mg calcites with lower $MgCO_3$ contents and low-Mg calcites are identified. From the expanded species range, $MgCO_3$ content in fish-derived carbonates ranges from *ca* 0·5 to > 40 mol%, and particle length is in the range 0·1 to >50 μm (typically <2 μm for individual crystals). Amorphous Mg-carbonates (with detectable $CaCO_3$ of <2 mol%) are also found to varying extent in the precipitates of many species. Dominant mineralogy and $MgCO_3$ content varies with producing species and crystal morphology (itself a species-dependent variable). Given the very small grain size and often high $MgCO_3$ contents of these carbonates, interesting questions arise about their preservation potential. Thus, the extent to which carbonates produced by different species may follow different post-excretion preservation pathways is considered.

Keywords Bahamas, carbonate mud, marine fish, Mg calcite, marine teleost, shallow tropical carbonates.

INTRODUCTION

Carbonate muds form a volumetrically significant component of many modern carbonate sediments and ancient limestones (Matthews, 1966; Purdy & Gischler, 2003; Pomar & Hallock, 2008). Consequently, they are important in controlling the depositional character (grain size, texture, etc.) of the sediments that accumulate in these environments, and understanding their origins can be important from the perspective of interpreting palaeo-environments (Flügel, 2004). The mineralogical composition of marine carbonate muds and, in particular, the presence and abundance of

Mg calcites can be important in determining sediment diagenetic pathways. Specifically, Mg calcite mud can influence the preservation of sediment textures and fabrics (Husseini & Matthews, 1972), and thus influence porosity and permeability patterns. Understanding the provenance and genesis of carbonate mud is, therefore, important; yet in limestones this is often problematic due to the pervasive recrystallization (to micrite and microspar) or the obliteration of fine-grained carbonate particles that often occurs during syn-depositional and burial diagenesis (Reid *et al.*, 1992; Walter *et al.*, 1993; Reid & MacIntyre, 1998). Thus, carbonate mud sources in modern settings are often used as analogues for sources in ancient settings.

Carbonate muds in contemporary depositional systems have been attributed to various sources: (i) direct physico-chemical precipitation from sea water, such as the aragonite needles and carbonate particles associated with 'whitings' (Black, 1933; Shinn *et al.*, 1989); (ii) mechanical and/or biological degradation of skeletal grains, such as calcareous green algae, coccolithophores and foraminifera (Lowenstam & Epstein, 1957; Matthews, 1966; Stockman *et al.*, 1967; Stieglitz, 1972; Futterer, 1974; Debenay *et al.*, 1999); and (iii) biogenically induced precipitation, such as that occurring within intertidal and shallow subtidal microbial mats (Chafetz & Buczynski, 1992). However, there is considerable debate as to the relative importance of each to carbonate sediment budgets in modern shallow marine environments (Broecker & Takahashi, 1966; Neumann & Land, 1975; Shinn *et al.*, 1989; Milliman *et al.*, 1993; Broecker *et al.*, 2000). Partly, this problem arises from difficulties in assigning mud-grade carbonates to a distinctive source; this being due both to grain degradation (itself a process invoked in the generation of mud-grade carbonate; Matthews, 1966) and/or the early recrystallization of fine-grained carbonates (Reid *et al.*, 1992; Reid & MacIntyre, 1998). Furthermore, some mud-grade carbonates, such as the aragonite needle products of whitings and calcareous green algae, can be difficult to distinguish due to morphological and chemical similarities (Boardman & Carney, 1991). Indeed, in recent studies of modern fine-grained carbonate sediments, as much as 60% of the mud fraction of some samples remained 'unidentified' (Gischler & Zingeler, 2002).

The Bahamian platform is one of the classic environments for research into carbonate mud production. Several studies (Lowenstam & Epstein, 1957; Cloud, 1962) identified aragonite as the predominant mud fraction mineralogy; this led to much work on the production of aragonite mud and, while this remains a topic of debate, its sources are now reasonably well-understood (Schlager, 2003). However, many studies also identify high-Mg calcite as an important component of shallow tropical muds, not only in The Bahamas, but also in other contemporary carbonate settings (Chave, 1962; Taft & Harbaugh, 1964; Matthews, 1966; Husseini & Matthews, 1972; Gischler, 2011), where it can constitute 70 to 90% of the mud fraction (Reid *et al.*, 1992). Thus, while some carbonate settings are dominated by aragonite mud and others by Mg calcite mud, it is clear that carbonate muds in most settings should be considered as a mixture of the two.

In a recent study, Perry *et al.* (2011) identified marine bony fish (teleosts) as a previously unknown, but prolific, primary source of morphologically distinctive high-Mg calcite mud-grade carbonate. Moreover, these authors emphasized the potential significance of this material in carbonate sediment budgets by showing that compositionally and morphologically similar high-Mg calcites are abundant in the finest fraction of surface sediments from a range of habitats sampled around the island of Eleuthera, The Bahamas. The genesis of these fish-derived carbonates involves primary precipitation within the intestines of bony marine fish (teleosts), and occurs as a by-product of an osmoregulatory requirement to continuously drink sea water in order to remain hydrated. Within their highly alkaline intestinal fluids (pH 8·3 to 9·3) high concentrations of imbibed Ca^{2+} and Mg^{2+} react with HCO_3^- and precipitate out of solution as carbonate crystals (Walsh *et al.*, 1991; Wilson *et al.*, 1996, 2002, 2009; Grosell, 2006; Mekuchi *et al.*, 2010). The levels of HCO_3^- within the intestine typically range from 30 to >100 mM, and are derived from metabolic CO_2 and secreted at high rates through the epithelial cells that line the lumen of the intestine. The resulting carbonate crystals are ultimately excreted as mucus-coated pellets along with faecal matter and, as shown in the preliminary studies of Perry *et al.* (2011), comprise loosely aggregated crystals of mainly high-Mg calcite (with measured $MgCO_3$ values in the range 18 to 39 mol%). These crystals are typically <0·5 to *ca* 30·0 μm in length, and exhibit a diverse array of morphologies, the nature of which varies between fish species. While primary carbonate production in marine bony fish has long been known and is well-documented by fish physiologists (Shehadeh &

Gordon, 1969; Humbert *et al.*, 1986, 1989; Walsh *et al.*, 1991; Wilson *et al.*, 1996, 2002, 2009; Grosell *et al.*, 2005), its potential significance as a source of mud-grade marine carbonate sediment has, until recently (Perry *et al.*, 2011), remained completely unrecognized. The present study provides a more extensive and expansive description of the morphological, compositional and mineralogical characteristics of the crystalline products excreted by tropical marine bony fish than that initially provided by Perry *et al.* (2011). Specifically, this description includes data from a much wider range of piscine functional groups, and thus provides an improved insight into the diversity of mud-grade carbonates produced by fish in shallow tropical marine environments. The study also considers the relevance of this material to fine-grained carbonate sediment production in shallow tropical marine settings, and considers some of the key research questions arising from the recognition of this novel marine carbonate mud source.

STUDY AREA

All of the fish species used in this study were collected from shallow water environments around Cape Eleuthera, Eleuthera Island, The Bahamas (24°50′ N, 76°20′ W; Fig. 1). The Eleuthera Sound, on the leeward side of the island, is characterized by warm shallow waters (up to 8 m in depth) that can be influenced by strong tidal currents. The southern margin of Eleuthera Sound is bordered by the deep-water Exuma Sound, running roughly parallel with the south-western coast of Cape Eleuthera. The sedimentary environments of the open bank are dominated by active and stabilized oolitic sands and skeletal sand veneers, with pelletal sands and pelleted lime muds dominating restricted bays and inlets (Dravis, 1979). The nearshore environment around Cape Eleuthera itself comprises numerous and widely distributed patch reefs, but is otherwise dominated by open sands, seagrass meadows and variously concentrated populations of calcareous green algae. Several large creeks and inlets also feed into the bay. These habitats support a large fish population that includes many species which are widespread and common in The Bahamas. For the purposes of this study, all fish species were collected from nearshore areas (in and around creeks and inlets) and patch reefs.

MATERIALS AND METHODS

Sampling was carried out over two periods at the Cape Eleuthera Research Institute (CEI), Eleuthera, The Bahamas, in November to December 2009 [sea surface temperature (sst) of *ca* 25 to 27°C] and July 2010 (sst of *ca* 28 to 30°C). Sea water salinity during both periods was between 36 and 37 (practical salinity scale). Twenty-three species of fish were captured from a range of shallow (<8 m) nearshore environments (patch reefs and inlets) in Eleuthera Sound using baited traps, seine nets and by hook and line. Immediately after capture, fish were transferred to tanks within the aquaculture facility at CEI. Fish were kept individually and in groups (arranged by size where possible), and all

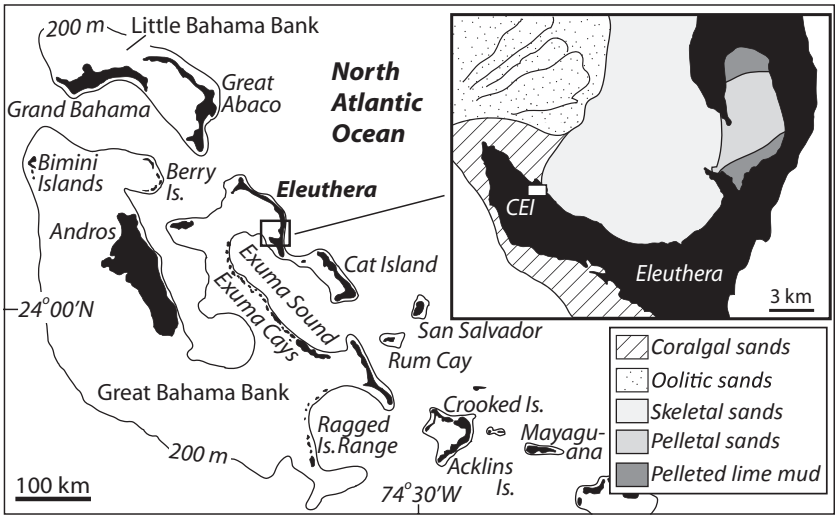

Fig. 1. Location map of the study area and the main sedimentary environments of Eleuthera Sound (inset; modified after Dravis, 1979). CEI = Cape Eleuthera Research Institute.

were left for two days prior to sampling to allow the excretion of any food material ingested prior to (or during) capture. Oxygen levels in each tank were maintained through quartz sand airstones linked to a central compressed air supply, and a continuous flow of one-pass sea water (pumped from *ca* 70 m offshore at a depth of 1 to 2 m) ensured that temperature and salinity remained close to ambient within local near-surface waters. Sea water flow was filtered to 5 μm to minimize influx of external material, thus preventing fish from ingesting material during sampling. Tanks were also fitted with false mesh floors to prevent fish re-ingesting excreted carbonate pellets (which typically sink after excretion). One species, yellowfin mojarra, was sampled during both sampling periods and acted as a control by ensuring that any variation in environmental conditions did not result in the production of different crystal forms.

Carbonates are excreted as mucus-coated pellets (see Perry *et al.*, 2011) and were collected within 24 h of excretion with plastic Pasteur pipettes. These pellets were immediately rinsed in distilled water to remove salts before being soaked for 6 h in 5·25% sodium hypochlorite (commercial bleach) to remove the organic components of mucus coatings. This treatment has no discernible effect on carbonate mineralogy or grain texture and causes no detectable dissolution (Gaffey & Bronnimann, 1993). However, along with other techniques commonly used to remove organics from carbonates (i.e. soaking in sodium hydroxide or hydrogen peroxide), hypochlorite treatments have been shown to cause minor changes in the trace element chemistry of aragonite (Love & Woronow, 1991), although the effect on calcite and Mg calcite is not known. Bleach was carefully removed with plastic Pasteur pipettes before two additional rapid rinses in distilled water to ensure removal of dissolved salt and bleach residues. Following the final rinse, precipitates were collected on 47 mm diameter, 0·45 μm pore size cellulose nitrate membranes or 47 mm diameter, 1 μm pore size glass fibre filters. Although the pore sizes of these filters exceed the width of many individual crystals (Perry *et al.*, 2011), pellets are able to tolerate gentle handling without disaggregating during the cleaning and filtration process, and thus most individual crystals of all sizes were retained. Precipitates were oven-dried on the membranes at 50°C. Using this methodology precipitates were readily liberated from filters/membranes and prepared either for morphological and/or compositional analysis.

The 23 fish species used for this study were selected to cover a range of key functional fish groups (Table 1), which include apex predators, macroinvertivores, piscivores, pisci-invertivores, omnivores and herbivores (Randall, 1967; Newman *et al.*, 2006). Thus, the sample set provides data from a range of common and ecologically important fish that occur within most shallow Caribbean environments. Functional groups not included are microinvertivores (for example, *Chaetodon* sp.) and planktivores, although several authors (Feddern, 1965; Clifton & Motta, 1998; White & Samhouri, 2011) consider bluehead wrasse to be largely planktivorous. Only two species did not excrete endogenously precipitated carbonates. Of these, it is noted that only a single specimen of doctorfish, *Acanthurus chirurgus*, was collected and that the absence of excreted carbonates does not necessarily apply to the entire species. Indeed, recent work indicates that sexually mature female fish may produce carbonates at significantly lower rates than males due to the uptake of large amounts of imbibed Ca^{2+} through the gut, driven by elevated oestrogen levels (Al-Jandal *et al.*, 2011), and this could explain the apparent absence of intestinally precipitated carbonates (sexing of fish was not carried out as this is difficult without histological information). The same may also apply to white mullet, *Mugil curema*, which also did not excrete endogenously precipitated carbonates.

Morphological analysis

Morphological analysis of crystals was undertaken using scanning electron microscopy (SEM) within a field emission gun (FEG) Zeiss Supra 40VP system (Carl Zeiss SMT Limited, Cambridge, UK). Loose pellets were tipped onto either adhesive carbon-coated tabs or a thin coating of silver epoxy resin upon 12 mm aluminium pin stubs (both methods yielding similar SEM image quality). In addition, some individual pellets were disaggregated in 1·5 ml microcentrifuge tubes filled with deionized water and placed in an ultrasonic bath operating at 44 kHz for periods of up to 30 sec (all pellets disaggregated easily and almost immediately upon sonication). Following disaggregation, the water-crystal mixture was homogenized by gently shaking and a 40 μl subsample was transferred onto a stub-mounted *ca* 0·5 cm^2 silicon plate, and the fluid was allowed to evaporate in a low-temperature (40°C) oven. All samples produced good secondary electron (SE) images when examined in high vacuum at a

Table 1. List of fish species sampled and the key data arising from each.

Species	Funct'l Group	Dominant (•) and subsidiary (^) crystal morphologies													$MgCO_3$ content (mol%)				
		m	e	r	w	d	s	x	l	p	a	b	n	Notes	EDX Dominant	EDX Subsidiary	LC	XRD*	Body mass of fish (g)
Category I																			
Lutjanes apodus (schoolmaster snapper)	P-I	•		^							^				22–37	–	20–34	30·4–39·6[a]	4·6–322
Ocyurus chrysurus (yellowtail snapper)	P-I	•												Coarse surface	34	–	26–33	26·4–30·1[a]	13–946
Cephalopholis cruentata (graysby grouper)	P-I	•				^									34	–	25–32	30·3–36·0[a]	58–185
Mycteroperca bonaci (black grouper)	AP	•		^	^	^				^	^	^			19–30 (m/r/w)	10–14 (d)	24–35	–	424–1653
Haemulon flavolineatum (French grunt)	M-I	•				^									20 (e)	6 (d)	22–24	–	11–25
Flounder sp.	?	•													36	–	–	–	81
Epinephelus guttatus (red hind)	P-I	•				^					^	^			39	–	33–35	–	205
Pterois volitans (red lionfish)	P-I	•								^				'Mesh' coating	35	–	24–32	–	25–381
Haemulon sp. (grunt sp.)	M-I			•	•										29	–	34	–	101
Sphyraena barracuda (great barracuda)	AP				•	^				^			•		25–35 (n/w)	3 (d/s)	22–33[†]	20·8–26·4	41–11364
Sub-category Ia																			
Gerres cinereus (yellowfin mojarra)	M-I	•				^	^	^	^						16–23 (m)	3–9 (d/s/x/l)	14–29	18·2[a]	107–202
Platybelone argalus argalus (keeltail needlefish)	P	•		•	•	^	^				^				11–16 (m/r/w)	2–5 (d/s)	16–22[†]	–	10–47
Category II																			
Pomacanthus arcuatus (grey angelfish)	O					•	•							Some twisted	2·3 (all)	–	–	–	429–460
Acanthostracion quadricornis (scrawled cowfish)	O					^	•					^			5 (s)	–	–	–	390

Table 1. (Continued)

Species	Funct'l Group	Dominant (•) and subsidiary (^) crystal morphologies													$MgCO_3$ content (mol%)				
		m	e	r	w	d	s	x	l	p	a	b	n	Notes	EDX Dominant	EDX Subsidiary	LC	XRD*	Body mass of fish (g)
Sphoeroides testudineus (checkered puffer)	M-I		•			^	•					^		Some twisted	1–3 (all)	9–14 (few d/s)	3–10	6·4 & 17·3[a]	118–207
Sparisoma chrysopterum (redtail parrotfish)	H		•			^	•	•	^			^		Some twisted	1·5 (all)	*ca* 4 (few s)	–	–	43–49
Category III																			
Thalassoma bifasciatum (bluehead wrasse)	Pk/M-I					•			^	•	•	•			*ca* 5 (d/b)	100 (p/a)	57–65‡	5·1[a]	1·1–7·7
Halichoeres bivittatus (slippery dick)	P-I					•				•	•	•			*ca* 5 (d/b)	100 (p/a)	–	–	1·5–5·9
Stegastes leucostictus (beaugregory)	H/O					•				•	•	•			*ca* 4 (d/b)	100 (p/a)	23–68‡	–	4·5–12·9
Category IV																			
Albula vulpes (bonefish)	M-I					^	•				^	^	•		19–23 (s)	35 (n)	32–35	13·5[a]	759–1506
Eucinostomus sp. (mojarra sp.)	M-I					•	•			^		^			19 (d/s)	–	22	–	11–30

Functional group codes: P-I = piscivore-invertivore; M-I = macroinvertivore; AP = apex predator; P = piscivore; O = omnivore; H = herbivore; Pk = planktivore.

Dominant morphology codes: m = monocrystalline ellipsoid; e = polycrystalline ellipsoid; r = rod; w = small dumb-bell/wheatsheaf; d = large dumb-bell; s = sphere; x = spherulite; l = lath/needle-like; p = platy (commonly forming rosettes or mesh-works); a = lacking clearly definable form; b = rhombohedron; *n* = nanosphere.

* X-ray diffraction (XRD) range limits represent estimates based on different calibration curves, applicable to all values of $MgCO_3$ >20 mol% (see *Mineralogical and chemical analysis* section). Results are based on one analysis for samples from all species except schoolmaster and barracuda. Upper and lower limits for these species are based on combined data from two analytical runs.

[a] Minor amounts of aragonite also detected in XRD.

Energy-dispersive X-ray spectroscopy (EDX) results are shown as mean values; where a range of values is shown this represents the range of mean values from different samples.

Liquid chromatography (LC) results are shown as the range of values based on analysis of multiple samples. Where only one value is shown, only one sample was analysed.

†Upper limit of LC results that represents the likely upper limit of $MgCO_3$ mol% in Mg calcite phases. Higher $MgCO_3$ values were recorded in some samples but are probably due to the presence of significant amounts of a Mg-carbonate phase.

‡Liquid chromatography values for $MgCO_3$ content are based on the combined influence of Mg calcite crystals and amorphous Mg-carbonates.

Categories refer to classification of fish species based on their carbonate products - see *Discussion* section.

working distance of 5 to 7 mm, accelerating voltage of 2 keV and aperture width of 30 μm.

Cross-sections of some larger particles were examined in polished resin blocks; these were made by placing sample pellets into foil moulds with a 2 ml mixture of 30% low-viscosity resin (TAAB Transmit LM; TAAB Laboratories Equipment Ltd, Aldermaston, UK) and 70% acetone. Air was removed from pellets by placing the moulds in a vacuum chamber at 94·7 kPa for 1 h, during which the acetone evaporated. Following this, a further 2 ml of resin was added and moulds were returned to the vacuum chamber for another hour. The resin was cured at 70°C for 18 h before sequential polishing down to 5 μm using Buehler P800, P1200 and P4000 silicon carbide abrasive grinding papers. A gold-palladium coating of several nanometres thickness was applied prior to analysis. Resin-embedding was only successful for samples with the largest crystals; sub-micron scale crystals, such as small ellipsoids, were ripped out of the resin during the polishing process.

Mineralogical and chemical analysis

Energy-dispersive X-ray spectroscopy

Compositional analyses of individual crystals utilized the SEM-integrated Oxford Instruments ISIS energy-dispersive X-ray spectroscopy (EDX) system (Oxford Instruments plc, Abingdon, UK), which allows standardless quantification of analytical results using EDAX ZAF quantification software. This system was used in combination with a backscatter electron (BSE) detector at a working distance of 15 mm, accelerating voltage of 15 keV and aperture width of 120 μm. Images produced using BSE, although lacking the clarity of SE images, were sufficient to identify and select the desired crystal types for analysis. Energy-dispersive X-ray spectroscopy requires flat polished sample surfaces for the most precise quantitative chemical analysis. However, because the smallest crystals could not be prepared and examined in this way, their analysis using EDX should be considered as semi-quantitative. Nevertheless, average results for samples from individual fish species are generally in close agreement with liquid ion chromatography and X-ray diffraction (XRD) results, and are thus taken as a good approximation of the accurate $MgCO_3$ mol%. It is also noted that the maximum resolution of EDX analysis is *ca* 1 μm. Given that many of the crystals are <1 μm in length, slight errors could be introduced due to analytical incorporation of other phases surrounding the subject crystal. Thus, for the smallest crystals, analyses were only conducted if they were surrounded by morphologically similar crystals.

X-ray diffraction

X-ray diffraction analysis was conducted on selected samples in order to: (i) confirm mineral phases; (ii) provide data to support the chemical compositions determined using EDX and liquid ion chromatography; and (iii) provide information on the crystallinity of the various precipitates. Samples were selected to cover a range of crystalline products: low-Mg calcite (LMC) spheres, dumb-bells and rods; LMC and high-Mg calcite (HMC) rhombohedra; and Mg-carbonates (with <2 mol% $CaCO_3$) that are platy or lacking clearly definable form. Various other crystal types, including monocrystalline ellipsoids, small dumb-bells and polycrystalline spheres [all HMC and 'very' high-Mg calcite (VHMC)], have been analysed previously (Perry *et al.*, 2011) and those data are incorporated here. In the present study the upper limit of LMC is, following convention, considered to be 4 mol% $MgCO_3$, and the lower limit for VHMC is arbitrarily designated as 25 mol%.

X-ray diffraction analyses were carried out using a Philips PW1710 X-ray diffractometer equipped with a Philips PW1729 X-ray generator (Cu$K\alpha$ radiation; Philips, Eindhoven, The Netherlands). Sub-samples (100 mg) were ground in an agate pestle and mortar and dispersed evenly over a glass plate with an adhesive coating. Samples were scanned with a step width of 0·02° 2θ at 1 sec per step. A silicon standard was used to check the goniometer position. Peak positions were compared with data from the RRUFF database (Downs, 2006) to confirm crystalline phases. In the case of Mg calcite, a systematic relationship exists between $d_{(104)}$ values and the amount of magnesium substituted for calcium in the crystal lattice, and numerous calibration curves have been published (Goldsmith *et al.*, 1961; Bischoff *et al.*, 1983; Zhang *et al.*, 2010). These curves, based on abiotic synthetic calcites and Mg calcites with up to 50 mol% $MgCO_3$, facilitate the estimation of $MgCO_3$ content in natural calcites, although several caveats apply. Firstly, estimates of $MgCO_3$ content for biogenic Mg calcites may vary by up to ±5 mol% due to: (i) line broadening associated with small (<1 μm) crystal size, defect density and relatively poor crystallinity; (ii) compositional heterogeneity; and (iii) lattice distortion

and disorder resulting from cation substitution (Bischoff *et al.*, 1983). Secondly, the influence of incorporated trace elements, such as Sr^{2+}, on calcite unit cell parameters is not well-constrained and may introduce further errors. The calibration curve of Goldsmith *et al.* (1961) and Bischoff *et al.* (1983) is based on the assumption of a linear solid-solution series between calcite and magnesite through stoichiometric dolomite. To address the problem of lattice disorder, Zhang *et al.* (2010) produced a different curve based on synthetic disordered HMC and disordered dolomite. At $MgCO_3$ contents greater than *ca* 20 mol% the two curves diverge, and at very high $MgCO_3$ contents (>40 mol%) values derived from these curves can differ by more than 10 mol%. As the degree of lattice disorder is not determined for fish-derived carbonates, a range of possible values based on both curves is presented.

Liquid ion chromatography

Cation (Ca^{2+} and Mg^{2+}) concentrations were measured by liquid ion chromatography (Dionex ICS-1000, Sunnyvale, CA, USA) using samples of cleaned excreted carbonates suspended in deionized water and dissolved using 0·02 N hydrochloric acid, followed by appropriate dilution. Occasionally, samples contained fragments of calcium phosphate scales and fin rays, and/or marine carbonate particles (excreted during sampling; the gut sometimes having taken longer than anticipated to become completely void of materials ingested prior to capture). The presence of such materials would alter Mg^{2+}/Ca^{2+} ratios measured by liquid ion chromatography and they were, therefore, removed with forceps prior to analysis.

RESULTS

Detailed SEM examination of fish-derived carbonates indicates that five predominant crystal morphologies are produced: ellipsoids, dumbbells, spheres, needles and euhedral rhombohedra. These range in length (or diameter, where appropriate) from 0·1 to >50 μm (Fig. 2) and, at least for crystals produced by the examined species range, most commonly occur in the range 0·4 to 3 μm. Chemical analyses indicate that, in addition to the mainly VHMC (18 to 39 mol% $MgCO_3$) products detailed by Perry *et al.* (2011), the excretion of predominantly LMC and/or HMC with 4 to 10 mol% $MgCO_3$ is recorded in seven of the 21 species that produced carbonates. Of these, three (all small specimens with a body mass of <13 g) excreted pellets dominated by a Mg-carbonate phase (often lacking clearly definable form) alongside subsidiary LMC and/or HMC. Below is a detailed description of the morphological and compositional characteristics of the different carbonate crystal products (summarized in Table 1). Following convention, fish species are referred to by their common English names; refer to Table 1 for a full list of species and their scientific names.

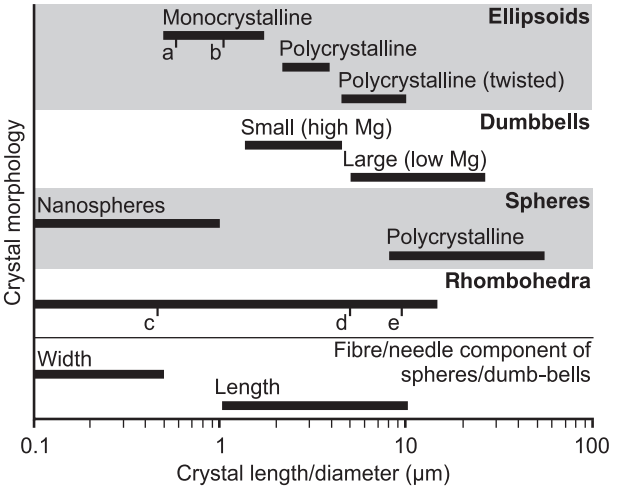

Fig. 2. Graph showing the lengths of common crystal forms precipitated within the intestines of marine fish: 'a' and 'b' mean lengths of monocrystalline ellipsoids produced by red hind and black grouper, respectively; 'c', 'd' and 'e' mean lengths of rhombohedra produced by black grouper, redtail parrotfish and bluehead wrasse, respectively. Note that small and large dumbbells are differentiated by means of $MgCO_3$ content as well as by size, and do not form a grain-size continuum.

Crystal morphology

Ellipsoids

In samples produced by eight fish species the dominant crystal form is ellipsoidal, representing >99% of excreted carbonates. Ellipsoids also represent the dominant crystal form in more heterogeneous samples produced by four other species, occurring alongside significant quantities of other crystal types (Table 1). In the majority of samples examined, ellipsoids take the form of monocrystalline prolate ellipsoids (Fig. 3A). These are typically 0·5 to 1·2 μm in length (although mean length can vary according to species) and are morphologically very uniform within most species, including yellowfin mojarra and keeltail needlefish which produce heterogeneous samples containing significant quantities of dumb-bell and sphere-shaped particles.

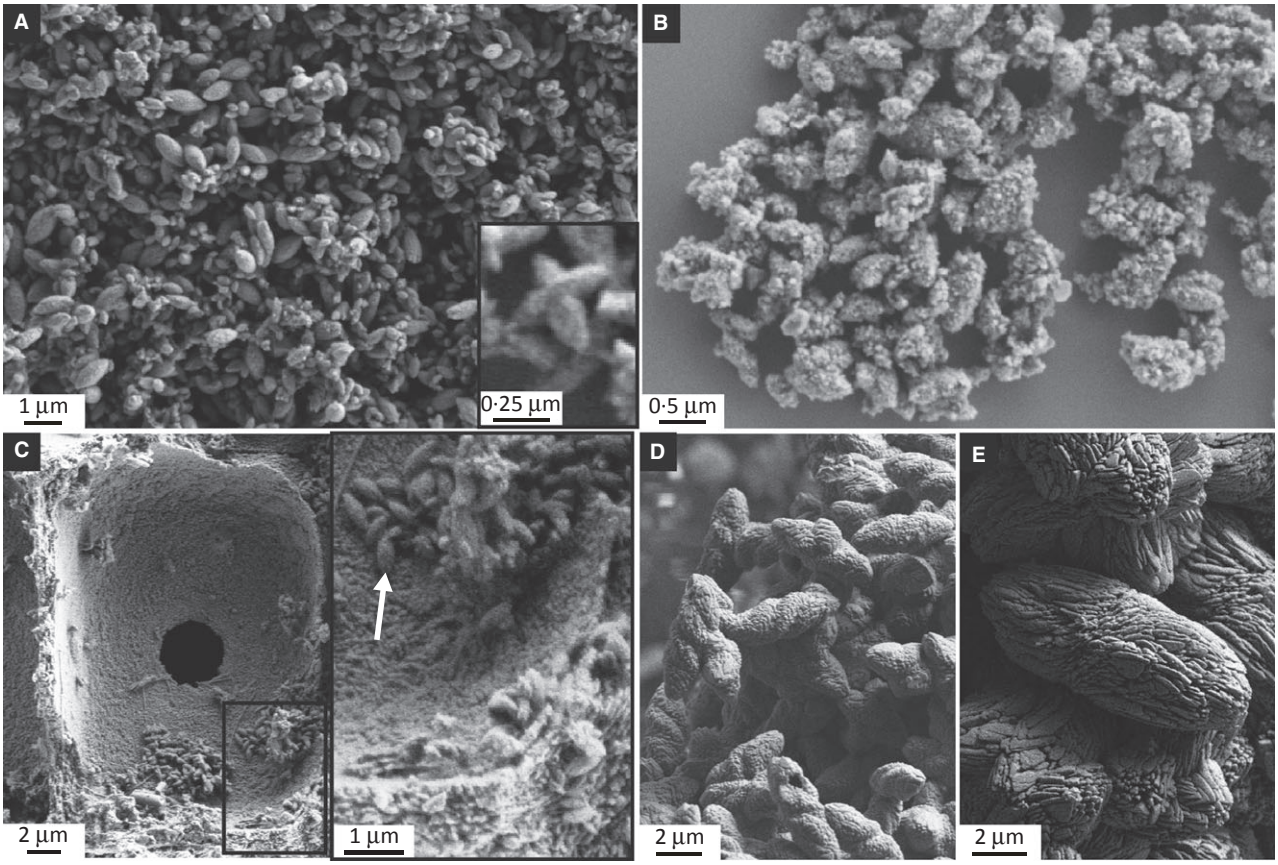

Fig. 3. Secondary electron (SE) images of various ellipsoidal crystalline forms produced by: (A) schoolmaster snapper; (B) and (C) yellowtail snapper; (D) checkered puffer; and (E) redtail parrotfish. (A) and (B) The majority of ellipsoidal forms examined herein are <2 µm in length and monocrystalline. Many exhibit smooth surfaces (A), but those produced by some species can exhibit rather coarse surfaces (B). (C) Monocrystalline ellipsoids (white arrow) exhibit the same characteristics when precipitated in the presence of ingested carbonate particles, such as *Amphiroa* shown here. (D) and (E) Checkered puffer and redtail parrotfish produce larger polycrystalline ellipsoids, at least some of which are hollow [(D) centre bottom]. As shown here, individual crystals that make up these ellipsoids are often arranged in a helical manner about the long axis. All ellipsoidal forms typically occur as individual particles, but it is not uncommon for intergrown clusters of two or more ellipsoids to occur [inset in (A)].

Variations on the monocrystalline ellipsoid form include: (i) the intergrowth of two or more ellipsoids that share a common centre and have long axes aligned perpendicular to one another (Fig. 3A, inset), occurring as rare particles in most samples dominated by monocrystalline ellipsoids; and (ii) subtle variations in the surface texture of crystals. For example, those produced by schoolmaster snapper are consistently very smooth-surfaced (Fig. 3A), while those produced by yellowtail snapper commonly have numerous surface protrusions that create a coarse surface appearance (Fig. 3B). In addition, ellipsoids can be difficult to discern in samples produced by some species (for example, red hind) due to large quantities of surrounding nano-particulate carbonates. Excreted carbonate samples are occasionally contaminated with 'foreign' carbonate particles ingested by fish prior to their capture. Importantly, these samples demonstrate that, at least for monocrystalline ellipsoids, crystal characteristics remain as described above when precipitated alongside these particles (i.e. as would happen during normal feeding behaviour) (Fig. 3C).

Morphologically different from the above described monocrystalline ellipsoids are polycrystalline ellipsoids that are the dominant crystalline form produced by redtail parrotfish. These comprise blade-like or platy sub-micron crystals that are aggregated to form ellipsoidal particles, occurring as one of two distinct forms (both larger than monocrystalline ellipsoids): (i) prolate ellipsoids, similar in shape to monocrystalline ellipsoids; or (ii) elongate 'twisted' ellipsoids, in which crystals are arranged about the long axis in a helical manner (Fig. 3D). Occasional broken surfaces of 'twisted' ellipsoids reveal a hollow internal structure (Fig.

3D). Similar polycrystalline forms are also produced by checkered puffer, although ellipsoids from this species tend to be larger (up to 10 μm in length) with more rounded ends, and individual crystals are aligned parallel to the long axes of particles (Fig. 3E), in contrast to the oblique alignment in ellipsoids produced by redtail parrotfish.

Dumb-bells

Dumb-bell-shaped particles are the dominant crystal form in some species (for example, great barracuda), and occur as an abundant to rare subsidiary form in samples produced by many other species. The basic dumb-bell structure comprises a narrow central core that broadens or splays perpendicular to the long axis, resulting in a particle that, in many cases, resembles a double-headed broccoli (Fig. 4A to F). However, the degree of broadening varies greatly, with end members resembling narrow wheatsheafs (Fig. 4A) and broad 'semi-spheres' (Fig. 4C). The largest dumb-bells commonly splay to such a degree that they eventually grow back on themselves, often merging to form a near-complete sphere. The structure of dumb-bells is highly variable, both across and within species, with both monocrystalline and polycrystalline forms occurring.

Dumb-bells typically range from 1·3 to 25 μm in length. Based on size relationships and chemical composition there appear to be two distinct types of dumb-bell: (i) small dumb-bells, which are chemically similar to monocrystalline ellipsoids (i.e. typically containing >20 mol% $MgCO_3$; see *Mineralogy and chemical composition* section) and are typically up to 4·4 μm in length (Fig. 4A and B); and (ii) large dumb-bells, which consistently have lower $MgCO_3$ contents (2 to 14 mol%) and typically occur with lengths in the range 5 to 25 μm (Fig. 4C to F). The former represent the dominant crystal form in samples produced by *Haemulon* sp. and great barracuda, and a subsidiary form in some other samples. The latter occur as a subsidiary form in samples produced by many species, usually present alongside dominant ellipsoids or spheres; in either case the length of large dumb-bells is commonly very variable (for example, in the range 5·2 to 18·4 μm in keeltail needlefish and 5·4 to 19·6 μm in checkered puffer). Chemical differences are recorded even when the two dumb-bell types occur in the same sample. For example, samples produced by keeltail needlefish typically comprise chemically similar monocrystalline ellipsoids and small dumb-bells, alongside large dumb-bells which have significantly lower magnesium contents.

The most commonly observed type of dumb-bell is polycrystalline, comprising needles or fibres that radiate from a common central point to create a double-headed broccoli-like form (Fig. 4D and E). These crystal aggregates form dumb-bells across the spectrum from 'wheatsheaf' to 'semi-sphere' and are present in samples produced by most species. Individual crystal fibres are typically very narrow (<0·1 μm in width), but occasionally they are broader (up to 0·5 μm in width), especially in the largest dumb-bells. Following gentle sonication, these dumb-bells partially disaggregate and release their individual component fibres (Fig. 4E). A second type of polycrystalline dumb-bell is that which comprises an aggregation of sub-micron equant rhombohedra (Fig. 4F). Occurring most commonly in samples produced by checkered puffer, *Eucinostomus* sp., bluehead wrasse, slippery dick and beaugregory, in most samples they are subsidiary to other dumb-bell types. Broadening in these particles appears to be controlled by the size of individual rhombohedra, increasing away from the dumb-bell core. A third form of dumb-bell-shaped particle is monocrystalline, and is common in carbonate samples excreted by a limited number of species (specifically bluehead wrasse, slippery dick and beaugregory). Crystals commonly are relatively large (5 to 15 μm in length) and of rhombohedral habit (see below), often tending towards dumb-bell-shaped.

As with ellipsoids, some of the large dumb-bell-shaped particles produced by redtail parrotfish, checkered puffer and grey angelfish have a twisted appearance, with individual crystals being arranged helically about the long axis. In carbonate particles excreted by redtail parrotfish the polycrystalline aspect commonly involves rather blade-like or platy crystals (as with ellipsoids excreted by this species), while dumb-bells produced by grey angelfish comprise fibres radiating and twisting from a common centre. Dumb-bells excreted by checkered puffer may comprise blade-like, fibrous or sub-micron rhombohedral crystals; only the former being arranged helically. Dumb-bells made up of blade-like crystals do not broaden to the same degree as those consisting of radial fibres, and thus do not form sphere-like morphologies. However, it is not uncommon for these dumb-bells to coalesce and form large multi-lobate structures that can constitute entire pellets (Fig. 4G).

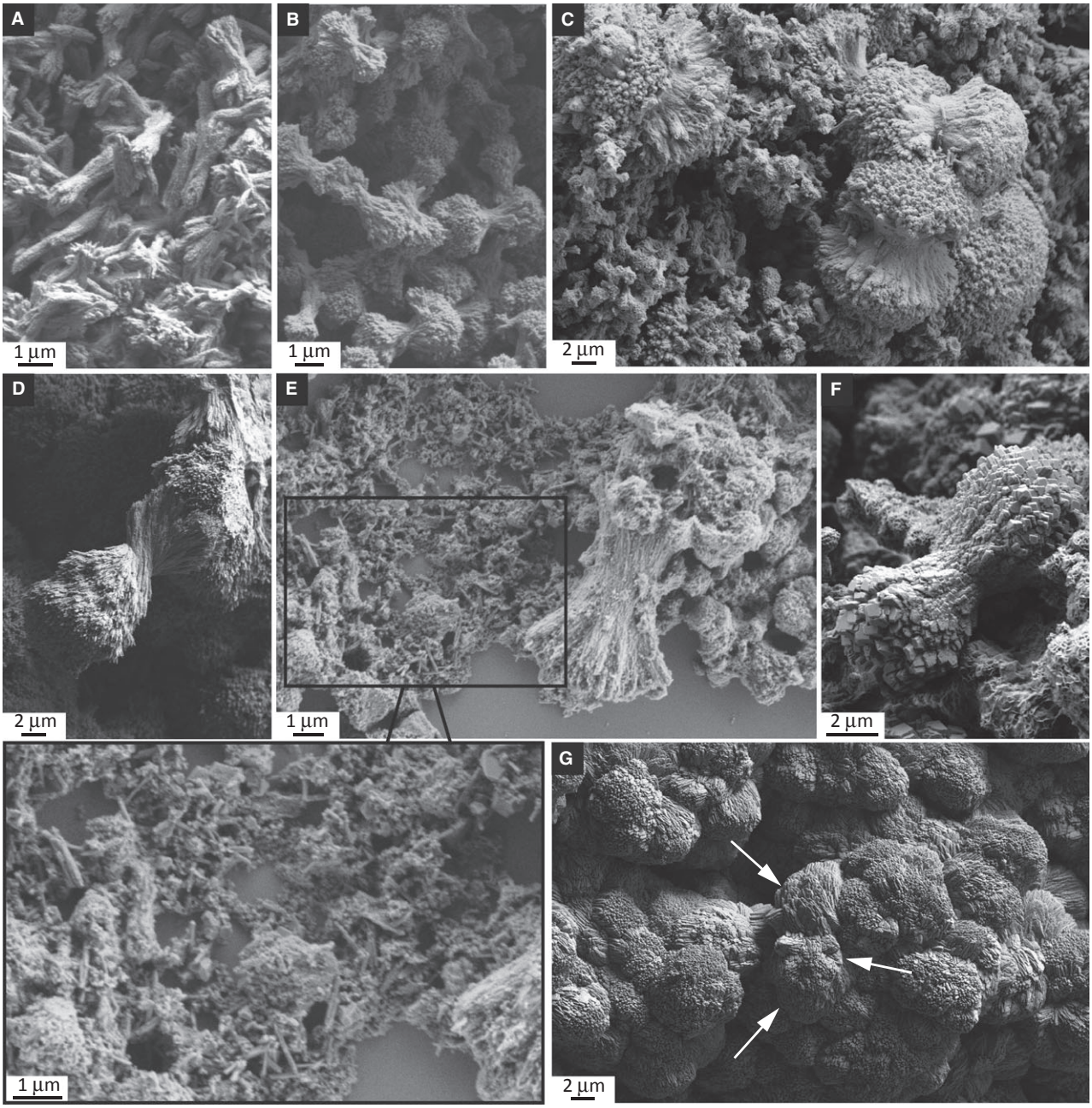

Fig. 4. Secondary electron (SE) images of various dumb-bell-shaped precipitates produced by (A) *Haemulon* sp.; (B) and (C) great barracuda; (D) grey angelfish; (E) great barracuda (after gentle sonication); (F) *Eucinostomus* sp.; (G) checkered puffer. (A) and (B) Some species produce carbonates dominated by small wheatsheafs (A) or dumb-bells (B) typically <4 µm in length. (C), (D) and (E) Larger dumb-bells (5 to 25 µm in length) typically comprise fibres that originate from a central point, forming 'semi-spheres' where they splay to the greatest degree (C). In dumb-bells produced by some species, these fibres are arranged helically about the long axis (D). After short periods of sonication dumb-bells release some of their individual component fibres [expanded portion of (E)]. (F) and (G) Large dumb-bells can also comprise numerous sub-micron rhombohedra (F) or micron-scale blade-like crystals (G). In some examples of the latter, dumb-bells appear to coalesce to form single multi-lobate particles; a dumb-bell-shaped particle is highlighted by white arrows (G).

Spheres

Spherical forms are the dominant crystalline product excreted by several species, including bonefish, checkered puffer, grey angelfish and scrawled cowfish; they also occur as subsidiary forms in carbonates produced by several other species (Table 1). Spheres are typically 8 to 50 µm in diameter. Within individual pellets sphere

diameter typically is reasonably uniform, but it commonly varies from one pellet to the next; mean diameter within individual pellets ranging from *ca* 10 to 30 μm (Fig. 5A). Occasionally, spheres occur as discrete particles (this is mostly restricted to the largest spheres), but most commonly they are intergrown with other spheres (Fig. 5A and B). While cohesion between ellipsoids appears to be a result of the interlocking of individual crystals, it is this intergrowth of spheres that allows these particles to coalesce and form pellets. Consequently, in many cases, spherical forms are not complete spheres, and the degree of coalescence can influence their appearance markedly. At one end of the spectrum a pellet may consist of large numbers of spheres that are in limited contact with one or more neighbouring spheres. At the opposite end of the spectrum the degree of coalescence is greater, and individual spheres are difficult to distinguish. In these cases, pellets have the appearance of single, multi-lobate particles.

In the majority of examples, spheres are polycrystalline, comprising densely packed, radially arranged fibres (Fig. 5B). Individual fibres are similar in size and structure to those that make up many polycrystalline dumb-bells and, when viewed end-on, a polycrystalline fibrous dumb-bell can be difficult to distinguish from a sphere. In some cases, spheres may be a manifestation of dumb-bells which have splayed to such a degree that they have grown back over themselves. Indeed, several apparent spheres have missing segments that reveal an internal structure indicating that they are composed of several well-developed, intergrown dumb-bells (Fig. 5C).

In contrast, externally identical spheres, when viewed in section, can also exhibit either a dense and continuous radial structure of fibres emanating from the central point (Fig. 5B and D) or an outer layer of radially arranged fibres (*ca* 1 μm in length) and a hollow, or partially hollow, centre (Fig. 5E and F). Internal structure variations are not particular to species; both bonefish and checkered puffer produce spheres with dense and hollow interiors. In samples produced by checkered puffer, spheres within individual pellets appear to be of only one type (i.e. either solid or hollow; never both) (Fig. 5D and E). Where spheres are partially hollow, the material that occupies the centre is commonly rather peloidal in character, at least in carbonates produced by bonefish. This material can include, or be dominated by, nanospheres that are typically <0·5 μm in diameter (Fig. 5F).

In addition to their presence within hollow spheres, nanospheres sometimes represent the dominant crystalline component of entire pellets. In either situation, their occurrence is limited to two species – bonefish and great barracuda; they range in diameter from <0·1 to 1·0 μm (typically being <0·4 μm). The continued growth of nanospheres to directly form larger spheres appears unlikely given the near-complete absence of spheres in the 1 to 5 μm diameter range. Thus nanospheres and larger spheres appear to be discrete crystal forms. The microstructure of nanospheres is difficult to ascertain at this scale, but they appear to have smooth surfaces and at least some have hollow interiors. Commonly they appear to coalesce in a similar manner to larger spheres, occasionally to such an extent that they amalgamate into a single uniform structure (Fig. 5G).

In addition to the spheroidal forms described above, spherulitic particles are commonly produced by yellowfin mojarra and redtail parrotfish (two species that produce a wide variety of crystal forms). In size and radial growth structure, these are similar to large spheres. However, individual crystals are less densely packed and much more blade-like in form, with flat faces and pointed terminations (Fig. 5H). Blades are up to 0·5 μm in width, and complete spherulites typically have diameters in the range 4 to 10 μm. Commonly they coalesce to form lobate structures that are similar, but less densely packed, than those formed by typical spheres.

Euhedral rhombohedra

The carbonate products excreted by bluehead wrasse, slippery dick and beaugregory differ significantly from those of other species. Pellets produced by all three are dominated by a Mg-carbonate phase (see *Mineralogy and chemical composition* section), but monocrystalline Mg calcite rhombohedra (5 to 15 μm in length) also represent a significant proportion of the excreted carbonates. In most pellets, Mg-carbonate forms a 'matrix' in which rhomobohedral Mg calcite is distributed uniformly. Crystal faces are commonly well-defined, but are typically repeated in a series of steps, with the overall effect of moderate crystal habit tending towards sphere-like or dumb-bell-like (Fig. 6A and B).

Rhombohedral particles are also a common, albeit volumetrically minor, product of many other species. These differ from the rhomobohedra described above, typically being smaller and of strong crystal habit. The redtail parrotfish, for example, produces rhombohedra of very

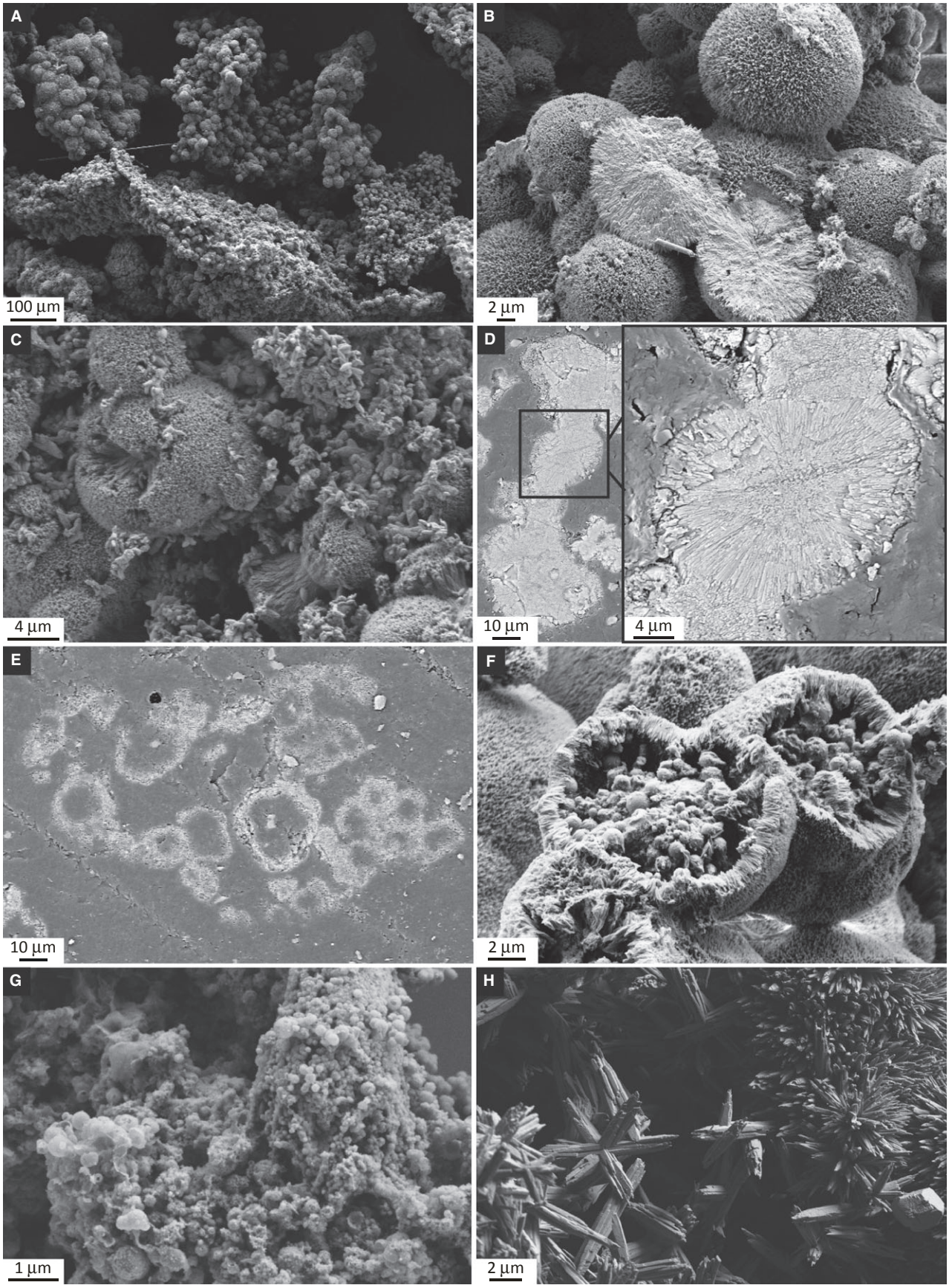

Fig. 5. Secondary electron (SE) images (unless stated otherwise) of the various forms of spherical precipitates. (A) Pellets comprising inter-connected spheres (bonefish). Sphere diameters are reasonably uniform within any given pellet, but can vary significantly from one pellet to the next. (B) Typical outward appearance of spheres (bonefish), with surfaces comprising the terminal points of densely packed radially arranged fibrous crystals. In this example, fibres radiate from a central point, as evidenced by two spheres in cross-section (centre bottom). (C) Incomplete sphere, left of centre (yellowfin mojarra). Missing segments reveal an internal structure that appears to comprise several intergrown dumb-bells. (D) and (E) Backscatter electron images of resin-embedded pellets (checkered puffer). (D) Solid spheres comprising radial fibres. (E) Hollow spheres (the nature of arrangement is not apparent due to damage caused during polishing). Individual pellets dominated by spheres typically comprise only one of these types. (F) Incomplete sphere revealing an outer layer of radial fibres *ca* 1 μm in length and a hollow centre containing nanospheres (bonefish). (G) Nanospheres (bonefish). Occasionally nanospheres appear to amalgamate, forming a single crystalline structure (top right). (H) Spherulitic forms (right) are less densely packed than typical spheres and comprise a radial arrangement of blade-like crystals (redtail parrotfish). Also shown are intersecting/intergrown fibrous needles with frayed terminations (left).

strong crystal habit that are typically up to 5 μm in length (Fig. 6C). Typically they occur as individual crystals distributed randomly through pellets that are dominated by other crystal morphologies. In samples produced by scrawled cowfish, rhombohedra identical to those produced by redtail parrotfish occasionally occur in clusters on sphere surfaces. The black grouper also produces similar rhombohedra, although crystals are typically smaller and more prismatic in form (Fig. 6D). In most pellets excreted by this species, rhombohedra are randomly distributed among dominant monocrystalline ellipsoids; in other pellets, however, they can occur in localized high concentrations.

Rods and needles

Rod-shaped crystals are produced as subsidiary forms by many species. Samples in which monocrystalline ellipsoids are the dominant form often also comprise monocrystalline rods, which average slightly greater lengths (mean *ca* 1·1 μm). Most examples have terminations that are flat, or at least are blunt relative to the pointed terminations of ellipsoids; they are typically straight-sided, although some crystals exhibit flat terminations and curved edges, thus having the appearance of an intergrade between ellipsoid and rod. Occasionally terminations appear frayed, indicating that some rods are partially fibrous. Indeed, such crystals produced by black grouper appear to show a succession of developmental stages, where rods with flat or blunt terminations develop into those with fibrous and frayed tips which, in turn, begin to splay to form possible precursors to small dumb-bells. It is therefore tempting to invoke a morphogenetic growth sequence that links ellipsoids, rods and small dumb-bells (Fig. 7).

In most other cases where the term 'rod' could be applied as a descriptor on the basis of straight-sided morphology, particles are polycrystalline, being similar in size and texture to polycrystalline dumb-bells. These particles are therefore considered end-members of the range of polycrystalline dumb-bells; that is, those which exhibit little or no splay perpendicular to the long axis. A rod or needle-like form of rather different character is occasionally observed in samples produced by redtail parrotfish and bluehead wrasse. Needles occur in the range 2 to 10 μm long and are straight-sided. The long faces differ from those of the rods described above by being of strong crystal habit. Rather frayed terminations are a manifestation of individual needles comprising several blade-like crystals. Needles and their component crystals are similar to the individual crystals that comprise spherulites, and in many cases they are intergrown in a similar radial manner. However, needles are less densely packed, usually with no more than three intersecting particles.

Other material

In addition to the common crystal morphologies described above, most of which are Mg calcite (see following section), samples from many species also comprise a Mg-carbonate phase. Typically this is a minor phase, occurring rarely and rather sporadic in distribution. In most cases, it is observed as discrete clusters of platy crystals (up to 2 μm in width) that interlock to form rosette-like structures on pellet surfaces (Fig. 8A). In samples produced by red lionfish, what is presumably a similar phase is more extensive and forms a pervasive mesh-like coating that covers nearly all of the dominant Mg calcite ellipsoids (Fig. 8B).

In samples produced by bluehead wrasse, slippery dick and beaugregory, Mg-carbonate represents the major phase (see *Energy-dispersive X-ray spectrometry* section). In these species, it

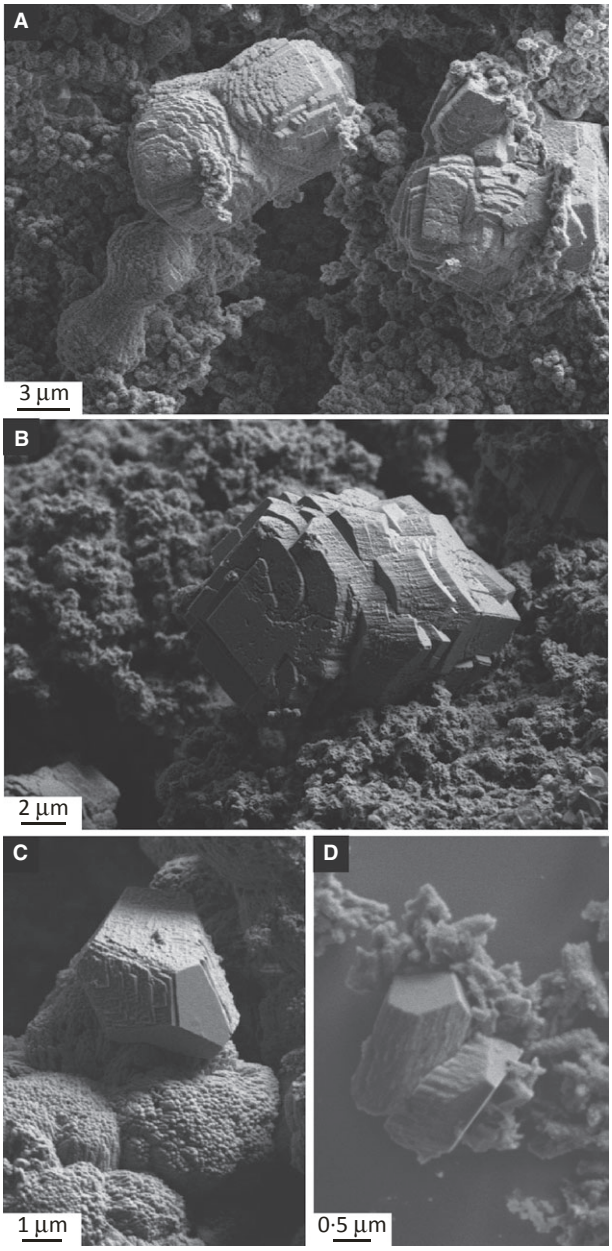

Fig. 6. Secondary electron (SE) images of representative examples of rhombohedral crystals produced by: (A) slippery dick; (B) bluehead wrasse; (C) redtail parrotfish; and (D) black grouper. (A) and (B) In samples produced by slippery dick, bluehead wrasse and beaugregory, rhombohedra have step-like structures and tend towards dumb-bell-shaped and equant, sub-spherical particles. Rhombohedra produced by these species are typically associated with a Mg-carbonate 'matrix' that consists of nanospheres comprising nanoscale interlocking plates (A). Rhombohedral crystals produced by other species are typically smaller and of a different structure, which varies according to species (C) and (D).

assumes three morphological forms: nanoscale plates that form extensive 'meshworks'; nanospheres or rosettes that comprise nanometre-scale

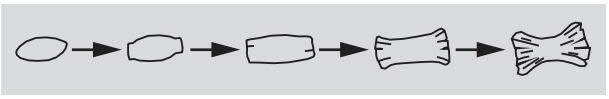

Fig. 7. Variations across a range of crystal forms suggest that each may be part of a morphogenetic sequence, in which continued growth of ellipsoids leads to the formation of rods, which begin to splay at their terminations to develop as wheatsheafs and dumb-bells.

interlocking plates (Fig. 8C); and a solid phase that lacks any clearly definable form (Fig. 8D) and commonly exhibits desiccation cracks in dried samples.

Mineralogy and chemical composition

X-ray diffraction

X-ray diffraction patterns indicate that for carbonates excreted by eight fish species (this study and Perry *et al.*, 2011) the dominant mineral phase is Mg calcite. This observation is based on the occurrence of lattice structures in the R-3c space group, with diffraction peaks close to those of pure calcite (Fig. 9; see also Perry *et al.*, 2011, supplementary online material). The d_{104} diffraction peak is also consistently shifted to values greater than 29·4° 2θ, further indicating Mg calcite as the dominant mineral phase. Estimates of $MgCO_3$ content based on d_{104} values are shown in Table 1. Given that the degree of lattice disorder in fish-derived crystals is unknown, values based on the curves for ordered (Goldsmith *et al.*, 1961; Bischoff *et al.*, 1983) and disordered (Zhang *et al.*, 2010) Mg calcites are used here to interpret $MgCO_3$ contents >20 mol%. These indicate that the $MgCO_3$ component of fish-derived Mg calcite varies with species and ranges from 5·1 to 39·6 mol%. However, SEM observations indicate that the majority of fish-derived crystals are <2 µm in length, and EDX results (see below) suggest significant compositional heterogeneity in carbonates from most species. This may explain the reasonably broad diffraction peaks observed (Fig. 9), although this could also reflect the fact that these carbonates have a low degree of crystallinity. In either case, broad peaks introduce potential errors in estimations of $MgCO_3$ contents (Bischoff *et al.*, 1983). Combined with problems of estimating $MgCO_3$ content at >20 mol% and the unknown influence of trace elements, these potential errors mean that crystal chemistry based on diffraction peak positions should be taken as semi-quantitative estimates of $MgCO_3$ content.

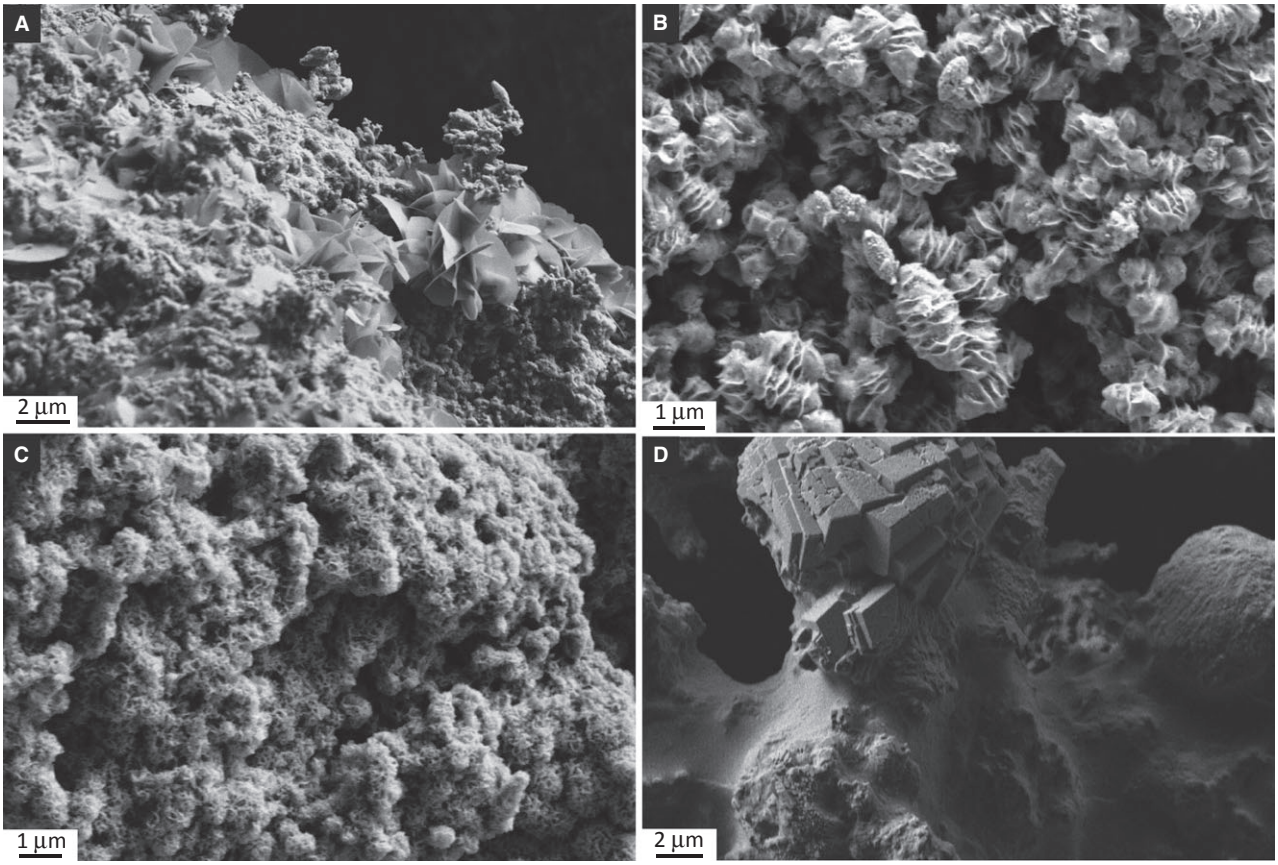

Fig. 8. Secondary electron (SE) images of various forms of Mg-carbonate. (A) Micron-scale plates occasionally form localized rosette-like structures on pellet surfaces (shown on pellet produced by black grouper). (B) Mesh-like coatings covering dominant Mg calcite particles are rare in samples produced by most species, but pervasive in those produced by red lionfish. (C) and (D) In pellets produced by bluehead wrasse, slippery dick and beaugregory, rhombohedral crystals are distributed throughout a 'matrix' of Mg-carbonate, which may consist of: (i) nanospheres, each comprising a 'meshwork' of interlocking nanoscale plates (C); or (ii) a solid that lacks any clearly definable form (D).

The presence of small amounts of aragonite in samples from some species is indicated by small diffraction peaks at 26·3° 2θ and 27·3° 2θ (Fig. 9; Perry *et al.*, 2011, supplementary online material); this is the only subsidiary crystalline phase detected. Samples produced by bluehead wrasse yield diffraction peak positions that clearly indicate the presence of Mg calcite containing *ca* 5 mol% $MgCO_3$ (Fig. 9), presumably referring to rhombohedral crystals. Despite the presence of a dominant Mg-carbonate phase in these samples (see EDX results below), no other diffraction peaks were detected, suggesting that it does not produce a diffraction pattern and is thus an amorphous phase.

Energy-dispersive X-ray spectrometry

$MgCO_3$ contents based on EDX analyses are generally in close agreement with estimates based on XRD analyses, thus confirming that magnesium detected by EDX is incorporated within the crystal lattice rather than being adsorbed or occluded. This analytical technique allows crystal chemistry to be determined on a crystal by crystal basis, thus addressing some of the issues apparent in XRD analysis. Mean values of mol% $MgCO_3$ for carbonate samples excreted by 21 fish species, based on 50+ individual EDX analyses per species, are shown in Table 1. Carbonates excreted by 13 out of 21 species have high Mg contents, falling within the range detailed by Perry *et al.* (2011) of 18 to 39 mol% $MgCO_3$. However, eight species are found to excrete carbonates with lower $MgCO_3$ contents, seven of which produce carbonates with a markedly different morphology and chemical composition (the carbonate products of keeltail needlefish, which have only slightly lower $MgCO_3$ contents than those previously reported for fish-derived carbonates, are morphologically similar).

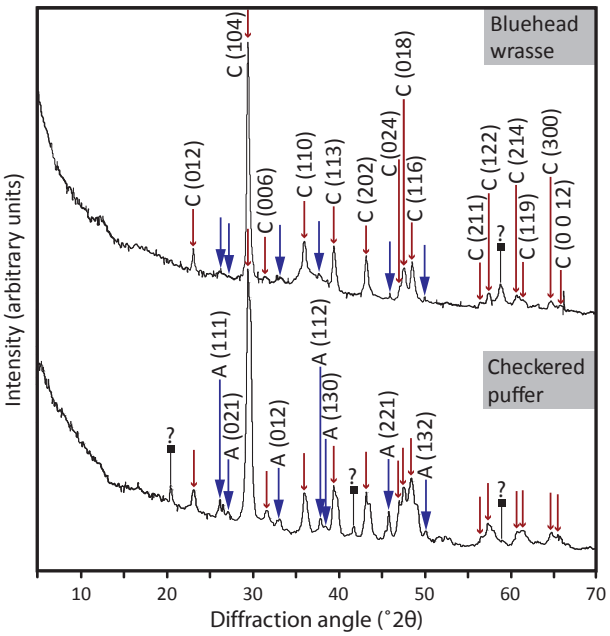

Fig. 9. X-ray diffraction patterns of carbonates produced by bluehead wrasse and checkered puffer. Large arrowheads (blue) indicate aragonite 'A' peaks; small arrowheads (red) indicate Mg calcite 'C' peaks. Note the broad $d_{(104)}$ peak for crystals produced by checkered puffer (relative to that for crystals produced by bluehead wrasse), probably indicating the presence of crystals with a broad range of $MgCO_3$ contents.

Four species (checkered puffer, redtail parrotfish, grey angelfish and scrawled cowfish) produce carbonates that comprise mainly LMC and which typically have relatively low Mg contents (1 to 5 mol% $MgCO_3$). Each of these species produces a wide range of crystal forms. In any given sample the Mg content may vary by a few mol% from one crystal to the next, but there is no relationship between crystal morphology and $MgCO_3$ content. However, it is noteworthy that some polycrystalline fibrous dumb-bells produced by checkered puffer have higher $MgCO_3$ contents (up to 14 mol%). This may explain the presence of a distinct shoulder on the d_{104} XRD peak for samples produced by this species, the position of which corresponds to a $MgCO_3$ content of 17 mol%.

The products of three other species (bluehead wrasse, slippery dick and beaugregory) differ greatly from those of the majority of species both in texture (see previous section) and in composition. The rhombohedral crystalline forms produced by these species typically have relatively low $MgCO_3$ contents (averaging approximately 5 mol% $MgCO_3$, but in the range 2 to 17 mol%). In contrast, the dominant phase (which either lacks any clearly definable form, or comprises a mesh-like network of sub-micron plates) has little or no calcium and appears to be a Mg-carbonate phase. These results, combined with XRD results, indicate that this is probably an amorphous form of magnesite or, given that EDX analyses are not capable of detecting the presence of hydrogen, any one of the various hydrous Mg-carbonate phases (for example, hydromagnesite, dypingite or nesquehonite). This phase is readily apparent in backscatter electron (BSE) images as a much darker phase than the associated Mg calcite crystals (Fig. 10). Backscatter electron imaging also reveals the limited presence of a similar phase in some samples produced by other

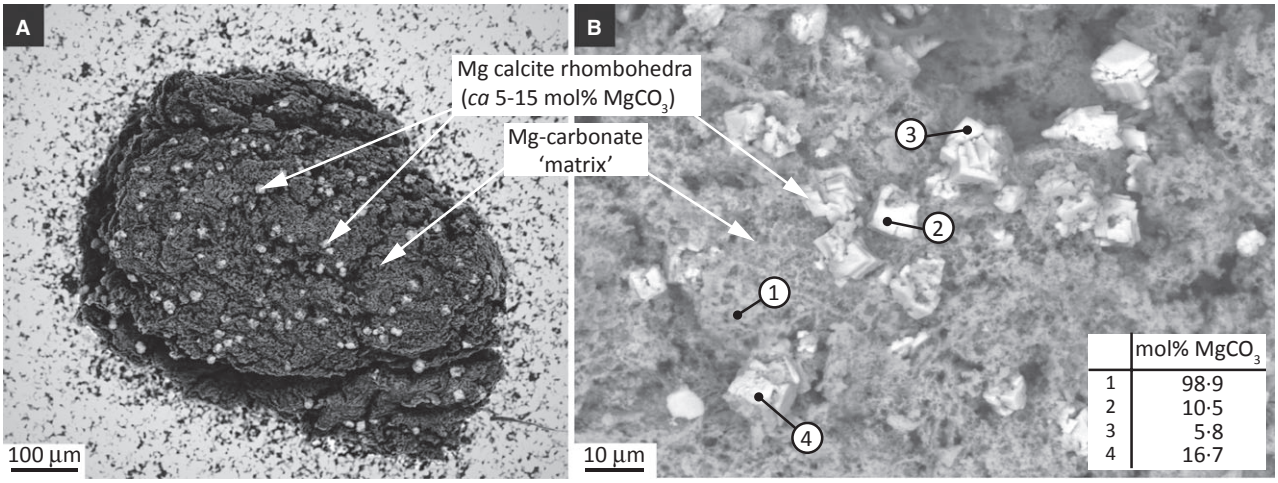

Fig. 10. Backscatter electron images of carbonate pellets produced by: (A) beaugregory; and (B) bluehead wrasse. Pale areas represent Mg calcite crystals; dark areas represent amorphous Mg-carbonates. Mg calcite crystals are typically uniformly distributed throughout the Mg-carbonate 'matrix' (A). Note the corresponding $MgCO_3$ contents, measured by EDX analysis (B).

species, such as black grouper and keeltail needlefish, in which Mg calcite monocrystalline ellipsoids represent the dominant phase. Larger-scale platy and rosette-like phases observed as a subsidiary form in carbonates produced by many species have a similar Mg-rich composition. The texture and composition of the latter is similar to some forms of nesquehonite ($MgCO_3{\cdot}3H_2O$) (Kloprogge *et al.*, 2003) and dypingite ($Mg_5(CO_3)_4(OH)_2{\cdot}5H_2O$) (Power *et al.*, 2007). The former occurs naturally as an evaporative mineral (Kloprogge *et al.*, 2003), and can form abiotically in highly alkaline environments enriched in magnesium, such as the hydromagnesite playas of the Cariboo Plateau, British Columbia, Canada (Power *et al.*, 2007). The occurrence of dypingite is less well-documented but it has been shown to be associated with microbial activity in similar settings (Power *et al.*, 2007).

The findings of this study also indicate that the $MgCO_3$ content of Mg calcite phases can actually vary more widely within samples from individual species than originally reported (Perry *et al.*, 2011). For example, the carbonate products of yellowfin mojarra are dominated by monocrystalline ellipsoids that have a mean $MgCO_3$ content of 21·1 mol%. Subsidiary products occurring alongside these include larger (*ca* 4 to 20 μm) polycrystalline dumb-bells and spheres that have consistently lower $MgCO_3$ contents (mean 5·5 mol%). Similarly, the products of keeltail needlefish are dominated by small (*ca* 1 to 2 μm) ellipsoids, rods and dumb-bells with a mean value of 13·2 mol% $MgCO_3$, but also comprise larger (*ca* 5 to 20 μm) dumb-bells and spheres with a mean of 2·5 mol% $MgCO_3$. Thus, for $MgCO_3$ values to be truly representative it is more appropriate to present them as mean values per crystal form for each species (Table 1).

In addition to variations according to species and crystal form, $MgCO_3$ content appears, in some samples, also to vary between different pellets that share a common dominant morphology and are excreted by the same species. For example, monocrystalline ellipsoids produced by schoolmaster snapper have an overall mean $MgCO_3$ content of 34·2 mol% (n = 62 crystals, 7 pellets), but the mean values for individual pellets range from 20·8 to 43·2 mol%. Samples produced by this species were collected from tanks holding several fish specimens. Thus, it could be the case that the $MgCO_3$ component of crystals varies with individual fish. Indeed, a separate group of schoolmaster snapper (comprising only the smallest specimens) produced HMC crystals with a mean $MgCO_3$ content of only 22·1 mol%. Several species show similar variations, usually to a lesser extent, across pellets, but many species produce pellets in which the $MgCO_3$ content is reasonably consistent. For example, mean values range from 17·5 to 21·5 mol% (n = 50 crystals, 5 pellets) in *Eucinostomus* sp.

In addition to quantifying the $MgCO_3$ component of fish-derived Mg calcites, EDX analysis also detects the presence of various trace elements in carbonates produced by most species. It is beyond the scope of this study to present these data in detail. However, it is worth mentioning that strontium, phosphorus and sulphur are frequently detected at levels of <1 wt. % in most crystal forms.

Liquid ion chromatography

Ion chromatography of dissolved carbonate samples produced by selected species reveals the bulk ionic concentrations of calcium and magnesium. Assuming that all calcium and magnesium originates from the initial Mg calcite, these data can provide quantification of the bulk $MgCO_3$ mol% for carbonates derived from each fish species. The results, shown in Table 1, are generally in close agreement with those derived from EDX (for dominant crystal forms) and XRD. Many species excrete HMC and VHMC (typically in the range 14 to 35 mol% $MgCO_3$), while checkered puffer excretes LMC and HMC (in the range 3 to 10 mol% $MgCO_3$). Of the samples examined using this technique, only those produced by bluehead wrasse, beaugregory, and some produced by great barracuda and keeltail needlefish have $MgCO_3$ contents significantly higher than those indicated by EDX and XRD. This finding is due to the presence of large amounts of amorphous Mg-carbonate in addition to Mg calcite crystals, and these values are therefore not representative of $MgCO_3$ content in Mg calcite crystals.

As with EDX data, ion chromatography data indicate that, while the $MgCO_3$ contents of carbonates produced by different individuals of the same species are generally comparable, there is clear variation (of up to 12·5 mol%) between individual fish within species. In addition, where analyses of multiple samples produced by a single fish (or group of fish) were carried out, it is apparent that these can exhibit significant differences (of up to 7·8 mol%) in $MgCO_3$ content. In each case there were no measured fluctuations in sea water temperature or salinity

during sampling, and all samples were checked carefully to ensure the absence of foreign particles. Thus the possibility arises that there could be some temporal variation in Mg^{2+} incorporation in crystals produced by some fish specimens. It is possible that such temporal and inter-specimen variations explain some of the discrepancies in measured $MgCO_3$ contents using different techniques (for example, bonefish; Table 1). It should be noted, however, that in many cases where multiple samples collected on different days were analysed, temporal variation in $MgCO_3$ content was limited to 0 to 2 mol%.

DISCUSSION

Fish-derived carbonates and their classification

By combining morphological and compositional (specifically $MgCO_3$ content) data it is possible to categorize fish species based on the carbonates they produce (Table 1). Firstly, all monocrystalline ellipsoids are HMC or VHMC with typical $MgCO_3$ contents in the range 20 to 35 mol%. Small wheatsheafs and dumb-bells typically have similar $MgCO_3$ contents. In samples where crystals of these morphologies represent >99% of the precipitates, subsidiary forms (larger polycrystalline dumb-bells and spheres) in the same samples have consistently lower $MgCO_3$ contents, in the range 3 to 14 mol%. All species producing carbonates of these descriptions (black grouper, schoolmaster snapper, yellowtail snapper, graysby grouper, red hind, flounder sp., grunt sp., French grunt, great barracuda and red lionfish) fall into Category I. Yellowfin mojarra and keeltail needlefish produce a suite of crystals that are morphologically similar to those of Category I and exhibit comparable compositional relationships (high $MgCO_3$ content in ellipsoids and small dumb-bells versus low $MgCO_3$ content in larger polycrystalline dumb-bells and spheres). However, samples are significantly more heterogeneous with respect to crystal morphology. Moreover, ellipsoids and small dumb-bells produced by these two species have significantly lower $MgCO_3$ contents (22·1 mol% and 13·2 mol%, respectively) than the equivalent products of most Category I species. Thus, yellowfin mojarra and keeltail needlefish are assigned to Sub-category Ia.

Category II consists of checkered puffer, grey angelfish, scrawled cowfish and redtail parrotfish. These species produce a wide range of crystal morphologies, with the notable absence of monocrystalline ellipsoids. Polycrystalline spheres dominate most samples, while other common products include polycrystalline ellipsoids and dumb-bells, rhombohedra, spherulites and needles. Only the products of these species include forms that appear twisted about the long axis. Compositionally, the products of these species differ from those of Category I species in their relatively low $MgCO_3$ content. Typically this falls in the range 0·8 to 7 mol%, with variability apparently not determined by species and/or crystal morphology.

The three species that constitute Category III are bluehead wrasse, slippery dick and beaugregory. The two features that define this category are the dominant presence of a Mg-carbonate phase and the Mg calcite phase being dominated by rhombohedral crystals with relatively low $MgCO_3$ contents (mean values range from 5 to 12 mol%). Other crystal morphologies are occasionally present (polycrystalline dumb-bells and spheres, and rare needles) but, as with Category II, monocrystalline ellipsoids are absent. Two species that do not fit the above categories are bonefish and *Eucinostomus* sp., both of which predominantly produce polycrystalline spheres and large dumb-bells with $MgCO_3$ contents of 19 to 23 mol%; significantly higher than equivalent products excreted by species in any other category. These species are assigned to Category IV.

Crystal growth mechanisms

Given the diverse range of crystal morphologies produced by fish it is clearly of interest to consider the potential controls on crystal growth and form, as this may provide an insight into why certain species produce different crystal forms. Although rarely described from natural settings, various $CaCO_3$ polymorphs, with morphologies similar to those described here, have been identified as common products in carbonate-precipitation experiments (Devery & Ehlmann, 1981; Morse *et al.*, 1997; Meldrum & Hyde, 2001; Kralj *et al.*, 2004; Rivadeneyra *et al.*, 2006; Gayathri *et al.*, 2007). Nearly all of the fish-derived carbonates identified in this study are Mg calcites, and thus it is clear that the precipitating solutions must contain at least some Mg^{2+}. Where inorganic precipitation is concerned, theoretical considerations invoke that the presence of Mg^{2+} in solution should inhibit the growth of calcite, instead favouring aragonite formation (Reddy & Wang, 1980; Falini *et al.*, 1994). However, Mg

calcites with similar morphologies to fish-derived carbonates have been precipitated inorganically; the inhibition of calcite growth being overridden in solutions with very high degrees of supersaturation, and by varying factors such as the concentrations of various impurities (Sr^{2+}, SO_4^{2-}, etc.) and the availability of CO_3^{2-} (Sawada *et al.*, 1990; Fernández-Díaz *et al.*, 1996; Kralj *et al.*, 2004). The inorganic chemistry of intestinal fluid in marine bony fish is very different to that of the sea water they ingest. In particular, the processing of ingested fluid: (i) reduces the salinity to about one-third that of oceanic sea water; (ii) reduces [Ca^{2+}] from 10 mM in sea water to about 2 to 5 mM due to continual precipitation; (iii) accumulates [Mg^{2+}] from 52 mM in sea water to over 200 mM in some cases, due to absorption of water into the blood without parallel removal of Mg^{2+} ions; and (iv) creates supersaturated conditions (with respect to common marine $CaCO_3$ polymorphs) as a result of alkaline pH (8·3 to 9·2) combined with very high alkalinity (from 30 to over 100 mM) as a result of substantial HCO_3^- secretion (Wilson *et al.*, 1996, 2002, 2009; Marshall & Grosell, 2005).

While it is possible that fish-derived carbonates are products of inorganic precipitation in a biologically facilitated environment (i.e. within the fish), it is difficult to envisage precipitation taking place in the intestine without at least some organic influence. Indeed, the majority of precipitation experiments that result in ellipsoidal, dumb-bell-shaped and spherical carbonate particles (comparable to those identified here) have involved the presence of various organic compounds or microbial strains, which are considered to be important controlling factors (Buczynski & Chafetz, 1991; Meldrum & Hyde, 2001; Rivadeneyra *et al.*, 2006; Sánchez-Román *et al.*, 2007; González-Muñoz *et al.*, 2008). The presence of organic additives in a precipitating solution alongside Mg^{2+} has also been shown to suppress aragonite growth and facilitate precipitation of Mg calcite (Meldrum & Hyde, 2001). Furthermore, Meldrum & Hyde (2001) show that when Mg^{2+} and organic additives are combined in the precipitating solution, Mg calcite crystals can exhibit curved or roughened crystal faces and form polycrystalline aggregates. The resultant particle morphologies can be very similar to those observed herein to be produced by fish and, thus, it is possible that similar factors are important controls on crystal morphology in both systems. The development of polycrystalline aggregates can be a result of calcite growth inhibition (Prieto *et al.*, 1994), perhaps caused by high Mg^{2+} concentrations (Kralj *et al.*, 2004), leading to the binding of sub-critical nuclei in order to facilitate continued growth. This process, which results in the growth of multiple aggregated crystals, may be enhanced by the presence of organic compounds, and possibly also by high pH levels (Van der Leeden & Van Rosmalen, 1987), the latter being characteristic of marine teleost intestinal fluids (Wilson *et al.*, 1996, 2002).

Carbonates produced in precipitation experiments where calcification is bacterially mediated (Rivadeneyra *et al.*, 2006), as well as those formed in nature in marine algal tidal flats and organic-rich inland lakes (Buczynski & Chafetz, 1991), can bear a striking resemblance to many fish-derived carbonates. It is thus tempting to invoke a major role for intestinal bacteria in the formation of fish-derived carbonates. Indeed, many crystal morphologies described herein (particularly nanospheres and ellipsoids) are reminiscent of coccoid and bacillus bacteria, and it is possible that individual bacteria create microenvironments conducive to carbonate precipitation, within which they eventually become encased; a mechanism similar to that proposed by several other workers (Greenfield, 1963; Chafetz & Folk, 1984; Buczynski & Chafetz, 1991). Such a process would go some way to explaining why some fish-derived carbonates appear to be hollow.

The large body of literature concerning $CaCO_3$ precipitation experiments considers various organic and inorganic influences on carbonate crystal growth and indicates that any of the above-mentioned factors, in various combinations, can result in mineralogies and crystal morphologies similar to those excreted by fish. A further consideration is that of the partitioning of varying amounts of trace elements (for example, Mg^{2+} and Sr^{2+}). In solutions where the precipitation of Mg calcite is favoured over aragonite, the amount of Mg^{2+} incorporated in the calcite crystal lattice increases with the Mg^{2+}/Ca^{2+} ratio of the precipitating solution (Mackenzie *et al.*, 1983; Meldrum & Hyde, 2001), and is independent of reaction rate (Mucci & Morse, 1983; Mucci *et al.*, 1985). The Mg^{2+}/Ca^{2+} ratio in the intestinal fluid of marine fish is much higher than in ambient sea water (for example, as indicated above, this can be >100 instead of *ca* 5), and this also varies depending on species due to different rates of absorption of water, Ca^{2+} and Mg^{2+}, as well as different rates of secretion of HCO_3^- ions (Marshall & Grosell, 2005). Other important factors influencing carbonate

precipitation, such as ion activity coefficients, ion pairing and ionic strength of the fluid (i.e. factors that determine the ion activity product; Morse & Mackenzie, 1990; Andrews *et al.*, 2004), although not previously determined, presumably differ significantly from known surface sea water values, and also vary with species. This variability of gut fluid chemistry between species could explain why, for example, Category II crystals typically have much lower $MgCO_3$ contents than Category I crystals. It may also be the case that such factors exert some influence on crystal morphology. Indeed, nearly all monocrystalline ellipsoids are VHMC, suggesting that crystals with this morphology might only form in solutions with high Mg^{2+}/Ca^{2+} ratios. However, the fact that individual carbonate pellets are often compositionally heterogeneous indicates that either: (i) Mg calcite crystals of various compositions can precipitate out of a single solution, suggesting that factors other than Mg^{2+}/Ca^{2+} ratio must also influence magnesium uptake; or (ii) there exist highly localized variations in precipitating conditions within the piscine gut.

Clearly the controls on morphological and compositional development in Mg calcite are complex, and it appears that a crystal with any specified morphology and composition can be derived through several pathways. However, with regard to carbonate precipitation in fish, it is reasonable to speculate that important drivers in the development of various crystal forms may include: (i) the presence of various organic components (mucus, microbial communities and organic compounds associated with digestion); (ii) high degrees of supersaturation; (iii) precipitating solutions with unique (in nature) ionic concentrations (and associated ion-activity products); (iv) metabolic rates and associated rates of HCO_3^- secretion in the intestine; and (v) high pH levels within the intestine. Variations in such factors according to species may explain why crystalline products are often species-specific. Preliminary observations indicate that fish body mass and functional group (and diet) may not be significant controls on precipitation. For example, numerous species sampled in this study produced morphologically and chemically uniform crystals across a large body mass range (for example, yellowtail snapper: 13·5 to 946 g), while macroinvertivores are included in all identified categories of crystal form (Table 1). However, it is not possible to completely rule out body mass as a factor, and it is interesting that all fish specimens that produced Category III precipitates had a body mass of <13 g (smaller than nearly all specimens of other species). Thus Category III precipitates could be species-controlled, but it is also possible that they are a product unique to very small fish (i.e. body mass-controlled). Further work to determine the species-dependent factors influencing crystal growth and form is ongoing and the nature of these interacting controls will be discussed elsewhere.

Relevance of fish-derived carbonates in carbonate muds

The great majority of fish-derived carbonates comprise individual crystals or polycrystalline particles of <4 μm, and typically <2 μm, length. Polycrystalline spheres and dumb-bells are commonly larger, up to 40 μm in diameter, but exposure to brief periods of gentle sonication indicates that these might ultimately break down into their component crystals (<1 to 10 μm) in a natural depositional setting. Figure 11 shows the grain-size distribution of fish-derived carbonates in the context of other major known carbonate mud producers within shallow tropical marine environments, and in the context of a typical carbonate mud fraction from a Bahamian surface sediment sample (Neumann & Land, 1975). This sample shows a rather bimodal grain-size distribution, with the majority of material occurring in the 16 to 63 μm and <4 μm fractions.

Various potential skeletal origins for this very fine carbonate material have been discussed in the literature. For example, the attrition of skeletal material, such as bivalve and gastropod shells (Matthews, 1966), is doubtless responsible for the generation of some material in the <4 μm fraction. In addition, numerous marine organisms, such as several species of calcareous green algae and foraminifera, precipitate skeletal carbonates in the form of aggregated anhedral equant nanograins and needles of <10 μm (Lowenstam & Epstein, 1957; Loreau, 1982; Debenay *et al.*, 1999). Upon post-mortem degradation of organic binding material, such organisms can release their individual component crystals to generate significant quantities of carbonate mud grains of <4 μm length (Lowenstam & Epstein, 1957; Stockman *et al.*, 1967; Neumann & Land, 1975; Multer, 1988; Debenay *et al.*, 1999). Abiotic precipitation of aragonite and Mg calcite needles of <4 μm length in whitings (Shinn *et al.*, 1989) also represents a possible source of mud-fraction carbonate. This study presents clear evidence that an additional and direct pathway for the

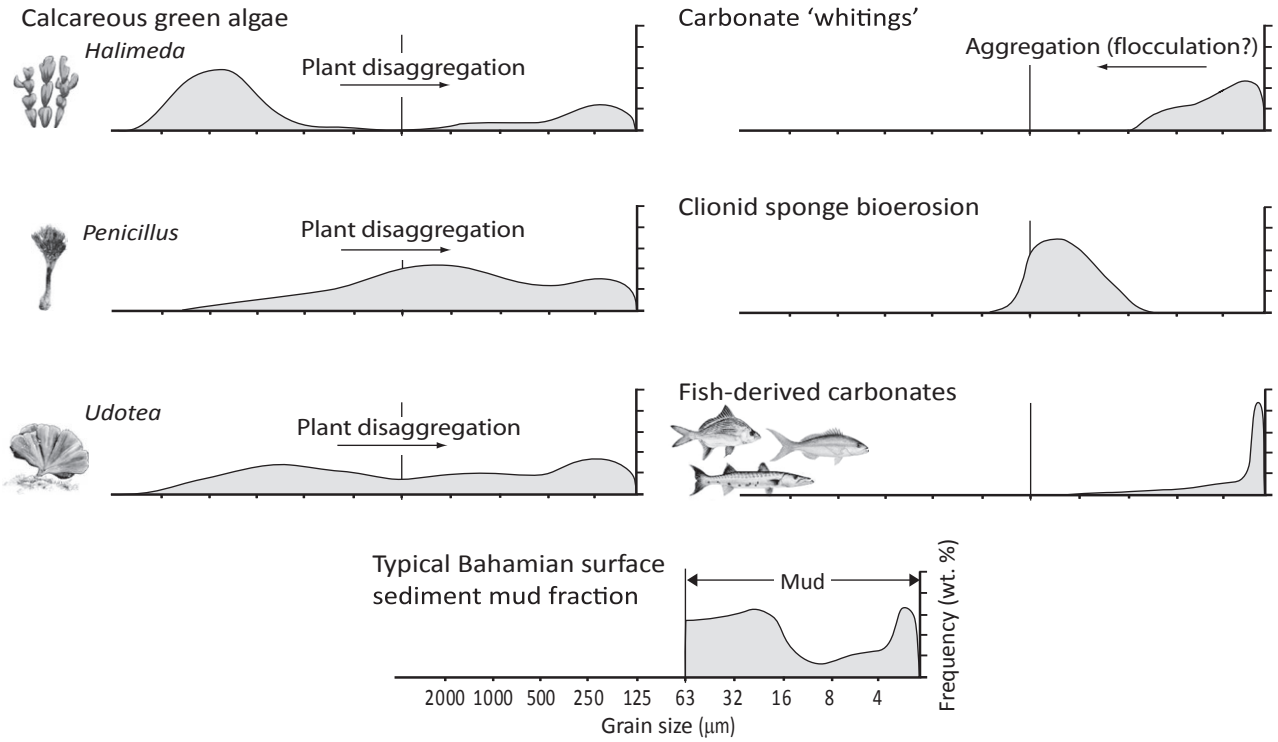

Fig. 11. Comparison of fish-derived carbonate grain-size distribution against those of other known carbonate mud producers and a typical mud fraction of Bahamian surface sediment. Calcareous green algae and surface sediment data from Neumann & Land (1975); whiting curve estimated based on data from Shinn *et al.* (1989) and Robbins & Blackwelder (1992); Clionid sponge data from Fütterer (1974).

production of such carbonate is from fish, the vast majority of which is directly precipitated Mg calcite and is <4 μm in size.

Many of the crystal morphologies described herein are not, however, typical of those commonly described in studies of tropical carbonate muds (Stieglitz, 1972; Gischler & Zingeler, 2002), although detailed investigations of the morphologies of the very finest size fraction carbonates are not exhaustive. However, Perry *et al.* (2011) document the presence of Mg calcite grains in Bahamian mud samples from a range of depositional settings that are morphologically and compositionally very similar to some of those precipitated within the intestines of marine fish. In light of this, and in the absence of morphologically similar grains originating from other known major mud producers, marine fish are considered to be a likely contributory source. This finding is perhaps not unexpected given the high measured production rates (Perry *et al.*, 2011), coupled with the fact that fish-derived carbonates precipitated and excreted alongside ingested carbonate particles (i.e. as occurs under normal dietary regimes) appear compositionally and morphologically similar to the crystals described herein. It is therefore likely that marine fish in their natural environments will precipitate and excrete carbonate crystals as described in this work. However, this study and previous work (Perry *et al.*, 2011) focus only on the production of fish-derived carbonates in The Bahamas; in order to understand the wider geographical production and significance of fish-derived carbonates, it will be necessary to extend this work into other contemporary shallow tropical settings, and also into temperate settings.

Post-excretion pathways

A key question arising from this work relates to the preservation potential of the fish-derived carbonates identified. High-Mg calcite is typically more soluble in sea water than other $CaCO_3$ polymorphs that commonly occur in marine settings, with numerous studies finding decreasing stability with increasing $MgCO_3$ content (Plummer & Mackenzie, 1974; Walter & Morse, 1984; Bischoff *et al.*, 1987; Busenberg & Plummer, 1989; Morse *et al.*, 2006). Mean $MgCO_3$ contents in modern Mg calcite muds are typically in the range 10 to 13 mol% (Bosence *et al.*, 1985; Reid *et al.*,

1992), and *ca* 15 mol% is considered the upper limit at which Mg calcite is thermodynamically stable in open shallow marine conditions at *ca* 25°C (Bertram *et al.*, 1991). Indeed, the $MgCO_3$ contents of many known producers of HMC mud are <15 mol%, with only some species of crustose coralline algae consistently producing Mg calcite with >15 mol% $MgCO_3$ (Fig. 12; Chave, 1954). The fish-derived carbonates identified in this study clearly exhibit a wide range of $MgCO_3$ contents, and some are very high at the point of excretion (Table 1; Fig. 12). It is thus reasonable to assume that a proportion of this material may be relatively unstable in sea water, and therefore subject to processes of recrystallization and/or dissolution. An additional force driving such processes may be the large amounts of excess free energy associated with such small crystals as fish-derived carbonates. Thus a fundamental consideration is that of the post-excretion pathways of fish-derived carbonates, with the very real possibility that different crystal types may undergo very different post-excretion preservation pathways. Clearly, significant further work is required to address this question, but several aspects of previous studies raise some interesting issues regarding preservation/diagenetic alteration potential.

For example, Morse *et al.* (2006) note that, in contrast to the findings of many solubility experiments, crystal solubility cannot be assumed to be a direct function of $MgCO_3$ content alone, especially when considering biogenic carbonates in natural environments. Indeed, the results of solubility experiments where samples were not cleaned prior to analysis (Plummer & Mackenzie, 1974) indicate significantly higher solubilities than samples that were cleaned (Bischoff *et al.*, 1987). Other factors that may influence crystal stability include composition of the original precipitating solution, degree of cation and carbonate anion lattice disorder (perhaps reflecting precip-

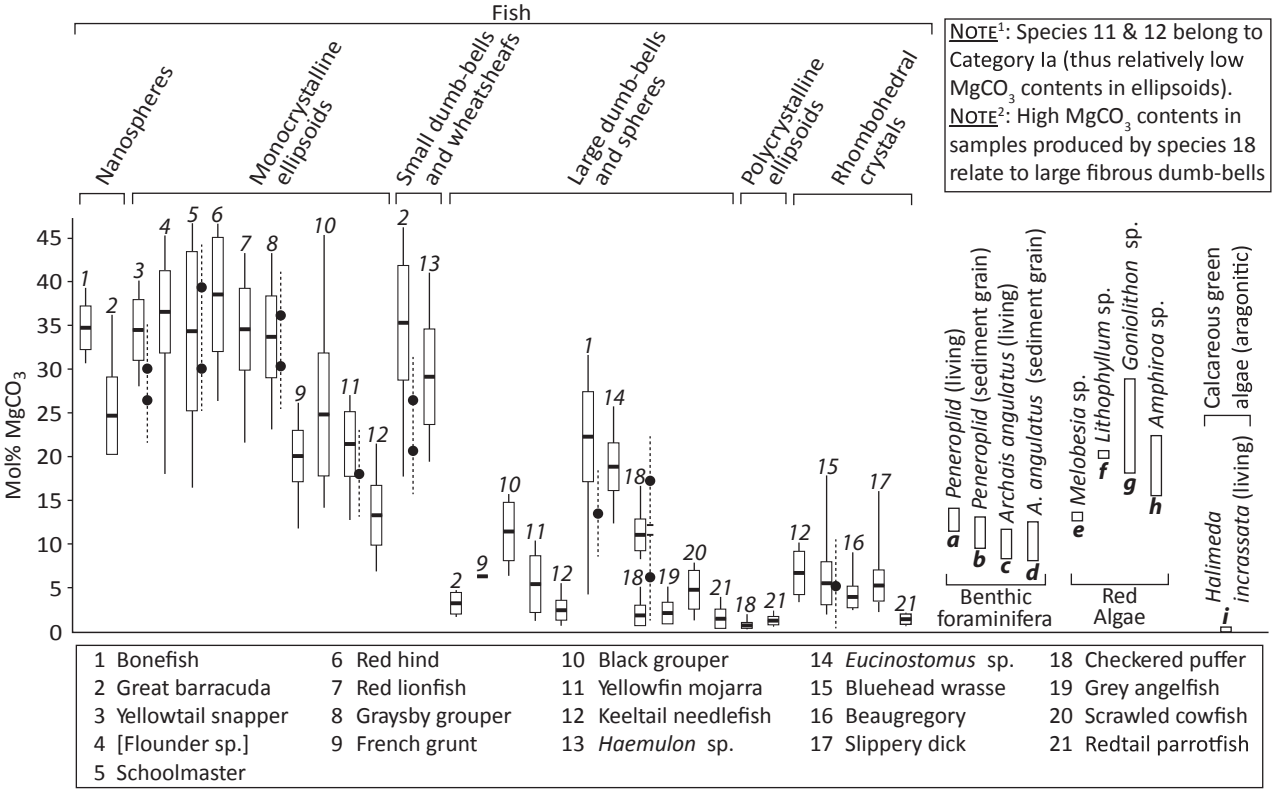

Fig. 12. Reported $MgCO_3$ compositional ranges for several known tropical marine carbonate mud producers compared with measured $MgCO_3$ contents of various carbonate crystal forms produced by a range of tropical fish species (this study). Fish data are based on EDX analyses and show mean $MgCO_3$ content per crystal form ±1 standard deviation (white boxes), and the full range of measured values (solid lines). Where measured, data based on XRD analyses are shown (solid circles; dashed lines represent error of ±5 mol%) adjacent to EDX data for the dominant crystal form produced by the species. Data on $MgCO_3$ content ranges of other carbonate mud producers based on: 'a' and 'b' – Hover *et al.* (2001); 'c' – Macintyre & Reid (1998); 'd' – Reid and Macintyre (1998); 'e' – Smith (1972); 'f' – Chave (1954); 'g' – Chave (1954); Walter & Morse (1984); 'h' – Chave (1954); Schmalz (1967); and 'i' – Hover *et al.* (2001).

itation rate) and sea water temperature (Bertram *et al.*, 1991; Morse *et al.*, 2006). In addition, the presence of impurities, such as Sr^{2+} and SO_4^{2-}, both of which are present to varying degrees in many fish-derived carbonates, and especially H_2O and OH^- (present in many biogenic Mg calcites; Bischoff *et al.*, 1983, 1987) could exert significant influence on crystal stability. Studies on the influence of incorporated Sr^{2+} on calcite solubility are scarce. However, Mucci & Morse (1983) suggest that, where incorporated at Ca^{2+} sites within the Mg calcite crystal lattice, the large ionic radius of Sr^{2+} may act to relieve some of the stress caused by the presence of Mg^{2+}, thus possibly increasing crystal stability. In addition, Wasylenki *et al.* (2005) note that calcite growth is enhanced when Sr^{2+} is incorporated in the crystal lattice, and speculate that a possible driver of this could be decreased solubility in response to the presence of Sr^{2+}. In contrast, biogenic Mg calcites are typically less stable than synthetic Mg calcites with similar $MgCO_3$ content, possibly due to the presence of impurities, such as H_2O and OH^- (Bischoff *et al.*, 1987). The factors that might influence Mg calcite solubility in nature are thus numerous and complex, and may not necessarily act to increase solubility. Furthermore, solubility studies typically only consider Mg calcites with up to 20 mol% $MgCO_3$. Empirical evidence for the stability of Mg calcites with very high (>25 mol%) $MgCO_3$ content in tropical sea water is extremely sparse and the post-excretion behaviour of fish-derived VHMC should not be assumed to be unstable.

The existing experimental data indicate that all fish-derived carbonates with <15 mol% $MgCO_3$ (i.e. most large polycrystalline dumb-bells and spheres, rhombohedral forms and polycrystalline ellipsoids) should be reasonably stable in shallow tropical sea water, while those with >15 mol% $MgCO_3$ (i.e. most nanospheres, monocrystalline ellipsoids and small dumb-bells) should have greater dissolution potential. Because these crystal forms are species-specific, even greater emphasis is placed on the need to understand species-dependent controls on precipitation. However, the crystal morphologies and compositions described in this study are representative only of fish-derived carbonates collected and processed within 24 h of excretion. The sustained presence of the mucus envelope and associated microbes may continue to influence crystal development and/or recrystallization for some time after excretion, and thus the final form in which fish-derived carbonates are incorporated as individual crystals within the surface sediment may vary. X-ray diffraction results also suggest that carbonate samples excreted by many fish species contain not only HMC and VHMC, but also minor amounts of aragonite and LMC. While the factors driving variations in these mineral phases are not yet understood, one of the major implications is that this may result in differential preservation potential of carbonates derived from individual fish species.

CONCLUSIONS

Marine bony fish are a prolific source of marine carbonate and the results of this study indicate that marine fish could make important sedimentary contributions to shallow marine carbonate muds. At the point of excretion, these aggregated carbonates exhibit a diverse array of monocrystalline and polycrystalline morphologies (including ellipsoids, dumb-bells, spheres, rods, needles and rhombohedra) and are typically <4 μm in length. Pellets readily disaggregate upon gentle sonication, indicating that individual crystals and particles may also be released in nature, possibly including individual fibrous components of polycrystalline spheres and dumb-bells. The dominant mineralogy in most fish carbonate samples analysed is high-Mg calcite, but low-Mg calcite and amorphous Mg-carbonates can represent the major phases in some samples. Magnesium contents of excreted Mg calcites occur over a wide range from *ca* 1 to 40 mol% $MgCO_3$; this value varying with producing species and crystal morphology (which, in most cases, is species-specific). Many of the crystal morphologies described herein are unique among known producers of marine carbonate mud, and more so for the very high magnesium contents of some crystal forms. However, their small size and often very high magnesium content raise important questions about the stability of fish-derived carbonates in sea water, such as whether or not they dissolve or recrystallize, when such processes might take place, and whether these processes vary according to crystal form and composition (and thus producing species). These aspects could have important implications with respect to the contribution these crystals make to carbonate depositional regimes.

Based on the different crystalline products identified, different fish species can be classified as producing different categories of carbonate crystals; each category presumably an expression of different precipitating conditions within the

intestine. An improved understanding of the controls on precipitation products is therefore important in order to elucidate the reasons for different fish species producing different crystal types, thus allowing improved modelling of carbonate production across fish populations and, ultimately, an improved understanding of the significance of potentially differential preservation processes. From this study it is apparent that body mass and functional group (and thus diet) may not be important factors controlling precipitation type. It is more likely that the variation of precipitating conditions within species can be attributed to one or more of the following: (i) different rates of cation absorption; (ii) different organic controls on precipitation (gut microbial populations, composition of the mucous membrane, etc.); (iii) different metabolic rates; or iv) different saturation states. Three major areas of future research are identified: (i) the need to understand the wider geographical significance and diversity of fish carbonate production both in other tropical, but also subtropical to temperate, regions; (ii) the need to more fully understand the species-dependent controls on the form and diversity of crystal products; and (iii) the need to investigate the preservation potential of fish-derived carbonates with respect to the variety of crystal morphologies and the chemical compositions.

ACKNOWLEDGEMENTS

This study forms part of the doctoral studies of MAS, funded through an MMU Studentship Bursary. CTP and RWW were funded through NERC Grants NE/G010617/1 and NE/H010092/1 and BBSRC Grants BB/D005108/1 and BB/F009364/1. The authors are grateful to Aaron Shultz, Annabelle Brooks, Tyler Sclodnick, Thiago Soligo and Sarah Briggs at CEI for assistance in the field. Erin Reardon and Jon Whittamore are thanked for assistance with LC analysis, and Norman Jenkinson (MMU) is acknowledged for assistance with XRD analysis.

REFERENCES

Al-Jandal, N.J., Whittamore, J.M., Santos, E.M. and **Wilson, R.W.** (2011) The influence of 17 beta-estradiol on intestinal calcium carbonate precipitation and osmoregulation in seawater-acclimated rainbow trout (*Oncorhynchus mykiss*). *J. Exp. Biol.*, **214,** 2791–2798.

Andrews, J.E., Brimblecombe, P., Jickells, T.D., Liss, P.S. and **Reid, B.J.** (2004) *An Introduction to Environmental Chemistry*. Blackwell Science, Oxford, 298 pp.

Bertram, M.A., Mackenzie, F.T., Bishop, F.C. and **Bischoff, W.D.** (1991) Influence of temperature on the stability of magnesian calcite. *Am. Mineral.*, **76,** 1889–1896.

Bischoff, W.D., Bishop, F.C. and **Mackenzie, F.T.** (1983) Biogenically produced magnesian calcite: inhomogeneities in chemical and physical properties; comparison with synthetic phases. *Am. Mineral.*, **68,** 1183–1188.

Bischoff, W.D., Mackenzie, F.T. and **Bishop, F.C.** (1987) Stabilities of synthetic magnesian calcites in aqueous solution: comparison with biogenic materials. *Geochim. Cosmochim. Acta*, **51,** 1413–1423.

Black, M. (1933) The precipitation of calcium carbonate on the Great Bahama Bank. *Geol. Mag.* **70,** 455–466.

Boardman, M.R. and **Carney, C.** (1991) Origin and accumulation of lime mud in ooid tidal channels, Bahamas. *J. Sediment. Petrol.*, **61,** 661–680.

Bosence, D.W.J., Rowlands, R.J. and **Quine, M.L.** (1985) Sedimentology and budget of a Recent carbonate mound, Florida Keys. *Sedimentology*, **32,** 317–343.

Broecker, W.S. and **Takahashi, T.** (1966) Calcium carbonate precipitation on the Bahama Banks. *J. Geophys. Res.*, **71,** 1575–1602.

Broecker, W.S., Sanyal, A. and **Takahashi, T.** (2000) The origin of Bahamian whitings revisited. *Geophys. Res. Lett.*, **27,** 3759–3760.

Buczynski, C. and **Chafetz, H.S.** (1991) Habit of bacterially induced precipitates of calcium carbonate and the influence of medium viscosity on mineralogy. *J. Sediment. Petrol.*, **61,** 226–233.

Busenberg, E. and **Plummer, L.N.** (1989) Thermodynamics of magnesian calcite solid solutions at 25 °C and 1 Atm total pressure. *Geochim. Cosmochim. Acta*, **53,** 1189–1208.

Chafetz, H.S. and **Buczynski, C.** (1992) Bacterially induced lithification of microbial mats. *Palaios*, **7,** 277–293.

Chafetz, H.S. and **Folk, R.L.** (1984) Travertines: depositional morphology and the bacterialy constructed constituents. *J. Sediment. Petrol.*, **54,** 289–316.

Chave, K.E. (1954) Aspects of biogeochemistry of magnesium: 1. Calcareous marine organisms. *J. Geol.*, **62,** 266–283.

Chave, K.E. (1962) Factors influencing the mineralogy of carbonate sediments. *Limnol. Oceanogr.*, **7,** 218–223.

Clifton, K.B. and **Motta, P.J.** (1998) Feeding morphology, diet, and ecomorphological relationships among five Caribbean labrids (Teleostei, Labridae). *Copeia*, **1998,** 953–966.

Cloud, P.E. (1962) Environment of calcium carbonate deposition west of Andros Island, Bahamas. *U.S. Geol. Surv. Prof. Papers*, **350,** 1–138.

Debenay, J.P., André, J.P. and **Lesourd, M.** (1999) Production of lime mud by breakdown of foraminiferal tests. *Mar. Geol.*, **157,** 159–170.

Devery, D.M. and **Ehlmann, A.J.** (1981) Morphological changes in a series of synthetic Mg-calcites. *Am. Mineral.*, **66,** 592–595.

Downs, R.T. (2006) The RRUFF Project: an integrated study of the chemistry, crystallography, Raman and infrared spectroscopy of minerals. *Program and Abstracts of the 19th General Meeting of the International Mineralogical Association in Kobe, Japan (July 2006)*, O03–13.

Dravis, J. (1979) Rapid and widespread generation of Recent oolitic hardgrounds on a high-energy Bahamian platform, Eleuthera Bank, Bahamas. *J. Sediment. Petrol.*, **49,** 195–207.

Falini, G., Gazzano, M. and **Ripamonti, A.** (1994) Crystallization of calcium carbonate in presence of magnesium and polyelectrolytes. *J. Cryst. Growth*, **137,** 577–584.

Feddern, H.A. (1965) The spawning, growth and general behaviour of the bluehead wrasse, *Thalassoma bifasciatum* (Pisces, Labridae). *Bull. Mar. Sci.*, **15,** 896–941.

Fernández-Díaz, L., Putnis, A., Prieto, M. and **Putnis, C.V.** (1996) The role of magnesium in the crystallization of calcite and aragonite in a porous medium. *J. Sediment. Res.*, **66,** 482–491.

Flügel, E. (2004) *Microfacies of Carbonate Rocks.* Springer, Berlin. 976 pp.

Futterer, D.K. (1974) Significance of boring sponge Cliona for origin of fine-grained material of carbonate sediments. *J. Sediment. Petrol.*, **44,** 79–84.

Gaffey, S.J. and **Bronnimann, C.E.** (1993) Effects of bleaching on organic and mineral phases in biogenic carbonates. *J. Sediment. Petrol.*, **63,** 752–754.

Gayathri, S., Lakshminarayanan, R., Weaver, J.C., Morse, D.E., Kini, R.M. and **Valiyaveettil, S.** (2007) In vitro study of magnesium-calcite biomineralization in the skeletal materials of the seastar *Pisaster giganteus*. *Chem. Eur. J.*, **13,** 3262–3268.

Gischler, E. (2011) Sedimentary facies of Bora Bora, Darwin's Type barrier reef (Society Islands, South Pacific): the unexpected occurrence of non-skeletal grains. *J. Sediment. Res.*, **81,** 1–17.

Gischler, E. and **Zingeler, D.** (2002) The origin of carbonate mud in isolated carbonate platforms of Belize, Central America. *Int. J. Earth Sci.*, **91,** 1054–1070.

Goldsmith, J.R., Graf, D.L. and **Heard, H.C.** (1961) Lattice constants of the calcium-magnesium carbonates. *Am. Mineral.*, **46,** 453–457.

González-Muñoz, M.T., De Linares, C., Martínez-Ruiz, F., Morcillo, F., Martín-Ramos, D. and **Arias, J.M.** (2008) Ca-Mg kutnahorite and struvite production by Idiomarina strains at modern seawater salinities. *Chemosphere*, **72,** 465–472.

Greenfield, L.J. (1963) Metabolism and concentration of calcium and magnesium and precipitation of calcium carbonate by marine carbonate. *Annal. N Y Acad. Sci.*, **109,** 25–45.

Grosell, M. (2006) Intestinal anion exchange in marine fish osmoregulation. *J. Exp. Biol.*, **209,** 2813–2827.

Grosell, M., Wood, C.M., Wilson, R.W., Bury, N.R., Hogstrand, C., Rankin, C. and **Jensen, F.B.** (2005) Bicarbonate secretion plays a role in chloride and water absorption of the European flounder intestine. *Am. J. Physiol. Regul. Integr. Comp. Physiol.*, **288,** R936–R946.

Hover, V.C., Walter, L.M. and **Peacor, D.R.** (2001) Early marine diagenesis of biogenic aragonite and Mg-calcite: new constraints from high-resolution STEM and AEM analyses of modern platform carbonates. *Chem. Geol.*, **175,** 221–248.

Humbert, W., Kirsch, R. and **Simonneaux, V.** (1986) Is mucus involved in biocrystallization: study of the intestinal mucus of the sea-water eel, *Anguilla anguilla*. *Cell Tissue Res.*, **245,** 599–604.

Humbert, W., Voegel, J.C., Kirsch, R. and **Simonneaux, V.** (1989) Role of intestinal mucus in crystal biogenesis: an electron-microscopical, diffraction and X-ray microanalytical study. *Cell Tissue Res.*, **255,** 575–583.

Husseini, S.I. and **Matthews, R.K.** (1972) Distribution of high-magnesium calcite in lime muds of Great Bahama Bank: diagenetic implications. *J. Sediment. Petrol.*, **42,** 179–182.

Kloprogge, J.T., Martens, W.N., Nothdurft, L., Duong, L.V. and **Webb, G.E.** (2003) Low temperature synthesis and characterization of nesquehonite. *J. Mater. Sci. Lett.*, **22,** 825–829.

Kralj, D., Kontrec, J., Brecevic, L., Falini, G. and **Nothig-Laslo, V.** (2004) Effect of inorganic anions on the morphology and structure of magnesium calcite. *Chem. Eur. J.*, **10,** 1647–1656.

Loreau, J.P. (1982) *Sédiments aragonitiques et leur genèse*. Musèum National D'Histoire Naturelle, Paris. Mémoires, Série C 47, 300 pp.

Love, K.M. and **Woronow, A.** (1991) Chemical changes induced in aragonite using treatments for the destruction of organic material. *Chem. Geol.*, **93,** 291–301.

Lowenstam, H.A. and **Epstein, S.** (1957) On the origin of sedimentary aragonite needles of the Great Bahama Bank. *J. Geol.*, **65,** 364–375.

Macintyre, I.G. and **Reid, R.P.** (1998) Recrystallization in living porcelaneous foraminifera (*Archaias angulatis*): textural changes without mineralogic alteration. *J. Sediment. Res.*, **68,** 11–19.

Mackenzie, F.T., Bischoff, W.B., Bishop, F.C., Loijens, M., Schoonmaker, J. and **Wollast, R.** (1983) Magnesian calcites: low-temperature occurrence, solubility and solid-solution behaviour. In: *Carbonates, Mineralogy and Chemistry* (Ed. R.J. Reeder), pp. 97–144. Bookcrafters, Chelsea, MI.

Marshall, W.S. and **Grosell, M.** (2005) Ion transport and osmoregulation in fish. In: *The Physiology of Fishes* (Ed. D. Evans), pp. 177–230. CRC Press, Boca Raton, FL.

Matthews, R.K. (1966) Genesis of recent lime mud in Southern British Honduras. *J. Sediment. Petrol.*, **36,** 428–454.

Mekuchi, M., Hatta, T. and **Kaneko, T.** (2010) Mg-calcite, a carbonate mineral, constitutes Ca precipitates produced as a byproduct of osmoregulation in the intestine of seawater-acclimated Japanese eel *Anguilla japonica*. *Fish. Sci.*, **76,** 199–205.

Meldrum, F.C. and **Hyde, S.T.** (2001) Morphological influence of magnesium and organic additives on the precipitation of calcite. *J. Cryst. Growth*, **231,** 544–558.

Milliman, J.D., Freile, D., Steinen, R.P. and **Wilber, R.J.** (1993) Great Bahama Bank aragonitic muds; mostly inorganically precipitated, mostly exported. *J. Sediment. Petrol.*, **63,** 589–595.

Morse, J.W. and **Mackenzie, F.T.** (1990) *Geochemistry of Sedimentary Carbonates*. Elsevier, Amsterdam, 707 pp.

Morse, J.W., Wang, Q.W. and **Tsio, M.Y.** (1997) Influences of temperature and Mg: Ca ratio on CaCO3 precipitates from seawater. *Geology*, **25,** 85–87.

Morse, J.W., Andersson, A.J. and **Mackenzie, F.T.** (2006) Initial responses of carbonate-rich shelf sediments to rising atmospheric pCO(2) and ''ocean acidification'': role of high Mg-calcites. *Geochim. Cosmochim. Acta*, **70,** 5814–5830.

Mucci, A. and **Morse, J.W.** (1983) The incorporation of Mg^{2+} and Sr^{2+} into calcite overgrowths: influences of growth-rate and solution composition. *Geochim. Cosmochim. Acta*, **47,** 217–233.

Mucci, A., Morse, J.W. and **Kaminsky, M.S.** (1985) Auger-spectroscopy analysis of magnesian calcite overgrowths precipitated from seawater and solutions of similar composition. *Am. J. Sci.*, **285,** 289–305.

Multer, H.G. (1988) Growth-rate, ultrastructure and sediment contribution of *Halimeda incrassata* and *Halimeda monile*, Nonsuch and Falmouth Bays, Antigua, WI. *Coral Reefs*, **6,** 179–186.

Neumann, A.C. and **Land, L.S.** (1975) Lime mud deposition and calcareous algae in Bight of Abaco, Bahamas: a budget. *J. Sediment. Petrol.*, **45,** 763–786.

Newman, M.J.H., Paredes, G.A., Sala, E. and **Jackson, J.B.C.** (2006) Structure of Caribbean coral reef communities across a large gradient of fish biomass. *Ecol. Lett.*, **9,** 1216–1227.

Perry, C.T., Salter, M.A., Harborne, A.R., Crowley, S.F., Jelks, H.L. and **Wilson, R.W.** (2011) Fish as major carbonate mud producers and missing components of the tropical carbonate factory. *Proc. Nat. Acad. Sci. U S A*, **108,** 3865–3869.

Plummer, L.N. and **Mackenzie, F.T.** (1974) Predicting mineral solubility from rate data; application to dissolution of magnesian calcites. *Am. J. Sci.*, **274,** 61–83.

Pomar, L. and **Hallock, P.** (2008) Carbonate factories: a conundrum in sedimentary geology. *Earth Sci. Rev.*, **87,** 134–169.

Power, I.M., Wilson, S.A., Thom, J.M., Dipple, G.M. and **Southam, G.** (2007) Biologically induced mineralization of dypingite by cyanobacteria from an alkaline wetland near Atlin, British Columbia, Canada. *Geochem. Trans.*, **8,** 13.

Prieto, M., Putnis, A., Fernández-Díaz, L. and **López-Andrés, S.** (1994) Metastability in diffusing-reacting systems. *J. Cryst. Growth*, **142,** 225–235.

Purdy, E.G. and **Gischler, E.** (2003) The Belize margin revisited: 1. Holocene marine facies. *Int. J. Earth Sci.*, **92,** 532–551.

Randall, J.E. (1967) Food habits of reef fishes of the West Indies. *Stud. Trop. Oceanogr.*, **5,** 665–847.

Reddy, M.M. and **Wang, K.K.** (1980) Crystallization of calcium carbonate in the presence of metal ions: 1. Inhibition by magnesium ion at pH 8.8 and 25 °C. *J. Cryst. Growth*, **50,** 470–480.

Reid, R.P. and **MacIntyre, I.G.** (1998) Carbonate recrystallization in shallow marine environments: a widespread diagenetic process forming micritized grains. *J. Sediment. Res.*, **68,** 928–946.

Reid, R.P., Macintyre, I.G. and **Post, J.E.** (1992) Micritized skeletal grains in Northern Belize lagoon: a major source of Mg-calcite mud. *J. Sediment. Petrol.*, **62,** 145–156.

Rivadeneyra, M.A., Delgado, R., Parraga, J., Ramos-Cormenzana, A. and **Delgado, G.** (2006) Precipitation of minerals by 22 species of moderately halophilic bacteria in artificial marine salts media: influence of salt concentration. *Folia Microbiol.*, **51,** 445–453.

Robbins, L.L. and **Blackwelder, P.L.** (1992) Biochemical and ultrastructural evidence for the origin of whitings: A biologically induced calcium carbonate precipitation mechanism. *Geology*, **20,** 464–468.

Sánchez-Román, M., Rivadeneyra, M.A., Vasconcelos, C. and **McKenzie, J.A.** (2007) Biomineralization of carbonate and phosphate by moderately halophilic bacteria. *FEMS Microbiol. Ecol.*, **61,** 273–284.

Sawada, K., Ogino, T. and **Suzuki, T.** (1990) The distribution coefficients of Mg^{2+} ion between $CaCO_3$ polymorphs and solution and the effects on the formation and transformation of $CaCO_3$ in water. *J. Cryst. Growth*, **106,** 393–399.

Schlager, W. (2003) Benthic carbonate factories of the Phanerozoic. *Int. J. Earth Sci.*, **92,** 445–464.

Schmalz, R.F. (1967) Kinetics and diagenesis of carbonate sediments. *J. Sediment. Res.*, **37,** 60–67.

Shehadeh, Z.H. and **Gordon, M.S.** (1969) The role of the intestine in salinity adaptation of the rainbow trout, *Salmo gairdneri*. *Comp. Biochem. Physiol.*, **21,** 7711–7717.

Shinn, E.A., Steinen, R.P., Lidz, B.H. and **Swart, P.K.** (1989) Whitings, a sedimentologic dilemma. *J. Sediment. Petrol.*, **59,** 147–161.

Smith, S.V. (1972) Production of calcium carbonate on the mainland shelf of Southern California. *Limnol. Oceanogr.*, **17,** 28–41.

Stieglitz, R.D. (1972) Scanning electron microscopy of the fine fraction of recent carbonate sediments from Bimini, Bahamas. *J. Sediment. Petrol.*, **42,** 411–426.

Stockman, K.W., Ginsburg, R.N. and **Shinn, E.A.** (1967) The production of lime mud by algae in South Florida. *J. Sediment. Petrol.*, **37,** 633–648.

Taft, W.H. and **Harbaugh, J.W.** (1964) *Modern Carbonate Sediments of Southern Florida, Bahamas, and Espiritu Santo Island, Baja, California: A Comparison of their Mineralogy and Chemistry, University Series, Geological Sciences*, pp. 1–133. Stanford University Press, Palo Alto, CA.

Van der Leeden, M.C. and **Van Rosmalen, G.M.** (1987) Aspects of additives in precipitation processes: performance of polycarboxylates in gypsum growth prevention. *Desalination*, **66,** 185–200.

Walsh, P.J., Blackwelder, P., Gill, K.A., Danulat, E. and **Mommsen, T.P.** (1991) Carbonate deposits in marine fish intestines: a new source of biomineralization. *Limnol. Oceanogr.*, **36,** 1227–1232.

Walter, L.M. and **Morse, J.W.** (1984) Magnesian calcite stabilities: a re-evaluation. *Geochim. Cosmochim. Acta*, **48,** 1059–1069.

Walter, L.M., Bischof, S.A., Patterson, W.P. and **Lyons, T.W.** (1993) Dissolution and recrystallization in modern shelf carbonates: evidence from porewater and solid-phase chemistry. *Philos. Trans. R. Soc. Lond. A Math. Phys. Eng.*, **344,** 27–36.

Wasylenki, L.E., Dove, P.M., Wilson, D.S. and **De Yoreo, J.J.** (2005) Nanoscale effects of strontium on calcite growth: an in situ AFM study in the absence of vital effects. *Geochim. Cosmochim. Acta*, **69,** 3017–3027.

White, J.W. and **Samhouri, J.F.** (2011) Oceanographic coupling across three trophic levels shapes source-sink dynamics in marine metacommunities. *Oikos*, **120,** 1151–1164.

Wilson, R.W., Gilmour, K.M., Henry, R.P. and **Wood, C.M.** (1996) Intestinal base excretion in the seawater-adapted rainbow trout: a role in acid-base balance? *J. Exp. Biol.*, **199,** 2331–2343.

Wilson, R.W., Wilson, J.M. and **Grosell, M.** (2002) Intestinal bicarbonate secretion by marine teleost fish - why and how? *Biochim. Biophys. Acta Biomembr.*, **1566,** 182–193.

Wilson, R.W., Millero, F.J., Taylor, J.R., Walsh, P.J., Christensen, V., Jennings, S. and **Grosell, M.** (2009) Contribution of fish to the marine inorganic carbon cycle. *Science*, **323,** 359–362.

Zhang, F.F., Xu, H.F., Konishi, H. and **Roden, E.E.** (2010) A relationship between d(104) value and composition in the calcite-disordered dolomite solid-solution series. *Am. Mineral.*, **95,** 1650–1656.

Manuscript received 7 December 2011; revision accepted 3 May 2012